

**VIBRATIONAL SPECTRAL ANALYSIS, QUANTUM
CHEMICAL CALCULATIONS AND MOLECULAR
DOCKING OF SOME POLYATOMIC MOLECULES**



Thesis submitted to

Bharathidasan University, Tiruchirappalli

in partial fulfillment of the requirements for the award of the degree of

DOCTOR OF PHILOSOPHY IN PHYSICS

by

K. VENIL

(Ref.No.40381/Ph.D.K3/Physics/Full-Time/Jan 2017)

Under the Guidance of

Dr. A. LAKSHMI M.Sc., M.Phil., Ph.D.



DEPARTMENT OF PHYSICS

GOVERNMENT ARTS COLLEGE

TIRUCHIRAPPALLI - 620022, TAMIL NADU

JULY 2021

Dr. A. LAKSHMI M.Sc., M.Phil., Ph.D.,

Assistant Professor,

Department of Physics,

Government Arts College,

Tiruchirappalli – 620 022.



Date:

CERTIFICATE

This is to certify that the work incorporated in this thesis titled, **“VIBRATIONAL SPECTRAL ANALYSIS, QUANTUM CHEMICAL CALCULATIONS AND MOLECULAR DOCKING OF SOME POLYATOMIC MOLECULES”** submitted to the Bharathidasan University in Partial fulfillment of the requirements for the degree of **“DOCTOR OF PHILOSOPHY IN PHYSICS”** is a bonafide record of work done by **K.VENIL (Ref.No.40381/Ph.D. K3/Full-Time/Physics/Jan’17)** who carried out the research under my supervision. Certified further that to the best of my knowledge, the contents of this thesis have not been formed the basis for the award of any degree, associate ship, diploma, fellowship or any other similar title of any university or institution.

Research Supervisor

K.VENIL, M.Sc., M.Phil.,

Research Scholar,

Department of Physics,

Government Arts College,

Tiruchirappalli – 620 022.

DECLARATION

This research work presented in this thesis titled, “**VIBRATIONAL SPECTRAL ANALYSIS, QUANTUM CHEMICAL CALCULATIONS AND MOLECULAR DOCKING OF SOME POLYATOMIC MOLECULES**” was carried out by me under the supervision of **Dr. A. LAKSHMI**, Assistant Professor, Department of Physics, Government Arts College, Tiruchirappalli. This work is original and has not been submitted in part or full for any other degree or diploma of this or any other university.

Place: Tiruchirappalli

Signature of the Candidate

Date :

Dr. A. LAKSHMI M.Sc., M.Phil., Ph.D.,

Assistant Professor,

Department of Physics,

Government Arts College,

Tiruchirappalli – 620 022.



CERTIFICATE OF PLAGIARISM













This is to certify that the thesis titled, “**VIBRATIONAL SPECTRAL ANALYSIS, QUANTUM CHEMICAL CALCULATIONS AND MOLECULAR DOCKING OF SOME POLYATOMIC MOLECULES**” was carried out by **K.VENIL (Ref.No. 40381/Ph.D. K3/Full-Time/Physics/Jan’17)** under my supervision. The work presented is original and own work of the author. The thesis has been checked using **Curiginal** plagiarism checker (copy of original report attached) and found within the limits as per the Ph.D regulations of the Bharathidasan University.

Research Supervisor

Document Information

Analyzed document	(Venil) plag pdf.pdf (D109686043)
Submitted	6/25/2021 10:21:00 AM
Submitted by	Srinivasa ragavan S
Submitter email	bdulib@gmail.com
Similarity	17%
Analysis address	bdulib.bdu@analysis.arkund.com

Sources included in the report

W	URL: https://www.researchgate.net/publication/278688704_Vibrational_spectra_HOMO_LUMO_NB_O_MEP_analysis_and_molecular_docking_study_of_22-diphenyl-4-piperidin-1-ylbutanamide Fetched: 3/10/2020 12:17:31 PM		1
W	URL: https://core.ac.uk/download/pdf/229209022.pdf Fetched: 12/29/2020 9:27:25 AM		5
W	URL: https://www.elixirpublishers.com/articles/1381908896_63%20(2013)%2018536-18554.pdf Fetched: 4/27/2021 7:28:33 AM		3
W	URL: https://hal.archives-ouvertes.fr/hal-01636270/file/revealing_strong_interactions_rev-1.pdf Fetched: 6/25/2021 10:23:00 AM		1
W	URL: https://www.ripublication.com/ijoms17spl/ijomsv12n2spl_23.pdf Fetched: 7/12/2020 4:14:33 PM		14
W	URL: https://core.ac.uk/download/pdf/229210724.pdf Fetched: 6/22/2021 12:34:10 PM		11
W	URL: http://www.journalcra.com/sites/default/files/issue-pdf/9784_0.pdf Fetched: 6/16/2021 8:10:02 AM		2
W	URL: https://rajpub.com/index.php/jac/article/view/1957/1915 Fetched: 2/10/2020 10:22:00 AM		14
W	URL: https://link.springer.com/article/10.1007/s13538-018-0613-5 Fetched: 6/12/2021 11:57:58 PM		6
W	URL: https://www.ncbi.nlm.nih.gov/pmc/articles/PMC6895590/ Fetched: 3/10/2020 8:26:00 PM		9
W	URL: https://www.degruyter.com/document/doi/10.1515/chem-2018-0005/html Fetched: 5/19/2021 8:30:09 AM		10
W	URL: https://isroset.org/pub_paper/IJSRPAS/12-IJSRPAS-01850-03.pdf Fetched: 6/21/2021 9:40:17 AM		26

ACKNOWLEDGEMENT

First and foremost I thank God Almighty for showered his blessings throughout my research work.

I express my sincere thanks to **Dr. S.S. Rosemary, M.Com., Ph.D**, Principal, Government Arts College, Trichy, for giving me permission to do my research work in this esteemed institution.

I would like to thank **Dr. M. Arivazhagan**, Head, Department of Physics, Government Arts College, Trichy, for permitting and providing me with all facilities to carry out the research work in the Department of Physics.

I express my sincere and heartfelt thanks to my research supervisor **Dr. A. Lakshmi, M.Sc., M.Phil., Ph.D**, Assistant Professor, Department of Physics, Government Arts College, Trichy, whose valuable guidance, suggestions and encouragement helped me for the successful completion of this research work.

I would like to thank the doctoral committee members **Dr. V. Balachandran**, Assistant Professor, PG and Research Department of Physics, Arignar Anna Government Arts College, Musiri and **Dr. M.K.Murali**, Assistant Professor and Head, Department of Physics, J.J. College of Arts and Science, Pudukkottai for their helpful comments and suggestions.

I would like to thank **Dr. W. Nirmala**, Assistant Professor, Department of Physics, Government Arts College, Trichy for helping me during the research work.

My special thanks to **Ms. N. Shanmugapriya, Ms. J. Jayasudha, Ms. S. Babiyana, Mrs. A. Viji, Mr. C. Sivakumar, Mr. R. Vijayakumar, Dr. K. Vanasundhari, Dr. K. Anitha**, who have helped me in many ways during my research work.

Finally I would like to express my thanks to my husband **Mr. M. Ravi** and my children **R. Siva Shankar, R. Elancheran** who helped and supported me a lot during my research work.

K. Venil

PREFACE

Vibrational spectroscopy is a frequently used tool to identify and characterize a molecule with the help of its vibrational modes.

The vibrational spectroscopy is useful in the identification of functional groups and the strength of the chemical bonding between atoms. The vibrational and rotational energies of molecules can be studied by infrared and Raman spectroscopy. The infrared and Raman spectroscopic methods yield complementary type of informations. For a complete vibrational analysis, both methods should necessarily be used. The observed frequencies obtained from IR and Raman spectra along with spectral parameters are used to carry out the normal coordinate analysis of some polyatomic molecules.

The quantum chemical calculations have been performed by GAUSSIAN 09W program package with the standard B3LYP/6-31G, 6-31G (d, p) basis sets. Optimized geometrical parameters, vibrational assignments, HOMO-LUMO, molecular electrostatic potential, Mulliken atomic charges were discussed. Natural Bond Orbital (NBO) analysis was carried out using NBO 3.1 program as implemented in the Gaussian 09 package. Reduced Density Gradient (RDG) analysis was calculated with the help of Multiwfn program and plotted by the Visual Molecular Dynamics program (VMD). Molecular docking studies were done by Autodock 4.2 software and the ligand-protein interaction was analyzed using Pymol and Discovery studio visualization software.

Chapter 1: In this chapter introduces the principles of vibrational spectroscopy and the necessary theory for the simplification of problems in vibrational spectroscopy. The

normal modes of vibrations and the theory of infrared absorption and Raman spectroscopy have been discussed.

Chapter 2: This theory deals with Quantum chemical calculations. The different quantum chemical calculations such as *Ab initio* methods, Density functional theory, semi-empirical methods were discussed. Different types of Basis sets are also presented here. Brief description about NBO, Molecular electrostatic potential, Fukui functions were discussed. Molecular Docking studies, reduced density gradient analysis were explained.

Chapter 3: This chapter includes the FT-IR and FT-Raman spectroscopic techniques, source, detectors, sample handling techniques and advantages.

Chapter 4: In this chapter we reported the molecular structure, optimized geometry of 5-(4-Propan-2-yl)benzylidene)-2-[3-(4-chlorophenyl)-5[4-(propan-2-yl)phenyl-4,5-dihydro-1*H*-pyrazol-1-yl]-1,3-thiazol-4(5*H*)-one based on quantum chemical calculations. The vibrational spectral assignments have been carried out using potential energy distribution (PED) analysis. The molecular electrostatic potential (MEP), HOMO-LUMO, RDG analysis, Fukui functions and Atoms In the Molecule (AIM) analysis were carried out. To study the biological activity of the title molecule, Molecular docking studies were done to identify the binding energy with different proteins.

Chapter 5: In this chapter the experimental and theoretical investigation of molecular structure, vibrational spectra of 5-(4-butoxybenzylidene)-2-[3-(4-chlorophenyl)-5[4-(propan-2-yl)-4,5-dihydro-1*H*-pyrazol-1-yl]-1,3-thiazol-4(5*H*)-one have been investigated using density functional theory (DFT) B3LYP method with 6-31G and 6-

31G (d,p) basis sets. The geometry of the molecule was fully optimized, vibrational spectra and fundamental vibrations were assigned on the basis of potential energy distribution (PED) analysis. In addition, molecular electrostatic potential (MEP), HOMO-LUMO, RDG analysis, Fukui functions and Atoms In the Molecule (AIM) analysis were carried out. The biological activity of the title compound has been made based on the prediction of Molecular docking results.

Chapter 6: This chapter deals with the conformational stability and vibrational analysis of (4Z)-4-(4-Methylbenzylidene)-2-phenyl-1,3-oxazol-5(4H)-one has been carried out by the application of B3LYP/6-31G and B3LYP/6-31G (d,p) basis sets based on scaled quantum mechanical method. The molecular stability and bond strength were investigated by applying the natural bond orbital analysis. The effect of substitution of electron withdrawing groups on the acceptor ring is studied by using HOMO-LUMO analysis. The molecular electrostatic potential (MEP), Fukui function, RDG analysis and AIM analysis were carried out. Besides, the docking has been performed by using variant proteins with the ligand i.e. the title molecule. The result obtained by docking suggests that the title molecule may possess the neuron disorder activity.

Chapter 7: This chapter comprises on quantum chemical calculations an experimental and theoretical study on molecular structure, vibrational spectra of (2E)-1-(anthracene-9-yl)-3-(4-ethoxyphenyl) prop-2-en-1-one were carried out. The FT-IR and FT-Raman spectra were recorded in the solid phase. From the MEP plot it is evident that the negative electrostatic potential regions are mainly localized. The natural bond orbital (NBO) analysis, Fukui function, RDG and AIM analysis were carried out. The molecular

docking studied was also done to identify the binding energy with different proteins and hydrogen bond length.

Chapter 8: This chapter includes the structure and spectroscopic studies of (2E) -1-(anthracene -9-yl)-3-(biphenyl-4-yl)prop-2-en-1-one has been studied based on quantum chemical calculations. Structure optimization by force field calculations based on density functional theory at the HF/6-31G and B3LYP/6-31G basis sets and the geometry of the molecule was fully optimized. In addition, the molecular electrostatic potential (MEP), Fukui function, RDG and AIM analysis were carried out. The biological effect of the title molecule has been made on the prediction of molecular docking results.

LIST OF PUBLICATIONS

1. FT-IR and FT-Raman investigation, quantum chemical analysis and molecular docking studies of 5-(4-propan-2-yl)benzylidene)-2-[3-(4-chlorophenyl)-5[4-(propan-2-yl)phenyl-4,5-dihydro-1*H*-pyrazol-1-yl]-1,3-thiazol-4(5*H*)-one, J Mol. Struct., 1225 (129070) (2021) 1-16.
2. Molecular docking, vibrational, structural and electronic studies of 5-(4-Butoxybenzylidene)-2-[3-(4-chlorophenyl)-5[4-(propan-2-yl)-4,5-dihydro-1*H*-pyrazol-1-yl]-1,3-thiazol-4(5*H*)-one, Annals of Romanian Society for Cell Biology, ISSN No: 1583-6258, 25 (5) (2021) 1587-1628.
3. FT-IR and FT-Raman Investigation, Quantum Chemical Analysis and Molecular Docking Studies of (4*Z*)-4-(4-Methylbenzylidene)-2-phenyl-1,3-oxazol-5(4*H*)-one, NOVYI MIR Research Journal, (ISSN: 0130-7673) Vol.6 Issue 3 pp 115-136.
4. Vibrational structural and electronic studies of (2*e*)-1-(anthracene-9-yl)-3-(4-ethoxyphenyl)prop-2-en-1-one, Journal of information and computational science, ISSN: 1548-7741) Vol. 10 Issue 4 pp 28-50.

PAPER PRESENTED IN CONFERENCES

1. Vibrational studies [FT-IR and FT-Raman], NBO, HOMO-LUMO and MEP of (2E)-1-(anthracene-9-yl)-3-(biphenyl-4-yl)prop-2-en-1-one based on quantum chemical calculation, International conference on recent advances in materials science (ICRAMS-2019) held on 04-06 Feb.2019 at National College, Trichy.
2. Vibrational studies [FT-IR and FT-Raman], NBO, HOMO-LUMO, RDG and MEP of 5-(4-Propan-2-yl)benzylidene)-2-[3-(4-chlorophenyl)-5[4-(propan-2-yl)phenyl-4,5-dihydro-1H-pyrazol-1-yl]-1,3-thiazol-4(5H)-one based on quantum chemical calculation, National conference on advanced materials and applications (NCAMA-2020) held on 27-28 Feb.-2020 at Urumu Dhanalakshmi College, Trichy.
3. FT-IR and FT-Raman investigation, quantum chemical analysis and molecular docking studies of (4Z)-4-(4-Methylbenzylidene)-2-phenyl-1,3-oxazol-5(4H)-one, National virtual conference on recent trends in materials science and technology (NCMST-2021) held on May 28, Kongunadu College of Engineering and Technology (Autonomous), Trichy.

CONTENT

Serial No.	Title	Page No.
	Certificate	ii
	Declaration	iii
	Certificate of Plagarism	iv
	Acknowledgement	v
	Preface	vi
	List of Publications	viii
	Paper presented in conferences	ix

Chapter – 1

An introduction to vibrational spectroscopy

1.1	Introduction	1
1.2	Vibrational Spectroscopy	1
1.3	Theory of infrared absorption and Raman spectroscopy.....	4
1.4	Molecular vibration	6
1.5	Normal coordinates	7
1.6	Molecular force constants.....	7
1.7	Force fields	8
1.8	Solution by symmetry and internal coordinates	9
1.9	Group theory and molecular vibrations.....	10

Chapter – 2

Quantum Chemical Calculations

2.1	Introduction	16
2.2	Survey of computational chemistry methods	16
2.3	Molecular Mechanics	17
2.4	Semi-empirical methods.....	19
2.5	<i>Ab-initio</i> method	20
2.6	Basis set	27

2.7	Properties arising from electron distribution.....	32
2.8	HOMO-LUMO analysis.....	33
2.9	Natural bond orbital analysis.....	34
2.10	Molecular electrostatic potential maps.....	39
2.11	Fukui function	40
2.12	Topological analysis	41
2.13	Reduced density gradient analysis	42
2.14	Molecular docking studies.....	43
2.15	Software used in the work	44

Chapter – 3

Instrumentation Techniques

3.1	Introduction	46
3.2	Dispersive infrared spectrometer.....	46
3.3	Fourier Transform Infrared spectrometer.....	47
3.4	Fourier Transform Raman spectrometer	57

Chapter – 4

FT-IR and FT-Raman investigation, quantum chemical analysis and molecular docking studies of 5-(4-Propan-2-yl)benzylidene)-2-[3-(4-chlorophenyl)-5[4-(propan-2-yl)phenyl-4,5-dihydro-1*H*-pyrazol-1-yl]-1,3-thiazol-4(5*H*)-one

4.1	Introduction	62
4.2	Experimental details	64
4.3	Computational details.....	64
4.4	Results and discussions	65
4.4.1	Optimized molecular geometrical parameters.....	65
4.4.2	Vibrational assignments	66
4.5	Mulliken population analysis	77
4.6	Molecular electrostatic potential (MEP) surface.....	79
4.7	Molecular orbital studies	81
4.8	Natural bond orbital analysis.....	83

4.9	Fukui Function.....	85
4.10	Reduced density gradient (RDG) analysis	87
4.11	Atoms in molecule analysis.....	87
4.12	Molecular docking studies	90
4.13	Conclusion.....	94

Chapter – 5

Molecular Docking, vibrational, structural and electronic studies of 5-(4-Butoxybenzylidene)-2-[3-(4-chlorophenyl)-5[4-(propan-2-yl)-4,5-dihydro-1H-pyrazol-1-yl]-1,3-thiazol-4(5H)-one

5.1	Introduction	112
5.2	Experimental details	113
5.3	Computational details.....	114
5.4	Results and discussions	114
5.4.1	Optimized molecular geometrical parameters.....	114
5.4.2	Vibrational assignments	117
5.5	Mulliken population analysis	130
5.6	Molecular electrostatic potential (MEP) surface.....	131
5.7	Frontier molecular orbital (FMO) study.....	133
5.8	Natural bond orbital analysis.....	134
5.9	Reduced density gradient analysis.....	137
5.10	Fukui Function.....	138
5.11	Topological analysis	139
5.12	Molecular docking studies	140
5.13	Conclusion.....	145

Chapter – 6

FT-IR and FT-Raman investigation, quantum chemical analysis and molecular docking studies of (4Z)-4-(4-Methylbenzylidene)-2-phenyl-1,3-oxazol-5(4H)-one

6.1	Introduction	166
6.2	Experimental details	167
6.3	Computational details.....	167

6.4	Results and discussions	168
6.4.1	Molecular geometry.....	168
6.4.2	Vibrational analysis.....	173
6.5	Mulliken atomic charge analysis.....	178
6.6	Frontier molecular orbital analysis.....	180
6.7	Natural bond orbital analysis.....	183
6.8	Molecular electrostatic potential (MEP) surface.....	184
6.9	Reduced density gradient analysis	185
6.10	Fukui Function.....	187
6.11	Topological analysis	189
6.12	Molecular docking studies	190
6.13	Conclusion.....	194

Chapter – 7

Molecular Docking, vibrational, structural and electronic studies of (2E)-1-(anthracene-9-yl)-3-(4-ethoxyphenyl) prop-2-en-1-one

7.1	Introduction	210
7.2	Experimental details	211
7.3	Computational details.....	212
7.4	Results and discussions	213
7.4.1	Optimized molecular geometrical parameters.....	213
7.4.2	Vibrational assignments	214
7.5	Mulliken population analysis	222
7.6	Natural bond orbital analysis.....	223
7.7	Frontier molecular orbital analysis.....	226
7.8	Molecular electrostatic potential (MEP) surface.....	227
7.9	Reduced density gradient (RDG) analysis	229
7.10	Fukui Function.....	232
7.11	Atom in molecule analysis	233
7.12	Molecular docking studies.....	234
7.13	Conclusion.....	239

Chapter – 8

Vibrational studies, Reduced Density Gradient and molecular docking studies of (2E)- 1-(anthracene-9-yl)-3-(biphenyl-4-yl) prop-2-en-1-one

8.1	Introduction	254
8.2	Experimental details	256
8.3	Computational details	256
8.4	Results and discussions	257
8.4.1	Optimized molecular geometrical parameters.....	257
8.4.2	Vibrational assignments	262
8.5	Mulliken population analysis	266
8.6	Frontier molecular orbital analysis.....	266
8.7	Natural bond orbital analysis.....	270
8.8	Molecular electrostatic potential surface analysis.....	271
8.9	Reduced density gradient analysis	274
8.10	Fukui Function.....	275
8.11	Atoms in molecules	277
8.12	Molecular docking studies	279
8.13	Conclusion.....	283
	Summary of Conclusion	293
	Reference	
	Reprints	

Chapter – 1

An Introduction to Vibrational Spectroscopy

CHAPTER – 1

An introduction to Vibrational spectroscopy

1.1 Introduction

Molecular spectroscopy is the study of the interactions between electromagnetic radiation and molecular systems. Modern spectroscopic methods covering the entire electromagnetic spectrum are becoming powerful tools for studying the physical properties of molecules, such as their molecular structure, chemical bonds, hydrogen bonding, isomerism and so on.

Vibrational spectroscopy is mainly concerned with vibrational transitions due to the absorption and emission of electromagnetic radiations. Vibrational transitions can be observed as Infrared and Raman spectra. It also provides information about intramolecular forces acting between the atoms in a molecule, the intermolecular forces in condensed phase and the nature of chemical bond.

1.2 Vibratioal spectroscopy

The vibrational spectroscopy of molecules probes the periodic oscillations of atoms. These oscillations do not occur at random, but are precisely defined. When considering an N-atomic molecule, there are $3N$ degrees of freedom, of which three (two) refer to translations and three (two) correspond to rotations in a nonlinear (linear) molecule structure. In this case, the remaining degrees of freedom are represented by the $3N-6$ ($3N-5$) vibrations of a nonlinear (linear) molecule. Every atom oscillates at the

same frequency and with the same phase although with different amplitude in each normal mode. Nevertheless, in vibrational spectroscopy, the first principle observable is the frequency, which is dependent on the forces acting on the individual atoms and on their masses. These forces are generated not only by chemical bonds between individual atoms, but also by nonbonding interactions inside the molecule and with the molecular environment.

In this approach, the frequencies of the normal modes serve as a characteristic signature of the molecule's chemical constitution, structure and electron density distribution in a specific chemical environment, i.e., all of the parameters required for an atomic-scale description of a molecule. These characteristics also determine the vibrational spectrum's second most important observable parameter: the band intensities, which, unlike the frequencies, are not independent of the method used to investigate the spectrum. IR and Raman spectroscopy are two commonly used techniques for obtaining vibrational spectra by different mechanisms. With IR spectroscopy, molecules are exposed to a continuous flow of IR radiation and the photons with energies corresponding to the frequencies of the normal modes can be absorbed to excite the respective vibrations. IR radiation with wavelengths corresponding to the frequency of molecular vibrations is typically found between 2.5 and 50 μm in wavelength. In Raman spectroscopy, the vibrational transitions occurred when monochromatic light is inelastically scattered by the molecule, so that the light's frequency is shifted by the vibrational frequency of the molecule. In molecules, absorption- and scattering-induced vibrational transitions have different probabilities, which are reflected in their IR and

Raman spectra and provide additional information about structural and electronic properties.

Nevertheless, Raman and IR spectroscopy have broader applications in the life sciences, as they are not limited to the study of minute structural changes. The use of these techniques may provide valuable insights into proteins, nucleic acids and membranes. Proteins are constructed from amino acids, which are linked by the same chemical entities as peptide bonds. In the same way, nucleic acids are composed of repeated units of sugar-phosphate linkages. A vibrational spectrum of these units can give insights into the secondary structures of proteins and nucleic acids, since some of the modes of vibration depend on the folding of the biopolymer chain. The lipid molecules that form bilayer membranes have the same conformations on a periodic basis, thus giving them global structural properties. For these conformations, characteristic vibrational marker bands can be monitored in order to determine phase transitions or other prolonged structural changes. Over the past few years, Raman and IR spectroscopy have seen substantial advances, but there has not been enough progress in the development of universal strategies for extracting structural information from spectra. Still, empirical approaches prevail that are based on the comparison with experimental data for related systems and model compounds.

In addition to vibrational analysis of proteins, genetic engineering enables individual amino acids to be assigned specific bands. A key strength of this approach is the close collaboration of spectroscopists and biologists, since it is essential to assess individual mutations' functional consequences before unambiguous interpretation can be

made of their spectra in terms of structure-function. As a consequence, these empirical approaches typically target only a small portion of the vibrational spectrum and thus obscure a vast amount of structural information. More comprehensive methods are based on the classical treatment of the vibrational Eigen state problem. With the increase in availability of powerful personal computers, the popularity of quantum chemical programs, the development of efficient program codes, and the development of efficient programs, all of these factors have helped to open up new possibilities for comprehensive and reliable vibrational analysis. The use of these approaches requires a good understanding of theoretical chemistry, but in time, they should become standard tools that experimentalists may also use.

1.3 Theory of infrared absorption and Raman spectroscopy

Molecular vibrations exhibited in two physical mechanisms: the absorption of light quanta and the inelastic scattering of photons [1]. A direct absorption of photons is achieved by irradiating molecules with polychromatic light that contains photons that have an energy difference $h\nu_k$ between an initial (e.g., ground state) and an excited (e.g., first excited state) vibrational state.

$$h\nu_k = h\nu_f - h\nu_i \quad \dots(1.1)$$

As these energy differences are in the order of 0.5 and 0.005 eV, light with wavelengths longer than 2.5 mm, that is infrared (IR) light, is sufficient to induce the vibrational transitions. Hence, vibrational spectroscopy, which is based on the direct absorption of light photons, means IR absorption or IR spectroscopy.

Unlike IR spectroscopy, the scattering process of exciting molecular vibrations requires monochromatic irradiation. Part of the incident photon is inelastically dissociated, so the energy of incident photon ($h\nu_0$) and the energy of scattered photon ($h\nu_R$) are different. A molecule's energy difference corresponds to the transition between two vibrational states, according to the law of conservation of energy. Thus, the energy differences

$$h\nu_0 - h\nu_R = h\nu_f - h\nu_i \quad \dots(1.2)$$

despite the fact that UV, visible, or near-infrared photons are used to cause scattering, the transitions investigated using direct absorption of mid-IR photons are in the same range as the transitions analyzed with direct absorption of mid-IR photons. This inelastic scattering of photons was first discovered by the Indian scientist C.V. Raman in 1928 and is thus denoted as the Raman Effect.

IR and Raman spectroscopy each probe different vibrational transitions of a molecule and in many cases both provide complementary information. In order to facilitate comparison, IR and Raman spectra are usually plotted analogously. An ordinate indicates the amount of light that is absorbed (IR) or scattered (Raman). When measuring IR absorption spectroscopy, the amount of absorption is expressed in units of absorbance, is less accurate, but commonly used in terms of optical density. Raman intensity, on the other hand, is measured in terms of the number of photons detected per second. In most instances, only relative intensities represent physically meaningful quantities as the value depends on many apparatus-specific parameters. In practice, Raman intensity scales are usually expressed using arbitrary units or omitted altogether. On the abscissa is shown the

vibrational energy, expressed in terms of wavenumbers (cm^{-1}), which correspond to the absorbed light frequency, ν_{abs} in IR spectroscopy, and difference between the excited and scattered light, $h\nu_0 - h\nu_R$ in Raman spectroscopy and it is depicted in Fig 1.1.

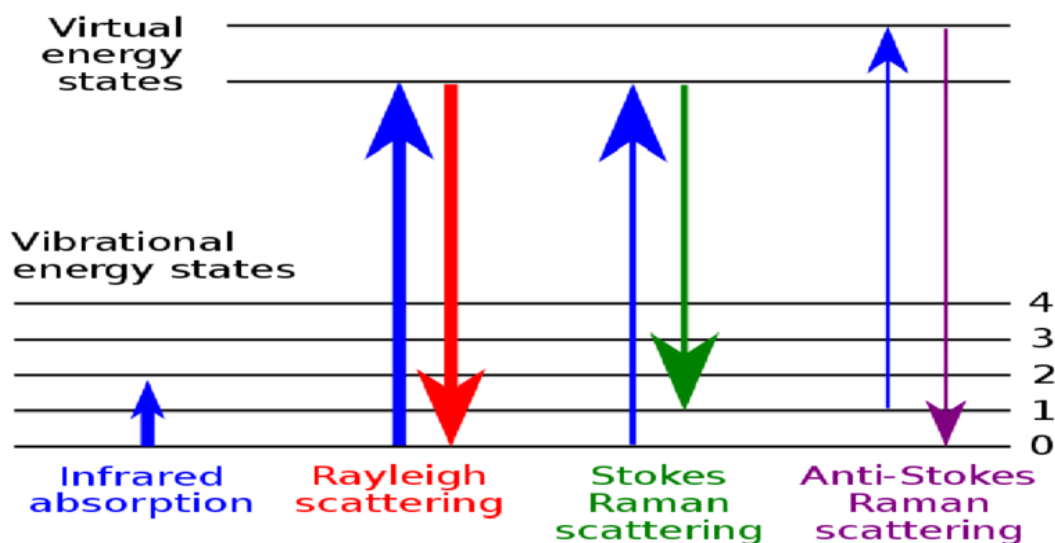


Fig. 1.1 Energy levels involved in Raman and Rayleigh scattering

1.4 Molecular vibration

In a molecular vibration, atoms in a molecule move periodically while the molecule rotates and translations constantly. Vibration frequency is defined as the frequency of periodic motion. Thus a diatomic molecule has only one normal mode of vibration. In polyatomic molecules, each normal mode of vibration is independent of the others, involving simultaneous vibrations of different parts. The vibration of a molecule is excited when a quantum of energy (E) is absorbed by it, corresponding to the vibration's frequency (ν), according to the relation $E=h\nu$. When a molecule absorbs a

quantum of energy in its ground state, a fundamental vibration is excited. Overtones are excited as two quanta are absorbed, and so on until higher overtones are excited.

1.5 Normal coordinates

According to a normal mode of vibration, the normal coordinates are the positions of atoms away from their equilibrium positions. Each normal mode has a single normal coordinate, which represents the "progress" along that normal mode. Formally, the normal modes are obtained by solving a secular determinant, which is then summarized over the Cartesian coordinates (over the atom positions) to obtain the normal coordinates. By working in normal modes, the matrix governing molecular vibrations is diagonalized, so that each normal mode has a spectrum of quantum mechanical states associated with it. In the presence of symmetries, a molecule will belong to a point group and its normal modes will "transform into" an irreducible representation. By applying group theory to the irreducible representation and projecting it onto the Cartesian plane, normal modes can be qualitatively determined [2].

1.6 Molecular force constants

Vibrational frequencies and structural data can be combined to determine the nature of forces binding the atoms together and to evaluate several molecular constants. Force constants represent the amount of force needed to restore a unit displacement or to stretch or bend an object, respectively. This quantity indicates the strength of chemical bonds between elements. As isotopic substitution does not alter the nature of the chemical bond, a molecule and its isotopic analogue have almost the same force constants. Using

the force field of a molecule, the fundamental wavenumbers of isotopic substitutes can be calculated. It is particularly useful when it is difficult to obtain the spectrum of an isotopic substitute. Alternatively, force constants can be evaluated more accurately with accurate knowledge of a molecule's spectra and its substituted isotopes.

Electron delocalization and interatomic interactions can be visualized with the help of force constants. The force constants also provide information regarding valence state of atoms in the molecule. As a result, we are also able to know the normal coordinates associated with each vibrational frequency, which is necessary for studies on absolute intensities. The bond dipole moments, polarizabilities, and derivatives of bond dipole moments can be calculated using Raman and infrared intensities along with force constants [3].

1.7 Force fields

The fundamental vibrational frequencies of a molecule can be determined from its Raman and infrared spectra and then used to solve the secular equations to determine its potential energy or force constant. The number of force constants to determine is generally greater than the number of equations; therefore, it is impossible to determine unique solutions to these equations. A way to overcome this difficulty is to select force constants from molecules with similar bonds and environments. The trail F matrix is set up and iterating them to give a weighted least square fit to all the observed frequencies. It is also possible to reduce the number of force constants to be determined by making

specific assumptions about the forces inside the molecules. There are several such force fields, each with its own strength and weakness.

1.8 Solution by symmetry and internal coordinates

Spectroscopic activity of a molecule is influenced by symmetry consideration. It has been proved that Howard and Wilson's [4] "symmetry coordinates" method is the best way to determine normal vibrations in symmetrical molecules. Each symmetry type or species is typically evaluated by determining the number of genuine vibrations. Generally there are $(2N-3)$ vibrations for in-plane modes and $(N-3)$ vibrations for out-of-plane modes. A symmetry coordinate is constructed to represent all the individual displacements of all the nuclei through the linear combination of equivalent internal coordinates. A quadratic function of symmetry coordinates represents the potential function. The choice of symmetry coordinates are governed by the following conditions:

- 1 There must be equal numbers of symmetry coordinates under each species for each symmetry type. It is necessary to have a pair of symmetry coordinates for doubly degenerate vibrations, and three such coordinates for triply degenerate vibrations.
- 2 They should be normalized.
- 3 They should be orthogonal.
- 4 As symmetry types, they should be transformed according to their characteristics.

1.9 Group theory and molecular vibrations

By applying group theory concepts, the normal vibrations of molecules can be classified based on their irreducible representations. This method allows qualitative analysis of the fundamental, overtone, and combination bands in infrared and Raman. The optical activity of a molecule can be determined by knowing its point group symmetry. Molecules with different symmetries have qualitatively different spectra [1, 5, 6].

Symmetry elements and symmetry operations

The symmetry element is a geometrical entity such as a point, an axis or a plane in which one or more symmetry operations take place. In the case of a molecule moving between configurations, the resulting configuration remains the same.

There is a close relationship between symmetry elements and symmetry operations, and one cannot exist without the other. Molecules have no translational motion while in symmetry operation. It is possible to treat all molecular symmetries as symmetry elements described in literature [7,8].

When a symmetry operation is applied to a molecule, a member of a set of degenerate vibrations will be transformed into a linear combination of those vibrations.

Point group and character tables

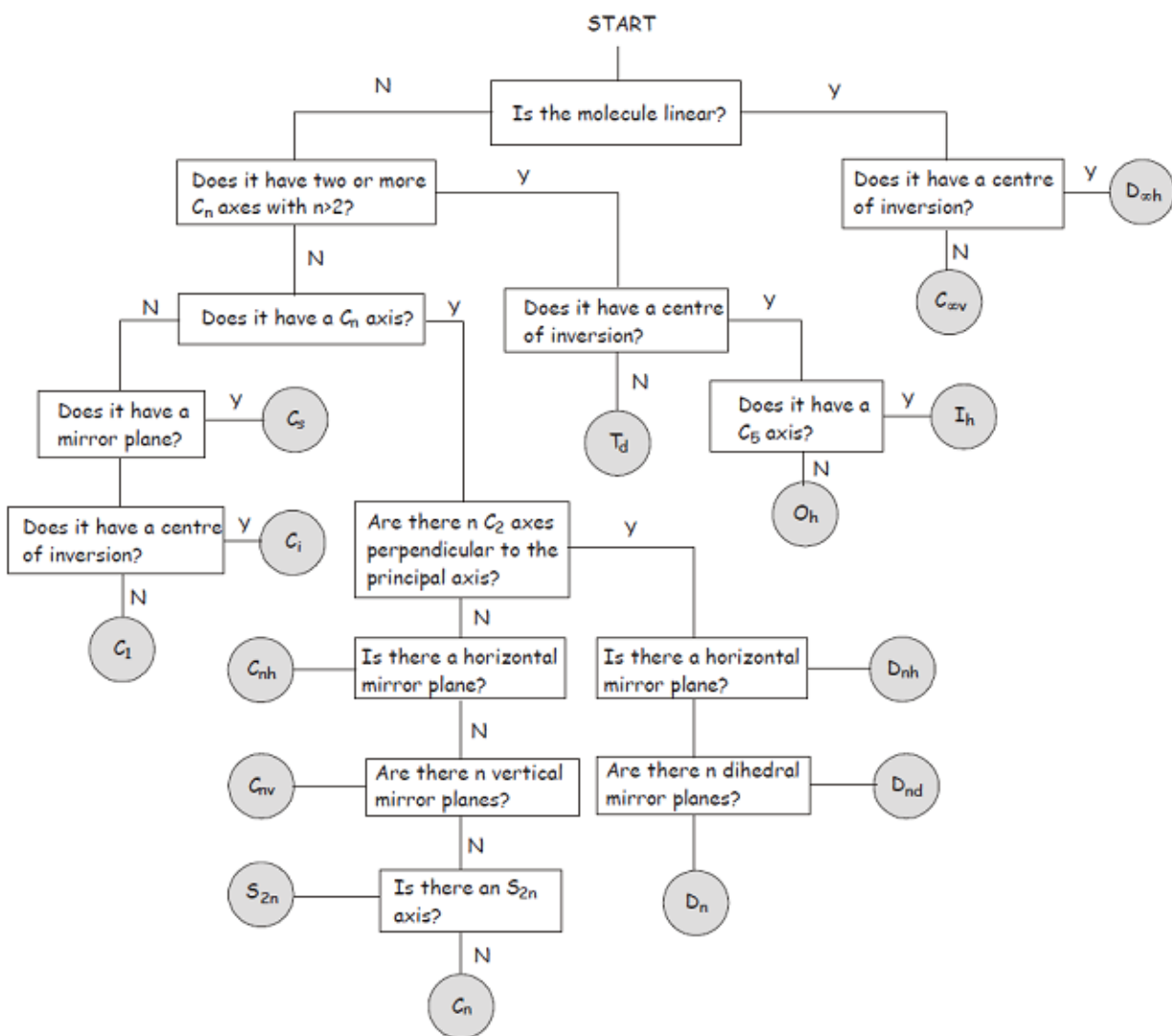
A possible combination of symmetry operations that leaves at least one point unchanged is called point group. This combination satisfies the group atoms. There are only a limited number of such combinations or point groups in mathematical group

theory. Most molecules belong to one of these point groups. The procedure for the identification of point groups of polyatomic molecules is given in the flow chart 1.1.

It is possible to list the characters of matrices in different irreducible representations of a point group in a character table. We can solve molecular vibrations with the help of character tables, which summarize the symmetry behavior of molecules of different point groups [7].

Group frequencies

When infrared spectra of series of compounds are examined critically, it is discovered that compounds containing a common group of atoms share some similarities, and this common group absorbs over a narrow range of frequencies, irrespective of the nature of the rest of the molecule. By examining infrared spectra, organic group frequencies can be used to identify atomic groups.



Flowchart 1.1 The procedure for the identification of point groups of polyatomic molecules

A group frequency is defined as the vibration of a particular group independent of the vibration of the rest of the molecule. The nuclei of a molecule oscillate harmonically as a result of normal vibration, so it is impossible to expect a polyatomic molecule to exhibit isolated vibrations. It is expected that isolated vibrations occur when a group contains either light atoms, such as hydrogen, or heavy atoms, such as iodine. When there are two or more double bonds in a group, it is considered independent if it is not part of a conjugated system [9]. It may not be possible to isolate group frequencies when atoms with similar masses are bonded through bonds of roughly the same force constant. For Raman or infrared spectra to confirm the presence or absence of a particular group frequency, studies on the structure of complicated molecules and their assignment of vibrations require critical examination. There may be a mixing of vibrations in a group that result in a significant change in the frequency of the group.

Fermi resonance

Overtone (or a combination of two vibrations) and fundamental vibrations may occur almost at the same frequency in certain molecules. According to quantum mechanical resonance, the frequency of one vibration (with higher energy) is raised while the frequency of the other (with lower energy) is lowered. Using the harmonic oscillator approximation, these levels are described by wave functions of the two vibrational excited states resulting from the mixing of two wave functions. Such a phenomenon was first observed by Fermi and known as Fermi resonance [10, 11]. There must be the same symmetry type between the two vibrations in order for the Fermi resonance to occur. Energy sharing may also occur in the presence of resonance. There is a possibility that

the intensity of overtones and combinations will become equal to the intensity of the fundamentals as they borrow energy from them. There is no longer a need to distinguish an overtone or combinational level from a fundamental level, since both the displaced levels will be partly one kind and partly the other. A deuteration or solvent effect that shifts the frequency of one vibration mode, while the other does not, will affect the Fermi resonance interaction. Thus, deuterating a sample or taking the spectrum in different solvents can be used to test the presence of Fermi resonance in compounds [7, 12].

Hydrogen bonding

Solids are also affected significantly by the formation of hydrogen bonds (H-bonds). The H-bond is defined as the bond between an atom X and the hydrogen atom of a covalent bond X–H, forming the group X–H...Y. Atoms X and Y have electronegativities greater than H.

Generally, it can be viewed as a proton shared by two electrons in a lone pair. Molecular association can be either intramolecular or intermolecular, and it is an important form of molecular interaction. If the H-bond is formed between groups within the same molecule, it's called intramolecular, but when it involves associations between two or more molecules, it's called intermolecular. Atoms with a higher electronegativity than hydrogen can form an H-bond. Oxygen, nitrogen and halogen atoms are the most frequent partners and may give rise to strong H-bond. Typically, oxygen, nitrogen, and halogen atoms form strong H-bonds. In order to understand the strength of H-bonds, spectroscopic methods are used. A large number of studies [13, 14] on H-bonded systems show the following effects with the formation of an H-bond,

- 1) When the H-bond becomes stronger, vibrations of the X-H stretching, shift to lower frequencies with broadening and increase in intensity.
- 2) Bending X-Y deformation band shifts to higher frequencies without appreciable changes in line width and intensity.
- 3) At low frequencies, new bands are observed corresponding to stretching and deformation of H...Y.
- 4) A shift in vibrational modes involving hydrogen bond acceptor atom Y. The shift is usually much smaller than that observed between donor X-H vibrations.
- 5) In IR and Raman spectroscopic studies, the focus is primarily on the ν_{X-H} frequencies, which occur in regions that are free of vibrations from other molecules. Therefore, IR studies are a powerful technique for understanding the nature and strength of hydrogen bonds in molecules.

Chapter – 2

Quantum Chemical Calculations

Quantum Chemical Calculations

2.1 Introduction

Computational chemistry aims to solve chemical problems by applying mathematical and theoretical principles. An important part of computational chemistry is molecular modeling, which predicts the behavior of molecules within chemical systems. The most accurate molecular models employ 'first principles' or *ab initio* methods to determine the electronic structure. These methods are based on quantum mechanical principles and are computer-intensive. Nevertheless, molecular modeling has been a rapidly developing and expanding field due to advancements in computer storage capacity and processor performance, allowing specialists to solve relevant problems in a reasonable amount of time.

The types of predictions possible for molecules and reactions include [15]: (1) Heats of formation (2) Bond and reaction energies (3) Molecular energies and structures (thermochemical stability) (4) Energies and structures of transition states (activation energies) (5) Reaction pathways, kinetics and mechanisms (6) Charge distribution in molecules (reactive sites) (7) Substituent effects (8) Electron affinities and ionization potentials (9) Vibrational frequencies (IR and Raman spectra) (9) Electronic transitions (UV/Visible spectra) (9) Magnetic shielding effects (NMR spectra).

2.2 Survey of computational chemistry methods

In general, molecular modeling techniques fall into three broad categories:

- (1) Molecular Mechanics
- (2) Semi-empirical methods and
- (3) *Ab initio* electronic structure calculations.

2.3 Molecular Mechanics

The simplest type of calculation is Molecular Mechanics (MM) by using the laws of classical physics, Molecular Mechanics (MM) predicts the structure and properties of molecules (i.e. no quantum mechanics are used; instead, parameters are derived from experimental or *ab initio* data. In the Born-Oppenheimer approximation, the nuclei motions are studied and the electrons are not explicitly treated. It is feasible to model large and non-symmetrical chemical systems such as polymers and proteins using Molecular Mechanics (MM). To predict the chemical properties of molecules, molecular mechanics relies upon the laws of classical physics without explicitly treating electrons. MM calculations are therefore unable to handle bond breaking or formation problems, where electronic or quantum effects are dominant. Additionally, MM models are totally dependent on the systems they are used to predict; as absolute quantities, they are not meaningful and can only be used for comparative studies. Although MM has some shortcomings, it has been extensively used in studying 'mesoscopic' effects in energetic materials due to its ability to bridge the gap between quantum mechanics and continuum mechanics. These applications include calculating reaction and dissociation energies on classical potential energy surfaces [16, 17], evaluating equilibrium crystal properties

(e.g., density, packing, specific heats) [18, 19], investigating shock interactions with crystals and defects [20], and simulating molecular crystal detonation.

The typical molecular mechanics method has some basic assumptions as listed below.

- Atoms (e.g., electrons and nuclei) are each considered to be a single particle with characteristic mass.
- The potential energy of interaction between two atoms is determined by the characteristic force constant of the chemical bond is considered to be a spring. Potential energy functions can characterize intramolecular stretching, bending, and torsion, as well as intermolecular phenomena such as electrical interactions or van der Waals forces.
- Potential energy functions based on experiments or other calculations derived from empirical parameters.

Strength of Molecular Mechanics

In comparison to *ab initio* computations, Molecular Mechanics computations are quite inexpensive, and this allows one to compute properties for large systems containing thousands of atoms, for example: (1) Energy optimization (2) Calculation of binding constants, (3) Simulating of protein folding kinetics (4) Examination of active site coordinates (5) Design of binding sites (6) MM can supply results in heat of formation if the zero of energy is taken into account.

Weaknesses of Molecular Mechanics

The performance of a force field parameterized for one class of compounds is unlikely to be as good for another class of compounds when it is parameterized for an inappropriate force field. It has been found that force fields produce good results for limited classes of molecules related to those for which they have been parameterized. The parameter transfer from one force field to another is invalid. Optimizing to a stationary point that may not be a minimum (it could be a "maximum", a transition state), and certainly may not be a global minimum. When a structure is not a minimum, rotate the bonds slightly and reoptimize; transition states should slide down toward nearby minimums. The solvent and nearby ions are ignored. Using the in vacuo structure can lead to incorrect geometries and energies in polar molecules. This is particularly important for biomolecules. The energies obtained by molecular mechanics do not possess any physical significance, but rather describe the difference in conformation (type of isomer). As MM methods ignore electrons, they cannot handle chemical problems dominated by electronic effects such as bond formation, bond breaking, etc.,

2.4 Semi-empirical methods

Molecular Mechanics provides mostly qualitative results, whereas *ab initio* methods are highly computationally demanding and Semi-empirical quantum methods (SE) offer both qualitative and quantitative results. Equations are parameterized using semi-empirical methods based on experimental data. A Hamiltonian and wave function are used like *ab initio* method. In other words, they are MO-LCAO methods derived from

Hartree-Fock model and they consider only the valence electrons. A minimal basis set is used for the valence shell. The numerical results are parametrized with experimental data by adjusting them to one and two-center integrals. A large number of properties can be quantitatively estimated with very efficient computational tools. It can be used to establish trends among classes of similar molecules and to scan a computational problem before undertaking high-level treatments. A lot of elements have not been parametrized such as transition metals.

Strength of Semi-empirical method

- 1) For molecules similar to those used for parametrization, semi-empirical methods are fast, produce accurate results, and can be applied to very large molecules.
- 2) In order to reproduce specific results, these equations must be parameterized, usually the geometry and heat of formation, but they can also be used in order to find other values.

Weaknesses of Semi-empirical method

- 1) The main weakness of SE methods is their unreliability. SE methods are less accurate than *ab initio* methods, especially in energies.
- 2) The SE heats of formation have errors of tens of kJ mol^{-1} , so heat (enthalpies) of reaction and activation can be in error by scores of kJ mol^{-1} .

2.5 *Ab initio* method

In Latin, *ab initio* means "from first principle". The computations are based on quantum mechanics and no experimental data is used. Schrödinger's equation is used in

the *ab initio* method, but with approximations. Model chemistry specifies how *ab initio* molecular orbital calculations should be performed. A model chemistry will include several factors, such as the choice of a method, a basis set, the general structure, state of the electrons in the molecular system under study (e.g., charge and spin states), and the way in which electron spin is treated. The properties of molecules can be assessed by using a user-specified input or by allowing the molecule to relax to a minimum energy configuration (geometry optimization). Because of their best mathematical approximation to the actual system, *ab initio* molecular orbital methods are the most accurate and consistent.

There are two strategies for solving equations based on *ab initio* methods: (1) Wavefunction-based methods, which concentrate on obtaining the electronic wavefunction, and (2) Density-based methods, which concentrate on determining the properties of the system through its electronic density without explicitly determining the wavefunction.

***Ab initio* method for molecular calculations must satisfy a set of stringent criteria**

(1) The structure and electronic states of the molecules must be well defined and specified for well defined and specified solutions, (2) the potential energy system of the molecule must vary smoothly and continuously with respect to displacements of the atomic nuclei, (3) the model must contain no bias (e.g., the assumption that a chemical bond exists between two atoms), (4) It is important to ensure that the model is 'size consistent', which requires that solutions and their associated errors scale proportionally to the molecule's size, (5) It is equally important that the model is 'variational', i.e.,

approximate solutions must provide an upper bound to the ‘true’ energy of the system. So, within the limitations of the method, the approximate solution with the lowest energy represents the closest fit to the true wavefunction.

Advantages of *ab initio* method

- A detailed analysis of the electronic distribution using the Schrödinger equation,
- It is possible to improve chemical accuracy systematically,
- It does not require parameterization or calibration in relation to experiments,
- Can describe structure, properties, energetic and reactivity.

Different levels of *Ab Initio* calculations

(a) Hartree-Fock (HF), (b) The Møller-Plesset Perturbation Theory (MP), (c) Density Functional Theory (DFT), (d) Configuration Interaction (CI).

(a) Hartree-Fock method

The Hartree-Fock method is a variational, wavefunction-based approach. It is a many-body technique, but the view is based on single-particle picture, which means that the electrons are assumed to occupy single-particle orbitals and make up the wavefunction. Through an effective potential, each electron perceives the presence of the other electrons indirectly. Thus, each orbital is affected by the presence of electrons in other orbitals.

In Hartree-Fock theory, the starting point is to construct a variational wave function from single particle orbitals. The simplest wavefunction that can be formed from these orbitals is their direct product

$$\phi(\vec{x}_1, \dots, \vec{x}_N) = \phi_1(\vec{x}_1)\phi_2(\vec{x}_2)\dots\phi_N(\vec{x}_N) \quad \dots (2.1)$$

This is the Hartree approximation and the variational lowest energy can be calculated by using this approximation from Equation 2.1. However, Hartree wavefunctions fail to satisfy antisymmetry, which states that a fermion wavefunction changes sign if the electronic variables are permuted in odd ways. The permutation operator is defined by its action on the wavefunction

$$\hat{P}_{ij}\phi_1(\vec{x}_1, \dots, \vec{x}_i, \dots, \vec{x}_j, \dots, \vec{x}_N) = \phi_1(\vec{x}_1, \dots, \vec{x}_j, \dots, \vec{x}_i, \dots, \vec{x}_N) = -\phi_1(\vec{x}_1, \dots, \vec{x}_i, \dots, \vec{x}_j, \dots, \vec{x}_N) \quad \dots (2.2)$$

When odd numbers of permutations of this kind are applied to the wavefunction, it takes on a negative sign, whereas when even numbers of permutations are applied there is no change in sign. In order to satisfy the anti-symmetry condition, a more sophisticated form of the Hartree wavefunction is needed [21, 22].

In terms of these orbitals, the Hartree-Fock Hamiltonian operator can be defined using the operators of Coulomb and exchange repulsion. For Hartree-Fock equations, the general procedure is to make the orbitals self-consistent with the potential field they generate. The result is reached through a trial-and-error computational procedure, for which reason the process is called the self-consistent field method.

Iterations to self consistency

(1) Start with an initial guess for the orbital; (2) construct all the operators in the Hamiltonian; (3) solve the Schrödinger equations for the single particle (compute the ground state); (4) using the newly constructed orbital, update the Hartree operators; (5) solve again and continue until convergence.

In practice, it is not desirable to construct the Hartree operator at every iteration. The previous charge densities may be modified a little bit to move in the direction of the new charge density to be calculated. The idea is to minimize the change in operators from one iteration to the next. The Hartree equations are coupled integral-differential equations.

The electron correlation and the Principle of antisymmetry wave function are missing in the Hartree equations.

(b) Møller-Plesset (MP)

Møller-Plesset (MP) treatment of electron correlation [23], a general approach used in physics to treat complex systems, is based on perturbation theory. This particular approach was described by Møller and Plesset in 1934 [24] and developed into a practical molecular computational method by Binkley and Pople [25] in 1975. Essentially, perturbation theory begins by treating a simple system, then progresses to a more complicated version of it. Møller-Plesset calculations are referred to as MP, MPPT (MP perturbation theory), or MBPT (many-body perturbation theory). MP energy levels fall into hierarchies: MP0, MP1 (these first two designations are rarely used), MP2, etc., which successively take into account more thoroughly interelectronic repulsion.

MP0 may use the electronic energy obtained by simply summing the HF one electron energies. It ignores interelectronic repulsion except for refusing to accommodate more than two electrons in a same spatial MO. MP1 corresponds to MP0 corrected with the coulomb and exchange integrals and simply it is the Hartree-Fock energy. MP2 is the first MP level to go beyond the HF treatment. MP2 energy represents the HF energy plus

a correction term (a perturbation adjustment) representing a lowering of energy as a result of the electrons being able to avoid one another more effectively than they did in the HF treatment:

$$E_{MP2} = E_{HF}^{TOTAL} + E^{(2)} \quad \dots(2.3)$$

The HF term includes internuclear repulsion S , and the perturbation correction $E^{(2)}$ is a purely electronic term. $E^{(2)}$ is a sum of terms each of which models the promotion of pairs of electron from occupied to unoccupied MOs.

Merits and demerits of Møller-Plesset Perturbation Theory

MP is an effective method for including electron correlations. The size extensive problem (but not variational) has no error bound for the energy differences. In other words, the error remains constant for different systems.

(c) Density Functional Theory

The method is considered as an *ab initio* method, but it is unique in that it uses electron density instead of wave function to describe the molecules. In DFT, electron correlation is modeled as a function of electron density (ρ). By using the Kohn-Sham equations [26, 27], current DFT methods partition electronic energy into several terms,

$$E = E^T + E^V + E^J + E^{XC} \quad \dots(2.4)$$

where E^T is the kinetic energy term (arising from the motion of the electrons), E^V is the potential energy term that includes nuclear-electron and nuclear-nuclear interactions, E^J is the electron-electron repulsion term and E^{XC} is the electron correlation term. With the exception of nuclear-nuclear repulsions, all the terms are functions of the electron

density. The terms $E^T + E^V + E^J$ represent the classical energy of the electron distribution, while E^{XC} represents both the quantum mechanical exchange energy, which accounts for electron spin, and the dynamic correlation energy due to the concerted motion of individual electrons.

It is the combination of an exchange functional and correlation functional those are used in pure DFT methods to calculate E^{XC} and so are designated by the choice of combination. For example, B3LYP combines Becke's gradient-corrected exchange functional with the gradient-corrected correlation functional of Lee, Yang and Parr [28]. DFT calculations fall into three general categories: local density approximations (LDA), generalized gradient approximations (GGA), and "hybrid" combinations of DFT and Hartree-Fock terms.

Local Density Approximations (LDA)

An approach that works for some bulk materials, but fails to predict isolated molecule properties accurately, because LDA exchange and correlation functionals only include electron density terms.

Generalized Gradient Approximations (GGA)

The GGA ("nonlocal") functional includes terms that depend on both electron density and density gradient. BLYP predicts intramolecular bond dissociation energies within a few kJ/mol using gradient-corrected density functional methods [29]. Since Coulomb's 'self-interaction' of electrons is neglected [30], the generalized gradient approximation significantly underestimates activation barriers. Combining Hartree-Fock

self-interaction corrections with density functional exchange and correlation is used to solve this problem.

Examples of hybrid methods are B3LYP and B3PW91, where B3 denotes Becke's three-parameter hybrid functional [31], while 'PW91' and 'LYP' are gradient-corrected correlation functional of Perdew and Wang [32] and, as above, Lee, Yang and Parr.

Hybrid

Hartree-Fock and DFT terms combine in this method.

Merits and demerits of DFT method

The computational expense is avoided with density functional methods. Molecular properties and reactions of larger energetic molecules can be studied using the DFT technique.

2.6 Basis set

A basis set is a mathematical description of the orbitals within a system that can be used for theoretical calculations. Atomic orbitals are categorized according to their size and description using standard *ab initio* software packages. The electron distribution around an atom is accounted for by several basis functions, and by combining atomic basis functions, this leads to the electron distribution within the entire molecule. Basis functions not centered on atoms can be considered to lie on "ghost atoms". More and a wider range of basis functions are included in larger basis sets. It is therefore possible to refine molecular wave functions more accurately by using larger basis sets; however, this requires correspondingly more computational power. In addition, electrons in atoms can

be treated in different ways to obtain accurate wave functions. Molecules containing large atoms ($Z > 30$) may be modeled using basis sets that incorporate relativistic treatments of inner-shell electrons. ‘Minimal’ basis sets contain the minimum number of AO basis functions needed to describe each atom (*e.g.*, 1s for H and He; 1s, 2s, 2p_x, 2p_y, 2p_z for Li to Ne). The general expression for a basis function is given as:

$$\text{Basis Function} = N * e^{(-\alpha * r)} \quad \dots(2.5)$$

where N is the normalization constant, α is the orbital exponent, r is the radius in angstroms.

Types of basis set and their uses

Basis sets are broadly classified into two types, one is minimal basis set and another one is extended basis set.

(1) Minimal basis set

As the minimal basis set contains only one function per occupied atomic orbital in the ground state, it is the smallest possible set. For elements from the first two groups of the periodic table, it always includes orbitals from partially occupied subshells and valence p-type functions. The most popular minimal basis sets are the STO-nG, where n denotes number of primitives in the contraction. It is common for minimal basis sets to provide insufficient results for research-quality publication, but they are generally much less expensive than their larger counterparts. STO-1G, STO-3G, STO-4G, STO-6G are the commonly used minimal basis sets of this type.

(2) Extended basis set

(a) Split valence basis sets

It is difficult to respond to changing molecular environments with minimal basis sets because they do not allow the orbitals to be altered. A p-orbital on oxygen in an ether compared to the same ether protonated. Comparisons between charged and uncharged species are unreliable when a basis set like STO-3G fails to reflect these changes. Anisotropic environments are another problem for minimal basis sets. In order to address these problems, split valence basis sets can be used. In this basis, the AOs are divided into two parts: an inner, compact orbit and an outer, more diffuse orbit. It is possible to vary the coefficients of the two kinds of orbitals independently during the construction of the MOs. By varying the inner and outer functions (below), the AO's size can be controlled. Basis sets that split only the valence orbitals are called split valence basis sets; basis sets that split both the core and valence orbitals are called double zeta, DZ (implying two different exponents).

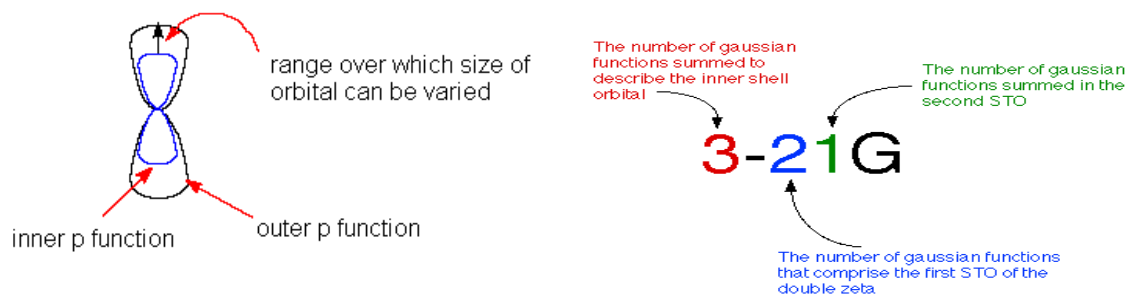


Fig. 2.1 Split valence basis set 3-21G

The simplest split valence basis set provided by GAUSSIAN is the 3-21G is shown in Fig. 2.1. According to this description, the core orbital has three Gaussian components, whereas the inner and outer valence orbitals have two and one Gaussian

components, respectively. GAUSSIAN offers two other split valence bases: the 6-31G and the 6-311G and both have six Gaussian cores. Based on the 6-311G, the inner orbital is represented by three Gaussians, and the middle and outer orbitals by single Gaussians. The triple split improves the description of the outer valence region.

(b) Polarization

Further improvement of basis functions is achieved by adding d-orbitals to all heavy (non-hydrogen) atoms. Unlike transition metal d-orbitals, these are not used to form bonds in typical organic compounds. They are used to allow a shift of the center of an orbital away from the position of the nucleus. In Pople notation, polarization functions are indicated by adding an asterisk to the set designator. The larger basis set 6-31G with polarization function is shown in Fig. 2.2. Typically, six *d*-functions (x^2 , y^2 , z^2 , xy , xz , and yz), equivalent to five *d*-orbital's and one *s*, are used (for computational convenience) Most programs can also use five "real" *d*-orbital's. DZP: double zeta, polarization is an alternative description of this kind of basis set. To provide polarization, a second asterisk, as in the 6-31G** basis set, implies adding p-orbitals to each hydrogen. Again, an alternative notation exists: DZ2P; double zeta 2 polarization. A polarization function is only added to elements in the second row when an asterisk appears in parentheses. This is the standard setup for the 3-21G basis set in GAUSSIAN. Another alternative to the asterisk for specifying polarization functions is (d), placed after the G.

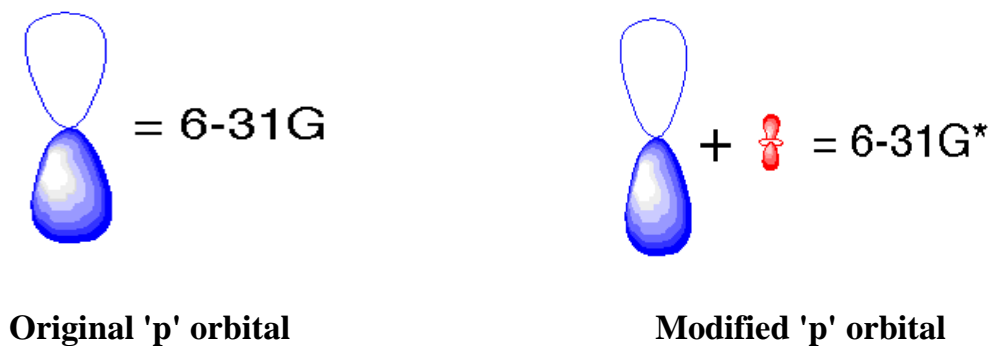


Fig. 2.2 Split Valence basis set 6-31G

(c) Diffuse Functions

In order to provide more accurate descriptions of neutral molecules with unshared pairs, diffuse functions may be added to basis sets. The purpose is to improve the basis set at large distances from the nuclei, improving the description of barely bound electrons in anions. If diffuse functions are included, processes involving changes in the number of unshared pairs, such as protonation, can be represented more accurately. In this case, the augmentation consists of a single set of very diffuse orbitals (exponents 0.1 - 0.01) on the *s* and *p* orbitals. The presence of diffuse functions is symbolized by the addition of a plus sign (+) to the basis set designator: 6-31+G. Since these are *s* and *p* orbital's, the symbol goes before the G. It should be noted that a second + implies diffusion functions are added to hydrogen's, however, unless hydride ions are included in the system under investigation, little improvement in results is observed. All of our *ab initio* programs offer at least one set of diffuse functions.

Ab initio programs in all of our programs offer diffuse functions at some point. Generally, we would like to use the largest available basis set, with the most extensive set

of diffuse and polarization functions, and the most extensive consideration of electron correlations.

2.7 Properties arising from electron distribution

Calculating the shapes (geometries), relative energies, and frequencies of stationary points on a potential energies surface are three applications of *ab initio* calculations. The shapes of a molecular species are one of its fundamental characteristics. Molecular vibrational frequencies provide information about the electronic nature of the bonds within a molecule, and experimentalists may be able to predict the spectra represented by these vibrational frequencies. It is possible to predict the dipole moment, the charge distribution, the bond orders, and the shapes of various molecular orbitals by calculating the electron density distribution.

(a) Dipole moments

A dipole moment [33] of a system of two charges Q and $-Q$ separated by r is, by definition, the vector Qr ; the direction of the vector is officially from $-Q$ toward $+Q$, but chemists usually assign molecular or bond dipoles the directions from positive to negative. The dipole moment of a collection of charges $Q_1, Q_2, Q_3, \dots, Q_n$, with corresponding position vectors $r_1, r_2, r_3, \dots, r_n$ is,

$$\mu = \sum_1^n Q_i r_i \quad \dots(2.6)$$

and the dipole moment of a molecule is seen to rise from the charges and positions of its component electrons and nuclei.

(b) Electrostatic potential

Molecule electrostatic potential surfaces can be calculated by using electron density and nucleus location. This surface represents the distance from a molecule at which a positive test charge experiences repulsion or attraction. Using the electrostatic potential, we can rationalize intermolecular interactions between polar species, identify regions of local negative and positive potential within a molecule, and predict the path charged reactants will take.

An electrostatic potential (ESP) measures charge distribution and offers other useful information as well [34]. The electrostatic potential at a point P of a molecule is defined as the amount of energy required to bring a unit point positive "probe charge" from infinity to P. It can be viewed as a measure of the molecule's positive or negative charge at the point: a positive value indicates repulsion as the probe charge was brought from infinity, while a negative value indicates attraction as the probe charge fell from infinity to P. The ESP at a point is the net result of the effect of the positive nuclei and the negative electrons.

2.8 HOMO–LUMO analysis

The acronyms HOMO and LUMO refer to the highest occupied molecular orbital (HOMO) and the lowest unoccupied orbital (LUMO). The HOMO is the molecular orbital of highest energy that is occupied by electrons. The LUMO is the molecular orbital of lowest energy that is not occupied by electrons. Molecular properties such as

reactivity and the ability of a molecule to absorb light are determined by the HOMO and LUMO.

To identify the reactive sites in a molecule, several approaches can be used. The choice of approach will depend on the size, type of molecule and the type of reaction. The use of atomic partial charges is useful for reactions that are charge controlled (e.g. protonation / deprotonation). Electrostatic potentials can be used where polar reagents are involved. HOMO and LUMO work best for predicting reactivity when these orbitals are well-separated in energy from the rest of the molecular orbitals. Larger molecules have a smaller energy difference between the HOMO and LUMO, as well as the other molecular orbitals. The molecular orbital close in energy to the HOMO or LUMO help to determine the reactivity, and various reactivity indices (electrophilic, nucleophilic, or radical susceptibilities, depending on the molecule).

2.9 Natural bond orbital analysis

Löwdin first introduced the "natural" orbital concept [35] to describe an array of orthonormal 1-electron functions $\theta_i(\vec{r})$ that are *intrinsic* to the N -electron wave function $\psi(1, 2, \dots, N)$. Mathematically, the θ_i 's can be considered as *Eigen* orbital of ψ (or, more precisely, of ψ 's first-order reduced density operator), therefore they are "best possible" (most rapidly convergent, in the mean-squared sense) for describing the electron density $\rho(\vec{r})$ of ψ . Natural orbitals are distinguished from many other orbitals that might be imagined or invented [e.g., the standard atomic orbital (AO) basis functions of electronic structure packages like Gaussian 2009 [36] by being referred to as "natural" by ψ itself.

In order to remove spurious effects associated with symmetry adaptation, one can formulate [37] a localized criterion for orbitals that have analogous maximum occupancy (natural) characteristics in localized 1-center and 2-center regions of the molecule. Since the Pauli Exclusion Principle limits the maximum occupancy of an orbital to a pair of electrons, local 1- and 2-center orbitals with occupancies sufficiently close to 2.000 may serve equally well as natural orbitals for describing ψ . As anticipated by G.N. Lewis, [38] localized orbitals of near-double occupancy can be found in the 1- and 2-center regions suggested by the elementary Lewis structure diagram. Such natural bond orbital's (NBOs) provide the most accurate possible "natural Lewis structure" picture of ψ , because all orbital details (polarization coefficients, atomic hybrid compositions, etc.) are mathematically chosen to include the highest possible percentage of the electron density. This gives us an idea as to how accurate the natural Lewis structure picture is, and is often found to be > 99% for common organic molecules, revealing the accuracy of Lewis's concept.

The NBOs are one of a sequence of natural localized orbital sets that include natural atomic (NAO), hybrid (NHO), and (semi-)localized molecular orbital (NLMO) sets, intermediate between basis AOs and canonical molecular orbital (MOs)



ψ can be described in terms of any of these natural localized sets, which are complete and orthonormal. Compared to standard AOs, e.g., the NAOs give a much more condensed description of ψ , with only a small number (i.e., corresponding to the formal "minimal basis") having appreciable occupancy. It is therefore often found that a "minimal"

description of NAOs in terms of their core and valence-shell provides a compact representation of ψ that is intimately related to standard valence concepts. Mutual orthogonality of natural localized orbitals may be seen as a conceptual liability, as the concept of "orbital overlap" may be lost. However, each orthogonal NAO (or NHO, NBO, etc.) can be uniquely associated with a corresponding "pre-orthogonal" PNAO (or PNHO, PNBO, etc.) which remains orthogonal to PNAOs on the same atom but has non vanishing overlap integrals with those on other atoms. In accordance with the Mulliken approximation, [39] the corresponding Hamiltonian interaction elements are found to be closely proportional to these overlap integrals. That is, if \hat{F} denotes the effective orbital Hamiltonian (Fock or Kohn-Sham operator), the interaction strength $\langle h_A | \hat{F} | h_B \rangle$ of bonding NHOs h_A, h_B can be approximated in terms of overlapping PNHOs \tilde{h}_A, \tilde{h}_B as

$$\langle h_A | \hat{F} | h_B \rangle \cong K \langle \tilde{h}_A | \tilde{h}_B \rangle \quad \dots(2.8)$$

where k is a proportionality constant of order unity. In accordance with the simple bond orbital picture each bonding NBO σ_{AB} can be written in terms of two directed valence hybrids (NHOs) h_A, h_B on atoms A and B, with corresponding polarization coefficients c_A, c_B ,

$$\sigma_{AB} = c_A h_A + c_B h_B \quad \dots(2.9)$$

that vary smoothly from covalent ($c_A = c_B$) to ionic ($c_A \gg c_B$) limit. Each valence bonding NBO must in turn be paired with a corresponding valence antibonding NBO

$$\sigma_{AB}^* = c_B h_A - c_A h_B \quad \dots(2.10)$$

to complete the span of the valence space. In an idealized Lewis structure picture, "Lewis"-type (donor) NBOs are complemented by "non-Lewis"-type (acceptor) NBOs that are formally empty. Weak valence antibonds occupancy results in irreducible departures from an idealized localized Lewis structure, that is, true "delocalization effects". The energetic stabilization due to such $\sigma \rightarrow \sigma^*$ donor acceptor interactions can be estimated by second-order perturbation theory, viz., for the $\sigma_i \rightarrow \sigma_j^*$ interaction,

$$\Delta E_{i \rightarrow j^*}^{(2)} = -2 \frac{\langle \sigma_i | \hat{F} | \sigma_j^* \rangle^2}{\varepsilon_{j^*} - \varepsilon_i} \quad \dots (2.11)$$

where \hat{F} is the effective orbital Hamiltonian (Fock or Kohn-Sham operator) and $\varepsilon_i = \langle \sigma_i | \hat{F} | \sigma_i \rangle$, $\varepsilon_{j^*} = \langle \sigma_j^* | \hat{F} | \sigma_j^* \rangle$ are the respective orbital energies of donor and acceptor NBOs. By considering valence antibonds, it is possible to broaden elementary Lewis structure concepts to include leading delocalization corrections in perturbative NBO estimates such as Equation (2.2). As a result of each $\sigma_i \rightarrow \sigma_j^*$ perturbation, the starting NBO acquires a weak antibonding "tail" in the final (doubly occupied) NLMO Ω_i . More generally, each semi localized NLMO Ω_i can be expressed as a linear combination of the parent Lewis-type NBO σ_i (with coefficient $c_{ii} \cong 1$) and residual weak contributions ($c_{ji} \cong 0$) from non-Lewis (NL) NBOs σ_j^*

$$\Omega_i = c_{ii} \sigma_i + \sum_j^{NL} c_{ji} \sigma_j^* \quad \dots (2.12)$$

that reflect the irreducible physical effect of $\sigma_i \rightarrow \sigma_j^*$ delocalizations. It is important to realize that the Slater determinant of doubly occupied NLMOs is equivalent to the usual MO wave function despite the compact form of NLMOs and their close connection to

chemical structure concepts. It is thus possible to achieve simplicity of such NBO-based expansions without losing the accuracy of describing ψ .

Two important physical effects distinguish NAOs from isolated-atom natural orbitals as well as standard basis orbitals:

- i. In NAOs, the spatial diffuseness is optimized for the effective atomic charge in the molecular environment (i.e., more contracted if A is somewhat cationic; more diffuse if A is somewhat anionic). As a result, NAOs incorporate the important "breathing" responses to local charge shifts, which typically require multiple basis functions of variable range (double zeta, triple zeta, or higher) to describe accurately.
- ii. The outer fringes of NAOs include the important nodal features caused by steric confinement (Pauli) in their molecular environment (more oscillatory features and higher kinetic energy with neighboring NAO interpenetration, which preserves interatomic orthogonality under Pauli exclusion principle). In this way, the valence NAOs of atom A include both inner nodes that maintain orthogonality to its atomic core and outer nodes that preserve orthogonality to filled orbitals on other atoms B. There are two features that are necessary for realistic steric properties in the molecular environment namely, the Fermi-Dirac anticommutators for the associated second-quantized NAO field operators [40], but they are commonly ignored in standard basis orbitals.

2.10 Molecular electrostatic potential maps

Molecular electrostatic potential provides a visual method to understand the relative polarity of the molecule. As a tool for predicting and analyzing molecular interactions, such as drug-receptor interactions and enzyme-substrate interactions, MEP is invaluable. For the study of biological discovery processes and hydrogen bonding interactions, MEP is very useful in elucidating the qualitative nature of electrophilic and nucleophilic reactions. Molecule size, shape, charge density, and site of chemical reactivity are depicted by an electron density isosurface mapped with electrostatic potential surface. Different colors represent different electrostatic potential values at the MEP surface: red or yellow, blue and green represent the most negative, most positive, and zero electrostatic potentials.

The molecular electrostatic potential of a molecule can be calculated from the expression,

$$V(\mathbf{r}) = \sum \frac{Z_A}{|\mathbf{r} - \mathbf{R}_A|} - \int \frac{\rho(\mathbf{r}')d^3r'}{|\mathbf{r} - \mathbf{r}'|} \quad (2.13)$$

where the first term is a contribution from the nuclear charges, which are considered to be point charges, and the second term arises from the electron density of the molecule, which is obtained from molecular orbital calculations or X-ray diffraction experiments.

The different colour ranging from red < orange < yellow < green < blue, gives the increasing positive potential.

2.11 Fukui function

Chemical reactivity in terms of hard-soft acid-base theory, the Fukui function $f(r)$, is defined from the change in electron density $\rho(r)$ at a given point r , where N , the total number of electrons is changed, by the most important local reactivity index [41].

$$\text{Fukui Function, } f(r) = (\partial\rho(r)/\partial N)_v \quad (2.14)$$

As well, it is defined as the functional derivative of chemical potential as compared to external potential with constant N .

$$\phi(\rho) = (\delta\epsilon/\delta\varpi)_N = (\delta^2E/\delta\varpi\delta N) = (\delta^2E/\partial N\partial\varpi) \quad (2.15)$$

The Fukui function, $f(r)$, plays a key role in linking frontier MO theory to the HSAB principle. Due to the derivative discontinuity problem at atoms and molecules with integral number of electrons [42, 43], both right- and left-hand derivatives are introduced.

$f^+(r) = (\partial\rho(r)/\partial N)_v^+ \approx \rho_{N+1}(r) - \rho_N(r) \approx \rho_{\text{LUMO}}(r)$ (for a nucleophilic sites provoking an electron increase in the system).

$f^-(r) = (\partial\rho(r)/\partial N)_v^- \approx \rho_N(r) - \rho_{N-1}(r) \approx \rho_{\text{HOMO}}(r)$ (for an electrophilic sites provoking an electron decrease in the system).

$$f^0(r) = f^+(r) + f^-(r)/2 \text{ (for radical attack).} \quad (2.16)$$

where ρ_N is the electron density at a point r in space around the molecule. The N corresponds to the number of electrons in the molecule. $N+1$ corresponds to an anion, with an electron added to the LUMO of the neutral molecule. $N-1$ correspondingly is the cation with an electron removed from the HOMO of the neutral. All calculations are done at the ground-state geometry. These functions can be condensed to the nuclei by using an atomic charge partitioning scheme, such as

Mulliken population analysis:

$$f_{k+} = q_k(N+1) - q_k(N) \quad (\text{for nucleophilic attack}) \quad (2.17)$$

$$f_{k-} = q_k(N) - q_k(N-1) \quad (\text{for electrophilic attack}) \quad \text{and} \quad (2.18)$$

$$f_k^0 = f_{k+} - f_{k-} / 2 \quad (\text{for radical attack}) \quad (2.19)$$

where $q_k(N)$ is the Mulliken charge on atom k for N total electrons. Merely run the appropriate calculations of the $(N+1)$, (N) or $(N-1)$ state using the same geometry, and subtract the resulting density volumes. Here the three different calculations are carried out that is for the molecule and also for the cation and anion.

2.12 Topological analysis

In general, topological analysis of atoms in the molecule provides us with more accurate information about the presence of strong and weak hydrogen bonds in terms of Topological parameters for intramolecular interactions in compound electron density electron (r_{BCP}), Laplacian (V_{BCP}^2), electron kinetic energy density (G_{BCP}), electron potential energy density (V_{BCP}), total electron energy density (H_{BCP}), hydrogen bond energy (E_{HB}) at bond critical point (BCP). The bond ellipticity index (ϵ) can provide information about the properties of intramolecular hydrogen bonds.

An atom is a region of space bounded by a surface not crossable by density gradient vectors is called as a 'zero-flux surface in $\text{grad } \rho$ '. This theory is known as the quantum theory of atoms in molecules (QTAIM). In charge distributions, the electron-nuclear force dominates, causing electron densities to peak at nuclear positions and imposing atomic structures on matter. Physically, the electron density provides the basis for partitioning space into atomic regions. All structural concepts such as open, cyclic,

and cage structures can be explained by the connectivity between the atomic regions defined by the maximum density lines connecting neighboring atoms. Structure and structural stability are both explained by changes in the topology of ρ due to nuclei motion. The existence of atoms in molecules or crystals is caused by the fact that atoms or functional groups of atoms exhibit characteristic static, reactive, and spectroscopic properties that vary within relatively narrow limits.

2.13 Reduced density gradient

RDG analysis approaches the weak interaction in real space based on electron density and derivatives. It is the first gradient in the literature and a dimensionless extent. Its main aim is to assess the effects of non-covalent interactions between dissimilar entities on the stability of crystal formation. Through NCI-RDG analysis, we are able to visualize the locations of non-covalent interactions graphically. Through the use of a simple colour code, it is demonstrated as a useful and effective technique to characterize repellent steric interactions, van der Waals interactions, as well as hydrogen bonds. RDG surface analysis can provide information about the quality of strength of the interaction. The red, green, and blue color codes represent destabilizing steric interactions, van der Waals interactions, and hydrogen bonding interactions, respectively. The RDG is defined from the following equation,

$$S(\mathbf{r}) = \frac{1}{C_s} \frac{|\Delta\rho(\mathbf{r})|}{\rho(\mathbf{r})^{\frac{4}{3}}} \quad (2.20)$$

2.14 Molecular docking studies

A computational technique called Molecular docking is used to determine the interaction energy between two molecules and the orientation of ligand forming a complex with minimum energy. As ligand fits within protein's cavity and these protein cavities become more active when they contact with any other compounds becomes as more active sites.

The docking sites and the interacting energy are calculated from a statistical scoring function. The Pymol, a visualizing tool, visualizing the 3D pose of bound ligand that shows the best fit of ligand. The details of the active site of the protein molecule are analyzed from the mode of protein-ligand interaction and further help in protein annotation. The molecular docking is mainly used in drug designing and discovery.

Different types of interactions

The different type of interactions between molecules can be defined based on the four different forces as follows:

1. The Electrostatic forces - Forces due to the charges on the particle such as charge-charge, charge-dipole and dipole-dipole.
2. Van der Waals interactions or Electrodynamical forces.
3. The Steric forces - When different molecules contact among them starts affecting their reactivity and the free energy of the system due to a force called Steric forces.

4. The Solvent-related forces - When a chemical reaction between the solvent and the protein or ligand generating a force is known as solvent related forces. eg; hydrophilic interactions and hydrophobic interactions.

Applications

The binding of ligands to enzyme proteins may result in either activation or inhibition of the enzyme due to force interactions, and as the enzyme protein is a receptor, ligand binding may show agonism or antagonism. In pharmaceuticals, docking is used mostly for drug design and discovery, along with lead optimization and bioremediation.

2.15 Software used in the work

Gaussian is a very high-end quantum chemical software package; available commercially through Gaussian, Inc. Gaussian is the most powerful software available to educators and student researchers through the North Carolina High School Computational Chemistry server. Gaussian is an industry standard in the area of molecular modeling and computational chemistry and it runs all of the major methods in molecular modeling, such as molecular mechanics, *ab initio*, semi-empirical, and DFT (density functional theory).

Gauss View is one of the most useful softwares, another Graphical User Interface, to prepare input for submission to Gaussian and permits us to graphically examine the output. All Gaussian 03 features including molecular specifications, graphical facilities for generating options and keywords are supported by Gauss View.

AutoDock Vina

A program known as AutoDock Vina is used in the field of pharmaceutical for drug design and discovery, molecular docking and virtual screening, which gives a good performance and good accuracy. This AutoDock Vina program was designed in 2010 in the Molecular Graphics Lab at The Scripps Research Institute. The grid maps and clusters are calculated automatically by using AutoDock Vina and it gives good results.

Chapter – 3

Instrumentation Techniques

Instrumentation Techniques

3.1 Introduction

An infrared spectroscopy is an extremely versatile experimental technique that can be used to gain spectra from solutions, liquids, solids or gases. In this chapter, we will examine how samples can be introduced into the instrument, the equipment needed to obtain spectra, as well as the pretreatment of samples in order to obtain spectra.

3.2 Dispersive infrared spectrometer

Prisms made of sodium chloride were used in the first dispersive infrared instruments. After the improved technology for grating construction enabled cheap, good quality gratings to be manufactured, prism instruments declined in popularity. The dispersive element in dispersive instruments is contained within a monochromator. An infrared spectrometer's optical path acts as grating monochromator. Dispersion occurs when energy falling on the entrance slit is collimated onto the dispersive element and the dispersed radiation is then reflected back to the exit slit, beyond which lies the detector. By rotating a suitable component within the monochromator, the dispersed spectrum is scanned across the exit slit. In order to compensate for the changes in the source energy with wavenumbers, the widths of the entrance and exit slits may be varied and programmed. During scanning of the spectrum without a sample, the detector receives radiation of approximately constant energy. The design of infrared instruments must take into account atmospheric absorption caused by CO₂ and H₂O in the instrument beam.

These contributions can be taken into account by using a double-beam arrangement in which radiation from a source is divided into two beams. These beams pass through a sample and a reference path of the sample compartment, respectively. The information from these beams is rationed to obtain the required sample spectrum.

In order for a detector to be effective, it must have adequate sensitivity to the radiation coming from the sample and be monochromatic over the entire spectrum. It is also necessary for the source to be sufficiently intense over a range of wavelengths and transmittances. Sources of infrared emission have included the Globar, which is constructed of silicon carbide. There is also the Nernst filament, which is a mixture of the oxides of zirconium, yttrium, erbium and conducts only electricity at elevated temperatures. Most detectors have consisted of thermocouples of varying characteristics.

A dispersive spectrometer's primary issue is its monochromatic nature. A dispersive spectrometer's primary issue is its monochromatic nature. By using a Fourier-transform infrared spectrometer, these limitations can be overcome.

3.3 Fourier transform infrared spectrometer

Fourier-transform infrared (FT-IR) spectroscopy [44] generates an interferogram by combining radiation from two beams. The latter is a signal produced as a function of the change of path length between the two beams. The two domains of distance and frequency are inter convertible by the mathematical method of *Fourier-transformation*. Before reaching a detector, radiation emitted from the source passes through an interferometer. As the signal is amplified and high-frequency contributions are removed

by a filter, the data are converted to digital form by an analog-to-digital converter and transferred to a computer for Fourier transformation. The basic components of an FT-IR spectrometer are shown in Fig.3.1.

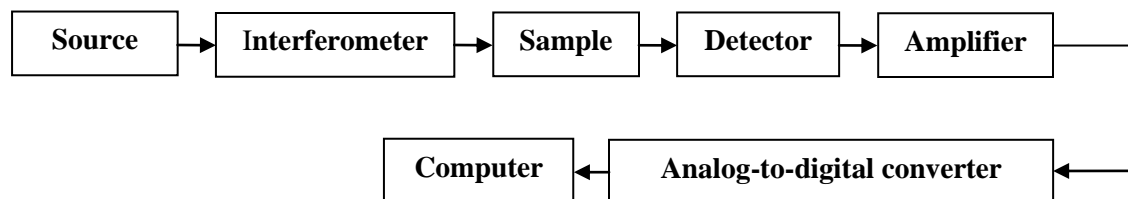


Fig. 3.1 Block diagram of FT-IR spectrophotometer

A Michelson interferometer is the most common interferometer used in FT-IR spectrometry. It consists of two perpendicular plane mirrors, one of which is able to travel in a direction perpendicular to the plane. The optical arrangement of FT-IR spectrophotometer is shown in Fig. 3.2. A semi-reflecting film, the *beam splitter*, bisects the planes of these two mirrors. Based on the region being examined, the beam splitter material should be chosen. Materials such as germanium or iron oxide are coated onto an ‘infrared-transparent’ substrate such as potassium bromide or cesium iodide to produce beam splitters for the mid- or near-infrared regions. Thin organic films, such as poly (ethylene terephthalate), are used in the far-infrared region.

When a collimated beam of monochromatic radiation of wavelength λ (cm) is passed through an ideal beam splitter, 50% of the incident radiation will be reflected, while 50% will be transmitted. Reflections from these mirrors recombine and interfere with each other at the beam splitter. Through the beam splitter, half of the beam (50%) reflected from the fixed mirror is transmitted and half (50%) is reflected back in the direction of the source. A beam that emerges from an interferometer at 90 to the input

beam is called a transmitted beam, and this beam is detected in FT-IR spectrometry. The moving mirror produces an optical path difference between the two arms of the interferometer. If the path difference between the two beams is $(n + 1/2) \lambda$, the transmitted beam interferes destructively, while the reflected beam interferes constructively.

Sources and detectors

A Globar or Nernst source is used in FT-IR spectrometers for the mid-infrared region. High-pressure mercury lamps can be used to examine the far-infrared region and for the near-infrared region, tungsten-halogen lamps are used as sources. In the mid-infrared region, two commonly used detectors are employed. Deuterium triglycine sulfate (DTGS) in a temperature resistant alkali halide window is commonly used as a pyroelectric detector for routine use.

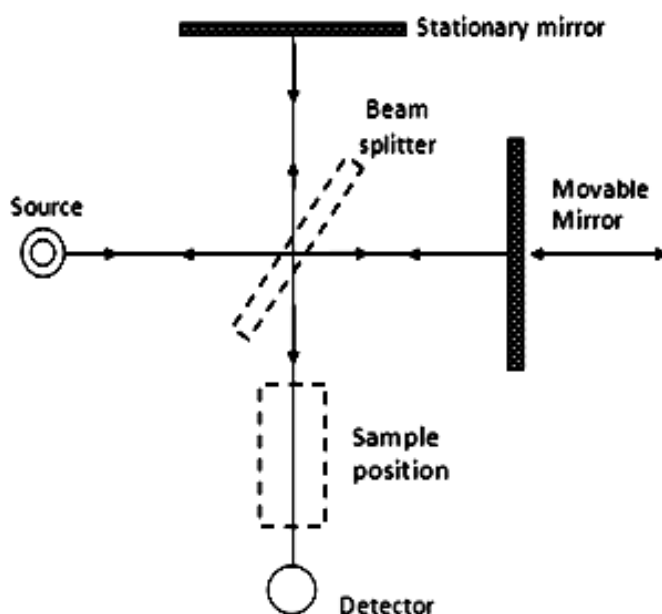


Fig. 3.2 Optical arrangement of FT-IR spectrophotometer

Mercury cadmium telluride (MCT) is used for more sensitive work, but it must be cooled to liquid nitrogen temperatures. The germanium or indium–antimony detectors are employed in the far-infrared region. They operate at liquid helium temperatures. In the near-infrared region, lead sulfide photoconductors are commonly used as detectors. The essential equations for a Fourier-transformation relating the intensity falling on the detector, $I(\delta)$, to the spectral power density at a particular wavenumbers, $\bar{\nu}$, given by $B(\bar{\nu})$ are as follows:

$$I(\delta) = \int_0^{+\infty} \bar{\nu} \cos(2\pi\bar{\nu}\delta) d\bar{\nu} \quad \dots(3.1)$$

which is one half of a cosine Fourier-transform pair, with the other being:

$$B(\bar{\nu}) = \int_0^{+\infty} I(\delta) \cos(2\pi\bar{\nu}\delta) d\delta \quad \dots(3.2)$$

A Fourier-transform pair consists of these two equations which can be transformed into one another. The first shows how power density changes as a function of path length differences, which is an interference pattern. The second shows the intensity variation as a function of wavenumber. With the help of the mathematical method of Fourier-transformation, each can be converted into the other.

In order to obtain an FT-IR spectrum, we must produce both an interferogram with and without a sample in the beam, and then transform the interferograms into spectra of (a) the source with sample absorptions and (b) the source without sample absorptions. The ratio of the former and the latter corresponds to a double-beam dispersive spectrum. With a new mathematical method (or algorithm) for fast Fourier-transformation (FFT), the mid-

infrared region underwent a major advance toward routine use. Combining this with advances in computers enabled these calculations to be performed quickly.

Moving mirrors

The moving mirror is one of the most important components of the interferometer. Ideally, it will align accurately and be able to scan two distances so that the path difference corresponds to a known value. When evaluating an infrared spectrum, a number of factors associated with the moving mirror have to be considered. In order to convert the interferogram into a conventional spectrum, the detector must digitalize the analogue signal. In converting the digitalized information from the interferogram to a spectrum, there are two major sources of error. To begin with, the transformation carried out in practice involves integration over a finite displacement rather than over an infinite displacement. The mathematical process of Fourier transformation assumes infinite boundaries. A suitable function is one that causes the interferogram's intensity to fall smoothly to zero at its ends. FT-IR spectrometers typically offer a wide range of apodization options, including the cosine function as follows:

$$F(D) = [1 + \cos(\pi D)]/2 \quad \dots(3.3)$$

where D is the optical path difference. Cosine functions provide a good compromise between reducing oscillations and deteriorating spectral resolution. More sophisticated mathematical functions may be needed, when accurate band shapes are required.

A second source of error is when the sample intervals are not identical on both sides of the maxima corresponding to zero path differences. There is a need for phase correction, but the correction procedure ensures that the sample intervals remain the same

on both sides of the first interval and should correspond to a path difference of zero. The resolution for an FT-IR instrument is limited by the maximum path difference between the two beams. There is a limiting resolution in wavenumbers (cm^{-1}) equal to the reciprocal of the path length difference (cm). For example, a path length difference of 10 cm is required to achieve a limiting resolution of 0.1 cm^{-1} . Based on this simple calculation, it appears to be quite easy to achieve high resolution. Unfortunately, this is not true, since the optics and mirror movement mechanism become less precise with longer path length displacements.

Signal-averaging

A rapid-scanning instrument's main advantage is the ability to increase signal-to-noise ratio (SNR) by signal-averaging, which results in an increase of signal-to-noise proportional to the square root of time, as follows:

$$\text{SNR} \propto n^{1/2} \quad \dots(3.4)$$

The diminishing returns of signal-averaging are that it takes an increasingly longer time to achieve greater and greater improvements. As a result of a large number of repeat scans, the instrument is placed under greater demands if it is to reproduce the conditions precisely. A monochromatic laser source is usually incorporated in the beam of the continuous source. Using the laser beam, successive scans can be aligned accurately, and the mirror displacement can be calculated and controlled at all times.

Advantages

In comparison with older dispersive instruments, FT-IR instruments have several significant advantages. Two of these are the *Fellgett* (or multiplex) advantage and the

Jacquinot (or throughput) advantage. As a result of Fellgett's advantage, the SNR per unit time is improved by a proportional amount to the square root of the number of resolution elements monitored. This results from the large number of resolution elements being simultaneously monitored. Additionally, since FT-IR spectrometry does not require any restricting devices, the entire source output can be passed continuously through the sample. This results in a significant increase in energy at the detector, thereby improving signals and SNRs. This is known as *Jacquinot's* advantage.

Strength of FT-IR spectrometry is its *speed advantage*. As a result of the mirror's ability to move short distances rather quickly, as well as improvements in the SNR due to the *Fellgett* and *Jacquinot* advantages, make it possible to obtain spectra on a millisecond time scale. In interferometry, the factor which determines the precision of the position of an infrared band is the precision with which the scanning mirror position is known. Using a helium–neon laser as a reference, the mirror position can be determined with high accuracy.

Computers

Infrared instruments are largely dependent on the computer, which performs a variety of functions. A computer controls the instrument, for example, setting scan speeds and limits, and starting and stopping scanning. By scanning the spectrum, it reads the spectrum into the computer memory, digitizing the spectrum. It is possible to manipulate the spectrum using the computer, for example, by adding and subtracting spectra or expanding areas of the spectrum that are of interest. Spectra can also be scanned continuously on the computer and averaged or added to the memory.

Spectra

Over a linear wavelength range, early infrared instruments recorded the percentage transmittance. Nowadays, routine samples are not measured by wavelength but by wavenumbers. The output from the instrument is referred as a spectrum. The wavenumbers of most commercial instruments decrease left to right in their spectrums. The infrared spectrum can be divided into three main regions: the *far-infrared* ($<400\text{ cm}^{-1}$), the *mid-infrared* ($4000\text{--}400\text{ cm}^{-1}$) and the *near-infrared* ($13000\text{--}4000\text{ cm}^{-1}$). Infrared applications typically use the mid-infrared region, but near- and far-infrared wavelengths are also important and provide information about some materials. Generally, there are many bands between 1800 cm^{-1} and 400 cm^{-1} region and less infrared bands in the $4000\text{--}1800\text{ cm}^{-1}$ region. Sometimes, the scale is changed so that the region between 1800 cm^{-1} and 400 cm^{-1} is expanded and the region between 4000 cm^{-1} and 1800 cm^{-1} is contracted to emphasize features of interest. The ordinate scale may be presented in % transmittance with 100% at the top of the spectrum. In terms of band intensity, absorbance and transmittance are commonly used.

Sample handling techniques in infrared spectroscopy

It is possible to measure the IR spectrum for samples in all three phases, namely solids, liquids, and gases. Recent improvements in instrumentation have resulted in an infrared spectrum covering a range of $12,500\text{ cm}^{-1}$ to 10 cm^{-1} . Generally, it is subdivided into three sections, namely, near infrared ($12,500\text{--}4000\text{ cm}^{-1}$), middle infrared ($4000\text{--}400\text{ cm}^{-1}$) and far infrared ($400\text{--}10\text{ cm}^{-1}$). Since it encompasses almost all vibrational and

rotational transitions, the middle infrared region is typically used for standard laboratory investigations.

The pellet technique has been employed for solid samples, to record the FT-IR spectrum. A finely ground sample is mixed with KBr powder until an intimate mixture is obtained is utilized by this technique. Transparent discs are then formed by pressing the mixture at high pressure under vacuum. In order to ensure good dispersion, the sample must be free of moisture and good dispersion must be achieved. There are several advantages of the pellet technique over the mull method, including lower scattering loss, high spectral resolution, no interference bands, better control over concentrations, homogeneity of sample in testing small samples, and the possibility of storing specimens for future analysis.

For recording liquid spectra, spacers are not used and liquids are examined neat or in solution. A film of thickness less than or equal to 0.1 mm is produced by pressing the liquid between two flat sodium chloride plates, transparent throughout the $4000\text{--}625\text{ cm}^{-1}$ region.

Cells of 0.1 to 1.0 mm thickness are used while examine solutions. In order to serve as a reference, a duplicate cell containing pure solvent is used. Solvents must be transparent in the region of interest and dry solvent must be used. The spectrum of the sample, dissolved in any of the solvents such as carbon tetrachloride and carbon disulphide, is determined after the sample is dissolved in a solvent with good infrared transparency. Despite its less symmetrical nature, chloroform is now preferred as a

solvent over carbon tetrachloride and carbon disulphide. Multiple reflection cells with path lengths up to several meters can be used to measure gas absorption spectra [45, 46].

Advantages of FT-IR over dispersive IR

There are several advantages of FT-IR over dispersive method. These are illustrated as follows:

- A better spectrum can be obtained with FT-IR since the spectrum is recorded in every 30 seconds at a resolution of 4 cm^{-1} .
- It is easier to achieve high resolution in FT-IR without sacrificing sensitivity.
- Polymeric samples of intractable nature can be analyzed using this technique.
- It can be used to obtain spectra from trace amounts of materials by depositing them on a micro MIR crystal.
- The response time of FT is much faster than that of dispersive spectroscopy. In dispersive spectroscopy, a small amount of energy is used slowly while FT uses a large amount of energy quickly.
- In FT instruments, the accuracy of wavenumber measurement is the same over the entire range while in dispersive instruments, there may be considerable variation.
- It is especially useful for examining small samples.

Through FT-IR, a digital process in which the data are handled in a computer, it is possible to subtract the spectrum of a pure compound from the spectrum of a mixture in order to reveal the spectrum of other components or components of the mixture [47].

3.4 Fourier transform Raman spectrometer

A FT-Raman spectrometer's optical arrangement is shown in Figure 3.3. The main advantage of FT-Raman over conventional dispersive Raman spectroscopy is that its lower excitation energy (Nd:YAG laser at 1064nm) renders spectra characterized by fluorescence interference. The spectrometer has a high through-put. The FT-IR and FT-Raman both have wavelength precision, which allows coadding of spectra, resulting in high signal-to-noise ratios (SNR). Using Nd:YAG lasers, sensitivity is reduced because the intensity of Raman lines is proportional to the fourth power of the excitation frequency. In contrast, the sensitivity of Fourier spectroscopy increases with multiplex gain. As a result of simultaneously detecting all frequencies, the experimental data is recorded in less time. Infrared and Raman spectrometers can be operated simultaneously by simply exchanging sources, beam splitters, and detectors on the FT spectrometer once its optical path is aligned. The optical arrangement of FT-Raman spectrometer is shown in Fig. 3.3.

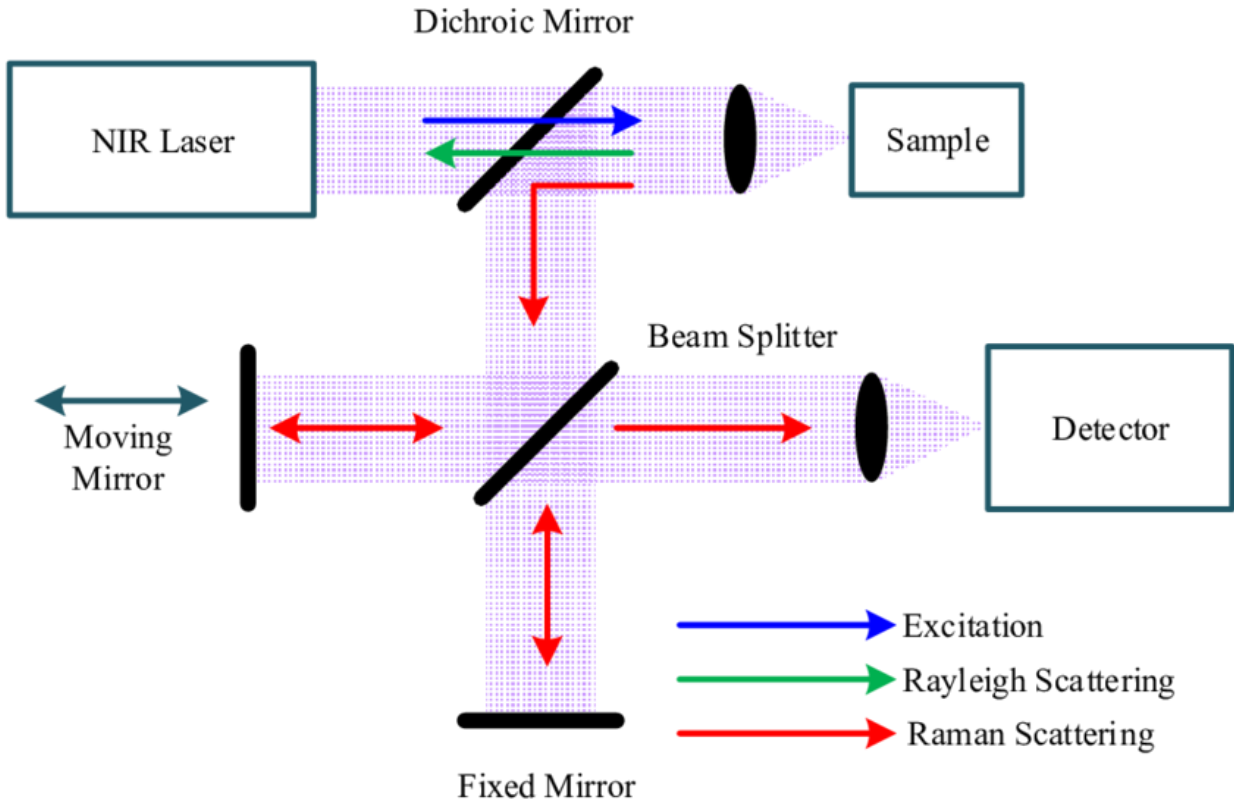


Fig. 3.3 Optical arrangement of FT-Raman spectrophotometer

Source

As the laser source in FT-Raman spectrometer, it is an air cooled, diode pumped Nd:YAG laser operating at a wavelength 1064 nm and with a maximum output power of 200 mW. A laser is attached to the rear of the FRA 106 and powered by its own source of electricity (110 V or 220 V). When the application program is running, laser radiation travels through the optics base plate to the front-mounted sample compartment, which can be switched on and off by computer software commands.

Monochromator

In order to eliminate even strong light radiation, a commercial Raman spectrometer is equipped with a double or triple monochromator. Double

monochromators have one monochromator coupled to another monochromator in sequence, allowing stray and Raman radiation to escape the first monochromator's exit slits, regardless of the monochromator's nominal frequency. The radiation, which escapes through the exit slit of the first monochromator, is redispersed in the second monochromator of the double monochromator, thereby removing the unwanted radiation. In this procedure, the laser is operated through a slit of some narrow width, causing a monochromator to shine. Afterward, the transmitted radiation is recorded at the laser frequency and then at the nominal monochromator frequency. This study uses a Raman spectrometer equipped with a triple monochromator that eliminates unwanted radiation more effectively than a double monochromator. Light enters the monochromator and passes through one or more narrow slits after being dispersed by the grating of the spectrometer. As a result, light entering a detector always has a narrow band width, consider being monochromatic. The detector of a spectrograph, however, displays a broad band of light due to wider slits.

Detectors

Raman spectrometers use photomultipliers as detectors. An electric signal is generated by collecting and focusing light from the monochromator on the cathode surface of the photomultiplier tube. A preamplifier further amplifies the electrical signal. Two factors enhance the detection efficiency of weak signals are (i) high efficiency and (ii) low thermionic dark current.

Quantum efficiency is defined as the ratio of signal pulses arriving at the anode per second to the number of photons reaching the cathode. This ratio is the function of

wavelength. As a detector, different types of photo surfaces are used depending on the laser wavelength. There should be few thermally excited electrons leaving the cathode of a photomultiplier tube in the absence of light. At room temperature, there are commercially available photo cathodes capable of producing five dark pulses per second. However, the photo cathodes are cooled to -30°C , which prevents dark pulses from appearing. This dark current is thus present at room temperature in the output of the photomultiplier tube. When considering the photomultiplier tube's output, this must be considered. Numbers of electron pulses are measured is called the output of the photomultiplier tube.

Data acquisition and control

Data acquisition and control are accomplished using a computer-enabled Raman spectrometer. Between the initial and final wavenumber positions, the position of the spectrometer is incremented by a predetermined step size. It is possible to select the data gathered for the entire run for the orthogonal orientation. The monitor screen displays Raman spectra after the run is complete. Several features of the library on the computer are useful, such as smoothing peaks, expanding selected peaks, and computing and comparing peak intensities. After the run has been completed, a plotter is used to take the printout displayed on the screen.

Sample handling techniques in the Raman spectroscopy

FT-Raman spectra of polycrystalline samples are recorded by grounding the sample and pressing it into a small depression on a metal disc. The disc is then mounted on the sample stage within the sample compartment, which then mounts the sample stage.

Polarized Raman spectra of the single crystal were recorded using a Nicolet 950 FT-Raman system in the near - infrared region using a Nd:YAG laser at wavelength 1064 nm. While the exciting laser beam has linear polarization, the plane of polarization remains unchanged. Hence the three different orientations are polarized so that all six orientations can be measured. A gas cell is used to handle gas samples. Multi-reflection gas cells contain pressure adjustment provisions [48].

Chapter – 4

FT-IR and FT-Raman investigation, quantum chemical analysis and molecular docking studies of 5-(4-Propan-2-yl)benzylidene)-2-[3-(4-chlorophenyl)-5[4-(propan-2-yl)phenyl-4,5-dihydro-1H-pyrazol-1-yl]-1,3-thiazol-4(5H)-one

FT-IR and FT-Raman investigation, quantum chemical analysis and molecular docking studies of 5-(4-Propan-2-yl)benzylidene)-2-[3-(4-chlorophenyl)-5[4-(propan-2-yl)phenyl]-4,5-dihydro-1*H*-pyrazol-1-yl]-1,3-thiazol-4(5*H*)-one

4.1 Introduction

Thiazole is used in the manufacturing of synthetic drugs, fungicides and dyes. The derivatives of thiazole like phenylthiazolyl, iso-thiazole are found to have a potent local anaesthetic, anti-inflammatory, analgesic and antipyretic activities [49-51]. Similarly, aminothiazoles are used to treat bacterial infections, inflammations, tumours [52-55] and play a vital role in insulin release [56-58]. Thiazole appears commonly in structures of various natural products and biologically active compounds, like thiamine (vitamin-B) and antibiotic drugs such as penicillin, micrococin which have revolutionized the therapy of bacterial diseases [59]. Phenyl and substituted phenyl-thiazoles are also common structures of a wide range of biologically active natural products [60]. Recently it has been found that phenyl-thiazole ring system provides a template for the design and synthesis of antiviral agents which inhibit the flaviviruses by targeting their E-protein [61]. Dyes are also prepared by employing thiazoles, especially isothiazole orange, containing thiazole moiety in the form of benzothiazole which has the binding capability with nucleic acids and other uses in biosensors and imaging [62-64]. Thiazoles used in material science due to its applications in liquid crystals, sensors and molecular switches. As far as the

pharmacological applications of 1,3-thiazoles are concerned, these scaffolds are antiviral [65], antifungal, antibacterial [66], anticancer [67], antitubercular [68] and anti-inflammatory [69]. Thiazoles are compounds which are used as antihyperglycemic compounds [70]. For this property, they have many applications in pharmacy and medicine industries [71].

Literature survey reveals that the results based on quantum chemical calculations, FT-IR and FT-Raman studies, NBO analysis, Reduced Density Gradient (RDG) analysis and docking studies of 5-(4-Propan-2-yl)benzylidene)-2-[3-(4-chlorophenyl)-5[4-(propan-2-yl)phenyl-4,5-dihydro-1*H*-pyrazol-1-yl]-1,3-thiazol-4(5*H*)-one (BPT1) have not been reported. Quantum chemical computational methods have proved to be an essential tool for interpreting and predicting the vibrational spectra. Hence, in this study, an attempt has been made to interpret the vibrational spectra of BPT1 by applying density functional theory calculations based on Becke-3-Lee-Yang-Parr (B3LYP) with 6-31G and 6-31G (d,p) basis sets. Further more, the HOMO-LUMO and NBO analysis of BPT1 have been studied by B3LYP level with 6-31G(d,p) basis set implemented in the Gaussian 09 program suite [36]. The Reduced Density Gradient (RDG) analysis has been carried out to investigate the presence of H-bond, Steric effect and Van der Waals interaction of the BPT1 molecule. Molecular docking studies have been carried out to evaluate the biological potential of the BPT1 molecule.

4.2 Experimental details

5-(4-Propan-2-yl)benzylidene)-2-[3-(4-chlorophenyl)-5[4-(propan-2-yl)phenyl]-4,5-dihydro-1*H*-pyrazol-1-yl]-1,3-thiazol-4(5*H*)-one was synthesized as per the reported procedure [72-74]. The Fourier transform infrared spectrum of the BPT1 molecule was recorded at room temperature within the interval at 4000-450 cm^{-1} in a resolution of $\pm 1 \text{ cm}^{-1}$ using an MCT detector with Perkin Elmer FT-IR spectrometer equipped for the Mid-IR range, and KBr pellets were utilized in the spectral measurements. The FT-Raman spectrum of the BPT1 molecule was recorded on a BRUKER RFS-66V model equipped with FRA-106 FT-Raman accessories within the interval at 4000-0 cm^{-1} using the 1064 nm line of an Nd: YAG laser device for excitation operated at 200 mW power.

4.3 Computational details

All calculations presented in this study were performed by using Gaussian 09 software [36] and Gauss view [75]. Several studies have been carried out regarding the calculations of vibrational spectra using B3LYP methods with the basis set 6-31G and 6-31G (d,p). RDG was calculated with the use of Multiwfn program [76] and plotted by visual molecule dynamics program (VMD) [77]. The reactivity descriptors, such as electrophilicity (ω), global hardness (η), the chemical potential (μ), ionization potential (I) and electron affinity (A) were determined from the energies of the frontier molecular orbital. The NBO and Mulliken population analysis is also reported for the local minima of the molecules. Molecular docking studies were made on Autodock 4.2 software [78]

and the result of docking was analyzed using Pymol [79] and Discovery studio [80] visualization software.

4.4 Results and discussions

4.4.1 Optimized molecular geometrical parameters

The optimized molecular structure and the geometrical parameters of the BPT1 molecule are shown in Fig.4.1 and Table 4.1 respectively, by using the B3LYP method with 6-31G, 6-31G (d,p) basis sets. The BPT1 molecule contains 32 C-C bonds, 30 C-H bonds, 5 C-N bonds, 2 C-S bonds and single N-N, C-O and C-Cl bonds.

The DFT calculated bond length of the C-C bond of the benzene rings are found at 1.419-1.388 Å [81]. The C-C bond length (DFT/XRD) in the phenyl rings in the range of 1.3866-1.4064/1.3763-1.4053 Å [82]. For our BPT1 molecule, the C-C bond length for phenyl ring are C4-C5 = 1.4082/1.4042 Å, C4-C6 = 1.4121/1.4082 Å, C5-C7 = 1.3979/1.3933 Å, C6-C9 = 1.3932/1.3882 Å, C7-C11 = 1.392/1.393 Å, C9-C11 = 1.3963/1.3979 Å for the above basis sets which was very close to experimental value [81]. The C-N bond lengths (DFT/XRD) are C11-N4 = 1.2891/1.2822, C6-N3 = 1.4847/1.4892 [82]. The bond lengths of thiazole ring for the BPT1 molecule are C42=N43 = 1.30/1.30 Å, C40-N43 = 1.41/1.40 Å respectively. These C-N bond lengths were found to be slightly shorter than the average value for a C-N single bond 1.47 Å, but longer than a C=N double bond 1.22 Å [83], suggesting that some multiple bond character is presented. The bond lengths of both the phenyl rings and regular hexagon falls between the normal values for a single (1.54Å) and a double (1.33Å) bond [84]. For the BPT1 molecule, bond lengths are C5-H8 = 1.0844/1.0851 Å, C6-H10 = 1.0835/1.0843 Å, C7-H12 = 1.0829/1.084 Å, C9-H13 =

1.0829/1.0841 Å. The reported values for C-S bond length are in the range 1.7675-1.8641 Å [85]. For the BPT1 compound, the bond length of C-S has C39-S41=1.86/1.79 Å, C42-S41=1.84/1.78 Å, which are in agreement with literature [86]. In the present study, the bond length of C40-O44 = 1.25/1.22 Å are in good agreement with the carbon-oxygen bond lengths (DFT/XRD) are reported at 1.2199/1.2212 Å [82]. C40-C39-S41= 108.92/108.73°, S41-C39-C45 = 118.14/118.67°, N25-C42-N43 = 122.95/122.14° which shows the interaction between the C=S and the neighbouring groups. Similarly at C40 position of the thiazole ring, the angles C39-C40-O44 is increased by 4.72/4.83° and the angle N43-C40-C39 is reduced by 6.54/7.30° from 120° which shows the interaction between the neighbouring atoms. From the Table, comparative analysis of the geometrical parameters such as bond length and bond angles was observed using DFT is in good agreement with each other.

4.4.2 Vibrational assignments

The BPT1 compound is constituted by 67 atoms and hence has 195 normal modes of vibration. The observed and calculated wavenumbers and potential energy distributions are discussed below. The fundamental modes of vibration were carried out and are depicted in Table 4.2. The comparison between theoretical and experimental FT-IR and FT-Raman spectra are given in Figs.4.2 and 4.3, respectively.

C-H vibrations

C-H stretching vibrations usually observed in a heteroaromatic compound in the frequency range 3200-2850 cm⁻¹ [86, 87]. The in-plane bending vibrations appear in the range of 1300-1000 cm⁻¹ and the out-of-plane bending occurs in the region 1000-750 cm⁻¹.

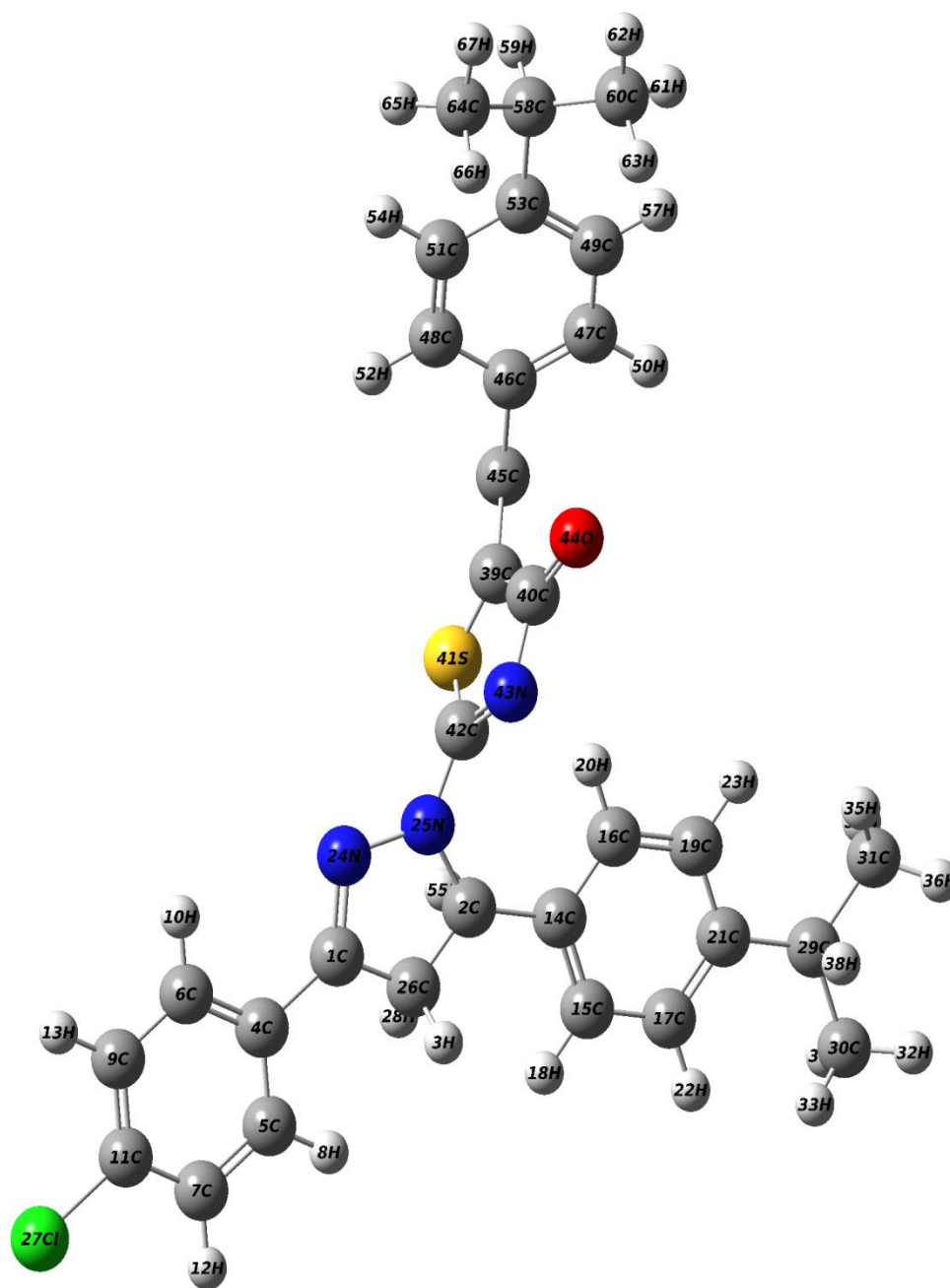


Fig. 4.1 Optimized molecular structure of 5-(4-Propan-2-yl)benzylidene)-2-[3-(4-chlorophenyl)-5[4-(propan-2-yl)phenyl-4,5-dihydro-1H-pyrazol-1-yl]-1,3-thiazol-4(5H)-one

Murugavel *et al* [88] reported that the C-H stretching vibrations at 2993, 3024 and 3061 cm^{-1} in FT-IR and calculated at 2944, 3022 and 3065 cm^{-1} . Al-Alshaikh *et al* [89] observed the C-H stretching vibrations at 3079, 3042 cm^{-1} theoretically and experimentally at 3060 cm^{-1} in FT-IR and 3068 cm^{-1} in FT-Raman spectrum. Minitha *et al* [90] reported the C-H stretching vibrations at 3195, 3157, 3106 3057 cm^{-1} in the FT-IR and at 3153, 3100, 3047 cm^{-1} in the FT-Raman spectrum. For the BPT1 molecule, the C-H stretching vibrations observed experimentally at 2870 cm^{-1} in FT-IR, 3102 cm^{-1} in FT-Raman and theoretically at 3135, 3129, 3120, 3104, 3095, 3074, 3056, 2986, 2873 cm^{-1} by B3LYP/6-31G and 3133, 3125, 3117 3100, 3093, 3070, 3055, 2986, 2871 cm^{-1} by B3LYP/6-31G (d,p) methods. Murugavel *et al* [88] reported that the in-plane bending vibration occurs at 1028 and 1282 cm^{-1} . Resmi *et al* [91] reported that the in-plane C-H bands are assigned at 1262, 1140, 1116, 1029 cm^{-1} and at 1250, 1103 cm^{-1} in FT- IR, 1250, 1136, 1105 cm^{-1} in FT-Raman, 1249, 1139, 1101, 1028 cm^{-1} by theoretically. Al-Alshaikh *et al* [89] observed the in-plane bending at 1063, 1013 cm^{-1} in IR and 1285, 1161, 1139, 1066 cm^{-1} in the Raman spectrum. Minitha *et al* [90] reported the C-H in-plane bending vibration occurs at 1514, 1425, 1287 cm^{-1} in IR spectrum , 1569, 1501, 1417, 1284 cm^{-1} in Raman spectrum and 1586, 1573, 1497, 1418,1281 cm^{-1} observed by theoretically. In the present study, 1267, 1248 cm^{-1} and 1462, 1390, 1300, 1250 cm^{-1} are assigned to C-H in-plane bending mode at FT-IR and FT-Raman spectrum, respectively and 1473, 1466,1456, 1391, 1360,1329, 1304, 1294, 1256,1235 cm^{-1} by B3LYP/6-31G and 1473, 1463, 1450, 1388, 1355, 1325, 1301, 1290, 1249, 1231 cm^{-1} theoretically obtained by B3LYP/6-31G(d,p) basis sets. C-H out-of-plane bending

vibrations are observed at 756, 826, 899 and 984 cm^{-1} by Murugavel *et al* [88]. Resmi *et al* [91] reported that the out-of-plane C-H deformations are assigned at 938, 904, 745 cm^{-1} FT-IR and 731 cm^{-1} in FT-Raman spectrum. Al-Alshaikh *et al* [89] observed the out-of-plane bending vibrations are assigned at 907, 825 cm^{-1} in the IR spectrum and 905, 827 cm^{-1} in the Raman spectrum. Minitha *et al* [90] reported the C-H out-of-plane bending vibration assigned at 964, 936, 881, 749 cm^{-1} in the IR spectrum, 989, 942, 744 cm^{-1} in Raman spectrum and 993, 931, 890, 731 cm^{-1} obtained by theoretically. For BPT1 molecule, the C-H out-of-plane bending vibrations occur at 908, 827 cm^{-1} in FT-IR and 910, 895, 810, 790 cm^{-1} in FT-Raman spectrum and 955, 928, 912, 906, 880, 856, 835, 816, 804 cm^{-1} by B3LYP/6-31G, 953, 924, 909, 875, 850, 830, 812, 800 cm^{-1} theoretically observed by B3LYP/6-31G (d,p) basis sets. These assignments are good agreement with the literature survey.

CH₃ vibrations

In general, the methyl group C-H stretching vibrations occur in the region 2975-3840 cm^{-1} [92, 93]. Normally, CH₃ group deformations are found in between 1450-1400 cm^{-1} [94]. For the present study, the asymmetric stretching vibration occurs at 3023, and 2959 in FT-IR spectrum, 3040 in FT-Raman spectrum and computed values are found at 3053, 3045, 3031, 3016, 3003, 2996, 2975, 2964, 2930, 2910, 2904, 2896 cm^{-1} by B3LYP/6-31G and 3049, 3041, 3032, 3025, 3012, 2999, 2991, 2972, 2960, 2928, 2906, 2900, 2891 cm^{-1} by B3LYP/6-31G (d,p). The symmetric stretching modes calculated for the title molecule at 2945, 2930, 2910, 2904, 2896 cm^{-1} by B3LYP/6-31G and 2941, 2928, 2906, 2900, 2891 cm^{-1} by B3LYP/6-31G (d,p) and 2904 cm^{-1} observed in FT-

Raman spectrum. In this study, the CH₃ in-plane bending vibrations are assigned at 1416 cm⁻¹ in FT-IR spectrum. The computed wavenumbers are predicted by $\delta_{ipb} = 1419, 1412, 1406, 1402 \text{ cm}^{-1}$, $\delta_{opb} = 1445, 1440, 1435, 1426 \text{ cm}^{-1}$, $\delta_{sb} = 1365, 1366 \text{ cm}^{-1}$, $\delta_{ipr} = 874, 866, 851, 849 \text{ cm}^{-1}$ by B3LYP/6-31G and $\delta_{ipb} = 1415, 1409, 1404, 1399 \text{ cm}^{-1}$, $\delta_{opb} = 1441, 1438, 1430, 1422 \text{ cm}^{-1}$, $\delta_{sb} = 1363, 1360 \text{ cm}^{-1}$, $\delta_{ipr} = 869, 861, 848, 845 \text{ cm}^{-1}$ by B3LYP/6-31G (d,p) methods. In this present work, the CH₃ out-of-plane bending vibrations are assigned at 1010 cm⁻¹ in FT-IR spectrum. The theoretically predicted values by B3LYP/6-31G $\gamma_{opr} = 1041, 1026, 1014, 1004 \text{ cm}^{-1}$ by B3LYP/6-31G and 1038, 1024, 1010, 999 cm⁻¹ by B3LYP/6-31G (d,p) method.

CH₂ vibrations

The CH₂ symmetric stretching vibrations are generally noticed in the vicinity of 2900-2800 cm⁻¹ and asymmetric stretch will appear at 3000-2800 cm⁻¹ [95, 96]. Mary *et al* [97] reported the stretching modes of CH₂ are assigned at 2971, 2925 cm⁻¹ by theoretically and at 2974, 2921 cm⁻¹ in the IR spectrum and the deformation modes of the CH₂ group are assigned at 1430, 1197, 1132 cm⁻¹ theoretically and at 1434, 1191 cm⁻¹ in the IR spectrum. Beegum *et al* [98] reported that the CH₂ stretching vibrations are assigned at 2926, 1465, 1340 cm⁻¹ in the IR spectrum, 2958, 2930, 1335 cm⁻¹ in the Raman spectrum and 2956, 2922, 1467, 1338, 1203, 947 cm⁻¹ theoretically obtained. Al-Shaikh *et al* [89] assigned the CH₂ stretching modes at 2965, 2921 cm⁻¹ in the FT-IR spectrum, 2999, 2965, 2944, 2918 cm⁻¹ in FT-Raman spectrum and the deformation modes of the CH₂ groups are assigned at 1444, 1415, 1366, 1294, 1269, 1252 cm⁻¹ in the

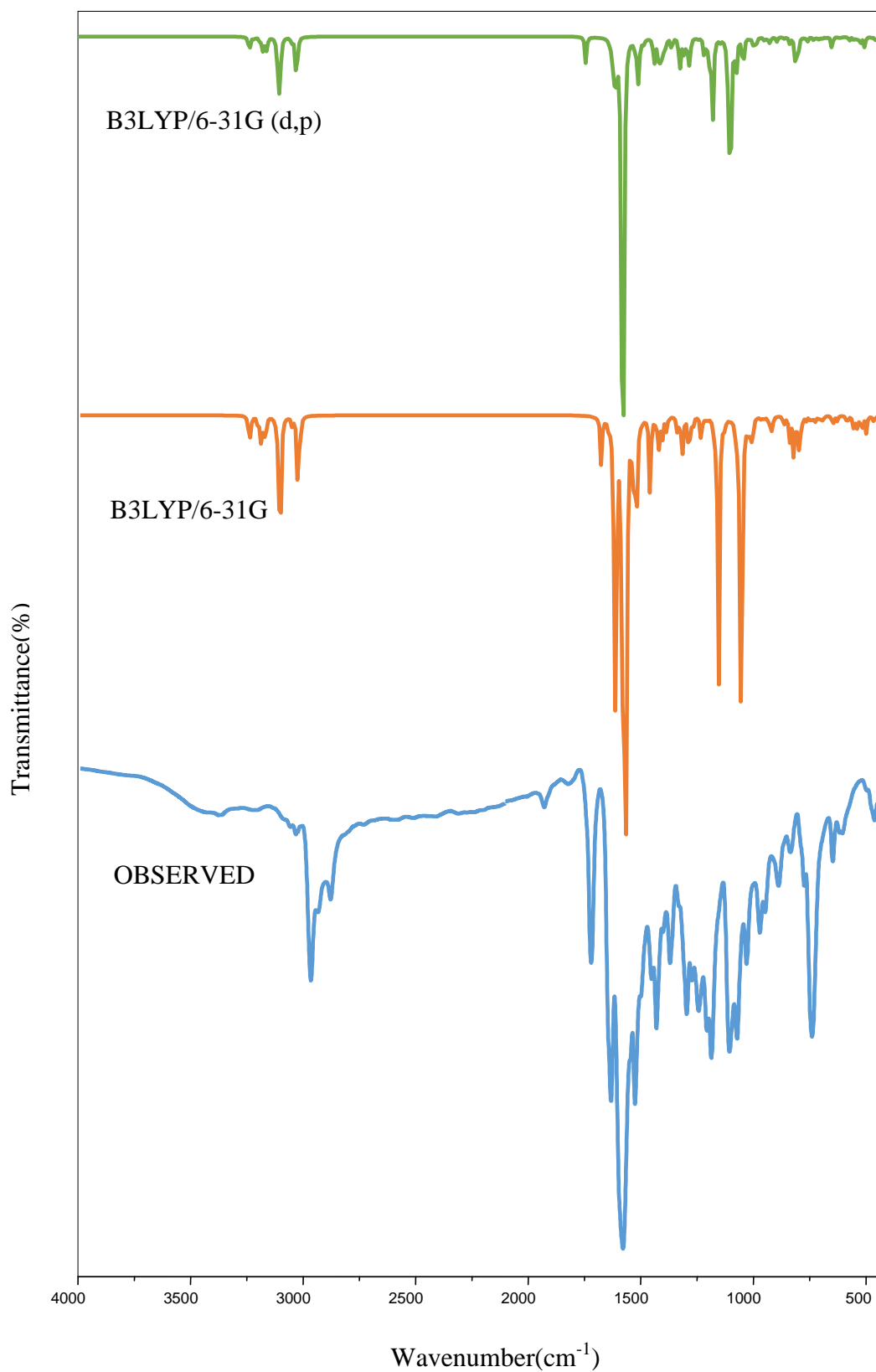


Fig. 4.2 Observed FT-IR and simulated spectra of 5-(4-Propan-2-yl)benzylidene)-2-[3-(4-chlorophenyl)-5[4-(propan-2-yl)phenyl-4,5-dihydro-1H-pyrazol-1-yl]-1,3-thiazol-4(5H)-one

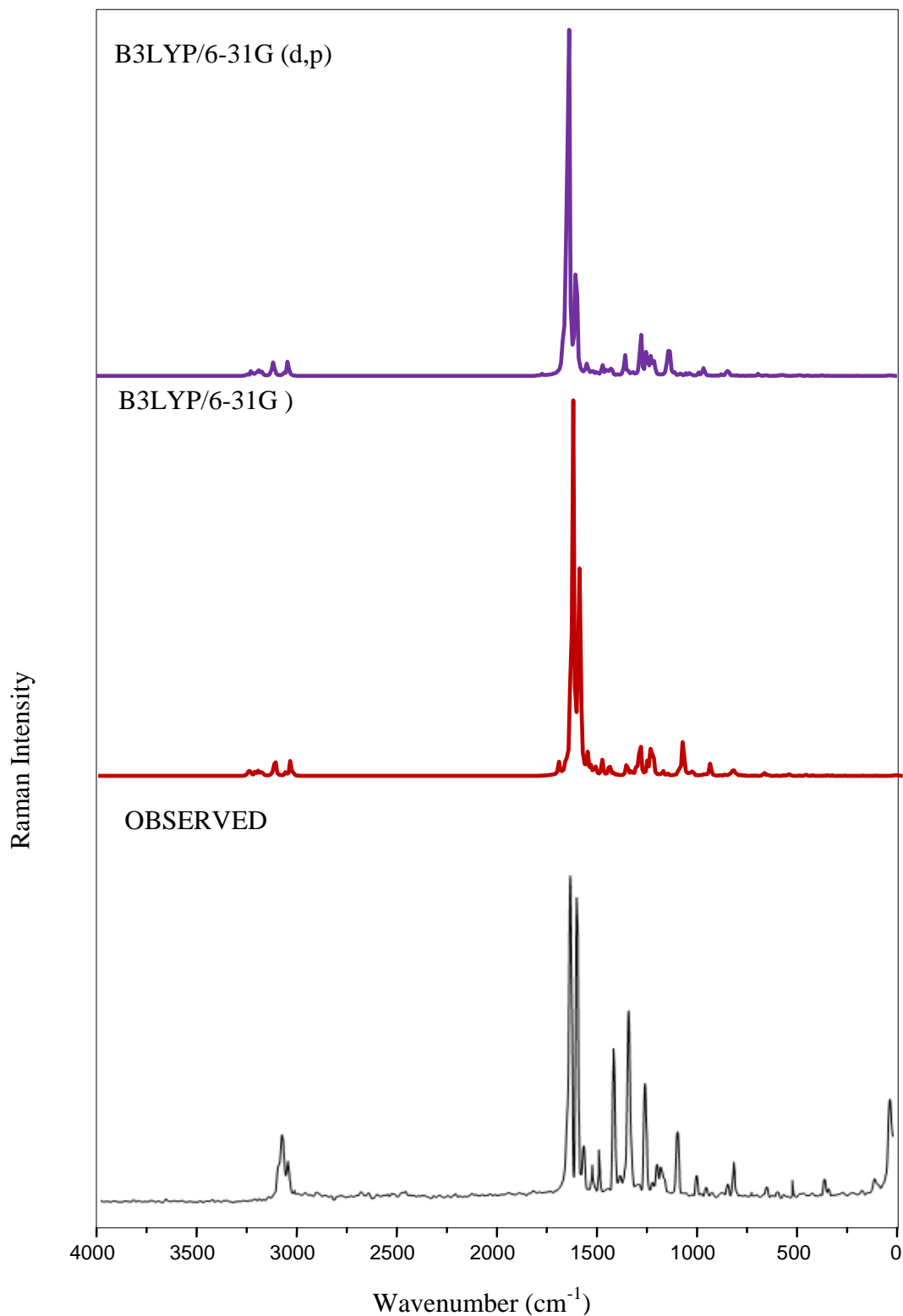


Fig 4.3 Observed FT-Raman and simulated spectra of 5-(4-Propan-2-yl)benzylidene)-2-[3-(4-chlorophenyl)-5[4-(propan-2-yl)phenyl-4,5-dihydro-1H-pyrazol-1-yl]-1,3-thiazol-4(5H)-one

FT-IR spectrum, 1444, 1415, 1370 1351, 1270 cm^{-1} in FT-Raman spectrum and at 1441, 1418 cm^{-1} for scissoring, 1362, 1355 cm^{-1} for wagging, 1296, 1267 cm^{-1} for twisting, 1254, 1132 cm^{-1} for rocking modes. For BPT1 molecule, the CH_2 stretching modes are observed at $\nu_{\text{ass}} = 3036 \text{ cm}^{-1}$, $\nu_{\text{ss}} = 2945 \text{ cm}^{-1}$, $\sigma_{\text{sci}} = 1398 \text{ cm}^{-1}$, $\rho_{\text{rock}} = 1206 \text{ cm}^{-1}$, $\tau = 1095 \text{ cm}^{-1}$, $\delta_{\text{wagg.}} = 935 \text{ cm}^{-1}$ by B3LYP/6-31G, $\nu_{\text{ass}} = 3032 \text{ cm}^{-1}$, $\nu_{\text{ss}} = 2941 \text{ cm}^{-1}$, $\sigma_{\text{sci}} = 1395 \text{ cm}^{-1}$, $\rho_{\text{rock}} = 1203 \text{ cm}^{-1}$, $\tau = 1091 \text{ cm}^{-1}$, $\delta_{\text{wagg.}} = 931 \text{ cm}^{-1}$ by B3LYP/6-31G (d,p) method respectively.

C-O vibrations

The stretching mode of C-O is expected in the range of 1850-1550 cm^{-1} [99]. The in-plane and out-of-plane bending modes of C-O were reported in the ranges $725 \pm 95 \text{ cm}^{-1}$ and $595 \pm 120 \text{ cm}^{-1}$ [99]. The calculated C-O stretching vibrational modes was obtained theoretically at 1788 cm^{-1} , 1782 cm^{-1} and 1694 cm^{-1} at FT-IR and 1689 cm^{-1} in FT-Raman by Ellakiya *et al* [100]. Parveen *et al* [101] observed the bands at 1657 cm^{-1} in the IR spectrum, 1662 cm^{-1} in the Raman spectrum and the in-plane and out-of-plane bending modes of C-O are assigned at 606, 569 cm^{-1} theoretically. In the present work, C-O stretching vibrations observed at 1689 cm^{-1} , in-plane bending at 944 cm^{-1} and out-of-plane bending at 753 cm^{-1} in FT-IR spectrum and observed theoretically at $\nu = 1896$, $\delta = 948$, $\gamma = 755$, 748 cm^{-1} by B3LYP/6-31G, $\nu = 1890$, $\delta = 945$, $\gamma = 751$, 745 cm^{-1} by B3LYP/6-31G (d,p) basis set.

C-Cl vibrations

The vibration between halogen atom attached to aromatic carbon is recognized around wave numbers 1285-485 cm^{-1} [102]. Generally, C-Cl absorption found in the vicinity 750-700 cm^{-1} [103] and C-Cl deformation bending around 460-175 cm^{-1} [104].

For Beegam *et al* [98], the C-Cl stretching mode is observed at 673 cm^{-1} in the Raman spectrum and theoretically at 671 cm^{-1} . Viji *et al* [105] observed the C-Cl stretching vibrations experimentally at 414 cm^{-1} and calculated at $\nu=416, 415 \text{ cm}^{-1}$ observed theoretically. Sebastian *et al* [81] observed this mode at 764 cm^{-1} in the IR spectrum and 760 cm^{-1} theoretically. For the C-Cl stretching mode, Resmi *et al* [91] are assigned at 876, 644, 581 cm^{-1} in Raman spectrum and 877, 646, 588 cm^{-1} theoretically. For the BPT1 molecule, the C-Cl stretching mode is observed theoretically at $\nu=690 \text{ cm}^{-1}$, $\delta=453 \text{ cm}^{-1}$, $\gamma=266, 160, 93 \text{ cm}^{-1}$ by B3LYP/6-31G and at $\nu=685 \text{ cm}^{-1}$, $\delta=449 \text{ cm}^{-1}$, $\gamma=262, 155, 88 \text{ cm}^{-1}$ by B3LYP/6-31G (d,p).

C-C vibrations

The C-C stretching vibrations usually occur at 1625-1465 cm^{-1} [106]. Murugavel *et al* [88] reported that the wavenumbers 1613, 1553, 1302, 1207, 1082 and 1036 cm^{-1} are recognized as C-C stretching modes. Resmi *et al* [91] reported that the C-C stretching vibrations are observed at 1570, 1545, 1284 cm^{-1} in the IR spectrum and at 1571 cm^{-1} in the Raman spectrum and theoretically observed at 1278, 1264 and 1571 cm^{-1} . For BPT1 molecule, the band observed in FT-IR spectrum at 1600, 1545, 1225, 1196, 1181, 1117, 1011 cm^{-1} and FT-Raman spectrum at 1600, 1545, 1501, 1210, 1160, 1110 cm^{-1} are assigned to C-C stretching vibrations. The computed C-C stretching values found at 1601,

1584, 1573, 1549, 1525, 1507, 1234, 1223, 1201, 1192, 1124 1104 cm^{-1} by B3LYP/6-31G and 1603, 1581, 1569, 1545, 1519, 1504, 1227, 1222, 1195, 1147, 1119, 1100 cm^{-1} by B3LYP/6-31G (d,p). Murugavel *et al* [88] reported that and C-C in-plane deformation was found at 429, 514, 580, 627, 652 cm^{-1} which is in accord with the experimental data at 428, 442, 459, 476, 515, 552, 575 and 627 cm^{-1} . For BPT1 molecule, the C-C in-plane bending occurs at 409 cm^{-1} in FT-IR spectrum, 835, 640, 410 cm^{-1} in FT-Raman spectrum and the computed values are found at 840, 836, 668, 644, 439, 424, 414, 396 cm^{-1} by B3LYP/6-31G and 837, 833, 666, 640, 438, 421, 410, 390 cm^{-1} by B3LYP/6-31G (d,p) method.

Ring vibration

The thiazole and phenyl ring in-plane bending vibrations are theoretically calculated at 520, 469, 437, 426, 418, 402, 354, 317,304 cm^{-1} in B3LYP/6-31G (d,p) and 515, 463, 433, 421, 415 399, 352, 312, 302 cm^{-1} in B3LYP/6-311G observed by Viji *et al* [107]. In the present work, the in-plane bending vibrations of thiazole ring are theoretically observed at 780, 767, 630, 621, 610, 605, 525, 515, 503, 490, 470, 376, 370, 335, 320, 83, 71, 60, 52, 45, 41, 36 cm^{-1} in B3LYP/6-31G and 777, 763, 625, 616, 607, 602, 523, 512, 500, 487, 468, 374, 368, 333, 318, 80, 68, 57, 49, 40, 38, 32 cm^{-1} in by B3LYP/6-31G (d,p) methods. The observed values at 608, 501 cm^{-1} in FT-IR spectrum and 600, 510, 375, 42 cm^{-1} in FT-Raman spectrum. The out-of-plane bending vibrations observed at 720, 556 cm^{-1} in FT-IR spectrum, 28 cm^{-1} in FT-Raman spectrum and computed values are 736, 725,584, 560 551, 405 399, 385,364,306, 182, 173, 145 cm^{-1} in B3LYP/6-31G and 732,

720, 581, 555, 544, 400, 394, 382, 361, 304, 179, 171, 142 cm^{-1} in by B3LYP/6-31G (d,p) method.

N-N vibrations

N-N stretching mode occurs at 1417-1372 cm^{-1} [108]. The N-N stretching mode is reported at 1120 cm^{-1} in the IR spectrum and 1130 cm^{-1} theoretically assigned by Parveen *et al* [101]. In the present work, 981, 980 cm^{-1} observed by FT-IR and FT-Raman spectrum and 986, 982 cm^{-1} obtained by theoretically by B3LYP/6-31G, 6-31G (d,p) methods.

C-S vibrations

This vibration cannot be identified easily as it results in weak infrared bands, which is susceptible to coupling effects and is also of variable intensity. In general, the C-S stretching vibration was reported in 750-600 cm^{-1} [109]. In the present work, the C-S stretching vibration assigned at 854 cm^{-1} in the IR spectrum, 860,786 cm^{-1} and 854, 785 cm^{-1} obtained theoretically by B3LYP/6-31G, 6-31G (d,p) methods. Aswathy *et al* [110] observed the band at 728 cm^{-1} in the IR spectrum, 729 cm^{-1} in the Raman spectrum and 728 cm^{-1} theoretically is assigned as the C-S stretching mode.

C-N vibrations

According to literature, the C-N stretching modes are expected in the region 1100-1300 cm^{-1} [111-113]. Murugavel *et al* [88] reported that the C-N stretching peaks appeared at 1188, 1222, 1229, 1440 and 1503 cm^{-1} . Kuruvilla *et al* [114] observed the C-N stretching vibrations theoretically at 1537 and 966 cm^{-1} and experimentally observed at 1395 cm^{-1} in the FT-IR spectrum. The C-N vibration observed at 1612 cm^{-1} in the FT-Raman spectrum

by Alphonsa *et al* [115]. For BPT1 molecule, the C-N stretching mode in the FT-IR spectrum exhibited at 1491, 1332 cm^{-1} . The calculated wavenumbers predicted at $\nu = 1530$, 1493, 1485, 1336, 847 cm^{-1} , $\gamma = 593$ in B3LYP/6-31G, $\nu = 1528$, 1490, 1481, 1333, 840 cm^{-1} , $\gamma = 590 \text{ cm}^{-1}$ in by B3LYP/6-31G (d,p) methods are assigned for C-N stretching vibrations.

4.5 Mulliken population analysis

The natural population analysis of the BPT1 molecule obtained by Mulliken [116] population analysis with B3LYP level using 6-31G and 6-31G (d,p) basis set. Mulliken atomic charge calculation has an important role in the application of quantum chemical calculation to the molecular system because of atomic charge affect, dipole moment, molecular polarizability, electronic structure and a lot of properties of molecule systems. The calculated Mulliken charge values are shown in Fig. 4.4. The charge changes with basis set due to polarization.

In the title compound, the Mulliken atomic charge of 8 carbon atoms, 30 hydrogen atoms and one sulphur atom exhibit a strong positive region and 22 carbon atoms, 3 nitrogen and one oxygen atoms are as a negative region which is tabulated in Table 4.3. In the present structure, the carbon atoms have both positive and negative charges so they were highly influenced by their substituent atoms [117]. For our BPT1 molecule, C40 was highly positive (C40=4.489/0.361) because that atom was attached with the two electronegative oxygen and nitrogen atoms and these two electronegative atoms withdrawing an electron charges from the carbon atom and become negative. The nitrogen

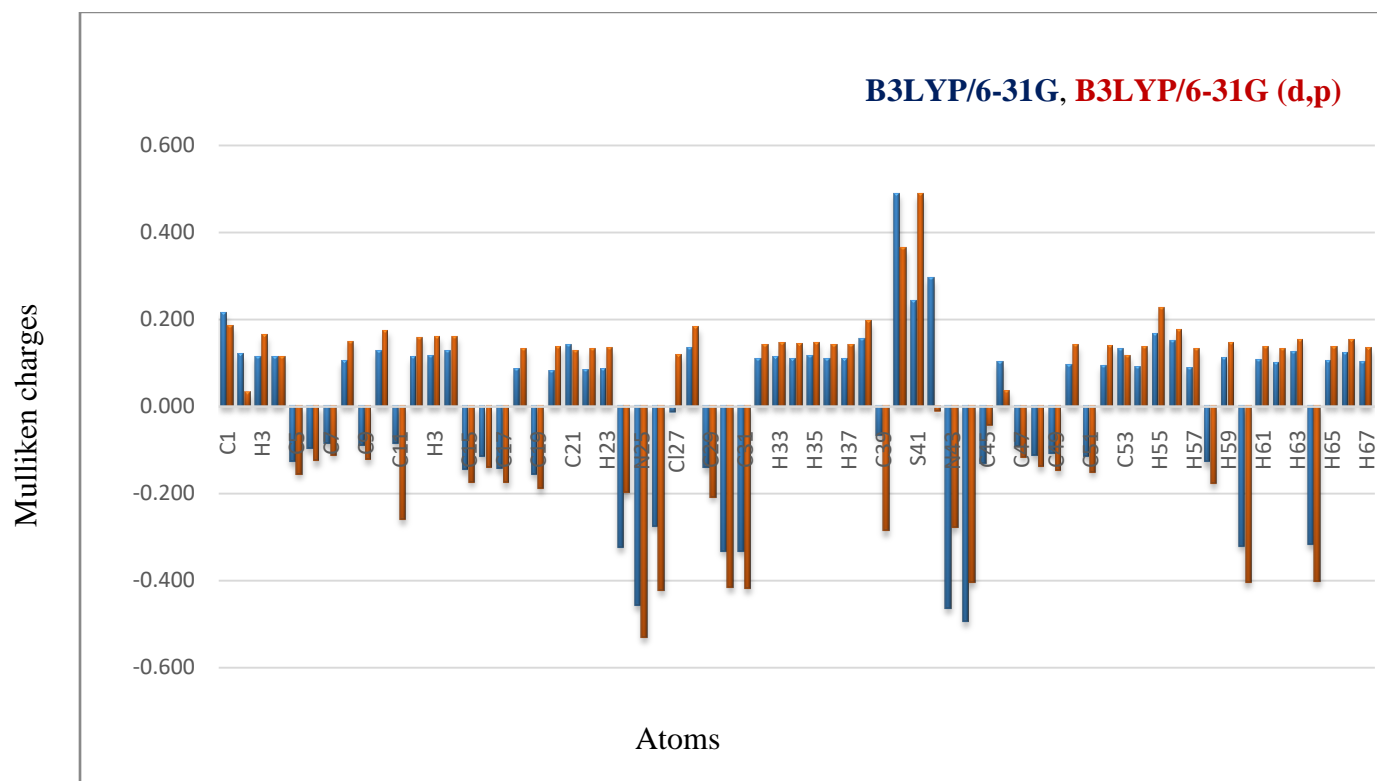


Fig. 4.4 Mulliken atomic charges of 5-(4-Propan-2-yl)benzylidene)-2-[3-(4-chlorophenyl)-5[4-(propan-2-yl)phenyl-4,5-dihydro-1H-pyrazol-1-yl]-1,3-thiazol-4(5H)-one

atom N25 was more negative than other nitrogen which is due to the influence of surrounding hydrogen atoms is N24=-0.324/-0.198, N25=-0.458/-0.531 and N43=-0.465/-0.278. All the hydrogen atoms in the BPT1 molecule have a positive charge and among the atoms, H35, H55, H56, H63, H66 were highly positive. The eight positive carbon atoms C1=0.215/0.184, C2=0.119/0.032, C4=0.112/0.113, C14=0.126/0.16, C21= 0.14/0.126, C40=0.489/0.361, C46=0.102/0.036, C53= 0.13/ 0.116. The carbon present in the negative region depends upon the neighbouring atoms and the carbon-negative range are given as C5=-0.127/-0.155, C6=-0.097/-0.126, C7=-0.086/-0.112, C9=-0.9/-0.121, C11=-0.085/-0.26, C15=-0.145/-0.174, C30=-0.332/-0.417, C31=-0.332/-0.418 respectively. Atoms C127 and C42 have both positive and negative charges. Distribution of positive and negative charges is vital to increase or decreasing bond length between the atoms.

4.6 Molecular electrostatic potential (MEP) surface

For investigating chemical reactivity of the molecule, molecular electrostatic potential (MEP) surface is plotted over the optimized electronic structure of the BPT1 molecule using density functional B3LYP method with 6-31G (d,p) basis set is shown in Fig.4.5. The MEP generated in the molecule by the charge distribution is very helpful in understanding the reactive sites for the nucleophilic and electrophilic region in hydrogen bonding interactions. The colour scheme for the MEP surface is the red, electron-rich, partially negative charge; blue, slightly electron-deficient, partially positive charge; light blue, slightly electron-deficient region; yellow slightly electron-rich region respectively. The colour order of the MEP of the BPT1 molecule originates with red colour (-7.132×10^{-2}

-7.132×10^{-2} a.u



-7.132×10^{-2} a.u

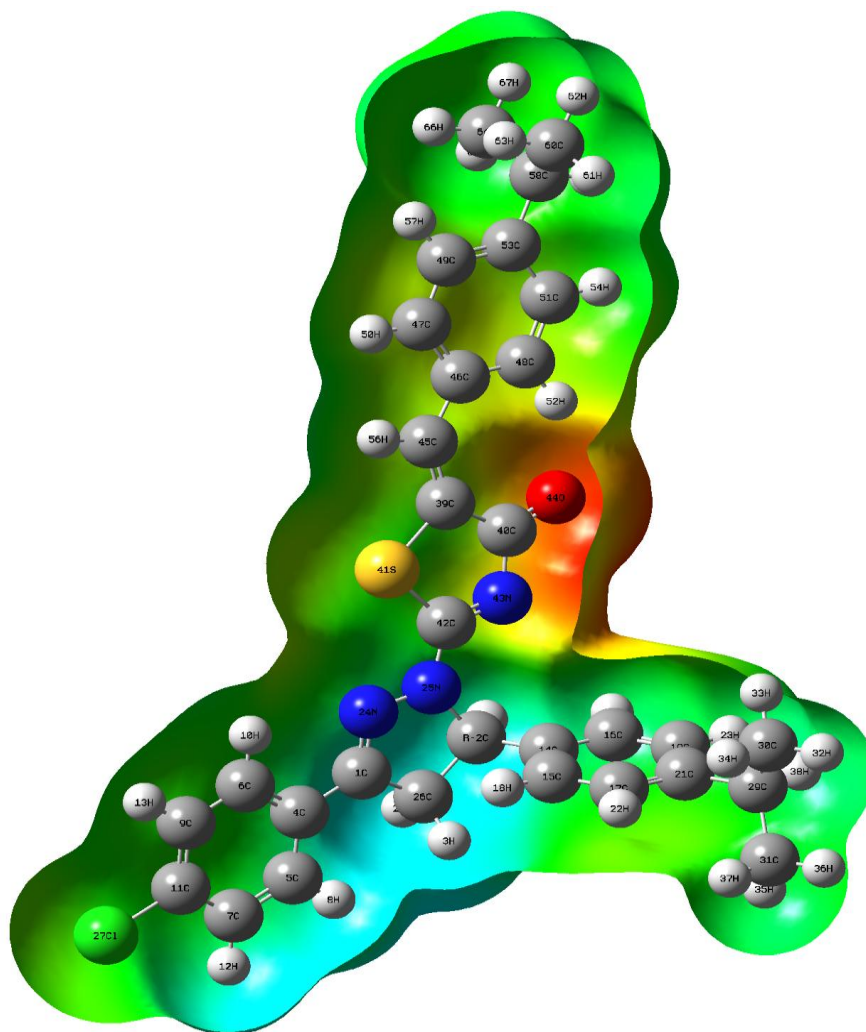


Fig.4.5 Molecular electrostatic potential surfaces of 5-(4-Propan-2-yl)benzylidene)-2-[3-(4-chlorophenyl)-5[4-(propan-2-yl)phenyl-4,5-dihydro-1H-pyrazol-1-yl]-1,3-thiazol-4(5H)-one

a.u) and terminated with dark blue colour (7.132×10^{-2} a.u) which shows the separate values of the electrostatic potential at the exterior of the molecule. The MEP total density of the BPT1 molecule clearly shows the presence of more electron density around the carbonyl group is characterized by red colour. The predominance of the green region in the MEP surfaces corresponds to a potential halfway between the two extremes red and blue colour. As seen from the 2D diagram of MEP of BPT1 molecule, more reactive sites are close to ketone (C=O) group which is present in thiazole group, the region having the most negative potential over oxygen atom O44 and the positive potential regions are most of the hydrogen atoms and it represents the possible site of the nucleophilic sites.

4.7 Molecular orbital studies

The most widely used theory by chemists is the molecular orbital (MO) theory. Ionization Potential (I), electron affinity (A), electronegativity (χ), electrophilic index (ω), hardness (η) and chemical potential (μ) must be put into a MO framework. The orbital energies of the Frontier molecular orbital are given by Fig.4.6. The FMO energy parameters and global reactivity descriptors at B3LYP/6-31G (d,p) method are tabulated in Table 4.4. We focus on the HOMO and LUMO energies to determine interesting molecular/atomic properties and chemical quantities.

$$\text{The softness of the molecule } S = \frac{1}{2\eta}$$

$$\text{The hardness of the molecule} = \frac{I + A}{2}$$

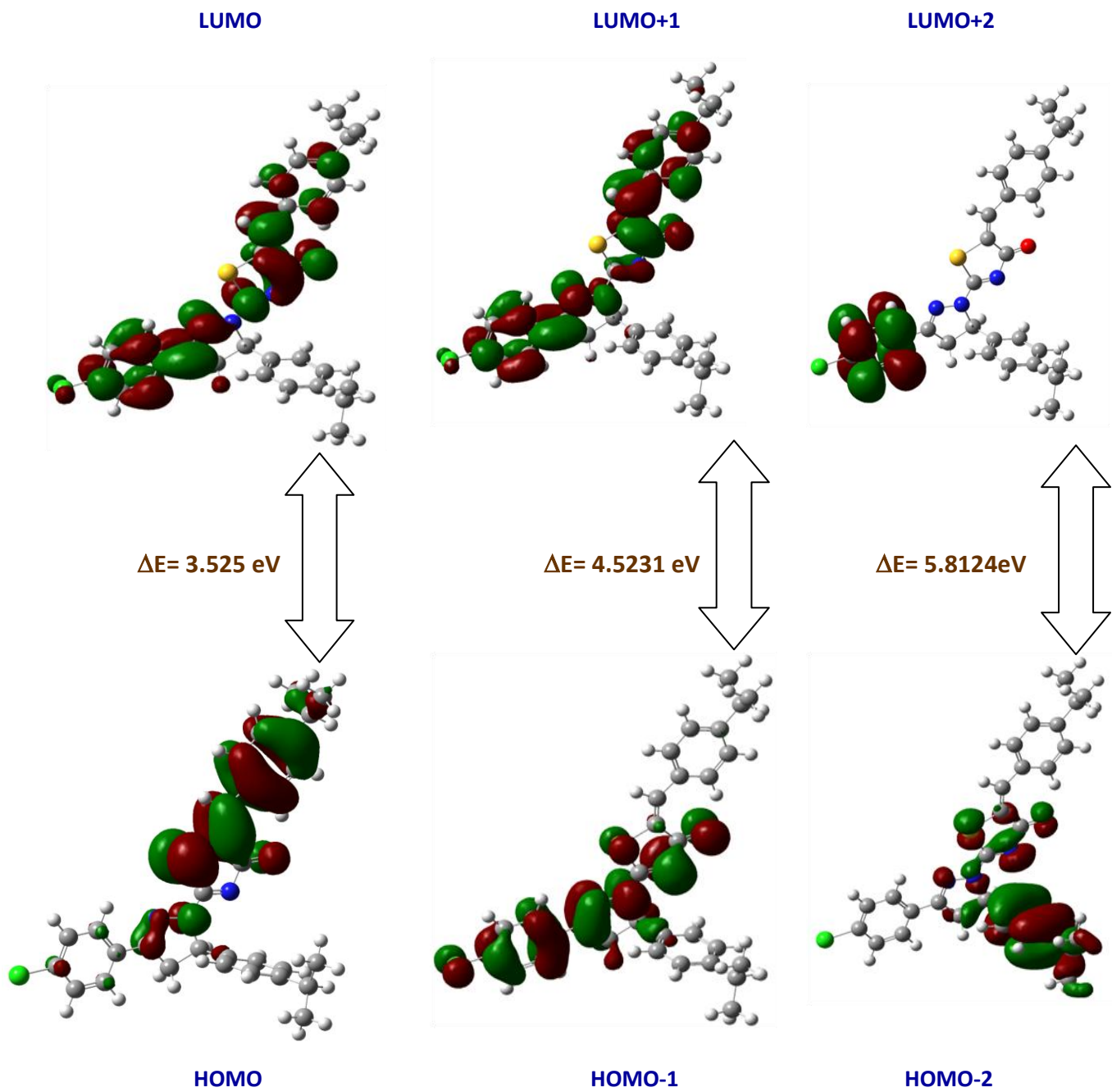


Fig.4.6 Patterns of the principle highest occupied and lowest unoccupied molecular orbital of 5-(4-Propan-2-yl)benzylidene)-2-[3-(4-chlorophenyl)-5[4-(propan-2-yl)phenyl-4,5-dihydro-1H-pyrazol-1-yl]-1,3-thiazol-4(5H)-one

$$\text{Electrophilic index } (\omega) \text{ or Global reactivity} = \frac{\mu^2}{2\eta}$$

where η is the chemical potential the electronegativity and hardness are used to make predictions about chemical behaviour and these are used to explain aromaticity in organic compounds [118]. A hard molecule has a large and a soft molecule has a small HOMO-LUMO gap. Like the same, soft molecule will be more reactive than the hard one. Based on a fully optimized ground state structure, the DFT/B3LYP/6-31G calculation predicts one intense electronic transition from the ground to the first excited state and is mainly described by one electron excitation from the highest occupied molecular orbital (HOMO) to the lowest unoccupied molecular orbital (LUMO). The less value of ΔE confirms that the molecule is more polarized and has bioactivity [119, 120]. Computed E_{HOMO} , E_{LUMO} and ΔE by DFT estimates that 401 molecular orbital with 139 occupied and remaining unoccupied for BPT1 molecule. Orbital 139 is identified as highest occupied HOMO orbital and 140 as lowest unoccupied LUMO orbital with energies 5.7579eV and 2.2329eV respectively. The HOMO-LUMO energy gap ΔE is 3.525eV, Ionization potential (I) = 5.758 eV, Electron affinity (A) = 2.233 eV, Global hardness (η) = 1.763 eV, Softness (η) = 0.567 eV, Chemical potential (μ) = -3.995 eV, Electrophilic index (ω) = 4.529 eV. The values for chemical potential and electrophilic index are small that indicates the reactive nature of the BPT1 molecule which confirms the bioactivity of the title molecule by the positive value of chemical softness.

4.8 Natural bond orbital analysis

In quantum chemistry, a natural bond orbital (NBO) is a computed bonding orbital with maximum electron density. Natural bond orbital is used in computational chemistry to calculate bond orbital, donor-acceptor interactions and the distribution of electron density between atoms. The natural bond orbital (NBO) calculations were performed using NBO 3.1 program [121] as implemented in the Gaussian 09 package at the DFT/B3LYP level with 6-31G (d,p) basis set in order to understand various second-order interactions and it provides an efficient method for studying interesting features of molecular structure and also provides a convenient basis for investigation of charge transfer or conjugative interaction in the molecular system. The second-order Fock matrix was carried out to evaluate the donor-accepter interactions in the NBO analysis [122]. For each donor (i) and acceptor (j) the stabilization energy (E2) associated with the delocalization $i \rightarrow j$ is determined as

$$E(2) = \Delta E_{ij} = q_i \frac{(F_{i,j})^2}{(E_j - E_i)}$$

where q_i is the donor orbital occupancy, E_i, E_j are diagonal elements (orbital energies) and $F_{(i,j)}$ is the off-diagonal NBO Fock matrix element. All the interactions of the BPT1 compound were tabulated in Table 4.5. The important hyper-conjugative interactions are C42-N43 from S41 of LP(2)S41 \rightarrow $\sigma^*(\text{C42-N43})$, C39-N45 from S41 of LP(2) S41 \rightarrow $\sigma^*(\text{C39-N45})$, C1-N24 from N25 of LP(1)N25 \rightarrow $\sigma^*(\text{C1-N24})$, C40-N43 from O44 of LP(2) O44 \rightarrow $\sigma^*(\text{C40-N43})$, C39-40 from O44 of LP(2) O44 \rightarrow $\sigma^*(\text{C39-C40})$, C39- C40

from O44 of LP(2) $O44 \rightarrow \sigma^*(C39-C40)$, C42-N43 from N25 of LP(N25) $\rightarrow \sigma^*(C42-N43)$ with stabilization energies, 100.22, 64.42, 26.81, 22.99, 18.59, 13.01 kJ/mol.

The perturbation energies of significant donor-acceptor interactions are presented in Table 6. The larger $E(2)$ value denotes is the interaction between electron donors (σ and π) and electron acceptors (σ^* and π^*). In Table 4.6, σ (C40-O44) orbital with 1.99418 a.u energy has 36.24% C40 character in $SP^{(2.02)}$ hybrid and has 63.76% O44 character in $SP^{(1.74)}$ hybrid. The idealized $SP^{(1.74)}$ hybrid has 66.86%, 63.51% p-character and 33.16%, 36.46% s-character. The two coefficients 0.6020 and 0.7985 are called polarization coefficients. σ C11-C127 orbital with 1.98945 a.u energy has 45.41% C11 character in $SP^{(3.42)}$ hybrid and has 54.59% C127 character in $SP^{(5.04)}$ hybrid. The idealized $SP^{(5.04)}$ hybrid has 77.38%, 83.45% p-character and 22.62%, 16.55% s-character. The two coefficients 0.6739 and 0.7389 are called polarization coefficients. The oxygen (O44) has a larger percentage of this NBO, 63.76% and gives the larger polarization coefficient 0.6777 because it has a higher electronegativity. Similarly, the carbon (C48) has a larger percentage of this NBO, 62.63% and gives the larger polarization coefficient 0.6113. The carbon and nitrogen have a lesser percentage of NBO and give a lesser polarization coefficient. The carbon (C40) has a lower percentage of this NBO, 36.24% and gives the lesser polarization coefficient 0.6020.

4.9 Fukui Function

In computational chemistry, the Fukui function describes the electron density when some electrons are added or removed from it. It is a local density functional descriptor,

which helps in predicting the chemical reactivity and selectivity. The Fukui function helps one to predict the most reactive sites for electrophilic and nucleophilic sites within a molecule [123, 124]. The condensed or atomic Fukui functions on the r th atomic site for an electrophilic f_r^- , nucleophilic f_r^+ and free radical f_r^0 on the reference molecule can be defined as

$$\begin{aligned} f_k^+ &= qk(N+1) - qk(N), \\ f_k^- &= qk(N) - qk(N-1) \\ f_k^0 &= \frac{1}{2} \{qk(N+1) - qk(N-1)\} \end{aligned}$$

In these equations, q_r is the atomic charge (evaluated from Mulliken population analysis, electrostatic derived charge, etc.) at the r th atomic site in the neutral (N), anionic (N+1), cationic (N-1) chemical species [125]. Dual descriptor ($\Delta f(r)$) combines the two Fukui functions f_r^+ and f_r^- as

$$\Delta f(r) = [f_+(r) - f_-(r)]$$

The dual descriptors $\Delta f(r)$ distinguishes between the nucleophilic and electrophilic attack at a particular site with their sign. If $\Delta f(r) > 0$, the site is favoured for a nucleophilic site, whereas if $\Delta f(r) < 0$, the site may be favoured for electrophilic sites. From Table 4.7, some of nucleophilic sites for the BPT1 molecule are C127, N43, H56, S41, C45, O44 and these sites have positive values i.e $\Delta f(r) > 0$. Similarly some of electrophilic sites are C64, C2, C26, C46, H20 and these sites have negative values i.e $\Delta f(r) < 0$. Among these nucleophilic and electrophilic sites, C46 and H20 have higher negative and positive charge values and O44, C45 are found in thiazole and phenyl group respectively of the BPT1 molecule.

4.10 Reduced density gradient (RDG) analysis

The reduced density gradient (RDG) can be used to reveal the intermolecular, intramolecular and even covalent interactions in real space based on the electron density and their derivatives are developed by Johnson et al [126]. It is defined as

$$\text{RDG}(\mathbf{r}) = \frac{1}{2(3\pi^2)^{1/2}} \frac{|\nabla\rho(\mathbf{r})|}{\rho(\mathbf{r})^{4/3}}$$

In order to explore the features associated with small reduced gradients, we examined plots of RDG versus $\text{sign}(\lambda_2(\mathbf{r})\rho(\mathbf{r}))$. The λ_2 sign was utilized to distinguish the bonded ($\lambda_2 < 0$) interactions from nonbonding ($\lambda_2 > 0$) interactions. The plot of the RDG versus the electron density ρ increased by the sign of λ_2 and visualization to a whole wide range of interactions types. The RDG spikes are found in the low gradient region and have low density and depicted in Fig.4.7. According to the 2d graph, the strong interactive interaction indicates in blue colour which represents the interaction between H-bond, C-Cl bonds, weak interaction represents in green colours such as Van der Waals interaction and steric repulsion in red colour. The reduced density gradient, RDG is -0.010 a.u.

4.11 Atoms in molecules (AIM) analysis

According to Atoms in molecules (AIM) hypothesis, any chemical bond involving in H-bonding is explained by bond critical points (BCPs). The topological parameters suited at each BCP decide the peculiarity of the interaction between two adjacent atoms. Here, AIM analysis is accomplished to examine the intermolecular interactions with in the BPT1 molecule. The molecular diagram of the BPT1 molecule using the AIM

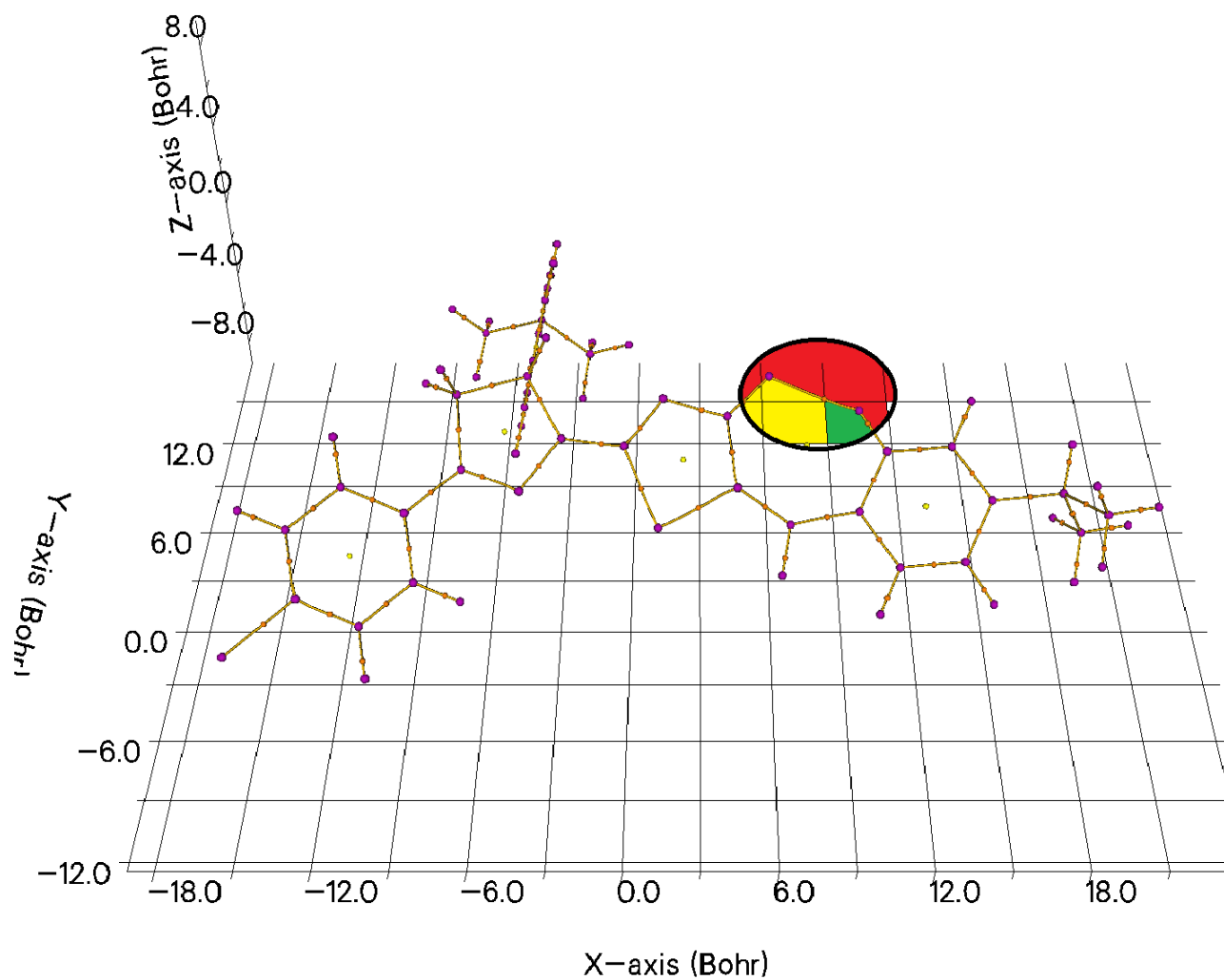


Fig.4.8 Molecular graph of 5-(4-Propan-2-yl)benzylidene)-2-[3-(4-chlorophenyl)-5[4-(propan-2-yl)phenyl-4,5-dihydro-1H-pyrazol-1-yl]-1,3-thiazol-4(5H)-one

program calculated at B3LYP/6-31G (d, p) approximation was presented in Fig.4.8 and the energy of intermolecular H-bond presenting is showed in Table 4.8. According to Rozas et al [127] hypothesis, Nature of hydrogen bond can be represented by values of $\nabla^2\rho(r) > 0$ and $V(r) < 0$ intimate intermediate type hydrogen bonds, values of $\nabla^2\rho(r) > 0$ and $G(r)+V(r) > 0$ associated weak hydrogen bond interactions. From the table, all interaction of hydrogen bond of the BPT1 molecule has positive values of Laplacian of electron density $\nabla^2\rho(r) > 0$ and $V(r) < 0$, depict that they are intermediate closed-shell type hydrogen bond interactions. The hydrogen bond energy 0.0159 kcal/mol as calculated with the help of Multiwfn.

4.12 Molecular docking studies

Molecular docking is a powerful computational tool that predicts the preferred binding orientation, affinity and protein targets. BPT1 molecule can be used for treating microbacterial diseases and cancer. To explore the biological activity of the BPT1 molecule, molecular docking simulations have been performed using AutoDock/Vina software [78]. The BPT1 molecule (ligand) was docked into the active site of the protein 4QXM, 5T6N, 4YJ3, 3S9Y and 4I50 associated with antitubercular, antiviral and anticancer activity. The 3D crystal structure of the protein was obtained from the protein data bank. Initially, the co-crystalline ligands co-factors and water molecules were removed from protein using Auto Dock Tools (ADT) graphical user interface. Subsequently, polar hydrogen was attached and atomic charges were computed by Kollman and Gasteiger method. The active site of protein was defined with 60Å x 60Å x 60Å grid size and the Lamarckian Genetic Algorithm (LGA) was used to carry out the

process. The molecular docking binding energies (kcal/mol), intermolecular energy (kcal/mol) and inhibition constants (μm) were obtained and are tabulated in Table 4.9. Binding energy gives a measure of the affinity of ligand-protein complex whereas the intermolecular energy indicates the energy between non-bounded atoms. Interaction of antitubercular protein shows three van der waals and one conventional hydrogen bond was found in 4QXM interacting with amino acids (3.12Å; MET A:98, 4.06Å; ILE A:47, 4.46Å; TYR A:158, 2.8Å; THR A:196) with different binding energy (-9.03, -7.24, -7.23, -6.73 kcal/mol), inhibition constant (239.32nm, 4.95mm, 5.06mm, 11.75mm) and RMSD values are (45.171, 32.143, 51.17, 39.7)Å. Interaction of antiviral protein shows two conventional hydrogen bonds, three pi-pi stacked bonds were found in 5T6N interacting with amino acids (3.49Å; GLN A-210, 1.92Å; GLN A:210, 3.15Å; TRP A:234, 3.13Å; TRP A:234, 3.15Å TRP A:234) with different binding energies (-7.63, -5.71, -6.23, -5.67, -5.37) kcal/mol, inhibition constant (2.57, 65.29, 27.26, 69.34, 115.39 μm) and RMSD values are (46.93, 61.645, 48.102, 49.815, 82.058) Å. Interaction of anticancerous protein shows existence of three van der waals interactions and Pi-donor hydrogen bond were found in 4YJ3interacting with amino acids (2.21Å; GLN A:358, 2.62 Å; PRO A:364, 2.81 Å; THR A:365, 2.94 Å; GLY A:365) with different binding energies (-6.47, -6.18, -6.14, -6.12) kcal/mol, inhibition constant (18.02, 29.66, 31.72, 32.56) μm) and RMSD values are (262.039, 229.467, 269.206, 267.117) Å. Interaction of anticancerous protein shows three conventional hydrogen bonds and a van der waals bond were found in 3S9Y interacting with amino acids (3.01Å;ASP A:160, 3.03 Å; LYS A:158, 2.61 Å; ASP A:160; 2.93Å; MET A:1) with different binding energies (-7.71, -7, -6.51, -7.79) kcal/mol, inhibition constant (2.24, 7.4, 16.78, 1.94) μm and RMSD values are (17.797,

56.79, 23.213, 39.362)Å. Two conventional hydrogen bonds, two pi-pi stacked interactions and a van der waals bond were found in another anticancerous protein 4I50 with amino acids (1.91 Å; ALA A:247, 1.92 Å; LEU A: 248, 3.01 Å; TYR A:357, 3.21 Å; TYR A:357, 3.83 ; GLY A:246) with different binding energies (-7.52, -7.09, -7.06, -7.03, -6.38) kcal/mol, inhibition constant (3.07, 6.37, 6.64, 7.01, 21.08) μm and RMSD values are (123.143, 123.075, 114.455, 113.872, 122.855) Å. The docked ligand interactions with amino acids of the receptor and the ligand at the active sites of the receptor are shown in Fig.4.9. These docked preliminary results suggest that the title compound might exhibit the inhibitory activity against protein inhibitors.

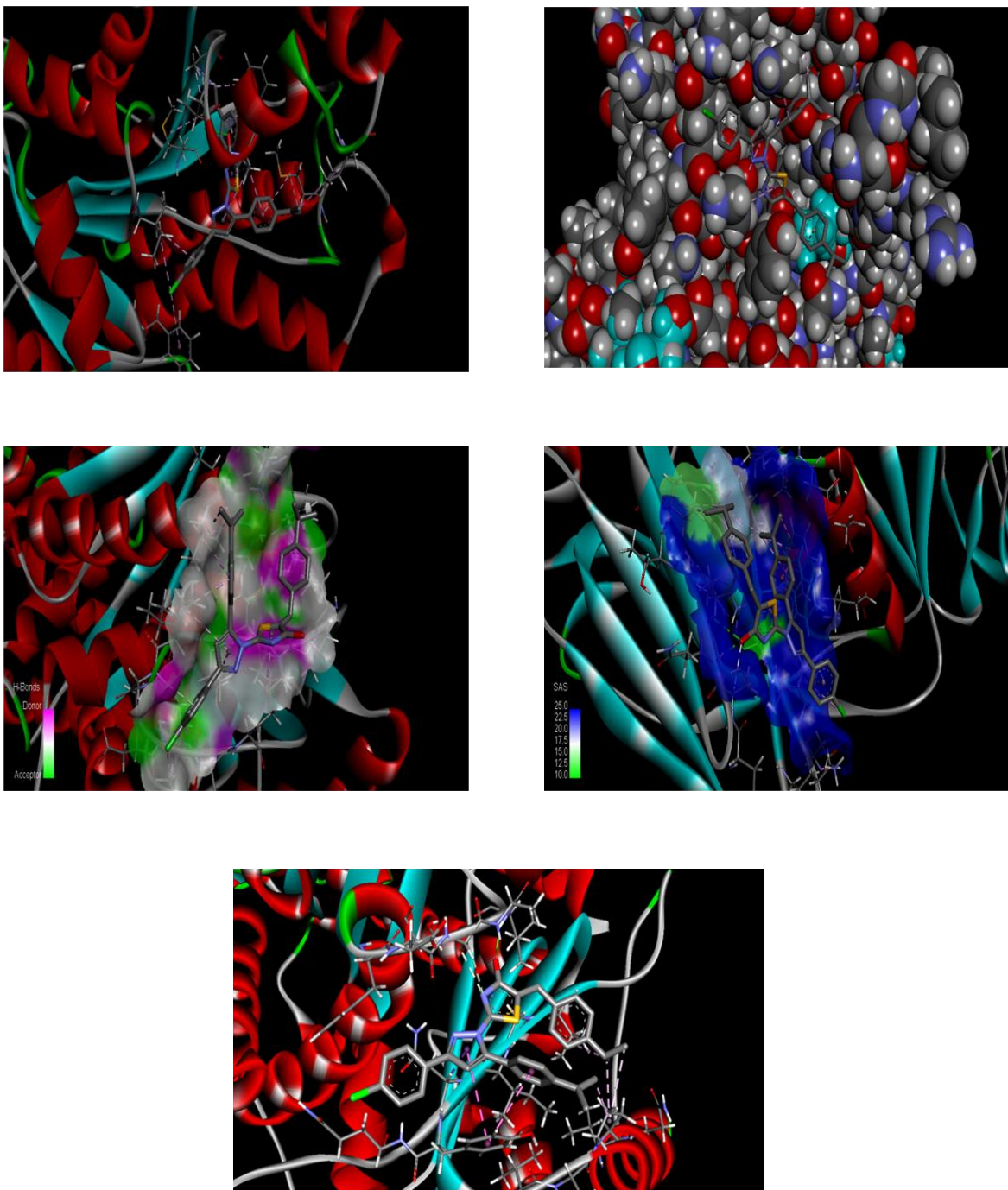


Fig.4.9 Ligand 5-(4-Propan-2-yl)benzylidene)-2-[3-(4-chlorophenyl)-5[4-(propan-2-yl)phenyl-4,5-dihydro-1H-pyrazol-1-yl]-1,3-thiazol-4(5H)-one - Protein – 4QXM, 3S9Y,4YJ3,5T6N and 4I5O

4.13 Conclusion

The optimized geometries and vibrational frequencies of the BPT1 molecule have been determined using DFT/B3LYP/6-31G and 6-31G (d,p) basis sets. Experimentally observed frequencies are in good agreement with the theoretical values as well as literature data. In HOMO and LUMO, the lower energy gaps i.e. 3.525eV, depict the presence of biological activity of the BPT1 molecule. From the MEP analysis, it is evident that the electrophilic regions are oxygen atoms and nucleophilic regions are mainly over hydrogen atoms. Stability of the molecule arising from hyper conjugative interaction and charge delocalization has been analysed using natural bond orbital analysis. The electron density between atoms revealed two relatively strong intramolecular noncovalent interactions. The molecular docking results referred that the BPT1 molecule might be an inhibitory activity against anti-cancer and antiviral agents. The anticancer protein 4YJ3 is having higher binding energy, inhibition constant and RMSD values such as -6.47 kcal/mol. 18.02 μ M and 262.039 than 3S9Y, 4I5O. Thus the BPT1 molecule may be observed as an efficient antitubercular, anticancer and antiviral drug.

Table 4.1 Optimized structural parameters of 5-(4-Propan-2-yl)benzylidene)-2-[3-(4-chlorophenyl)-5[4-(propan-2-yl)phenyl-4,5-dihydro-1H-pyrazol-1-yl]-1,3-thiazol-4(5H)-one using B3LYP/6-31G and B3LYP/6-31G (d,p) method

Parameters	Bond length (Å°)		Parameters	Bond angle (°)		Parameters	Dihedral angles (°)	
	B3LYP/6-31G	B3LYP/6-31G(d,p)		B3LYP/6-31G	B3LYP/6-31G(d,p)		B3LYP/6-31G	B3LYP/6-31G(d,p)
C1-C4	1.46	1.46	C4-C1-N24	121.69	121.78	N24-C1-C4-C5	178.97	178.57
C1-N24	1.31	1.29	C4-C1-C26	125.18	125.08	N24-C1-C4-C6	-0.80	-1.17
C2-N25	1.51	1.49	N24-C1-C26	113.12	113.13	C26-C1-C4-C5	0.14	-0.29
C2-H55	1.09	1.09	C14-C2-N25	112.42	112.52	C24-C1-C4-C6	-179.64	179.97
H3-C26	1.09	1.09	C14-C2-C26	115.12	114.92	C4-C1-N24-N25	-179.90	179.80
C4-C5	1.41	1.40	C14-C2-H55	109.25	109.07	C26-C1-N24-N25	-0.93	-1.22
C4-C6	1.41	1.41	N25-C2-C26	100.18	100.19	C4-C1-C26-C2	-174.61	-174.90
C5-C7	1.40	1.39	N25-C2-H55	107.27	107.64	C4-C1-C26-H3	-54.52	-54.77
C5-H8	1.08	1.09	C26-C2-H55	112.12	112.08	C4-C1-C26-H28	65.51	65.17
C6-C9	1.39	1.39	C1-C4-C5	120.64	120.60	C24-C1-C26-C2	6.47	6.16
C6-H10	1.08	1.08	C1-C4-C6	120.60	120.83	C24-C1-C26-H3	126.56	126.28
C7-C11	1.39	1.39	C5-C4-C6	118.76	118.57	C24-C1-C26-H28	-113.41	-113.77
C7-H12	1.08	1.08	C4-C5-C7	120.89	121.04	N25-C2-C14-C15	67.62	63.88
C9-C11	1.40	1.40	C4-C5-H8	120.26	120.20	N25-C2-C14-C16	-112.24	-116.40
C9-H13	1.08	1.08	C7-C5-H8	118.85	118.76	C26-C2-C14-C15	-46.25	-49.94
C17-H22	1.09	1.09	C4-C6-C9	120.75	120.86	C26-C2-C14-C16	133.89	129.79
C19-C21	1.40	1.40	C4-C6-H10	119.06	119.07	H55-C2-C4-C15	-173.42	-176.75

C19-H23	1.09	1.09	C9-C6-H10	120.20	120.07	H55-C2-C14-C16	6.72	2.97
C21-C29	1.53	1.52	C5-C7-C11	118.79	119.15	C14-C2-N25-N24	-113.77	-114.45
N24-N25	1.39	1.37	C5-C7-H12	120.73	120.69	C14-C2-N25-C42	69.30	71.09
N25-C42	1.35	1.35	C1-C7-H12	120.48	120.17	C26-C2-N25-N24	8.96	8.10
C29-H38	1.10	1.10	C6-C9-C11	118.97	119.36	C26-C2-N25-C42	-167.97	-166.37
C30-H32	1.10	1.10	C6-C9-H13	120.71	120.65	H55-C2-N25-N24	126.12	125.36
C39-C40	1.50	1.51	C11-C9-H13	120.33	119.98	H55-C2-N25-C42	-50.81	-49.11
C39-S41	1.86	1.79	C7-C11-C9	121.84	121.02	C14-C2-C26-C1	112.34	113.07
C39-C45	1.36	1.36	C7-C11-C127	119.10	119.54	C4-C2-C26-H3	-8.49	-7.64
C40-N43	1.41	1.40	C9-C11-C127	119.05	119.44	C14-C2-C26-H28	-128.62	-128.10
C40-O44	1.25	1.22	C2-C14-C15	121.40	121.26	N25-C2-C26-C1	-8.47	-7.77
S41-C42	1.84	1.78	C2-C14-C16	119.97	120.21	N25-C2-C26-H3	-129.30	-128.47
C42-N43	1.30	1.30	C15-C14-C16	118.63	118.53	N25-C2-C26-H28	110.57	111.07
C48-H52	1.08	1.08	C14-C15-C17	120.63	120.65	H55-C2-C26-C1	-121.96	-121.67
C49-C53	1.41	1.40	C40-C39-S41	108.92	108.73	H55-C2-C26-H3	117.21	117.62
C49-H57	1.09	1.09	C40-C39-C45	132.94	132.60	H55-C2-C26-H28	-2.92	-2.84
C58-C60	1.55	1.54	S41-C39-C45	118.14	118.67	C1-C4-C5-C7	-179.71	-179.67
C58-C64	1.55	1.54	C39-C40-O44	124.72	124.83	C1-C4-C5-H8	0.23	0.27
C64-H66	1.10	1.10	N43-C40-O44	121.81	122.47	C6-C4-C5-C7	0.07	0.08
C64-H67	1.10	1.10	S41-C39-C45	118.14	118.67	C6-C4-C5-H8	-179.99	-179.98

Table 4.2 Vibrational assignments of 5-(4-Propan-2-yl)benzylidene)-2-[3-(4-chlorophenyl)-5[4-(propan-2-yl)phenyl-4,5-dihydro-1H-pyrazol-1-yl]-1,3-thiazol-4(5H)-one using B3LYP/6-31G and B3LYP/6-31G (d,p) method

Modes	Observed wavenumbers (cm ⁻¹)		Calculated wavenumbers (cm ⁻¹)		Vibrational assignments (% PED)
			B3LYP/6-31G	B3LYP/6-31G (d,p)	
	FT-IR	FT-Raman			
1			3135	3133	vCH (98)
2			3129	3125	vCH (98)
3			3120	3117	vCH (98)
4			3113	3109	vCH (98)
5		3102	3104	3100	vCH (98)
6			3101	3098	vCH (98)
7			3095	3093	vCH (98)
8			3091	3089	vCH (98)
9			3085	3082	vCH (98)
10			3080	3076	vCH (98)
11			3074	3070	vCH (98)
12			3071	3063	vCH (98)
13			3056	3055	vCH (98)
14			3053	3049	v _{ass} CH ₃ (95)
15		3040	3045	3041	v _{ass} CH ₃ (95)
16			3036	3032	v _{ass} CH ₂ (95)
17	3023		3031	3025	v _{ass} CH ₃ (95)
18			3016	3012	v _{ass} CH ₃ (95)
19			3003	2999	v _{ass} CH ₃ (95)
20			2996	2991	v _{ass} CH ₃ (95)
21			2986	2980	vCH (98)
22			2975	2972	v _{ass} CH ₃ (95)
23	2959		2964	2960	v _{ass} CH ₃ (95)
24			2945	2941	v _{ss} CH ₂ (96)
25			2930	2928	v _{ss} CH ₃ (97)
26		2904	2910	2906	v _{ss} CH ₃ (97)

27			2904	2900	$\nu_{ss} \text{CH}_3$ (97)
28			2896	2891	$\nu_{ss} \text{CH}_3$ (97)
29			2891	2888	νCH (97)
30	2870		2891	2871	νCH (97)
31	1689		1896	1890	νCO (71), νCC (18), δCH (10)
32	1600	1601	1606	1603	νCC (70), δCH (22)
33			1584	1581	νCC (70), δCH (20)
34			1573	1569	νCC (70), δCH (20)
35	1545	1545	1549	1545	νCC (62), νCN (11), δCH (10)
36			1530	1528	νCN (63), νCC (12), δCH (10)
37			1525	1519	νCC (62), δCH (12), δCC (10)
38		1501	1507	1504	νCC (60), νCCl (16), νCN (10)
39	1491		1493	1490	νCN (62), νCC (18), δCH (10)
40			1485	1481	νCN (60), νCC (18), δCO (12)
41			1473	1470	δCH (63) νCC (18)
42		1462	1466	1463	δCH (63) νCC (18)
43			1456	1450	δCH (62) νCC (20)
44			1445	1441	$\nu_{opb} \text{CH}_3$ (71)
45			1440	1438	$\nu_{opb} \text{CH}_3$ (70)
46			1435	1430	$\nu_{opb} \text{CH}_3$ (70)
47			1426	1422	$\nu_{opb} \text{CH}_3$ (71)
48	1416		1419	1415	$\nu_{ipb} \text{CH}_3$ (73)
49			1412	1409	$\nu_{ipb} \text{CH}_3$ (73)
50			1406	1404	$\nu_{ipb} \text{CH}_3$ (72)
51			1402	1399	$\nu_{ipb} \text{CH}_3$ (73)
52	1397		1398	1395	$\sigma_{sci} \text{CH}_2$ (81)
53		1390	1391	1388	δCH (66) νCC (19)
54			1375	1371	δCH (66) νCC (21)
55	1364		1365	1363	$\delta_{sb} \text{CH}_3$ (75)
56			1366	1360	$\delta_{sb} \text{CH}_3$ (75)
57			1360	1355	δCH (68), νCC (20)
58			1357	1351	δCH (68), νCC (22)
59			1350	1346	$\delta_{sb} \text{CH}_3$ (76)
60			1345	1340	$\delta_{sb} \text{CH}_3$ (76)
61	1332		1336	1333	γCN (65)

62			1329	1325	$\delta\text{CH}(68)$
63			1320	1317	$\delta\text{CH}(68)$
64		1300	1304	1301	$\delta\text{CH}(66)$
65			1294	1290	$\delta\text{CH}(66)$
66			1385	1281	$\delta\text{CH}(69)$
67	1267		1369	1267	$\delta\text{CH}(65), \nu\text{CC}(12)$
68	1248	1250	1256	1249	$\delta\text{CH}(65), \nu\text{CC}(12)$
69			1244	1240	$\delta\text{CH}(66), \nu\text{CC}(12)$
70			1235	1231	$\delta\text{CH}(66), \nu\text{CC}(12)$
71	1225		1234	1227	$\nu\text{CC}(63), \delta\text{CH}(12)$
72			1228	1222	$\nu\text{CC}(65), \delta\text{CH}(16)$
73			1223	1218	$\nu\text{CC}(65), \delta\text{CH}(15)$
74		1210	1216	1212	$\nu\text{CC}(65)$
75			1206	1203	$\rho_{\text{rock}}\text{CH}_2(70), \delta\text{CH}(12)$
76	1196		1199	1195	$\nu\text{CC}(65), \delta\text{CH}(15)$
77			1192	1188	$\nu\text{CC}(65), \delta\text{CH}(16)$
78	1181		1183	1180	$\nu\text{CC}(65), \delta\text{CH}(15)$
79		1160	1167	1161	$\nu\text{CC}(65), \delta\text{CH}(15)$
80			1150	1147	$\nu\text{CC}(66)$
81	1117		1124	1119	$\nu\text{CC}(66)$
82			1122	1115	$\nu\text{CC}(65)$
83		1110	1114	1110	$\nu\text{CC}(66)$
84			1104	1100	$\nu\text{CC}(66)$
85	1090		1095	1091	$\tau\text{CH}_2(96)$
86			1086	1082	$\gamma\text{CH}(53)$
87			1079	1075	$\nu\text{CC}(66), \delta\text{CH}(13)$
88			1070	1063	$\nu\text{CC}(65), \delta\text{CH}(13)$
89	1056		1059	1055	$\nu\text{CC}(65), \delta\text{CH}(12)$
90			1041	1038	$\gamma_{\text{opr}}\text{CH}_3(63), \gamma\text{CC}(12)$
91	981	980	1026	1024	$\gamma_{\text{opr}}\text{CH}_3(63), \gamma\text{CC}(12)$
92			1021	1016	$\nu\text{CC}(72), \nu\text{CO}(13), \delta\text{CH}(10)$
93			1014	1010	$\gamma_{\text{opr}}\text{CH}_3(63), \gamma\text{CC}(13)$
94			1004	999	$\gamma_{\text{opr}}\text{CH}_3(63), \gamma\text{CC}(13)$
95			986	982	$\nu\text{NN}(64), \delta\text{CH}(22)$
96			981	978	$\nu\text{CC}(62), \delta_{\text{wagg}}, \text{CH}_2(12)$

97			975	971	vCC (63), δ CH(18)
98			970	967	vCC (64), δ CH(19)
99			955	953	γ CH (58)
100	944		948	945	δ CO (65), δ CH(19)
101			935	931	δ_{wagg} , CH ₂ (59), vCC (18)
102			928	924	γ CH (58), γ_{ring} (22)
103			916	913	γ CH (58), γ_{ring} (20)
104	908	910	912	909	γ CH (58), γ_{ring} (22)
105			906	901	γ CH (60), γ_{ring} (22)
106		895	899	895	γ CH (61), γ_{ring} (21)
107			880	875	γ CH (60), γ_{ring} (20)
108			874	869	δ_{ipr} CH ₃ (66)
109			866	861	δ_{ipr} CH ₃ (66)
110	854		860	854	vCS (75), δ CH(21)
111			856	850	γ CH (60)
112			851	848	δ_{ipr} CH ₃ (68)
113			849	845	δ_{ipr} CH ₃ (68)
114			847	840	vCN (65), vCC(18)
115		835	840	837	δ CC(61), δ_{ipr} CH ₃ (12)
116			836	833	δ CC(60), δ_{ipr} CH ₃ (12)
117	827		835	830	γ CH (61)
118			827	824	γ CH (60)
119			822	819	γ CH (60)
120		810	816	812	γ CH (60)
121			810	807	γ CH (59)
122			804	800	γ CH (58)
123		790	798	791	γ CH (60)
124			786	785	vCS (75), δ CH(20)
125			780	777	δ_{ring} (60)
126			767	763	δ_{ring} (60)
127	753		755	751	γ CO (53), γ_{ring} , CC(17)
128			748	745	γ CO (51), γ_{ring} (18)
129			736	732	γ_{ring} (51), γ CC (13)
130	720		725	720	γ_{ring} (50)
131		715	719	716	γ CC (48), γ_{ring} (23)

132		690	685	γ_{CCl} (67), δ_{ring} (27)
133		668	666	δ_{CC} (61), $\delta_{\text{ipr CH}_3}$ (12)
134	640	644	640	δ_{CC} (61),
135		630	625	δ_{ring} (67)
136		621	616	δ_{ring} (66)
137	608	610	607	δ_{ring} (66)
138	600	605	602	δ_{ring} (65)
139		593	590	γ_{CN} (57), γ_{ring} (27)
140		584	581	γ_{ring} (58)
141	556	560	555	γ_{ring} (58)
142		551	544	γ_{ring} (57)
143	535	540	536	γ_{CC} (60), γ_{ring} (22)
144		525	523	δ_{ring} (65)
145	510	515	512	δ_{ring} (65)
146	501	503	500	δ_{ring} (66)
147		490	487	δ_{ring} (66)
148		470	468	δ_{ring} (65)
149		453	449	δ_{CCl} (62), δ_{ring} (18)
150		439	438	δ_{CC} (62)
151		424	421	δ_{CC} (60)
152	409	410	410	δ_{CC} (60)
153		405	400	γ_{ring} (55)
154		399	394	γ_{ring} (55)
155		396	390	δ_{CC} (60)
156		385	382	γ_{ring} (56)
157	375	376	374	δ_{ring} (58)
158		370	368	δ_{ring} (60)
159	360	364	361	γ_{ring} (55)
160		335	333	δ_{ring} (61)
161		320	318	δ_{ring} (61)
162		306	304	γ_{ring} (52)
163		286	283	δ_{CC} (63)
164		280	275	δ_{CC} (63)
165	260	266	262	γ_{CCl} (59)
166		254	250	γ_{CC} (55)

167		242	241	γ CC (54)
168		235	230	τ CH ₃ (58)
169		222	219	τ CH ₃ (58)
170		208	204	τ CH ₃ (58)
171		200	198	τ CH ₃ (58)
172		196	191	γ CC (55)
173		189	185	γ CC (55)
174		182	179	γ_{ring} (54)
175		173	171	γ_{ring} (53)
176		160	155	γ CC (54)
177	150	156	150	γ CC (54)
178		145	142	γ_{ring} (55)
179		140	136	γ CC (55)
180	128	135	130	γ CC (54)
181		110	103	γ CC (54)
182		93	88	γ CC (54)
183		83	80	δ_{ring} (58)
184		71	68	δ_{ring} (60)
185		60	57	δ_{ring} (58)
186		52	49	δ_{ring} (58)
187	42	45	40	δ_{ring} (56)
188		41	38	δ_{ring} (56)
189		36	32	δ_{ring} (58)
190	28	32	28	γ_{ring} (54)
191		30	25	γ_{ring} (53)
192		25	21	γ_{ring} (53)
193		20	16	γ_{ring} (54)
194		140	11	γ_{ring} (55)
195		8	5	γ_{ring} (55)

ν -stretching, ν_{sym} -sym stretching, ν_{asym} -asym stretching, δ -in-plane bending, γ -out-of-plane bending, ρ -scissoring, ω -wagging, σ -rocking, τ -twisting.

Table 4.3 Mulliken atomic charges for 5-(4-Propan-2-yl)benzylidene)-2-[3-(4-chlorophenyl)-5[4-(propan-2-yl)phenyl-4,5-dihydro-1H-pyrazol-1-yl]-1,3-thiazol-4(5H)-one using B3LYP/6-31G and B3LYP/6-31G (d,p) method

Atom Numbering	Charge		Atom Numbering	Charge	
	B3LYP/6- 31G	B3LYP/6- 31G(d,p)		B3LYP/6- 31G	B3LYP/6- 31G(d,p)
C1	0.215	0.184	H35	0.116	0.147
C2	0.119	0.032	H36	0.108	0.139
H3	0.114	0.163	H37	0.108	0.140
C4	0.112	0.113	H38	0.155	0.194
C5	-0.127	-0.155	C39	-0.068	-0.287
C6	-0.097	-0.126	C40	0.489	0.361
C7	-0.086	-0.112	S41	0.242	0.488
H8	0.103	0.149	C42	0.293	-0.013
C9	-0.090	-0.121	N43	-0.465	-0.278
H10	0.126	0.173	O44	-0.495	-0.404
C11	-0.085	-0.260	C45	-0.131	-0.043
H12	0.113	0.157	C46	0.102	0.036
H13	0.115	0.159	C47	-0.092	-0.115
C14	0.126	0.160	C48	-0.111	-0.138
C15	-0.145	-0.174	C49	-0.109	-0.147
C16	-0.114	-0.140	H50	0.094	0.139
C17	-0.143	-0.175	C51	-0.113	-0.151
H18	0.084	0.131	H52	0.093	0.137
C19	-0.155	-0.190	C53	0.130	0.116
H20	0.080	0.135	H54	0.089	0.135
C21	0.140	0.126	H55	0.166	0.224
H22	0.083	0.130	H56	0.152	0.174
H23	0.085	0.133	H57	0.088	0.131
N24	-0.324	-0.198	C58	-0.128	-0.178
N25	-0.458	-0.531	H59	0.111	0.144
C26	-0.275	-0.424	C60	-0.321	-0.406
C127	-0.014	0.117	H61	0.106	0.136
H28	0.134	0.182	H62	0.100	0.131
C29	-0.142	-0.208	H63	0.123	0.153
C30	-0.332	-0.417	C64	-0.317	-0.402
C31	-0.332	-0.418	H65	0.104	0.134
H32	0.109	0.139	H66	0.122	0.152
H33	0.113	0.143	H67	0.101	0.132
H34	0.108	0.141			

Table 4.4 HOMO-LUMO energies for 5-(4-Propan-2-yl)benzylidene)-2-[3-(4-chlorophenyl)-5[4-(propan-2-yl)phenyl]-4,5-dihydro-1H-pyrazol-1-yl]-1,3-thiazol-4(5H)-one by B3LYP/6-31(d,p) basis set.

Molecular properties	Energy (eV)	Energy gap (eV)	Ionisation potential (I)	Electron affinity (A)	Global hardness (η)	Electron negativity (χ)	Global softness (σ)	Chemical potential (μ)	Global Electrophilicity (ω)
E_{HOMO}	5.7579	3.5250	5.7579	2.2329	1.7625	3.995	0.5674	-3.9954	4.5286
E_{LUMO}	2.2329								
$E_{\text{HOMO-1}}$	6.1868	4.5231	6.1868	1.6637	2.2616	3.9252	0.4422	-3.9253	3.4064
$E_{\text{LUMO-1}}$	1.6637								
$E_{\text{HOMO-2}}$	6.5852	5.8124	6.5852	0.7725	2.9064	3.6789	0.3441	-3.6788	2.3282
$E_{\text{LUMO-2}}$	0.7725								

Table 4.5 Second order perturbation theory analysis of Fock matrix in NBO basis corresponding to intra molecular bands of 5-(4-Propan-2-yl)benzylidene)-2-[3-(4-chlorophenyl)-5[4-(propan-2-yl)phenyl-4,5-dihydro-1H-pyrazol-1-yl]-1,3-thiazol-4(5H)-one

Donor	Acceptor	E(2)(kcal/mol)	E(J)-E(i) (a.u)	F _(ij) (a.u)
		BMP	BMP	BMP
LP (1) N 24	BD*(1) C2 - N25	4.81	0.82	0.056
LP (1) N 25	BD*(2) C1 - N24	26.81	0.24	0.072
LP (1) N 25	BD*(1) C2 - C14	1.04	0.65	0.024
LP (1) N 25	BD*(1) C2 - H55	4.15	0.65	0.049
LP (1) N 25	BD*(1) S41 - C42	6.94	0.75	0.068
LP (1) N 25	BD*(1) C42 - N43	13.01	0.68	0.088
LP (1)Cl 27	BD*(1) C7 - C11	1.21	1.48	0.038
LP (1)Cl 27	BD*(1) C9 - C11	1.21	1.48	0.038
LP (2)Cl 27	BD*(1) C7 - C11	3.88	0.87	0.052
LP (2)Cl 27	BD*(1) C9 - C11	3.85	0.87	0.052
LP (3)Cl 27	BD*(2) C7 - C11	12.37	0.32	0.061
LP (1) S 41	BD*(1) N25 - C42	0.61	0.92	0.021
LP (1) S 41	BD*(1) C39 - C40	7.94	0.99	0.08
LP (1) S 41	BD*(1) C40 - O44	0.78	1.04	0.026
LP (1) S 41	BD*(1) C42 - N43	8.55	0.94	0.08
LP (2) S 41	BD*(2) C39 - C45	64.42	0.2	0.111
LP (2) S 41	BD*(1) S41 - C42	0.56	0.76	0.022
LP (2) S 41	BD*(2) C42 - N43	100.22	0.21	0.133
LP (1) N 43	BD*(1) N25 - C42	1.76	0.75	0.033
LP (1) N 43	BD*(1) C39 - C40	5.99	0.81	0.062
LP (1) N 43	BD*(1) C39 - C45	0.71	0.69	0.02
LP (1) N 43	BD*(1) C40 - O44	1.54	0.87	0.033
LP (1) N 43	BD*(1) S41 - C42	5.63	0.84	0.062
LP (1) O 44	BD*(1) C39 - C40	3.04	1.13	0.053
LP (1) O 44	BD*(1) C40 - N43	2.31	1.1	0.046
LP (2) O 44	BD*(1) C39 - C40	18.59	0.69	0.102
LP (2) O 44	BD*(1) C40 - N43	22.99	0.65	0.111

aE(2) means energy of hyperconjugative interactions (stabilization energy).

b Energy difference between donor and acceptor i and j NBO orbitals.

c F(i,j) is the Fock matrix element between i and j NBO orbitals.

Table 4.6 NBO analysis of bonding and antibonding orbit of 5-(4-Propan-2-yl)benzylidene)-2-[3-(4-chlorophenyl)-5[4-(propan-2-yl)phenyl-4,5-dihydro-1H-pyrazol-1-yl]-1,3-thiazol-4(5H)-one

Band (A-B)	ED/Energy (a.u.)	ED %	ED %	NBO	S (%)	P (%)
BD (1) C 1 - C 4	1.9716	50.07	49.93	0.7076 SP ^(1.72)	36.83	63.17
	-0.63785			0.7066 SP ^(2.42)	29.21	70.79
BD (1) C 1 - N 24	1.98458	41.16	58.84	0.6416 SP ^(2.53)	28.3	71.7
	-0.8076			0.7671 SP ^(2.53)	35.15	64.85
BD (1) C 1 - C 26	1.97344	47.4	52.6	0.6884 SP ^(1.87)	34.83	65.17
	-0.71293			0.7253 SP ^(2.48)	28.73	71.27
BD (1) C 2 - C 14	1.96717	52.32	47.68	0.7233 SP ^(2.08)	32.46	67.54
	-0.62256			0.6905 SP ^(2.5)	28.53	71.47
BD (1) C 2 - N 25	1.97706	39.6	60.4	0.6293 SP ^(2.92)	25.51	74.49
	-0.79968			0.7772 SP ^(1.85)	35.07	64.93
BD (1) C 2 - C 26	1.96518	50.3	49.7	0.7092 SP ^(2.03)	33.04	66.96
	-0.71183			0.7050 SP ^(2.48)	28.73	71.27
BD (1) C 2 - H 55	1.89411	63.49	36.51	0.7968 SP ^(9.94)	9.14	90.86
	-0.45971			0.6042 S ⁽¹⁾	100	
BD (1) C 4 - C 5	1.97386	51.06	48.94	0.7146 SP ^(1.8)	35.68	64.32
	-0.71778			0.6996 SP ^(1.87)	34.85	65.15
BD (1) C 4 - C 6	1.97513	51.33	48.67	0.7146 SP ^(1.85)	35.11	64.89
	-0.71245			0.6977 SP ^(1.86)	34.98	65.02
BD (1) C 5 - C 7	1.96991	50.02	49.98	0.7072 SP ^(1.81)	35.55	64.45
	-0.71264			0.7070 SP ^(1.8)	35.76	64.24
BD (1) C 6 - C 9	1.97082	49.7	50.3	0.7050 SP ^(1.86)	34.99	65.01
	-0.70774			0.7092 SP ^(1.79)	35.82	64.18
BD (1) C 7 - C 11	1.98087	49.11	50.89	0.7008 SP ^(1.88)	34.78	65.22
	-0.73664			0.71334 SP ^(1.59)	38.64	61.36
BD (1) C 9 - C11	1.98117	48.98	51.02	0.6999 SP ^(1.89)	34.66	65.34
	-0.73613			0.7142 SP ^(1.58)	38.74	6.26
BD (1) C 11 -Cl 27	1.98945	45.41	54.59	0.6739 SP ^(3.42)	22.62	77.38
	-0.72439			0.7389 SP ^(5.04)	16.55	83.45
BD (1) C 14 - C 15	1.97179	51.33	48.67	0.7165 SP ^(1.78)	36.02	63.98
	-0.70373			0.6976 SP ^(1.88)	34.77	65.23
BD (1) C 14 - C 16	1.97342	51.24	48.76	0.7158 SP ^(1.83)	35.37	64.63
	-0.70241			0.6983 SP ^(1.88)	34.71	65.29
BD (1) C 15 - C 17	1.97468	50.24	49.76	0.7088 SP ^(1.78)	35.97	64.03
	-0.69235			0.7054 SP ^(1.83)	35.36	64.64
BD (1) C 21 - C 29	1.97443	49.85	50.15	0.7060 SP ^(2.34)	29.96	70.04
	-0.60045			0.7082 SP ^(2.34)	29.98	70.02
BD (1) N 24 - N 25	1.97516	44.85	55.15	0.6697 S ^(3.87)	20.53	79.47
	-0.78565			0.7456 SP ^(2.67)	27.25	72.75
BD (1) N 25 - C 42	1.98191	59.48	40.52	0.7713 SP ^(1.67)	37.41	62.59
	-0.84614			0.6365 S ^(2.05)	32.8	67.2

BD (1) C 31 - H 35	1.98711	61.78	38.22	0.7860 SP ^(2.93)	25.45	74.55
	-0.5137			0.6182 S ⁽¹⁾	100	
BD (1) C 39 - C 40	1.97996	54.86	45.14	0.7407 SP ^(2.03)	33.04	66.96
	-0.73079			0.6719 SP ^(1.84)	35.18	64.82
BD (1) C 39 - S 41	1.9775	53.45	46.55	0.7311 SP ^(1.98)	33.55	66.45
	-1.04732			0.6823 SP ^(2.03)	33.03	66.97
BD (1) C 39 - C 45	1.97473	54.08	45.92	0.7354 SP ^(2.00)	33.34	66.66
	-0.66995			0.6777 SP ^(2.10)	32.25	67.75
BD (1) C 40 - N 43	1.98023	41.39	58.61	0.6433 SP ^(2.21)	31.13	68.87
	-0.78333			0.7656 SP ^(2.28)	30.46	69.54
BD (1) C 40 - O 44	1.99418	36.24	63.76	0.6020 SP ^(2.02)	33.14	66.86
	-1.01591			0.7985 SP ^(1.74)	36.46	63.51
BD (1) S 41 - C 42	1.9822	47.49	52.5	0.6891 SP ^(2.07)	32.57	67.43
	-1.06292			0.7247 SP ^(1.77)	36.15	63.85
BD (1) C 42 - N 43	1.9797	44.91	55.09	0.6702 SP ^(2.07)	30.79	69.21
	-0.80862			0.7422 SP ^(2.26)	30.71	69.29
BD (1) C 45 - C 46	1.98017	49.8	50.2	0.7057 SP ^(1.88)	34.72	65.28
	-0.64355			0.7085 SP ^(2.53)	28.3	71.7
BD (1) C 46 - C 47	1.96938	51.35	48.65	0.7166 SP ^(1.81)	35.57	64.43
	-0.70742			0.6975 SP ^(1.87)	34.86	65.14
BD (1) C 46 - C 48	1.9671	51.25	48.75	0.7169 SP ^(1.77)	36.12	63.88
	-0.71003			0.6982 SP ^(1.87)	34.86	65.14
BD (1) C 47 - C 49	1.97519	50.04	49.96	0.7074 SP ^(1.81)	35.65	64.35
	-0.69378			0.7069 SP ^(1.87)	34.79	65.21
BD (1) C 48 - C 51	1.97445	50.17	49.83	0.7083 SP ^(1.79)	35.79	64.21
	-0.69711			0.7059 SP ^(1.85)	35.08	64.92
BD (1) C 48 - H 52	1.98197	62.63	37.37	0.7914 SP ^(2.41)	29.34	70.66
	-0.52131			0.6113 S ⁽¹⁾	100	
BD (1) C 49 - C 53	1.97437	49.41	50.59	0.7029 SP ^(1.88)	34.75	65.25
	-0.69549			0.7113 SP ^(1.89)	34.6	65.4
BD (1) C 51 - C 53	1.97499	49.43	50.57	0.7031 SP ^(1.84)	35.2	64.8
	-0.69798			0.7111 SP ^(1.89)	34.6	65.4
BD (1) C 53 - C 58	1.97214	50.82	49.18	0.7129 SP ^(2.25)	30.81	69.19
	-0.59158			0.7013 SP ^(2.96)	25.23	74.77
BD (1) C 58 - C 60	1.98234	50.65	49.35	0.7117 SP ^(2.94)	25.38	74.62
	-0.57515			0.7025 SP ^(2.79)	26.35	73.65
BD (1) C 58 - C 64	1.98097	50.69	49.31	0.7120 SP ^(2.94)	25.39	74.61
	-0.57507			0.7022 SP ^(2.8)	26.34	73.66
BD (1) C 60 - H 61	1.98862	61.54	38.46	0.7845 SP ^(3.11)	24.34	75.66
	-0.50495			0.6201 S ⁽¹⁾	100	
BD (1) C 39-S 41	1.9775	53.45	46.55	0.7311 SP ^(1.98)	33.55	66.45
	-1.04732			0.6201 S ^(2.03)	33.03	66.97

Table 4.7 Fukui function (f_i^+ , f_i^- , Δf) for 5-(4-Propan-2-yl)benzylidene)-2-[3-(4-chlorophenyl)-5[4-(propan-2-yl)phenyl-4,5-dihydro-1H-pyrazol-1-yl]-1,3-thiazol-4(5H)-one

Atoms	Natural atomic charges			Fukui functions(eV)			Electro -philicity	Nucleo -philicity
	qN	qN-1	qN+1	F+	F-	F0		
C 1	0.184	0.160	0.237	-0.077	0.024	-0.039	-0.102	0.102
C 2	0.032	0.037	0.010	0.026	-0.005	0.013	0.031	-0.031
H 3	0.163	0.138	0.245	-0.107	0.025	-0.053	-0.131	-0.131
C 4	0.113	0.115	0.113	0.001	-0.001	0.001	0.003	-0.003
C 5	-0.155	-0.163	-0.142	-0.021	0.007	-0.010	-0.028	0.028
C 6	-0.126	-0.132	-0.111	-0.022	0.006	-0.011	-0.028	0.028
C 7	-0.112	-0.114	-0.104	-0.011	0.003	-0.005	-0.013	0.013
H 8	0.149	0.140	0.160	-0.019	0.008	-0.010	-0.028	0.028
C 9	-0.121	-0.125	-0.114	-0.011	0.004	-0.006	-0.015	0.015
H 10	0.173	0.171	0.196	-0.025	0.002	-0.012	-0.027	0.027
C 11	-0.260	-0.263	-0.256	-0.008	0.003	-0.004	-0.011	0.011
H 12	0.157	0.137	0.191	-0.054	0.020	-0.027	-0.074	-0.074
H 13	0.159	0.142	0.194	-0.053	0.018	-0.026	-0.070	0.070
C 14	0.160	0.143	0.157	-0.014	0.016	-0.007	-0.031	0.031
C 15	-0.174	-0.176	-0.160	-0.016	0.003	-0.008	-0.019	0.019
C 16	-0.140	-0.137	-0.126	-0.012	-0.003	-0.006	-0.008	0.008
C 17	-0.175	-0.182	-0.160	-0.022	0.007	-0.011	-0.029	0.029
H 18	0.131	0.116	0.150	-0.034	0.015	-0.017	-0.049	0.049
C 19	-0.190	-0.200	-0.176	-0.025	0.010	-0.012	-0.035	0.035
H 20	0.135	0.196	0.160	0.036	-0.060	0.018	0.096	-0.096
C 21	0.126	0.127	0.128	-0.001	-0.001	0.000	0.000	0.000
H 22	0.130	0.107	0.168	-0.061	0.024	-0.031	-0.085	0.085
H 23	0.133	0.132	0.168	-0.035	0.001	-0.018	-0.036	0.036
N 24	-0.198	-0.193	-0.163	-0.031	-0.005	-0.015	-0.025	0.025
N 25	-0.531	-0.511	-0.474	-0.036	-0.020	-0.018	-0.016	0.016
C 26	-0.424	-0.410	-0.477	0.066	-0.014	0.033	0.080	-0.080
Cl 27	0.117	0.076	0.197	-0.121	0.041	-0.060	-0.162	0.162
H 28	0.182	0.158	0.240	-0.082	0.023	-0.041	-0.105	0.105
C 29	-0.208	-0.203	-0.222	0.019	-0.005	0.009	0.024	-0.024
C 30	-0.417	-0.417	-0.419	0.001	0.000	0.001	0.001	-0.001
C 31	-0.418	-0.417	-0.419	0.002	-0.001	0.001	0.003	-0.003
H 32	0.139	0.126	0.163	-0.037	0.013	-0.019	-0.051	0.051

H 33	0.143	0.141	0.147	-0.005	0.002	-0.003	-0.007	0.007
H 34	0.141	0.131	0.162	-0.031	0.011	-0.016	-0.042	0.042
H 35	0.147	0.155	0.149	0.006	-0.008	0.003	0.014	-0.014
H 36	0.139	0.124	0.163	-0.040	0.016	-0.020	-0.055	0.055
H 37	0.140	0.134	0.160	-0.027	0.006	-0.013	-0.033	0.033
H 38	0.194	0.188	0.217	-0.029	0.007	-0.015	-0.036	0.036
C 39	-0.287	-0.325	-0.309	-0.016	0.037	-0.008	-0.053	0.053
C 40	0.361	0.328	0.376	-0.048	0.033	-0.024	-0.082	0.082
S 41	0.488	0.386	0.521	-0.135	0.102	-0.067	-0.236	0.236
C 42	-0.013	-0.064	-0.015	-0.049	0.051	-0.025	-0.100	0.100
N 43	-0.278	-0.355	-0.265	-0.089	0.077	-0.045	-0.166	0.166
O 44	-0.404	-0.546	-0.372	-0.174	0.142	-0.087	-0.316	0.316
C 45	-0.043	-0.147	-0.009	-0.138	0.104	-0.069	-0.242	0.242
C 46	0.036	0.079	0.026	0.052	-0.042	0.026	0.095	-0.095
C 47	-0.115	-0.114	-0.115	0.001	-0.002	0.001	0.003	-0.003
C 48	-0.138	-0.142	-0.135	-0.007	0.005	-0.004	-0.012	0.012
C 49	-0.147	-0.159	-0.140	-0.018	0.012	-0.009	-0.030	0.030
H 50	0.139	0.114	0.146	-0.032	0.024	-0.016	-0.056	0.056
C 51	-0.151	-0.162	-0.145	-0.017	0.011	-0.009	-0.029	0.029
H 52	0.137	0.114	0.141	-0.027	0.023	-0.013	-0.049	0.049
C 53	0.116	0.118	0.116	0.002	-0.001	0.001	0.003	-0.003
H 54	0.135	0.097	0.152	-0.055	0.038	-0.027	-0.092	0.092
H 55	0.224	0.221	0.294	-0.072	0.003	-0.036	-0.075	0.075
H 56	0.174	0.091	0.197	-0.106	0.084	-0.053	-0.190	0.190
H 57	0.131	0.095	0.148	-0.053	0.036	-0.027	-0.089	0.089
C 58	-0.178	-0.171	-0.182	0.010	-0.007	0.005	0.017	-0.017
H 59	0.144	0.119	0.157	-0.038	0.025	-0.019	-0.063	0.063
C 60	-0.406	-0.402	-0.408	0.006	-0.004	0.003	0.010	-0.010
H 61	0.136	0.128	0.140	-0.012	0.008	-0.006	-0.020	0.020
H 62	0.131	0.106	0.145	-0.040	0.026	-0.020	-0.065	0.065
H 63	0.153	0.155	0.151	0.004	-0.002	0.002	0.006	-0.006
C 64	-0.402	-0.398	-0.404	0.006	-0.004	0.003	0.011	-0.011
H 65	0.134	0.127	0.138	-0.011	0.007	-0.005	-0.018	0.018
H 66	0.152	0.154	0.150	0.004	-0.002	0.002	0.006	-0.006
H 67	0.132	0.106	0.146	-0.040	0.026	-0.020	-0.067	0.067

Table 4.8 Topological parameters for intramolecular interactions in compound electron density (ρ_{BCP}), Laplacian of electron density (∇^2_{BCP}), electron kinetic energy density (G_{BCP}), electron potential energy density (V_{BCP}), total electron energy density (H_{BCP}), Hydrogen bond energy (E_{HB}) at bond critical point(BCP)

Interactions	ρ_{BCP}	∇^2_{BCP}	G_{BCP}	V_{BCP}	H_{BCP}	E_{HB}
O40.....H50	0.02952	0.1168	0.0318	-0.0345	-0.0026	-0.0159

Table 4.9 Binding affinity for docking in 5-(4-Propan-2-yl)benzylidene)-2-[3-(4-chlorophenyl)-5[4-(propan-2-yl)phenyl-4,5-dihydro-1H-pyrazol-1-yl]-1,3-thiazol-4(5H)-one

Drug	Protein	Type of activity	Binding affinity (kcal/mol)	Etimated inhibition constant Ki(μM)	Bonded residues	Nature of bond	Bond distance (\AA)	RMSD
5-(4-Propan-2-yl)benzylidene)-2-[3-(4-chlorophenyl)-5[4-(propan-2-yl)phenyl-4,5-dihydro-1H-pyrazol-1-yl]-1,3-thiazol-4(5H)-one	4QXM	Antitubercular	-9.03	239.32 (Nm)	MET A:98	van der waals	3.12	45.171
			-7.24	4.95 (M)	ILE A:47	van der waals	4.06	32.143
			-7.23	5.06(M)	TYR A:158	van der waals	4.46	51.17
			-7.03	7.05 (M)	ILE A:36	Alkyl	3.01	30.178
			-6.73	11.75(M)	THR A:196	Conventional hydrogen bond	2.8	39.7
	5T6N	Antiviral	-7.63	2.57	GLN A:210	Conventional hydrogen bond	3.49	46.93
			-6.23	27.26	TRP A:234	π - π stacked	3.15	48.102
			-5.71	65.29	GLN A:210	Conventional hydrogen bond	1.92	61.645
			-5.67	69.34	TRP A:234	π - π stacked	3.13	49.815
			-5.37	115.39	TRP A:234	π - π stacked	3.15	82.058
	4YJ3	Anticancer	-6.47	18.02	GLN A:358	van der waals	2.21	262.039
			-6.18	29.66	PRO A:364	van der waals	2.62	229.467

			-6.14	31.72	THR A:365	van der waals	2.81	269.206
			-6.12	32.56	GLY A:365	Pi-donor hydrogen bond	2.94	267.117
			-6.02	38.85	VAL A:26	Pi-alkyl	3.01	258.416
3S9Y	Anticancer		-7.63	2.57	GLN A:210	Conventional hydrogen bond	3.49	46.93
			-6.23	27.26	TRP A:234	π - π stacked	3.15	48.102
			-5.71	65.29	GLN A:210	Conventional hydrogen bond	1.92	61.645
			-5.67	69.34	TRP A:234	π - π stacked	3.13	49.815
			-5.37	115.39	TRP A:234	π - π stacked	3.15	82.058
4I5O	Anticancer		-7.52	3.07	ALA A:247	Conventional hydrogen bond	1.91	123.143
			-7.09	6.37	LEU A:248	Conventional hydrogen bond	1.92	123.075
			-7.06	6.64	TYR A:357	π - π stacked	3.01	114.455
			-7.03	7.01	TYR A:357	π - π stacked	3.21	113.872
			-6.38	21.08	GLY A:246	van der waals	3.83	122.866

Chapter – 5

Molecular Docking, vibrational, structural and electronic studies of 5-(4-Butoxybenzylidene)-2-[3-(4-chlorophenyl)-5[4-(propan-2-yl)-4,5-dihydro-1H-pyrazol-1-yl]-1,3-thiazol-4(5H)-one

Molecular Docking, vibrational, structural and electronic studies of 5-(4-Butoxybenzylidene)-2-[3-(4-chlorophenyl)-5[4-(propan-2-yl)-4,5-dihydro-1H-pyrazol-1-yl]-1,3-thiazol-4(5H)-one**5.1 Introduction**

Thiazole is a heterocyclic compound that contains both sulphur and nitrogen and a large family of derivatives. Thiazole itself is a pale yellow liquid with a pyridine-like odor and they have extensive applications in agriculture and medicinal chemistry [128, 129]. Varieties of biologically active molecules accommodate the thiazole and its derivatives, aminothiazoles [130]. They are used as important fragments in different drugs related to anti-tuberculosis, anti-inflammatory, [131,69, 132] , anti-allergic [133], anti-hypertensive [134], schizophrenia [135], anti-bacterial, HIV infections [131,136] and human lymphatic filarial parasites [137]. Various thiazole derivatives are used as fungicides and herbicides and have numerous applications in agricultural field [138]. Hydantoin derivatives, in particular phenytoin, are important antiepileptic drugs.

We have found from literature survey that no results have been reported on quantum chemical calculations, FT-IR, FT-Raman spectral analysis, NBO analysis, AIM analysis, Reduced Density Gradient (RDG) and Molecular Docking studies on 5-(4-Butoxybenzylidene)-2-[3-(4-chlorophenyl)-5[4-(propan-2-yl)-4, 5-dihydro-1H-pyrazol-1-yl]-1,3-thiazol-4(5H)-one (BPT2). Hence in this study, an attempt has been made to

interpret the vibrational spectra of the BPT2 molecule by applying density functional theory calculations based on Becke-3-Lee-Yang-Parr (B3LYP) with 6-31G and 6-31G (d,p) basis sets. The Mulliken atomic charge analysis has been reported using the above basis sets. Further more, the HOMO-LUMO, MEP analysis and NBO analysis of BPT2 molecule have been studied by B3LYP level with 6-31G (d,p) implemented in the Gaussian 09 program suite [36]. The AIM analysis has been carried out to find out the presence of strong and weak H-bond in the BPT2 molecule. The Reduced Density Gradient (RDG) analysis has been carried out to investigate the presence of Steric effect, Van der Waals interaction and Hydrogen bond of the BPT2 molecule. Herewith the molecular docking studies have been carried out for the BPT2 molecule to assess its biological potential.

5.2 Experimental details

5-(4-Butoxybenzylidene)-2-[3-(4-chlorophenyl)-5[4-(propan-2-yl)-4, 5-dihydro-1H-pyrazol-1-yl]-1,3-thiazol-4(5H)-one (BPT2) was synthesized as per the reported procedure [72-74]. The Fourier Transform infrared (FT-IR) spectrum of the BPT2 molecule was recorded using Perkin Elmer Spectrometer fitted with a KBr beam splitter around 4000-450 cm^{-1} . The Bruker RFS 27 FT-Raman spectrometer in the region 4000-0 cm^{-1} using a 1064 nm Nd:YAG laser source was used to reported the FT-Raman spectrum. Both the spectral measurements were performed at the Sophisticated Analytical Instrumentation Facility (SAIF), IIT, Madras, India.

5.3 Computational details

All calculations of the BPT2 molecule were carried out using Gaussian 09 program [36] was performed with Becke's three-parameter hybrid model and therefore the Lee-Yang-Parr correlation was a useful functional (B3LYP) in DFT [139, 140] technique. The electronic structure of the molecule has to be proven with the density functional theory. The visual representations for fundamental modes are also checked by the Gauss view program [75]. Electron density map and reduced density gradient (RDG) were calculated with the use of Multiwfn program [76] and plotted by visual molecule dynamics program (VMD) [77]. The reactivity descriptors, such as electrophilic index (ω), global hardness (η), the chemical potential (μ), ionization potential (I) and electron affinity (A) were determined from the energies of frontier molecular orbitals. The NBO and Mulliken population analysis are also reported for the local minima of the molecules. The molecular docking calculation was performed by the AutoDock 4.2 software [141], which was also applied to detect the docking input files and analyze the docking result. Using Discovery studio visualize software, one of the best active site was visualized for ligand-protein interactions.

5.4 Results and discussions

5.4.1 Optimized molecular geometrical parameters

The geometrical structure and parameters of 5-(4-Butoxybenzylidene)-2-[3-(4-chlorophenyl)-5[4-(propan-2-yl)-4,5-dihydro-1H-pyrazol-1-yl]-1,3-thiazol-4(5H)-one (BPT2) are depicted in Fig. 5.1 and Table 5.1 by using B3LYP/6-31G and B3LYP/6-31G

(d,p) methods. The C-C bond length are in the range of 1.3952-1.3984 Å (DFT), 1.3815-1.4041 Å(XRD) [84], while for the BPT2 molecule, the C-C bond length for pyrazole ring of C1-C26, C2-C26 are 1.5223/1.5184, 1.5576/1.5519 Å, for thiazole ring for C39-C40 is 1.493/1.5081 Å for the B3LYP/6-31G and B3LYP/6-31G (d,p) methods and these values are in between the single and double bond (1.54 Å and 1.33 Å) [84].

In the present work, the C-O bond length are observed at C40-O44=1.2485/1.2232 Å, C53-O58 = 1.3842 / 1.3595Å, O58-C59=1.4618/1.4285Å which are in good agreement with the reported values for a similar derivatives (1.3871 Å and 1.3653 Å) [142]. The C-N bond length for the BPT2 molecule are C1-N24, C2-N25, N25-C42, C40-N43, C42-N43 are 1.3062/1.294 Å, 1.5078/1.4931 Å, 1.3483/1.3513 Å, 1.4066/1.3966 Å, 1.3043/1.2987 Å which are in agreement with the literature [143]. The C-S bond length for the BPT2 molecule are 1.8656/1.794 Å for C39-S41 and for S41-C42 is 1.8656/1.794 Å, 1.8391 /1.776 Å and is similar to Kuruvilla *et al* [144] observed the C-S value at C5-S9= 1.748 Å and C8-S9=1.733 Å theoretically and experimentally at 1.8642, 1.862 Å. In the case of C-H bond lengths, (DFT/XRD) it is observed that aromatic C-H bonds measure 1.10/1.09 Å, which is equal to the experimental value. For the BPT2 molecule, the bond lengths for C2-H55, C6-H10, C9-H13, C31-H35, C47-H50, C65-H66, C68-H70, C68-H71 are 1.0919/1.0919, 1.0835/1.0843, 1.083/1.0842, 1.0956/1.0944, 1.0867/1.0872, 1.1/1.0984, 1.0958/1.0945 and 1.0969/1.0956 Å observed. It was also very confined to experimental value [145]. The N-N bond lengths (DFT/XRD) are reported in the range 1.3409-1.3886 Å [146] and in the present case, the N-N bond length is found at 1.3915/1.37 Å for N24-N25. The thiazole ring is tilted from the phenyl ring as is evident from the torsion angles

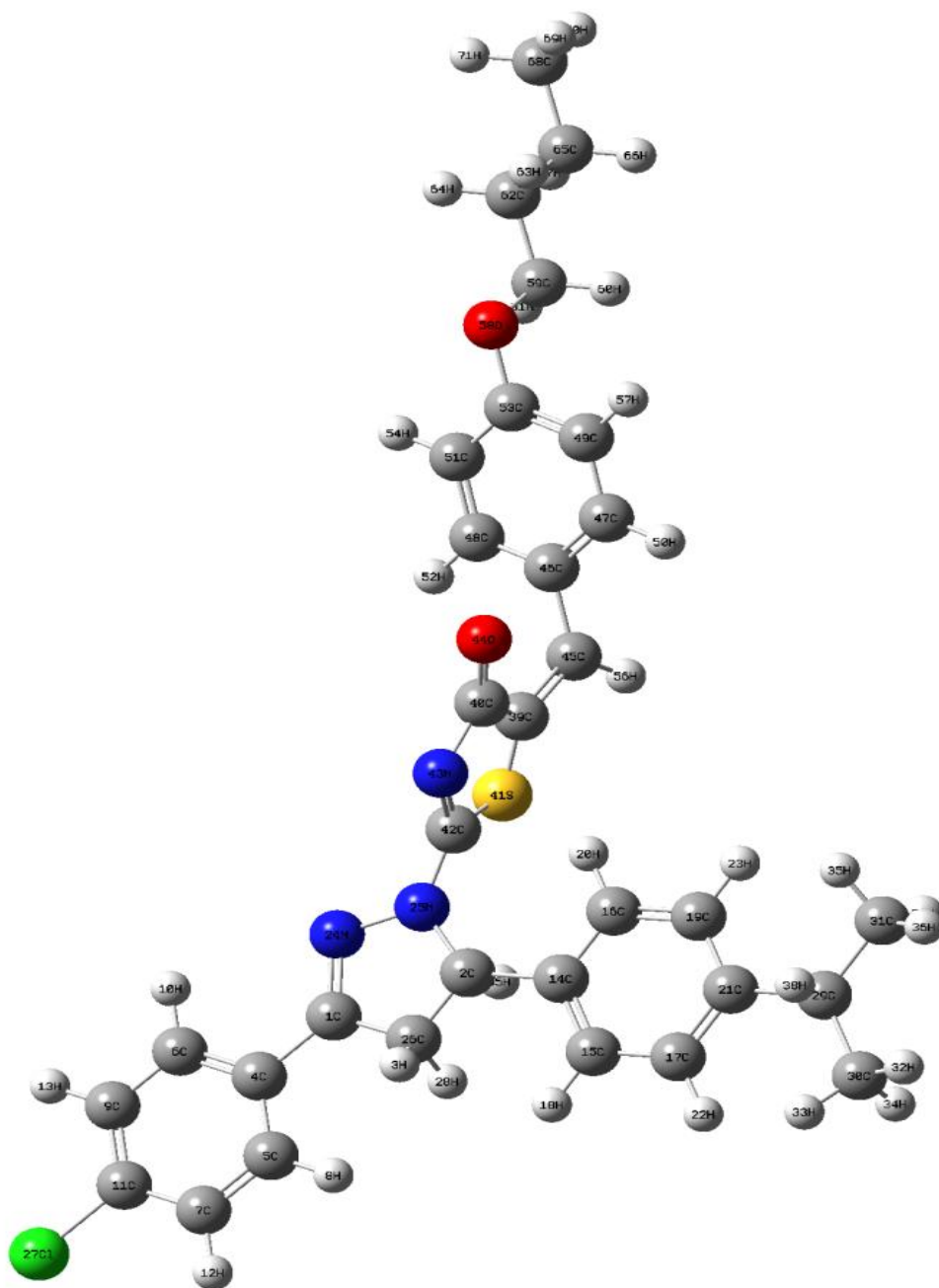


Fig.5.1 Optimized molecular structure of 5-(4-Butoxybenzylidene)-2-[3-(4-chlorophenyl)-5[4-(propan-2-yl)-4,5-dihydro-1H-pyrazol-1-yl]-1,3-thiazol-4(5H)-one

C45-C39-C40-N43=179.99/179.97°, S41-C39-C40-H43 = -0.1457/-0.2921°, C40-C39-S41-C42= 0.3713/ 0.414° and C45-C39-S41-C42= -179.74/-179.81°.

For the BPT2 molecule, the interactions between the thiazole and pyrazole groups are C40-C39-C45 = 132.917/132.571, S41-C39-C45 = 118.135/118.669, C39-C40-N43 = 113.471 /112.705, C39-C40-O44 = 124.813 / 124.954, N43-C40-O44 = 121.716/ 122.339, C39-S41-C42 = 86.313/87.757, N25-C42-S41= 119.688/119.294, N25-C42-N43 = 122.861 / 122.033, S41-C42-N43 = 117.447/118.672, C40-N43-C42 = 113.818 / 112.104 respectively.

5.4.2 Vibrational assignments

The BPT2 molecule is consist of 71 atoms and has 207 fundamental modes of vibrations. The observed and simulated FT-IR and FT-Raman spectra of 5-(4-Butoxybenzylidene)-2-[3-(4-chlorophenyl)-5[4-(propan-2-yl)-4,5-dihydro-1H-pyrazol-1-yl]-1,3-thiazol-4(5H)-one (BPT2) at B3LYP level using 6-31G and 6-31G(d,p) basis sets are shown in Figs. 5.2 and 5.3. The elaborated vibrational assignments of the BPT2 molecule along with the calculated IR and Raman frequencies and normal mode descriptions are given in Table 5.2.

C-H vibrations

The substituted aromatic structures show the presence of C-H stretching vibration in the region 3100-3000 cm⁻¹ which is the characteristic region for the identification of C-H stretching vibrational modes [147, 112, 148].

Soleymani *et al* [149] observed the C-H vibrations at 3112, 3113 3071, 2978 cm⁻¹ theoretically and 3050, 3128 cm⁻¹ experimentally. Saruadevi *et al* [150] reported the C-H

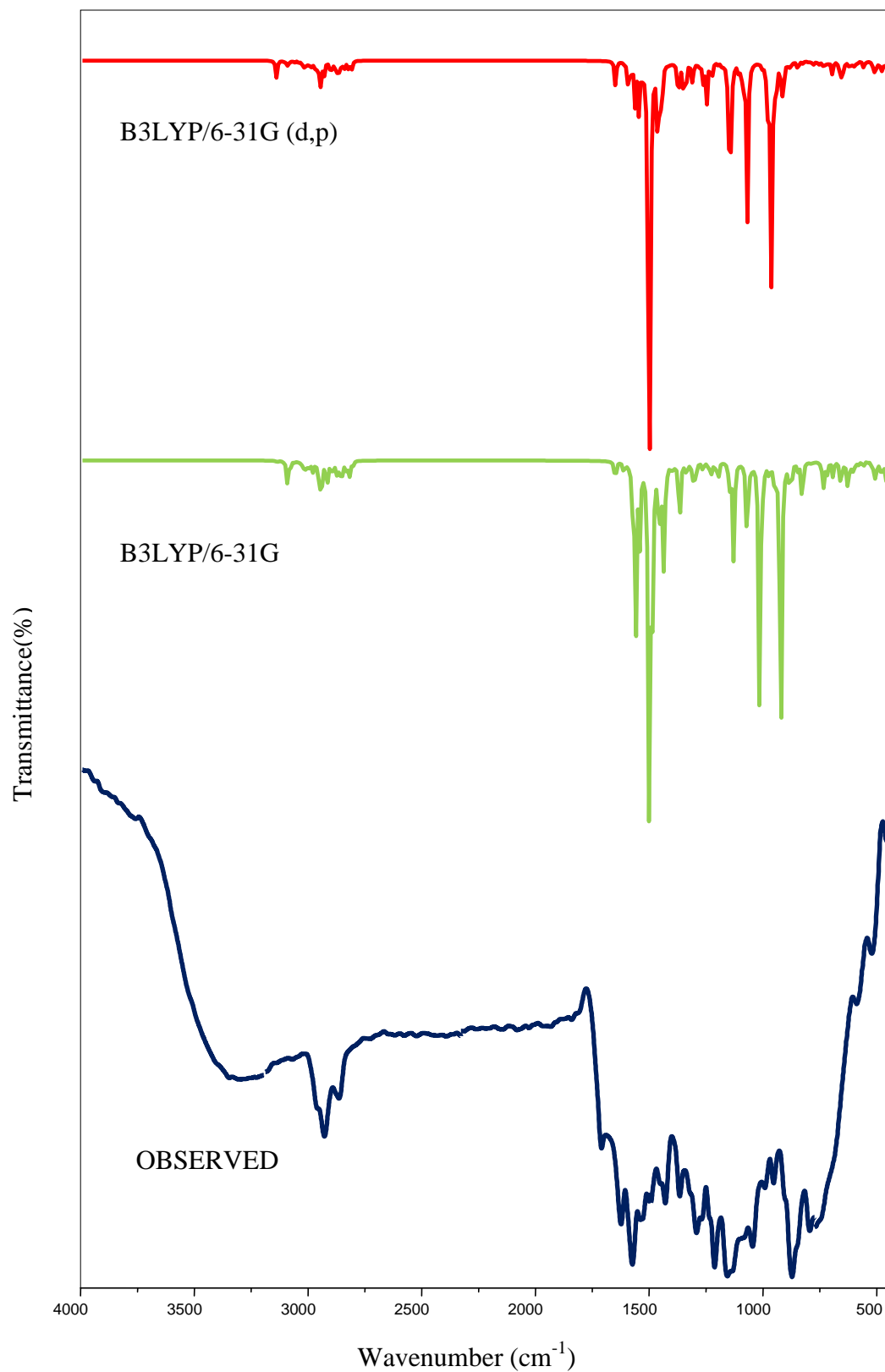


Fig.5.2 Observed FT-IR and simulated spectra of 5-(4-Butoxybenzylidene)-2-[3-(4-chlorophenyl)-5[4-(propan-2-yl)-4,5-dihydro-1H-pyrazol-1-yl]-1,3-thiazol-4(5H)-one

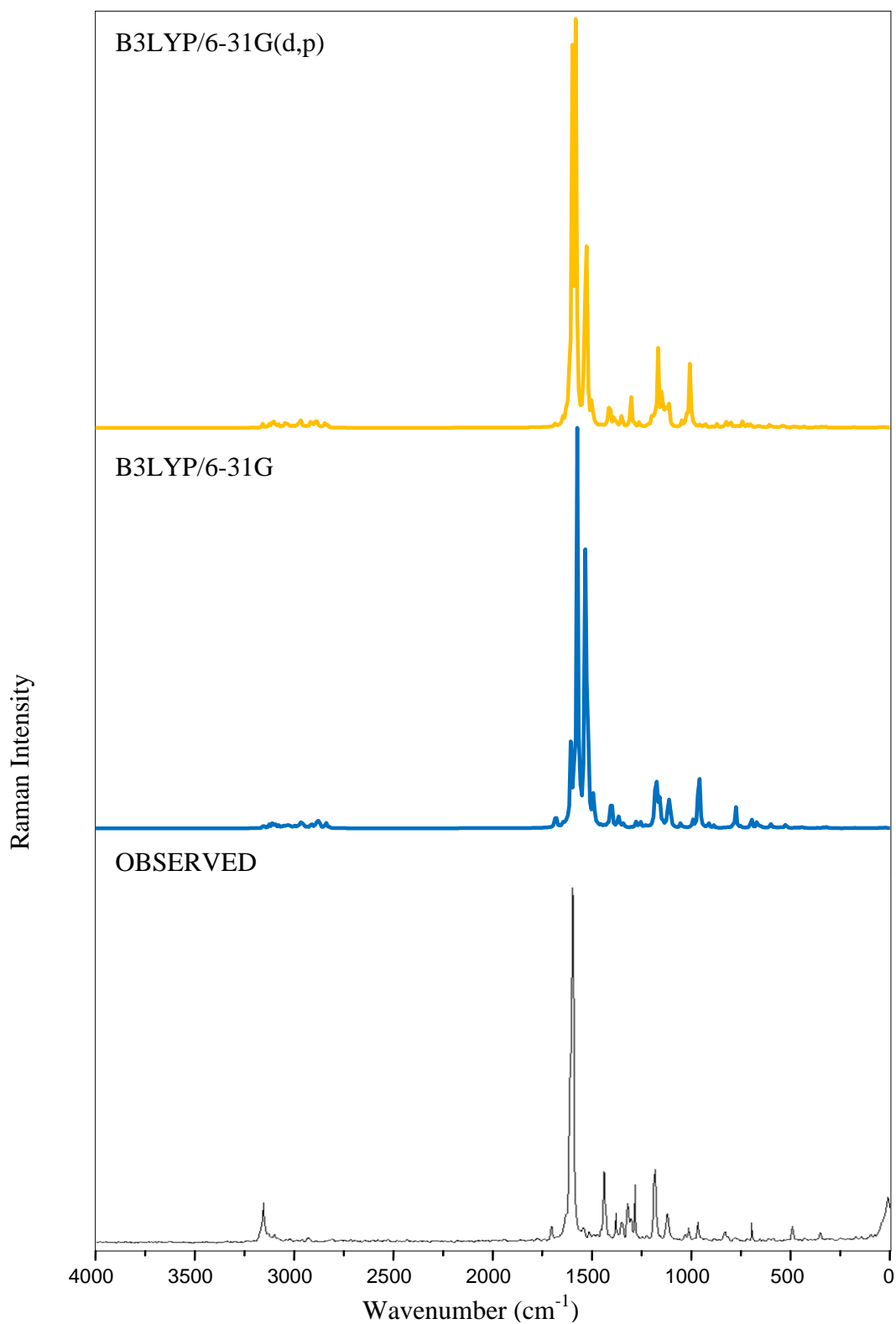


Fig. 5.3 Observed FT-Raman and simulated spectra of 5-(4-Butoxybenzylidene)-2-[3-(4-chlorophenyl)-5[4-(propan-2-yl)-4,5-dihydro-1H-pyrazol-1-yl]-1,3-thiazol-4(5H)-one

stretching modes are observed at 3096 cm^{-1} in the IR spectrum and at $3097, 3063, 3038\text{ cm}^{-1}$ in the Raman spectrum experimentally and at $3098, 3075, 3072, 3066, 3055, 3044\text{ cm}^{-1}$ theoretically. Pillai *et al* [151] reported the C-H stretching vibrations at $3097, 3086, 3081, 3057, 3055\text{ cm}^{-1}$ in the IR spectrum and $3077, 3064\text{ cm}^{-1}$ in the Raman spectrum. Kuruvilla *et al* [144] reported the C-H stretching vibrations are found at $3090, 3062, 2964, 2940\text{ cm}^{-1}$ in FT-Raman and at $2934, 2771\text{ cm}^{-1}$ in FT-IR spectrum. Kuruvilla *et al* [145] observed the C-H vibrations experimentally at $3050, 2900\text{ cm}^{-1}$ in FT-IR spectrum and $3042, 2976, 2891, 2850\text{ cm}^{-1}$ in FT- Raman spectrum. For our BPT2 molecule, the C-H stretching vibrations observed at $3150, 3075, 3002\text{ cm}^{-1}$ for FT-Raman spectrum, $3156, 3125, 3110, 3099, 3094, 3078, 3058, 3045, 3038, 3033, 3026, 3016, 3010, 2936, 2846\text{ cm}^{-1}$ and $3152, 3123, 3107, 3095, 3088, 3074, 3055, 3043, 3034, 3029, 3021, 3011, 3003, 2935, 2843\text{ cm}^{-1}$ are calculated by B3LYP method with 6-31G and 6-31G(d,p) basis sets.

Jeyasheela *et al* [103] observed the C-H in-plane bending vibrations at $1179, 1059\text{ cm}^{-1}$ in Raman spectrum and at $1167, 1086, 1046\text{ cm}^{-1}$ in IR spectrum and computed bands appeared at $1318, 1170, 1094, 1059\text{ cm}^{-1}$. Tamilelakkia *et al* [100] observed the C-H stretching mode at $1543, 1440\text{ cm}^{-1}$ in IR spectrum and $1540, 1477\text{ cm}^{-1}$ in Raman spectrum and was calculated in the range of $1511-1445\text{ cm}^{-1}$. Saraudevi *et al* [150] reported the C-H bands theoretically at $1277, 1248, 1170, 1140, 1108, 1102, 1042\text{ cm}^{-1}$ and experimentally observed at $1250, 1114, 1044\text{ cm}^{-1}$ in IR spectrum and $1279, 1246, 1168, 1038\text{ cm}^{-1}$ in Raman spectrum. In our BPT2 molecule, the C-H in-plane bending vibrations occurs at $1506, 1485, 1329\text{ cm}^{-1}$ and $1510, 1485, 1310, 1280\text{ cm}^{-1}$ observed in FT-IR and FT-Raman spectrum and calculated theoretically at $1512, 1499,$

1490, 1420, 1414, 1335, 1327, 1308, 1285, 1278, 1266, 1248 cm^{-1} and 1508, 1493, 1486, 1475, 1408, 1403, 1330, 1323, 1302, 1281, 1275, 1263, 1244 cm^{-1} for the same basis set.

Saraudevi *et al* [150] observed the CH out-of-plane bending vibrations theoretically at 930, 897, 895, 858, 818, 811, 731 cm^{-1} and experimentally at 931, 896, 855, 816 cm^{-1} for IR, 788, 729 cm^{-1} for Raman spectrum. In the present work, the C-H out-of-plane bending vibrations occurs at 948, 827 cm^{-1} and 950 cm^{-1} for FT-IR and FT-Raman spectrum and calculated values found at 960, 953, 935, 932, 889, 840, 833, 823, 796, 779, 706 cm^{-1} and 956, 948, 933, 929, 885, 865, 834, 829, 820, 795, 790, 773, 700 cm^{-1} respectively. These assignments are good agreement with the literature data.

CH₃ vibrations

The CH₃ modes are occurs in the region 2900-3050 cm^{-1} [152]. Asymmetric and symmetric stretching modes of a methyl group attached to the benzene ring are usually downshifted because of electronic effects and are expected near 2925 and 2865 cm^{-1} for asymmetric and symmetric stretching vibrations [153].

The asymmetric stretching modes of the methyl group are calculated at 3047, 3039, 3022, 3003 cm^{-1} by Paniker *et al* [154]. For the BPT2 molecule, asymmetric stretching vibrations observed at 2922 cm^{-1} for IR spectrum, theoretically found at 3001, 2986, 2976, 2964, 2950, 2930 cm^{-1} and 2995, 2983, 2971, 2959, 2947, 2926 cm^{-1} by B3LYP/6-31G and B3LYP/6-31G(d,p) respectively.

The symmetric modes are observed at 3038, 2946 cm^{-1} in the IR spectrum and theoretically obtained at 2948, 2943 cm^{-1} by Paniker *et al* [154]. Saraudevi *et al* [150]

reported the CH₃ stretching mode at 3027, 2970, 2908 cm⁻¹ and experimentally observed at 3002, 2972, 2970 cm⁻¹. Parveen *et al* [142] observed the CH₃ stretching modes are assigned at 3002, 2980, 2958, 2914 cm⁻¹ in the IR spectrum, 2960, 2938 cm⁻¹ in the Raman spectrum and theoretically occurs in the range 3032-2906 cm⁻¹. Murugavel *et al* [88] theoretically the C-H stretching modes of methyl group at 3056, 3022, 2984, 2964, 2944, 2917 and 2911 cm⁻¹ is the experimental values 3024 and 2943 cm⁻¹. Alphonsa *et al* [115] reported CH₃ stretching mode for FT-IR spectrum at 2983, 2924 cm⁻¹ and for FT-Raman at 2983, 2944, 2923 cm⁻¹ and asymmetric and symmetric stretching vibrations observed at 3059, 3053 cm⁻¹ for FT-IR, Raman spectrum and theoretically at 3012 cm⁻¹. For the BPT2 molecule, symmetric stretching vibrations observed at 2856 cm⁻¹ for IR spectrum, theoretically found at 2888, 2882, 2860 cm⁻¹ and 2884, 2878, 2854 cm⁻¹ by B3LYP/6-31G and B3LYP/6-31G(d,p) respectively.

In this work, the CH₃ in-plane bending vibrations theoretically obtained at $\delta_{\text{opb}} = 1481, 1477, 1472 \text{ cm}^{-1}$, $\delta_{\text{ipb}} = 1455, 1442, 1437 \text{ cm}^{-1}$, $\delta_{\text{sb}} = 1388, 1385, 1376 \text{ cm}^{-1}$, $\delta_{\text{ipr}} = 768, 760, 741 \text{ cm}^{-1}$, $\tau_{\text{CH}_3} = 230, 218, 210 \text{ cm}^{-1}$ by B3LYP/6-31G method and $\delta_{\text{opb}} = 1475, 1470, 1466 \text{ cm}^{-1}$, $\delta_{\text{ipb}} = 1436, 1430, 1422 \text{ cm}^{-1}$, $\delta_{\text{sb}} = 1383, 1379, 1370 \text{ cm}^{-1}$, $\delta_{\text{ipr}} = 765, 756, 748 \text{ cm}^{-1}$, $\tau_{\text{CH}_3} = 221, 212, 206 \text{ cm}^{-1}$ by B3LYP/6-31G(d,p) method. For the BPT2 molecule, the out-of-plane bending vibration occurs at 1002 cm⁻¹ for FT-IR spectrum. The theoretically predicted values by B3LYP/6-31G $\gamma_{\text{opr}} = 1032, 1021, 1003 \text{ cm}^{-1}$ by B3LYP/6-31G and 1028, 1017, 1000 cm⁻¹ by B3LYP/6-31G (d,p) methods. These assignments are good agreement with experimental observation as well as literature data.

CH₂ group

The stretching vibrations of the CH₂ group and deformation modes of CH₂ group (scissoring, wagging, twisting and rocking modes) appears in the regions 3000 ± 20 , 2900 ± 25 , 1450 ± 30 , 1330 ± 35 , 1245 ± 45 , 780 ± 55 cm⁻¹ respectively [152, 155, 112].

Parveen *et al* [142] observed the CH₂ stretching modes at 2923 cm⁻¹ in the Raman spectrum and at 2926, 2966 cm⁻¹ theoretically. The deformation modes of CH₂ are assigned at 1439, 1295, 1220, 1148 cm⁻¹ in the IR spectrum, 1146 cm⁻¹ in the Raman spectrum. Murugavel *et al* [88] the CH₂ stretching vibrations are calculated at 2991 cm⁻¹ (asymmetric) and 2944 cm⁻¹ (symmetric). Asymmetric bending of is found at 1275 cm⁻¹ which is consistent with the DFT value of 1274 cm⁻¹. Minithra *et al* [90] observed CH₂ asymmetric and symmetric stretching at 2982, 2932 cm⁻¹ and 2905, 2893 cm⁻¹ and assigned at 2978, 2930, 2885 cm⁻¹ in the IR spectrum and at 2971, 2935, 2898 cm⁻¹ in the Raman spectrum. For the BPT2 molecule, the asymmetric CH₂ stretching calculated at 2970, 2922, 2910, 2872 by B3LYP/6-31G method and 2933, 2919, 2906, 2869 by B3LYP/6-31G(d,p) method. The symmetric CH₂ stretching observed at 2910 in FT-Raman spectrum and the computed values are 2915, 2896, 2841, 2830 by B3LYP/6-31G method and 2912, 2893, 2835, 2822 by B3LYP/6-31G(d,p) method. For the BPT2 molecule, CH₂ scissoring band observed at 1394, rocking at 1173 in the IR spectrum and scissoring at 1415, 1400, rocking at 1200, wagging at 800 in the Raman spectrum. For the BPT2 molecule, the CH₂ stretching modes are observed at $\sigma_{\text{sci}} = 1429, 1423, 1408, 1402$ cm⁻¹, $\rho_{\text{rock}} = 1214, 1210, 1179, 1165$ cm⁻¹, $\tau = 1118, 1110, 1056, 1044$ cm⁻¹, $\delta_{\text{wagg.}} = 817, 805, 785, 775$ cm⁻¹ by B3LYP/6-31G, $\sigma_{\text{sci}} = 1422, 1415, 1399, 1395$ cm⁻¹, $\rho_{\text{rock}} =$

1207, 1200, 1175, 1163 cm^{-1} , $\tau = 1113, 1105, 1051, 1040 \text{ cm}^{-1}$, $\delta_{\text{wagg.}} = 812, 802, 780, 769 \text{ cm}^{-1}$ by B3LYP/6-31G (d,p) method respectively.

C-O vibrations

The C-O stretching vibrations [156, 152] are expected in the region 1715-1600 cm^{-1} . The in-plane deformation of C-O found in the region $625 \pm 70 \text{ cm}^{-1}$ and out-of-plane bending is in the range $540 \pm 80 \text{ cm}^{-1}$ [152].

Lucose *et al* [157] observed C-O stretching vibrations at 1632 cm^{-1} in IR spectrum and theoretically found at 1636 cm^{-1} (DFT). In-plane bending observed at 569 cm^{-1} in IR and 555 cm^{-1} in DFT is assigned as this mode and out-of-plane bending observed at 673, 676 cm^{-1} in the IR spectrum.

The C=O stretching vibration appears both in the FT-IR and FT-Raman spectra due to intra molecular charge transfer from donor atom to acceptor atom through σ and π bonds conjugated path, which can induce large variation in dipole and molecular polarizability of the molecule and hence high activity in both spectra [152]. Pillai *et al* [151] observed the C-O modes at 1625 at IR and 1614, 1626 cm^{-1} at Raman spectrum. The C-O stretching modes are reported at 1786, 1603, 1027 cm^{-1} and at 1726, 1629 cm^{-1} in the FT-IR, Raman spectrum and 1184, 1083, 1010, 974, 696 cm^{-1} assigned theoretically by Sakthivel *et al* [158]. Benzon *et al* [159] reported the C-O stretching mode at 1212 cm^{-1} (IR), 1228 cm^{-1} (Raman) and at 1229 cm^{-1} theoretically. For the BPT2 molecule, C-O stretching vibrations observed at 1679, 1254 cm^{-1} in IR spectrum and 1680, 1295 cm^{-1} in Raman spectrum. The reported values for $\nu_{\text{C-O}} = 1683, 1301, 1260 \text{ cm}^{-1}$, $\delta_{\text{CO}} = 1346, 984, 965 \text{ cm}^{-1}$, $\gamma_{\text{CO}} = 685, 630, 620 \text{ cm}^{-1}$ by B3LYP/6-31G method,

$\nu_{\text{C-O}} = 1680, 1297, 1254 \text{ cm}^{-1}$, $\delta_{\text{CO}} = 1342, 980, 963 \text{ cm}^{-1}$, $\gamma_{\text{CO}} = 679, 626, 620 \text{ cm}^{-1}$ by B3LYP/6-31G (d,p) method respectively.

C-C vibrations

C-C stretching vibrations occur in the range of $1625\text{-}1465 \text{ cm}^{-1}$ [106]. The in-plane and out-of plane bending modes of C-C were reported at 725 ± 95 and $595 \pm 120 \text{ cm}^{-1}$ [113].

The C-C band observed by Kuruvilla *et al* [144] at 1579, 1531, 1439, 1380, 1123 for FT-Raman and for FT-IR bands at 1428, 1235, 1002 cm^{-1} . Soleymani *et al* [149] observed C-C stretching band at 1625, 1590, 1575, 1540, 1470, 1465, 1430, 1380, 1280 cm^{-1} . Tamil elakkiya *et al* [100] observed the C-C stretching band at 1313, 1039 cm^{-1} and calculated at 1600, 1625, 1319, 1054 cm^{-1} . In the present work, the C-C stretching vibrations observed at 1591, 1230, 1118, 909 cm^{-1} in IR spectrum, 1215, 910 cm^{-1} in Raman spectrum. The reported values at 1644, 1625, 1613, 1596, 1538, 1236, 1221, 1195, 1186, 1162, 1145, 1140, 1131, 1125, 1080, 1013, 992, 925, 924, 914, 845 cm^{-1} by B3LYP/6-31G method, 1641, 1623, 1604, 1590, 1533, 1231, 1217, 1191, 1182, 1158, 1143, 1136, 1127, 1120, 1075, 1009, 989, 921, 916, 910, 842 cm^{-1} by B3LYP/6-31G (d,p) methods respectively. The C-C in-plane bending observed at 503 cm^{-1} and 502, 345 cm^{-1} in IR and Raman spectrum and the reported values are 792, 715, 690, 616, 608, 590, 575, 565, 539, 510, 503, 477, 480, 360, 349 cm^{-1} by B3LYP/6-31G method and 786, 711, 688, 612, 603, 586, 573, 561, 535, 506, 500, 472, 466, 354, 345 cm^{-1} by B3LYP/6-31G (d,p) method. The C-C out-of-plane bending vibration assigned at 150, 135, 120 cm^{-1} in Raman spectrum and the calculated values are at 330, 319, 303, 296, 291, 273, 262, 246,

197, 189, 176, 158, 141, 126 cm^{-1} by B3LYP/6-31G method, 325, 314, 299, 293, 286, 275, 268, 242, 191, 185, 173, 151, 136, 120 cm^{-1} by B3LYP/6-31G (d,p) method respectively.

C-N vibrations

The C-N stretching modes are expected in the region 1400-1200 cm^{-1} Sandhyarani *et al* [160] reported the C-N stretching mode at 1319 cm^{-1} . Benzon *et al* [159] reported at 1247, 129, 938 cm^{-1} theoretically, 1268, 11135, 926 cm^{-1} in the Raman spectrum and 924 cm^{-1} in the IR spectrum. The C-N stretching modes were reported at 1268, 1220, 1151 cm^{-1} theoretically by Malek *et al* [161]. Al-Alshaikh *et al* [89] observed C-N stretching mode at 1329, 1092, 997 cm^{-1} in the IR spectrum, 1328 cm^{-1} in the Raman spectrum and theoretically at 1479, 1472, 1331, 1097, 998 cm^{-1} . Bhagyasree *et al* [162] reported C-N stretching modes at 1247 and 1236 cm^{-1} . Shana parveen *et al* [146] assigned the C-N stretching mode at 1579 cm^{-1} and IR spectrum at 1553 cm^{-1} . In the present work, C-N stretching vibrations obtained at 1541 cm^{-1} and 1350, 720 cm^{-1} in IR and Raman spectrum. The calculated values are obtained at 1579, 1533, 1525, 1370, 1356, 726 cm^{-1} and 1572, 1529, 1517, 1362, 1351, 720 cm^{-1} by the B3LYP/6-31G and B3LYP/6-31G (d,p) method respectively.

N-N vibrations

N-N stretching mode occurs at 1417-1372 cm^{-1} [163]. The ν N-N has been reported at 1151 cm^{-1} by Crane *et al* [164], 1121 cm^{-1} by Bezerra *et al* [165] and 1130 cm^{-1} El-behery and El-Twigry *et al* [166] and 1083 cm^{-1} theoretically by Sundaragengan *et al* [167]. Binil *et al* [85] reported the N-N stretching mode at 1138 cm^{-1} in IR, 1139 cm^{-1} in

Raman and 1136 cm^{-1} theoretically. For Murugavel *et al* [88], N-N stretching vibrations allocated at $1083, 1119\text{ cm}^{-1}$ by DFT technique and experimentally at 1082 cm^{-1} in FT-IR spectrum. For the BPT2 molecule, N-N stretching mode is calculated at 883 and 879 cm^{-1} by B3LYP/6-31G and 6-31G (d,p) method respectively.

C-S vibrations

This vibration cannot be identified easily as it results in weak infrared bands, which is susceptible to coupling effects and is also of variable intensity. In general, the C-S stretching vibration was reported in $750\text{-}600\text{ cm}^{-1}$ [109].

Benson *et al* [159] reported value this mode at 1515 cm^{-1} in the IR spectrum, 1520 cm^{-1} in the Raman spectrum, 1517 cm^{-1} theoretically. The C-S stretching mode observed for Sarau *et al* [150] assigned at $759, 660\text{ cm}^{-1}$ theoretically and experimentally observed at $756, 665\text{ cm}^{-1}$ and $756, 658\text{ cm}^{-1}$ in the IR and Raman spectrum. Kuruvilla *et al* [144] observed these vibrations at $822, 714\text{ cm}^{-1}$ theoretically and FT-IR spectrum obtained experimentally observed at 714 cm^{-1} . The C-S stretching modes were observed by Coates *et al* [109] in the range $710\text{-}687\text{ cm}^{-1}$ while Kwastkowski *et al* [168] reported the vibration at 839 and 608 cm^{-1} . The C-S stretching vibrations are reported at $783, 632\text{ cm}^{-1}$ and 633 cm^{-1} IR, Raman spectrum and $785, 635\text{ cm}^{-1}$ theoretically found by El-Azab *et al* [169]. The C-S stretching vibrations are reported at 770 cm^{-1} in the IR spectrum, and at $770, 636\text{ cm}^{-1}$ theoretically assigned by Shaheen Fatma *et al* [106]. In the present work, C-S vibrations calculated at $738, 697$ and $731, 694\text{ cm}^{-1}$ by B3LYP/6-31G and 6-31G (d,p) method respectively.

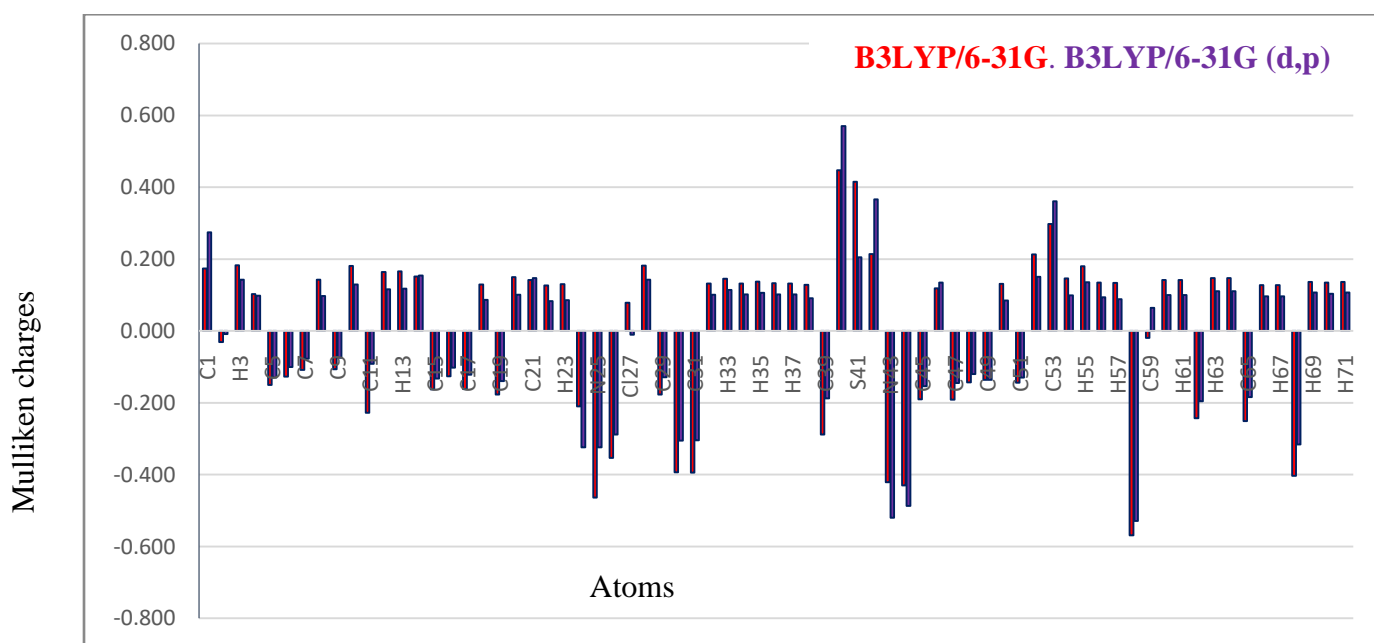


Fig.5.4 Mulliken atomic charges of 5-(4-Butoxybenzylidene)-2-[3-(4-chlorophenyl)-5[4-(propan-2-yl)-4,5-dihydro-1H-pyrazol-1-yl]-1,3-thiazol-4(5H)-one

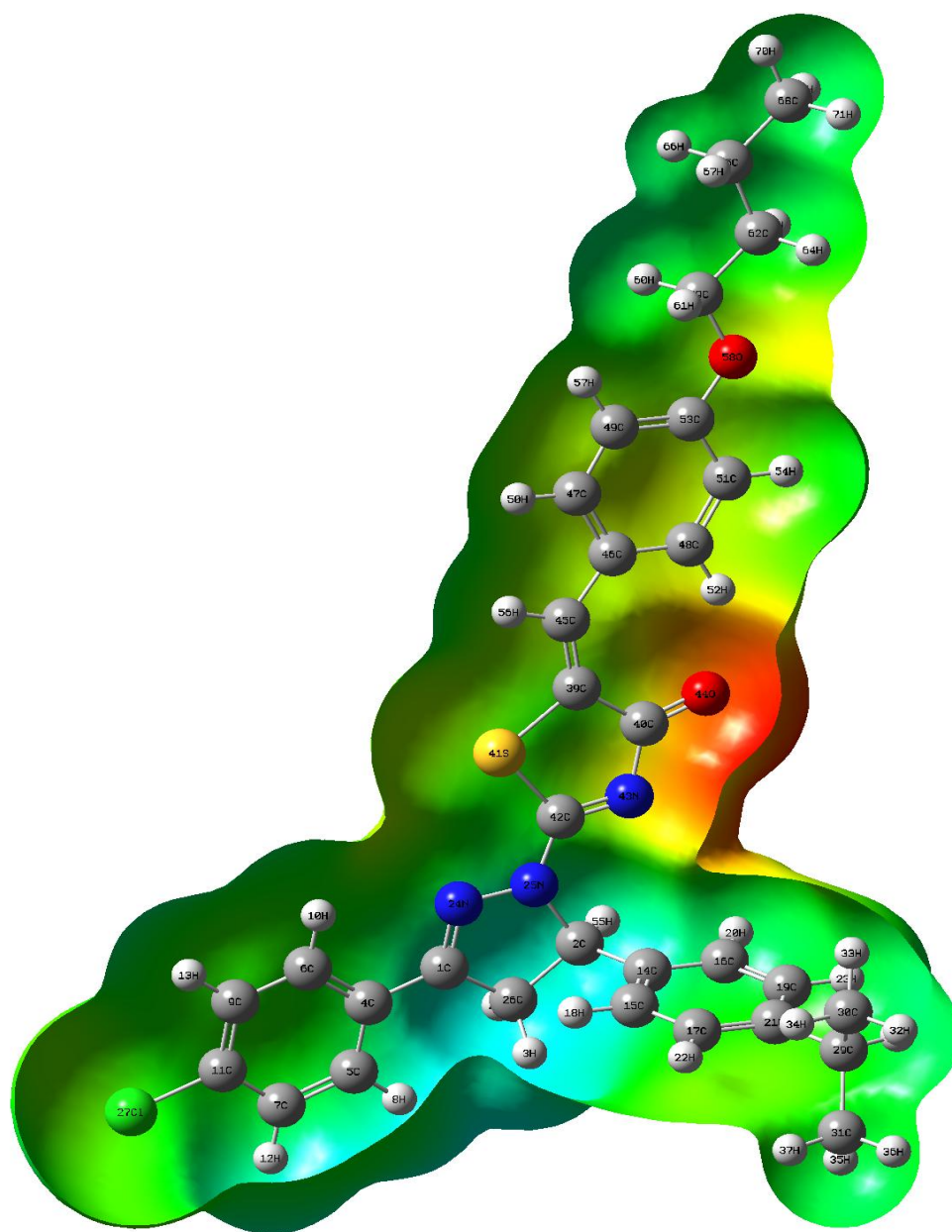


Fig.5.5 Molecular electrostatic potential surfaces of 5-(4-Butoxybenzylidene)-2-[3-(4-chlorophenyl)-5[4-(propan-2-yl)-4,5-dihydro-1H-pyrazol-1-yl]-1,3-thiazol-4(5H)-one
5.5 Mulliken population analysis

C-Cl vibrations

The vibrations belong to C-Cl absorption is obtained in the region between 850-550 cm^{-1} [170]. Kuruvilla1 *et al* [144] observed theoretically at C-Cl vibration at 694 cm^{-1} and 415 cm^{-1} and experimentally at 710-505 cm^{-1} . Jayasheela *et al* [103] reported this band at 725 cm^{-1} and 720 cm^{-1} 4-chlorophenyl ([(1E)-3-(1Himidazol-1-yl)-1-phenylpropylidene] amino}oxy) methanone for theoretically and experimentally. For the BPT2 molecule, the vibrations occurs at for $\nu_{\text{C-Cl}}=597$, $\delta_{\text{C-Cl}}=438$ in FT-IR spectrum and theoretically at $\nu_{\text{C-Cl}}=602$ and 598 cm^{-1} , $\delta_{\text{C-Cl}}=473$ and 440 cm^{-1} , $\gamma_{\text{C-Cl}}=280$ and 275 cm^{-1} by B3LYP/6-31G and 6-31G (d,p) methods respectively.

Ring vibration

The thiazole ring in-plane bending vibrations are observed for the BPT2 molecule at 551, 457, 411 cm^{-1} by FT-IR spectrum and theoretically at 588, 553, 545, 531, 522, 487, 463, 427, 417, 407, 392, 381, 166, 146, 112, 52, 48 cm^{-1} by B3LYP/6-31G method and 580, 550, 541, 523, 518, 481, 460, 422, 410, 401, 389, 375, 162, 142, 102, 49, 46, 43 cm^{-1} by B3LYP/6-31G(d,p) method. The ring out-of-plane bending observed at 35 cm^{-1} in FT-Raman spectrum, theoretically at 135, 95, 86, 80, 75, 66, 41, 37, 30, 25, 23, 17, 12, 7 cm^{-1} by B3LYP/6-31G method and 128, 89, 79, 74, 69, 57, 35, 30, 24, 22, 20, 16, 10, 6 cm^{-1} by B3LYP/6-31G(d,p) method.

5.5 Mulliken population analysis

Mulliken atomic charge calculation [116] has an important role in the application of quantum chemical calculation to molecular system. Because of atomic charges affects

dipole moment, polarizability, electronic structure and more properties of molecular system. The Mulliken atomic charges of the methyl group hydrogen atoms are higher than the aromatic group hydrogen atoms. It denotes that the methyl group hydrogen atoms are more acidic than the aromatic group hydrogen atoms. Atomic charges has been used to describe the process of electro negativity equalization and charge transfer in chemical reactions [171,172] and to model the electrostatic potential outside the molecular surfaces. Mulliken atomic charges calculated at the B3LYP/6-31G and 6-31G (d,p) methods are tabulated in Table 5.3 and Fig. 5.4. For the BPT2 molecule, the Mulliken atomic charges of C40, S41, C42, H52, C53 are occupies the more positive and becomes high acidic and N24, N25, C26, C30, C31, N43, O44 and O58 are have more negative and become less acidic.

5.6 Molecular electrostatic potential (MEP) surface analysis

Molecular electrostatic potential at a point in space around a molecule gives information about the net electrostatic effect produced at that point by total charge distribution (electron + proton) of the molecule and correlates with dipole moments, electro-negativity, partial charges and chemical reactivity of the molecules. It provides a visual method to understand the relative polarity of the molecule [173, 174]. An electron density iso-surface mapped with electrostatic potential surface depicts the size, shape, charge density and site of chemical reactivity of the molecules. Fig.5.5 illustrates the charge distributions of the molecule two dimensionally. As it can be seen from the figure, the different values of the electrostatic potential at the surface are represented by different colours; red represents region of most electronegative electrostatic potential, blue represents region of the most positive electrostatic potential and green represents region of

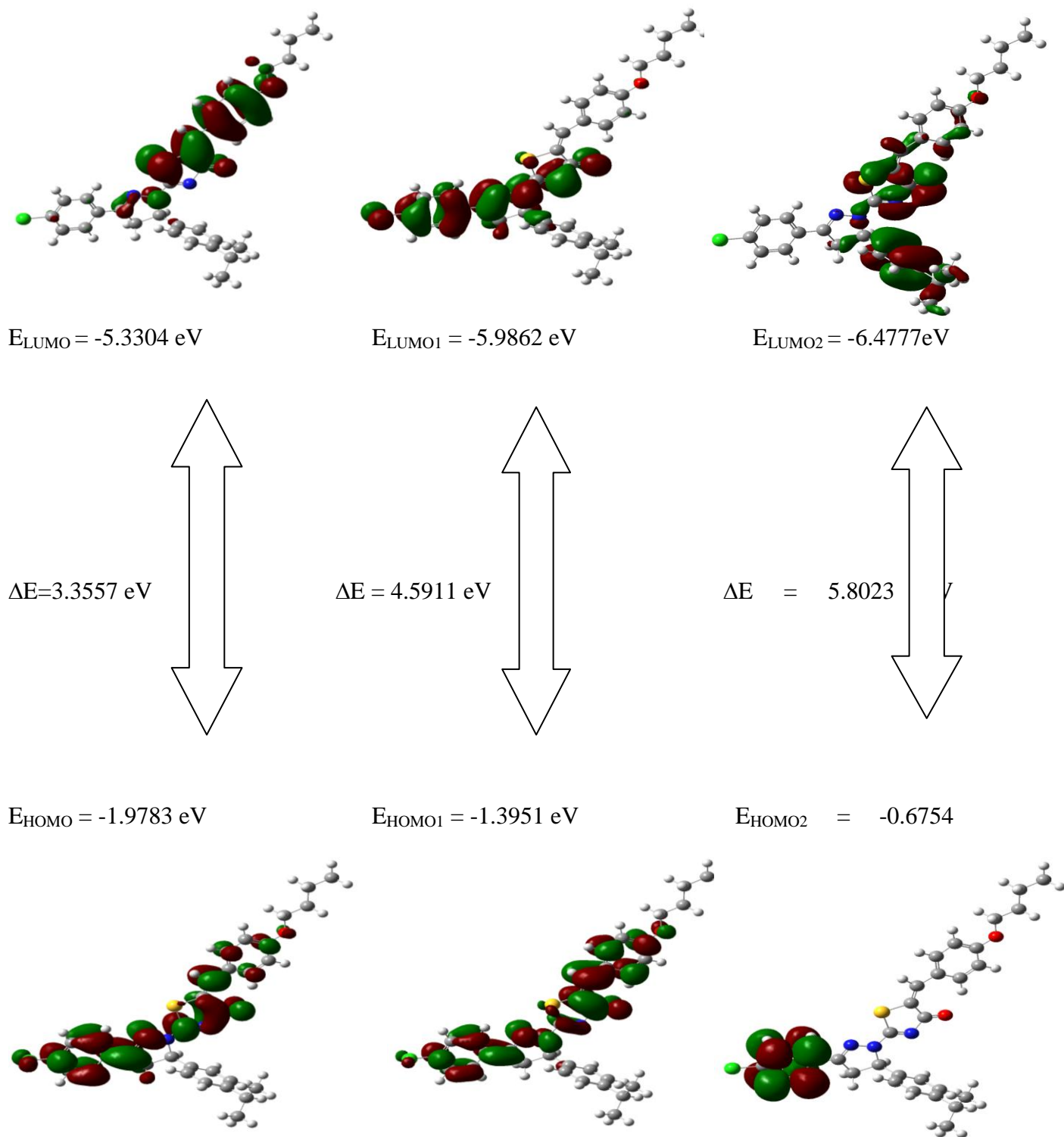


Fig. 5.6 Patterns of the principle highest occupied and lowest unoccupied molecular orbital 5-(4-Butoxybenzylidene)-2-[3-(4-chlorophenyl)-5[4-(propan-2-yl)-4,5-dihydro-1H-pyrazol-1-yl]-1,3-thiazol-4(5H)-one

zero potential. Potential increases in the order red < orange < yellow < green < blue. Blue indicates the strongest attraction and red indicates the strongest repulsion. Region of negative potential are usually associated with the lone pair of electronegative atoms. From the MEP map of the BPT2 molecule, more reactive sites are close to C=O (C40-O44) groups, the region having the most negative potential over oxygen atom O44 and O58, then all the hydrogen atoms have positive potential. The negative potential which is represented by red colour corresponds to an interaction of a proton by aggregate the electron density of the molecule represented by red yellow shade and blue region is positive which corresponds to the repulsion of the proton represented by blue shades. The strong negative region spread over the phenyl rings, nitrogen atom and oxygen atom of the hydroxyl group and these are possible sites of electrophilic sites. The positive electrostatic potential regions are fully covered all the hydrogen atoms and it represents the possible site of the nucleophilic sites in the MEP plot.

5.7 Frontier molecular orbital (FMO) study

DFT method with 6-31G (d,p) basis set is applied to compute the energy of HOMO and LUMO levels and the energies are shown in Table 5.4. The Frontier molecular orbitals (FMO) play a significant function in the electric and quantum chemistry [175]. The pictorial demonstration of these different FMOs is shown in Fig.5.6. The HOMO is the donor and LUMO is acceptor orbital and the energy difference between HOMO and LUMO have been used to investigate the global reactivity descriptors. The electrophilic index (ω), hardness (η) and chemical potential (μ) are known reactivity parameters. These parameters are considered as highly successful

descriptors for biological activity. Moreover, electronegativity (χ), electron affinity (A), ionization potential (I) are also determined using the energies of frontier molecular orbitals and these reactivity parameters used in understanding the site selectivity and the reactivity. The compounds that possess positive electron affinity are known as electron acceptors and might participate in charge transfer reactions. The electron donation strength for any donor compound can be measured using ionisation potential is the energy which need to take off an electron from the HOMO. Electronegativity is known as one of the most important chemical properties which defined as power of species to attract electrons towards itself. The large $E_{\text{HOMO}} - E_{\text{LUMO}}$ differences define a hard species, which means compound is more stable and less reactive. While, small $E_{\text{HOMO}} - E_{\text{LUMO}}$ gap defines a soft species is less stable and more reactive. The calculated energy of HOMO is -5.3304 eV and LUMO is -1.9783 eV and the energy gap for the BPT2 molecule is 3.3521 eV and is a hard one. Ionization potential (I) =5.3304 eV, Electron affinity (A) = 1.9783 eV, Global hardness (η) = 1.6761 eV, Softness (η) = 0.5966 eV, Chemical potential (μ) = -3.6544 eV, Electrophilic index (ω) = 3.9838 eV. The values for chemical potential and electrophilic index are small that indicates the reactive nature of the BPT2 molecule which confirms the bioactivity of the title molecule by the positive value of chemical softness.

5.8 Natural bond orbital analysis

Natural bond orbital (NBO) analysis helps in understanding the delocalization of electron density from occupied Lewis-type (donor) NBOs to properly unoccupied non-

Lewis type (acceptor) NBOs within the molecule [176]. It is an efficient method for investigating charge transfer or conjugative interactions in molecular systems. To explain the intermolecular hydrogen bonding, intermolecular charge transfer (ICT), rehybridization and delocalization of electron density, NBO analysis was done for the BPT2 molecule. The corresponding results are given in Table 5.5. As the value of E (2) increases, the interaction of electron donors and electron acceptors also increases. As a result, the extent of conjugation of the system shows an increasing tendency to donate electrons from donors to the electron acceptors.

The important hyper-conjugative interactions are C42 - N43 from S41 of $\pi(2)$ S41 $\rightarrow \sigma^*(2)$ C42 - N43, C39 - C45 from S41 of $\pi(2)$ S41 $\rightarrow \sigma^*(2)$ C39 - C45, C1 - N24 from N25 of $\pi(1)$ N25 $\rightarrow \sigma^*(2)$ C1-N24, C40 - N43 from O44 of $\pi(2)$ O44 $\rightarrow \sigma^*(1)$ C40 - N43, C39 - C40 from O44 of $\pi(1)$ O44 $\rightarrow \sigma^*(2)$ C39 -C40, C42 - N43 from N25 of $\pi(1)$ N25 $\rightarrow \sigma^*(2)$ C42-N43, C7 - C11 from C127 of $\pi(3)$ C127 $\rightarrow \sigma^*(2)$ C7 - C11, C42 - N43 from S41 of $\pi(1)$ S41 $\sigma^*(1) \rightarrow$ C42 - N43, C39 - C40 from S41 of $\pi(1)$ S41 $\rightarrow \sigma^*(1)$ C39 -C40, C 49 - C53 from O59 of $\pi(1)$ O59 $\sigma^*(1) \rightarrow$ C49 - C53, with electron densities, 0.133, 0.112, 0.072, 0.111, 0.102, 0.088, 0.061, 0.08, 0.08, 0.068 eV and stabilization energies, 99.81, 65.56, 26.71, 22.98, 18.59, 13.03, 12.39, 8.55, 7.95 and 5.89 kcal/mol.

In Table 5.6, σ C40-O44 orbital with 1.99419 a.u energy has 36.24% of C40 character in SP^{2.02} hybrid and has 63.75% O44 character in (SP)^{2.29} hybrids. The idealized SP^{2.02} hybrid has 63.56% p-character and 36.44% s-character. The two coefficients 0.6020 and 0.7985 are called polarization coefficients. σ C53-O58 orbital

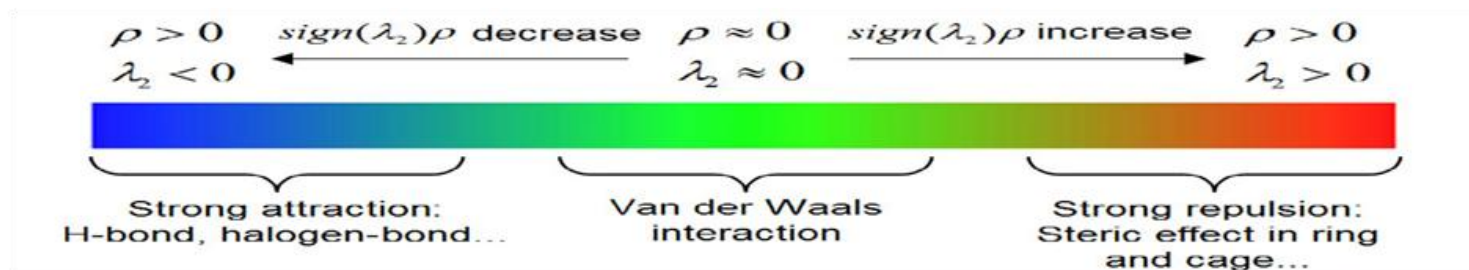
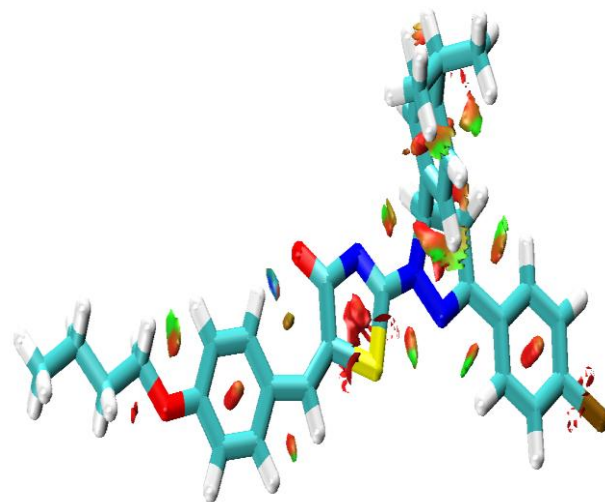
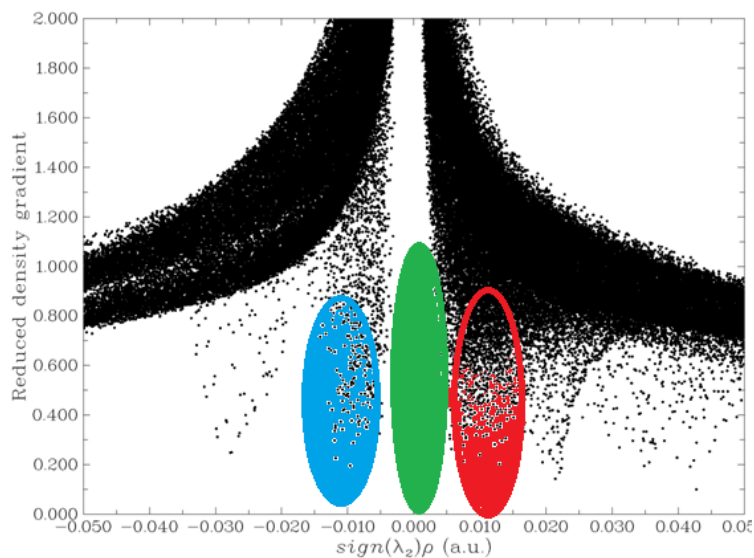


Fig.5.7. Plots of the RDG versus $\lambda_2\rho$ of 5-(4-Butoxybenzylidene)-2-[3-(4-chlorophenyl)-5[4-(propan-2-yl)-4,5-dihydro-1H-pyrazol-1-yl]-1,3-thiazol-4(5H)-one

with 1.98738 a.u energy has 33.44 % of C53 character in $SP^{3.11}$ hybrid and has 66.01 % O58 character in $SP^{2.83}$ hybrids. The idealised $SP^{3.11}$ hybrid has 24.31%, 26.09% s-characters and 75.69%, 73.92% p-characters. The two coefficients 0.5830 and 0.8124 are called polarization coefficients. The oxygen (O58) has a larger percentage of NBO, 67.56% and gives the larger polarization coefficient 0.8219 because it has a higher electronegativity. The carbon, nitrogen and sulphur have a lesser percentage of NBO and gives a lesser polarization coefficient.

5.9 Reduced density gradient

RDG is a pictorial visualization of various kinds of non-covalent interactions directly in the real space using Multiwfn and plotted by visual molecular dynamics (VMD) program [76, 77]. Noncovalent interactions are very weak when compared with covalent bonds and hence play a vital role in nature. To understand the nature of intermolecular interaction of the BPT2 molecule, RDG analyses were carried out and the resultant graphs are shown in Fig.5.7. According to this graph, the green regions represent weak attractive interactions ($\lambda_2 \approx 0$) such as Van der Waals interaction; strong attractions like H-bond, C-Cl bonds are represented by blue colour. The red colour represents steric repulsion appears in the inside of phenyl rings, pyrazole, and 4-Butoxybenzylidene while Van der Waals interactions took place near 4(propan-2-yl) and over hydrogen atoms. The negative values of $\lambda(2)\rho$ indicates strong attractive interactions, while the positive values mean the repulsive interactions.

5.10 Fukui functions

Fukui functions indicate how electron density changes with the addition or removal of the charge. If the charge is added it is useful to track where electron density increased. On the other side if the charge is removed than it is useful to track where electron density decreased. This is done by the so called f^+ and f^- functions, which are in Jaguar defined in the finite difference approximation as following:

$$f^* = (\rho^{N+\delta}(r) - \rho^N(r)) / \delta$$

$$f^* = (\rho^{N-\delta}(r) - \rho^N(r)) / \delta$$

where N denotes the number of electrons in the reference state of the molecule and δ represents the fraction of electron, which is set to be 0.01 [177]. Values of Fukui f^+ and f^- functions have been mapped to electron density surface.

Morell *et al* [178] have introduced a new dual descriptor ($\Delta f(r)$), which is defined as the difference between nucleophilic and electrophilic Fukui function and is given by, $\Delta f(r) = [f^+ - f^-]$. When $\Delta f(r) < 0$, the site is favoured for an electrophilic attack, $\Delta f(r) > 0$, the site is favoured for a nucleophilic attack. These sites of the BPT2 molecule based on Mulliken atomic charges and these sites are listed in Table 5.7. Most favourable electrophilic and nucleophilic sites of the BPT2 molecule is in the order of $H20 > N25 > H55 > H3 > Cl27$ and $N43 > S41 > C45 > O44$. The higher positive charge values obtained for H20 (= 0.0846), N25 (=0.0784), H20 lies in the phenyl ring and N25 in the pyrazole ring. The higher negative values obtained at O44 (= -0.0845), C45(=-0.0832) whereas O44 in the thiazole ring and C45 in between the thiazole and phenyl ring.

5.11 Topological analysis

The topological analysis of atoms in the molecule provides an effective information about the presence of strong and weak hydrogen bonds in terms of Topological parameters for intramolecular interactions in compound electron density (ρ_{BCP}), Laplacian of electron density (V^2_{BCP}), electron kinetic energy density (G_{BCP}), electron potential energy density (V_{BCP}), total electron energy density (H_{BCP}), Hydrogen bond energy (E_{HB}) at bond critical point (BCP) [179]. To contemplate the noncovalent interactions of the BPT2 molecule, AIM analysis was performed using Multiwfn [138] package. According to the topological theory of AIM, the Bond Critical Point (BCP) appears when the two neighbouring atoms are chemically bonded or those atoms have weak interactions. The weak H-bonds, medium, strong and their electrostatic partially covalent and covalent nature can be denoted by ($V^2_{\text{BCP}} > 0$ and $H_{\text{BCP}} > 0$), ($V^2_{\text{BCP}} > 0$ and $H_{\text{BCP}} < 0$) and ($V^2_{\text{BCP}} < 0$ and $H_{\text{BCP}} < 0$) [180]. The topology analysis of the BPT2 molecule was carried out to (3,-1) bond critical points. The paths generated are pictured in Fig. 5.8. The bond interactions and their values are provided in Table 5.8 and indicated that O44...H50 is weak interactions having V^2_{BCP} and H_{BCP} values greater than zero. $\nabla^2\rho(r) > 0$ and $G(r)+V(r) < 0$, depict that they are intermediate closed shell type hydrogen bond interactions. The strength of hydrogen bond can be also characterized by evaluating the hydrogen bonding energy (E_{HB}). The negative value of E_{HB} of hydrogen bonds designate the conformation of the hydrogen bonds is thermodynamically favoured [181].

5.12 Molecular docking studies

Molecular docking is a computer-assisted drug design (CADD) method used to predict the favourable orientation of a ligand (drug) to a target (receptor) when bound to each other to form a stable complex. By understanding the favoured orientation can be used to find out the strength of binding affinity between ligand and target site, e.g. by docking score [182]. Moreover, docking study can be used to find out type of interactions between ligand and receptor like hydrogen bonding and hydrophobic interactions. Hence, molecular docking can be considered as first-line technique for a pharmaceutical lead discovery [183]. Molecular docking studies were carried out to understand the binding profile of thiazole derivatives and to support the *in vitro* anticancerous activity. Automated docking was used to determine the orientation of inhibitors bound in the active site of Tubulin (PDB ID=4YJ2), which the protein has anti-cancerous activity. Protein 4YZJ has antiviral and 1OQE, 4YJE has anti tumor activity.

A Lamarckian genetic algorithm method, implemented in the program AutoDock Vina software was employed. The ligand used for docking was the optimized structure at B3LYP/6-31G (d, P). The files were prepared in a pdb format. The protein structure file (PDB ID: 4YZJ) taken from RCSB Protein Data Bank (PDB) was prepared for docking by removal of water molecules, adding polar hydrogens and Kollman charges to the structure file. *In silico* prediction of amino acids involved in the active site of protein responsible for binding with the ligands are obtained from the co-crystallized endogenous ligand from the PDB file. The ligand was docked in the functional sites of the selected protein and minimum docking energy value was examined. Docked conformation which

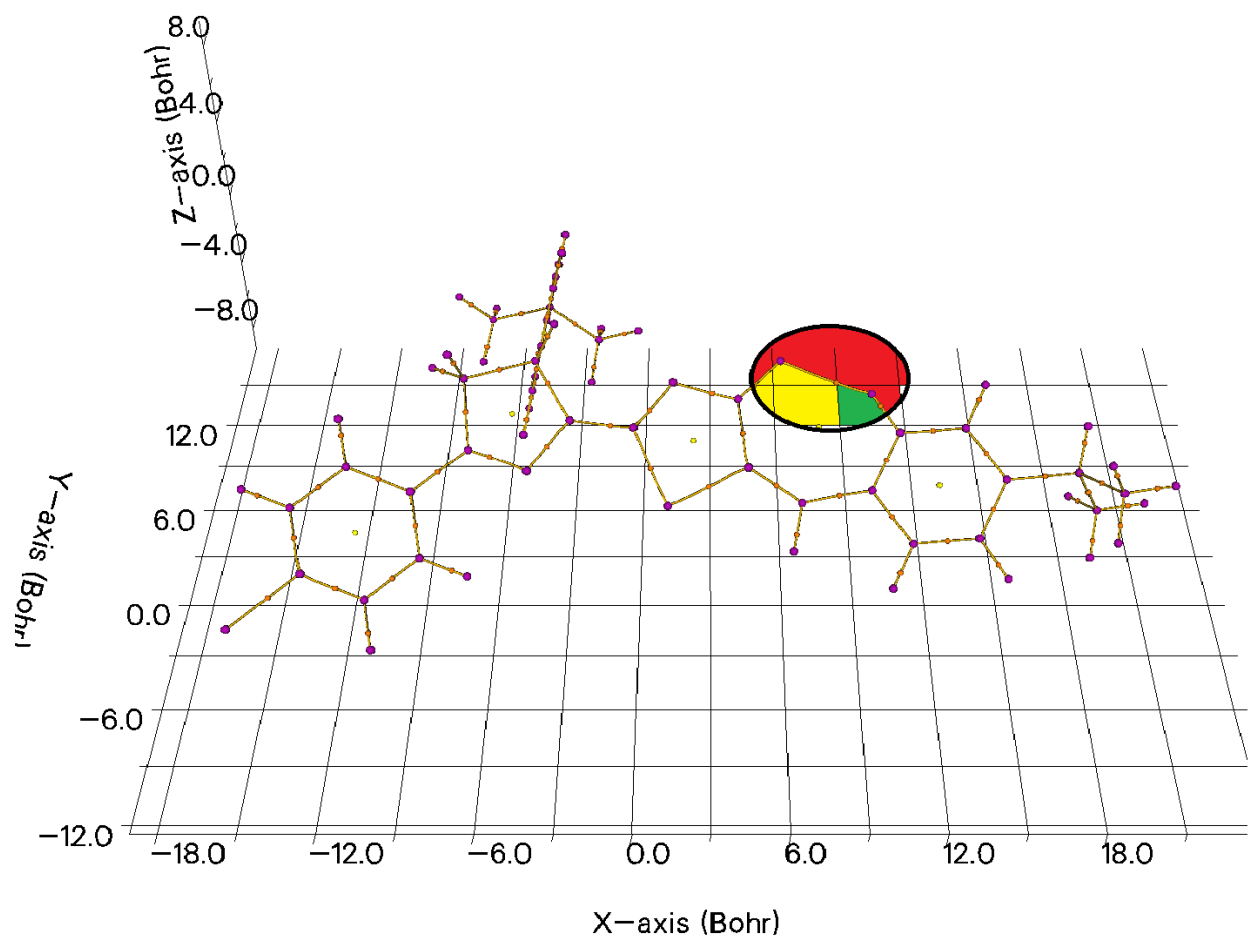


Fig. 5.8 Molecular graph of 5-(4-Butoxybenzylidene)-2-[3-(4-chlorophenyl)-5[4-(propan-2-yl)-4,5-dihydro-1H-pyrazol-1-yl]-1,3-thiazol-4(5H)-one

had the lowest binding energy was chosen to scrutinize the molecule mode of binding. The molecular docking binding energies and inhibition constants were also obtained and listed in Table 5.9. The BPT2 molecule taken as the ligand interactions with proteins are shown in Figs. 5.9.

Anti-tumor activity

Interaction of antitumor protein 1OQE shows the existence of many conventional bonds such as three conventional hydrogen bonds and two alkyl bond interaction with amino acid (ASN A: 42, GLU A: 41, ASN A: 42, PRO A: 15, ILE A: 15) with different binding energies (-4.7, -3.97, -3.8, -4.33, -4.19)kcal/mol, inhibition constants (360.43, 1.23 (mM), 1.54 (mM), 667.85, 845.86)ki(μ M) RMSD values are (87.206, 81.106, 82.083, 71.635, 78.414) \AA . Interaction of antitumor protein 4YJE shows the existence of many conventional bonds such as five conventional hydrogen bond interaction with amino acid (MET A: 438, MET A: 438, TYR A: 486, MET A: 438, MET A: 438) with different binding energies (-5.42, -5.32, -5.2, -4.95, -4.45)kcal/mol, inhibition constants (106.41, 126.67, 155.59, 234.91, 544.29)ki(μ M) RMSD values are (49.944, 48.812, 33.732, 25.064, 25.158) \AA .

Anticancerous activity

Interaction of anticancerous protein 4YJ2 shows the existence of many conventional bonds such as one Alkyl bonds, two π -alkyl bond and one carbon hydrogen bond interaction with amino acid (LEU A: 397, PRO A: 175, PRO A: 173, PRO A: 184, GLN A: 176) with different binding energies (-4.7, -4.6, -4.21, -4.57, -4.53)kcal/mol,

inhibition constants (358.4, 426.72, 817.23, 447.01, 482.07)ki(μ M) RMSD values are (80.983, 121.029, 111.228, 87.283, 94.627) \AA .

Antiviral activity

Interaction of antiviral protein 4JZJ shows the existence of many conventional bonds such as three van der waals bonds and two π - π stacked bond interaction with amino acid (PHE A: 107, TRP A: 47, PHE A: 107, TRP A: 105, LEU A: 45) with different binding energies (-5.17, -4.95, -4.49, -4.23, -4.2)kcal/mol, inhibition constants (163.56, 236.07, 514.73, 790.86, 838.87)ki(μ M) RMSD values are (36.106, 36.427, 30.374, 38.123, 32.471) \AA .

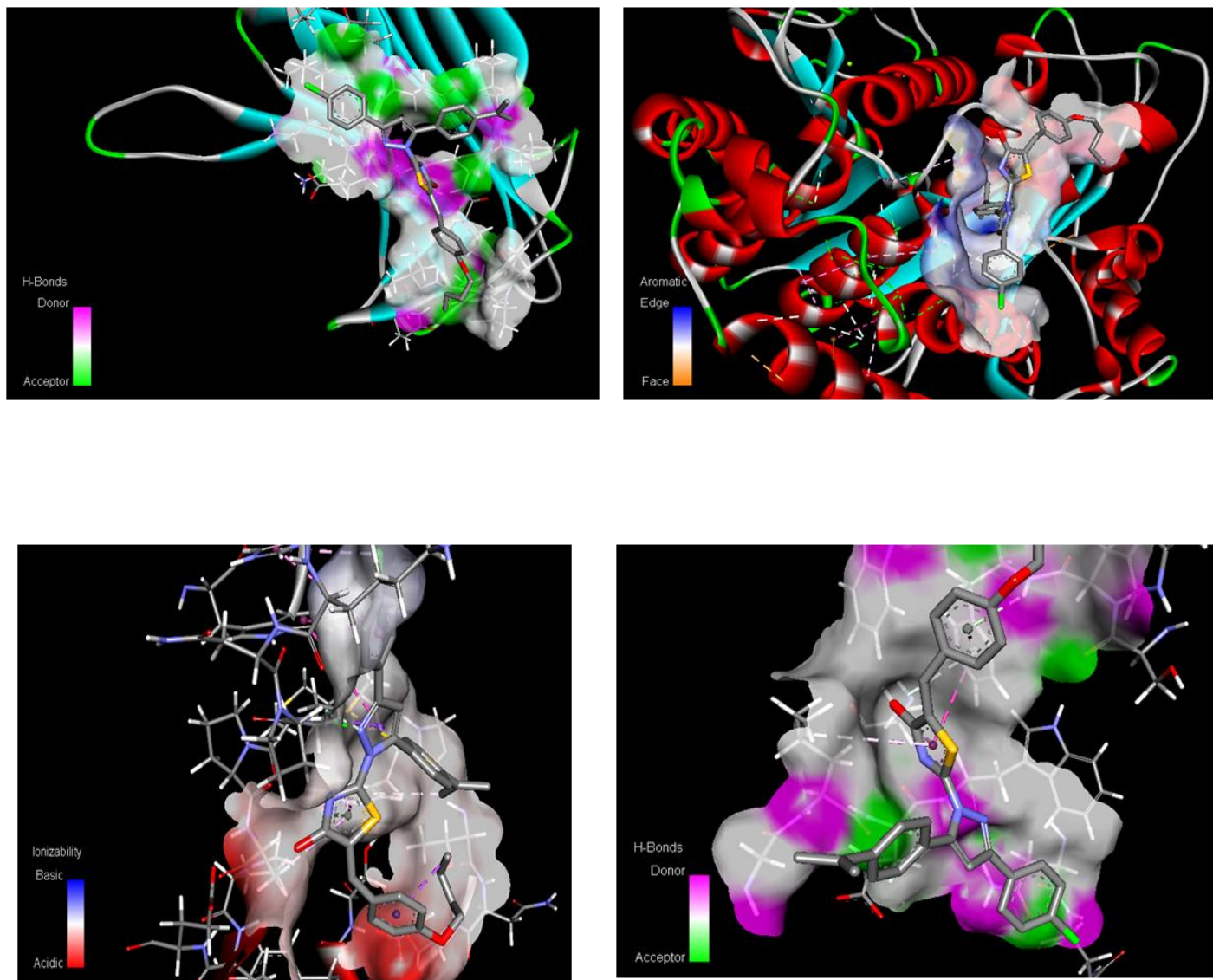


Fig 5.9 Ligand - 5-(4-Butoxybenzylidene)-2-[3-(4-chlorophenyl)-5[4-(propan-2-yl)-4,5-dihydro-1H-pyrazol-1-yl]-1,3-thiazol-4(5H)-one, Proteins – 1JH5,1OQE, 4YJ2 and 4JZJ

5.13 Conclusion

Structure of the BPT2 molecule was investigated using high-level quantum chemistry calculation. The optimized geometrical parameters and vibrational frequency assignment of the fundamental modes of BPT2 molecule have been obtained from DFT/B3LYP/6-31G and DFT/B3LYP/6-31G (d, p) level of calculation. The observed and theoretical wavenumbers are compared and assigned on the basis of potential energy calculations shows the excellent agreement of the calculated and observed spectra. In the Mulliken atomic charges, C40 (=0.448/0.57) has high values for both basis sets. The stability of the molecule arising from hyper-conjugative interaction and charge delocalization has been studied using NBO analysis. The HOMO and LUMO analysis are used to determine the charge transfer within the molecule and the calculated HOMO and LUMO energies show the chemical activity of the molecule. The energy gap of the title molecule is $\Delta E = 3.3557\text{eV}$. From the molecular electrostatic potential plot, it is evident that the negative charge covers the carbonyl group and the positive region is over the remaining groups and the more electronegativity in the carbonyl group makes it the most reactive part of the molecule. The preferred active sites for the electrophilic and nucleophilic reactions are also identified by the Fukui indices of the BPT2 molecule. Weak interaction profile shows that the presence of Van der Waals interactions and steric effect are present in the molecule. Molecular docking analysis reveals that the BPT2 molecule can act as a good inhibitor against the proteins 1JH5, 1OQE, 4YJ2 and 4JZJ.

Table 5.1 Optimized structural parameters of 5-(4-Butoxybenzylidene)-2-[3-(4-chlorophenyl)-5[4-(propan-2-yl)-4,5-dihydro-1H-pyrazol-1-yl]-1,3-thiazol-4(5H)-one obtained by B3LYP/6-31G and B3LYP/6-31G (d,p) basis sets.

Parameters	Bond length (Å)		Parameters	Bond angle (°)		Parameters	Dihedral angle (°)	
	B3LYP/ 6-31G	B3LYP/ 6-31G(D,P)		B3LYP/ 6-31G	B3LYP/ 6-31G(d,p)		B3LYP/ 6-31G	B3LYP/ 6-31G(D,P)
C1-C4	1.4604	1.4628	C4-C1-N24	121.7147	121.788	N24-C1-C4-C5	179.171	178.663
C1-N24	1.3062	1.294	C4-C1-C26	125.171	125.091	N24-C1-C4-C6	-0.574	-1.023
C1-C26	1.5223	1.5184	N24-C1-C26	113.104	113.11	C26-C1-C4-C5	0.425	-0.056
C1-C14	1.5184	1.5174	C14-C2-N25	112.3446	112.421	C26-C1-C4-C6	-179.319	-179.743
C2-N25	1.5078	1.4931	C14-C2-C26	115.1468	114.938	C4-C1-N24-N25	-179.833	179.898
C2-C26	1.5576	1.5519	C14-C2-N25	109.2771	109.088	C26-C1-N24-N25	-0.948	-1.241
C2-H55	1.0919	1.0919	N25-C2-C26	100.1893	100.201	C4-C1-N26-C2	-174.604	-174.939
H3-C26	1.0937	1.0932	N25-C2-H55	107.2673	107.668	C4-C1-C26-H3	-54.509	-54.804
C4-C5	1.4082	1.4042	C26-C2-H55	121.7147	121.788	C4-C1-C26-H28	65.533	65.160
C4-C6	1.4121	1.4083	C1-C4-C5	125.171	125.091	N24-C1-C26-C2	6.557	6.245
C5-C7	1.3979	1.3933	C1-C4-C6	113.104	113.11	N24-C1-C26-H3	126.652	126.379
C5-C8	1.0844	1.0852	C5-C4-C6	112.3446	112.421	N24-C1-C26-H28	-113.306	-113.657
C6-C9	1.3932	1.3882	C4-C5-C7	115.1468	114.9386	N25-C2-C14-C15	68.304	64.354
C6-H10	1.0835	1.0843	C4-C5-H8	109.2771	109.088	N25-C2-C14-C16	-111.460	-115.788
C7-C11	1.392	1.3929	C7-C5-H8	100.1893	100.201	C26-C2-C14-C15	-45.540	-49.422
C7-H12	1.0829	1.084	C4-C6-C9	107.2673	107.668	C26-C2-C14-C16	134.697	130.437
C9-C11	1.3963	1.3978	C4-C6-H10	121.7147	121.788	H55-C2-C14-C15	-172.766	-176.292
C9-H13	1.083	1.0842	C9-C6-H10	125.171	125.091	H55-C2-C14-C16	7.471	3.566
C11-C127	1.8237	1.7554	C5-C7-C11	113.104	113.11	C14-C2-N25-N24	-113.650	-114.317
C14-C15	1.4058	1.4019	C5-C7-H12	112.3446	112.421	C14-C2-N25-C42	69.525	71.318
C14-C16	1.4006	1.3959	C11-C7-H12	115.1468	114.938	C26-C2-N25-N24	9.079	8.210
C15-C17	1.3957	1.3917	C6-C9-C11	109.2771	109.088	C26-C2-N25-C42	-167.745	-166.155

C15-H18	1.0867	1.0872	C6-C9-H13	100.1893	100.201	H55-C2-N25-N24	126.247	125.504
C16-C19	1.3982	1.3951	C11-C9-H13	107.2673	107.668	H55-C2-N25-C42	-50.578	-48.861
C16-H20	1.0849	1.0859	C7-C11-C9	121.7147	121.788	C14-C2-C26-C1	112.154	112.861
C17-C21	1.4076	1.4037	C7-C11-C127	125.171	125.091	C14-C2-C26-C3	-8.727	-7.907
C17-C22	1.086	1.0865	C9-C11-C127	113.104	113.11	C14-C2-C26-H28	-128.840	-128.348
C19-C21	1.4035	1.399	C2-C14-C15	112.3446	112.421	N25-C2-C26-C1	-8.582	-7.874
C19-H23	1.0862	1.087	C2-C14-C16	115.1468	114.939	N25-C2-C26-C3	-129.463	-128.642
C21-C29	1.5261	1.5226	C15-C14-C16	109.2771	109.088	N25-C2-C26-H28	110.424	110.917
N24-N25	1.3915	1.37	C14-C15-C17	100.1893	100.201	H55-C2-C26-C1	-122.075	-121.822
N25-C42	1.3483	1.3513	C14-C15-H18	107.2673	107.668	H55-C2-C26-C3	117.044	117.409
C26-H28	1.0969	1.096	C17-C15-H18	121.7147	121.788	H55-C2-C26-H28	-3.069	-3.032
C29-C30	1.5465	1.5402	C14-C16-C19	125.171	125.091	C1-C4-C5-C7	-179.695	-179.612
C29-C30	1.546	1.5402	C14-C16-H20	113.104	113.11	C1-C4-C5-H8	0.260	0.318
C29-H38	1.0993	1.0978	C19-C16-H20	112.3446	112.421	C6-C4-C5-C7	0.054	0.082
C30-H32	1.0965	1.0953	C15-C17-C21	115.1468	114.938	C6-C4-C5-C8	-179.991	-179.988
C30-H33	1.0953	1.094	C15-C17-H22	109.2771	109.088	C1-C4-C6-C9	179.712	179.627
C30-H34	1.0968	1.0955	C21-C17-H22	100.1893	100.201	C1-C4-C6-H10	-0.241	-0.339
C31-H35	1.0956	1.0944	C16-C19-C21	107.2673	107.668	C5-C4-C6-C9	-0.037	-0.066
C31-H36	1.0966	1.0954	C16-C19-H23	121.7147	121.788	C5-C4-C6-H10	-179.990	179.968
C31-H37	1.0968	1.0956	C21-C19-H23	125.171	125.091	C4-C5-C7-C11	-0.039	-0.047
C39-C40	1.493	1.5081	C17-C21-C19	113.104	113.11	C4-C5-C7-H12	179.976	179.971
C39-S41	1.8656	1.794	C17-C21-C29	112.3446	112.421	H8-C5-C7-C11	-179.994	-179.978
C39-C45	1.3602	1.3596	C19-C21-C29	115.1468	114.939	H8-C5-C7-H12	0.020	0.040
C40-N43	1.4066	1.3966	C1-N24-N25	109.2771	109.088	C4-C6-C9-C11	0.006	0.015
C40-O44	1.2485	1.2232	C2-N25-N24	100.1893	100.201	C4-C6-C9-H13	-179.979	-179.983
S41-C42	1.8391	1.776	C2-N25-C42	107.2673	107.668	H10-C6-C9-C11	179.958	179.981
C42-N43	1.3043	1.2987	N24-N25-C42	121.7147	121.788	H10-C6-C9-H13	-0.027	-0.018

C45-C46	1.4585	1.4571	C1-C26-C2	125.171	125.091	C5-C7-C11-C9	0.006	-0.006
C45-C56	1.0902	1.0904	C1-C26-H3	113.104	113.11	C5-C7-C11-C127	-179.973	-179.967
C46-C47	1.416	1.4105	C1-C26-H28	112.3446	112.421	H12-C7-C11-C9	179.992	179.977
C46-C48	1.4198	1.4156	C2-C26-H3	115.1468	114.939	H12-C7-C11-C127	0.013	0.016
C47-C49	1.3931	1.3906	C2-C26-H28	109.2771	109.088	C6-C9-C11-C7	0.010	0.021
C47-H50	1.0867	1.0872	H3-C26-H28	100.1893	100.201	C6-C9-C11-C127	179.989	179.982
C48-C51	1.3882	1.3839	C21-C29-C30	107.2673	107.668	H13-C9-C11-C7	179.995	-179.980
C48-H52	1.0817	1.082	C21-C29-C31	121.7147	121.788	H13-C9-C11-C127	-0.026	-0.019
C49-C53	1.4036	1.4017	C21-C29-H38	125.171	125.091	C2-C14-C15-C17	179.751	179.385
C49-H57	1.0828	1.0831	C30-C29-C31	113.104	113.11	C2-C14-C15-H18	-0.979	-1.326
C51-C53	1.4054	1.4049	C30-C29-H38	112.3446	112.421	C16-C14-C15-C17	-0.483	-0.476
C51-H54	1.0837	1.0851	C31-C29-H38	115.1468	114.939	C16-C14-C15-H18	178.787	178.813
C53-O58	1.3842	1.3595	C29-C30-H32	109.2771	109.088	C2-C14-C15-C19	-179.424	-179.063
O58-C59	1.4618	1.4285	C29-C30-H33	100.1893	100.201	C2-C14-C16-H20	2.293	2.184
C59-H60	1.0988	1.0996	C29-C30-H34	107.267	107.668	C15-C14-C16-C19	0.806	0.799
C59-H61	1.0988	1.0996	C40-C39-C45	113.104	113.11	C15-C14-C16-H20	-177.477	-177.954
C59-C62	1.5233	1.5217	S41-C39-C45	118.135	118.670	C14-C15-C17-C21	-0.126	-0.137
C62-H63	1.0976	1.0969	C39-C40-N43	113.471	112.705	C14-C15-C17-H22	179.731	179.737
C62-H64	1.0976	1.0969	C39-C40-O44	124.813	124.954	H18-C15-C17-C21	-179.403	-179.432
C62-C65	1.5402	1.5336	N43-C40-O44	121.716	122.339	H18-C15-C17-H22	0.454	0.442
C65-H66	1.1	1.0984	C39-S41-C42	86.313	87.757	C14-C16-C19-C21	-0.532	-0.522
C65-H67	1.1	1.0984	N25-C42-S41	119.688	119.294	C14-C16-C19-H23	-179.815	-179.889
C65-C68	1.5369	1.5315	N25-C42-N43	122.861	122.033	H20-C16-C19-C21	177.745	178.228
C68-H69	1.0969	1.0956	S41-C42-N43	117.447	118.672	H20-C16-C19-H23	-1.538	-1.139
C68-H70	1.0958	1.0945	C40-N43-C42	113.818	112.104	C15-C17-C21-C19	0.407	0.421
C68-H71	1.0969	1.0956	S41-C39-C45	118.135	118.670	C15-C17-C21-C29	179.921	-179.872

Table 5.2 Vibrational assignments of 5-(4-Butoxybenzylidene)-2-[3-(4-chlorophenyl)-5[4-(propan-2-yl)-4,5-dihydro-1H-pyrazol-1-yl]-1,3-thiazol-4(5H)-one by B3LYP/6-31G and B3LYP/6-31G (d,p) method.

Modes	Observed wavenumbers (cm ⁻¹)		Calculated wavenumbers (cm ⁻¹)		Vibrational assignments (%PED)
	FT-IR	FT-Raman	B3LYP/6-31G	B3LYP/6-31G(d,p)	
1		3150	3156	3152	vCH(98)
2			3125	3123	vCH(98)
3			3110	3107	vCH(98)
4			3099	3095	vCH(98)
5			3094	3088	vCH(98)
6		3075	3078	3074	vCH(98)
7			3058	3055	vCH(98)
8			3045	3043	vCH(98)
9			3038	3034	vCH(98)
10			3033	3029	vCH(98)
11			3026	3021	vCH(98)
12			3016	3011	vCH(98)
13		3002	3010	3003	vCH(98)
14			3001	2995	v _{ass} CH ₃ (96)
15			2986	2983	v _{ass} CH ₃ (97)
16			2976	2971	v _{ass} CH ₃ (97)
17			2970	2966	v _{ass} CH ₂ (95)
18			2964	2959	v _{ass} CH ₃ (96)
19			2950	2947	v _{ass} CH ₃ (97)
20			2936	2935	vCH(98)
21	2922		2930	2926	v _{ass} CH ₃ (98)
22			2922	2919	v _{ass} CH ₂ (96)
23		2910	2915	2912	v _{ss} CH ₂ (96)
24			2910	2906	v _{ass} CH ₂ (97)
25			2896	2893	v _{ss} CH ₂ (96)
26			2888	2884	v _{ss} CH ₃ (97)
27			2882	2878	v _{ss} CH ₃ (96)
28			2872	2869	v _{ass} CH ₂ (97)
29	2856		2860	2854	v _{ss} CH ₃ (96)
30			2846	2843	vCH(98)

31			2841	2835	vssCH ₂ (96)
32			2830	2822	vssCH ₂ (96)
33	1679	1680	1683	1680	vCO(72), vCC(20)
34			1644	1641	vCC(70), δCH(18)
35			1625	1623	vCC(71), δCH(20)
36			1613	1604	vCC(70), δCH(22)
37	1591		1596	1590	vCC(68), vCN(12), δCH(10)
38			1579	1572	vCN(65), vCC(14), δCH(10)
39			1563	1559	vCC(64), δCH(14), δCC(11)
40			1538	1533	vCC(60), δCCl(18), vCN(10)
41	1541		1533	1529	vCN(65), vCC(15), δCH(12)
42			1525	1517	vCN(65), vCC(16), δCH(12)
43	1506	1510	1512	1508	δCH(64), vCC(18)
44			1499	1493	δCH(64), vCC(20)
45	1485	1485	1490	1486	δCH(65), vCC(18)
46			1481	1475	δ _{opb} CH ₃ (72)
47			1477	1470	δ _{opb} CH ₃ (75)
48			1472	1466	δ _{opb} CH ₃ (73)
49			1455	1451	δ _{ipb} CH ₃ (73)
50			1442	1436	δ _{ipb} CH ₃ (72)
51			1437	1430	δ _{ipb} CH ₃ (72)
52			1429	1422	σ _{sci} CH ₂ (80)
53		1415	1423	1415	σ _{sci} CH ₂ (80)
54			1420	1408	δCH(65), vCC(21)
55			1414	1403	δCH(66), vCC(22)
56		1400	1408	1399	σ _{sci} CH ₂ (80)
57	1394		1402	1395	σ _{sci} CH ₂ (81)
58			1388	1383	δ _{sb} CH ₃ (75)
59			1385	1379	δ _{sb} CH ₃ (75)
60			1376	1370	δ _{sb} CH ₃ (74)
61			1370	1362	vCN(64)
62		1350	1356	1351	vCN(65), δCH(14)
63			1346	1342	δCO(67)
64	1329		1335	1330	δCH(67)
65			1327	1323	δCH(68)
66		1310	1318	1312	δCH(66), vCC(14)

67			1308	1302	$\delta\text{CH}(66)$, $\nu\text{CC}(15)$
68		1295	1301	1297	$\nu\text{CO}(66)$, $\delta\text{CH}(12)$
69		1280	1285	1281	$\delta\text{CH}(66)$, $\nu\text{CC}(12)$
70			1278	1275	$\delta\text{CH}(66)$, $\nu\text{CC}(12)$, $\nu\text{CN}(10)$
71			1266	1263	$\delta\text{CH}(64)$, $\nu\text{CN}(18)$, $\nu\text{CC}(10)$
72	1254	1250	1260	1254	$\nu\text{CO}(65)$, $\delta\text{CH}(17)$, $\nu\text{CCl}(10)$
73			1248	1244	$\delta\text{CH}(66)$, $\nu\text{CC}(12)$, $\nu\text{CN}(10)$
74	1230		1236	1231	$\nu\text{CC}(63)$, $\delta\text{CH}(16)$, $\nu\text{CN}(12)$
75		1215	1221	1217	$\nu\text{CC}(65)$, $\delta\text{CH}(18)$
76			1214	1207	$\rho\text{rockCH}_2(70)$, $\delta\text{CH}(12)$
77		1200	1210	1200	$\rho\text{rockCH}_2(70)$, $\delta\text{CH}(12)$
78			1195	1191	$\nu\text{CC}(65)$, $\delta\text{CH}(14)$
79			1186	1182	$\nu\text{CC}(66)$, $\delta\text{CH}(15)$
80	1173		1179	1175	$\rho\text{rockCH}_2(70)$
81			1165	1163	$\rho\text{rockCH}_2(69)$
82			1162	1158	$\nu\text{CC}(68)$
83			1145	1143	$\nu\text{CC}(68)$
84			1140	1136	$\nu\text{CC}(68)$
85			1131	1127	$\nu\text{CC}(66)$
86	1118		1125	1120	$\nu\text{CC}(66)$
87			1118	1113	$\tau\text{CH}_2(75)$
88			1110	1105	$\tau\text{CH}_2(75)$
89			1102	1097	$\gamma\text{CH}(60)$
90			1093	1088	$\gamma\text{CH}(60)$
91			1080	1075	$\nu\text{CC}(65)$, $\delta\text{CH}(13)$
92			1056	1051	$\tau\text{CH}_2(75)$
93			1044	1040	$\tau\text{CH}_2(74)$
94			1032	1028	$\gamma_{\text{opr}}\text{CH}_3(62)$, $\nu\text{CC}(10)$
95			1021	1017	$\gamma_{\text{opr}}\text{CH}_3(63)$, $\nu\text{CC}(10)$
96			1013	1009	$\nu\text{CC}(74)$, $\nu\text{CO}(16)$
97	1002		1003	1000	$\gamma_{\text{opr}}\text{CH}_3(64)$
98			992	989	$\nu\text{CC}(66)$, $\delta\text{CH}(15)$
99			984	980	$\delta\text{CO}(66)$, $\delta\text{CH}(14)$
100			965	963	$\delta\text{CO}(65)$, $\delta\text{CH}(12)$
101			960	956	$\gamma\text{CH}(58)$, $\gamma_{\text{ring}}(26)$
102	948	950	953	948	$\gamma\text{CH}(58)$, $\gamma_{\text{ring}}(26)$

103			935	933	$\gamma\text{CH}(58), \gamma_{\text{ring}}(25)$
104			932	929	$\gamma\text{CH}(58), \gamma_{\text{ring}}(21)$
105			925	921	$\nu\text{CC}(72), \nu\text{CO}(15), \delta\text{CH}(10)$
106			924	916	$\nu\text{CC}(63), \delta\text{CH}(18)$
107	909	910	914	910	$\nu\text{CC}(64), \delta\text{CH}(20)$
108			889	885	$\gamma\text{CH}(58), \gamma_{\text{ring}}(18)$
109			883	879	$\nu\text{NN}(65), \delta\text{CH}(18)$
110			867	865	$\gamma\text{CH}(55), \gamma\text{CC}(18)$
111			845	842	$\gamma\text{CC}(18), \delta\text{wagg CH}_2(12)$
112			840	834	$\gamma\text{CH}(62), \gamma_{\text{ring}}(18)$
113	827		833	829	$\gamma\text{CH}(58), \gamma\text{CC}(21)$
114			823	820	$\gamma\text{CH}(58), \gamma\text{CC}(20)$
115			817	812	$\delta_{\text{wagg}} \text{CH}_2(58), \gamma\text{CC}(20)$
116		800	805	802	$\delta_{\text{wagg}} \text{CH}_2(58), \gamma\text{CC}(21)$
117			800	795	$\gamma\text{CH}(56), \gamma\text{CC}(18)$
118			796	790	$\gamma\text{CH}(55), \gamma\text{CC}(17)$
119			792	786	$\delta\text{CC}(63), \delta\text{CH}(18)$
120			785	780	$\delta_{\text{wagg}} \text{CH}_2(57)$
121			779	773	$\gamma\text{CH}(58), \gamma_{\text{ring}}(18)$
122			775	769	$\delta_{\text{wagg}} \text{CH}_2(58), \gamma\text{CC}(20)$
123			768	765	$\delta_{\text{ipr}} \text{CH}_3(68)$
124			760	756	$\delta_{\text{ipr}} \text{CH}_3(68)$
125	747		741	748	$\delta_{\text{ipr}} \text{CH}_3(68)$
126			738	731	$\nu\text{CS}(74), \delta\text{CH}(20)$
127		720	726	720	$\nu\text{CN}(64), \nu\text{CC}(16)$
128			715	711	$\delta\text{CC}(60), \delta_{\text{ipr}} \text{CH}_3(19)$
129			706	700	$\gamma\text{CH}(58), \gamma_{\text{ring}}(16)$
130			697	694	$\nu\text{CS}(75), \delta\text{CH}(20)$
131			690	688	$\delta\text{CC}(60), \delta_{\text{ipr}}(17)$
132			685	679	$\gamma\text{CO}(58)$
133			670	666	$\gamma\text{CC}(68)$
134			664	659	$\gamma\text{CC}(68)$
135			658	655	$\gamma\text{CC}(68)$
136			653	648	$\delta_{\text{ring}}(56)$
137			646	643	$\delta_{\text{ring}}(56)$
138			640	638	$\delta_{\text{ring}}(56)$

139			635	631	$\gamma_{CC}(66)$
140			630	626	$\gamma_{CO}(51), \gamma_{ring}(17)$
141			625	620	$\gamma_{CO}(50), \gamma_{ring}(17)$
142			616	612	$\delta_{CC}(58)$
143			608	603	$\delta_{CC}(59)$
144	597		602	598	$\nu_{CCl}(68), \delta_{ring}(25)$
145			590	586	$\delta_{CC}(58)$
146			588	580	$\delta_{ring}(52)$
147			575	573	$\delta_{CC}(58)$
148			565	561	$\delta_{CC}(58)$
149	551		553	550	$\delta_{ring}(52)$
150			545	541	$\delta_{ring}(53)$
151			539	535	$\delta_{CC}(59)$
152			531	523	$\delta_{ring}(52)$
153			522	518	$\delta_{ring}(50)$
154			510	506	$\delta_{CC}(58)$
155	503	502	503	500	$\delta_{CC}(58)$
156			487	481	$\delta_{ring}(54)$
157			477	472	$\delta_{CC}(59)$
158			480	466	$\delta_{CC}(59)$
159	457		463	460	$\delta_{ring}(55)$
160	438		445	440	$\delta_{CCl}(60), \delta_{ring}(15)$
161			427	422	$\delta_{ring}(52)$
162	411		417	410	$\delta_{ring}(54)$
163			407	401	$\delta_{ring}(50)$
164			392	389	$\delta_{ring}(52)$
165			381	375	$\delta_{ring}(52)$
166			371	366	$\delta_{CC}(53)$
167			360	354	$\delta_{CC}(54)$
168		345	349	345	$\delta_{CC}(54)$
169			337	332	$\delta_{CC}(54)$
170			330	325	$\gamma_{CC}(55)$
171			319	314	$\gamma_{CC}(54)$
172			303	299	$\gamma_{CC}(53)$
173			296	293	$\gamma_{CC}(55)$
174			291	286	$\gamma_{CC}(54)$

175		280	275	γ CCl(55)
176		273	268	γ CC(50)
177		262	259	γ CC(54)
178		246	242	γ CC(50)
179		230	221	τ CH ₃ (55)
180		218	212	τ CH ₃ (54)
181		210	206	τ CH ₃ (54)
182		197	191	γ CC(55)
183		189	185	γ CC(55)
184		176	173	γ CC(55)
185		166	162	δ_{ring} (58)
186	150	158	151	γ CC(55)
187		146	142	δ_{ring} (55)
188	135	141	136	γ CC(56)
189		135	128	γ_{ring} (56)
190	120	126	120	γ CC(56)
191		112	102	δ_{ring} (53)
192	92	95	89	γ_{ring} (54)
193		86	79	γ_{ring} (53)
194		80	74	γ_{ring} (54)
195		75	69	γ_{ring} (53)
196		66	57	γ_{ring} (51)
197		60	49	δ_{ring} (58)
198		52	46	δ_{ring} (58)
199		48	43	δ_{ring} (58)
200	35	41	35	γ_{ring} (54)
201		37	30	γ_{ring} (53)
202		30	24	γ_{ring} (54)
203		25	22	γ_{ring} (54)
204		23	20	γ_{ring} (53)
205		17	16	γ_{ring} (54)
206		12	10	γ_{ring} (54)
207		7	6	γ_{ring} (54)

v-stretching, v_{sym} -sym stretching, v_{asym} -asym stretching, δ -in-plane bending, γ -out-of-plane bending, ρ -scissoring, ω -wagging, σ -rocking, τ -twisting.

Table 5.3 Mulliken atomic charges for 5-(4-Butoxybenzylidene)-2-[3-(4-chlorophenyl)-5[4-(propan-2-yl)-4,5-dihydro-1H-pyrazol-1-yl]-1,3-thiazol-4(5H)-one one by B3LYP/6-31G and B3LYP/6-31G (d,p) basis sets

Atom Numbering	Charge		Atom Numbering	Charge	
	B3LYP/6- 31G	B3LYP/6- 31G(d,p)		B3LYP/6- 31G	B3LYP/6- 31G(d,p)
C1	0.173	0.274	H37	0.132	0.102
C2	-0.031	-0.009	H38	0.129	0.091
H3	0.182	0.142	C39	-0.289	-0.188
C4	0.102	0.098	C40	0.448	0.570
C5	-0.151	-0.130	S41	0.416	0.205
C6	-0.127	-0.101	C42	0.214	0.366
C7	-0.109	-0.078	N43	-0.422	-0.520
H8	0.143	0.097	O44	-0.430	-0.487
C9	-0.107	-0.075	C45	-0.190	-0.154
H10	0.181	0.129	C46	0.118	0.135
C11	-0.228	-0.092	C47	-0.192	-0.145
H12	0.164	0.116	C48	-0.144	-0.120
H13	0.166	0.118	C49	-0.136	-0.137
C14	0.151	0.154	H50	0.131	0.084
C15	-0.163	-0.132	C51	-0.145	-0.130
C16	-0.126	-0.102	H52	0.212	0.150
C17	-0.162	-0.122	C53	0.298	0.361
H18	0.129	0.086	H54	0.146	0.099
C19	-0.178	-0.140	H55	0.180	0.135
H20	0.150	0.101	H56	0.135	0.094
C21	0.142	0.147	H57	0.134	0.088
H22	0.127	0.083	O58	-0.569	-0.529
H23	0.130	0.086	C59	-0.020	0.065
N24	-0.210	-0.324	H60	0.142	0.100
N25	-0.464	-0.324	H61	0.141	0.100
C26	-0.354	-0.289	C62	-0.243	-0.196

Cl27	0.079	-0.010	H63	0.147	0.111
H28	0.182	0.143	H64	0.147	0.111
C29	-0.178	-0.129	C65	-0.251	-0.184
C30	-0.394	-0.305	H66	0.127	0.096
C31	-0.394	-0.304	H67	0.127	0.096
H32	0.132	0.101	C68	-0.403	-0.317
H33	0.145	0.114	H69	0.137	0.107
H34	0.132	0.102	H70	0.134	0.103
H35	0.137	0.106	H71	0.137	0.107
H36	0.133	0.102			

Table 5.4 HOMO-LUMO energies for 5-(4-Butoxybenzylidene)-2-[3-(4-chlorophenyl)-5[4-(propan-2-yl)-4,5-dihydro-1H-pyrazol-1-yl]-1,3-thiazol-4(5H)-one by B3LYP/6-31G (d,p) basis set

Molecular properties	Energy (eV)	Energy gap (eV)	Ionisation potential (I)	Electron affinity (A)	Global hardnessn (η)	Global softness (σ)	Chemical potential (μ)	Global Electroplicity (ω)
E_{HOMO}	-5.3304	3.3521	5.3304	1.9783	1.6761	0.5966	-3.6544	3.9838
E_{LUMO}	-1.9783							
$E_{\text{HOMO-1}}$	-5.9862	4.5911	5.9862	1.3951	2.2955	0.4356	-3.6907	2.9669
$E_{\text{LUMO-1}}$	-1.3951							
$E_{\text{HOMO-2}}$	-6.4777	5.8023	6.4777	0.6754	2.9012	0.3447	-3.5765	2.2045
$E_{\text{LUMO-2}}$	-0.6754							

Table 5.5 Second order perturbation theory analysis of Fock matrix in NBO basis corresponding to intra molecular bands of 5-(4-Butoxybenzylidene)-2-[3-(4-chlorophenyl)-5[4-(propan-2-yl)-4,5-dihydro-1H-pyrazol-1-yl]-1,3-thiazol-4(5H)-one

Donor	Acceptor	E(2)(kcal/mol) ^a	E(J)-E(i) (a.u) ^b	F _(ij) (a.u) ^c
		BMP	BMP	BMP
π (1) N25	$\sigma^*(2)$ C1-N24	26.71	0.24	0.072
π (1) N25	$\sigma^*(1)$ C2 - C14	1.03	0.65	0.024
π (1) N25	$\sigma^*(1)$ C2 - H55	4.15	0.65	0.049
π (1) N25	$\sigma^*(1)$ S41- C42	6.95	0.75	0.068
π (1) N25	$\sigma^*(1)$ C42 - N43	13.03	0.68	0.088
π (1)Cl27	$\sigma^*(1)$ C7 - C11	1.21	1.48	0.038
π (1)Cl27	$\sigma^*(1)$ C9 - C11	1.21	1.48	0.038
π (2)Cl27	$\sigma^*(1)$ C7 - C11	3.88	0.87	0.052
π (2)Cl27	$\sigma^*(1)$ C9 - C11	3.85	0.87	0.052
π (3)Cl27	$\sigma^*(2)$ C7 - C11	12.39	0.32	0.061
π (1) S41	$\sigma^*(1)$ N25 - C42	0.61	0.92	0.021
π (1) S41	$\sigma^*(1)$ C39 - C40	7.95	0.99	0.08
π (1) S41	$\sigma^*(1)$ C40 - O44	0.78	1.04	0.026
π (1) S41	$\sigma^*(1)$ C42 - N43	8.55	0.94	0.08
π (2) S41	$\sigma^*(2)$ C39 - C45	65.56	0.2	0.112
π (2) S41	$\sigma^*(1)$ S41 - C42	0.57	0.76	0.022
π (2) S41	$\sigma^*(2)$ C42 - N43	99.81	0.21	0.133
π (1) N43	$\sigma^*(1)$ N25 - C42	1.76	0.75	0.033
π (1) N43	$\sigma^*(1)$ C39 - C40	5.99	0.81	0.062
π (1) N43	$\sigma^*(1)$ C39 - C45	0.71	0.69	0.02
π (1) N43	$\sigma^*(1)$ C40 - O44	1.54	0.87	0.033
π (1) N43	$\sigma^*(1)$ S41 - C42	5.63	0.84	0.062
π (1) O44	$\sigma^*(1)$ C39 - C40	3.05	1.13	0.054
π (1) O44	$\sigma^*(1)$ C40 - N43	2.31	1.1	0.046
π (2) O44	$\sigma^*(1)$ C39 - C40	18.59	0.69	0.102
π (2) O44	$\sigma^*(1)$ C40 - N43	22.98	0.65	0.111
π (1) O58	$\sigma^*(1)$ C49 - C53	5.89	0.98	0.068
π (1) O58	$\sigma^*(1)$ C51 - C53	1.32	0.98	0.032
π (1) O58	$\sigma^*(2)$ C51 - C53	2.06	0.43	0.029

π (1) O58	$\sigma^*(1)$ C59 - H60	5.28	0.89	0.062
π (1) O58	$\sigma^*(1)$ C59 - H61	0.77	0.89	0.023
π (1) O58	$\sigma^*(1)$ C59 - H62	0.65	0.78	0.02
π (2) O58	$\sigma^*(1)$ C51 - C53	4.53	1.02	0.061
π (2) O58	$\sigma^*(2)$ C51 - C53	3.73	0.47	0.041
π (2) O58	$\sigma^*(1)$ C59 - H61	4.6	0.93	0.059
π (2) O58	$\sigma^*(1)$ C59 - H62	0.54	0.83	0.019

aE(2) means energy of hyperconjugative interactions (stabilization energy).

b Energy difference between donor and acceptor i and j NBO orbitals.

c F(i,j) is the Fock matrix element between i and j NBO orbitals.

Table 5.6 NBO analysis of bonding and antibonding orbit of 5-(4-Butoxybenzylidene)-2-[3-(4-chlorophenyl)-5[4-(propan-2-yl)-4,5-dihydro-1H-pyrazol-1-yl]-1,3-thiazol-4(5H)-one

Band (A-B)	ED/Energy (a.u.)	ED %	ED %	NBO	S(%)	P(%)
BD (1)C1 - C4	1.97159	50.09	49.91	0.7077 SP ^(1.71)	36.84	63.16
	-0.63884			0.7065 SP ^(2.42)	29.2	70.8
BD(1)C1-N24	1.98456	41.16	58.84	0.6416 SP ^(2.53)	28.3	71.7
	-0.80876			0.7671 SP ^(1.84)	35.16	64.84
BD(1) C1 -C26	1.97344	47.4	52.6	0.6885 SP ^(1.87)	34.82	65.18
	-0.71406			0.6416 SP ^(2.48)	28.72	71.28
BD (1) C2 - C14	1.96718	52.33	47.67	0.7234 SP ^(2.08)	32.46	67.54
	-0.62372			0.6905 SP ^(2.51)	28.53	71.47
BD (1)C2 - N25	1.97696	39.59	60.41	0.6292 SP ^(2.92)	25.5	74.5
	-0.801			0.7773 SP ^(1.85)	35.08	64.92
BD(1) C2 - C26	1.96517	50.31	49.69	0.7093 SP ^(2.03)	33.04	66.96
	-0.71298			0.7049 SP ^(2.48)	28.73	71.27
BD(1) C4 - C5	1.97386	51.06	48.94	0.7146 SP ^(1.80)	35.69	64.31
	-0.71857			0.6995 SP ^(1.87)	34.84	65.16
BD (1) C4 - C6	1.97513	51.33	48.67	0.7165 SP ^(1.85)	35.12	64.88
	-0.71323			0.6976 SP ^(1.86)	34.97	65.03
BD(1) C5 - C7	1.96991	50.02	49.98	0.7073 SP ^(1.81)	35.55	64.45
	-0.71337			0.7070 SP ^(1.80)	35.76	64.24

BD (1) C6 - C9	1.97082	49.7	50.3	0.7050 SP ^(1.86)	35	65
	-0.70844			0.7092 SP ^(1.79)	35.82	64.18
BD(1) C7 - C11	1.98087	49.11	50.89	0.7008 SP ^(1.88)	34.78	65.22
	-0.73732			0.7134 SP ^(1.59)	38.63	61.37
BD(1) C9 - C11	1.98117	48.98	51.02	0.6999 SP ^(1.89)	34.66	65.34
	-0.7368			0.7142 SP ^(1.58)	38.73	61.27
BD(1)C11 -C127	1.98944	45.42	54.58	0.6740 SP ^(3.42)	22.62	77.38
	-0.72494			0.7388 SP ^(5.04)	16.55	83.45
BD(1) C14 - C15	1.97178	51.34	48.66	0.7165 SP ^(1.78)	36.03	63.97
	-0.70477			0.6976 SP ^(1.88)	34.77	65.23
BD(2) C14 - C15	1.67259	49.99	50.01	0.7070 SP ^(99.99)	0.08	99.92
	-0.25609			0.7072 SP ⁽¹⁾		100
BD(1) C14 -C16	1.97342	51.23	48.77	0.7158 SP ^(1.83)	35.37	64.63
	-0.70356			0.6983 SP ^(1.88)	34.72	65.28
BD(1) C15 - C17	1.97468	50.24	49.76	0.7088 SP ^(1.78)	35.97	64.03
	-0.69332			0.7054 SP ^(1.83)	35.36	64.64
BD(1)C16 - C19	1.97521	50.2	49.8	0.7085 SP ^(1.80)	35.74	64.26
	-0.69142			0.7057 SP ^(1.83)	35.38	64.62
BD(1) C17 - C21	1.97314	49.13	50.87	0.7009 SP ^(1.85)	35.07	64.93
	-0.69629			0.7132 SP ^(1.86)	34.98	65.02
BD(1) C21 - C29	1.97443	49.86	50.14	0.7061 SP ^(2.34)	29.97	70.03
	-0.60131			0.7081 SP ^(2.34)	29.98	70.02
BD(1) N24 -N25	1.97507	44.83	55.17	0.6695 SP ^(3.88)	20.51	79.49
	-0.78688			0.7428 SP ^(2.67)	27.27	72.73
BD(1) N25 - C42	1.98189	59.45	40.55	0.770 SP ^(1.68)	37.38	62.62
	-0.84789			0.6368 SP ^(2.05)	32.83	67.17
BD(1) C29 - C30	1.98383	51.43	48.57	0.7171 SP ^(2.35)	29.89	70.11
	-0.58926			0.6969SP ^(2.88)	25.8	74.2
BD(1) C29 - C31	1.98381	51.46	48.54	0.7173 SP ^(2.34)	29.91	70.09
	-0.58907			0.6967SP ^(2.88)	25.78	74.22
BD(1) C39 - C40	1.98003	54.87	45.13	0.7407 SP ^(2.03)	33.02	66.98
	-0.73383			0.6718 SP ^(1.84)	35.17	64.83

BD(1) C39 - S41	1.9775	53.47	46.53	0.7407 SP ^(2.03)	33.57	66.43
	-1.05001			0.6718 SP ^(1.84)	33	67
BD(1) C39 - C45	1.97467	5.05	45.95	0.7352 SP ^(2.00)	33.34	66.66
	-0.67297			0.6778 SP ^(2.1)	32.3	67.7
BD(1) C40 - N43	1.98023	41.41	58.59	0.6435 SP ^(2.21)	31.15	68.85
	-0.78584			0.7655 SP ^(2.29)	30.42	69.58
BD(1) C40 - O44	1.99419	36.24	63.76	0.6020 SP ^(2.02)	33.14	66.86
	-1.01876			0.7985 SP ^(2.29)	36.44	63.56
BD(1) C45 - C46	1.97996	49.65	50.35	0.7046 SP ^(1.89)	34.63	65.37
	-0.64813			0.7096 SP ^(2.52)	28.44	71.56
BD(1) C46 - C47	1.97007	51.3	48.7	0.7162 SP ^(1.82)	35.49	64.51
	-0.71492			0.6979 SP ^(1.86)	34.91	65.09
BD(1) C46 - C48	1.96789	51.21	48.79	0.7156 SP ^(1.77)	36.06	63.94
	-0.71737			0.6985 SP ^(1.87)	34.9	65.1
BD(2) C46 - C48	1.66959	52.13	47.87	0.7220 SP ^(99.99)	0.02	99.98
	-0.26411			0.6919 SP ^(99.99)	0.02	99.98
BD(1) C47 - C49	1.97212	50.01	49.99	0.7072 SP ^(1.83)	35.34	64.66
	-0.70351			0.7070 SP ^(1.84)	35.17	64.83
BD(1) C49 - C53	1.97919	50.13	49.87	0.7080 SP ^(1.89)	34.61	65.39
	-0.71706			0.7062 SP ^(1.65)	37.72	62.28
BD(1) C51 - C53	1.9797	50.14	49.86	0.7080 SP ^(1.86)	35.01	64.99
	-0.71924			0.7061 SP ^(1.65)	37.79	62.21
BD(2) C53 - O58	1.98738	33.99	66.01	0.5830 SP ^(3.11)	24.31	75.69
	-0.81114			0.8124 SP ^(2.83)	26.08	73.92
BD(1) O58 - C59	1.97868	67.56	32.44	0.8219 SP ^(2.9)	25.61	74.39
	-0.79178			0.5696 SP ^(4.02)	19.92	80.08
BD(1) C59 - C62	1.98311	50.39	49.61	0.7099 SP ^(2.58)	27.96	72.04
	-0.58843			0.7043 SP ^(2.98)	25.12	74.88
BD(1) C62 - C65	1.97916	50.45	49.81	0.7085 SP ^(2.85)	26	74
	-0.57455			0.7057 SP ^(2.88)	25.78	74.22

Table 5.7 Fukui function (f_i^+ , f_i^- , Δf) for 5-(4-Butoxybenzylidene)-2-[3-(4-chlorophenyl)-5[4-(propan-2-yl)-4,5-dihydro-1H-pyrazol-1-yl]-1,3-thiazol-4(5H)-one

Atoms number	Neutral (N)	Cation (N-1)	Anion (N+1)	f_k^+	f_k^-	f_k^0	Δf	S_k^+	S_k^-	S_k^0	ω_k^+	ω_k^-	ω_k^0
C1	0.1848	0.1603	0.2373	0.0525	0.0245	0.0385	0.0280	0.0202	0.0094	0.0148	0.1716	0.0801	0.1258
C2	0.0320	0.0368	0.0097	-0.0223	-0.0048	-0.0135	-0.0175	-0.0086	-0.0019	-0.0052	-0.0728	-0.0157	-0.0443
H3	0.1634	0.1388	0.2464	0.0830	0.0246	0.0538	0.0584	0.0320	0.0095	0.0207	0.2713	0.0804	0.1758
C4	0.1136	0.1148	0.1135	-0.0001	-0.0012	-0.0006	0.0011	0.0000	-0.0005	-0.0002	-0.0002	-0.0039	-0.0021
C5	-0.1550	-0.1625	-0.1416	0.0134	0.0075	0.0104	0.0060	0.0052	0.0029	0.0040	0.0438	0.0244	0.0341
C6	-0.1261	-0.1322	-0.1106	0.0155	0.0061	0.0108	0.0094	0.0060	0.0024	0.0042	0.0507	0.0201	0.0354
C7	-0.1118	-0.1145	-0.1037	0.0081	0.0027	0.0054	0.0054	0.0031	0.0010	0.0021	0.0264	0.0087	0.0176
H8	0.1488	0.1406	0.1599	0.0112	0.0082	0.0097	0.0030	0.0043	0.0032	0.0037	0.0365	0.0268	0.0316
C9	-0.1213	-0.1250	-0.1139	0.0074	0.0037	0.0056	0.0037	0.0029	0.0014	0.0021	0.0243	0.0122	0.0182
H10	0.1735	0.1716	0.1968	0.0233	0.0019	0.0126	0.0214	0.0090	0.0007	0.0048	0.0762	0.0062	0.0412
C11	-0.2604	-0.2633	-0.2557	0.0047	0.0030	0.0038	0.0017	0.0018	0.0011	0.0015	0.0152	0.0097	0.0125
H12	0.1571	0.1369	0.1913	0.0342	0.0202	0.0272	0.0140	0.0132	0.0078	0.0105	0.1118	0.0660	0.0889
H13	0.1597	0.1420	0.1951	0.0354	0.0177	0.0266	0.0177	0.0136	0.0068	0.0102	0.1157	0.0579	0.0868
C14	0.1599	0.1434	0.1575	-0.0023	0.0164	0.0070	-0.0188	-0.0009	0.0063	0.0027	-0.0077	0.0537	0.0230
C15	-0.1739	-0.1764	-0.1598	0.0141	0.0026	0.0083	0.0115	0.0054	0.0010	0.0032	0.0461	0.0084	0.0272
C16	-0.1404	-0.1373	-0.1256	0.0148	-0.0031	0.0058	0.0179	0.0057	-0.0012	0.0022	0.0483	-0.0102	0.0190
C17	-0.1747	-0.1817	-0.1596	0.0151	0.0071	0.0111	0.0081	0.0058	0.0027	0.0043	0.0494	0.0231	0.0362
H18	0.1309	0.1161	0.1509	0.0200	0.0148	0.0174	0.0053	0.0077	0.0057	0.0067	0.0655	0.0483	0.0569
C19	-0.1898	-0.2003	-0.1750	0.0149	0.0105	0.0127	0.0044	0.0057	0.0040	0.0049	0.0486	0.0342	0.0414
H20	0.1341	0.1947	0.1580	0.0240	-0.0607	-0.0183	0.0846	0.0092	-0.0234	-0.0071	0.0783	-0.1983	-0.0600
C21	0.1260	0.1273	0.1282	0.0022	-0.0014	0.0004	0.0036	0.0009	-0.0005	0.0002	0.0073	-0.0045	0.0014
H22	0.1307	0.1070	0.1692	0.0386	0.0236	0.0311	0.0149	0.0149	0.0091	0.0120	0.1261	0.0773	0.1017
H23	0.1333	0.1321	0.1685	0.0352	0.0012	0.0182	0.0340	0.0136	0.0005	0.0070	0.1151	0.0040	0.0595
N24	-0.1983	-0.1929	-0.1623	0.0360	-0.0054	0.0153	0.0414	0.0139	-0.0021	0.0059	0.1177	-0.0176	0.0501
N25	-0.5314	-0.5112	-0.4731	0.0582	-0.0202	0.0190	0.0784	0.0224	-0.0078	0.0073	0.1905	-0.0660	0.0622

C26	-0.4241	-0.4103	-0.4772	-0.0532	-0.0137	-0.0335	-0.0394	-0.0205	-0.0053	-0.0129	-0.1738	-0.0450	-0.1094
C127	0.1175	0.0766	0.1986	0.0811	0.0409	0.0610	0.0401	0.0312	0.0158	0.0235	0.2651	0.1339	0.1995
H28	0.1818	0.1585	0.2410	0.0592	0.0233	0.0412	0.0359	0.0228	0.0090	0.0159	0.1936	0.0761	0.1348
C29	-0.2083	-0.2031	-0.2222	-0.0138	-0.0053	-0.0096	-0.0086	-0.0053	-0.0020	-0.0037	-0.0452	-0.0172	-0.0312
C30	-0.4171	-0.4174	-0.4187	-0.0016	0.0003	-0.0006	-0.0019	-0.0006	0.0001	-0.0002	-0.0052	0.0009	-0.0021
C31	-0.4180	-0.4172	-0.4195	-0.0015	-0.0007	-0.0011	-0.0008	-0.0006	-0.0003	-0.0004	-0.0050	-0.0024	-0.0037
H32	0.1395	0.1262	0.1641	0.0246	0.0134	0.0190	0.0112	0.0095	0.0051	0.0073	0.0804	0.0437	0.0621
H33	0.1434	0.1413	0.1467	0.0033	0.0021	0.0027	0.0012	0.0013	0.0008	0.0010	0.0107	0.0068	0.0088
H34	0.1411	0.1306	0.1627	0.0216	0.0105	0.0161	0.0111	0.0083	0.0040	0.0062	0.0706	0.0344	0.0525
H35	0.1465	0.1548	0.1489	0.0024	-0.0083	-0.0030	0.0107	0.0009	-0.0032	-0.0011	0.0078	-0.0271	-0.0097
H36	0.1396	0.1239	0.1642	0.0247	0.0156	0.0201	0.0090	0.0095	0.0060	0.0078	0.0806	0.0511	0.0659
H37	0.1400	0.1336	0.1612	0.0212	0.0064	0.0138	0.0149	0.0082	0.0025	0.0053	0.0695	0.0208	0.0451
H38	0.1946	0.1881	0.2177	0.0231	0.0065	0.0148	0.0165	0.0089	0.0025	0.0057	0.0755	0.0214	0.0484
C39	-0.2852	-0.3236	-0.2976	-0.0123	0.0383	0.0130	-0.0507	-0.0048	0.0148	0.0050	-0.0404	0.1253	0.0425
C40	0.3617	0.3282	0.3673	0.0056	0.0335	0.0195	-0.0279	0.0021	0.0129	0.0075	0.0182	0.1095	0.0638
S41	0.4886	0.3866	0.5339	0.0453	0.1020	0.0736	-0.0568	0.0174	0.0393	0.0284	0.1480	0.3337	0.2408
C42	-0.0124	-0.0630	-0.0243	-0.0120	0.0506	0.0193	-0.0625	-0.0046	0.0195	0.0074	-0.0391	0.1654	0.0632
N43	-0.2757	-0.3528	-0.2499	0.0257	0.0772	0.0514	-0.0514	0.0099	0.0297	0.0198	0.0841	0.2523	0.1682
O44	-0.4001	-0.5431	-0.3416	0.0585	0.1430	0.1008	-0.0845	0.0225	0.0551	0.0388	0.1913	0.4677	0.3295
C45	-0.0456	-0.1487	-0.0257	0.0199	0.1031	0.0615	-0.0832	0.0077	0.0397	0.0237	0.0651	0.3373	0.2012
C46	0.0363	0.0787	0.0267	-0.0096	-0.0424	-0.0260	0.0328	-0.0037	-0.0163	-0.0100	-0.0313	-0.1386	-0.0850
C47	-0.1131	-0.1109	-0.1165	-0.0034	-0.0021	-0.0028	-0.0013	-0.0013	-0.0008	-0.0011	-0.0113	-0.0070	-0.0091
C48	-0.1357	-0.1405	-0.1362	-0.0005	0.0047	0.0021	-0.0052	-0.0002	0.0018	0.0008	-0.0016	0.0155	0.0069
C49	-0.1117	-0.1230	-0.1069	0.0048	0.0113	0.0081	-0.0065	0.0018	0.0044	0.0031	0.0157	0.0370	0.0264
H50	0.1466	0.1225	0.1493	0.0027	0.0241	0.0134	-0.0215	0.0010	0.0093	0.0052	0.0088	0.0790	0.0439
C51	-0.1149	-0.1250	-0.1104	0.0045	0.0102	0.0073	-0.0057	0.0017	0.0039	0.0028	0.0147	0.0333	0.0240
H52	0.1449	0.1226	0.1447	-0.0002	0.0223	0.0111	-0.0225	-0.0001	0.0086	0.0043	-0.0006	0.0729	0.0362
C53	0.2482	0.2348	0.2526	0.0045	0.0134	0.0089	-0.0089	0.0017	0.0052	0.0034	0.0146	0.0437	0.0292
H54	0.1470	0.1064	0.1614	0.0144	0.0406	0.0275	-0.0262	0.0055	0.0156	0.0106	0.0470	0.1327	0.0899

H55	0.2243	0.2211	0.2943	0.0700	0.0032	0.0366	0.0668	0.0270	0.0012	0.0141	0.2289	0.0103	0.1196
H56	0.1751	0.0915	0.1894	0.0143	0.0836	0.0490	-0.0694	0.0055	0.0322	0.0189	0.0467	0.2735	0.1601
H57	0.1420	0.1029	0.1569	0.0149	0.0391	0.0270	-0.0241	0.0057	0.0150	0.0104	0.0487	0.1277	0.0882
O58	-0.5454	-0.5607	-0.5382	0.0072	0.0152	0.0112	-0.0080	0.0028	0.0059	0.0043	0.0236	0.0498	0.0367
C59	-0.0223	-0.0026	-0.0313	-0.0091	-0.0196	-0.0143	0.0106	-0.0035	-0.0076	-0.0055	-0.0296	-0.0642	-0.0469
H60	0.1280	0.1187	0.1320	0.0040	0.0093	0.0067	-0.0053	0.0016	0.0036	0.0026	0.0132	0.0304	0.0218
H61	0.1278	0.1196	0.1311	0.0033	0.0082	0.0057	-0.0049	0.0013	0.0032	0.0022	0.0108	0.0268	0.0188
C62	-0.2397	-0.2380	-0.2406	-0.0009	-0.0017	-0.0013	0.0008	-0.0003	-0.0007	-0.0005	-0.0029	-0.0056	-0.0043
H63	0.1433	0.1344	0.1473	0.0040	0.0089	0.0064	-0.0048	0.0015	0.0034	0.0025	0.0131	0.0290	0.0211
H64	0.1416	0.1334	0.1451	0.0034	0.0082	0.0058	-0.0048	0.0013	0.0032	0.0022	0.0113	0.0268	0.0191
C65	-0.2554	-0.2517	-0.2572	-0.0018	-0.0037	-0.0028	0.0019	-0.0007	-0.0014	-0.0011	-0.0060	-0.0121	-0.0090
H66	0.1282	0.1242	0.1300	0.0018	0.0040	0.0029	-0.0021	0.0007	0.0015	0.0011	0.0060	0.0129	0.0095
H67	0.1279	0.1244	0.1294	0.0014	0.0035	0.0025	-0.0021	0.0006	0.0014	0.0010	0.0047	0.0116	0.0081
C68	-0.4018	-0.4019	-0.4016	0.0002	0.0001	0.0001	0.0001	0.0001	0.0000	0.0001	0.0007	0.0003	0.0005
H69	0.1370	0.1319	0.1397	0.0027	0.0052	0.0039	-0.0025	0.0010	0.0020	0.0015	0.0088	0.0169	0.0128
H70	0.1324	0.1208	0.1386	0.0063	0.0115	0.0089	-0.0053	0.0024	0.0044	0.0034	0.0205	0.0377	0.0291
H71	0.1367	0.1318	0.1391	0.0024	0.0049	0.0036	-0.0025	0.0009	0.0019	0.0014	0.0077	0.0160	0.0119

Table 5.8 Topological parameters for intramolecular interactions in compound electron density (ρ_{BCP}), Laplacian of electron density (∇^2_{BCP}), electron kinetic energy density (G_{BCP}), electron potential energy density (V_{BCP}), total electron energy density (H_{BCP}), Hydrogen bond energy (E_{HB}) at bond critical point (BCP).

Interactions	ρ_{BCP}	∇^2_{BCP}	G_{BCP}	V_{BCP}	H_{BCP}	E_{HB}
O44.....H52	0.03021	0.1179	0.03249	-0.0355	0.0263	-0.0177

Table 5.9 Binding affinity for docking in 5-(4-Butoxybenzylidene)-2-[3-(4-chlorophenyl)-5[4-(propan-2-yl)-4,5-dihydro-1H-pyrazol-1-yl]-1,3-thiazol-4(5H)-one

Drug	Protein	Type of activity	Binding affinity(kcal/mol)	Etimated inhibition constant Ki(μ M)	Bonded residues	Nature of bond	Bond distance (\AA)	RMSD
In 5-(4-Butoxybenzylidene)-2-[3-(4-chlorophenyl)-5[4-(propan-2-yl)-4,5-dihydro-1H-pyrazol-1-yl]-1,3-thiazol-4(5H)-one	1OQE	Antitumer	-4.7	360.43	ASN A-42	Conventional hydrogen bond	3.31	87.206
			-4.33	667.85	PRO A-15	Alkyl	4.1	71.635
			-4.19	845.86	ILE A-15	Alkyl	4.17	78.414
			-3.97	1.23(mM)	GLU A-41	Conventional hydrogen bond	4.32	81.106
			-3.8	1.64 (mM)	ASN A-42	Conventional hydrogen bond	4.55	82.083
	4YJ2	Anticancer	-4.7	358.4	LEU A-397	Alkyl	3.72	80.983
			-4.6	426.72	PRO A-175	Alkyl	3.82	121.029
			-4.21	817.23	PRO A-173	π -alkyl	4.24	111.228
			-4.57	447.01	PRO A-184	π -alkyl	4.39	87.283
			-4.53	482.07	GLN A-176	Carbon hydrogen bond	4.55	94.627
	4YJE	Antitumer	-5.42	106.41	MET A-438	Conventional hydrogen bond	3.64	49.944
			-5.42	106.79	MET A-438	Conventional hydrogen bond	3.8	47.995
			-5.32	126.67	TYR A-486	carbon hydrogen bond	3.89	48.812
			-5.2	155.59	MET A-438	Conventional hydrogen bond	4.02	33.732
			-4.95	234.91	MET A-438	Conventional hydrogen bond	4.17	25.064
	4JZJ	Antiviral	-5.17	163.56	PHE A: 107	van der waals	3.85	36.106
			-4.95	236.07	TRP A: 47	van der waals	4.65	36.427
-4.49			514.73	PHE A: 107	van der waals	4.94	30.374	
-4.23			790.86	TRP A: 106	π - π Stacked	5.05	38.123	
-4.2			838.87	LEU A: 45	π - π Stacked	5.08	32.471	

Chapter – 6

FT-IR and FT-Raman investigation, quantum chemical analysis and molecular docking studies of (4Z)-4-(4-Methylbenzylidene)-2-phenyl-1,3-oxazol-5(4H)-one

FT-IR and FT-Raman investigation, quantum chemical analysis and molecular docking studies of (4Z)-4-(4-Methylbenzylidene)-2-phenyl-1,3-oxazol-5(4H)-one

6.1 Introduction

The biological study of heterocyclic compounds has been interesting field for a long time [184] and oxazole is one such moiety which has gained attention in recent times due to its increasing importance in the field of medicinal chemistry. Oxazole is an important heterocyclic nucleus having a wide spectrum of biological activities and its derivatives used in various biological activities. Oxazole derivatives play a pivotal role in delineating the biological activities like antimicrobial [185], anticancer [186], antitubercular [187], anti-inflammatory [188], antidiabetic [189], antiobesity [190] and antioxidant [191]. Based on the literature review, we have found that quantum chemical calculations, FT-IR, FT-Raman spectroscopic studies, Reduced density gradient (RDG) analysis and docking studies of (4Z)-4-(4-Methylbenzylidene)-2-phenyl-1,3-oxazol-5(4H)-one (MBO) have not been reported. To interpret and predict the vibrational spectra of the MBP compound, the quantum chemical computational methods have been used as an effective tool. Hence, in this study, the results reported here are based on the experimental and theoretical interpretations of the infrared and Raman spectra, which agree and support each other. In addition to vibrational spectra, electrostatic potential should aid in understanding the structural, spectral, and bioactive properties of the MBO

compound of this class. Furthermore, the HOMO-LUMO, NBO analysis and Fukui function of MBO compound have been studied by B3LYP level with 6-31G (d,p) basis set implemented in the Gaussian 09 program suite [36]. RDG analysis has been performed on the molecule to analyze H-bonds, steric effects, and Van der Waals interactions. The Molecular Docking studies have been conducted to evaluate the biological potential of the MBO compound.

6.2 Experimental details

Fourier transform infrared (FT-IR) spectrum of (4Z)-4-(4-Methylbenzylidene)-2-phenyl-1,3-oxazol-5(4H)-one (MBO) was recorded employing the Perkin Elmer spectrometer fitted with a KBr beam splitter around 4000-450 cm^{-1} . Bruker RFS 27 FT-Raman spectrometer was used to report the FT-Raman spectrum in the region 4000-0 cm^{-1} using a 1064 nm Nd: YAG laser source. Both the spectral measurements were performed at the Sophisticated Analytical Instrumentation Facility (SAIF), IIT, Chennai, India.

6.3 Computational details

All calculations presented in this study were performed with the Gaussian 09W program [36] and Gauss view [75]. By DFT calculations, B3LYP functional combined with 6-31G and 6-31G (d,p) basis sets to predict the molecular structure and vibrational wave numbers. The natural bonding orbital calculations were performed using the NBO program as implemented in Gaussian 09 Package. The Reduced Density Gradient (RDG) analysis of the MBO molecule are graphed by Multiwfn [76] and plotted by the VMD

program [77]. The molecular docking calculations were performed with the Autodock Tools version 1.5.6 software package [78] and the docking results were analyzed using Pymol [79] and Discovery studio [80] visualization software. The three dimensional crystal structure of DNA was obtained from the Protein data bank PDB ID.

6.4 Results and discussions

6.4.1 Molecular geometry

The optimized geometrical structure and parameters of the MBO compound obtained using DFT at B3LYP/6-31G and B3LYP/6-31G (d,p) level are shown in Fig.6.1 and Table 6.1 respectively. The MBO compound contains 17 C-C bonds, 12 C-H bonds, 3 C-O bonds and 2 C-N bonds.

The bond length C1-C2, C1-C6, C2-C3, C5-C6, C15-C16, C19-C20, C19-C21, C22-C26, C24-C26 values are 1.3965 / 1.3932, 1.4003 / 1.396, 1.4071 / 1.4034, 1.4026 / 1.3986, 1.4987 / 1.5023, 1.4361 / 1.4327, 1.436 / 1.4333, 1.4122 / 1.4089 which are high due to the presence of benzene ring and also are good agreement with Benzon *et al* [192] that C22-C24, C21-C23 are 1.4988 and 1.4923 Å. For the MBO compound, C18-C19, C20-C22, C21-C24 has bond length values are 1.3737/1.3692, 1.3857/1.3823, 1.3858/1.3814 which is good agreement with the reported value [193].

The C-H bond length lies between 1.08 and 1.09 Å for the phenyl ring. Here for the MBO compound, C1-H7, C2-H8, C4-H9, C5-H10, C6-H11, C20-H23, C21-H25, C22-H27, C24-H28, C29-H30, C29-H31, C29-H32 are 1.0849/1.0857, 1.0834/1.0841, 1.084/1.0845, 1.085/1.0857, 1.0854/1.086, 1.0841/1.0845, 1.0841/1.0846, 1.0863/1.087, 1.0863/1.0871, 1.0952/1.0938, 1.0995/1.098, 1.0952/1.0944 are very close to the reported

value. The C-O bond length of the MBO compound of C12-O14, C16-O14, C16-O17 are 1.4204/1.3899, 1.4316/1.4015, 1.2189/1.1976 which are close agreement with reported values C3-O11 = 1.3959 Å and C12-O11 = 1.4565 Å [194].

The C-N bond distance for the MBO compound, C12-N13, N13=C15 has 1.3003/1.2894, 1.4354/1.416 Å was found to be much shorter than the average value for a C-N single bond (1.47Å) but significantly longer than a C=N double bond (1.22Å) [195], suggesting that some multiple bond character is presented. Haress *et al* [194] assigned the C-N bond length of C24-N5 = 1.2951/1.2933 Å and C7-N4 = 1.2947/1.2923 Å which are close to the MBO compound. Purkayastha and Chattopadhyay *et al* [196] reported N14-C13, N14-C19 bond lengths as 1.3270 Å, 1.400 Å which are close related to our title compound. For the MBO compound, the bond angle for C2-C1-C6, C1-C2-C3 is 120.19/120.18°, 119.77/119.81° which is in good agreement with the reported values (120.4° and 120°) and C3-C4-C5, C1-C6-C5 has 119.83°/119.87°, 120.05°/120.06° are close to Benzon *et al* [194] observed at 120.7° and 118.1°. For the MBO compound, N13-C15-C16 = 108.11°/107.91°, N13-C15-C18 = 126.37°/127.53°, C16-C15-C18 = 126.52°/124.56° which is due to the interaction between the oxazole and the benzene ring.

It is clearly seen that the dihedral angles C4-C3-C12-O14, C2-C3-C12-N13 are 180° and C2-C3-C12-O14, C4-C3-C12-N13 are 0°. This indicates that the benzene ring and the oxazole ring moieties of the MBO compound is planner.

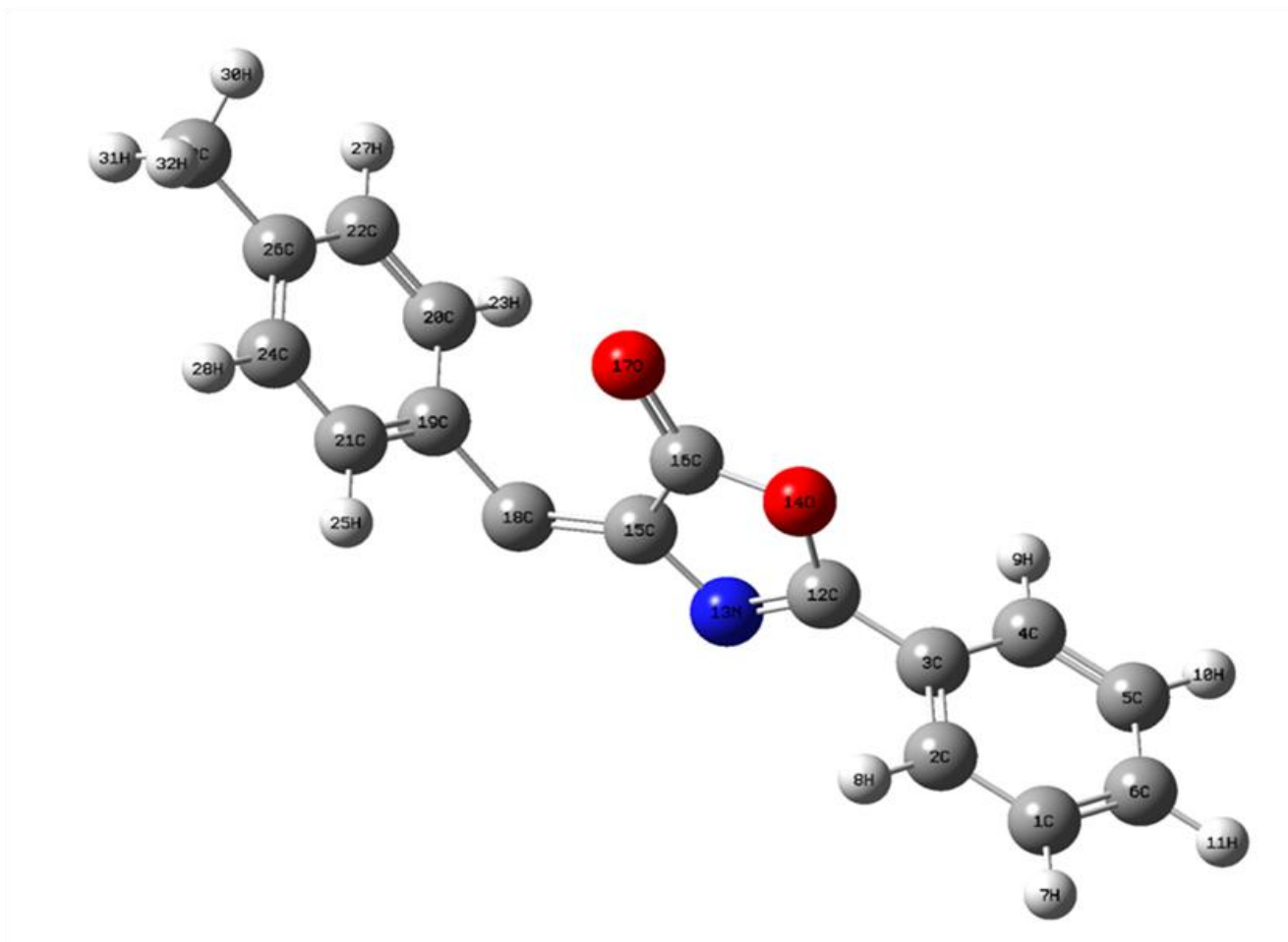


Fig 6.1 Optimized molecular structure of (4Z)-4-(4-Methylbenzylidene)-2-phenyl-1,3-oxazol-5(4H)-one

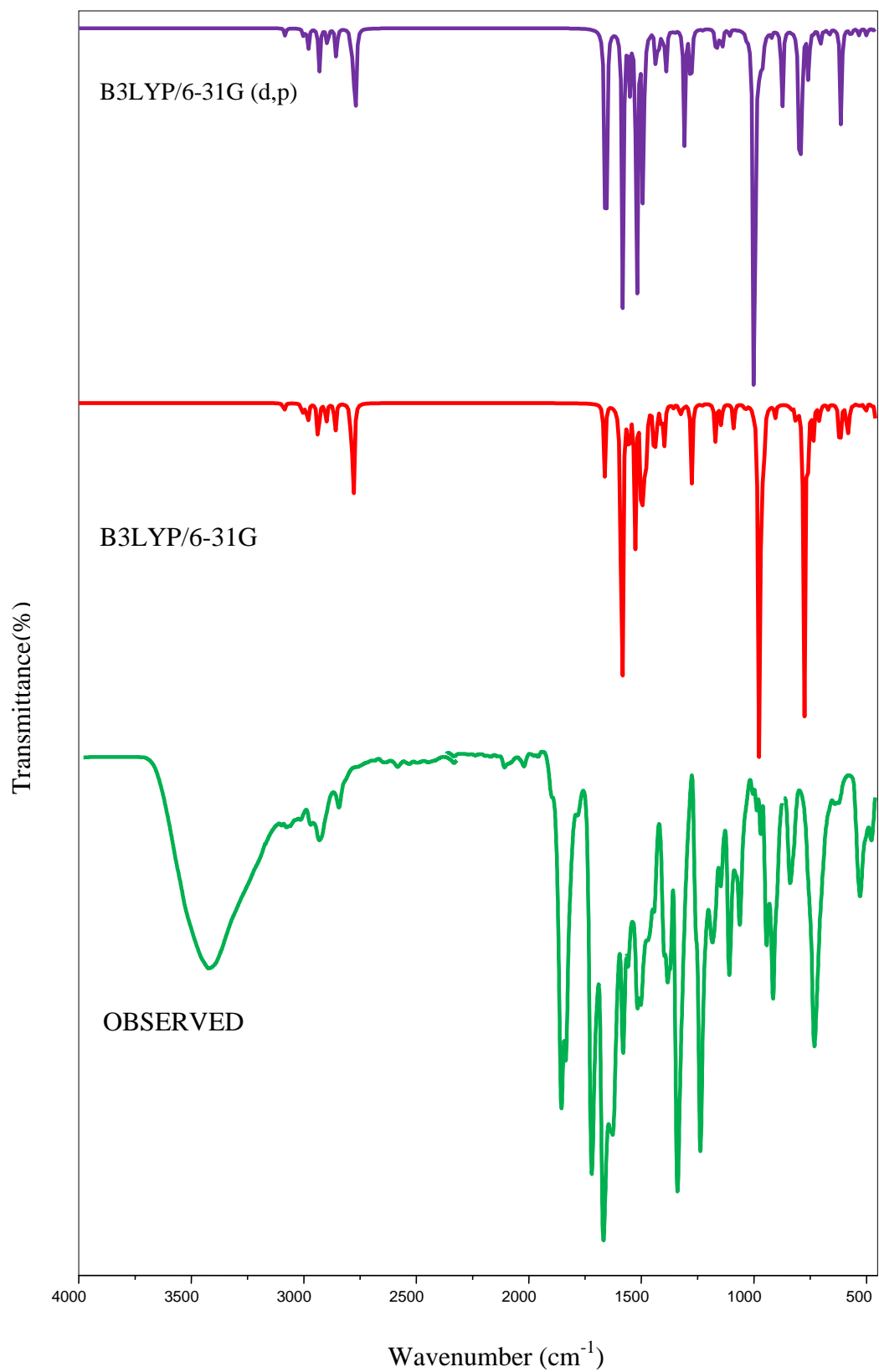


Fig 6.2 Observed FT-IR and simulated spectra of (4Z)-4-(4-Methylbenzylidene)-2-phenyl-1,3-oxazol-5(4H)-one

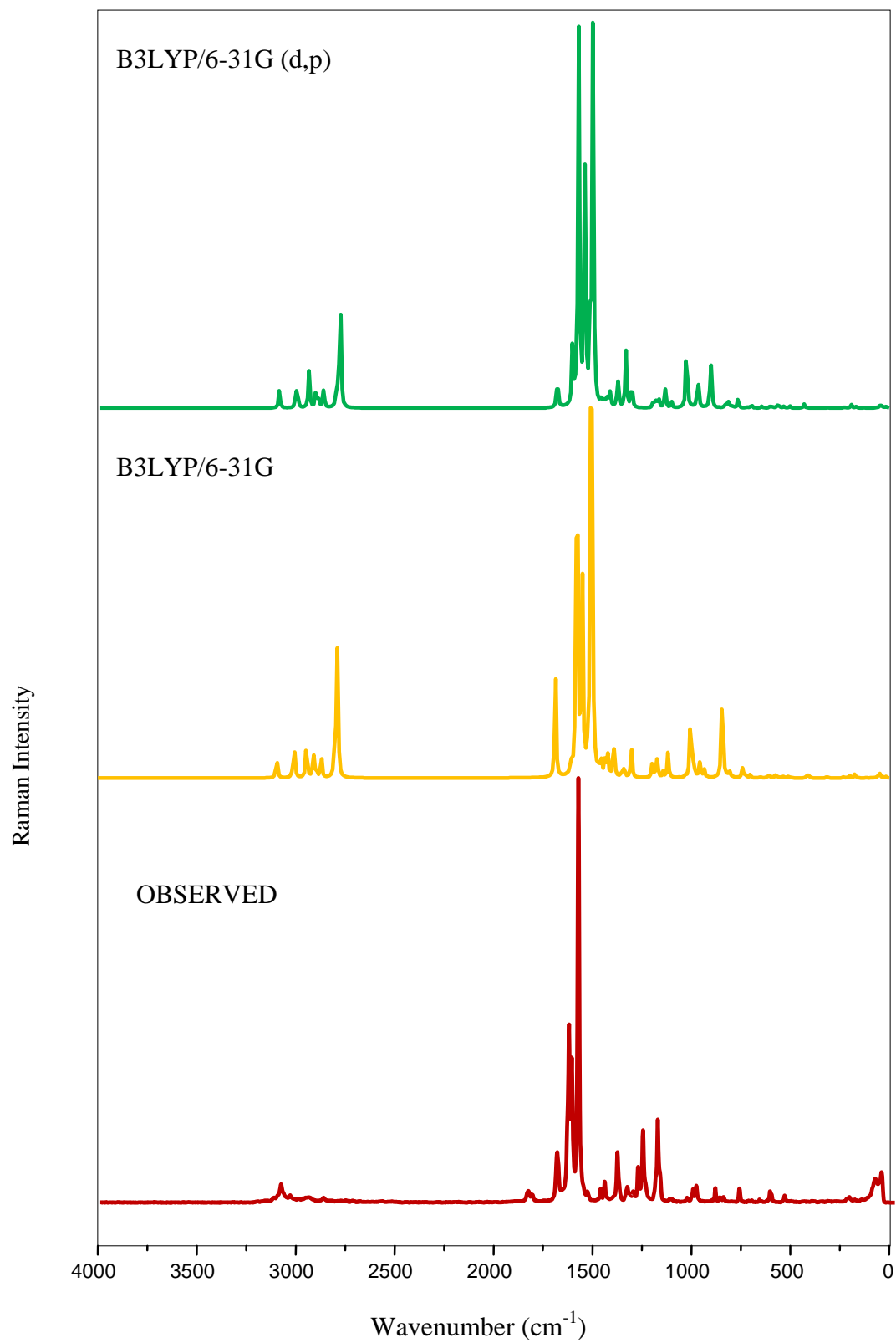


Fig 6.3 Observed FT-Raman and simulated spectra of (4Z)-4-(4-Methylbenzylidene)-2-phenyl-1,3-oxazol-5(4H)-one

6.4.2 Vibrational analysis

The MBO compound is constituted by 32 atoms and has 90 normal modes of vibrations. Among 90 fundamental modes of vibrations are classified into 36 stretching and the remaining is divided into in-plane and out-of-plane bending vibrations. The observed and simulated FT-IR and FT-Raman spectra of the MBO compound at DFT-B3LYP level using 6-31G and 6-31G (d,p) basis sets are shown in Figs. 6.2 and 6. 3. The elaborated vibrational assignments of the MBO compound along with the calculated IR and Raman frequencies and normal mode descriptions are given in Table 6.2.

CH₃ vibrations

The stretching vibrations of CH₃ are expected in the range 3050-2850 cm⁻¹ for asymmetric and symmetric vibrations [152, 155]. The deformed modes of methyl group are expected in the range of 1485-1355 cm⁻¹. The methyl rocking wavenumbers are expected in the range 1100±95 cm⁻¹ and 1080± 80 cm⁻¹ [152].

Benzon *et al* [159] assigned the asymmetric CH₃ stretching vibrations at 3023, 2997, 2961 cm⁻¹ in IR spectrum, 3037, 3016, 2992, 2967 cm⁻¹ in Raman spectrum and for symmetric CH₃ stretching vibrations at 2934, 2916 cm⁻¹ theoretically and 2924 cm⁻¹ for IR spectrum, 2928, 2903 cm⁻¹ at Raman spectrum. Parveen *et al* [146] observed the CH₃ vibrations at 2980 cm⁻¹ and 2978 cm⁻¹ in the IR and Raman spectrum and theoretically observed at 3011, 2988, 2925 cm⁻¹. Benzon *et al* [192] asymmetric CH₃ groups are theoretically obtained at 3063, 2996 cm⁻¹ and experimentally observed at 3063 cm⁻¹ in IR spectrum, 2998 cm⁻¹ in Raman spectrum. For our MBO compound, the assCH₃ stretching vibrations occurs 2785 cm⁻¹ in FT-Raman spectrum and theoretically observed at 2796,

2790 cm^{-1} and 2791, 2786 cm^{-1} for B3LYP/6-31G and B3LYP/6-31G (d,p) basis sets. The symmetric stretching vibrations observed at 2788 cm^{-1} and 2780 cm^{-1} for the same basis sets.

Benzon *et al* [192] observed the CH_3 deformation modes at 1458, 1455 1450, 1435 cm^{-1} by theoretically and 1442, 1446 in FT-IR, FT-Raman spectrum. Parveen *et al* [146] observed the deformed methyl group at 1355 cm^{-1} at IR and theoretically at 1449, 1434, 1358 cm^{-1} . Benzon *et al* [159] observed the CH_3 modes at 1468 cm^{-1} (IR), 1470, 1435 cm^{-1} (Raman) and calculated at 1464, 1458, 1455, 1435 cm^{-1} . In the present work, the CH_3 in-plane bending vibrations are assigned at 1374, 911 cm^{-1} and 1420, 991 cm^{-1} in FT-IR and FT-Raman spectrum. The computed wavenumbers are predicted by B3LYP/6-31G method at $\delta_{\text{opb}} = 1435 \text{ cm}^{-1}$, $\delta_{\text{ipb}} = 1426 \text{ cm}^{-1}$, $\delta_{\text{sb}} = 1380 \text{ cm}^{-1}$, $\delta_{\text{opr}} = 993 \text{ cm}^{-1}$, $\delta_{\text{ipr}} = 915 \text{ cm}^{-1}$ and for B3LYP/6-31G (d,p) method at $\delta_{\text{opb}} = 1431 \text{ cm}^{-1}$, $\delta_{\text{ipb}} = 1422 \text{ cm}^{-1}$, $\delta_{\text{sb}} = 1374 \text{ cm}^{-1}$, $\delta_{\text{opr}} = 990 \text{ cm}^{-1}$, $\delta_{\text{ipr}} = 913 \text{ cm}^{-1}$. In this study, the out-of-plane twisting vibration is observed at 38/31 cm^{-1} for the above basis sets.

C-H stretching

The C-H stretching vibrations occur at 3120-3000 cm^{-1} [152]. The C-H in-plane and out-of-plane bending occurs at 1315-995 cm^{-1} and 1000-700 cm^{-1} [152].

Parveen *et al* [146] observed the C-H stretching vibrations at 3088, 3038 cm^{-1} in IR spectrum and 3102, 3072, 3035 cm^{-1} in Raman spectrum. Haress *et al* [194] reported the C-H stretching at 2921, 2917, 2915 cm^{-1} . Renjith *et al* [151] observed the CH stretching vibration at 3081 cm^{-1} and 3077, 3064 cm^{-1} in IR and Raman spectrum, found

theoretically in the range of 3097-3057 cm^{-1} . For the MBO compound, the CH stretching vibrations observed at 3001, 2900, 2802 cm^{-1} in FT-IR spectrum, 3095, 3010, 2940 cm^{-1} in FT-Raman spectrum and theoretically at 3095, 3015, 3006, 2991, 2945, 2910, 2896, 2870, 2802 cm^{-1} by B3LYP/6-31G and 3091, 3010, 3001, 2989, 2941, 2905, 2891, 2866, 2800 cm^{-1} by B3LYP/6-31G (d,p) method.

The C-H in-plane bending for IR spectrum observed at 1294, 1145, 1115, 1035 cm^{-1} and 1288, 1148 cm^{-1} for FT-Raman spectrum for Parveen *et al* [146]. Haress *et al* [194] observed the in-plane bending for 2-(Adamantan-1-yl)-5-(4-nitrophenyl)-1,3,4-oxadiazole at 1349, 1299, 1085 cm^{-1} theoretically. Renjith *et al* [151] observed the in-plane bending at 1272, 1202, 1077 cm^{-1} in IR spectrum and 1266, 1197, 1174, 1150 cm^{-1} in Raman spectrum. In the present work, the in-plane bending vibrations observed at 1455, 1411, 1300, 1135, 1100, 1056 cm^{-1} in FT-IR spectrum and 1460, 1386, 1304, 1295, 1102 cm^{-1} in FT-Raman spectrum and theoretically obtained at 1464, 1453, 1420, 1391, 1309, 1300, 1170, 1140, 1115, 1064, 1004 cm^{-1} by B3LYP/6-31G and 1458, 1447, 1412, 1385, 1304, 1296, 1167, 1134, 1101, 1057, 1000 cm^{-1} by B3LYP/6-31G (d,p) method.

The out-of-plane bending by Parveen *et al* [146] assigned at 947, 922, 820, 808 cm^{-1} for IR spectrum and 820, 920 cm^{-1} for Raman spectrum. Haress *et al* [194] reported the out-of-plane bending at 943, 845, 821 cm^{-1} theoretically. Renjith *et al* [151] observed the out-of-plane bending for IR spectrum at 1272, 1202, 1077 cm^{-1} and Raman spectrum at 1266, 1197, 1174, 1150 cm^{-1} . In the present work, the out-of-plane bending vibrations occurs at 888, 861, 733 cm^{-1} in FT-IR spectrum, 875, 836, 785 cm^{-1} in FT-Raman spectrum and 933, 890, 879, 863, 841, 805, 801, 790, 738, 722, 648 cm^{-1} by B3LYP/6-

31G and 931, 886, 877, 860, 838, 802, 795, 786, 735, 718, 643 cm^{-1} by B3LYP/6-31G (d,p) method.

C-O vibrations

The C-O band is expected in the region $1220 \pm 40 \text{ cm}^{-1}$ [156, 197,198]. Benzon *et al* [159] reported the stretching of C-O appears at 1212 cm^{-1} in the IR spectrum, 1228 cm^{-1} in Raman spectrum and the calculated value is 1229 cm^{-1} . Ulahannan *et al* [199] reported that the stretching of C-O at 1215 cm^{-1} in IR and theoretically at 1208 cm^{-1} . Varghese *et al* [200] reported the C-O stretching at 1255 cm^{-1} in both IR and Raman spectra. Sagdinc *et al* [201] reported the C-O vibration at 1680, 1725, 1717 cm^{-1} for IR spectrum, at 1723 cm^{-1} Raman spectrum and at 1726 cm^{-1} observed theoretically. Veenakumar *et al* [202] assigned the C-O stretching vibrations at 1214, 1050 and 1396, 1208, 1050 in IR and Raman spectrum. For the MBO compound, the C-O stretching vibrations reported at 1680 and 1682 in FT-IR and FT-Raman spectrum. Theoretically at 1685, 1337 and 1680, 1332 in B3LYP/6-31G and B3LYP/6-31G (d,p) method. The in-plane bending vibrations occurs at 1007 in FT-Raman spectrum, 1011, 830 and 1009, 824 in B3LYP/6-31G and B3LYP/6-31G (d,p) method.

C-C vibrations

The C=C stretching is expected around $1600 \pm 50 \text{ cm}^{-1}$ [92]. Benzon *et al* [159] is observed at 1653 cm^{-1} , 1647 cm^{-1} in IR, Raman spectrum and assigned theoretically at 1630 cm^{-1} . Felfoldi *et al* [203] reported the C-C stretching vibrations at 1625 cm^{-1} theoretically. For the MBO compound, C-C vibrations observed at 1602, 1580, 1510, 1251, 1183, 980 in FT-IR spectrum, 1605, 1502, 1304, 1251, 1190 in FT-Raman

spectrum and theoretically at 1607, 1576, 1520, 1504, 1491, 1351, 1254, 1196, 1183, 982 and 1603, 1573, 1514, 1500, 1487, 1340, 1250, 1192, 1180, 978 B3LYP/6-31G and B3LYP/6-31G (d,p) methods. The in-plane bending vibrations observed at 563 and 224,65 in FT-IR and FT-Raman spectrum and 571, 353, 228, 211 and 565, 348, 225, 208 in the B3LYP/6-31G and B3LYP/6-31G (d,p) method. The out-of-plane bending vibrations observed at 648, 312, 170, 29, 13 and 612, 309, 166, 25, 10 at B3LYP/6-31G and B3LYP/6-31G (d,p) method.

C-N vibrations

Normally C-N stretching vibrations of aromatic rings are observed in the region at 1330-1260 cm^{-1} due to stretching of the phenyl carbon-nitrogen bond [155].

Parveen *et al* [146] assigned the C-N stretching modes at 1211, 1208 cm^{-1} in the IR, Raman and at 1270, 1209 cm^{-1} theoretically. Bhagyasree *et al* [204] reported C-N stretching modes at 1247 and 1236 cm^{-1} and Mary *et al* [205] reported the C-N stretching modes at 1238 cm^{-1} in Raman spectrum and theoretically at 1233, 1209 cm^{-1} . Sandhyarani *et al* [206] reported the C-N stretching at 1318 cm^{-1} and Benzoni *et al* [159] C-N is assigned at 1247, 1183, 1131, 1122 cm^{-1} theoretically and experimentally observed at 1247, 1181, 1140, 1120 cm^{-1} in Raman spectrum, 1153 cm^{-1} in IR spectrum. Veenakumar *et al* [202] reported the C-N stretching mode at 1609, 1132 cm^{-1} for IR spectrum and 1605, 1520, 1288, 1170, 1009, 971 cm^{-1} at FT-Raman spectrum, and observed theoretically in the range of 1607-969 cm^{-1} . Hareeas *et al* [194] observed the C-N stretching at 1535, 1520 cm^{-1} and 1540, 1521 cm^{-1} in the IR and Raman spectra and calculated wavenumber at 1531, 1516 cm^{-1} . For the MBO compound, the C-N vibrations

observed at 1545 in FT-Raman spectrum and theoretically at 1549, 1028 and 1542, 1025 at B3LYP/6-31G and B3LYP/6-31G (d,p) method. These assignments are good agreement with the literature data.

Ring vibrations

The ring breathing mode of the 1,4-disubstituted benzenes with entirely different substituent has been reported in the interval 780-880 cm^{-1} [197]. Mary *et al* [97] reported the ring breathing modes are assigned at 977, 748 cm^{-1} for benzene ring theoretically. For our MBO compound, the ring breathing modes are observed at 968 cm^{-1} in FT-Raman spectrum, 970 and 967 cm^{-1} assigned theoretically by B3LYP method with 6-3.1G and 6-31G (d,p) basis sets.

For the MBO compound, the in-plane bending vibrations of oxazole and benzene rings are observed at 902, 812, 693, 503 cm^{-1} in FT-IR spectrum and 694, 602, 527,101 cm^{-1} in FT-Raman spectrum and theoretically reported at 954, 906, 815, 765, 700, 606, 590, 560, 535, 506, 431, 195, 110, 89 cm^{-1} in B3LYP/6-31G and 950, 902, 812, 763, 695, 600, 587, 554, 530, 501, 428, 189, 102, 85 cm^{-1} in B3LYP/6-31G (d,p) method. The out-of-plane bending vibrations observed at 402 cm^{-1} in IR spectrum and obtained theoretically at 631, 491, 470, 408, 376, 128, 61 cm^{-1} in B3LYP/6-31G, 627, 488, 467, 401, 373, 123, 56 cm^{-1} in B3LYP/6-31G (d,p) method.

6.5 Mulliken atomic charge analysis

The charge distribution analysis is leading to the application of quantum mechanical calculations to the molecular systems. The charge distribution of a molecule

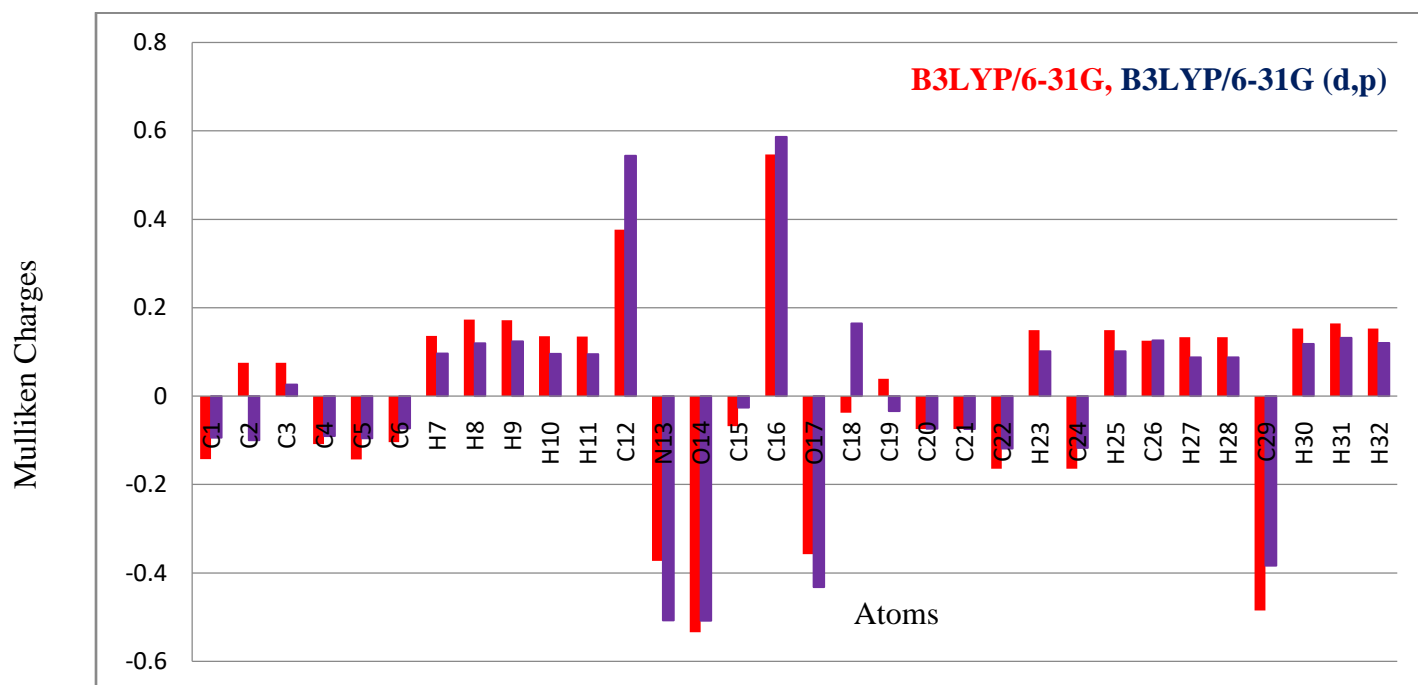


Fig.6.4 Mulliken atomic charges of (4Z)-4-(4-Methylbenzylidene)-2-phenyl-1,3-oxazol-5(4H)-one

has significant influence on dipole moment, polarizability, electronic structure and vibrational modes [207]. Mulliken atomic charge distribution analysis was performed for the present molecular structure using DFT/B3LYP method with 6-31G and 6-31G (d,p) basis sets and values are compared and tabulated it in Table 6.3 and shown in Fig 6.4 in order to assess the sensitivity of the calculated charges to changes in the choice of the basis set and the choice of the quantum mechanical method. Generally, carbon atoms bonded to electronegative atoms such as nitrogen, oxygen are negatively charged atoms N13= -0.3728/-0.5075, O14= -0.5344/-0.5084, O17= -0.3576/-0.4321. For the MBO compound, all the hydrogen atoms has positive values, such as H8= 0.1735/0.1199, H9=0.1713/0.1237, H30= 0.1527/0.1180, H31= 0.1641/0.1319, H32 = 0.1527/0.1206 and the charges in the ring carbon atoms have both positive and negative charge (C2 = 0.0751/-0.0996, C19=0.0395/-0.0336) that indicates that carbon atoms are highly influenced by their neighboring atoms [208].

6.6. Frontier molecular orbital analysis

The HOMO energy characterizes the electron donating ability and LUMO is the electron retreating ability and the energy gap between the HOMO and LUMO levels describes the molecular chemical stability. The energy gap has low which corresponds to low kinetic stability and large chemical reactivity [209-212]. The electron transition from ground state to first excited state was described by an electron transition from HOMO to LUMO. The HOMO, LUMO energy gap and quantum chemical parameters of the MBO compound have been calculated by DFT method with B3LYP/6-31G (d, p) basis set. The

orbital energies of the Frontier orbital are given by Fig.6.5. Quantum chemical quantities such as ionization potential (I), electron affinity (A), chemical potential (μ), global hardness (η), global softness (ν), global electrophilic index (ω) and electronegativity (χ) can be calculated using the HOMO and LUMO energy values and tabulated in Table 6.4. Hardness, chemical potential and electronegativity are outlined using Koopman's theorem as $I = E_{\text{HOMO}}$; $A = E_{\text{LUMO}}$; $\mu = -(I+A)/2$, $\eta = (I-A)/2$, $\sigma = 1/\eta$ and $\omega = \mu^2/2\eta$

For the MBO compound, $E_{\text{HOMO}} = -5.2126$ eV, $E_{\text{LUMO}} = -2.3157$ eV, Energy gap (E_g) = 2.8969 eV, Ionization potential (I) = 5.2126 eV, Electron affinity (A) = 2.3157 eV, Chemical hardness (μ) = 1.4485eV, Softness (σ) = 0.6904 eV, Chemical potential (μ) = -2.7642 eV, Electrophilic index (ω) = 2.6375eV. It is seen that the chemical potential of the MBO compound is negative; it means that the compound is stable. The global hardness (η) parameter is related to the E_g and defined as measurement from the resistance of an atom or a group of atoms to charge transfer [213]. The molecular structure with a small energy gap (E_g) has a high chemical reactivity, kinetic stability and is a soft molecule, whereas a hard molecule has high energy gap. For MBO compound, the calculated global hardness for H-1 and H-2 are 2.8082, 3.3778 respectively. Hence the MBO compound is a soft molecule.

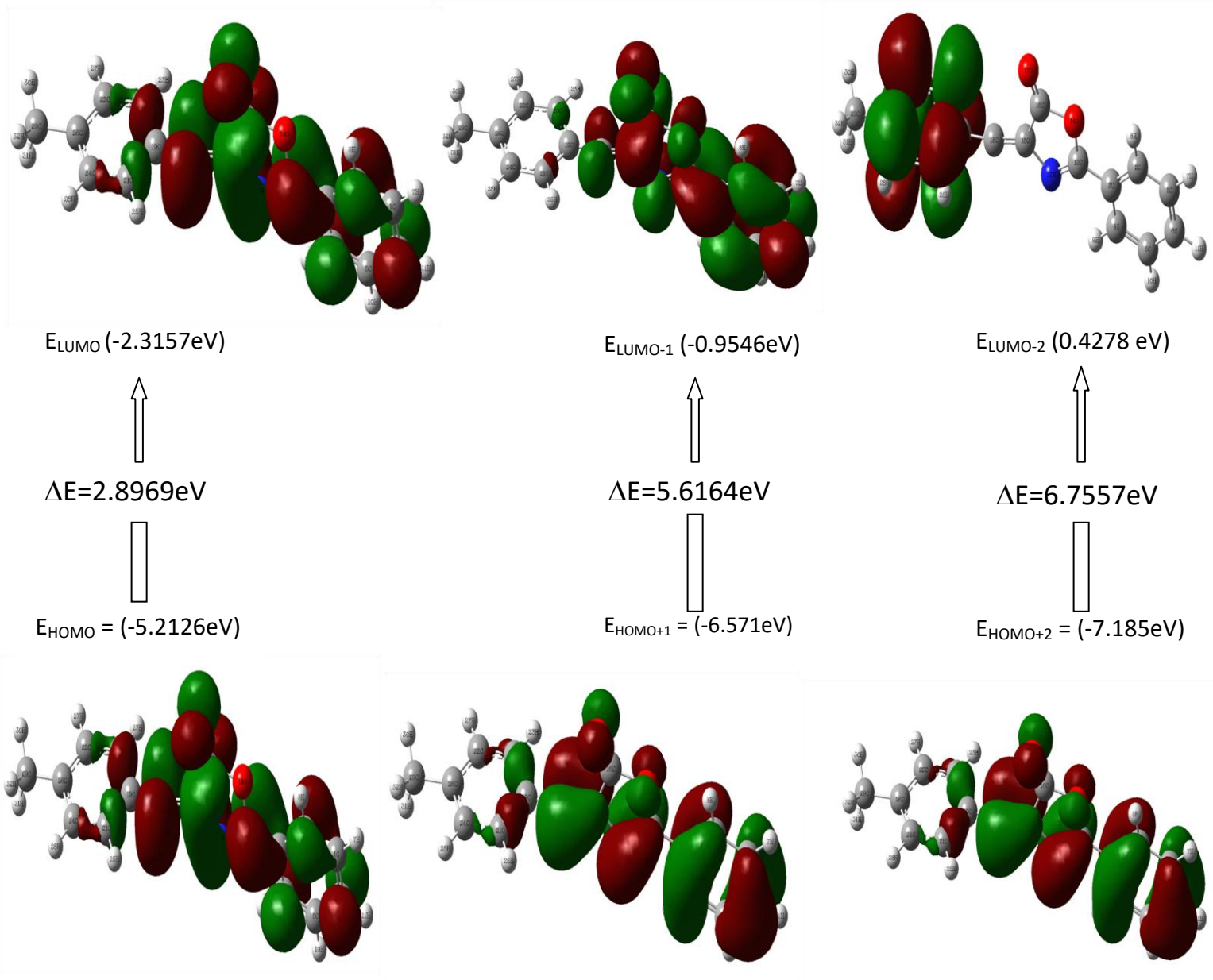


Fig 6.5 Patterns of the principle highest occupied and lowest unoccupied molecular orbital of (4Z)-4-(4-Methylbenzylidene)-2-phenyl-1,3-oxazol-5(4H)-one

6.7 Natural bond orbital analysis

The natural bond orbital (NBO) analysis is an effective tool for determining the chemical interpretation of hyper conjugative interactions and electron density transfer from filled lone pair orbital of one subsystem to a vacant orbital of another subsystem. The DFT calculations are used to analyze various second order interactions between the filled and vacant orbital's of a system which gives a measure of delocalization and hyper conjugation [214]. The hyper conjugation interaction energy can be obtained from the second order perturbation method [215] as follows:

$$E(2) = \Delta E_{ij} = q_i \frac{(F_{i,j})^2}{(E_j - E_i)}$$

where q_i is the donor orbital occupancy, E_i and E_j are the diagonal elements and $F(i, j)$ is the off diagonal NBO Fock matrix element. The NBO analysis shows the various possible donors and acceptors in the molecule with their occupancy value in each position are tabulated in Table 6.5. The important hyper-conjugative interactions are C12-N13 from O14 of LP(2) $O41 \rightarrow \sigma^*(C12-N13)$, C16-O17 from O14 of LP(2) $O14 \rightarrow \sigma^*(C16-O17)$, O14-C16 from O17 $\rightarrow \sigma^*(O14-C16)$, C12-O14 from N13 $\rightarrow \sigma^*(C12-O14)$, C15-C16 from C18 $\rightarrow \sigma^*(C15-C16)$ with stabilization energies 19.37, 16.14, 11.1, 4.66, 4.09 kJ/mol.

Also, the various possible transitions among these donors and acceptors are provided. The larger the $E(2)$ values the more intense will be the interaction between the electron donors and electron acceptor groups i.e. more electron donating tendency and greater the extent of conjugation of the whole system tabulated on Table 6.6. $\sigma(C15-$

C16) orbital with 0.99659 a.u. energy has 50.91% C15 character in $SP^{(1.98)}$ hybrid and has 49.08% C16 character in $SP^{(1.44)}$ hybrid. The idealized $SP^{(1.44)}$ hybrid has 66.49%, 58.95% p-character and 33.51%, 41.05% s-character. The two coefficients 0.7136 and 0.7006 are called polarization coefficients. σ (C16-O17) orbital with 0.99543 a.u energy has 40.43% C16 character in $SP^{(1.99)}$ hybrid and has 59.57% O17 character in $SP^{(3.85)}$ hybrid. The idealized $SP^{(3.75)}$ hybrid has 66.61%, 79.37% p-character and 33.39%, 20.63% s-character. The two coefficients 0.6358 and 0.7718 are called polarization coefficients. The oxygen (O17) has a larger percentage of this NBO, 79.37% and gives the larger polarization coefficient 0.7718 because it has a higher electronegativity. Similarly, the carbon (C29) has a larger percentage of this NBO, 74.12% and gives the larger polarization coefficient 0.6988. The carbon and nitrogen have a lesser percentage of NBO and give a lesser polarization coefficient. The carbon (C16) has a lower percentage of NBO, 25.22% and gives the lesser polarization coefficient 0.5514.

6.8 Molecular electrostatic potential functions

Molecular electrostatic potential (MEP) is related to the electronic density which is very useful descriptor in understanding nucleophilic and electrophilic sites as well as hydrogen bonding interaction [216]. This analysis is also used to predict the biological activity of a molecule as well as its ability to form hydrogen bonding with its target protein. To predict the reactive sites such as electrophilic and nucleophilic sites for the title molecule, MEP at the B3LYP/6-31G (d,p) optimized geometry was calculated. The color range of the MEP diagram of the MBO molecule is shown in Fig.6.6 which starts

with red color and ends with dark blue color which means different values of electrostatic potential at the surface of the molecule in the following decreasing order: Red > orange > yellow > blue > green, red, blue and green represent the regions of most negative, most positive and zero electrostatic potential respectively. The negative electrostatic potential corresponds to an attraction of the proton by the aggregate electron density in the molecule (shades of red), while the positive electrostatic potential corresponds to the repulsion of the proton by the atomic nuclei (shade of blue). The negative, (red) region of MEP were related to electrophilic reactivity and the positive (blue) regions to nucleophilic reactivity.

From the MEP plot of the MBO compound, it is evident that the negative charge covers the nitrogen in the oxazole ring and the positive region is over all the hydrogen atoms in the methylbenzylidene and benzene ring. The more electronegativity in the nitro group makes it the more reactive part in the molecule.

6.9 Reduced density gradient analysis

Reduced density gradient is a dimensionless quantity and Johnson *et al* [128] derived the methodology for RDG from electron density and it was the first gradient found in the literature.

$$\text{RDG}(\mathbf{r}) = \frac{1}{2(3\pi r^2)^{1/2}} \frac{|\nabla\rho(r)|}{\rho(r)^{4/3}}$$

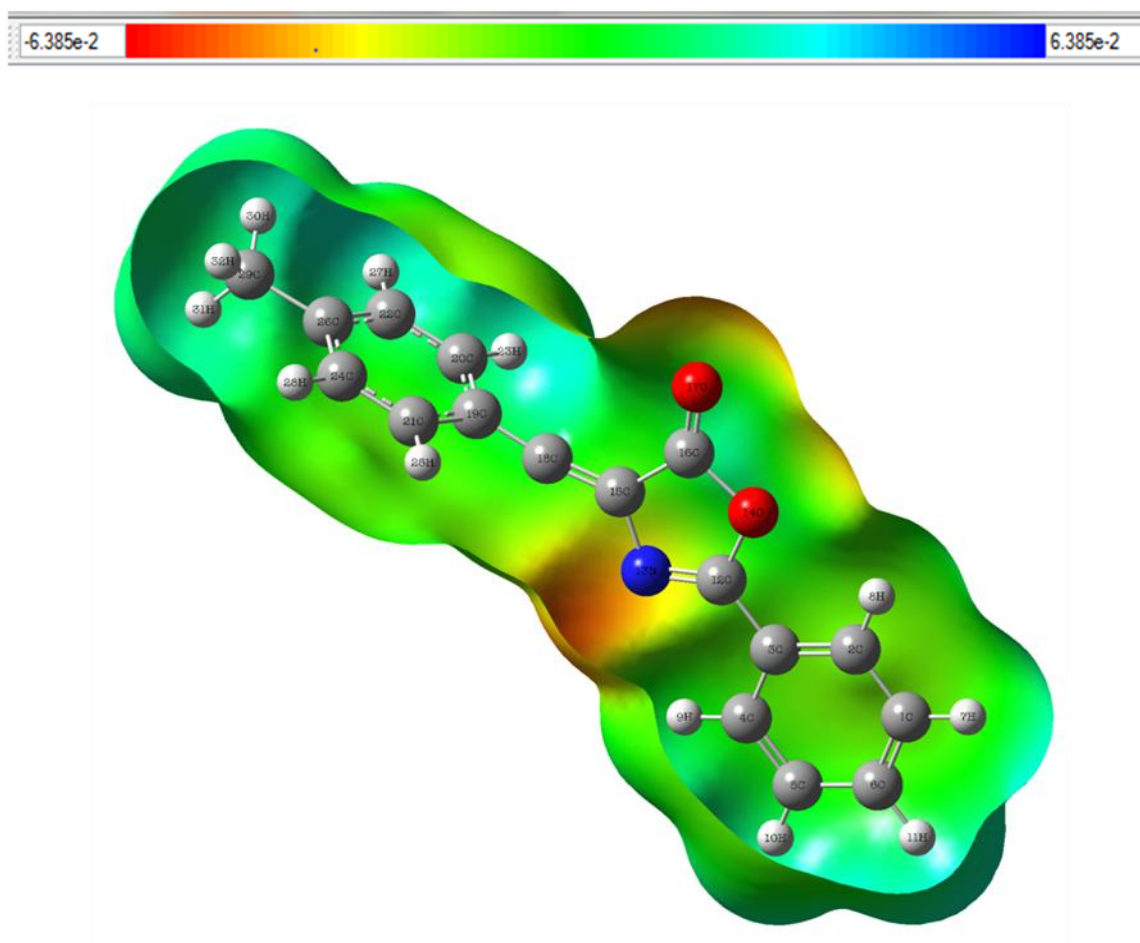


Fig 6.6 Molecular electrostatic potential surfaces of (4Z)-4-(4-Methylbenzylidene)-2-phenyl-1,3-oxazol-5(4H)-one

The plot $\rho(r)$ against λ_2 sign will help to understand the nature and strength of the interactions. The sign of λ_2 the second largest value of hessian matrix of electron density and is used to find the nature of interaction. If $\lambda_2 > 0$, for non bonded and if $\lambda_2 < 0$ for bonded. The red color in scale in Fig.6.7 represents a strong repulsion for the stric effect. The green colour representing the non-covalent interaction i.e Van der Waals interaction and the blue indicate the strong attractions of the MBO compound.

6.10 Fukui function

Fukui function is defined as the partial derivative of the electron density $\rho(r)$ with respect to the total number of electron N , at constant external potential $V(r)$ or the partial derivatives of the chemical potential μ with respect to external potential $V(r)$, at constant number of electrons N

$$f(r) = \left(\frac{\partial \rho(r)}{\partial N} \right)_{V(r)} = \left(\frac{\partial \mu}{\partial V(r)} \right)_N$$

The Fukui function is a function defined at each point of space, but it is helpful to define a condensed Fukui function. For this, the Fukui functions are defined as condensed to an atom, by a partial scheme and the condensed form of Fukui functions for an atom k in a molecules are expressed as,

$$f_{k+} = q_k(N+1) - q_k(N) \quad (\text{for nucleophilic attack})$$

$$f_{k-} = q_k(N) - q_k(N-1) \quad (\text{for electrophilic attack}) \text{ and}$$

$$f_k^0 = f_{k+} - f_{k-}/2 \quad (\text{for radical attack})$$

where q_k is the atomic charge (evaluated from Mulliken population analysis) at the k th atomic site in the neutral (N), anionic (N+1) and cationic (N-1) chemical species [217]. From Table 6.7, according to the condition for dual descriptor $\Delta f(r)$, which is defined as the difference between the nucleophilic and electrophilic Fukui function and some of the nucleophilic sites are N13, C16, C19, C22, H23 and C24 are positive values i.e $\Delta f(r) > 0$. Similarly the electrophilic sites are C12, C15, O17, C18 and C29 are some of the negative values i.e $\Delta f(r) < 0$.

6.11 Topological analysis

In the frame of AIM (Atoms in Molecule) hypothesis [218], any chemical bond or those atoms have interactions involving in H-bonding is explained by bond critical points (BCPs). One can acquire about the characteristics of intramolecular hydrogen bond interactions through on the bond elliptic index (ϵ), AIM analysis was performed using Multiwfn package to contemplate the noncovalent interactions of the MBO compound. The strong, medium, weak H-bonds and their covalent, partially covalent and electrostatic nature can be denoted by ($V^2_{BCP} < 0$ and $H_{BCP} < 0$), ($V^2_{BCP} > 0$ and $H_{BCP} < 0$) and ($V^2_{BCP} > 0$ and $H_{BCP} > 0$) [182]. The molecular diagram of the title molecule using the AIM program calculated at B3LYP/6-31G (d, p) approximation was presented in Fig. 6.8. The bond critical point is not observed for the MBO compound.

6.12 Molecular docking studies

The molecular interactions between the lead molecule and target protein of biological interest have become great importance within the field of drug design. Title molecule can be used for treating cancer, tubercular and convulsant. To explore the biological activity of the MBO molecule, molecular docking studies were carried out. The molecular mechanism of selectivity [219] can be observed by docking analysis of the lead molecule with many protein targets. The MBO compound was docked into the active sites of proteins 5FDC, 1EOU, 5H8V, 1PCV, 2RER and 1NNU associated with convulsant, cancer, fungal, tubercular and human lymphatic filarial parasites activity. The molecular docking binding energies (kcal/mol), intermolecular energy (kcal/mol) and inhibition constants (μm) were obtained and are tabulated in Table 6.8. The proteins were downloaded from the protein data bank website. The docking macromolecule i.e protein was prepared by removing the water, co-factors, co-crystallized ligands and AutoDock tools (ADT) graphical computer program was accustomed calculate Kollman charges and polar hydrogens. The active site of the macromolecule was defined to incorporate residues of the active site within the grid size of $60\text{\AA} \times 60\text{\AA} \times 60\text{\AA}$. The common method to evaluate the quality of docking result is to calculate the Root Mean Square Deviation (RMSD) between the docked cause and the well known crystal structure conformation. RMSD values up to 2\AA are considered reliable for a docking protocol [220]. Amongst the docked conformations of the co-crystallized ligand and scored well was visualized for ligand-protein interactions in Discovery Studio Visualizer 4.1 software. The docked ligand interactions with amino acids of the receptor and the ligand at the active sites of the receptor are stated in Fig.6.9.

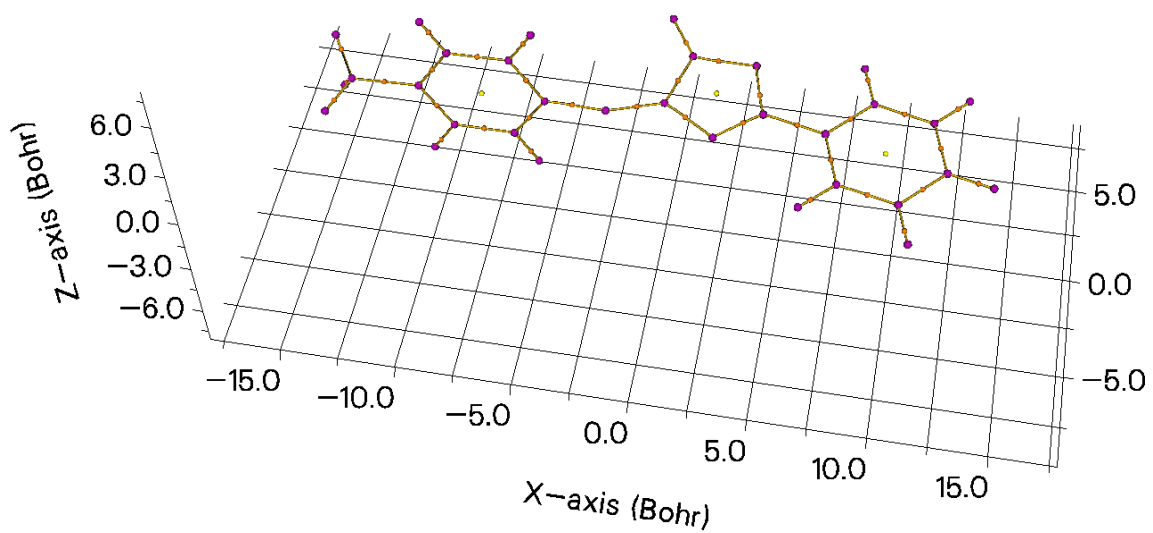
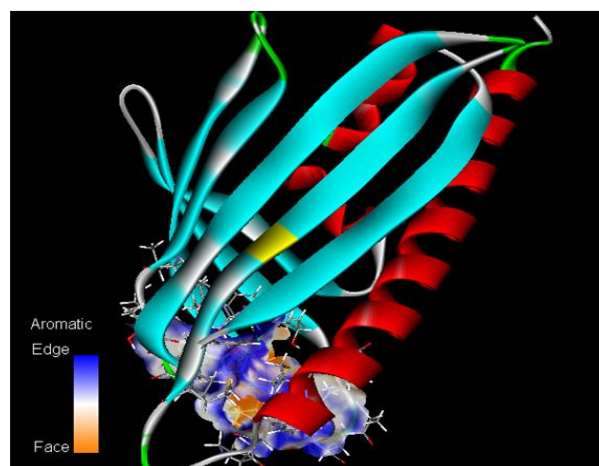
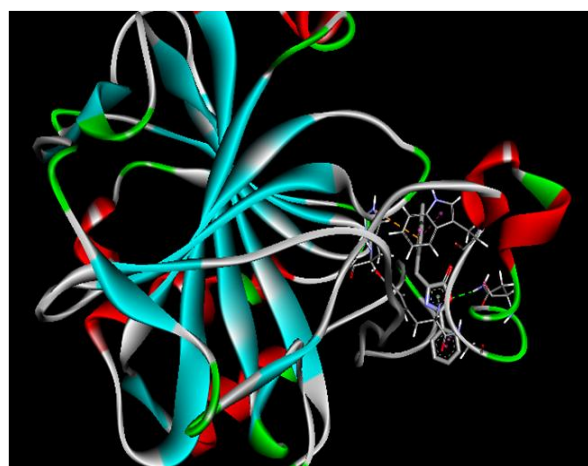
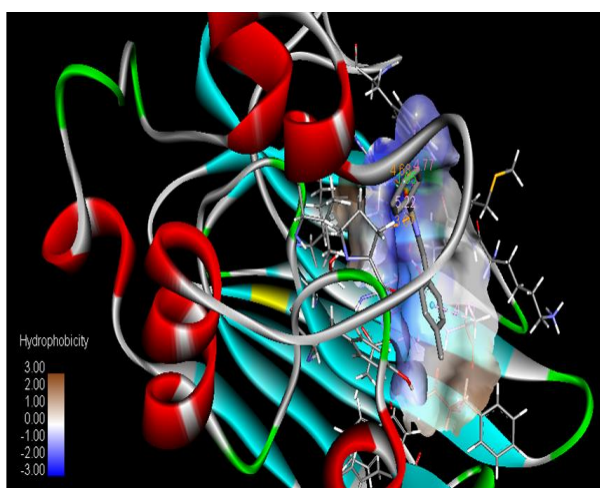
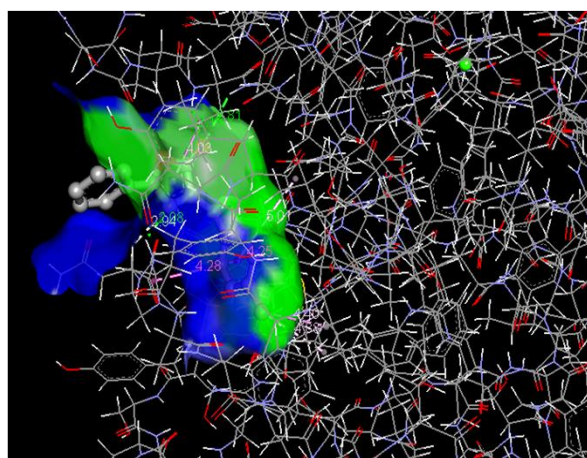
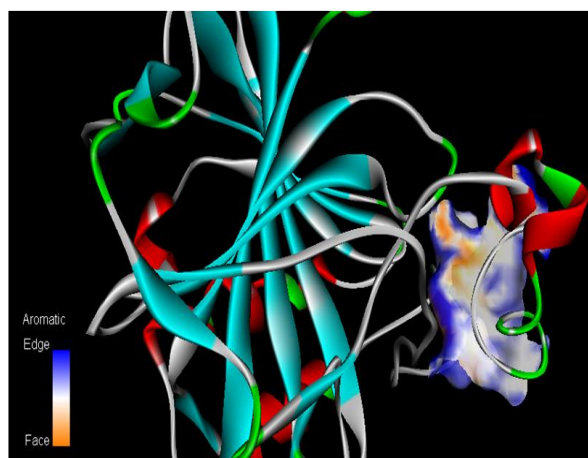


Fig.6.8 Molecular graph of (4Z)-4-(4-Methylbenzylidene)-2-phenyl-1,3-oxazol-5(4H)-one



**Fig. 6.9 Ligand (4Z)-4-(4-Methylbenzylidene)-2-phenyl-1,3-oxazol-5(4H)-one
Protein – 5FDC, 5H8X, 1PCV, 1NNU, 1EOU, 2RER.**

Anticonvulsant

Interaction of anticonvulsant proteins shows existence of many conventional bonds which are as follows: two Conventional hydrogen bond and one van der Waals bond was found in 5FDC interacting with amino acids (1.92 Å; TYR A: 7, 2.01 Å; HIS A:64, 3.14 Å; GLY A:63) with different binding energy(-7.05, -6.71, -5.99) kcal/mol, inhibition constant (6.85, 12.12, 40.43) μM and RMSD value is (8.468, 25.279, 13.263) Å. One conventional bond, one π -donor hydrogen bond and one van der waals bond was found in 1EOU interacting with amino acids (2.3 Å; ASN A:11, 2.93 Å; TYR A:7, 3.5 Å; GLY A:63) with different binding energy(-7.23, -6.42, -6.23) kcal/mol, inhibition constant (5.02, 19.84, 27.11) μM and RMSD value is (9.016, 13.611, 8.945) Å.

Anticancer

Interaction of anticancer proteins shows existence of many conventional bonds which are as follows: three Conventional hydrogen bond and one π - π stacked bond was found in 5H8V interacting with amino acids (2.26 Å; LEU A:160, 2.18 Å; TYR A:219, 3.66 Å; ALA A:161, 3.21 Å; VAL A:194) with different binding energy(-7.97, -7.63, -5.3, -5.18) kcal/mol, inhibition constant (1.44, 2.53, 129.56, 158.36) μM and RMSD value is (27.135, 26.811, 9.135, 19.745) Å.

Antifungal

Interaction of antifungal proteins shows existence of many conventional bonds which are as follows: two Conventional hydrogen bond, two van der Waals bond and one π - π stacked bond was found in 1PCV interacting with amino acids (1.97 Å; ARG A:44,

2.62 Å; ARG A:44, 2.74 Å; PHE A:95, 3.12 Å; MET A: 42, 2.12 Å; TRP A: 75) with different binding energy (-6.6, -5.97, -5.7, -5.63, -6.14) kcal/mol, inhibition constant (14.5, 42.39, 65.97, 73.29, 31.45) µM and RMSD value is (35.044, 44.564, 46.382, 46.842, 32.706) Å.

Antitubercular

Interaction of antitubercular proteins shows existence of many conventional bonds which are as follows: two Conventional hydrogen bond and one carbon-hydrogen bond was found in 2RER interacting with amino acids (1.83 Å; ARG A:82, 2.22 Å; ARG A:82, 2.35 Å; PRO A:87) with different binding energy(-7.61, -7.34, -6.95) kcal/mol, inhibition constant (2.63, 4.14, 8.03) µM and RMSD value is (49.626, 55.046, 53.908) Å.

Human lymphatic filarial parasites

Interaction of human lymphatic filarial parasites proteins shows existence of many conventional bonds which are as follows: two carbon-hydrogen bond and two van der Waals bond was found in 1NNU interacting with amino acids (2.03 Å; ALA A:169, 2.01 Å; SER A:170, 2.12 Å; GLY A:104, 4.1 Å; ASN A:218) with different binding energy (-7.67, -7.01, -7.49, -6.71) kcal/mol, inhibition constant (2.37, 7.31, 3.23, 11.99) µM and RMSD value is (99.845, 111.129, 103.844, 108.043) Å.

6.13 Conclusion

The FT-IR and FT-Raman spectral measurements have been performed for (4Z)-4-(4-Methylbenzylidene)-2-phenyl-1,3-oxazol-5(4H)-one (MBO). In the present work, to

calculate the geometrical parameters of the optimized structure, quantum chemical techniques have been used.

The stability of the molecule arising hyper-conjugative interaction and charge delocalization has been studied using NBO analysis. The HOMO-LUMO analysis is used to determine the charge transfer within the molecule and the calculated HOMO-LUMO energies show the chemical reactivity of the molecule. The energy gap (ΔE) is 2.8969 eV.

From the MEP plot, it is evident that the negative charge covers the nitrogen in the oxazole group and in the positive region all are hydrogen atoms.

The strong, weak and van der Waals interactions can be studied by the Reduced Density Gradient.

Molecular docking studies were carried out for various proteins such as 5FDC, 1EOU, 5H8V, 1PCV, 2RER and 1NNU.

Table 6.1 Optimized structural parameters of (4Z)-4-(4-Methylbenzylidene)-2-phenyl-1,3-oxazol-5(4H)-one using B3LYP/6-31G and B3LYP/6-31G (d,p) method

Parameters	Bond length (Å)		Parameters	Bond angle (°)		Parameters	Dihedral angle (°)	
	B3LYP/	B3LYP/		B3LYP/	B3LYP/		B3LYP/	B3LYP/
	6-31G	6-31G(d,p)		6-31G	6-31G(d,p)		6-31G	6-31G(d,p)
C1-C2	1.3965	1.3932	C2-C1-C6	120.1941	120.1864	C6-C1-C2-C3	-0.0001	0.0015
C1-C6	1.4003	1.396	C2-C1-H7	119.7215	119.7025	C6-C1-C2-H8	180.0005	-179.999
C1-H7	1.0849	1.0857	C5-C1-H7	120.0845	120.1111	H7-C1-C2-C3	-179.9999	-179.999
C2-C3	1.4071	1.4034	C1-C2-C3	119.7765	119.8103	H7-C1-C2-H8	0.0007	-0.0001
C2-H8	1.0834	1.0841	C1-C2-H8	120.837	120.6321	C2-C1-C6-C5	0.0002	-0.0017
C3-C4	1.4088	1.405	C2-C3-H8	119.3865	119.5577	C2-C1-C6-H11	180.0003	179.9971
C3-C12	1.4529	1.4608	C2-C3-C4	119.9757	119.9049	H7-C1-C6-C5	180	179.9992
C4-C5	1.394	1.3903	C2-C3-C12	120.7341	120.887	H7-C1-C6-H11	0.0001	-0.002
C4-H9	1.084	1.0845	C4-C3-C12	119.2902	119.2081	C1-C2-C3-C4	0.0002	-0.0002
C5-C6	1.4026	1.3986	C3-C4-C5	119.8256	119.8754	C1-C2-C3-C12	179.9995	-179.998
C5-H10	1.085	1.0857	C3-C4-H9	118.9188	118.8525	H8-C2-C3-C4	-180.0004	-180
C6-H11	1.0854	1.086	C5-C4-H9	121.2556	121.272	H8-C2-C3-C12	-0.0011	0.0031
C12-N13	1.3003	1.2894	C4-C5-C6	120.1699	120.1597	C2-C3-C4-C5	-0.0003	-0.0008
C12-O14	1.4204	1.3833	C4-C5-H10	119.7888	119.7752	C2-C3-C4-H9	179.9995	-180
N13-C15	1.4354	1.416	C6-C5-H10	120.0413	120.0651	C12-C3-C4-C5	-179.9996	179.9965
O14-C16	1.4316	1.4015	C1-C6-C5	120.0582	120.0633	C12-C3-C4-H9	0.0002	-0.0023
C15-C16	1.4987	1.5023	C1-C6-H11	119.9885	119.9712	C2-C3-C12-N13	180.0027	-179.974
C15-C18	1.3172	1.3152	C5-C6-H11	119.9532	119.9656	C2-C3-C12-O14	0.0004	0.0307
C16-O17	1.2189	1.1976	C3-C12-N13	127.9771	126.7808	C4-C3-C12-N13	0.002	0.0284

C18-C19	1.3737	1.3692	C3-C12-O14	117.0539	116.6691	C4-C3-C12-O14	179.9997	-179.967
C19-C20	1.4361	1.4327	N13-C12-O14	114.969	116.5501	C3-C4-C5-C6	0.0003	0.0006
C19-C21	1.436	1.4333	C12-N13-C15	106.6147	105.3947	C3-C4-C5-H10	180.001	-179.998
C20-C22	1.3857	1.3823	C12-O14-C16	106.1513	106.2689	H9-C4-C5-C6	-179.9995	179.9994
C20-H23	1.0841	1.0845	N13-C15-C16	108.106	107.9065	H9-C4-C5-H10	0.0012	0.0007
C21-C24	1.3858	1.3814	N13-C15-C18	126.3724	127.5269	C4-C5-C6-C1	-0.0003	0.0006
C21-H25	1.0841	1.0846	C16-C15-C18	125.5216	124.5665	C4-C5-C6-H11	179.9996	-179.998
C22-C26	1.4122	1.4079	O14-C16-C15	104.1591	103.8798	H10-C5-C6-C1	-180.0009	179.9993
C22-H27	1.0863	1.087	O14-C16-O17	122.5165	122.6714	H10-C5-C6-H11	-0.0011	0.0005
C24-C26	1.4122	1.4089	C15-C16-O17	133.3244	133.4487	C3-C12-N13-C15	-180.0066	-179.986
C24-H28	1.0863	1.0871	C15-C18-C19	171.1948	179.9605	O14-C12-N13-C15	-0.0044	0.009
C26-C29	1.5093	1.5069	C18-C19-C20	121.2321	121.2464	C3-C12-O14-C16	180.0039	179.9899
C29-H30	1.0952	1.0938	C18-C19-C21	121.236	121.2185	N13-C12-O14-C16	0.002	-0.0056
C29-H31	1.0995	1.098	C20-C19-C21	117.5283	117.5336	C12-N13-C15-C16	0.005	-0.0086
C29-H32	1.0952	1.0944	C19-C20-C22	120.5149	120.4589	C12-N13-C15-C18	179.9974	-179.992

Table 6.2 Vibrational assignments of (4Z)-4-(4-Methylbenzylidene)-2-phenyl-1,3-oxazol-5(4H)-one using B3LYP/6-31G and B3LYP/6-31G (d,p) method

Modes	Observed		Calculated		Vibrational assignments (% PED)
	wavenumbers (cm ⁻¹)		wavenumbers (cm ⁻¹)		
	FT-IR	FT-Raman	B3LYP/ 6-31G	B3LYP/ 6-31G (d,p)	
1		3095	3095	3091	vCH (98)
2		3010	3015	3010	vCH (99)
3	3001		3006	3001	vCH (98)
4			2991	2989	vCH (98)
5		2940	2945	2941	vCH (99)
6	2900		2910	2905	vCH (98)
7			2896	2891	vCH (98)
8			2870	2866	vCH (99)
9	2802		2802	2800	vCH (98)
10			2796	2791	v _{ass} CH ₃ (97)
11		2785	2790	2786	v _{ass} CH ₃ (97)
12			2788	2780	v _{ss} CH ₃ (97)
13	1680	1682	1685	1680	vCO(78), vCC (16)
14	1602	1605	1607	1603	vCC(84), vCO (12)
15	1580		1576	1573	vCC (78), δCH (17)
16		1545	1549	1542	vCN (76), δCC (19)
17	1510		1520	1514	vCC (76), δCH (18)
18		1502	1504	1500	vCC (76), δCH (18)
19			1491	1487	vCC (78), δCH (16)
20	1455	1460	1464	1458	δCH (69), vCC (22)
21			1453	1447	δCH (68), vCC (20)
22			1435	1431	δ _{opb} CH ₃ (88)
23		1420	1426	1422	δ _{ipb} CH ₃ (86)
24	1411		1420	1412	δCH (68), δCC (19)
25		1386	1391	1385	δCH (70), vCC (21)
26	1374		1380	1374	δ _{sb} CH ₃ (86)

27			1351	1340	vCC (75), δ CH (21)
28			1337	1332	vCO (69), δ CH (13), vCC (10)
29	1300	1304	1309	1304	δ CH (72), vCO (13)
30		1295	1300	1296	δ CH (69), vCC (13)
31	1250	1251	1254	1250	vCC (76), δ CH (18)
32		1190	1196	1192	vCC (68), δ CH (12)
33	1183		1183	1180	vCC (70), δ CH (12), δ CC (10)
34			1170	1167	δ CH (78)
35	1135		1140	1134	δ CH (75)
36	1100	1102	1115	1101	δ CH (73)
37	1056		1064	1057	δ CH (75)
38			1028	1025	vCN (66), vCC (13), δ CO (10)
39		1007	1011	1009	δ CO (67), vCC (12), δ CH (10)
40			1004	1000	δ CH (68)
41		991	993	990	$\delta_{\text{opr}} \text{CH}_3$ (70)
42	980		982	978	vCC (72), δ CH (14)
43		968	970	967	Ring breathing (75)
44			954	950	δ_{ring} (69)
45			933	931	γ CH (64)
46	911		915	912	$\delta_{\text{ipr}} \text{CH}_3$ (69), δ CH (10)
47	902		906	902	δ_{ring} (70)
48	888		890	886	γ CH (65)
49		875	879	877	γ CH (65)
50	861		863	860	γ CH (65)
51		836	841	838	γ CH (66)
52			830	824	δ CO (72), δ_{ring} (16)
53	812		815	812	δ_{ring} (66)
54			805	802	γ CH (67)
55			801	795	γ CH (67)
56		785	790	786	γ CH (67)
57			765	763	δ_{ring} (70)
58	733		738	735	γ CH (68)
59			722	718	γ CH (68)

60	693	694	700	695	δ ring (72)
61			648	643	γ CH (68)
62			631	627	γ ring (63), γ CC (14)
63			615	612	γ CC (66), γ ring (15)
64		602	606	600	δ ring (68)
65			590	587	δ ring (68)
66	563		571	565	δ CC (60), δ CO (18)
67			560	554	δ ring (66)
68		527	535	530	δ ring (65)
69	503		506	501	δ ring (65)
70			491	488	γ ring (62)
71			470	467	γ ring (62)
72			431	428	δ ring (66)
73	402		408	401	γ ring (63)
74			376	373	γ ring (62)
75			353	348	δ CC (68)
76			312	309	γ CC (62)
77			290	285	δ CCH ₃ (64)
78		224	228	225	δ CC (66)
79			211	208	δ CC (66)
80			195	189	δ ring (68)
81			170	166	γ CC (61)
82			128	123	γ ring (60)
83		101	110	102	δ ring (65)
84			89	85	δ ring (65)
85		65	72	67	δ CC (66)
86			61	56	γ ring (60)
87			47	40	δ CC (58)
88			38	31	τ CH ₃ (67)
89			29	25	γ CC (62)
90			13	10	γ CC (60)

v-stretching, v_{sym} -sym stretching, v_{asym} -asym stretching, δ -in-plane bending, γ -out-of-plane bending, ρ -scissoring, ω -wagging, σ -rocking, τ -twisting.

Table 6.3 Mulliken atomic charges for (4Z)-4-(4-Methylbenzylidene)-2-phenyl-1,3-oxazol-5(4H)-one using B3LYP/6-31G and B3LYP/6-31G (d,p) method

Atom Numbering	Charge		Atom Numbering	Charge	
	B3LYP/6- 31G	B3LYP/6- 31G(d,p)		B3LYP/6- 31G	B3LYP/6- 31G(d,p)
C1	-0.1424	-0.0940	O17	-0.3576	-0.4321
C2	0.0751	-0.0996	C18	-0.0373	0.1646
C3	0.0751	0.0262	C19	0.0395	-0.0336
C4	-0.1083	-0.0904	C20	-0.0745	-0.0741
C5	-0.1435	-0.0952	C21	-0.0744	-0.0743
C6	-0.1043	-0.0728	C22	-0.1639	-0.1184
H7	0.1363	0.0964	H23	0.1490	0.1016
H8	0.1735	0.1199	C24	-0.1639	-0.1173
H9	0.1713	0.1237	H25	0.1490	0.1017
H10	0.1356	0.0960	C26	0.1255	0.1262
H11	0.1349	0.0948	H27	0.1331	0.0879
C12	0.3769	0.5437	H28	0.1331	0.0879
N13	-0.3728	-0.5075	C29	-0.4852	-0.3838
O14	-0.5344	-0.5084	H30	0.1527	0.1180
C15	-0.0682	-0.0258	H31	0.1641	0.1319
C16	0.5467	0.5862	H32	0.1527	0.1206

Table 6.4 HOMO-LUMO energies for (4Z)-4-(4-Methylbenzylidene)-2-phenyl-1,3-oxazol-5(4H)-one by using B3LYP/6-31G (d,p) level of theory

Molecular properties	Energy (eV)	Energy gap (eV)	Ionisation potential (I)	Electron affinity (A)	Global hardness(η)	Global softness(σ)	Chemical potensial (μ)	Global Electroplicity (ω)
E_{HOMO}	-5.2126	-2.8969	5.2126	2.3157	1.4485	0.6904	-2.7642	2.6375
E_{LUMO}	-2.3157							
$E_{\text{HOMO-1}}$	-6.571	-5.6164	6.571	0.9546	2.8082	0.3561	-3.7628	2.5609
$E_{\text{LUMO-1}}$	-0.9546							
$E_{\text{HOMO-2}}$	-7.1835	-6.7557	7.1835	0.4278	3.3778	0.2961	3.8057	2.1439
$E_{\text{LUMO-2}}$	-0.4278							

Table 6.5 Second order perturbation theory analysis of Fock matrix in NBO basis corresponding to intra molecular bands of (4Z)-4-(4-Methylbenzylidene)-2-phenyl-1,3-oxazol-5(4H)-one

Donor	Acceptor	E(2)(kcal/mol)	E(j)-E(i) (a.u)	F _(ij) (a.u)
		BMP	BMP	BMP
LP (1) N 13	BD*(1) C 12 - O 14	4.66	0.62	0.068
LP (1) N 13	BD*(1) C 15 - C 16	2.71	0.82	0.06
LP (1) N 13	BD*(1) C 15 - C 18	0.35	0.72	0.02
LP (1) N 13	BD*(1) C 16 - O 17	0.4	0.63	0.02
LP (1) O 14	BD*(1) C 12 - N 13	1.89	0.99	0.055
LP (1) O 14	BD*(1) C 15 - C 16	1.58	1.04	0.051
LP (1) O 14	BD*(1) C 16 - O 17	0.39	0.84	0.023
LP (2) O 14	BD*(2) C 12 - N 13	19.37	0.31	0.1
LP (2) O 14	BD*(2) C 16 - O 17	16.14	0.29	0.089
LP (1) O 17	BD*(1) O 14 - C 16	0.86	1.02	0.038
LP (1) O 17	BD*(1) C 15 - C 16	1.48	1.23	0.054
LP (2) O 17	BD*(1) O 14 - C 16	11.1	0.5	0.094
LP (2) O 17	BD*(1) C 15 - C 16	2.95	0.71	0.059
LP (2) O 17	BD*(2) C 19 - C 20	0.28	0.28	0.012
LP (1) C 18	BD*(1) N 13 - C 15	0.6	0.77	0.027
LP (1) C 18	BD*(1) C 15 - C 16	4.09	0.82	0.073
LP (1) C 18	BD*(1) C 19 - C 20	0.34	0.93	0.023
LP (1) C 18	BD*(2) C 19 - C 20	4	0.38	0.054
LP (1) C 18	BD*(1) C 19 - C 21	0.35	0.93	0.023

a E(2) means energy of hyperconjugative interactions (stabilization energy).

b Energy difference between donor and acceptor i and j NBO orbitals.

c F(i,j) is the Fock matrix element between i and j NBO orbitals.

Table 6.6 NBO analysis of bonding and antibonding orbit of (4Z)-4-(4-Methylbenzylidene)-2-phenyl-1,3-oxazol-5(4H)-one

Band (A-B)	ED/Energy (a.u.)	ED %	ED %	NBO	S(%)	P(%)
σ C 1-C 2	0.98877	49.7	50.3	0.7050 sp ^(1.85)	35.12	64.88
				0.7092 sp ^(1.81)	35.59	64.41
σ C 1-C 6	0.99014	50.01	49.99	0.7072 SP ^(1.84)	35.26	64.74
				0.7070 SP ^(1.84)	35.26	64.75
σ C 2-C 3	0.9825	48.22	51.78	0.6944 SP ^(1.88)	34.74	65.26
				0.7178 SP ^(1.83)	35.17	64.83
σ C 3-C 4	0.98248	51.79	48.21	0.7196 SP ^(1.85)	35.13	64.87
				0.6944 SP ^(1.88)	34.71	65.29
σ C 3-C 12	0.98717	50.62	49.38	0.7115 SP ^(2.37)	29.67	70.33
				0.7027 SP ^(1.31)	43.28	56.72
σ C 3-C 12	0.98879	50.29	49.71	0.7092 SP ^(1.81)	35.61	64.39
				0.7050 SP ^(1.85)	35.14	64.86
σ C 4-C 5	0.98879	50.29	49.71	0.7092 SP ^(1.81)	35.61	64.39
				0.705 SP ^(1.85)	35.14	64.86
σ C 5-C 6	0.99013	50.01	49.99	0.7072 SP ^(1.84)	35.24	64.76
				0.707 SP ^(1.84)	35.25	64.75
σ C 12-N 13	0.99155	41.08	58.92	0.641 SP ^(2.13)	31.98	68.02
				0.7676 SP ^(2.13)	31.91	68.09
σ C 12-O 14	0.99353	30.56	69.44	0.5528 SP ^(3.04)	24.77	75.23
				0.8333 SP ^(2.17)	31.58	68.42
σ N 13-C 15	0.99006	58.41	41.59	0.7643 SP ^(2.07)	32.58	67.42
				0.6449 SP ^(2.34)	29.93	70.07
σ O14-C 16	0.9935	69.59	30.41	0.8342 SP ^(2.38)	29.58	70.42
				0.5514 SP ^(2.97)	25.22	74.78
σ C 15-C 16	0.99659	50.91	49.08	0.7136 SP ^(1.98)	33.51	66.49
				0.7006 SP ^(1.44)	41.05	58.95
σ C 15-C 18	0.98694	54.63	45.37	0.7391 SP ^(1.74)	36.43	63.57
				0.6736 SP ^(2.43)	29.2	70.8

σ C 16-O 17	0.99543	40.43	59.57	0.6358 SP ^(1.99)	33.39	66.61
				0.7718 SP ^(3.85)	20.63	79.37
σ C 18-C 19	0.9882	46.62	53.38	0.5828 SP ^(2.19)	31.31	68.69
				0.7306 SP ^(2.55)	28.16	71.84
σ C 19-C 20	0.98691	50.97	49.03	0.714 SP ^(1.78)	35.92	64.08
				0.7002 SP ^(1.86)	35.02	64.98
σ C 19-C 21	0.9869	50.97	49.03	0.714 SP ^(1.78)	35.92	64.08
				0.7002 SP ^(1.85)	35.03	64.97
σ C 20-C 22	0.98822	50.25	49.75	0.7098 SP ^(1.82)	35.49	64.51
				0.7053 SP ^(1.85)	35.07	64.93
σ C 21-C 24	0.98821	50.25	49.75	0.7089 SP ^(1.82)	35.46	64.54
				0.7053 SP ^(1.85)	35.05	64.95
σ C 22-C 26	0.98822	49.26	50.74	0.7019 SP ^(1.83)	35.32	64.68
				0.7123 SP ^(1.87)	34.9	65.1
σ C 26-C 29	0.99118	51.17	48.83	0.7154 SP ^(2.31)	30.17	69.83
				0.6988 SP ^(2.86)	25.88	74.12

Table 6.7 Fukui function (f_i^+ , f_i^- , Δf) for (4Z)-4-(4-Methylbenzylidene)-2-phenyl-1,3-oxazol-5(4H)-one

Atom numbering	Neutral (N)	Cation (N-1)	Anion (N+1)	f_k^+	f_k^-	f_k°	Δ	s_k^+	s_k^-	s_k°	ω_k^+	ω_k^-	ω_k°
C1	-0.1396	-0.1442	-0.1339	0.0058	0.0046	0.0052	0.0013	0.0022	0.0018	0.0020	0.0191	0.0149	0.0170
C2	-0.0914	-0.0954	-0.0864	0.0050	0.0040	0.0045	0.0010	0.0019	0.0016	0.0017	0.0164	0.0132	0.0148
C3	0.0539	0.0546	0.0518	-0.0021	-0.0007	-0.0014	-0.0014	-0.0008	-0.0003	-0.0005	-0.0068	-0.0022	-0.0045
C4	-0.0912	-0.0953	-0.0854	0.0059	0.0041	0.0050	0.0018	0.0023	0.0016	0.0019	0.0193	0.0132	0.0163
C5	-0.1398	-0.1443	-0.1347	0.0050	0.0045	0.0048	0.0005	0.0019	0.0018	0.0018	0.0164	0.0149	0.0156
C6	-0.1072	-0.1145	-0.0992	0.0081	0.0072	0.0076	0.0008	0.0031	0.0028	0.0029	0.0263	0.0237	0.0250
H7	0.1409	0.1108	0.1693	0.0283	0.0302	0.0292	-0.0019	0.0109	0.0116	0.0113	0.0924	0.0986	0.0955
H8	0.1543	0.1443	0.1643	0.0100	0.0100	0.0100	0.0000	0.0039	0.0038	0.0038	0.0327	0.0326	0.0327
H9	0.1543	0.1443	0.1647	0.0104	0.0100	0.0102	0.0005	0.0040	0.0038	0.0039	0.0340	0.0325	0.0333
H10	0.1409	0.1108	0.1689	0.0279	0.0302	0.0290	-0.0023	0.0107	0.0116	0.0112	0.0911	0.0987	0.0949
H11	0.1394	0.1061	0.1704	0.0310	0.0334	0.0322	-0.0024	0.0119	0.0129	0.0124	0.1013	0.1092	0.1053
C12	0.2781	0.2378	0.3002	0.0222	0.0403	0.0312	-0.0181	0.0085	0.0155	0.0120	0.0725	0.1317	0.1021
N13	-0.4033	-0.4208	-0.3628	0.0405	0.0175	0.0290	0.0230	0.0156	0.0067	0.0112	0.1324	0.0573	0.0949
O14	-0.4701	-0.5091	-0.4292	0.0408	0.0390	0.0399	0.0018	0.0157	0.0150	0.0154	0.1335	0.1276	0.1305
C15	0.0771	-0.0305	0.0919	0.0148	0.1075	0.0612	-0.0926	0.0057	0.0414	0.0236	0.0485	0.3515	0.2000
C16	0.4974	0.4625	0.5621	0.0647	0.0348	0.0498	0.0299	0.0249	0.0134	0.0192	0.2116	0.1139	0.1627
O17	-0.4489	-0.5592	-0.3981	0.0507	0.1103	0.0805	-0.0596	0.0195	0.0425	0.0310	0.1658	0.3608	0.2633
C18	0.0994	-0.0434	0.1941	0.0947	0.1428	0.1188	-0.0480	0.0365	0.0550	0.0457	0.3098	0.4669	0.3883
C19	-0.0246	0.0044	-0.0286	-0.0040	-0.0290	-0.0165	0.0250	-0.0015	-0.0112	-0.0064	-0.0131	-0.0948	-0.054
C20	-0.1014	-0.1284	-0.0683	0.0331	0.0270	0.0301	0.0061	0.0127	0.0104	0.0116	0.1083	0.0884	0.0983
C21	-0.1013	-0.1283	-0.0681	0.0332	0.0271	0.0301	0.0061	0.0128	0.0104	0.0116	0.1086	0.0885	0.0985

C22	-0.1462	-0.1523	-0.1244	0.0218	0.0061	0.0140	0.0157	0.0084	0.0024	0.0054	0.0713	0.0200	0.0456
H23	0.149	0.0965	0.2171	0.0683	0.0522	0.0603	0.0161	0.0263	0.0201	0.0232	0.2234	0.1708	0.1971
C24	-0.1465	-0.1526	-0.1247	0.0218	0.0061	0.0140	0.0157	0.0084	0.0023	0.0054	0.0713	0.0199	0.0456
H25	0.1488	0.0965	0.2172	0.0684	0.0523	0.0604	0.0161	0.0264	0.0201	0.0232	0.2238	0.1710	0.1974
C26	0.1009	0.0933	0.1153	0.0143	0.0077	0.0110	0.0066	0.0055	0.0030	0.0042	0.0468	0.0253	0.0360
H27	0.1367	0.0775	0.2068	0.0701	0.0592	0.0647	0.0109	0.0270	0.0228	0.0249	0.2294	0.1936	0.2115
H28	0.1367	0.0775	0.2069	0.0702	0.0592	0.0647	0.0110	0.0270	0.0228	0.0249	0.2296	0.1937	0.2116
C29	-0.4696	-0.4728	-0.4701	-0.0005	0.0032	0.0014	-0.0037	-0.0002	0.0012	0.0005	-0.0016	0.0104	0.0044
H30	0.1548	0.1248	0.1975	0.0426	0.0300	0.0363	0.0126	0.0164	0.0116	0.0140	0.1394	0.0981	0.1188
H31	0.1639	0.1247	0.2182	0.0543	0.0392	0.0467	0.0150	0.0209	0.0151	0.0180	0.1774	0.1282	0.1528
H32	0.1546	0.1246	0.1971	0.0425	0.0300	0.0363	0.0126	0.0164	0.0115	0.0140	0.1391	0.0981	0.1186

Table 6.8 Binding affinity for docking in (4Z)-4-(4-Methylbenzylidene)-2-phenyl-1,3-oxazol-5(4H)-one

Drug	Protein	Type of activity	Binding affinity (kcal/mol)	Etimated inhibition constant Ki(μ M)	Bonded residues	Nature of bond	Bond distance (Å)	RMSD
(4Z)-4-(4-Methylbenzylidene)-2-phenyl-1,3-oxazol-5(4H)-one	5FDC	Anticonvulsant	-7.05	6.85	TYR A:7	Conventional Hydrogen bond	1.92	8.468
			-6.71	12.12	HIS A:64	Conventional Hydrogen bond	2.01	25.279
			-6.25	26.17	GLY A: 6	π -Anion	3.02	13.607
			-5.99	40.43	GLY A: 63	Van der waals	3.14	13.263
			-5.78	58.01	PHE A: 231	π - π Alkyl	3.16	35.532
	5H8X	Anticancer	-7.97	1.44	LEU A: 160	Conventional Hydrogen bond	2.26	27.135
			-7.63	2.53	TYR A: 219	Conventional Hydrogen bond	2.18	26.811
			-5.3	129.56	ALA A:161	Conventional Hydrogen bond	3.66	9.135
			-5.18	158.36	VAL A: 194	π - π Stacked	3.21	19.745
			-4.99	221.37	LEU A: 194	Alkyl	2.76	14.536
			-4.96	232.75	HIS A: 197	Amide-Pi Alkyl	4.37	14.701
	1PCV	Antifungal	-6.6	14.5	ARG A: 44	Conventional	1.97	35.044

						Hydrogen bond		
			-6.14	31.45	TRP A: 75	π - π Stacked	2.12	32.706
			-5.97	42.39	ARG A:44	Conventional Hydrogen bond	2.62	44.564
			-5.7	65.97	PHE A:95	Van der waals	2.74	46.382
			-5.64	73.29	MET A:42	Van der waals	3.12	46.842
			-5.63	74.76	GLU A:84	π -Anion	5.4	21.728
			-5.59	80.5	ALA A;86	π -Alkyl	5.37	47.042
	1E0U	Anticonvulsant	-7.23	5.02	ASN A: 11	Conventional Hydrogen bond	2.3	9.016
			-7.01	7.29	HIS A: 64	π -Cation	2.93	11.272
			-6.42	19.84	TYR A: 7	π -Donar Hydrogen bond	3.27	13.611
			-6.23	27.11	GLY A: 63	Van der waals	3.5	8.945
			-6.03	37.84	TYR A: 5	π - π T-Stacked	5.02	16.602
	2RER	Antitubercular	-7.61	2.63	ARG A: 82	Conventional Hydrogen bond	1.83	49.626
			-7.34	4.14	ARG A: 82	Conventional Hydrogen bond	2.22	55.046
			-7.2	5.27	TRP A: 63	π - π Stacked	2.24	53.799
			-6.95	8.03	PRO A: 87	Carbon - Hydrogen	2.35	53.908

						Bond			
			-6.65	13.4	TRP A: 65	π -Sigma	4.12	53.525	
1NNU	Human lymphatic filarial parasites		-7.67	2.37	ALA A: 169	Carbon - Hydrogen Bond	2.03	99.845	
			-7.49	3.23	GLY A: 104	Van der waals	2.12	103.844	
			-7.01	7.31	SER A: 170	Carbon Hydrogen Bond	2.01	111.129	
			-6.94	8.12	LYS A:240	π -Cation	2.6	107.16	
			-6.78	10.74	ASP A: 168	π -Anion	3.3	105.347	
			-6.71	11.99	ASN A:218	Van der waals	4.1	108.043	

Chapter – 7

Molecular Docking, vibrational, structural and electronic studies of (2E)-1-(anthracene-9-yl)-3-(4-ethoxyphenyl) prop-2-en-1-one

Molecular Docking, vibrational, structural and electronic studies of (2E)-1-(anthracene-9-yl)-3-(4-ethoxyphenyl) prop-2-en-1-one

7.1 Introduction

Anthracene derivatives such as Anthraquinone are a significant building block for the synthesis of dyes and pigments [221,222] pharmaceuticals [223, 224], agrochemicals [225], light-emitting devices [226], additives of paper making [227] as well as potentially used as a significant insecticide since it is postulated as the chemical which gives teak its resistance to insect and fungi attacks. Anthracene finds applications as photoelectric material in areas of photo-induced electron transfer, photochemical reactions and photon absorption [228-230]. They also have been widely used as fluorescent sensors, electronic donor or receptors with chromospheres, triple state sensitization agent and polymer of energy transfer detection agent 3-D memory material [231-234]. Hence, anthracene and its derivatives have been the subject matter for ongoing spectroscopic and theoretical investigations from the viewpoint of application and basic science.

Literature survey reveals that to the best of our knowledge, the results based on quantum chemical calculations, FT-IR and FT-Raman studies, HOMO-LUMO analysis, NBO analysis, Reduced Density Gradient (RDG) analysis and molecular studies of (2E)-1-(anthracene-9-yl)-3-(4-ethoxy phenyl)prop-2-en-1-one (ANC1) have not been reported. Quantum Chemical computational methods have proved to be an effective tool for

interpreting and predicting the vibrational spectra. Hence, in this study, an attempt has been made to interpret the vibrational spectra of (2E)-1-(anthracene-9-yl)-3-(4-ethoxy phenyl)prop-2-en-1-one (ANC1) by applying density functional theory calculations based on B3LYP with 6-31G and 6-31G (d,p) basis sets. In addition, the HOMO-LUMO analysis, NBO analysis, Mulliken atomic charge analysis of ANC1 molecule have been studied by B3LYP level with 6-31G (d,p) basis set implemented in the Gaussian 09 program suite [36]. The reduced density gradient (RDG) analysis has been carried out to evaluate steric effect, Van der Waals and Hydrogen bond of the ANC1 molecule using Multiwfn software. The structure of the target protein can be obtained from the protein data bank (PDB) format. The molecular docking can predict the preferred orientation of the ligand concerning the protein concerned with complex. We Hope that the theoretical and experimental results carried out in the current study would be helpful for future research work.

7.2 Experimental details

The infrared and Raman spectra of (2E)-1-(anthracene-9-yl)-3-(4-ethoxy phenyl)prop-2-en-1-one (ANC1) was recorded at Sophisticated Analytical Instrumentation Facility (SAIF), Indian Institute of Technology, Chennai. The FT-IR spectrum of the title compound was recorded in the frequency region 4000-450 cm^{-1} at a resolution of $\pm 1 \text{ cm}^{-1}$ Perkin Elmer spectrometer equipped with an MCT detector, a KBr beam splitter and global source. The spectrum of FT-Raman has been recorded using the 1064 nm line of an Nd-YAG laser as excitation wavelength in the region of 4000-0

cm⁻¹ BRUKER model interferometer. The reported wavenumbers are expected to be accurate within ± 1 resolution with 250 mW of power at the sample in both techniques.

7.3 Computational details

The quantum chemical computations have been carried out to determine the molecular structure, vibrational frequencies with intensities and characteristics of the molecule using density functional triply-parameter hybrid model DFT/B3LYP [235,20] employing 6-31G and 6-31G (d, p) basis sets by Gaussian 09w software package [36]. The natural bonding orbital (NBO) calculations were performed using NBO 3.1 [123] program as implemented in Gaussian 09W package at the 6/31G(d,p) level to understand various second-order interactions between another subsystem which is the measure of the intramolecular delocalization or hyper-conjugation. The HOMO-LUMO analysis was also investigated with the same level, to confirm the intramolecular charge transfer and also molecular electrostatic potential (MEP) contour map shows the various electrophilic region of the ANC1 compound. In order to detect adsorption interactions in real space based on the electron density, the reduced density gradients (RDG) analysis have been studied. The molecular docking calculation was performed by the AutoDock 4.0.1 software [236] which was also applied to detect the docking input files and analyze the docking result. Due to the different potential biological activity, molecular docking of the ANC1 molecule is also reported.

7.4. Results and discussions

7.4.1 Optimized molecular geometrical parameters

The ANC1 compound is optimized using the B3LYP method with the 6-31G and 6-31G (d,p) basis set. The complete geometrical optimization was accomplished by accepting the C1 point group symmetry. The experimental and calculated molecular geometrical parameters were given in Table 7.1 and the observed and calculated bond parameters are compatible with each other. The molecular structure of the ANC1 compound is shown in Fig.7.1. The experimental value of C-C bond length in the range of 1.4747-1.356 Å, which is much shorter than the typical C-C single bond (1.54Å) and longer than the C=C double bond (1.34Å) [237, 238]. The ANC1 compound contains 28 C-C bonds, 21 C-H bonds, 3 C-O bonds and a single H-O bond.

For the ANC1 compound, C1-C2, C1-C6, C3-C4, C5-C6, C7-C10, C9-C10, C11-C13, C14-C15, C24-C26, C26-C28, C28-C30, C30-C32, C31-C33, C32-C35 and C35-C37 bond length are computed as 1.3727, 1.4258, 1.4486, 1.3754, 1.4005, 1.4497, 1.372, 1.3748, 1.4747, 1.356, 1.4571, 1.411, 1.3885, 1.3942 and 1.4055 Å for the basis set B3LYP/6-31G and for 6-31G(d,p) basis set the bond length are observed as 1.3685, 1.4233, 1.4451, 1.3709, 1.3977, 1.4459, 1.3678, 1.3703, 1.4814, 1.3513, 1.4558, 1.4067, 1.3848, 1.3905 and 1.4045Å respectively which are good agreement with 1.406 Å by X-ray crystal data [239]. The C=O bond length (1.1988Å) given by DFT calculation agree with the reported literature values [239] and for the ANC1 compound is C24=O25= 1.2587/1.2298 Å.

According to the calculations for the ANC1 compound, the exocyclic angle C8-C24-O25 and O25-C24-C26 are reduced by 1.0° which shows the interaction between C24 and O25 (C8-C24-O25 = $121.1^\circ/121.06^\circ$ and O25-C24-C26 = $121.19^\circ/121.92^\circ$) for the B3LYP/6-31G and /6-31G(d,p) basis sets. This departure of the exocyclic angles from 120° can be found in the crystal structure of the anthraquinone [240]. For the ANC1 compound, the bond angle for C33-C37-O40, C37-O40-C41, and O40-C41-C44 has $115.7^\circ/115.9^\circ$, $119.7^\circ/119.1^\circ$ and $106.7^\circ/107.5^\circ$ is reduced by 4.3° , 0.3° and 3.3° due to the interaction between the C37 and O40. C35-C37-O40 is increased by 4.3° due to the interaction between the ethoxy group and O40. O40-C41-H42, O40-C41-H43 (= $109.3^\circ/109.7^\circ$, $109.3^\circ/109.7^\circ$) is reduced by 0.3° , 0.7° due to the interaction between H42 and O40.

7.4.2 Vibrational assignments

The ANC1 compound has 47 atoms and 135 modes of fundamental vibrations which span the irreducible representation as A. The observed and simulated FT-IR and FT-Raman spectra of the ANC1 compound at DFT-B3LYP level using 6-31G and 6-31G(d, p) basis sets are shown in Figs. 7.2 and 7.3. The experimental and theoretical wavenumbers along with their intensities are given in Table 7. 2. The assignments of fundamental modes are based on the reported literature and Gauss View visualization program. The observed and calculated wavenumber and potential energy distribution are discussed below.

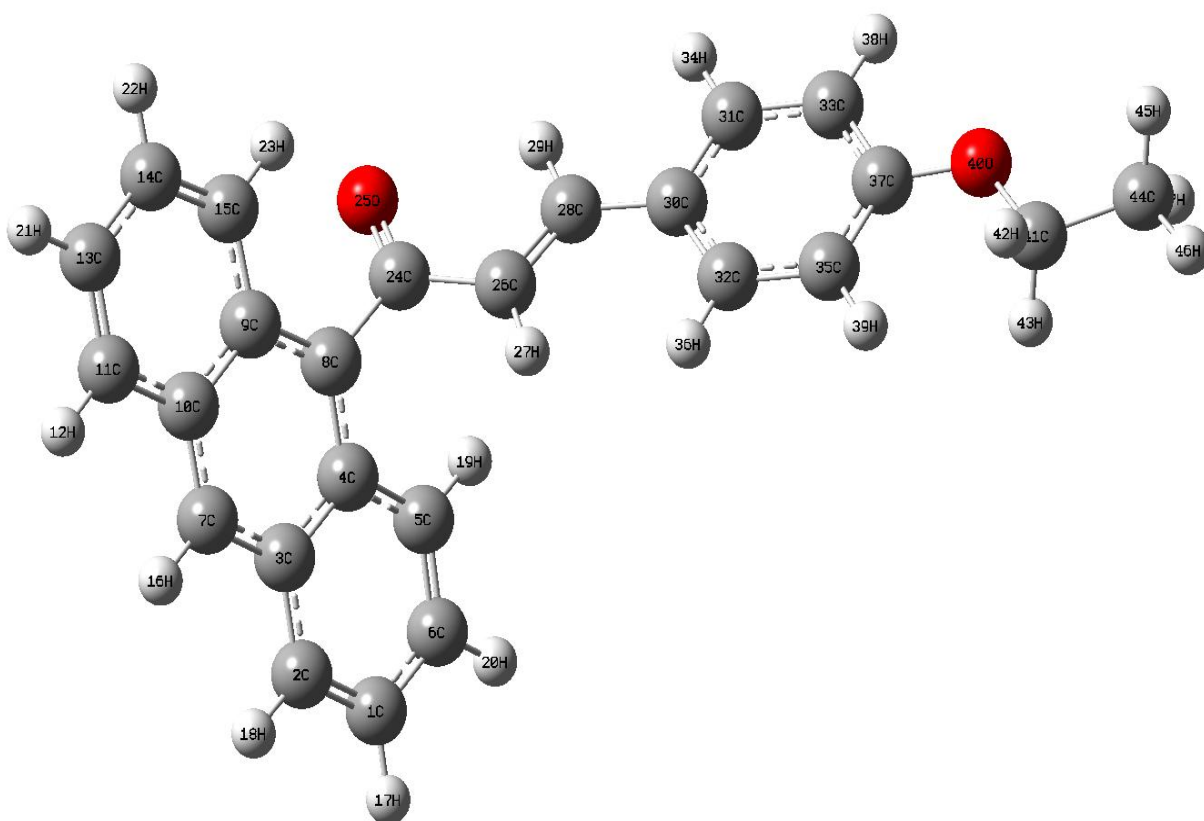


Fig.7.1 Optimized molecular structure of (2E)-1-(anthracene-9-yl)-3-(4-ethoxyphenyl) prop-2-en-1-one

C-H vibrations

The C-H stretching vibrations of aromatic compounds are exhibit in the region 3100-2800 cm^{-1} [59]. The C-H in-plane bending and out-of-plane bending vibrations occur at 1300-1000 cm^{-1} and 1000-700 cm^{-1} [59].

In the present work, the CH stretching vibrations, the band appeared at 3127vw, 3050 vw, 2971 vw, 2923 vw, 2885 vw, 2851 vw cm^{-1} in IR spectrum and 3060s, 2990 vw, 2950 vw, 2860 vw, 2758 vw cm^{-1} in Raman spectrum. The computed values at B3LYP/6-31G method are 3065, 3055, 3045, 3038, 3032, 3025, 3017, 3010, 3002, 2986, 2978, 2971, 2960, 2948, 2940 cm^{-1} and 3062, 3051, 3043, 3036, 3029, 3022, 3015, 3007, 2999, 2982, 2975, 2966, 2957, 2936, 2918, 2907, 2896, 2887 cm^{-1} obtained by by B3LYP/6-31G(d,p) method. Alaşalvar *et al* [241] reported that the CH in-plane bending modes are found at 1466, 1458, 1377, 1264, 1181, 1169, 1160, 1118, 1091, 1078, 1017 cm^{-1} for IR spectrum and 1467, 1385, 1186, 1162, 1123, 1093, 1078 cm^{-1} for Raman spectrum. In the present work, the C-H in-plane bending vibrations reported at 1443, 1313, 1174, 1041 cm^{-1} in the IR spectrum and 1435, 1325, 1216, and 1033 cm^{-1} in the Raman spectrum. The computed values by B3LYP/6-31G method are obtained at 1471, 1445, 1440, 1406, 1392, 1340, 1327, 1273, 1179, 1160, 1078, 1043, 1040 cm^{-1} for B3LYP/6-31G and 1469, 1442, 1438, 1401, 1390, 1337, 1325, 1270, 1175, 1158, 1075, 1040, 1036, 1032 cm^{-1} obtained by B3LYP/6-31G(d,p) method. The C-H out-of-plane bending modes are observed at 727, 813, 841, 846, 864, 905, 919 cm^{-1} for IR spectrum and 817, 841, 863, 924 cm^{-1} for Raman spectrum by Alaşalvar *et al* [241]. In the present

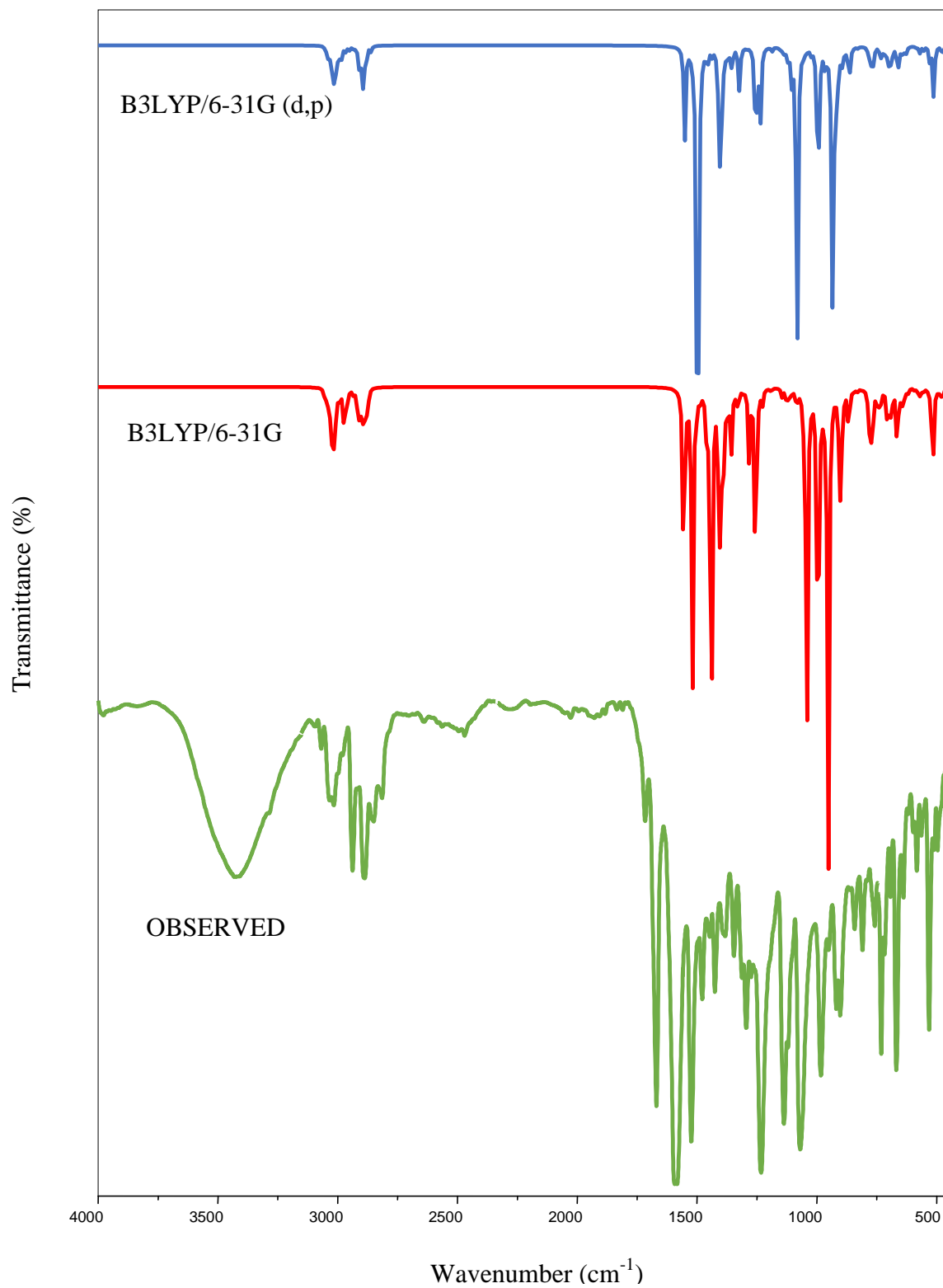


Fig. 7.2 Observed FT-IR and simulated spectra of (2E)-1-(anthracene-9-yl)-3-(4-ethoxyphenyl)prop-2-en-1-one

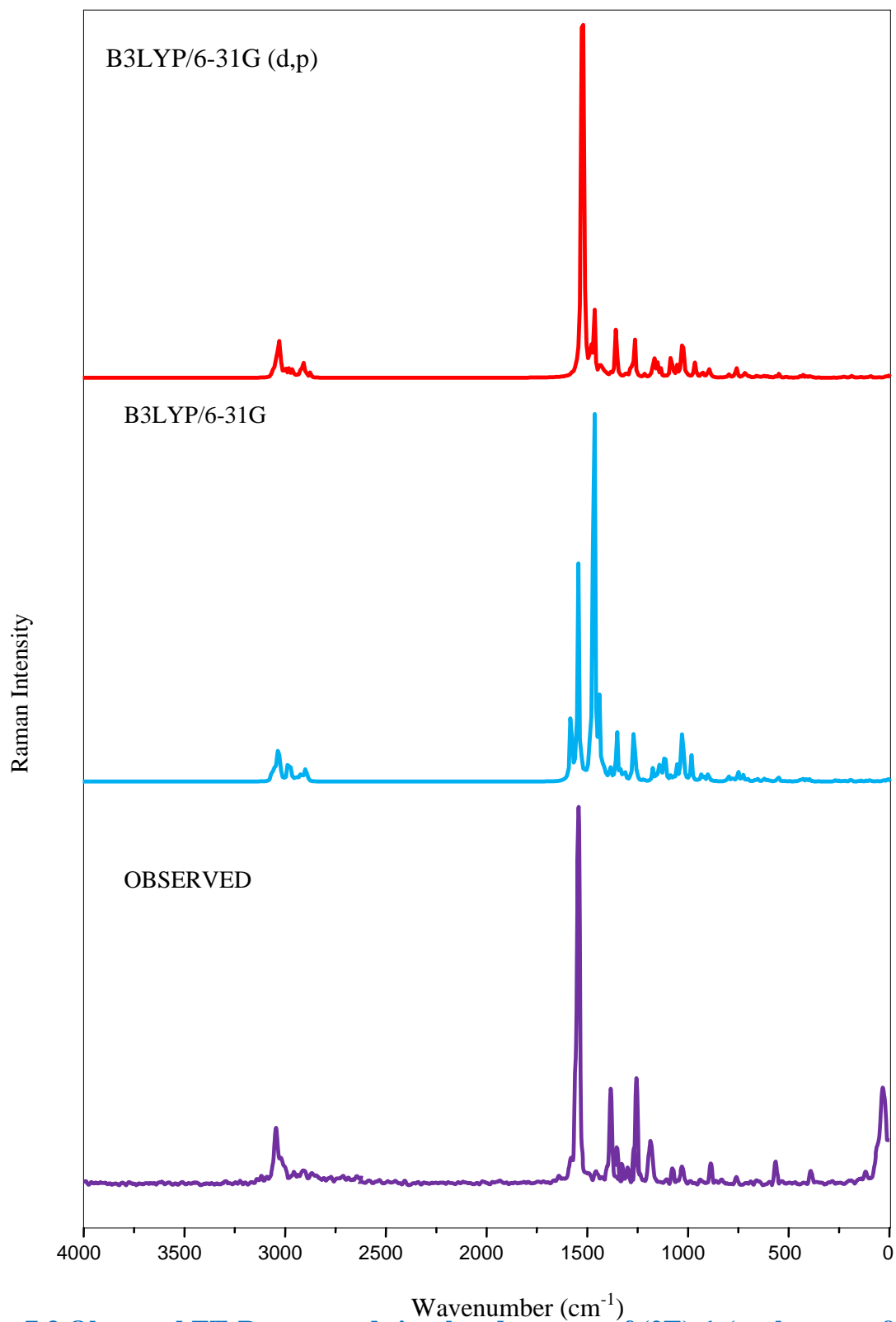


Fig. 7.3 Observed FT-Raman and simulated spectra of (2E)-1-(anthracene-9-yl)-3-(4-ethoxyphenyl)prop-2-en-1-one

work, the C-H out-of-plane bending vibrations are assigned to 918, 890, 864, 798, 734 cm^{-1} in FT-IR and 880, 800, 732 cm^{-1} in FT-Raman. The computed values by B3LYP/6-31G method are 926, 924, 896, 885, 870, 849, 810, 802, 788, 775, 745, 735, 718 cm^{-1} and 930, 923, 918, 892, 881, 867, 845, 809, 799, 785, 771, 741, 733, 715 cm^{-1} obtained by B3LYP/6-31G(d,p) method.

Ring vibrations

The anthracene ring and phenyl ring in-plane bending vibrations were calculated at 784, 770, 648, 636, 628, 615, 600, 439, 420, 406, 388, 304, 125, 105 cm^{-1} for B3LYP/6-31G and 779, 765, 645, 632, 613, 597, 436, 418, 401, 385, 301, 121, 103 cm^{-1} obtained by B3LYP/6-31G(d,p) method. The peaks were observed at 696, 643, 623, 599 cm^{-1} for IR and 765, 600, 450, 400, 120 cm^{-1} for Raman spectrum was assigned to ring in-plane bending vibrations. The ring out-of-plane bending vibrations were calculated at 682, 500, 455, 431, 360, 163, 120, 98, 82, 65, 45, 34, 20, 13 cm^{-1} for B3LYP/6-31G and 681, 497, 451, 427, 361, 160, 117, 95, 80, 62, 40, 29, 17, 10 cm^{-1} obtained by B3LYP/6-31G (d,p) method and the Raman spectrum was observed at 82 cm^{-1} .

C-O vibration

The C-O stretching mode is expected in the region 1750-1680 cm^{-1} [242, 161, 243]. The in-plane and out-of-plane C-O bending modes are expected in the regions 625 ± 70 and $540 \pm 80 \text{ cm}^{-1}$, respectively. In the present work, C-O stretching mode, in-plane bending and out-of-plane bending vibrations are observed at 1116 cm^{-1} , 669 cm^{-1} and 557 cm^{-1} by FT-IR and at $\nu=1580 \text{ cm}^{-1}$ and $\gamma=557 \text{ cm}^{-1}$ by FT-Raman. Hence in

the present work, the calculated C-O stretching vibrations by B3LYP/ 6-31G method at = 1585, 1120, 1007 cm^{-1} , C-O in-plane bending = 734, 673, 575 cm^{-1} , C-O out-of-plane bending = 559 cm^{-1} and ν_{CO} =1581, 1118, 1001 cm^{-1} , δ_{CO} = 729, 670, 571 cm^{-1} , γ_{CO} = 555 cm^{-1} by B3LYP/6-31G (d, p).

CH₃ vibrations

The wavenumber of the vibrational modes of methoxy group is known to be influenced by a many interactions such as electronic effects, intermolecular hydrogen bonding and Fermi resonance [244]. Electronic effect such as back donation and induction are caused by the presence of oxygen atom adjacent to CH₃ group that can shift the position of CH stretching and bending modes [245, 246]. ν_{asCH_3} absorb with a weak medium intensity ($2985\pm 25 \text{ cm}^{-1}$ and $2970\pm 30 \text{ cm}^{-1}$) and regularly seen above 3000 cm^{-1} . In the present work, CH₃ stretching vibrations for the ANC1 compound, the bands appeared at $\nu_{\text{ass}}=2923_{\text{vw}} \text{ cm}^{-1}$ in FT- IR spectrum and 2900, 2890 cm^{-1} for FT- Raman spectrum. The computed values for $\nu_{\text{ass}} = 2928, 2920 \text{ cm}^{-1}$, $\nu_{\text{ss}}= 2910$, $\delta_{\text{opb}}=1420 \text{ cm}^{-1}$, $\delta_{\text{sb}}=1358, 1315 \text{ cm}^{-1}$, $\delta_{\text{ipb}}=1415 \text{ cm}^{-1}$, $\gamma_{\text{opr}}=1131 \text{ cm}^{-1}$, $\delta_{\text{ipr}}=1024 \text{ cm}^{-1}$ computed wave-numbers by B3LYP/6-31G method and at $\nu_{\text{ass}}=2925, 2918 \text{ cm}^{-1}$, $\delta_{\text{opb}}=1417 \text{ cm}^{-1}$, $\delta_{\text{ipb}}=1410 \text{ cm}^{-1}$, $\delta_{\text{sb}}=1355, 1312 \text{ cm}^{-1}$, $\gamma_{\text{opr}}=1129 \text{ cm}^{-1}$ computed wavenumber by B3LYP/6-31G(d,p) method.

CH₂ vibrations

The main fundamental vibrations associated with each CH₂ group is classified as CH₂ symmetric stretching, asymmetric stretching, rocking and scissoring modes belong to in-plane vibration, whereas CH₂ twisting and wagging modes assigned to out-of-plane

bending vibration. This CH₂ symmetric and asymmetric stretching vibrations occur in the range 3000- 2800 cm⁻¹ [247]. For the ANC1 compound, the methyl group, symmetric stretching is observed at $\nu_{\text{ssCH}_2} = 2889, 2887 \text{ cm}^{-1}$ and $\nu_{\text{asCH}_2} = 2898, 2896 \text{ cm}^{-1}$ theoretically obtained by B3LYP/6-31G and B3LYP/6-31G (d,p) method. Scissoring modes reported at 1313 cm⁻¹ (IR), 1435 cm⁻¹ (Raman) and 1440, 433, 1420 cm⁻¹ observed theoretically for B3LYP/6-31G, 1438, 1431, 1417 cm⁻¹ for B3LYP/6-31G (d,p). Rocking modes are observed at 1356, 1313 cm⁻¹ for IR spectrum and 1355 cm⁻¹ for Raman spectrum. Theoretically δ_{rock} observed at 1358, 1315, 1024 cm⁻¹ by B3LYP/6-31G, 1355, 1312, 1188 cm⁻¹ $\gamma_{\text{wag}} = 758, 752 \text{ cm}^{-1}$ by B3LYP/6-31G (d,p) methods. $\tau_{\text{CH}_2} = 1131, 1129 \text{ cm}^{-1}$ for the same basis set. Varasanyi *et al* [197] observed the τ_{CH_2} scissoring mode at 1465, 1420 cm⁻¹ and CH₂ twisting and wagging at 1350, 1150 cm⁻¹. For methyl group, two asymmetric stretching modes are calculated at 2974, 2975, 2978 and 3006 cm⁻¹, while one symmetric stretching vibrational frequency is observed at 2921 and 2926 cm⁻¹ by Alasalvar *et al* [241].

C-C vibration

The C-C stretching vibrations in aromatic rings generally appear at 1600-1400 cm⁻¹ [248-250, 251, 252]. In the present work, the C-C stretching vibrations observed at 1424, 1387, 1257 in FT-IR and 1565, 1515, 1294, 1259 cm⁻¹ in FT-Raman spectrum. These C-C stretching modes are calculated at 1571, 1560, 1549, 1531, 1518, 1489, 1429, 1388, 1366, 1289, 1260, 1145 cm⁻¹ B3LYP/6-31G method and 1566, 1557, 1545, 1528, 1516, 1487, 1425, 1385, 1362, 1288, 1258, 1221, 1141 cm⁻¹ by B3LYP/6-31G(d,p) method. In the present study, The C-C in-plane deformation were calculated at 806, 728, 707, 474,

338, 228 cm^{-1} by B3LYP/6-31G method and 804, 722, 703,470, 334, 226 cm^{-1} by B3LYP/6-31G (d,p) method. The C-C out-of-plane deformation were calculated at 661, 535, 520, 285, 260, 241 cm^{-1} for B3LYP/6-31G and 657, 531, 519, 282, 258, 239 cm^{-1} for B3LYP/6-31G (d,p).

7.5 Mulliken atomic charges

The natural population analysis of the ANC1 compound is obtained by Mulliken population analysis with B3LYP level using 6-31G and 6-31G (d,p) basis sets. The Mulliken charge values are tabulated in Table 7.3 and the plot is shown in Fig. 7.4. The calculation has an important role in the application of quantum chemical calculation to the molecular system because of atomic charge affect, dipole moment, molecular polarizability and electronic structure. The charge changes with the basis set to polarization. For example, the charge of C(24) and C(37) atoms has 0.22 a.u, 0.32 a.u and 0.3 a.u, 0.36 a.u for the B3LYP /6-31G and B3LYP /6-31G (d,p) basis set are more positive, which are acceptor atoms The charge distribution for C(33) and C(35) atoms has -0.13 a.u, -0.12 a.u and -0.14 a.u, -0.13 a.u charges. The charges of O(25) and O(40) atoms have -0.45 a.u, -0.49 a.u and -0.56 a.u, -0.52 a.u are more negative which are donor atoms. MEP and Mulliken charge analysis can be used for interpreting and predicting the reactive sites of a wide variety of chemical systems in both nucleophilic and electrophilic reactions.

7.6 NBO analysis

The natural bond orbital (NBO) calculations for the ANC1 compound were performed using NBO 3.1 program [123] as implemented in the Gaussian 09 package at the DFT / B3LYP level with 6-31G (d,p) basis set. The NBO method demonstrates the bonding concept like atomic charge, Lewis structure, bond type, hybridization, bond order, charge transfer and resonance possibility. The stabilization of orbital interaction is proportional to the energy difference between interacting orbitals. The bonding – antibonding stabilization energies within the molecule are calculated, to investigate the intermolecular interactions. The bonding - antibonding interactions can be qualitatively described employing second-order perturbation interaction energy $E(2)$ [255, 256,189,257, 258]. This energy represents the estimate of the off-diagonal NBO Fock matrix elements and the Fock matrix was carried out to evaluate donor (i) and acceptor (j). The stabilization energy $E(2)$ associated with delocalization $i \rightarrow j$ is estimated as follows

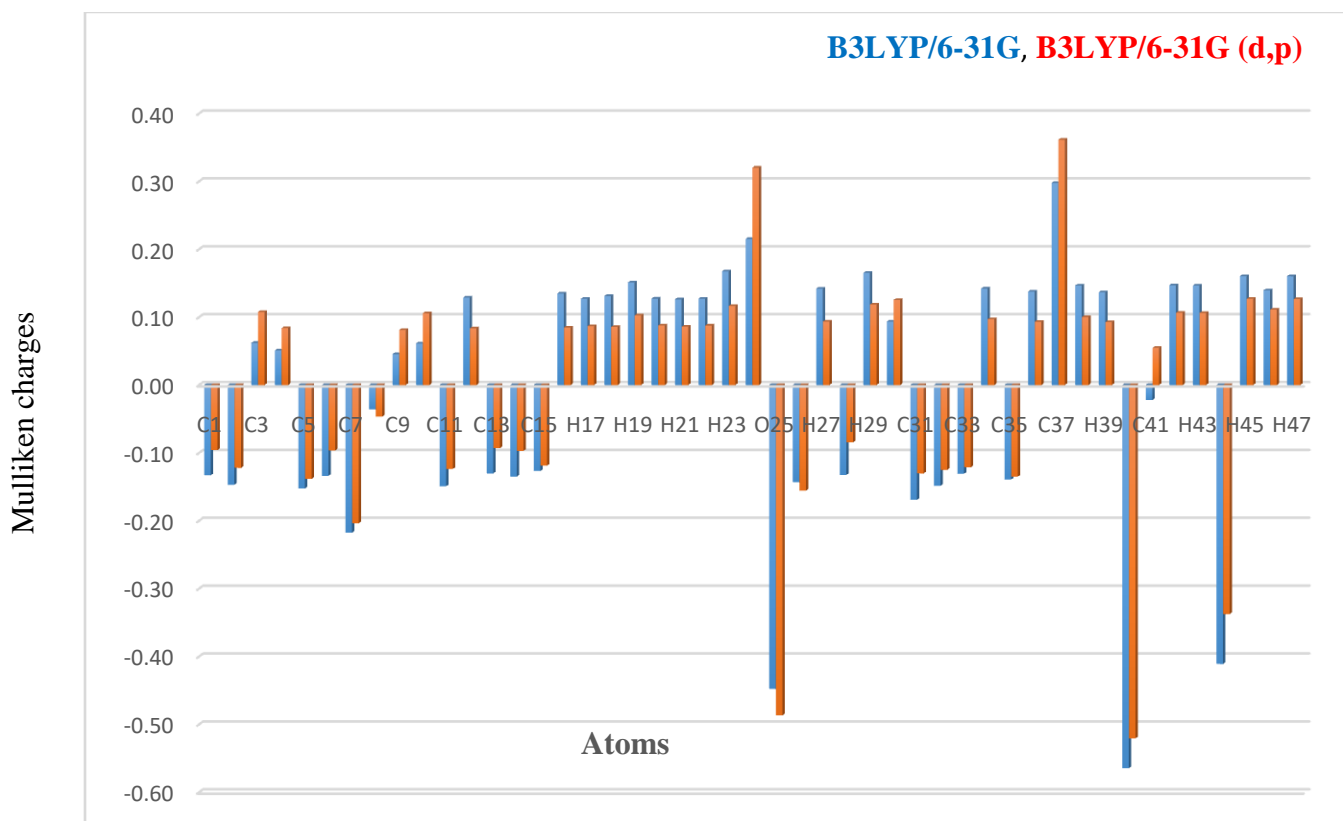


Fig.7.4 Mulliken atomic charges of (2E)-1-(anthracene-9-yl)-3-(4-ethoxyphenyl)prop-2-en-1-one

$$E(2) = \Delta E_{ij} = \frac{q_i F_{2(i,j)}}{\epsilon_j - \epsilon_i}$$

where q_i is the donor orbital occupancy ϵ_j and ϵ_i are diagonal elements and $F(i,j)$ is the offdiagonal NBO Fock matrix element.

The occupancy of bond orbitals, atomic and hybrid contributions of different bonds of the ANC1 compound are presented in Table 7.4. The NBO analysis BD (C37-O40) orbital with 1.99005 electrons has 33.04% C37 character in a $sp^{1.14}$ hybrid and has 66.96% O40 character in a $sp^{2.33}$ hybrid. The $sp^{1.14}$ hybrid on C37 has 75.64 p-characters and the $sp^{2.33}$ hybrid on O40 has 69.97 p-character. For BD (C41-C44) orbital with 1.98962 electrons has 50.54% C41 character in a $sp^{2.55}$ hybrid and has 49.46% C44 character in a $sp^{2.9}$ hybrid. The $sp^{2.55}$ hybrid on C41 has 71.87% p-character and the $sp^{2.9}$ hybrid on C44 has 74.33% p-character for the ANC1 compound. The two coefficients, 1.99005 and 1.98962 are called polarization coefficients. The sizes of these coefficients show the importance of the two hybrids in the formation of the bond. The oxygen has a larger percentage of this NBO, 66.96% and gives the larger polarization coefficient 0.8183 because it has the higher electronegativity. Similarly, BD (C5-H19), BD (C1-H17), BD (C2-H18) having a lesser percentage of NBO and give the lesser polarization coefficients as compared to BD (C37-O40) bond. This shows that oxygen and carbon in the above bonding orbitals have less electronegativity as compared to BD (C37-O40).

The donor-accepter interaction can be estimated by the second-order perturbation theory. Table 7.5 lists the calculated second-order interaction energies $E(2)$ between the donor-accepter orbital of the ANC1 compound. The most important interaction energies

related to the resonance in the anthracene ring are electron-donating from the BD (C1-C2), BD (C3-C4), LP(2) O25, LP(2) O25, LP(2) O40, LP(2) O40 to the anti-bonding acceptor BD*(2) C3-C4, BD*(2) C8-C9, BD*(1) C24-C26, BD*(1) C8-C24, BD*(2) C35-C37, BD*(1) C41-H43, orbitals and their corresponding energies are 24.47, 44.72, 19.57, 8.82, 8.35 and 5.56 kcal/mol, respectively. These interactions indicate that the strongest interaction increase in the stabilization energy of electron delocalization occurs due to the substitution of the molecule.

7.7 Frontier molecule orbitals

The highest occupied molecular orbital (HOMO) and lowest unoccupied molecular orbital (LUMO) are called as the frontier molecule orbitals (FMOS) that have an important role in chemical reactions [209]. The HOMOs and LUMOs can be considered as donor and acceptor groups occupied, unoccupied by electrons respectively. The energy values between HOMO and LUMO also determines the molecular electronic properties such as ionization potential ($I = -E_{\text{HOMO}}$), electron affinity ($A = E_{\text{LUMO}}$), chemical hardness ($\eta = (I-A)/2$), Chemical softness ($\epsilon = 1/2(I-A)$), Chemical potential ($\mu = -(I+A)/2$), Electronegativity ($\chi = (I+A)/2$), electrophilic index ($\omega = \mu^2 / 2\eta$) chemical reactivity and chemical stability that are important parameters in a quantum chemistry [257, 120, 258]. To understand the bonding schemes of the ANC1 compound, the surfaces of FMOs are given in Fig.7.5 and Table 7.6. The energy gap, the difference between H-L, H-1-L-1, H-2-L-2 orbital are the parameters in determining molecular electrical transport properties because it is a measure of electronic conductivity and the

energy gaps were calculated as 3.1197, 4.3785 and 6.1495eV respectively. This energy gap also indicates the colour of these compounds as electrons are constantly shifting between these orbitals and further dictates their interaction with receptor site at the cellular level. Simultaneously, it also explains that charge transfer interactions are occurring within the molecules. From the energy gap, one can find whether the molecule is hard or soft. The molecules having a large energy gap are known as hard and having small energy gap is known as soft. The energy gap of the ANC1 compound is 3.12 eV. Hence we conclude that the ANC1 compound belongs to hard material. The soft molecules are more polarizable than the hard one because they need small energy for excitation. The calculated values of the hardness and softness of the molecules were 0.115eV and 8.722eV. The chemical potential of the title compound is negative and it means that the ANC1 compound is stable.

7.8 Molecular electrostatic potential

The molecular electrostatic potential (MEP) has been used to predict the behaviour and reactivity of the molecule. It is very useful in understanding the potential sites for electrophilic (negative region) and nucleophilic (negative region) reactions [259]. MEP is also well suited for analyzing process based on the “recognition” of one molecule by another, as in drug-receptor and enzyme-substrate interactions because it is through their potential that the two species first “see” each other [260]. To predict reactive sites for electrophilic and nucleophilic sites for the investigated molecule, MEP is calculated at

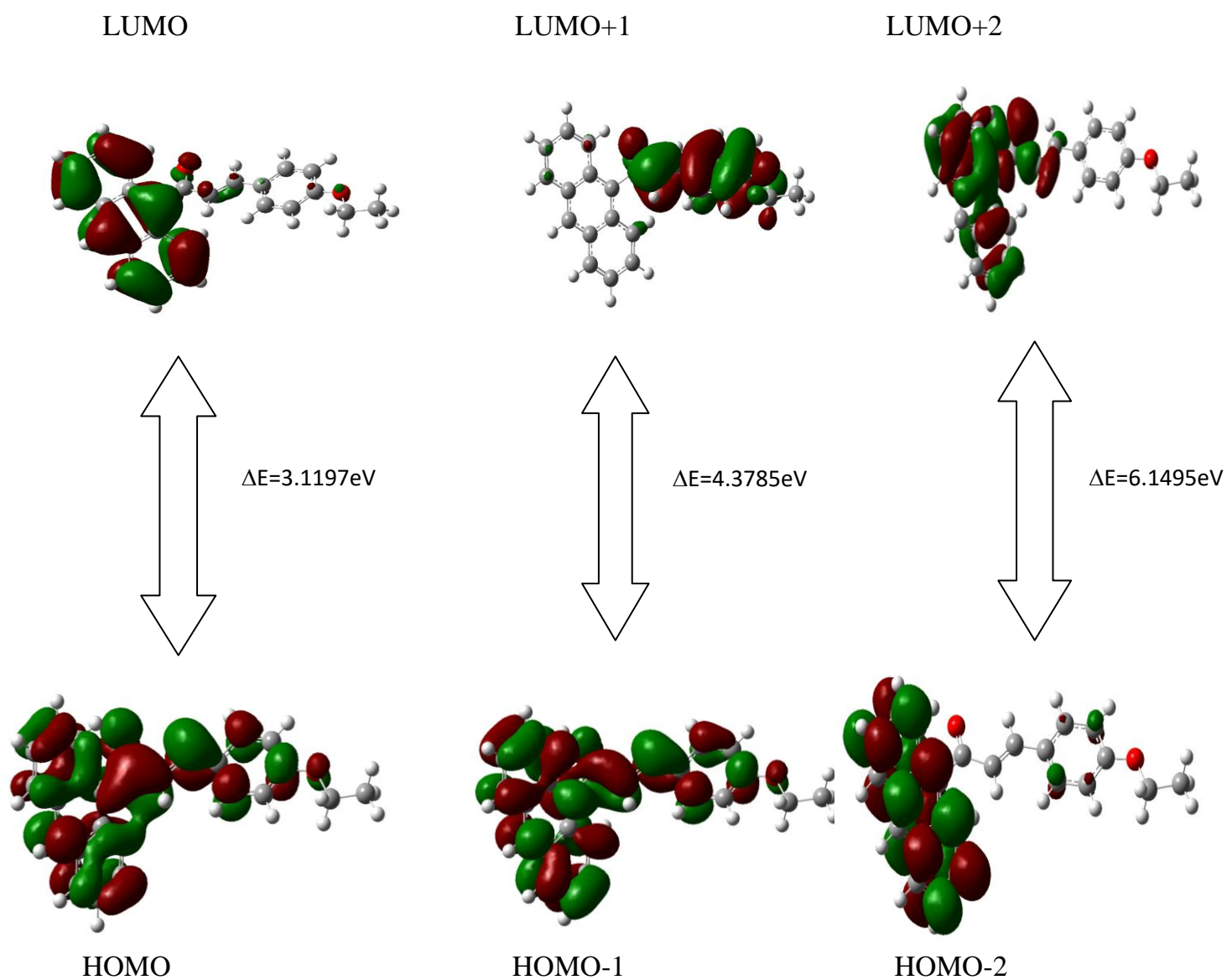


Fig 7.5 Patterns of the principle highest occupied and lowest unoccupied molecular orbital of (2E)-1-(anthracene-9-yl)-3-(4-ethoxyphenyl) prop-2-en-1-one

the B3LYP/6-31G(d,p) optimized geometries and shown in Fig. 7.6. The colour scheme for the MEP surface is, red represents a rich region which is an absolute negative charge, yellow represents the slightly electron-rich region, light blue represents a slightly electron-deficient region, green represents the neutral region and blue represents electron-deficient which is a partially positive charge. Potential increases in the order red < orange < yellow < green < blue [261].

For the ANC1 compound, more reactive sites are close to the C=O group, the regions having the most negative potential over the oxygen atom O25 ketone group then all the hydrogen atoms have positive potential. The red colour is a negative potential which corresponds to the interaction of a proton and blue region is positive which corresponds to the repulsion of the proton. It is seen that negative electrostatic potential (red) is located maximum around oxygen atom and the hydrogen atoms attached to the ethylene group possess the bang of positive charge (blue).

7.9 Reduced density gradient (RDG) analysis

The reduced density gradient (RDG) [128] analysis can be used to reveal the intermolecular, intramolecular and covalent interactions in real space based on the electron density using Multiwfn and plotted by visual molecular dynamics (VMD) program [262, 77]. In order to explore the features associated with reduced gradients, we examined plots of RDG versus sign ($\lambda_2(r)\rho(r)$) and the resultant graph is shown in Fig.7.7.

$-6.480 e^{-2}$



$-6.480 e^{-2}$

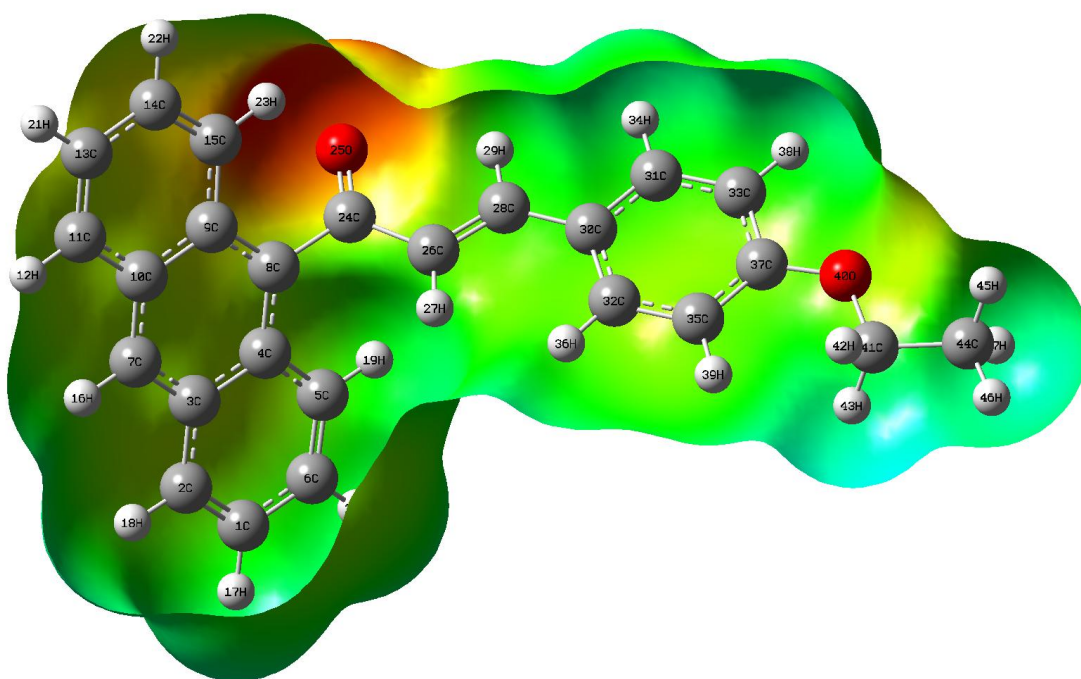


Fig 7.6 Molecular electrostatic potential surfaces of (2E)-1-(anthracene-9-yl)-3-(4-ethoxyphenyl)prop-2-en-1-one

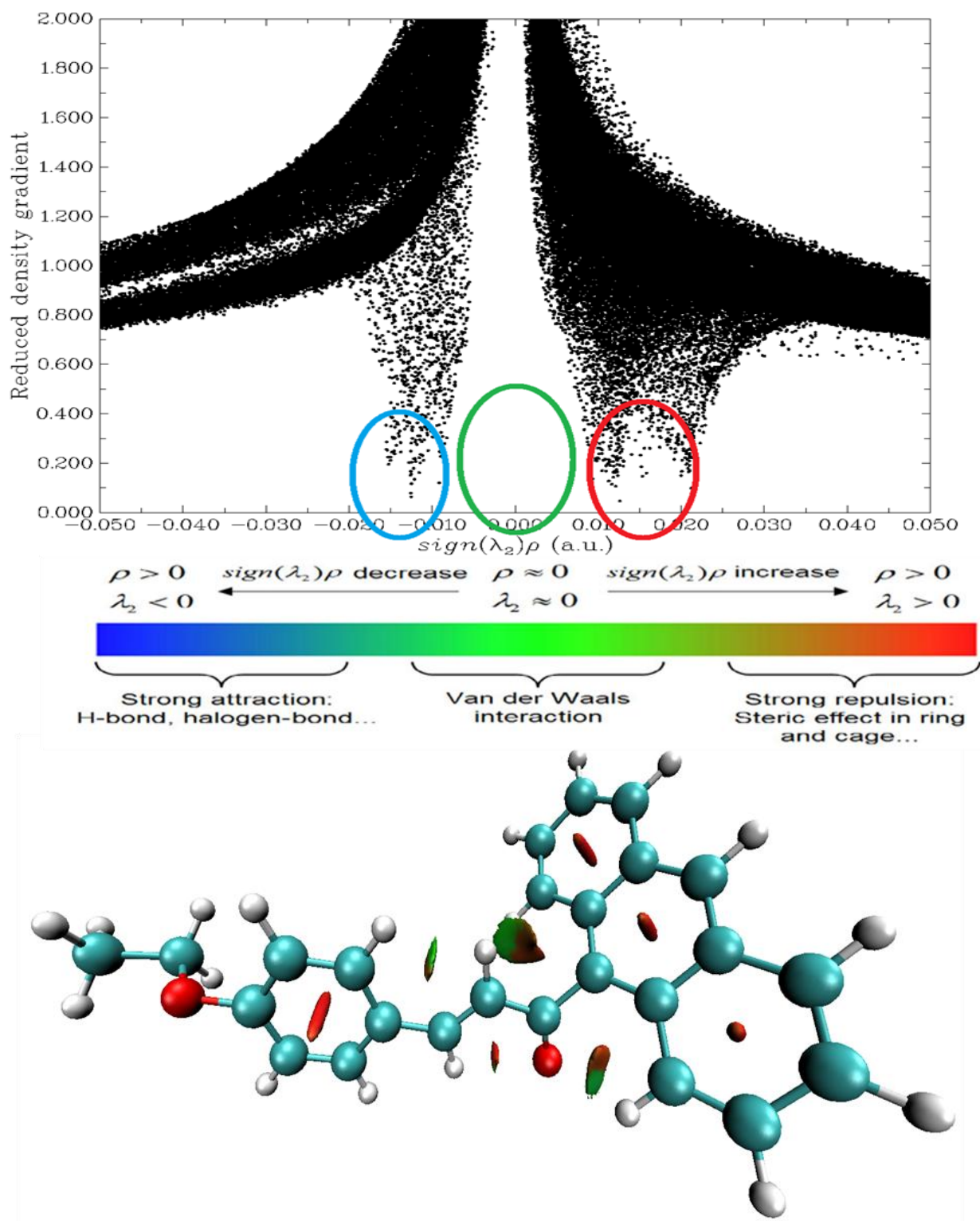


Fig 7.7 Plots of the RDG versus $\lambda(2)\rho$ of (2E)-1-(anthracene-9-yl)-3-(4-ethoxyphenyl)prop-2-en-1-one

According to graph, the green regions represent weak attractive interactions ($\lambda^2 \approx 0$) such as Van der Waals interaction, blue color ring represents strong interaction like hydrogen bond and red color represents steric repulsion. For the ANC1 compound, the phenyl ring showed more steric effect than anthracene ring and benzene ring. The negative values of $\lambda(2)\rho$ indicates strong attractive interactions, while the positive values mean the repulsive interactions. The color on the RDG isosurface between the carbon and oxygen showed that strong Van der Waals interaction formed. The Van der Waals interaction in the ANC1 compound has two strong spikes observed.

7.10 Fukui functions

The Fukui function is a local reactivity descriptor that indicates the preferred regions where chemical species will change its density when the number of electrons is modified and hence, it indicates propensity of the electronic density to deform at a given position upon donating or accepting electrons. Condensed Fukui functions can be defined using finite differences of the electronic density [263]. Electrophilic and nucleophilic attack is given by

$$f_{k-} = q_k(N) - q_k(N-1)$$

$$f_{k+} = q_k(N+1) - q_k(N)$$

where q_k is the atomic charge (N-1) is the densities of the cation, (N) is the neutral and (N+1) is the densities of anionic charges.

The Fukui function is a function defined at each point of space, but it's helpful to define a condensed Fukui function. In this case, the Fukui functions are defined as

condensed to an atom, by a partition scheme. The condensed forms of Fukui functions for an atom k in a molecule are expressed as: $f^+ = (N+1)-(N)$, (for a nucleophilic sites), $f^- = (N)-(N-1)$, (for an electrophilic sites). From Table, 7.7 C=0.0859, 3C=0.1244, 4C=0.1077, 9C=0.1258, 10C= .1165, 14C=0.0887, 15C=0.0099, 25O=0.0624, 26C=0.0989, 30C=0.1132, 31C=0.0339, 33C=0.0872, 35C=0.0871 and 44C=0.0448 are positive values $f(r)>0$. 7C=-0.0226, 12H=-0.0723, 16H=-0.0776, 17H=-0.0671, 18H=-0.0738, 19H=-0.0957, 20H=-0.0652, 21H=-0.0674, 24C=-0.1307, 27H=-0.0775, 28C=-0.1081, 29H=0.0783, 34H=-0.0898, 36H=-0.0854, 37C=-0.101, 38H=-0.0956, 39H=-0.0935, 41C=-0.0372, 45H=-0.0208, 46H=-0.0189 and 47H=-0.0202 are some of the negative values ie $f(r)<0$.

7.11 Atom in molecule analysis

The topological analysis of atoms in the molecule gives as more information about the presence of strong and weak hydrogen bonds in terms of in terms of Topological parameters for intramolecular interactions in compound electron density (ρ_{BCP}), Laplacian of electron density (V^2_{BCP}), electron kinetic energy density (G_{BCP}), electron potential energy density (V_{BCP}), total electron energy density (H_{BCP}), Hydrogen bond energy (E_{HB}) at bond critical point (BCP) [181]. The criteria contribute a basis to discriminate these interactions from Van der Waals interactions and have been establish to be sufficient for slandered and nonconventional H-bonds. Here, AIM analysis is accomplished to examine the intermolecular interactions with in the ANC1 compound. The molecular diagram of the ANC1 compound using the AIM program calculated at

B3LYP/6-31G (d, p) approximation was presented in Fig. 7.8. The topology of electron density of different intra and intermolecular interactions is counterpoint to validate the strength of interactions. The strength of hydrogen bond can also be characterized by evaluating the hydrogen bond energy (E_{HB}). The bond interactions and their values are enrolled in Table 7.8.

7.12 Molecular docking studies

Molecular docking is an efficient tool to get insight into ligand-receptor interactions. This is usually helpful in designing novel inhibitors possessing specific activities. Molecular docking calculations were performed on AutoDock-Vina software [78]. The 3D crystal structure was obtained from Protein Data Bank (PDB ID: 5T6N). The Auto Dock Tools (ADT) graphical user interface was used to add polar hydrogen. Atomic charges for the protein were calculated by Kollman method. Protein was cleaned by removing waters and co-crystallized ligands. The ligand (2E)-1-(Anthracene-9-yl) -3-(4-ethoxyphenyl) prop-2-en-1-one (ANC1) was prepared for docking by minimizing its energy at B3LYP/6-31G (d,p) level of theory. Partial charges were calculated by Geistenger method. The active site of the enzyme was defined to include residues of the active site within the grid size of $40\text{\AA} \times 40\text{\AA} \times 40\text{\AA}$. The most popular algorithm, Lamarckian Genetic Algorithm (LGA) [264] available in Autodock was employed for docking. The docking protocol was tested by extracting co-crystallized inhibitor from the

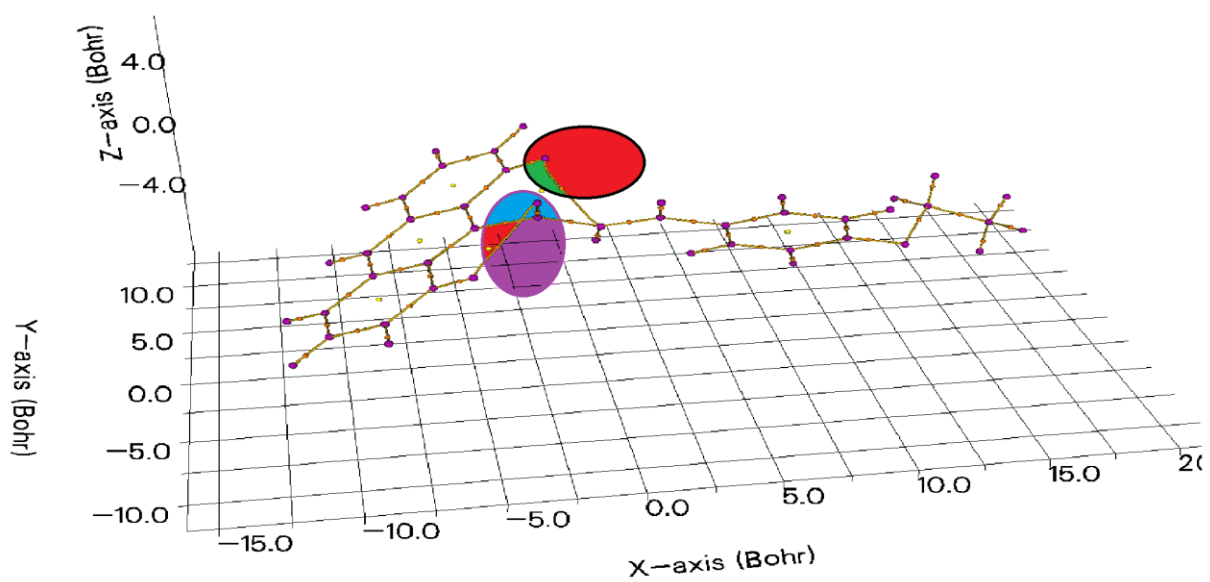


Fig.7.8. Molecular graph of (2E)-1-(anthracene-9-yl)-3-(4-ethoxyphenyl)prop-2-en-1-one

protein and then docking the same. The docking protocol predicted the same conformation as was present in the crystal structure with RMSD value well within the allowed range of 2Å. Amongst the docked conformations the best scored conformation predicted by AutoDock scoring function was visualized for ligand-enzyme interactions in Discover Studio Visualizer 4.0. The molecular docking binding energies and inhibition constants were obtained and listed in Table 7.9. The ANC1 compound taken as the ligand interactions with proteins are shown in Fig. 7.9 respectively. The docking of the ANC1 compound with the protein inhibitors to forms a stable complex and it gives the better binding affinity (-6.81 ΔG in kcal/mol) value and bond distance is 1.8 Å. Hence it can be concluded that the ANC1 compound may be used for design and synthesis of a new drug for anti-viral. However, biological tests should be carried out before support the results.

Anticancer activity

Interaction of anticancer protein 4G9R shows the existence of many conventional bonds such as two van der waals bonds, one carbon-hydrogen bond and one π -donar hydrogen bond interaction with amino acid (THR A: 269, THR A: 269, TYR A: 277, THR A: 279) with different binding energies (-5.5, -5, -5.98, -5.17) kcal/mol, inhibition constants (93.22, 217.31, 41.02, 162.63) μM RMSD values are (48.225, 47.159, 46.819, 47.159)Å.

Interaction of anticancer protein 4D8S shows the existence of many conventional bonds such as one van der waals bonds, two π -sulfur bond and two Alkyl bond interaction with amino acid (VAL A: 449, CYS A: 129, CYS A: 129, VAL A: 163, LEU A: 4120) with different binding energies (-5.23, -6.7, -5.06, -6.07, -5.9)kcal/mol,

inhibition constants (147.57, 12.3, 198.84, 35.58, 47.14)ki(μ M) RMSD values are (5.785, 35.313, 30.141, 45.9, 141.131) Å.

Antiviral activity

Interaction of antiviral protein 5T6S shows the existence of many conventional bonds such as two van der waals bonds, two π -cation bond and two Carbon-Hydrogen bond interaction with amino acid (ASN A: 133, MET A: 151, ARG A: 141, ARG A: 141, ALA A: 149, ALA A: 149) with different binding energies (-4.11, -3.99, -3.75, -3.62, -3.22, -3.02)kcal/mol, inhibition constants (964.52, 1.2(mM), 1.79(mM), 2.24(mM), 4.35(mM), 6.06 (mM))ki(μ M) RMSD values are (282.655, 268.727, 258.241, 274.112, 257.795, 279.965)Å.

Interaction of antiviral protein 5T6N shows the existence of many conventional bonds such as two π - π stacked, two van der waals bonds, one π - p stacked bonds interaction with amino acid (TRP A: 234, TRP A: 234, ASP A: 104, PRO A: 103, TRP A: 234) with different binding energies (-5.69, -5.32, -5.18, -3.52, -3.59)kcal/mol, inhibition constants (67.22, 127.03, 160.76, 2.65(mM), 2.35(mM))ki(μ M) RMSD values are (59.851, 59.328, 60.614, 100.194, 86.7)Å.

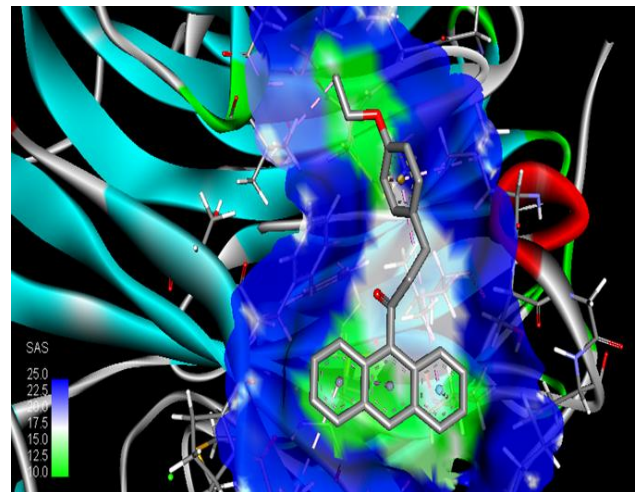
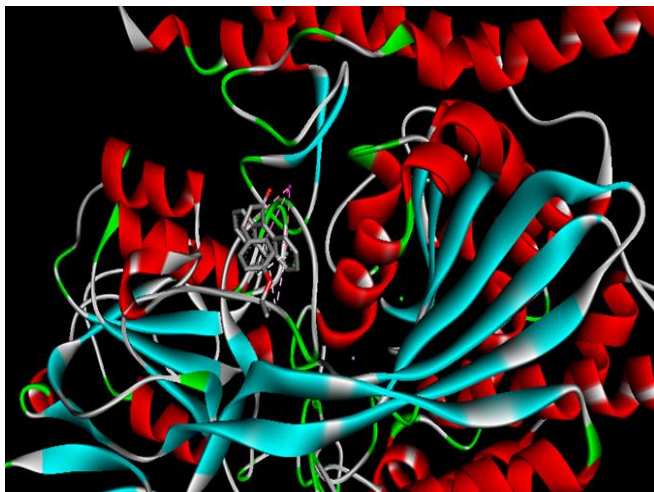
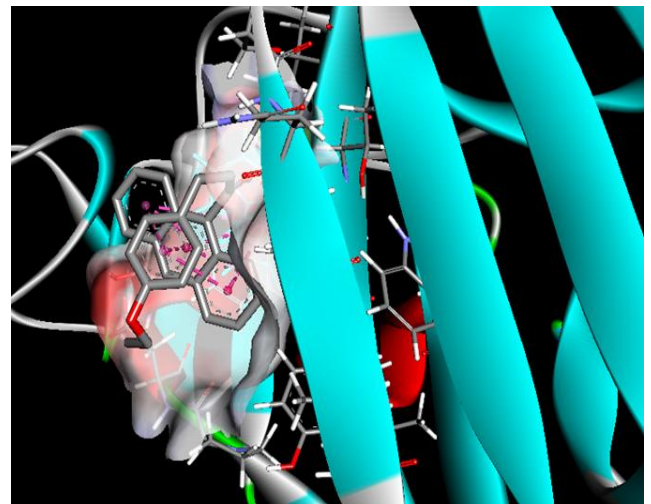
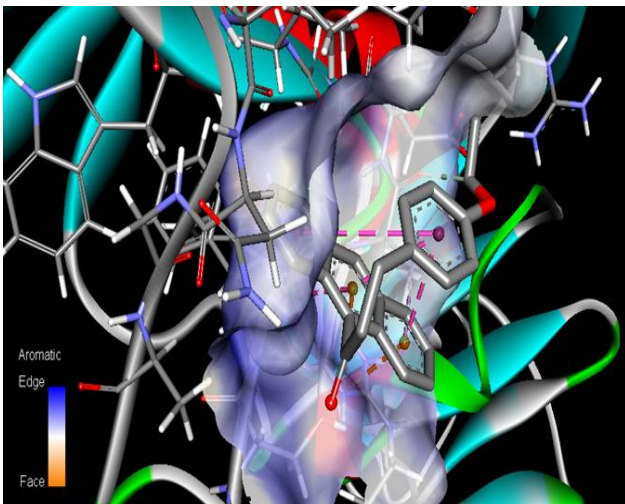


Fig.7.9. Molecular docking studies of (2E)-1-(anthracene-9-yl) -3-(4-ethoxyphenyl) prop-2-en-1-one, Proteins -4GNR, 4D8S, 5T6S, 5T6N

7.13 Conclusion

The FT-IR and FT-Raman spectra of (2E)-1-(Anthracene-9-yl) -3-(4-ethoxy phenyl) prop-2-en-1-one (ANC1) was recorded and the vibrational spectra have been investigated experimentally and theoretically by using B3LYP and 6-31G, 6-31G (d,p) method. Experimentally observed frequencies are in good agreement with the theoretical values. The stability of the molecule arising from hyper-conjugative interaction and charge delocalization has been analyzed using NBO analysis. The LUMO and HOMO energy provides information regarding ionization potential, chemical potential and other chemical descriptors. As seen from the MEP map of the ANC1 compound, negative region is mainly localized over the C=O group, anthracene ring and the maximum positive region is localized on the phenyl groups. Weak interaction profile shows that the presence of van der Waals interactions and the steric effect is present in the molecule. The anticancer protein 4G9R has higher binding energy, inhibition constant and RMSD values such as -5.98kcal/mol, 41.02(μ M) and 46.819 than 4D8S.

Table 7.1 Optimized structural parameters of (2E)-1-(anthracene-9-yl)-3-(4-ethoxyphenyl) prop-2-en-1-one by using B3LYP method and 6-31G, 6-31G (d,p) basis sets.

Parameters	Bond length (Å)		Parameters	Bond angle (°)		Parameters	Dihedral angle (°)	
	B3LYP/ 6-31G	B3LYP/ 6-31D(D,P)		B3LYP/ 6-31G	B3LYP/ 6-31D(D,P)		B3LYP/6- 31G	B3LYP/ 6-31D(D,P)
C1-C2	1.373	1.365	C2-C1-C6	119.798	120.447	C6-C1-C2-C3	-0.653	0.161
C1-C6	1.426	1.426	C2-C1-H17	120.516	120.959	C6-C1-C2-H18	178.648	179.972
C1-H17	1.085	1.100	C6-C1-H17	119.679	118.594	H17-C1-C2-C3	-179.690	-179.854
C2-C3	1.433	1.433	C1-C2-C3	121.125	120.764	H17-C1-C2-H18	-0.389	-0.043
C2-H18	1.086	1.101	C1-C2-H18	120.695	121.155	C2-C1-C6-C5	0.980	0.001
C3-C4	1.449	1.429	C3-C2-H18	118.177	118.081	C2-C1-C6-H20	-178.164	179.909
C3-C7	1.400	1.399	C2-C3-C4	119.410	118.790	H17-C1-C6-C5	-179.975	-179.984
C4-C5	1.436	1.433	C2-C3-C7	121.245	121.701	H17-C1-C6-H20	0.881	-0.077
C4-C8	1.421	1.399	C4-C3-C7	119.343	119.509	C1-C2-C3-C4	-1.068	-0.253
C5-C6	1.375	1.365	C3-C4-C5	117.372	118.787	C1-C2-C3-C7	178.379	179.764
C5-H19	1.083	1.101	C3-C4-C8	119.496	119.515	H18-C2-C3-C4	179.614	179.931
C6-H20	1.085	1.100	C5-C4-C8	123.092	121.699	H18-C2-C3-C7	-0.939	-0.052
C7-C10	1.401	1.399	C4-C5-C6	121.411	120.765	C2-C3-C4-C5	2.403	0.184
C7-H16	1.087	1.101	C4-C5-H19	119.192	118.076	C2-C3-C4-C8	-179.832	-179.923
C8-C9	1.423	1.399	C6-C5-H19	119.381	121.159	C7-C3-C4-C5	-177.054	-179.833
C8-C24	1.503	1.540	C1-C6-C5	120.838	120.448	C7-C3-C4-C8	0.710	0.061
C9-C10	1.450	1.429	C1-C6-H20	119.400	118.563	C2-C3-C7-C10	-178.066	-179.953
C9-C15	1.436	1.433	C5-C6-H20	119.756	120.990	C2-C3-C7-H16	1.225	-0.021
C10-C11	1.433	1.433	C3-C7-C10	121.868	120.976	C4-C3-C7-C10	1.381	0.064
C11-H12	1.086	1.101	C3-C7-H16	119.073	119.499	C4-C3-C7-H16	-179.328	179.996
C11-C13	1.372	1.365	C10-C7-H16	119.056	119.525	C3-C4-C5-C6	-2.129	-0.028
C13-C14	1.426	1.426	C4-C8-C9	120.457	120.976	C3-C4-C5-H19	176.396	-179.980
C13-H21	1.085	1.100	C4-C8-C24	120.270	119.499	C8-C4-C5-C6	-179.807	-179.919
C14-C15	1.375	1.365	C9-C8-C24	119.265	119.525	C8-C4-C5-H19	-1.281	0.129

C14-H22	1.085	1.100	C8-C9-C10	119.150	119.510	C3-C4-C8-C9	-3.287	-0.097
C15-H23	1.081	1.101	C8-C9-C15	123.293	121.695	C3-C4-C8-C24	175.679	179.999
H19-C26	2.529	1.536	C10-C9-C15	117.535	118.795	C5-C4-C8-C9	174.344	179.794
H23-O25	2.277	2.036	C7-C10-C9	119.580	119.514	C5-C4-C8-C24	-6.690	-0.111
C24-O25	1.259	1.227	C7-C10-C11	120.998	121.704	C4-C5-C6-C1	0.465	-0.067
C24-C26	1.475	1.540	C9-C10-C11	119.422	118.782	C4-C5-C6-H20	179.606	-179.973
C26-H27	1.085	1.070	C10-C11-H12	118.188	118.075	H19-C5-C6-C1	-178.058	179.883
C26-C28	1.356	1.540	C10-C11-C11	121.011	120.768	H19-C5-C6-H20	1.083	-0.023
C28-H29	1.090	1.070	H12-C11-H12	120.800	121.158	C3-C7-C10-C9	-0.893	-0.152
C28-C30	1.457	1.790	C11-C13-C14	119.826	120.449	C3-C7-C10-C11	179.193	179.900
C30-C31	1.416	1.395	C11-C13-H21	120.485	120.973	H16-C7-C10-C9	179.816	179.916
C30-C32	1.411	1.395	C14-C13-H21	119.689	118.578	H16-C7-C10-C11	-0.098	-0.032
C31-C33	1.389	1.395	C13-C14-C11	121.048	120.442	C4-C8-C9-C10	3.761	0.009
C31-H34	1.086	1.100	C13-C14-H22	119.317	118.580	C4-C8-C9-C15	-177.992	-179.920
C32-C35	1.394	1.395	C15-C14-H22	119.634	120.977	C24-C8-C9-C10	-175.215	179.913
C32-H36	1.085	1.100	C9-C15-C14	121.158	120.764	C24-C8-C9-C15	3.033	-0.016
C33-C37	1.405	1.395	C9-C15-H23	118.799	118.073	C4-C8-C24-O25	129.436	126.861
C33-H38	1.083	1.100	C14-C15-H23	120.017	121.163	C4-C8-C24-C26	-54.308	-0.002
C35-C37	1.406	1.395	C8-C24-O25	121.120	91.051	C9-C8-C24-O25	-51.586	-53.045
C35-H39	1.083	1.100	C8-C24-C26	117.575	115.550	C9-C8-C24-C26	124.670	-179.908
C37-O40	1.384	1.430	O25-C24-C26	121.196	122.225	C8-C9-C10-C7	-1.682	0.115
O40-C41	1.464	1.430	C33-C37-C35	119.926	119.994	H22-C14-C15-C9	-179.569	-179.937
C41-H42	1.098	1.070	C33-C37-O40	115.735	120.003	H22-C14-C15-H23	-1.448	0.075
C41-H43	1.098	1.070	C35-C37-O40	124.339	120.003	C8-C24-C26-C27	-0.860	-76.523
C41-C44	1.519	1.540	C37-O40-C41	119.699	120.000	C8-C24-C26-C28	-179.254	163.478
C44-H45	1.094	1.070	O40-C41-H42	109.268	109.471	O25-C24-C26-H27	175.393	174.490
C44-H46	1.096	1.070	O40-C41-H43	109.305	109.471	O25-C24-C26-C28	-3.001	54.490
C44-H47	1.094	1.070	C40-C41-C44	106.690	109.471	C24-C26-C28-H29	-1.574	4.367

Table 7.2 Vibrational assignments of (2E)-1-(anthracene-9-yl)-3-(4-ethoxyphenyl) prop-2-en-1-one using B3LYP method and 6-31G, 6-31G (d,p) basis sets

Modes	Observed wavenumbers (cm ⁻¹)		Calculated wavenumber (cm ⁻¹)		Vibrational assignments (% PED)
	FT-IR	FT-Raman	B3LYP/6-31G	B3LYP/6-31G (d,p)	
1		3060	3065	3062	vCH(98)
2	3050		3055	3051	v CH(98)
3			3045	3043	v CH(98)
4			3038	3036	v CH(98)
5			3032	3029	v CH(97)
6			3025	3022	v CH(98)
7			3017	3015	v CH(99)
8			3010	3007	v CH(98)
9	3000		3002	2999	v CH(98)
10			2986	2982	v CH(97)
11			2978	2975	v CH(98)
12			2971	2966	v CH(99)
13			2960	2957	v CH(98)
14			2948	2945	v CH(98)
15			2940	2936	v CH(98)
16			2928	2925	v _{ass} CH ₃ (96)
17			2920	2918	v _{ass} CH ₃ (96)
18			2910	2907	v _{ss} CH ₃ (96)
19			2898	2896	v _{ass} CH ₂ (98)
20			2889	2887	v _{ss} CH ₂ (98)
21		1580	1585	1581	vCO(69),vCC(20), δCH(10)
22			1571	1566	vCC(68), δCH(22)
23		1565	1560	1557	vCC(68), δCH(22)
24			1549	1545	vCC(72), vCO(12),δCH(10)
25			1531	1528	vCC(70), δCH(23)

26		1515	1518	1516	$\nu_{\text{CC}}(72)$, $\delta_{\text{CH}}(20)$
27			1489	1487	$\nu_{\text{CC}}(72)$, $\delta_{\text{CH}}(22)$
28			1471	1469	$\delta_{\text{CH}}(68)$, $\nu_{\text{CC}}(22)$
29	1443		1445	1442	$\delta_{\text{CH}}(69)$, $\nu_{\text{CC}}(22)$, $\sigma_{\text{SCl}}\text{CH}_2(21)$
30	1313	1435	1440	1438	$\delta_{\text{CH}}(68)$, $\sigma_{\text{SCl}}\text{CH}_2(21)$
31			1433	1431	$\sigma_{\text{SCl}}\text{CH}_2(83)$
32	1424		1429	1425	$\nu_{\text{CC}}(70)$, $\delta_{\text{CH}}(13)$
33			1420	1417	$\delta_{\text{OPB}}\text{CH}_3$ (69), $\sigma_{\text{SCl}}\text{CH}_2(13)$
34		1408	1415	1410	$\delta_{\text{IPB}}\text{CH}_3$ (74)
35			1406	1401	$\delta_{\text{CH}}(69)$, $\nu_{\text{CC}}(14)$
36			1392	1390	$\delta_{\text{CH}}(69)$, $\nu_{\text{CC}}(14)$
37	1387		1388	1385	$\nu_{\text{CC}}(72)$, $\delta_{\text{CH}}(16)$,
38			1366	1362	$\nu_{\text{CC}}(74)$, $\delta_{\text{CH}}(12)$
39	1356	1355	1358	1355	$\delta_{\text{SB}}\text{CH}_3$ (71), $\rho_{\text{rock}}\text{CH}_2(10)$
40			1340	1337	$\delta_{\text{CH}}(68)$, $\nu_{\text{CC}}(18)$
41		1325	1327	1325	$\delta_{\text{CH}}(72)$, $\nu_{\text{CC}}(14)$
42	1313		1315	1312	$\rho_{\text{rock}}\text{CH}_2(68)$, $\delta_{\text{SB}}\text{CH}_3$ (13)
43		1294	1289	1288	$\nu_{\text{CC}}(67)$, $\delta_{\text{CO}}(13)$, $\delta_{\text{CH}}(10)$
44			1273	1270	$\delta_{\text{CH}}(67)$, $\nu_{\text{CC}}(18)$, $\nu_{\text{CO}}(10)$
45	1257	1259	1260	1258	$\nu_{\text{CC}}(69)$, $\delta_{\text{CH}}(16)$
46			1225	1221	$\nu_{\text{CC}}(68)$, $\delta_{\text{CH}}(18)$
47	1174	1216	1179	1175	$\delta_{\text{CH}}(68)$, $\nu_{\text{CC}}(16)$
48			1160	1158	$\delta_{\text{CH}}(68)$, $\nu_{\text{CC}}(15)$
49		1173	1145	1141	$\nu_{\text{CC}}(68)$, $\delta_{\text{CH}}(12)$
50			1131	1129	$\gamma_{\text{OPR}}\text{CH}_3$ (76), τ_{CH_2} (13)
51	1116		1120	1118	$\nu_{\text{CO}}(60)$, $\delta_{\text{CH}}(18)$
52		1109	1091	1089	$\nu_{\text{CC}}(66)$, $\delta_{\text{CH}}(16)$
53			1078	1075	$\delta_{\text{CH}}(68)$, $\nu_{\text{CC}}(18)$
54			1060	1059	$\nu_{\text{CC}}(68)$, $\delta_{\text{CH}}(18)$
55	1041		1043	1040	$\delta_{\text{CH}}(65)$, $\nu_{\text{CC}}(20)$
56			1040	1036	$\delta_{\text{CH}}(66)$, $\nu_{\text{CC}}(18)$

57		1033	1033	1032	δ CH(65), ν CC(21)
58			1030	1027	ν CC(66), δ CH(18)
59			1024	1020	$\delta_{\text{ipr}} \text{CH}_3$ (74), $\rho_{\text{rock}} \text{CH}_2$ (12)
60	1012	1013	1015	1012	ν CC(66), δ CH(18)
61			1007	1001	ν CO(62), δ CH(13)
62	985		989	986	ν CC(63), δ CH(16)
63			980	979	ν CC(63), δ CH(18)
64	970	970	973	970	ν CC(66), ν CO(18), δ CH(10)
65			958	953	ν CC(68), ν CO(20)
66			943	941	ν CC(68), δ CH(18)
67			939	935	ν CC(66), δ CH(16)
68			934	930	γ CH(58)
69			930	928	ν CC(66), δ CH(13)
70			926	923	γ CH(58)
71	918		924	918	γ CH(59)
72			905	903	ν CC(67), ν CO(14)
73	890		896	892	γ CH(59)
74		880	885	881	γ CH(60)
75			870	867	γ CH(60)
76	846		849	845	γ CH(62)
77			825	823	ν CC(60), δ CH(16)
78	816		818	815	ν CC(70), ν CO(12)
79			810	809	γ CH(69)
80			806	804	δ CC(61), δ CO(12)
81	798	800	802	799	γ CH(67)
82			788	785	γ CH(68)
83			784	779	δ_{ring} (58)
84			775	771	γ CH(66)
85	765		770	765	δ_{ring} (58)
86			758	752	$\gamma_{\text{wag}} \text{CH}_2$ (65)
87			745	741	γ CH(68)

88	734	732	735	733	γ CH(68)
89			734	729	δ CO(57)
90			728	722	δ CC(66)
91			718	715	γ CH(67)
92			707	703	δ CC(59)
93	696		697	695	δ CC(60)
94			682	681	γ_{ring} (52)
95	669		673	670	δ CO(58)
96			661	657	γ CC(52)
97	643		648	645	δ_{ring} (62)
98			636	632	δ_{ring} (63)
99	623		628	625	δ_{ring} (63)
100			615	613	δ_{ring} (63)
101	599	600	600	597	δ_{ring} (62)
102			575	571	δ CO(58)
103	557	557	559	555	γ CO(53)
104	530		535	521	γ CC(52)
105			520	519	γ CC(53)
106			500	497	γ_{ring} (52)
107			474	470	δ CC(59)
108	456	450	455	451	γ_{ring} (50)
109			439	436	δ_{ring} (57)
110	436		431	427	γ_{ring} (51)
111			420	418	δ_{ring} (58)
112		400	406	401	δ_{ring} (57)
113			388	385	δ_{ring} (57)
114			360	361	γ_{ring} (52)
115			338	334	δ CC(58)
116			304	301	δ_{ring} (58)
117		280	285	282	γ CC(51)
118			275	271	Butterfly(55)

119		260	258	$\gamma_{\text{CC}}(50)$
120		241	239	$\gamma_{\text{CC}}(51)$
121		228	226	$\delta_{\text{CC}}(58)$
122		202	199	$\tau_{\text{CH}_3}(68)$
123	190	194	192	Butterfly(55)
124		163	160	$\gamma_{\text{ring}}(51)$
125		150	149	$\tau_{\text{CH}_2}(66)$
126	120	125	121	$\delta_{\text{ring}}(52)$
127		120	117	$\gamma_{\text{ring}}(51)$
128		105	103	$\delta_{\text{ring}}(53)$
129		98	95	$\gamma_{\text{ring}}(51)$
130	82	82	80	$\gamma_{\text{ring}}(52)$
131		65	62	$\gamma_{\text{ring}}(52)$
132		45	40	$\gamma_{\text{ring}}(51)$
133		34	29	$\gamma_{\text{ring}}(51)$
134		20	17	$\gamma_{\text{ring}}(50)$
135		15	10	$\gamma_{\text{ring}}(50)$

v-stretching, v_{sym} -sym stretching, v_{asym} -asym stretching, δ -in-plane bending, γ -out-of-plane bending, ρ -scissoring, ω -wagging, σ -rocking, τ -twisting.

Table 7.3 Mulliken atomic charges for (2E)-1-(anthracene-9-yl)-3-(4-ethoxyphenyl) prop-2-en-1-one by B3LYP/ 6-31G, 6-31G (d,p) level of theory

Atom Numbering	Charge		Atom Numbering	Charge	
	B3LYP/ 6-31 G	B3LYP/ 6-31 G (d,p)		B3LYP/ 6-31 G	B3LYP/ 6-31 G (d,p)
C1	-0.13	-0.10	O25	-0.45	-0.49
C2	-0.15	-0.12	C26	-0.14	-0.16
C3	0.06	0.11	H27	0.14	0.09
C4	0.05	0.08	C28	-0.13	-0.08
C5	-0.15	-0.14	H29	0.17	0.12
C6	-0.13	-0.10	C30	0.09	0.13
C7	-0.22	-0.20	C31	-0.17	-0.13
C8	-0.04	-0.05	C32	-0.15	-0.13
C9	0.05	0.08	C33	-0.13	-0.12
C10	0.06	0.11	H34	0.14	0.10
C11	-0.15	-0.12	C35	-0.14	-0.13
H12	0.13	0.08	H36	0.14	0.09
C13	-0.13	-0.09	C37	0.30	0.36
C14	-0.13	-0.10	H38	0.15	0.10
C15	-0.13	-0.12	H39	0.14	0.09
H16	0.13	0.08	O40	-0.56	-0.52
H17	0.13	0.09	C41	-0.02	0.05
H18	0.13	0.09	H42	0.15	0.11
H19	0.15	0.10	H43	0.15	0.11
H20	0.13	0.09	C44	-0.41	-0.34
H21	0.13	0.09	H45	0.16	0.13
H22	0.13	0.09	H46	0.14	0.11
H23	0.17	0.12	H47	0.16	0.13
C24	0.22	0.32			

Table 7.4 Second order perturbation theory analysis of Fock matrix in NBO basis corresponding to intra molecular bands of (2E)-1-(anthracene-9-yl)-3-(4-ethoxyphenyl) prop-2-en-1-one

Donor	Acceptor	E(2)(kcal/mol)	E(J)-E(i) (a.u)	F _(ij) (a.u)
		BMP	BMP	BMP
π (2) O25	$\sigma^*(2)$ C8-C9	2.8	0.68	0.043
π (2) O25	$\sigma^*(1)$ C8-C24	8.82	1.08	0.088
π (2) O25	$\sigma^*(1)$ C14-C15	0.58	1.42	0.026
π (2) O25	$\sigma^*(2)$ C14-C15	1.02	0.71	0.025
π (2) O25	$\sigma^*(1)$ C24-C26	19.57	1.06	0.13
π (2) O25	$\sigma^*(1)$ C26-H27	0.57	1.19	0.023
π (2) O40	$\sigma^*(1)$ C33-C 37	3.02	1.4	0.058
π (2) O40	$\sigma^*(1)$ C 35-C 37	8.4	1.4	0.097
π (2) O40	$\sigma^*(2)$ C 35-C 37	1.16	0.72	0.028
π (2) O40	$\sigma^*(1)$ C41-H 42	7.65	1.31	0.09
π (2) O40	$\sigma^*(1)$ C41-H 43	1.49	1.31	0.04
π (2) O40	$\sigma^*(1)$ C41-C 44	0.92	1.17	0.029
π (2) O40	$\sigma^*(1)$ C33-C37	3.8	1.51	0.068
π (2) O40	$\sigma^*(2)$ C35-C37	8.35	0.83	0.081
π (2) O40	$\sigma^*(1)$ C41-H43	5.56	1.42	0.08
π (2) O40	$\sigma^*(1)$ C41-C44	1.03	1.28	0.033
π (1) C1-C2	$\sigma^*(1)$ C6-H20	2.28	1.66	0.055
π (2) C3-C4	$\sigma^*(2)$ C8-C9	44.72	0.45	0.129
π (2) C1-C2	$\sigma^*(2)$ C3-C4	24.47	0.49	0.107
π (1) C2-H18	$\sigma^*(1)$ C3-C4	5.13	1.51	0.079
π (2) C3-C4	$\sigma^*(1)$ C2-C3	4.11	1.68	0.074
π (2) C4-C5	$\sigma^*(1)$ C6-H20	3.18	1.59	0.064
π (2) C30-C32	$\sigma^*(1)$ C26-C28	1.2	0.92	0.032
π (2) C30C32	$\sigma^*(2)$ C 35-C 37	37.8	0.49	0.122

a E(2) means energy of hyperconjugative interactions (stabilization energy).

b Energy difference between donor and acceptor i and j NBO orbitals.

c F(i,j) is the Fock matrix element between i and j NBO orbitals.

Table 7.5 NBO analysis of bonding and antibonding orbit of (2E)-1-(anthracene-9-yl)-3-(4-ethoxyphenyl) prop-2-en-1-one

Band (A-B)	ED/Energy (a.u.)	ED %	ED %	NBO	S(%)	P(%)
σ C1-C2	1.98066	49.84	50.16	0.7060 SP ^(1.73)	36.64	63.36
				0.7082 SP ^(1.71)	36.96	63.04
σ C2-C3	1.97394	48.47	51.53	0.6962 SP ^(1.97)	33.65	66.35
				0.7179 SP ^(2.02)	33.1	66.9
σ C4-C5	1.97022	51.74	48.26	0.7193 SP ^(2.04)	32.9	67.1
				0.6947 SP ^(2.11)	32.15	67.85
σ C7-C10	1.97451	48.7	51.3	0.6978 SP ^(1.82)	35.4	64.6
				0.7163 SP ^(1.9)	34.51	65.49
σ C8-C24	1.97312	51.47	48.53	0.7174SP ^(2.66)	27.31	72.69
				0.6966 SP ^(2.16)	31.63	68.37
σ C9-C15	1.97195	51.85	48.15	0.7201 SP ^(2.04)	32.91	67.09
				0.6939 SP ^(2.03)	32.98	67.02
σ C13-C14	1.97925	50.16	49.84	0.7083 SP ^(1.94)	34.04	65.96
				0.7060 SP ^(1.97)	33.69	66.31
σ C24-O25	1.99274	34.52	65.48	0.5875 SP ^(2.38)	29.56	70.44
				0.8092 SP ^(1.68)	37.29	62.71
σ C28-C30	1.98055	50.6	49.4	0.7113 SP ^(2.53)	28.32	71.68
				0.7029 SP ^(3.21)	23.78	76.22
σ C35-C37	1.97967	50.28	49.72	0.7091 SP ^(1.87)	34.79	65.21
				0.7051 SP ^(1.66)	37.56	62.44
σ C37-O40	1.99005	33.04	66.96	0.5748 SP ^(3.14)	24.36	75.64
				0.8183 SP ^(2.33)	30.03	69.97
σ O40-C41	1.98638	30.64	30.64	0.8329 SP ^(2.32)	30.11	69.89
				0.5535 SP ⁽⁴⁾	20.02	79.98
σ C41-C44	1.98962	50.54	49.46	0.7109 SP ^(2.55)	29.13	71.87
				0.7033 SP ^(2.9)	25.67	74.33

Table 7.6 HOMO-LUMO energies for (2E)-1-(Anthracene-9-yl)-3-(4-ethoxyphenyl) prop-2-en-1-one using B3LYP/6-31G (d,p) method

Energy (eV)	Energy gap (eV)	Ionisation potential (I)	Electron affinity (A)	Global hardness (η)	Electron negativity (χ)	Global softness (σ)	Chemical potential (μ)	Global Electroplicity (ω)
5.2966	3.1197	0.19465	0.08	0.11465	0.1373	8.7222	-0.1373	0.0822
2.1769								
5.8787	4.3785	0.21604	0.05513	0.16091	0.1356	6.2146	-0.1356	0.05713
1.5002								
6.4559	6.1495	0.23725	0.01126	0.22599	0.1242	4.4249	-0.1242	0.03413
0.3064								

Table 7.7 Fukui function (f_i^+ , f_i^- , Δf) for (2E)-1-(anthracene-9-yl)-3-(4-ethoxyphenyl) prop-2-en-1-one

Atoms	Natural atomic charges			Fukui functions(eV)			Electro-philicity	Nucleo-philicity
	qN	qN+1	qN+1	F0	F+	F-		
C1	-0.207	-0.129	-0.112	-0.094	0.077	-0.008	0.086	-0.086
C2	-0.163	-0.168	-0.125	-0.038	-0.005	-0.021	0.017	-0.17
C3	-0.035	0.101	0.078	-0.113	0.136	0.011	0.124	-0.124
C4	-0.127	-0.049	0.011	-0.138	0.078	-0.030	0.108	-0.108
C5	-0.094	-0.025	-0.041	-0.053	0.069	0.008	0.061	-0.061
C6	-0.267	-0.217	-0.171	-0.097	0.050	-0.023	0.073	-0.073
C7	-0.188	-0.256	-0.166	-0.022	-0.067	-0.045	-0.023	0.023
C8	-0.103	-0.090	-0.095	-0.007	0.013	0.003	0.010	-0.01
C9	-0.073	0.030	0.076	-0.149	0.103	-0.023	0.126	-0.126
C10	-0.039	0.088	0.068	-0.106	0.127	0.010	0.117	-0.117
C11	-0.170	-0.167	-0.129	-0.041	0.003	-0.019	0.022	-0.022
H12	0.208	0.091	0.179	0.028	-0.116	-0.044	-0.072	0.072
C13	-0.206	-0.135	-0.117	-0.089	0.070	-0.009	0.080	-0.08
C14	-0.237	-0.166	-0.130	-0.107	0.071	-0.018	0.089	-0.089
C15	-0.088	-0.082	-0.075	-0.013	0.007	-0.003	0.010	-0.01
H16	0.218	0.085	0.196	0.022	-0.133	-0.056	-0.078	0.078
H17	0.197	0.078	0.183	0.014	-0.120	-0.053	-0.067	0.067
H18	0.210	0.088	0.184	0.026	-0.122	-0.048	-0.074	0.074
H19	0.255	0.141	0.179	0.077	-0.115	-0.019	-0.096	0.096
H20	0.197	0.084	0.180	0.017	-0.113	-0.048	-0.065	0.065
H21	0.198	0.081	0.181	0.017	-0.118	-0.050	-0.067	0.067

H22	0.197	0.084	0.182	0.015	-0.113	-0.049	-0.064	0.064
H23	0.237	0.154	0.190	0.047	-0.083	-0.018	-0.065	0.065
C24	0.423	0.252	0.332	0.091	-0.171	-0.040	-0.131	0.131
O25	-0.481	-0.499	-0.338	-0.143	-0.018	-0.080	0.062	-0.062
C26	-0.334	-0.232	-0.238	-0.096	0.102	0.003	0.099	-0.099
H27	0.241	0.103	0.224	0.017	-0.138	-0.061	-0.077	0.077
C28	-0.024	-0.197	-0.066	0.043	-0.173	-0.065	-0.108	0.108
H29	0.232	0.100	0.207	0.025	-0.131	-0.053	-0.078	0.078
C30	-0.057	0.064	0.047	-0.105	0.122	0.009	0.113	-0.113
C31	-0.214	-0.187	-0.174	-0.040	0.027	-0.006	0.034	-0.034
C32	-0.216	-0.188	-0.177	-0.039	0.028	-0.006	0.033	-0.033
C33	-0.201	-0.121	-0.107	-0.094	0.080	-0.007	0.087	-0.087
H34	0.238	0.136	0.160	0.078	-0.102	-0.012	-0.090	0.09
C35	-0.202	-0.122	-0.107	-0.095	0.080	-0.007	0.087	-0.085
H36	0.224	0.126	0.150	0.074	-0.097	-0.012	-0.085	0.085
C37	0.361	0.249	0.272	0.090	-0.112	-0.011	-0.101	0.101
H38	0.236	0.110	0.170	0.066	-0.125	-0.030	-0.096	0.096
H39	0.230	0.107	0.166	0.064	-0.123	-0.030	-0.093	0.093
O40	-0.766	-0.585	-0.560	-0.206	0.181	-0.012	0.193	-0.193
C41	0.032	0.010	-0.020	0.052	-0.023	0.015	-0.037	0.037
H42	0.151	0.121	0.134	0.017	-0.030	-0.006	-0.023	0.023
H43	0.154	0.125	0.133	0.021	-0.029	-0.004	-0.025	0.025
C44	-0.452	-0.409	-0.406	-0.046	0.044	-0.001	0.045	-0.045
H45	0.176	0.146	0.164	0.012	-0.030	-0.009	-0.021	0.021
H46	0.153	0.122	0.147	0.007	-0.031	-0.012	-0.019	0.019
H47	0.173	0.145	0.160	0.013	-0.028	-0.008	-0.020	0.02

Table 7.8 Topological parameters for intramolecular interactions in compound electron density (ρ_{BCP}), Laplacian of electron density (∇^2_{BCP}), electron kinetic energy density (G_{BCP}), electron potential energy density (V_{BCP}), total electron energy density (H_{BCP}), Hydrogen bond energy (E_{HB}) at bond critical point(BCP) for (2E)-1-(anthracene-9-yl)-3-(4-ethoxyphenyl) prop-2-en-1-one

Interactions	ρ_{BCP}	∇^2_{BCP}	G_{BCP}	V_{BCP}	H_{BCP}	E_{HB}
H23....C26	0.0154	0.0726	0.0159	-0.0136	-0.0023	-0.0068
H19....O25	0.0127	0.0455	0.0102	-0.0089	0.0012	-0.0049

Table 7.9 Binding affinity for docking in (2E)-1-(anthracene-9-yl)-3-(4-ethoxyphenyl) prop-2-en-1-one

Drug	Protein	Type of activity	Binding affinity (kcal/mol)	Etimated inhibition constant Ki (μ M)	Bonded residues	Nature of bond	Bond distance (\AA)	RMSD
(2E)-1-(Anthracene-9-Yl)-3-(4-ethoxyphenyl) prop-2-en-1-one	4NGR	Anticancer	-5.98	41.02	TYR A: 277	Carbon-Hydrogen bond	2.71	46.819
			-5.5	93.22	THR A:269	van der waals	2.15	48.225
			-5.17	162.63	TYR A: 279	Pi-donor hydrogen bond	3.24	47.206
			-5	217.31	THR A:269	van der waals	4.01	47.159
			-4.43	561.81	TYR A:272	π -p stacked	4.16	66.425
			-4.2	834.57	TYR A:272	π -p stacked	4.49	31.124
			-4.08	1.03 (mM)	ALA A: 278	Pi-alkyl	4.1	66.658
	4D8S	Anticancer	-6.7	12.3	CYS A: 129	Pi-Sulfur	3.65	35.313
			-6.07	35.68	VAL A: 163	Alkyl	4.75	45.9
			-5.9	47.14	LEU A: 4120	Alkyl	4.55	14.131
			-5.81	55.33	CYS A: 447	Pi-alkyl	4.23	46.29
			-5.23	147.57	VAL A: 449	van der waals	5.45	5.785
			-5.15	167.05	VAL A:419	Alkyl	4.8	24.661
			-5.06	196.84	CYS A: 129	Pi-Sulfur	6.54	30.141
	5T6S	Antiviral	-4.11	964.52	ASN A: 133	van der waals	2.71	282.655
-3.99			1.2 (mM)	MET A: 151	van der waals	3.02	268.727	

			-3.75	1.79 (mM)	ARG A: 141	Pi-cation	3.46	258.241		
			-3.62	2.24 (mM)	ARG A: 141	Pi-cation	3.94	274.112		
			-3.36	3.47 (mM)	ALA A: 135	van der waals	4.02	282.169		
			-3.22	4.35 (mM)	ALA A: 149	Carbon-Hydrogen bond	4.36	257.795		
			-3.02	6.06 (mM)	ALA A: 149	Carbon-Hydrogen bond	4.86	279.965		
	5T6N	Antiviral	-5.69	67.22	TRP A: 234	p-p stacked	3.74	59.851		
					-5.32	127.03	TRP A: 234	p-p stacked	3.82	59.328
					-5.18	160.76	ASP A: 104	van der waals	3.24	60.614
					-3.59	2.35 (mM)	TRP A: 234	π -p stacked	3.52	86.7
					-3.52	2.65 (mM)	PRO A: 103	van der waals	4.36	100.194

Chapter – 8

*Vibrational studies, Reduced Density Gradient
and molecular docking studies of (2E)- 1-
(anthracene-9-yl)-3-(biphenyl-4-yl) prop-2-en-
1-one* Summary of

Vibrational studies, Reduced Density Gradient and molecular docking studies of (2E)- 1-(anthracene-9-yl) -3-(biphenyl-4-yl) prop-2-en-1-one

8.1 Introduction

Anthracene is a polycyclic aromatic hydrocarbon (PAH), consisting of three fused benzene rings. It is a component of coal tar and is used in the production of red dye alizarin and other dyes. It is converted into anthraquinone, a precursor to dyes. It is colourless but exhibits a blue (400-500 nm peak) fluorescence under ultraviolet radiation. Anthracene derivatives have been extensively investigated in many fields such as, material chemistry, thermochromic chemistry and organic light emitting devices. It is used in optical, electronic and magnetic switches. In biological systems, anthracene skeletal compounds are useful for probing DNA cleavage. In medical field its derivatives act as a good anti-cancerous drug and they are carcinogenic to many living beings. It has a biological activity against L210 in vitro tumor cells [265]. Psedourea is anthracene-based drugs tested in clinical trials [266] and it is very effective against specific skin ailments [267]. The planer, linear, three-ring system of the anthracene nucleus has potential for overlapping with the DNA base pairs [268]. It absorbs moderately in the near UV region and gives fluorescence quantum yields that are useful to monitor ligand to DNA by spectroscopic methods [269]. Binding studies of small molecules with

deoxyribonucleic acid (DNA) [270] and the investigations are going on the binding and interactions between small molecules and biomolecules, especially with DNA [271] are in progress. This will be helpful for preventing and curing diseases [272]. Anthracene, the first material producing electroluminescence and along with its derivatives has still been attracting attention from the view point of its application and the basic science [273].

Based on the literature survey, we have found that quantum chemical calculations, FT-IR, FT-Raman spectroscopic studies, Topological analysis, Reduced density gradient (RDG) analysis and docking studies of (2E)-1-(anthracene-9-yl)-3-(biphenyl-4-yl)prop-2-en-1-one (ANC2) have not been reported. Quantum chemical computational methods have proved to be an essential tool for interpreting and predicting the vibrational spectra. In addition, an attempt has been made to interpret the vibrational spectra of ANC2 molecule, by applying density functional theory calculations based on Becke-3-Lee-Yang-Parr (B3LYP) with 6-31G and 6-31G (d,p) basis sets. Furthermore, the HOMO-LUMO and NBO analysis of ANC2 have been studied by B3LYP level with 6-31G (d,p) basis set implemented in the Gaussian 09 program suite [36]. The Reduced Density Gradient (RDG) analysis has been carried out to investigate the presence of Hydrogen bond, steric effect and Van der Waals interaction of the ANC2 molecule. Molecular docking studies have been carried out to evaluate the biological potential of the ANC2 molecule.

8.2 Experimental details

(2E)-1-(anthracene-9-yl)-3-(biphenyl-4-yl)prop-2-en-1-one (ANC2) was synthesized as per the reported procedure. The FT-IR spectrum of the ANC2 molecule was recorded in the frequency region 4000-450 cm^{-1} at a resolution of $\pm 1 \text{ cm}^{-1}$ Perkin Elmer spectrometer equipped with an MCT detector, a KBr pellet technique and global source. The spectrum of FT-Raman of the ANC2 molecule has been recorded using the 1064nm line of an Nd-YAG laser as excitation wavelength in the region of 4000-0 cm^{-1} BRUKER model interferometer. The reported wavenumbers are expected to be accurate within ± 1 resolution with 200 mW of power at the sample in both techniques.

8.3 Computational details

The entire calculations were performed using Gaussian 09W [36] program package. Subsequently, the vibrations in association with the molecule were derived along with their IR intensity and Raman activity. By DFT calculations, the B3LYP/6-31G and HF/6-31G basis set can be used to predict the geometrical parameters and the vibrational assignments. The potential energy distributions (PEDs) are done with the help of (VEDA) [274] program and it is viewed by GaussView [78] program. The polarizability, hyper polarizability and dipole moments of ANC2 molecule have been calculated by the same method. The charge transfer within the molecule is explained by the HOMO-LUMO analysis. The global hardness (η), global softness (ν), electronegativity (χ), and chemical potential (μ) have been calculated using the highest occupied molecular orbital (HOMO) and lowest unoccupied molecular orbital (LUMO).

The NBO analysis was performed at the B3LYP/6-31G level by means of the NBO 3.1 program within the Gaussian 09 W package [36] at DFT level in order to understand various second order interactions between the another subsystem, which is a measure of the intra molecular delocalization or hyper- conjugation. Reduced density gradient (RDG) analysis are calculated with the use of Multiwfn program [76] and plotted by visual molecule dynamics program (VMD) [77] Autodock 4.2 software [78] is used for molecular docking. The three-dimensional crystal structure of DNA was obtained from the Protein data bank PDB ID. Using Discovery studio visualize software, the ligand-protein interaction was visualized.

8.4 Result and discussion

8.4.1 Molecular geometrical parameter

The optimized molecular structure of the ANC2 molecule was depicted in Fig.8.1. The experimental and calculated molecular geometrical parameters such as bond lengths, bond angles and dihedral angles are determined and presented in Table 8.1.

The C-C bond length of the anthracene ring falls in the range 1.335 to 1.501 Å [275]. Chandran *et al* [240] reported the bond length of anthracene are C7-C3, C2-C3, C2-C1, C1-C6, C4-C3, C8-C9, C9-C15, C9-C10, C14-C15, C14-C13, H23-C15, H22-C14 are 1.3995 Å, 1.4322 Å, 1.3719 Å, 1.4231 Å, 1.4475 Å, 1.4344 Å, 1.4325 Å, 1.4488 Å, 1.3781 Å, 1.4229 Å, 1.0798 Å, 1.0855 Å which are in good agreement with the ANC2 molecule has 1.4/1.388 Å, 1.432/1.434 Å, 1.373/1.351 Å, 1.426/1.427 Å and 1.449/1.427 Å, 1.424/1.403 Å, 1.436/1.439 Å, 1.45/1.428 Å, 1.375/ 1.353Å, 1.426/1.428 Å,

1.081/1.069 Å, 1.085/1.073 Å for HF/ B3LYP methods. For the ANC2 molecule, C26-C28=1.335Å and C8-C24=1.501Å is the lower and higher bond length due to the presence of the neighboring C=O group. The C=O bond length (1.1988Å) given by DFT calculation agree with the reported literature values [276] and C=O has 1.258/1.227 Å obtained for the ANC2 molecule. The value of C1-H17, C6-H20, C13-H2, C14-H22, C33-H38, C35-H39, C41-H44, C42-H46, C43-H48, C45-H49, C47-H50 all the C-H bond has the bond length 1.085 for HF and 1.073Å for B3LYP method.

The bond angle of anthracene for the ANC2 molecule C9-C8-C24, C9-C8-C4, C8-C9-C10, C15-C9-C10, C9-C15-C14, C15-C14-C13 are 119.316°/119.275°, 120.78°/120.471°, 119.173°/119.113°, 117.664°/117.511°, 121.077°/121.157°, 120.994°/121.07° which are in agreement with Zilberg *et al* [277] observed as 123.0°, 119.8°, 119.3°, 117.0°, 121.3°, 121.3° respectively. C3-C7-C10=121.683° / 121.893°, C7-C3-C4 = 119.366°/119.335°, C2-C3-C4=119.273°/119.434°, C1-C2-C3 = 121.083° / 121.12°, C2-C1-C6 = 119.93°/119.783° is the bond angle of anthracene for the ANC2 molecule is close to Chandran *et al* [240] observed as 121.5°, 119.3°, 119.3°, 120.9° and 120.1° for (E)-4-((anthracen-9-ylmethylene)amino)-N-carbamimidoyl benzene sulfonamide. The phenyl ring is tilted from prop -2-en-1-one which is concluded from the torsion angles C26-C28-C30-C31=178.77°/179.629° and C26-C28-C30-C32 = -1.262°/-0.306°. The two phenyl rings are tilted as C33-C37-C40-C41= -136.507°/-144.455° and C33-C37-C40-C42 = 43.463°/35.49°. The comparative analysis of parameters associated with the structure was attained using DFT structural parameters are in good agreement with each other.

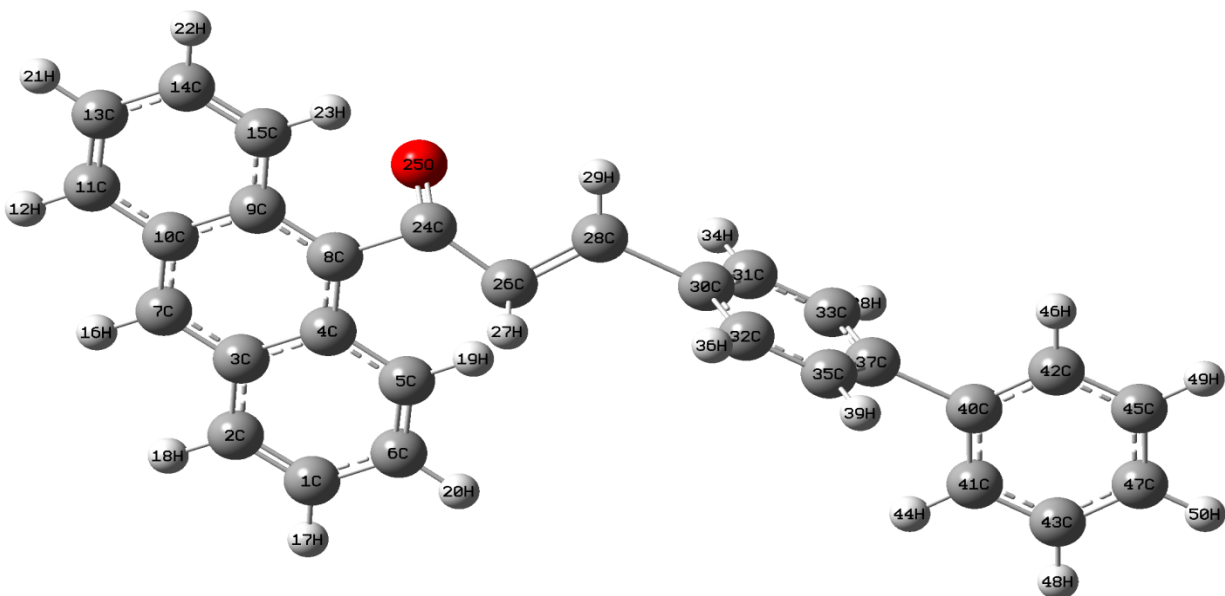


Fig.8.1 Optimized molecular structure of (2E)- 1-(anthracene-9-yl) -3-(biphenyl-4-yl) prop-2-en-1-one

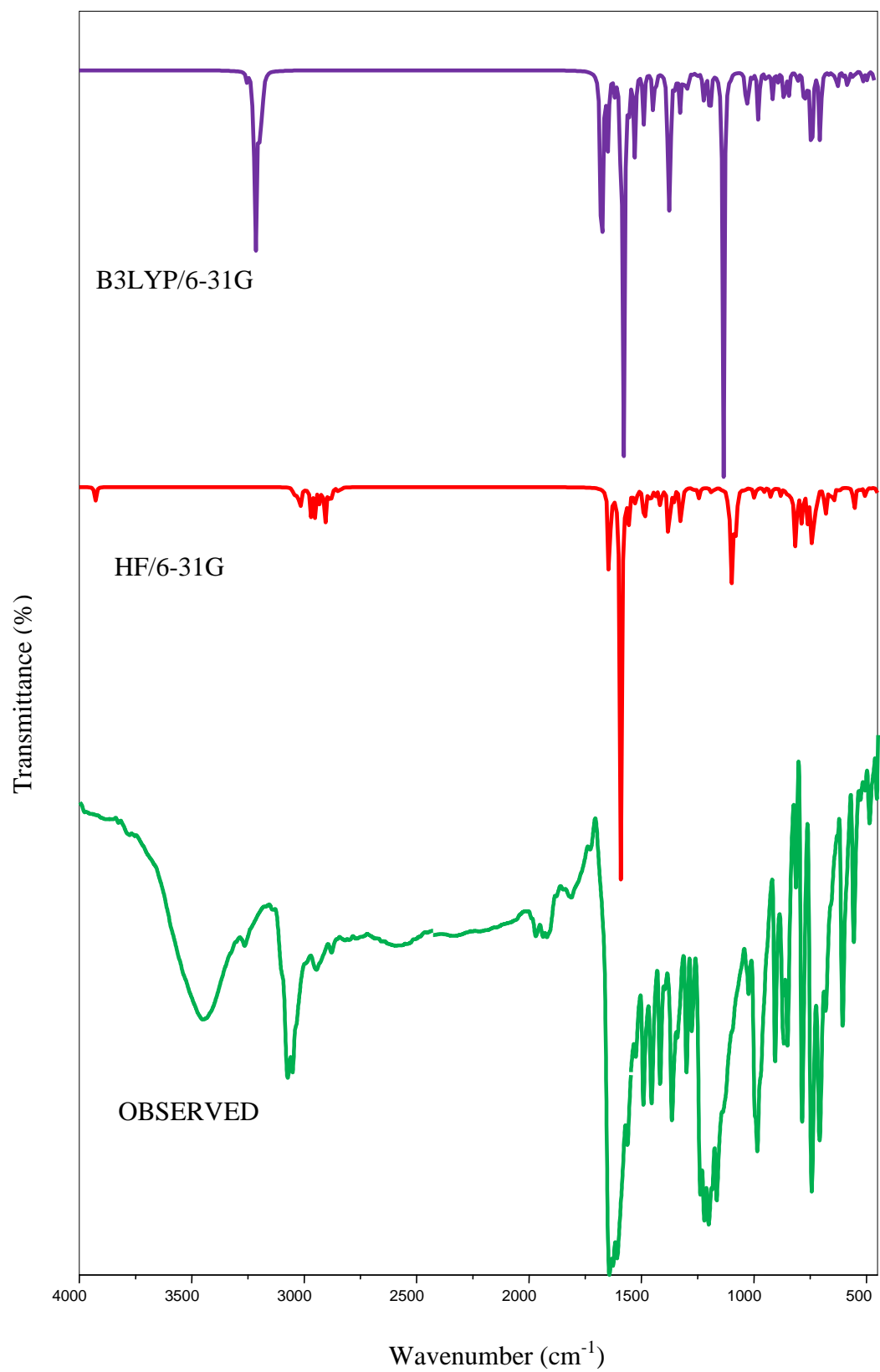


Fig. 8.2 Observed FT-IR and simulated spectra of (2E)- 1-(anthracene-9-yl) -3-(biphenyl-4-yl) prop-2-en-1-one

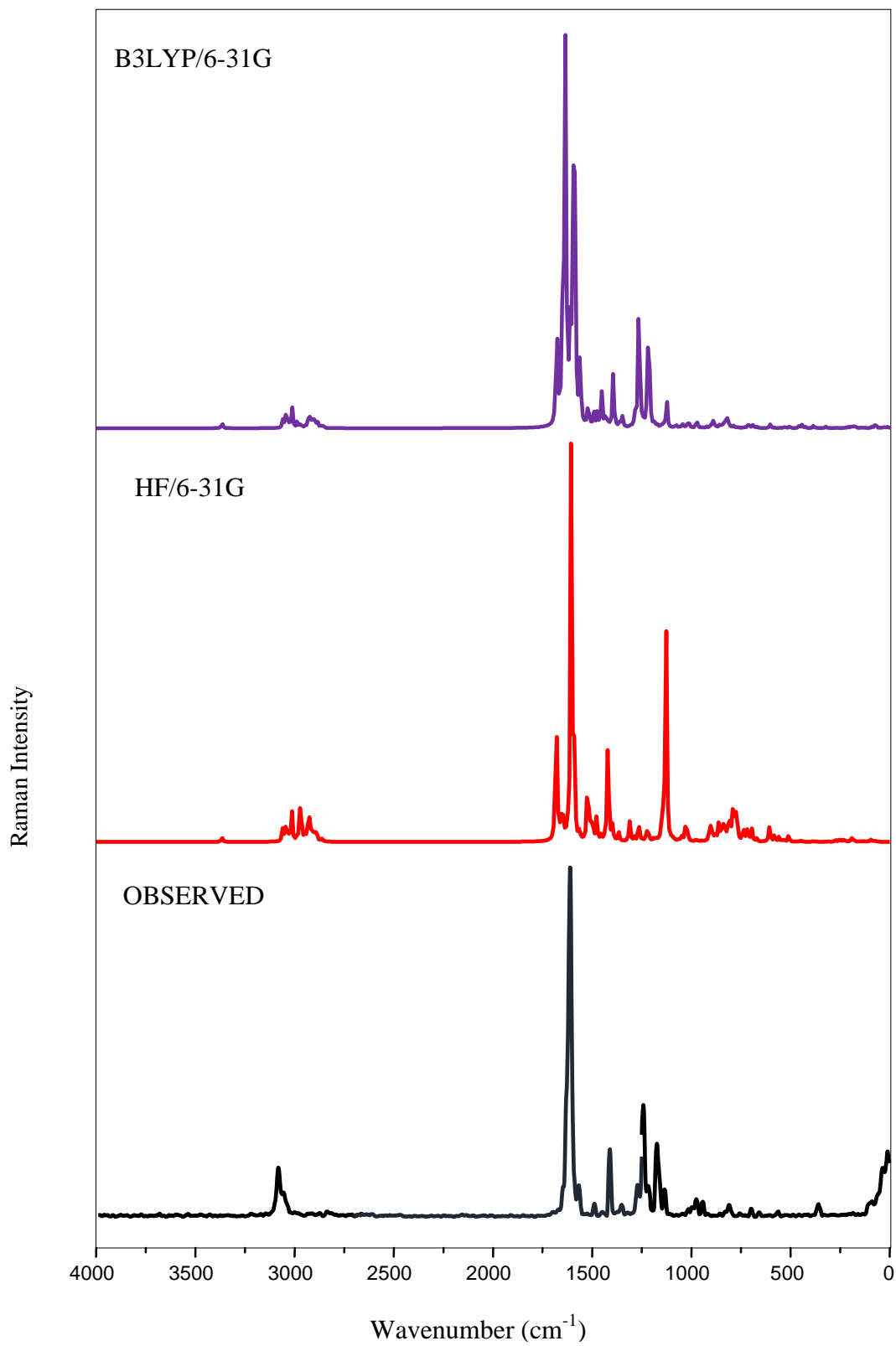


Fig.8.3 Observed FT-Raman and simulated spectra of (2E)-1-(anthracene-9-yl)-3-(biphenyl-4-yl) prop-2-en-1-one

8.4.2 Vibrational assignments

The detailed vibrational assignments of observed and calculated frequencies, normal mode descriptions have been reported in Table 8.2. The comparison between theoretical and experimental FT-IR and FT Raman of the ANC2 molecule are given in Figs. 8.2 and 8.3, respectively. The ANC2 molecule consists of 50 atoms with 144 normal modes of vibrations. It is convenient to discuss the vibrational spectral regions for the basis set HF/6-31G and B3LYP/6-31G as described below.

C-H vibrations

Aromatic compounds commonly exhibit multiple weak bands in the region 3100 - 3000 cm^{-1} [59] due to C-H stretching vibration. The C-H in-plane bending vibrations are observed in the region 1300-1000 cm^{-1} [59]. The C-H out-of-plane bending vibrations occur in the region of 1000-700 cm^{-1} [59].

In the present investigation, the bands identified at 3051, 3029, 2919, 2851 cm^{-1} and 3059 cm^{-1} are observed in FT-IR and FT-Raman spectrum respectively and are assigned to C-H stretching vibration. The computed values by HF/6-31G method are assigned in the range of 3060-2850 cm^{-1} and by B3LYP/6-31G are 3066-2854 cm^{-1} respectively. Pavithra *et al* [239] observed the C-H stretching vibration at 3186, 3166, 3158, 3117, 3113, 3111, 3104, 3102 and 3085 cm^{-1} for IR spectrum for 2-[(Anthracene-9-ylmethylene)amino]-2-methylpropane-1,3-diol. The C-H stretching modes are assigned by Renjith *et al* [278] at 3088, 3081, 3069, 3048, 3045, 3041 cm^{-1} by theoretical and these bands are observed experimentally, at 3074 cm^{-1} for IR spectrum, 3075, 3062 cm^{-1} for Raman spectrum.

Mary *et al* [279] observes the CH stretching modes at 3024 cm^{-1} in the Raman spectrum and observed theoretically at $3077, 3022\text{ cm}^{-1}$.

The C-H in-plane bending vibrations are observed at $1224, 1206, 1187, 1150\text{ cm}^{-1}$ for FT-IR and $1228, 1188, 1152\text{ cm}^{-1}$ for FT-Raman spectra for the ANC2 molecule. Kumar *et al* [280] assigned the in-plane C-H vibrations at $1439, 1250, 1215$ and 1153 cm^{-1} . The C-H in-plane bending modes are appear near the band $1322, 1303, 1262, 1202, 1194, 1172, 1154, 1054$ and 1032 cm^{-1} by Pavithra *et al* [239]. Vatsal *et al* [281] observed the in-plane bending vibration at $1224, 1159, 1032, 1003\text{ cm}^{-1}$. In this work, the computed values for δCH vibrations by HF/6-31G method predicted in the range of $1675\text{-}1130\text{ cm}^{-1}$ and for B3LYP/6-31G the range is $1635\text{-}1090\text{ cm}^{-1}$.

The C-H out -of -plane bending vibrations of our ANC2 molecule are observed at $1020, 1004, 971, 964, 824\text{ cm}^{-1}$ for FT-IR spectrum and $998, 962, 883, 850, 834\text{ cm}^{-1}$ for FT-Raman spectrum. The computed values by HF/6-31G method are predicted in the range of $1075\text{-}820\text{ cm}^{-1}$ and for B3LYP/6-31G $1079\text{-}825\text{ cm}^{-1}$ respectively. Kumar *et al* [280] observed C-H out -of -plane bending vibrations at $960, 884\text{ cm}^{-1}$ in the IR spectrum and in the range $973\text{-}748\text{ cm}^{-1}$ theoretically. Alasalvar *et al* [241] assigned the C-H out-of-plane bending modes are observed at $905, 841, 727\text{ cm}^{-1}$ and $924, 919, 863, 864, 841, 817, 813\text{ cm}^{-1}$ for FT-IR and FT-Raman spectrum. Pavithra *et al* [239] observed the C-H out-of-plane bending modes at $994, 989, 980, 975, 882, 864, 839, 770\text{ cm}^{-1}$. Vatsal *et al* [281] assigned the out-of plane bending vibration at $927, 945$ and 740 cm^{-1} . Mary *et al* [279] reported the out-of-plane C-H vibrations at $990, 978, 875\text{ cm}^{-1}$ in the IR spectrum, $991, 877\text{ cm}^{-1}$ in the Raman spectrum and at $983, 981, 877, 869\text{ cm}^{-1}$ theoretically

observed. Renjith *et al* [278] observed the γ CH modes at 971, 960, 930, 846, 835, 827, 825, 811 cm^{-1} (IR), at 966, 930, 811 cm^{-1} (Raman) and theoretically these modes are assigned at 983, 958, 956, 826, 823, 811 cm^{-1}

C-C vibrations

The C-C stretching vibration usually occurs in the region 1626-1285 cm^{-1} [282]. Mary *et al* [279] observed the C-C bands for bis[(E)-Anthranlyl-9-acrylic]anhydride theoretically at 1604, 1598 cm^{-1} and 1609, 1608 cm^{-1} in the IR and Raman spectrum. Alasalvar *et al* [241] observed at 1580, 1591 cm^{-1} and 1596 cm^{-1} in the IR and Raman spectrum and calculated values for N-(12-amino-9, 10- dihydro-9,10-ethanoanthracen-11-yl)-4-methylbenzenesulfonamide at 1589, 1582, 1577, 1567, 1562 and 1522 cm^{-1} . The FT-IR spectra are observed at 1771, 1446, 1154, 1132 cm^{-1} by Vatsal *et al* [281]. In the present study, the frequencies observed in the FT-IR spectrum at 1618, 1601, 1485, 1447, 1408, 1386, 1350, 1288, 1264, 1117 cm^{-1} and 1602, 1485, 1413, 1359, 1282, 1255 cm^{-1} for FT-Raman are assigned to C-C stretching vibrations. The computed values by HF/6-31G method are observed at 1662, 1657, 1643, 1624, 1618, 1602, 1567, 1486, 1471, 1415, 1407, 1392, 1385, 1360, 1351, 1304, 1285, 1280, 1262, 1253, 1136, 1123, 1115 cm^{-1} and for B3LYP/6-31G the wave numbers are 1666, 1662, 1648, 1627, 1622, 1609, 1575, 1492, 1475, 1420, 1414, 1395, 1389, 1364, 1356, 1309, 1289, 1285, 1266, 1260, 1174, 1140 cm^{-1} .

The observed C-C-C out of plane bending vibrations for the ANC2 molecule reported at 503 cm^{-1} in IR and 500, 175, 75, 68 cm^{-1} in Raman spectrum. It is calculated by HF/6-31G method at 383, 365, 321, 269, 245, 223, 209, 193, 186, 179, 174, 160, 75,

70, 67, 20, 12 cm^{-1} and for B3LYP/6-31G are 387, 368, 325, 270, 248, 225, 210, 195, 188, 181, 176, 164, 77, 73, 70, 24, 10 cm^{-1} respectively.

C-O vibration

The C-O stretching vibrations occur in the region 1260-1000 cm^{-1} [239]. In our present work, the C=O stretching vibrations are assigned at 730 cm^{-1} near 1650-1400 cm^{-1} in FT-Raman spectrum. According to literature [283], the C=O vibration is occurred at the lower region by the inflation of other vibrations. In this work, the calculated C=O stretching vibrations are 1675, 1624 cm^{-1} and 1679, 1627 cm^{-1} . Vatsal *et al* [281] observed C-O band experimental and theoretically at 1702 and 1675 cm^{-1} . 1665, 1607 cm^{-1} are C-O stretching modes observed theoretically and experimentally observed at 1674, 1609 cm^{-1} (IR) and 1671, 1609 cm^{-1} (Raman) by Renjith *et al* [278]. C=O stretching vibrations reported by Joseph *et al* [285] at 1669, 1600 cm^{-1} in the IR spectrum for 1-(4-methoxyphenyl)-4-methylantraquinone.

Ring modes

The ring modes are usually appears in IR and weak or absent in Raman spectrum For the ANC2 compound, in IR spectra, the in- plane bending ring modes occurs at 724 and 666 cm^{-1} and out-of-plane bending ring mode occurs at 789, 764, 550, 523 and 454 cm^{-1} . The δ_{ring} modes are calculated by HF/6-31G method at 943, 921, 899, 893, 855, 819, 812, 725, 714, 706, 690, 681, 665, 602 cm^{-1} and by B3LYP/6-31G method are 945, 925, 903, 896, 859, 823, 815, 717, 710, 708, 692, 683, 668, 605 cm^{-1} . The ν_{ring} modes are calculated by HF/6-31G method at 795, 790, 785, 780, 765, 598, 575, 551, 536, 525, 441, 453, 425, 300, 103 and 799, 794, 788, 783, 767, 601, 578, 555, 540, 529, 445, 458, 428,

304, 128 cm^{-1} by B3LYP/6-31G method. The observed values at 523, 503, 454 and 705, 600 cm^{-1} in FT-IR and Raman spectrum are assigned to ring in-plane bending vibrations. Joseph *et al* [285] observed the Raman Spectra at 234 and 383 cm^{-1} by theoretically and experimentally at 230 and 385 cm^{-1} .

8.5 Mulliken atomic charges

The Mulliken atomic charges calculation [286] has an important role in the application of quantum mechanical calculation to molecular system. Atomic charges are very important because they affect its dipole moment, molecular polarizability, electronic structure and more properties of molecular systems. Mulliken atomic charges are calculated by the HF, B3LYP/6-31G methods are presented in Table 8.3 and calculated atomic charges of the graph is shown in Fig.8.4. It is worthy to mention that the Mulliken atomic charges of C24 ($=0.22/0.43$) atom occupies the highest positive value and high acidic presentation and O25 ($=-0.44/-0.56$), C26 ($=-0.44/-0.27$) has the negative value and has electro negativity. H12= $0.13/0.21$, H19= $0.15/0.23$, H20= $0.13/0.29$, H23= $0.17/0.25$ are some positive values of the ANC2 molecule. Atoms like C1, C3, C10, H27, C30, H29, C45, H48 having both positive and negative charges. Distribution of positive and negative charges is vital to increasing or decreasing bond length between the atoms.

8.6 Frontier molecular orbitals

The analysis of the wave function indicates that the electron absorption corresponds to a transition from the ground to the first excited state and is mainly

described by one electron excitation from HOMO to LUMO. Both HOMO and LUMO are the main orbital taking part in chemical reaction. The HOMO energy characterizes the capability of electron giving; LUMO characterizes the capability of electron accepting [287]. The frontier orbital gap helps to characterize the chemical reactivity, optical polarizability and chemical hardness-softness of a molecule [209]. The aromatic orbital components of the frontier molecular orbitals are calculated by using B3LYP/6-31G levels of density functional theory shown in Fig.8.5.

The chemical hardness and softness of a molecule indicates the chemical stability of it. From the HOMO-LUMO energy gap, one can find whether the molecule is hard or soft. If the molecule having large energy gap it shows it is hard and having a small energy gap it is soft. Soft molecules have more polarizable than the hard one. The energy gap (eV), Ionization potential (I), Electron affinity (A), Global hardness (η), Electron negativity (χ), Global softness (σ), Chemical potential (μ), Global Electrophilic index (ω) of the ANC2 molecule has been calculated and tabulated in Table 8.4. For the ANC2 molecule, $E_{\text{HOMO}} = -5.3595$ eV, $E_{\text{LUMO}} = -0.9812$ eV, Ionization potential (I) = 5.3595 eV, Electron affinity (A) = 0.9812 eV, Global hardness (η) = 2.1892 eV, Softness (η) = 0.4568 eV, Chemical potential (μ) = 3.1703 eV, Electrophilic index (ω) = 2.2955 eV. It is seen that the chemical potential of the ANC2 molecule are negative and it means that the compound is stable.

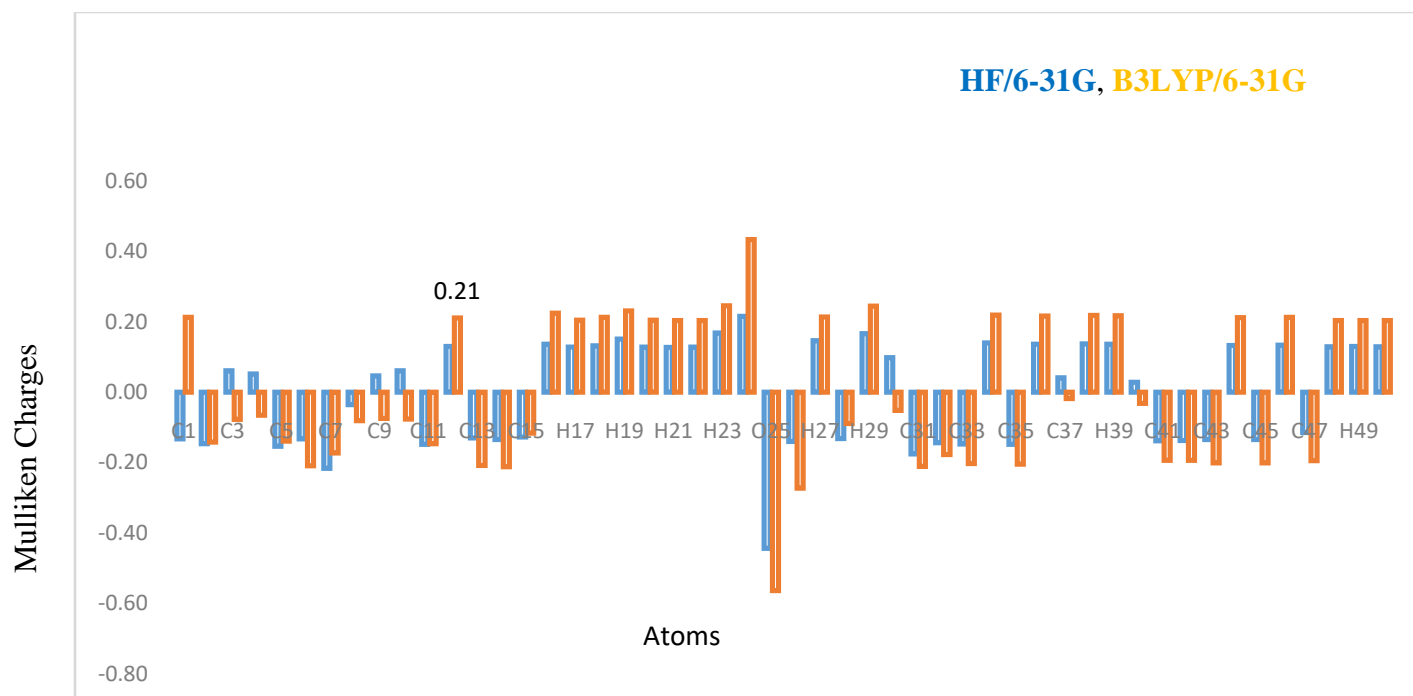


Fig. 8.4 Mulliken atomic charges for (2E)- 1-(anthracene-9-yl) -3-(biphenyl-4-yl) prop-2-en-one

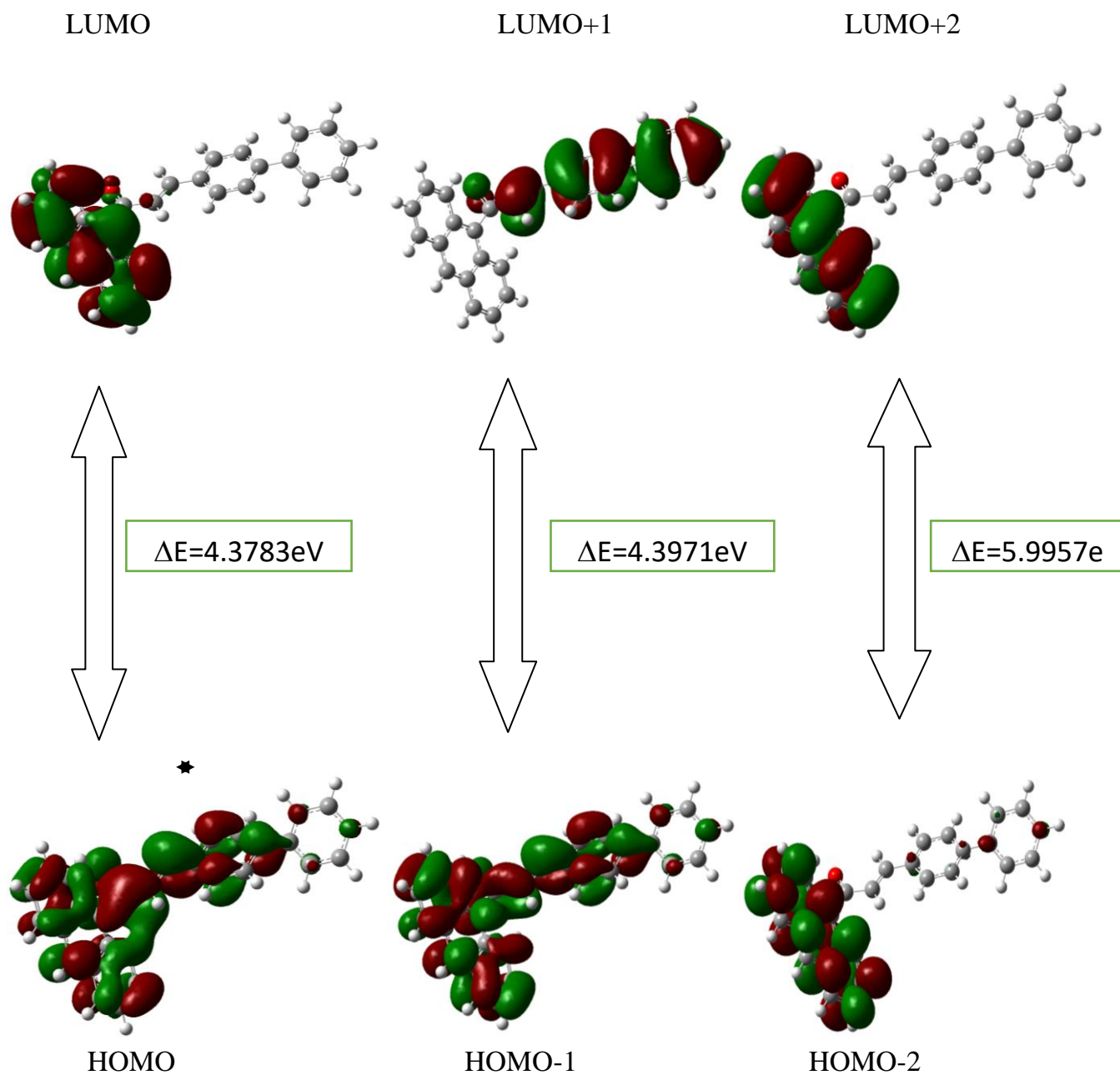


Fig.8.5 Patterns of the principle highest occupied and lowest unoccupied molecular orbital of (2E)-1-(anthracene-9-yl)-3-(biphenyl-4-yl) prop-2-en-1-one

8.7 Natural bond orbital analysis

Natural bond orbital analysis gives information about the interaction in both filled and virtual orbital spaces that could enhance the analysis of inter and intramolecular interactions. NBO calculations of ANC2 molecule are performed using NBO 3.1 program [288] as implemented in the Gaussian 09 package Delocalization of the electron density between occupied Lewis type (bond (or) lone pair) NBO orbitals and formally unoccupied (antibond (or) Rydberg) non- Lewis NBO orbitals corresponding to a stabilizing donor- acceptor interaction. The energy of this interaction can be estimated by the second order perturbation theory. Table 8.5, lists the calculated second order interaction energies $E^{(2)}$ between the donor-acceptor orbitals in the ANC2 molecules. The important interaction energies are 1.43, 2.68, 7.23, 0.03, 0.52 kcal/mol for the title molecule. These values are identified at LP (2) donor NBOs and their corresponding acceptors NBOs are BD*(1) C4-C8, BD*(2) C8-C9, BD*(1) C8-C24, BD*(2) C14-C15, BD*(1)C24-C25, BD*(1)C24-C26, BD*(1)C26-C27, respectively.

In Table 8.6, σ (C26-C28) orbital with 1.98666 electrons has 50.97% C26 character in a $sp^{2.6}$ hybrid and has 49.03 % C28 character in a $SP^{1.76}$ hybrid. For σ (C33-C37), the $sp^{1.83}$ hybrid on C33 has 49.78% p character and the $sp^{1.71}$ hybrid on C37 has 50.22% p character for the ANC2 molecule. For σ (C30-C32) orbital with 1.97886 electrons has 50.23 % C30 character in a $sp^{1.63}$ hybrid and 49.77 % C32 character in a $sp^{1.85}$ hybrid. For σ (C30-C31) orbital with 1.96978 electrons has 50.17% C30 character in a $sp^{1.8}$ hybrid and 49.83 % C31 character in a $sp^{1.83}$ hybrid. The coefficients 0.7140,

0.7002, 0.7055, 0.7087, 0.7087, 0.7055, 0.7094, 0.7048 are called polarization coefficient of the ANC2 molecule. The size of these coefficients shows the importance of the two hybrids in the formation of the bond. In our ANC2 molecule, the carbon has large percentage of NBO and gives the large polarization coefficient because it has higher electronegativity. It is noted that the maximum occupancies 1.98096, 1.97624, 1.97111, 1.98668, 1.97842, 1.97886, 1.96978, 1.97799. These values are found at BD(C1-C2), BD(C1-C6), BD(C8-C24), BD(C26-C28), BD(C30-C31), BD(C30-C32), BD(C31-C33), BD(C33-C37) orbital respectively.

8.8 Molecular electrostatic potential surface analysis

The molecular electrostatic potential (MEP) have been used for interpreting and predicting the reactive behavior of wide variety of chemical and nucleophilic reaction processes and hydrogen bonding interactions and in biological recognition process [289].

The plot of MEP surface of the ANC2 molecule calculated by DFT/B3LYP method is shown in Fig.8.6. It shows the computationally derived electrostatic potential and electrostatic point charges on its individual atoms. Different values of the electrostatic potential are represented by different colour. Red represents the regions of the most negative electrostatic potential and blue represents the regions of most positive electrostatic potential. Potential increases in the order of red < orange < yellow < green < blue. The colour grading of resulting surface simultaneously displays molecular size, shape and electrostatic potential value which are very useful in research of molecular structure with its physiochemical property relationship [290]. For the ANC2 molecule, it

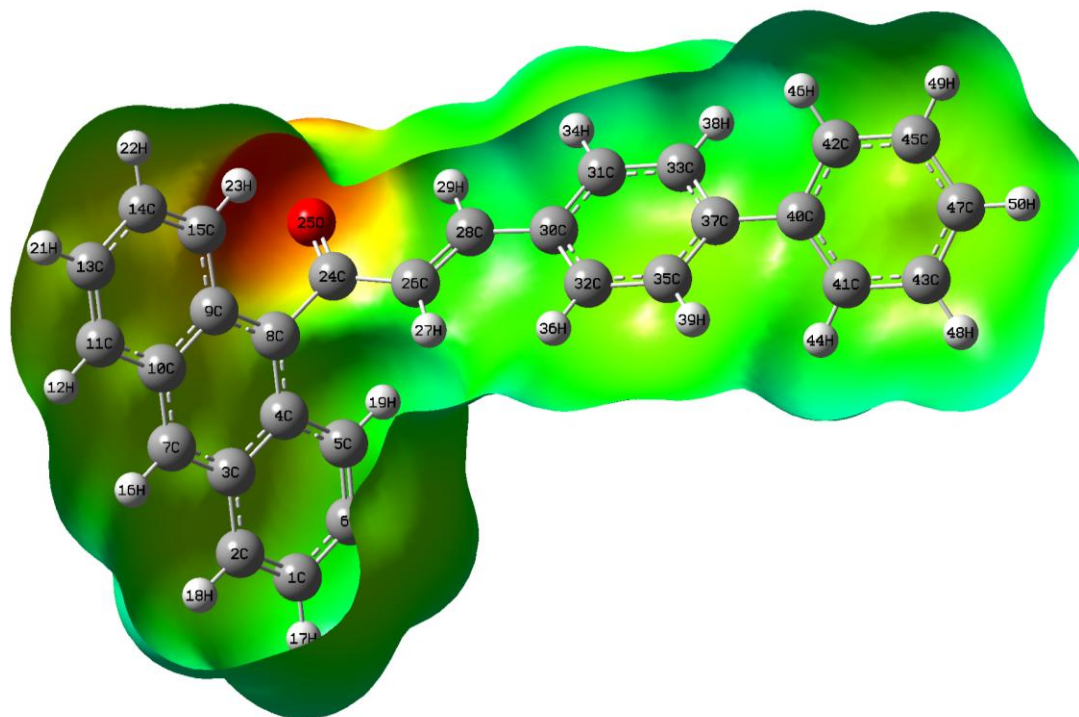


Fig.8.6 Molecular electrostatic potential surfaces of (2E)-1-(anthracene-9-yl)-3-(biphenyl-4-yl) prop-2-en-1-one

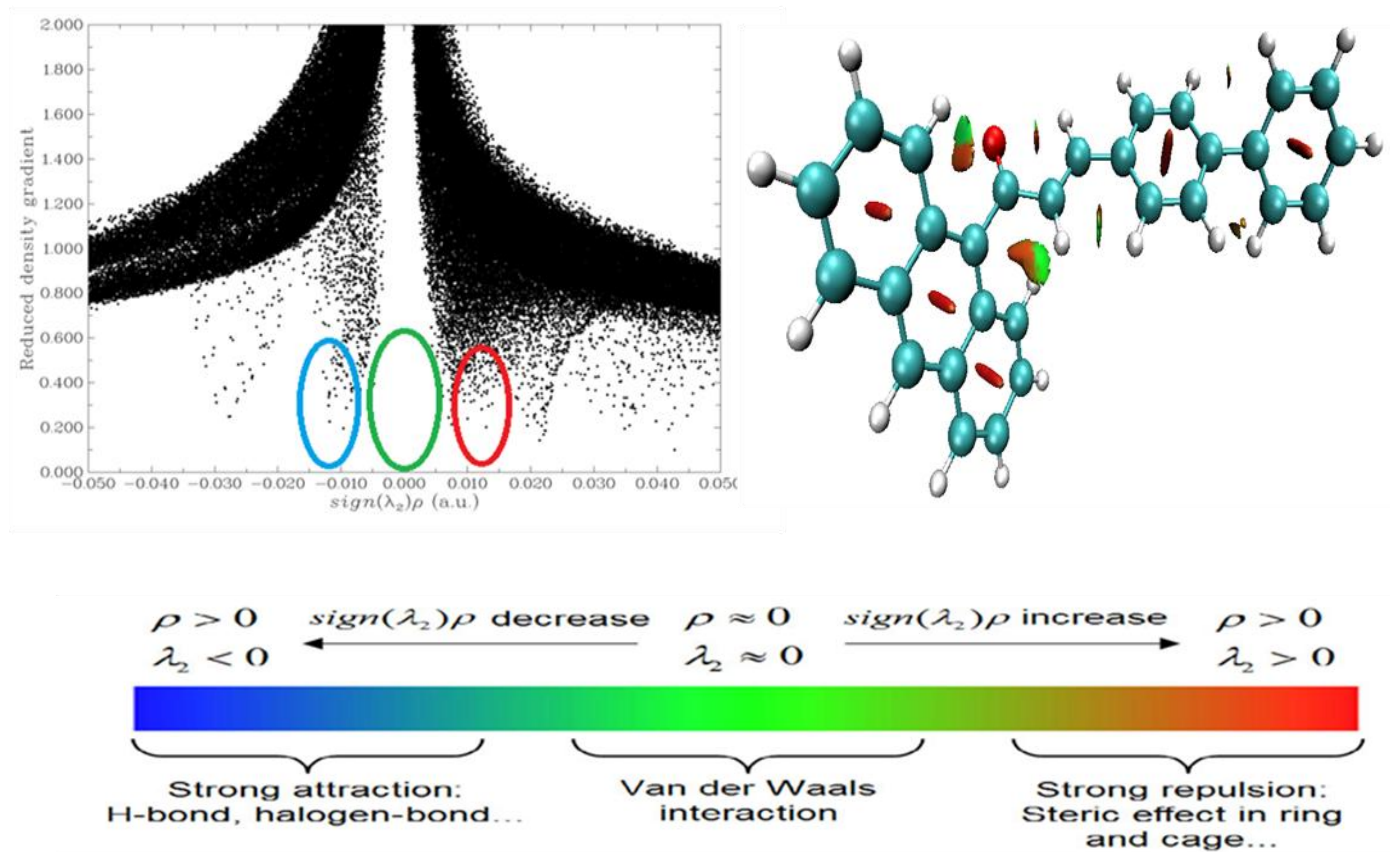


Fig.8.7 Plots of the RDG versus $\lambda(2)\rho$ of (2E)- 1-(anthracene-9-yl)-3-(biphenyl-4-yl) prop-2-en-1-one

is easily represents that the regions having the most positive potential are the hydrogen atoms and the regions having the negative potential are over the electronegative atom ie oxygen atom. The most negative sites are near C=O group, the region having the most negative potential over the oxygen atom O₂₅. The negative potential value is -7.027×10^{-2} indicate the strongest electrophilic attack. A most positive region localized around the hydrogen atoms. These sites give information about the region from where the compound can have intermolecular interactions.

8.9 Reduced density gradient analysis

The reduced density gradient can be used to reveal the intermolecular, intramolecular and covalent interactions in real space based on the electron density. The spikes can be classified to three types as (i) large, negative values indicative of attractive interactions, such as dipole - dipole or H-bonding. (ii) Large and positive sign indicating nonbonding interaction, such as strong repulsion or steric effect in the ring and (iii) values near zero indicating very weak interactions, such as van der Waals interaction.

Johnson *et al* [126] derived the methodology for reduced density gradient (RDG) from electron density as a dimensionless quantity and it was the first gradient found in the literature

$$RDG = (r) = \frac{1}{2(3\pi)^{\frac{1}{3}}} \frac{\Delta\rho(r)}{\rho(r)^{\frac{4}{3}}}$$

The plot $\rho(r)$ against λ_2 sign will help to understand the nature and strength of the interactions. The sign of λ_2 , the second largest value of hessian matrix of electron density,

is used to find the nature of an interaction. If $\lambda_2 > 0$, for non-bonded and if $\lambda_2 < 0$ for bonded. The RDG iso-surface of the ANC2 molecule was drawn with isosurface value of 0.5 as illustrated in Fig.8.7. The software utilized for plotting RDG surface is Multiwfn software and it was plotted by VMD program. The red color represents for steric effect, blue indicates stronger attraction and non-covalent or Van der Waals interaction represents by green color. A strong Van der Waals interaction took place between the carbon (C5, C24) and oxygen (O25) molecule and strong interaction between the hydrogen molecules in the anthracene ring.

8.10 Fukui function

Fukui indices are, in short, reactivity indices they give us information concerning that atoms during a molecule have a large tendency to either loose or accept an electron, which we tend to chemist interpret as that are alot of susceptible to endure a nucleophilic or an electrophilic sites, respectively. The Fukui function is defined using finite differences of the electron density as [263].

$$f = (\delta \rho(r) / \delta (N))_r$$

where $\delta(r)$ is that the electronic density. N is the number of electrons and r is that the external potential exerted by the enzyme. Fukui Function (FF) is one of the wide useful local density functional descriptors to model chemical reactivity and selectivity. The Fukui Function may be a local reactivity descriptor that indicates the number of electron is modified. Therefore, it indicates the propensity of the electronic density to perform at a

given position upon accepting or donating electrons [291]. Also, it is possible to define the corresponding condensed or atomic Fukui Functions on the j th atom site as,

$$f_j^+ = q(N+1) - q_j(N)$$

$$f_j^- = q(N) - q_j(N-1)$$

$$f_j^0 = 1/2[q(N+1) - q_j(N-1)]$$

wherever f^+ , f^- , f^0 are nucleophilic, electrophilic and free radical on the reference molecule, respectively. In these equations, q_j is that the atomic charge (evaluated from Mulliken population, electrostatic derived charge, etc.) at the j th atomic site is the neutral (N), anionic (N+1) or (N-1) chemical species. Morell *et al* [292] have recently planned a dual descriptor (Δf , which is defined as the difference between the nucleophilic and electrophilic Fukui function and is given by the equation,

$$\Delta f(r) = [f^+(r) - f^-(r)]$$

$\Delta f(r) > 0$, then the site is favored for a nucleophilic site, whereas if $\Delta f(r) < 0$, then the site could also be favored for an electrophilic site. According to dual descriptor Δf give a transparent distinction between nucleophilic and electrophilic attack at a particular site with their sign. That is they provide positive value prone for electrophilic sites. From Table 8.7, some of the nucleophilic sites for the ANC2 molecule are C5, H23, C8, H19 and C15 are positive values i.e $\Delta f(r) > 0$ among them, the carbon in the anthracene ring is the highest positive value, C5 (has 0.0666) Similarly, the electrophilic sites are C28, C4, H29, C26 and H27 are some of negative values i.e $\Delta f(r) < 0$ and C28 has high negative value of -0.0425.

8.11 Atoms in molecules

According to the topological analysis of atoms in the molecule gives us more information about the presence of strong and weak hydrogen bonds in terms of Topological parameters for intramolecular interactions in compound electron density (ρ_{BCP}), Laplacian of electron density (V_{BCP}^2), electron kinetic energy density (G_{BCP}), electron potential energy density (V_{BCP}), total electron energy density (H_{BCP}), Hydrogen bond energy (E_{HB}) at bond critical point (BCP) [181].

AIM analysis was performed using Multiwfn package to contemplate the noncovalent interactions of the ANC2 molecule. According to the topological theory of AIM, the two neighbouring atoms are chemically bonded or those atoms have weak interactions that appear in the Bond Critical Point (BCP). The strong, medium, weak H-bonds and their covalent, partially covalent and electrostatic nature can be denoted by ($V_2 \text{ BCP} < 0$ and $H_{\text{BCP}} < 0$), ($V_2 \text{ BCP} > 0$ and $H_{\text{BCP}} < 0$) and ($V_2 \text{ BCP} > 0$ and $H_{\text{BCP}} > 0$) [233]. The topology analysis of the ANC2 molecule was carried out to (3,-1) bond critical points. The paths generated are pictured in Fig. 8.8. ρ_{BCP} and H_{BCP} are Laplacian of electron density and total electron density at bond critical point respectively. From the Table 8.8, it can be seen that the all interaction of hydrogen bond for the ANC2 molecule having positive values of Laplacian of electron density $\nabla^2\rho(r) > 0$ and $V(r) < 0$, shows that they are intermediate closed-shell type hydrogen bond interactions. The strength of hydrogen bond can be also characterized by evaluating the hydrogen bonding energy (E_{HB}). The negative value of E_{HB} of hydrogen bonds designate the conformation of the hydrogen bonds is thermodynamically favoured

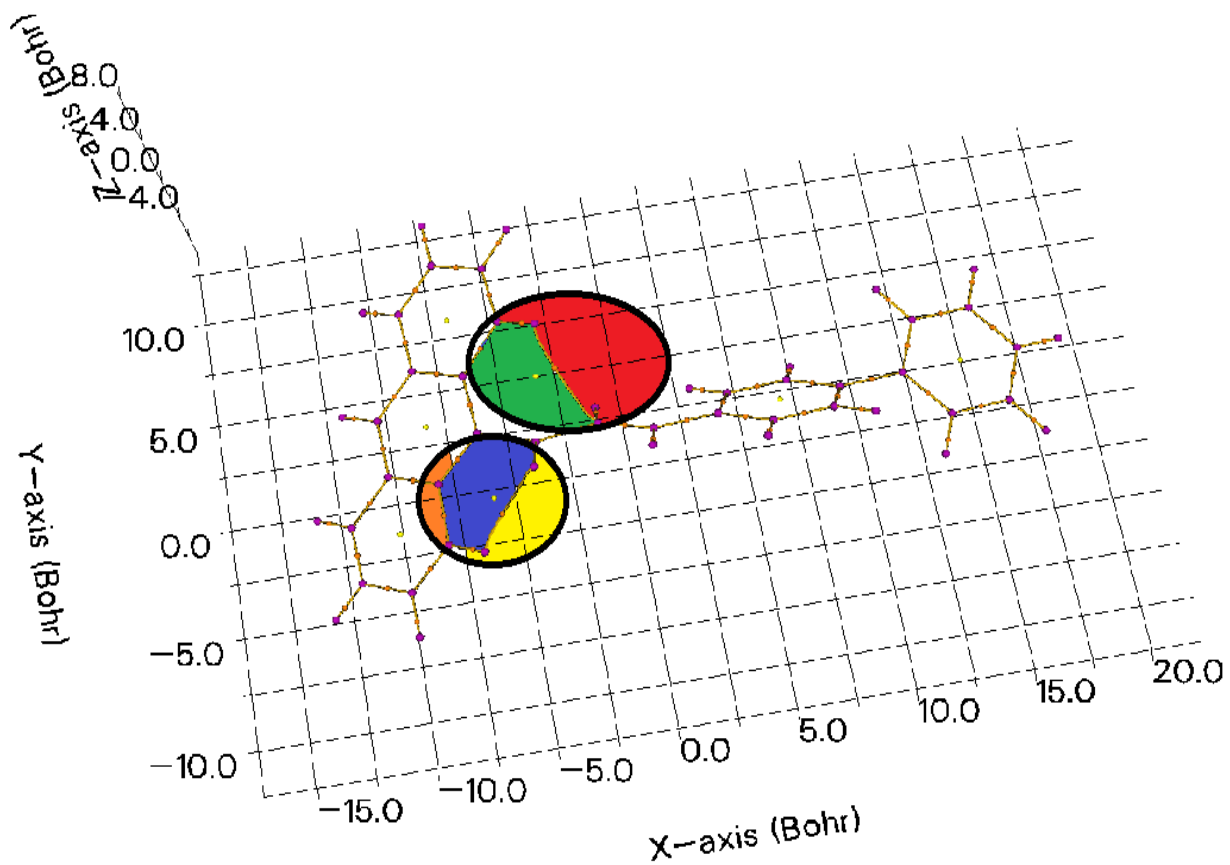


Fig.8.8 Molecular graph of (2E)-1-(anthracene-9-yl)-3-(biphenyl-4-yl)prop-2-en-1-one

8.12 Molecular docking studies

Molecular docking is an efficient tool to get an insight into ligand receptor interactions. The ANC2 compound can be used for treating ubiquinol, cancer and tumor. To explore the biological activity, molecular docking calculations were performed on AutoDock-Vina software [78] which makes use of the Lamarckian Genetic Algorithm (LGA) [293] required in the LGA, all water molecules were removed and the polar hydrogen atoms were added followed by the calculation of Gasteiger charges. The ligand was prepared for docking by minimizing its energy at B3LYP/6-31G level of theory. The ANC2 molecule (ligand) was docked into the active site of the protein 1SQB, 1NTM, 2B7F and 1JH5 associated with ubiquinol, anticancer and antitumor activity. Torsion and rotatable bonds were defined. The active site of the enzyme was defined to include residues of the active site within the grid size of $60 \text{ \AA} \times 60 \text{ \AA} \times 60 \text{ \AA}$. The docking protocol was tested by removing co-crystallized inhibitor from the protein and then docking it at the same site. To evaluate the quality of docking results, the common way is to calculate the Root Mean Square Deviation (RMSD) between the docked pose and the known crystal structure confirmation. RMSD values up to 2 \AA are considered reliable for the docking protein [220]. Amongst the docked conformations, the best scored conformation predicted by AutoDock scoring function was visualized for ligand-enzyme interactions in Discover Studio Visualizer 4.0 and pymol software. Surface view of the proteins with docked ligand embedded in the active site is shown in Fig.8.9. The binding energy (kcal/mol), inhibition constants (nm/ μm), intermolecular energy (kcal/mol) and bonded residues were calculated and the results were tabulated in Table 8.9.

Antitumor

Interaction of antitumor protein 1JH5 shows the existence of many conventional bonds such as four van der waals bonds, one conventional hydrogen bond and one π - π stacked bond interaction with amino acid (LEU A: 361, ALA A: 364, ARG A: 398, ALA A: 263, CYS A: 313, TRP A: 395) with different binding energies (-4.99, -4.64, -4.29, -4.06, -3.95, -3.86)kcal/mol, inhibition constants (218.12, 394.65(μ M), 717.09(μ M), 1.06(mM), 1.26(mM), -3.85(mM)) and RMSD values are (65.462, 71.011, 72.27, 78.998, 85.889, 76.484) \AA .

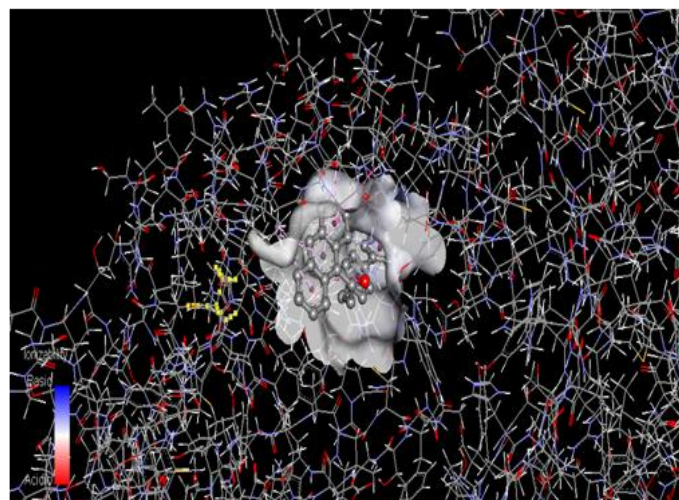
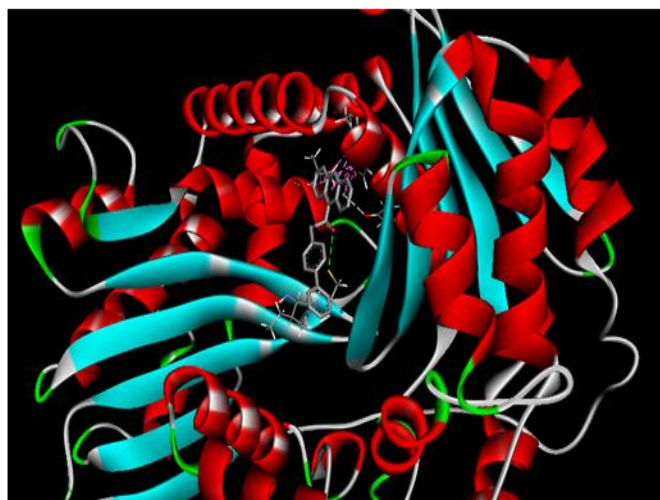
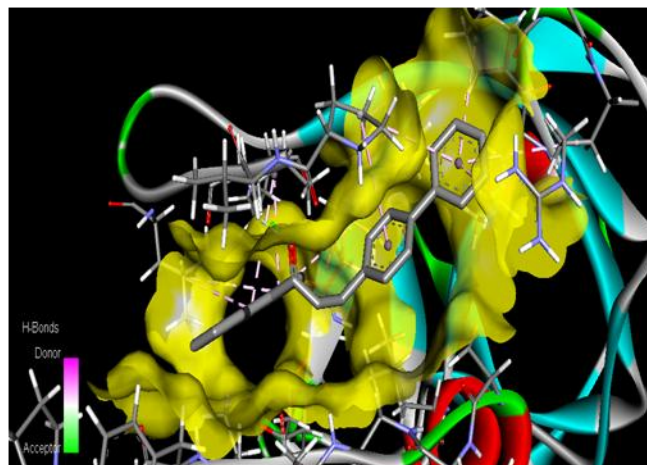
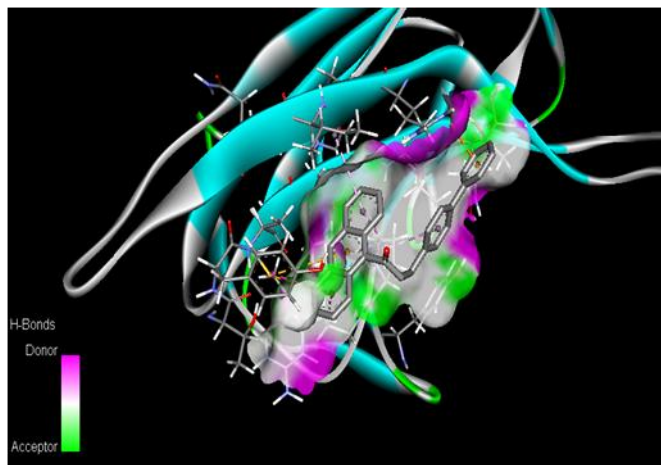
Anticancer

The anticancer protein 2B7F interact with ligand shows the existence of many conventional bonds such as three van der waals bonds and one conventional hydrogen bond interaction with amino acid (VAL A:2, PRO A: 11, ILE A: 13, ILE A: 3) with different binding energies (-9.41, -9.09, -5.23, -9.1)kcal/mol, inhibition constants (127.16(nm), 218.81(nm), 147.58(μ M)) and RMSD values are (126.598, 123.132, 139.504, 123.757) \AA .

Ubiquinol

The interaction of ubiquinol protein 1SQB shows the existence of many conventional bonds such as three van der waals bonds, one conventional hydrogen bond and one π - π stacked bond interaction with amino acid (TRP A: 262, LEU A:365, THR A: 91, CYS A: 313, TRP A: 395) with different binding energies (-7.19, -6.47, -6.28, -5.32, -6.17) kcal/mol, inhibition constants (5.61, 18.15, 25.08, 125.13, 30.17) μ M and RMSD

values are (147.926, 121.518, 149.195, 140.387, 150.448)Å. The ubiquinol protein 1NTM interact with ligand shows the existence of many conventional bonds such as five van der waals bonds, one π - Sulfur bond and one π - π stacked bond interaction with amino acid (LEU A:70, LEU A:70, LEU A:70,ALA A:66, TYR A: 22, TYR A:65, MET A:67) with different binding energies (-7.78, -7.6, -7.23, -7.19, -7.17, -7.47, -5.99)kcal/mol, inhibition constants (1.99, 2.7, 5.02, 5.33, 5.58, 40.57, 3.34) μ M) and RMSD values are (151.809, 151.435, 167.519, 151.242, 150.142, 135.719, 150.611)Å.



Fog.8.9 Ligand (2E)-1-(anthracene-9-yl) -3-(biphenyl-4-yl) prop-2-en-1-one, Protein – 1JHF, 2B7F, 1SQX, 1NTM

8.13 Conclusion

Structure of the ANC2 molecule was investigated using high-level quantum chemistry calculation. The optimized geometrical parameters are theoretically determined and compared with the experimental results. Vibrational frequencies including Infrared intensities and Raman intensities were derived from the computed Raman scattering activities, corresponding vibrational spectra interpreted with the aid of normal coordinate analysis based on scaled *ab initio* and density functional force field, atomic charges were analysed using HF/B3LYP with 6-31G method. It was found that the optimized molecular structures and vibrational frequencies have shown a good agreement with the experimental results and the chosen calculation level is powerful approach for understanding the molecular structure and vibrational spectra of (2E)-1-(anthracene-9-yl)-3-(biphenyl-4-yl) prop-2-en-one (ANC2). The MEP map shows that the negative potential sites are on oxygen atom as well as the positive potential sites are around the hydrogen atoms. This gives information about the region from where the compound can have intramolecular interactions. The NBO analysis is more compatible with the molecular structure of the ANC2 molecule and it is a very useful method for molecular modelling. The HOMO and LUMO analysis are used to determine the charge transfer within the molecule and the calculated HOMO and LUMO energies show the chemical activity of the molecule i.e. the energy gap ΔE is 4.3783eV. The colour on the RDG isosurface indicates that the green regions represent weak attractive interactions ($\lambda_2 \approx 0$) such as Van der Waals interaction; strong attractions like Hydrogen bond were represented by blue color. The red color represents steric repulsion. Molecular docking

analysis reveals that the ANC2 molecule can act as a good inhibitor against the 1SQB, 1NTM, 2B7F and 1JH5 and has maximum binding energy for 2B7F (-9.41kcal/mol) and hence it is suitable ligand for docking studies.

Table 8.1 Optimized structural parameters of (2E)-1-(anthracene-9-yl)-3-(biphenyl-4-yl)prop-2-en-1-one using HF/6-31G and B3LYP/6-31G method

Parameters	Bond length(Å)		Parameters	Bond Angle (°)		Parameters	Dihedral Angle (°)	
	HF/ 6-31G	B3LYP/ 6-31G		HF/ 6-31G	B3LYP/ 6-31G		HF/ 6-31G	B3LYP/ 6-31G
C1-C2	1.373	1.351	C2-C1-C6	119.930	119.783	C6-C1-C2-C3	-0.407	-0.696
C1-C6	1.426	1.427	C2-C1-H17	120.652	120.527	C6-C1-C2-H18	179.256	178.602
C1-H17	1.085	1.073	C6-C1-H17	119.416	119.683	H17-C1-C2-C3	-179.824	-179.709
C2-C3	1.432	1.434	C1-C2-C3	121.083	121.120	H17-C1-C2-H18	-0.161	-0.410
C2-H18	1.086	1.074	C1-C2-H18	120.714	120.696	C2-C1-C6-C5	0.610	1.011
C3-C4	1.449	1.427	C3-C2-H18	118.202	118.181	C2-C1-C6-H20	-178.779	-178.109
C3-C7	1.400	1.388	C2-C3-C4	119.273	119.434	H17-C1-C6-C5	-179.965	-179.968
C4-C5	1.436	1.438	C2-C3-C7	121.360	121.228	H17-C1-C6-H20	0.646	0.912
C4-C8	1.421	1.403	C4-C3-C7	119.366	119.335	C1-C2-C3-C4	-0.654	-1.096
C5-C6	1.376	1.353	C3-C4-C5	117.631	117.351	C1-C2-C3-C7	179.155	178.328
C5-H19	1.083	1.071	C3-C4-C8	119.422	119.486	H18-C2-C3-C4	179.675	179.588
C6-H20	1.085	1.073	C5-C4-C8	122.929	123.122	H18-C2-C3-C7	-0.517	-0.988
C7-C10	1.401	1.388	C4-C5-C6	121.219	121.414	C2-C3-C4-C5	1.473	2.511
C7-H16	1.087	1.075	C4-C5-C9	119.360	119.243	C2-C3-C4-C8	179.985	-179.780
C8-C9	1.424	1.403	C6-C5-H19	119.413	119.325	C7-C3-C4-C5	-178.340	-176.924
C8-C24	1.501	1.501	C1-C6-C5	120.846	120.848	C7-C3-C4-C8	0.173	0.786
C9-C10	1.450	1.428	C1-C6-H20	119.186	119.400	C2-C3-C7-C10	-178.937	-178.015
C9-C15	1.436	1.439	C5-C6-H20	119.965	119.747	C2-C3-C7-H16	0.739	1.256
C10-C11	1.433	1.434	C3-C7-C10	121.683	121.893	C4-C3-C7-C10	0.872	1.409
C11-H12	1.086	1.074	C3-C7-H16	119.164	119.060	C4-C3-C7-H16	-179.452	-179.320

C11-C13	1.372	1.351	C10-C7-H16	119.152	119.043	C3-C4-C5-C6	-1.301	-2.250
C13-C14	1.426	1.428	C4-C8-C9	120.781	120.471	C3-C4-C5-H19	177.641	176.178
C13-H21	1.085	1.073	C4-C8-C24	119.897	120.244	C8-C4-C5-C6	-179.758	-179.870
C14-C15	1.375	1.353	C9-C8-C24	119.319	119.275	C8-C4-C5-H19	-0.816	-1.442
C14-H22	1.085	1.073	C8-C9-C10	119.173	119.113	C3-C4-C8-C9	-1.779	-3.435
C15-H23	1.081	1.069	C8-C9-C15	123.150	123.353	C3-C4-C8-C24	177.578	175.377
H19-C26	2.522	2.649	C10-C9-C15	117.664	117.511	C5-C4-C8-C9	176.651	174.136
H23-O25	2.267	2.460	C7-C10-C9	119.537	119.589	C5-C4-C8-C24	-3.992	-7.052
C24-O25	1.258	1.227	C7-C10-C11	121.156	120.964	C4-C5-C6-C1	0.271	0.519
C24-C26	1.478	1.476	C9-C10-C11	119.307	119.448	C4-C5-C6-H20	179.656	179.635
C26-H27	1.085	1.071	C10-C11-H12	118.203	118.188	H19-C5-C6-C1	-178.670	-177.908
C26-C28	1.355	1.335	C10-C11-C13	121.007	121.007	H19-C5-C6-H20	0.714	1.209
C28-H29	1.090	1.076	H12-C11C13	120.790	120.806	C3-C7-C10-C9	-0.320	-0.950
C28-C30	1.459	1.467	C11-C13-C14	119.950	119.808	C3-C7-C10-C11	179.799	179.144
C30-C31	1.412	1.394	C11-C13-H21	120.631	120.495	H16-C7-C10-C9	-179.996	179.779
C30-C32	1.413	1.397	C14-C13-H21	119.419	119.697	H16-C7-C10-C11	0.123	-0.127
C31-C33	1.393	1.385	C13-C14-C15	120.994	121.070	C4-C8-C9-C10	2.322	3.879
C42-H46	1.085	1.073	H29-C28-C31	115.566	116.082	C10-C9-C15-C14	0.189	-0.003
C43-C47	1.400	1.387	C28-C30-C31	118.729	118.889	C10-C9-C15-H23	-178.248	-178.147
C43-H48	1.086	1.073	C28-C30-C32	123.404	123.499	C7-C10-C11-H12	-0.127	-0.027
C45-C47	1.400	1.387	C31-C30-C32	117.867	117.612	C7-C10-C11-C13	179.866	-179.985
C45-H49	1.086	1.073	C30-C31-C33	121.270	121.357	C9-C10-C11-H12	179.991	-179.932

Table 8.2 Vibrational assignments of (2E)-1-(anthracene-9-yl) -3-(biphenyl-4-yl) prop-2-en-1-one performed by HF/6-31G and B3LYP/ 6-31G method

Modes	Observed wavenumbers (cm ⁻¹)		Calculated wavenumbers (cm ⁻¹)		Vibrational Assignments (% PED)
	FT-IR	FT-Raman	HF/6-31G	B3LYP/6-31G	
	1		3059	3060	
2	3051		3050	3058	vCH(98)
3			3035	3041	vCH(98)
4	3029		3027	3030	vCH(97)
5			3006	3013	vCH(98)
6			2984	2986	vCH(98)
7			2966	2969	vCH(97)
8			2945	2950	vCH(98)
9			2939	2944	vCH(97)
10			2925	2931	vCH(98)
11	2919		2919	2926	vCH(98)
12			2919	2923	vCH(97)
13			2904	2914	vCH(98)
14			2899	2907	vCH(97)
15			2893	2899	vCH(98)
16			2889	289	vCH(98)
17			2874	2886	vCH(97)
18			2863	2871	vCH(98)
19			2856	2862	vCH(98)
20	2851		2850	2854	vCH(98)
21			1675	1679	vCO(58), vCC(27), δCH(12)
22			1662	1666	vCC(68), δCH(28)
23			1657	1662	vCC(69), δCH(29)
24			1643	1648	vCC(68), δCH(25)
25	1634		1630	1635	δCH(68), vCC(24)
26			1624	1627	vCC(65), δCO(20)
27	1618		1618	1622	vCC(66), vCH(22)
28			1609	1614	δCH(67), vCC(25)

29	1601	1602	1602	1609	vCC(67), δCH(24)
30			1588	1592	δCH(65), vCC(23)
31			1567	1575	vCC(67), δCH(22)
32	1556	1559	1558	1562	δCH(71), vCC(23)
33	1520		1521	1524	δCH(70), vCC(24)
34			1517	1520	δCH(68), vCC(23)
35			1501	1507	δCH(70), vCC(23)
36			1493	1499	δCH(71), vCC(22)
37	1485	1485	1486	1492	vCC(70), δCH(20)
38			1471	1475	vCC(71), δCH(23)
39	1447	1448	1450	1453	δCH(70), vCC(23)
40			1431	1436	δCH(66), vCC(21)
41			1422	1426	δCH(68), vCC(20)
42		1413	1415	1420	vCC(70), δCH(23)
43	1408		1407	1414	vCC(70), δCH(22)
44			1392	1395	vCC(82)
45	1386		1385	1389	vCC(71), δCH(12)
46		1359	1360	1364	vCC(70), δCH(14)
47	1350		1351	1350	vCC(80)
48			1304	1309	vCC(80)
49	1288		1285	1289	vCC(75), vCH(12)
50		1282	1280	1285	vCC(73), δCH(11)
51	1264		1262	1266	vCC(80) , δCH(10)
52		1255	1253	1260	vCC(82)
53			1240	1244	δCH(72), vCC(12)
54	1224	1228	1225	1228	δCH(70), vCC(14)
55			1214	1217	δCH(71), vCC(14)
56	1206		1205	1210	δCH(83)
57	1187	1188	1180	1186	δCH(83)
58			1171	1174	vCC(71), δCH(13)
59	1150	1152	1150	1155	δCH(82)
60			1142	1146	δCH(80)
61			1136	1140	vCC(70), δCO(14)
62			1130	1135	δCH(78)
63			1123	1125	vCC(68), δCH(13)

64	1117		1115	1120	vCC(67), δ CH(13)
65			1086	1090	δ CH(77)
66			1075	1079	γ CH(77)
67			1059	1062	γ CH(78)
68			1043	1046	γ CH(80)
69			1037	1040	γ CH(70)
70	1020		1022	1026	γ CH(68)
71			1015	1017	γ CH(68)
72	1004		1007	1011	γ CH(68)
73		998	995	998	γ CH(68)
74	971		971	975	γ CH(67)
75	964	962	965	968	γ CH(67)
76			943	945	δ Ring(63)
77			921	925	δ Ring(68)
78			899	903	δ Ring(65)
79			893	896	δ Ring(66)
80			889	890	Ring breathy(63)
81		883	885	888	γ CH(67)
82			873	878	γ CH(67)
83		862	860	864	vCC(58), δ CH(27)
84			858	861	γ CH(69)
85			855	859	δ Ring(65)
86		850	851	855	γ CH(65)
87			844	849	γ CH(65)
88		834	836	840	γ CH(65)
89			833	835	γ CH(58), γ CC(23)
90			830	832	γ CH(60)
91	824		827	830	γ CH(65)
92			820	825	γ CH(64)
93			819	823	δ Ring(65)
94			812	815	δ Ring(66)
95		800	803	807	γ CC(60), γ CH(21)
96			795	799	γ Ring(66)
97	789		790	794	γ Ring(65)
98			785	788	γ Ring(65)

99			780	783	γ Ring(66)
100			771	775	γ CC(65)
101	764		765	767	γ Ring(65)
102		730	731	735	γ CO(67)
103	724		725	717	δ Ring(66)
104			714	710	δ Ring(65)
105		705	706	708	δ Ring(64)
106			700	704	δ CC(64)
107			690	692	δ Ring(65)
108			681	683	δ Ring(65)
109	666		665	668	δ Ring(68)
110		600	602	605	δ Ring(64)
111			598	601	γ Ring(65)
112	596		596	598	γ CC(68)
113			575	578	γ Ring(65)
114	550		551	555	γ Ring(66)
115			536	540	γ Ring(64)
116	523		525	529	γ Ring(60)
117	503	500	500	506	γ CCC(64)
118			441	458	γ Ring(65)
119	454		453	445	γ Ring(66)
120			425	428	γ Ring(64)
121			383	387	γ CCC (65)
122			365	368	γ CCC (64)
123			321	325	γ CCC (64)
124			300	304	γ Ring(64)
125			269	270	γ CCC (64)
126			245	248	γ CCC (65)
127			223	225	γ CCC (60)
128			209	210	γ CCC (58)
129			193	195	γ CCC (59)
130			186	188	γ CCC (60)
131			179	181	γ CCC (61)
132		175	174	176	γ CCC (60)
133			160	164	γ CCC (61)

134		141	145	γ CHC (58)
135		125	128	γ Ring(58)
136		103	106	γ CC (58)
137		88	91	γ CC (58)
138	75	75	77	γ CCC (60)
139		70	73	γ CCC (61)
140	68	67	70	γ CCC (54)
141		47	51	δ CCC (58)
142		31	33	δ CCC (58)
143		20	24	γ CCC (54)
144		12	10	γ CCC (54)

v-stretching, v_{sym} -sym stretching, v_{asym} -asym stretching, δ -in-plane bending, γ -out-of-plane bending, ρ -scissoring, ω -wagging, σ -rocking, τ -twisting.

Table 8.3 Mulliken atomic charges for (2E)-1-(anthracene-9-yl)-3-(biphenyl-4-yl)prop-2-en-1-one at HF/6-31G and B3LYP/6-31G basis set

Atom Numbering	Charge		Atom Numbering	Charge	
	HF/6-31G	B3LYP/ 6-31G		HF/6-31G	B3LYP/ 6-31G
C1	-0.13	0.21	C26	-0.44	-0.27
C2	-0.15	-0.14	H27	-0.14	0.21
C3	0.06	-0.08	C28	0.15	-0.09
C4	0.05	-0.07	H29	-0.13	0.24
C5	-0.15	-0.14	C30	0.17	-0.05
C6	-0.13	-0.21	C31	0.10	-0.21
C7	-0.22	-0.17	C32	-0.18	-0.18
C8	-0.04	-0.08	C33	-0.14	-0.20
C9	0.05	-0.07	H34	-0.15	0.22
C10	0.06	-0.08	C35	0.14	-0.20
C11	-0.15	-0.15	H36	-0.15	0.22
H12	0.13	0.21	C37	0.14	-0.02
C13	-0.13	-0.21	H38	0.04	0.22
C14	-0.13	-0.21	H39	0.14	0.22
C15	-0.13	-0.12	C40	0.14	-0.03
H16	0.14	0.22	C41	0.03	-0.19
H17	0.13	0.20	C42	-0.14	-0.19
H18	0.13	0.21	C43	-0.14	-0.20
H19	0.15	0.23	H44	-0.13	0.21
H20	0.13	0.20	C45	0.13	-0.20

H21	0.13	0.20	H46	-0.13	0.21
H22	0.13	0.20	C47	0.13	-0.19
H23	0.17	0.25	H48	-0.11	0.20
C24	0.22	0.43	H49	0.13	0.20
O25	-0.44	-0.56	H50	0.13	0.20

Table 8.4 HOMO-LUMO energies for (2E)-1-(anthracene-9-yl)-3-(biphenyl-4-yl) prop-2-en-1-one at B3LYP/6-31G basis set.

Molecular properties	Energy (eV)	Energy gap (eV)	Ionisation potential (I)	Electron affinity(A)	Global hardness (η)	Global softness (σ)	Chemical potential (μ)	Global Electroplicity (ω)
E_{HOMO}	-5.3595	4.3783	5.3595	0.9812	2.1892	0.4568	-3.1703	2.2955
E_{LUMO}	-0.9812							
$E_{\text{HOMO-1}}$	-6.0398	4.3971	6.0398	1.6427	2.1985	0.4548	-3.8413	3.3558
$E_{\text{LUMO-1}}$	-1.6427							
$E_{\text{HOMO-2}}$	-6.5522	5.9957	6.5522	0.5565	2.9978	0.3336	-3.5544	2.1072
$E_{\text{LUMO-2}}$	-0.5565							

Table 8.5 Second order perturbation theory analysis of Fock matrix in NBO basis corresponding to intra molecular bands of (2E)- 1-(anthracene-9-yl)-3-(biphenyl-4-yl) prop-2-en-1-one.

Donor	Acceptor	$E(2)^a$ (kcal/mol)	$E(j)-E(i)^b$ (a.u)	$F_{(ij)}^c$ (a.u)
		BMP	BMP	BMP
LP(2)O 25	BD*(1)C4-C8	1.43	0.88	0.032
LP(2)O 25	BD*(2)C8-C9	2.68	0.33	0.029
LP(2)O 25	BD*(1)C8-C24	7.23	0.63	0.061
LP(2)O 25	BD*(2)C14-C15	1.03	0.34	0.017
LP(2)O 25	BD*(1)C24-C26	17.40	0.62	0.094
LP(2)O 25	BD*(1)C26-C27	0.52	0.72	0.018
BD(2)C1-C2	BD*(2)C3-C4	14.50	0.29	0.063
BD(2)C11-C13	BD*(2)C7-C10	17.10	0.29	0.066
BD(2)C14-C15	BD*(2)C1-C13	17.40	0.29	0.064
BD(2)C24-O25	BD*(2)C8-C9	9.89	0.47	0.066
BD(2)C24-O25	BD*(2)C26-C28	4.05	0.35	0.34
BD(2)C35-C37	BD*(2)C30-C32	21.78	0.27	0.069
BD(2)C43-C47	BD*(2)C40-C41	20.59	0.28	0.068
BD(2)C1-C4	BD*(2)C3-C11	20.73	0.28	0.068

a $E(2)$ means energy of hyperconjugative interactions (stabilization energy).

b Energy difference between donor and acceptor i and j NBO orbitals.

c $F(i,j)$ is the Fock matrix element between i and j NBO orbitals

Table 8.6 NBO analysis of bonding and antibonding orbit for (2E)-1-(anthracene-9-yl)-3-(biphenyl-4-yl) prop-2-en-1-one.

Band (A-B)	ED/Energy (a.u.)	ED _A %	ED _B %	NBO	S(%)	P(%)
σC1-C2	1.98096	49.85%	50.15%	0.7060(sp ^{1.72})	36.74	63.26
				0.7082(sp ^{1.71})	36.93	63.07
σC1-C6	1.97624	50.02	49.7	0.7073(sp ^{1.93})	34.11	65.89
				0.7069(sp ^{1.94})	33.97	66.03
σC1-H17	1.98195	62.3	37.7	0.7893(sp ^{2.43})	29.16	70.84
				0.6140(s ¹)	100	0
σC2-C3	1.97295	48.53	51.47	0.6967(sp ^{1.95})	33.85	66.15
				0.7174(sp ^{2.03})	33.02	66.98
σC1-H18	1.98096	62.22	37.78	0.7888(sp ^{2.24})	29.22	70.78
				0.6146 (s ¹)	100	0
σC3-C4	1.95954	49.56	50.44	0.7040(sp ^{2.09})	32.33	67.67
				0.7102(sp ^{2.04})	32.92	67.08
σC3-C7	1.97423	51.36	48.64	0.7166(sp ^{1.89})	34.6	65.4
				0.6974(sp ^{1.82})	35.4	64.6
σC4-C5	1.96898	51.55	48.45	0.7180(sp ^{2.05})	32.8	67.2
				0.6961(sp ^{2.06})	32.71	67.29
σC4-C8	1.96222	50.28	49.72	0.7091(sp ^{1.92})	34.26	65.74
				0.7051(sp ^{1.8})	35.78	64.22
σC6-H20	1.98187	62.25	37.75	0.789(sp ^{2.42})	29.25	70.75
				0.644 (s ¹)	100	
σC7-C10	1.97442	48.72	51.28	0.698(sp ^{1.82})	35.48	64.52
				0.7161(sp ^{1.9})	34.43	34.43
σC8-C24	1.97111	51.56	48.44	0.7180(sp ^{2.67})	27.28	72.72
				0.6960(sp ^{2.09})	32.33	67.67
σC9-C10	1.96241	50.28	49.72	0.7091(sp ^{2.04})	32.89	67.11
				0.7051(sp ^{2.09})	32.41	67.59
σC9-C15	1.97094	51.75	48.25	0.7193(sp ^{2.04})	32.86	67.14
				0.6947(sp ^{2.01})	33.2	66.8
σC11-C13	1.9809	50.17	49.83	0.7083(sp ^{1.70})	36.98	63.02
				0.7059(sp ^{1.72})	36.71	63.29
σC13-C14	1.9783	50.11	49.89	0.7079(sp ^{1.93})	34.14	65.86
				0.7063(sp ^{1.96})	33.83	66.17

σ C13-H21	1.98237	62.26	37.74	0.7891(sp ^{2.43})	29.16	70.84
				0.6143(s) (s ¹)	100	
σ C24-O25	1.9929	34.44	65.56	0.5868(SP ^{2.42})	29.25	70.75
				0.8097(S ^{1.75})	36.33	63.67
σ C24-O25	1.93228	36.64	63.36	0.6053(SP ^{98.16})	1.01	98.99
				0.7960(SP ³⁰)	3.23	96.77
σ C24-C26	1.97785	49.76	50.24	0.7054(SP ^{1.67})	37.45	62.55
				0.7088(SP ^{2.82})	26.16	73.84
σ C26-H27	1.96057	63.77	36.23	0.7986(SP ⁹²)	34.2	65.8
				0.6019(SP ¹)	100	
σ C26-C28	1.98668	50.97	49.03	0.7140(SP ^{2.6})	27.76	72.24
				0.7002(SP ^{1.76})	36.19	63.81
σ C30-C31	1.97842	50.32	49.68	0.7094(sp ^{1.61})	38.37	61.63
				0.7048(sp ^{1.86})	34.98	65.02
σ C30-C32	1.97886	50.23	49.77	0.7087(sp ^{1.63})	38.06	61.94
				0.7055(sp ^{1.83})	35.07	64.93
σ 31-C33	1.96978	50.17	49.83	0.7083(sp ^{1.8})	35.69	64.31
				0.7059(sp ^{1.85})	35.12	64.88
σ C33-C37	1.97799	49.78	50.22	0.7055(sp ^{1.83})	35.33	64.67
				0.7087(sp ^{1.71})	36.88	63.12

Table 8.7 Topological parameters for intramolecular interactions in compound electron density (ρ_{BCP}), Laplacian of electron density (∇^2_{BCP}), electron kinetic energy density (G_{BCP}), electron potential energy density (V_{BCP}), total electron energy density (H_{BCP}), Hydrogen bond energy (E_{HB}) at bond critical point(BCP)

Interactions	ρ_{BCP}	∇^2_{BCP}	G_{BCP}	V_{BCP}	H_{BCP}	E_{HB}
H19....C26	0.0155	0.07289	0.01597	-0.0137	-0.0022	-0.0068
H28....O25	0.0127	0.04566	0.0102	-0.009	0.0012	-0.0045

Table 8.8 Fukui function (f_i^+ , f_i^- , Δf) for (2E)-1-(anthracene-9-yl) -3-(biphenyl-4-yl) prop-2-en-1-one

Atoms	Neutral (N)	Cation (N-1)	Anion (N+1)	f_k^+	f_k^-	f_k°	Δ
C1	-0.132	-0.129	-0.112	0.0194	-0.0025	0.0085	0.0219
C2	-0.150	-0.168	-0.125	0.0248	0.0179	0.0213	0.0069
C3	0.088	0.101	0.078	-0.0095	-0.0133	-0.0114	0.0038
C4	0.003	-0.049	0.011	0.0081	0.0514	0.0297	-0.0433
C5	-0.066	-0.025	-0.041	0.0251	-0.0409	-0.0079	0.0660
C6	-0.196	-0.217	-0.171	0.0253	0.0211	0.0232	0.0042
C7	-0.227	-0.256	-0.166	0.0610	0.0285	0.0448	0.0326
C8	-0.116	-0.090	-0.095	0.0209	-0.0267	-0.0029	0.0476
C9	0.057	0.030	0.076	0.0189	0.0269	0.0229	-0.0080
C10	0.079	0.088	0.068	-0.0115	-0.0086	-0.0100	-0.0029
C11	-0.155	-0.167	-0.129	0.0258	0.0117	0.0188	0.0140
H12	0.126	0.091	0.179	0.0530	0.0348	0.0439	0.0181
C13	-0.133	-0.135	-0.117	0.0157	0.0025	0.0091	0.0132
C14	-0.154	-0.166	-0.130	0.0233	0.0127	0.0180	0.0107
C15	-0.093	-0.082	-0.075	0.0178	-0.0110	0.0034	0.0288
H16	0.129	0.085	0.196	0.0672	0.0438	0.0555	0.0234
H17	0.121	0.078	0.183	0.0617	0.0433	0.0525	0.0184
H18	0.129	0.088	0.184	0.0545	0.0409	0.0477	0.0136
H19	0.137	0.141	0.180	0.0427	-0.0042	0.0192	0.0468
H20	0.122	0.085	0.181	0.0586	0.0370	0.0478	0.0216
H21	0.121	0.081	0.181	0.0603	0.0401	0.0502	0.0202
H22	0.120	0.083	0.182	0.0614	0.0368	0.0491	0.0246
H23	0.145	0.154	0.190	0.0453	-0.0087	0.0183	0.0539
C24	0.290	0.252	0.332	0.0422	0.0379	0.0401	0.0042
O25	-0.368	-0.499	-0.339	0.0290	0.1310	0.0800	-0.1020
C26	-0.206	-0.231	-0.238	-0.0315	0.0250	-0.0032	-0.0565
H27	0.203	0.103	0.225	0.0214	0.0998	0.0606	-0.0784
C28	-0.111	-0.198	-0.066	0.0443	0.0868	0.0656	-0.0425

H29	0.179	0.100	0.206	0.0262	0.0792	0.0527	-0.0530
C30	0.052	0.061	0.045	-0.0066	-0.0095	-0.0080	0.0029
C31	-0.167	-0.176	-0.165	0.0019	0.0096	0.0057	-0.0078
C32	-0.169	-0.178	-0.168	0.0014	0.0088	0.0051	-0.0075
C33	-0.140	-0.150	-0.135	0.0053	0.0098	0.0076	-0.0044
H34	0.152	0.135	0.156	0.0038	0.0173	0.0106	-0.0135
C35	-0.139	-0.149	-0.134	0.0053	0.0098	0.0076	-0.0046
H36	0.141	0.125	0.146	0.0055	0.0154	0.0104	-0.0099
C37	0.015	0.017	0.013	-0.0023	-0.0019	-0.0021	-0.0005
H38	0.149	0.113	0.169	0.0194	0.0365	0.0280	-0.0171
H39	0.147	0.111	0.167	0.0199	0.0362	0.0281	-0.0163
C40	0.015	0.011	0.018	0.0031	0.0040	0.0035	-0.0009
C41	-0.145	-0.146	-0.145	0.0005	0.0010	0.0007	-0.0004
C42	-0.145	-0.146	-0.144	0.0006	0.0010	0.0008	-0.0004
C43	-0.130	-0.132	-0.128	0.0017	0.0024	0.0021	-0.0007
H44	0.138	0.139	0.133	-0.0049	-0.0007	-0.0028	-0.0042
C45	-0.130	-0.132	-0.128	0.0017	0.0024	0.0021	-0.0007
H46	0.138	0.134	0.141	0.0032	0.0042	0.0037	-0.0010
C47	-0.121	-0.124	-0.118	0.0024	0.0037	0.0031	-0.0012
H48	0.132	0.115	0.142	0.0098	0.0169	0.0133	-0.0070
H49	0.132	0.113	0.145	0.0128	0.0187	0.0157	-0.0059
H50	0.130	0.110	0.144	0.0140	0.0207	0.0173	-0.0067

Table 8.9 Binding energy and inhibition constant of ligand (2E)-1-(anthracene-9-yl) -3-(biphenyl-4-yl) prop-2-en-1-one with protein

Drug	Protein	Type of activity	Binding affinity (kcal/mol)	Etimated inhibition constant Ki(μ M)	Bonded residues	Nature of bond	Bond distance (\AA)	RMSD
(2E)-1-(anthracene-9-yl) -3-(biphenyl-4-yl) prop-2-en-1-one	1JH5	Antitumor	-4.99	218.12	LEU A: 361	van der waals	2.43	65.462
			-4.64	394.65	ALA A: 364	van der waals	2.82	71.011
			-4.29	717.09	ARG A: 398	van der waals	3.01	72.27
			-4.06	1.06 (mM)	ALA A: 263	van der waals	3.24	78.998
			-3.95	1.26 (mM)	TRP A: 395	π - π stacked	4.67	86.889
			-3.86	1.47 (mM)	CYS A: 313	Conventional hydrogen bond	5.46	76.484
	2B7F	Anticancer	-9.41	127.16 (nm)	VAL A:2	van der waals	1.91	126.598
			-9.1	212.7 (nm)	ILE A: 3	Conventional hydrogen bond	2.23	123.757
			-9.09	218.81 (nm)	PRO A: 11	van der waals	2.55	123.132
			-5.23	147.58	ILE A: 13	van der waals	5.27	139.504
	1SQB	Ubiquinol	-7.16	5.61	TRP A: 262	van der waals	3.12	147.926
			-6.47	18.15	LEU A:365	van der waals	3.64	121.518
			-6.28	25.08	THR A: 91	van der waals	3.85	149.195
			-6.17	30.17	TRP A: 395	π - π stacked	4.67	150.448
			-5.32	125.13	CYS A: 313	Conventional hydrogen bond	5.46	140.387

	1NTM	Ubiquinol	-7.78	1.99	LEU A: 70	van der waals	2.21	151.809
			-7.6	2.7	LEU A: 70	van der waals	2.34	151.435
			-7.47	3.34	TYR A: 65	π - π T-shaped	2.6	150.611
			-7.23	5.02	LEU A: 70	van der waals	2.82	167.519
			-7.19	5.33	ALA A: 66	van der waals	3.01	151.242
			-7.17	5.58	TYR A: 22	van der waals	3.35	150.142
			-5.99	40.57	MET A:67	π - Sulfur	5.2	135.719

Conclusion

Summary of Conclusions

In the present work, FT-IR and FT-Raman spectra of polyatomic molecules have been observed experimentally. Theoretical calculations were performed based on the quantum mechanical approach by DFT (HF/B3LYP) calculations using different basis sets with 6-31G and 6-31G(d,p). The molecular geometry of investigated molecules have been provided with computed bond lengths, bond angles and dihedral angles and also calculated vibrational wavenumbers. The theoretically calculated spectra have good agreement with experimentally observed spectra. Natural bond orbital analysis reflects the charge transfer within the molecule that provides a good understanding of bond strength, aromatic character of ring and hyperconjugation interactions. Frontier molecular orbital, Molecular Electrostatic potential and Fukui function calculations provide the most appropriate atomic sites for the electrophilic and nucleophilic nature.

The analysis of Mulliken atomic charge indicates the charge distribution within the molecule. The results presented in this work, illustrate the vibrational spectroscopy in conjugation with quantum chemical calculations carried out for the polyatomic molecules. The topological analysis at bond critical point have been carried out by Quantum theory of atoms in molecules (QTAIM) and found that the natures of hydrogen bond present in molecules are moderate. The noncovalent interactions were identified from the molecular geometry and electron localization function. The molecular docking studies were predicting the favourable orientation of the ligand and protein to investigate the pharmaceutical properties.

Reference

References

- [1] G. Herzberg, *Molecular Spectra and Molecular Structure: II, Infrared and Raman Spectra of Polyatomic Molecules*, Van Nostrand Reinhold, New York, 1966.
- [2] E.B. Wilson, J.C. Decius, P.C. Cross, *Molecular Vibrations: The Theory of Infrared and Raman Vibrational Spectra*, McGraw-Hill, New York, 1955.
- [3] R.C. Clive, I.M. Mills, W.B. Person, B. Crawford, Jr., *J. Chem. Phys.* 25(1958) 1266.
- [4] J.B. Howard, E.B. Wilson. Jr., *J. Chem. Phys.* 2 (1934) 620.
- [5] B.P. Straughan, S. Walker, *Spectroscopy*, Chapman and Hall, London, 1976.
- [6] A.W. Joshi, *Elements of Group Theory of Physicists*, Wiley Eastern, 1973.
- [7] F. Albert Cotton, *Chemical Applications of Group Theory*, Wiley-Interscience, New York, 1963.
- [8] K.V. Raman, *Group Theory and its Applications to Chemistry*, TataMcGraw - Hill, New Delhi, 1990.
- [9] K. Nakamoto, *Infrared and Raman Spectra of Inorganic and Co-ordination Compounds*, third ed., John Wiley & Sons Inc., New York, 1978.
- [10] W.A. Gillory, *Introduction to Molecular Structure and Spectroscopy*, Allyn and Bacon Inc., Boston, 1977.
- [11] G. Davidson, *Group Theory for Chemists*, Macmillan, London, 1991.
- [12] C.N.R. Rao, *Chemical Applications of Infrared Spectroscopy*, Academic Press, New York, 1963.

- [13] S.N. Vinogradov, R.H. Linnell, Hydrogen bonding, Van nostrand, Reinhold Company, New York, 1971.
- [14] L.A. Woodward, Introduction to Theory of Molecular Vibrations and Vibrational Spectroscopy, Oxford University Press, New York, 1972.
- [15] J.B. Foresman, C. Frisch, Second Ed., Gaussian Inc., Pittsburgh, PA, 1996.
- [16] D.V. Shalashilin, D.L. Thompson, J. Phy. chem. A101 (1997) 961–966.
- [17] Y. Kohno, K. Ueda, A. Imamura, J. Phy. chem. 100 (1996) 4701–4712.
- [18] A.V. Dzyabchenko, T.S. Pivina, E.A. Arnautova, J. Mol. Struct. 378 (1996) 67–82.
- [19] G. Filippini, A. Gavezotti, Chem. Phy. Lett. 231 (1994) 86–92.
- [20] L. Phillips, R.S. Sinkovits, E.S. Oran, J.P. Boris, J. Phy. Cond. Matt. 5 (1993) 6357–6376.
- [21] C.C.J. Roothaan, Rev. Mod. Phys. 23 (1951) 69.
- [22] A. Messiah, Quantum Mechanics, North-Holland Pub., Amsterdam, 1961.
- [23] Errol Lewars, Computational Chemistry, Klumer Academic/Plenum Press, New York, Second Ed., 2008.
- [24] C. Møller, M.S. Plesset, Phys. Rev. 46 (1934) 618.
- [25] J.S. Binkley, J.A. Pople, Int. J. Quantum Chem. 9 (1975) 229.
- [26] R.G. Parr, W. Yang, R. Breslow, J.B. Goodenough, J. Halpern, J. Rolinson, Oxford University Press, New York, 1989.
- [27] D. Joubert, Density Functionals: Theory and Applications, Springer- Verlag, DE. Heidelberg, 1998.

- [28] C. Lee, W. Yang, R.G. Parr, *Phy. Rev.* B37 (2) (1988) 785–789.
- [29] W. Kohn, A.D. Becke, R.G. Parr, *J. Phy. Chem.* 100 (31) (1996) 12974–12980.
- [30] J.L. Durant, *Chem. Phy. Lett.* 256 (1996) 595–602.
- [31] A.D. Becke, *Phy. Rev.* A38 (6) (1998) 3098–3100.
- [32] J.P. Perdew, K. Burke, Y. Wang, *Phy. Rev.* B54 (23) (1996) 16533–16539.
- [33] O. Exner, *Dipole Moments in Organic Chemistry*, George Thieme Publishers, Stuttgart, 1975.
- [34] T. Brinck, C. Parkanyi, *Theoretical Organic Chemistry*, Elsevier New York, 1998.
- [35] P.O. Löwdin, *Phys. Rev.* 97 (1955) 1474–1489.
- [36] M. J. Frisch, G. W. Trucks, H. B. Schlegel, G. E. Scuseria, M. A. Robb, J. R. Cheeseman, G. Scalmani, V. Barone, B. Mennucci, G. A. Peterson, H. Nakatsuji, M. Caricato, X. Li, H. P. Hratchian, F. Izmaylov, J. Bloino, G. Zheng, J. I. Sonnenberg, M. Hada, M. Ehara, K. Toyota, R. Fukuda, J. Hasegawa, M. Ishida, T. Nakajima, Y. Honda, O. Kitao, H. Nagari, T. Vreven, T. A. Montgomery Jr., J. E. Peralta, F. Ogliaro, M. Bearpark, J. J. Heyd, Brothers E, Kudin K N, V. N. Staroverov, R. K. Kobayashi, J. Normand, K. Ragavachari, A. Rendell, J. C. Burant, S. S.B Iyengar, J. Tomasi, M. Cossi, N. Rega, J. M. Millam, M. Klene, J. E. Knox, J. B. Cross, V. Bakken, C. Adamo, J. Jaramillo, R. G. Gomperts, R. E. Strarmann, O. Yazyev, A. J. Austin, R. Cammi, C. Pomelli, J. W. Ochterski, R. I. Martin, K. Morokuma, V. G. Zakrzewski, G. A. Voth, P. Salvador, J. J. Dannenberg, S. Dapprich, O. Farkas, J. V. Ortiz, J. Cioslowski, D. J. Fox Gaussian, Inc., Wallingford CT, 2009.

- [37] J.P. Foster, F. Weinhold, *J. Am. Chem. Soc.* 102 (1980) 7211–7218.
- [38] G.N. Lewis, *J. Am. Chem. Soc.* 38 (1916) 762.
- [39] R.S. Mulliken, *J. Chem. Phys.* 46 (1944) 497.
- [40] P. Jorgensen, J. Simons, *J. Chem. Phys.* 79 (1983) 334.
- [41] R.G. Parr, W. Yang, Density functional approach to the frontier-electron theory of chemical reactivity, *J. Am. Chem. Soc.*, 106 (1984) 4049-4050.
- [42] J.P. Perdew, R.G. Parr, M. Levy, J.L. Balduz Jr., *Phys. Rev. Lett.*, 49 (1982) 1691-1694.
- [43] Y. Zhang, W. Yang, “Perspective on Density-functional theory for fractional particle number: derivative discontinuities of the energy” *Theor. Chem. Acc.*, 103 (2000) 346-348.
- [44] P.R. Griffiths, J.A. De Haseth, *Fourier Transform Infrared Spectrometry*, Wiley, New York, 1986.
- [45] R.J. Bell, *Introducing Fourier Transform Spectroscopy*, Academic Press, New York, 1972.
- [46] Jag Mohan, *Organic Spectroscopy - Principles and Applications*, Sixth Ed., Narosa, Publishing House, New Delhi, 2010.
- [47] Jag Mohan, *Organic Analytical Chemistry - Theory and Practice*, Narosa Publishing House, New Delhi, 2003.
- [48] T. Hirschfeld, E.R. Schildkraut, M. Lapp, *Laser Raman Gas Diagnostics*, Plenum, New York, 1974.

- [49] N. Klose, K. Niedbolla, K. Schwartz, I. Bottcher, 4,5Bis(4-methoxyphenyl)2-cycloalkylthioimidazole mit antiphlogistischer Wirkung, Arch.Pharm. 316 (1983) 941-951.
- [50] R.K. Satsangi, S.M. Zaidi, V.C. Misra, 1-(4-substituted-thiazol-2-yl)hydantoins as anti-inflammatory and CNS-active agents, Pharmazie 38 (1983) 341-342.
- [51] E. Daniel Lynch, Ian McClenaghan, E. Mark Light, L. Simon Coles, The Hydrogenbonding networks of 2- amino-4-phenyl-1,3-thiazole derivatives, Cryst. Eng. 5 (2002) 123-136.
- [52] C.T. Supuran, A. Scozzafava, B.C. Jurca, M. A. Lises, Eur.J. Med. Chem. 33 (1998) 83-93.
- [53] G. Renzi, A. Scozzafava, C.T. Supuran, Bioorg. Med. Chem. Lett., 10 (2000) 4570-4577.
- [54] J.J. Li, D. Anderson, E.G. Burton, J.N. Cogburn, J.T. Collins, D.J. Garland, S. A. Gregory, H.G. Huang, P.C. Isakson, Med. Chem. 38 (1995) 4570-4578;
- [55] K. Asada, M. Watanabe, T. Nagasu, T. Tsukhara, L.K. Iijima, A. K. Kitoh, J. Med. Chem. 38 (1992) 2496-2497.
- [56] A. K. Gadad, C.S. Maharajanshetti, S. Nimbalkar, A. Raichurkar, Eur. J. Med. Chem. (2000) 853-857;
- [57] F. Zani, P. Vicini, Antimicrobial activity of some 1,2-benzisothiazoles having a benzenesulfonamide moiety, Arch.Pharm. (1998) 219-223.
- [58] T.H. Maren, Relations between structure and biological activity of sulfonamides, Ann.Rev.Pharmacol., Toxicol. (1976) 309-327.

- [59] M.J. Rogers, E. Cundliffe, T.F. Mccutchan, *Antimicrob. Agents Chemother.* 42 (1998) 715-716.
- [60] M.C. Bagley, J.W. Dale, E. A. Merritt, X. Xiong, Thiopeptide antibiotics, *Chem. Rev.* 105 (2005) 685-714.
- [61] A. S. Mayhoub, M. Khaliq, C. Botting, Z. Li, R.J. Kuhn, M. Cushman, *Bioorg. An investigation of phenylthiazole antflaviviral agents*, *Med. Chem.* 19 (2011) 3845–3854.
- [62] O. Seitz, F. Bergmann, D. Heindl, A Convergent Strategy for the Modification of Peptide Nucleic Acids: Novel Mismatch Specific PNA Hybridization Probes, *Angew. Chem. Int. Ed.* 38(15) (1999) 2203-2206.
- [63] O. Köhler, D.V. Jarikote, O. Seitz, Forced intercalation probes (FIT Probes): thiazole orange as a fluorescent base in peptide nucleic acids for homogeneous single-nucleotide-polymorphism detection, *Chembiochem* 6(1) (2005) 69-77.
- [64] O. Koehler, O. Seitz, Thiazole orange as fluorescent universal base in peptide nucleic acids, *Chem. Commun.* (23) (2003) 2938-2939.
- [65] O.I. El-Sabbagh, M.M. Baraka, S.M. Ibrahim, C. Pannecouque, G. Andrei, R. Snoeck, J. Balzarini, A. A. Rashad, *Eur. J. Med. Chem.* 44(9) (2009) 3746-3753.
- [66] S.K. Bharti, G. Nath, R. Tilak, S. Singh, *Eur. J. Med. Chem.* 45(2) (2010) 651-660.
- [67] M.I. Soares, A. F. Brito, M. Laranjo, J. A. Paixão, M.F. Botelho, T. M. P. Melo, *Eur. J. Med. Chem.* 60 (2013) 254-262.

- [68] F. Mjambili, M. Njoroge, K. Naran, C. De Kock, P.J. Smith, V. Mizrahi, D. Warner, K. Chibale *Bioorg. Med. Chem. Lett.* 24(2) (2014) 560-564.
- [69] M. Helal, M. Salem, M. El-Gaby, M. Aljahdali, *Eur. J. Med. Chem.* 65 (2013) 517-526.
- [70] H.W. Lee, B.Y. Kim, J.B. Ahn, S.W. Kang, J.H. Lee, J.S. Shin, S.K. Ahn, S.J. Lee, S.S. Yoon, *J Med Chem* , 40 (2005) 862.
- [71] A. Ceriello, Oscillating Glucose Is More Deleterious to Endothelial Function and Oxidative Stress Than Mean Glucose in Normal and Type 2 Diabetic Patients *Diab Met Res Rev*, 24: 14 (2008).
- [72] V. V. Salian, B. Narayana, B. K. Sarojini, M. S. Kumar, K. Sharath Chandra, A. G.Lobo, *J. Mol. Struct.*, 1192 (2019) 91-104.
- [73] V. V. Salian, B. Narayana, B. K. Sarojini, E. S. Sindhupriya, L. N. Madhu, S. Rao, *Lett. Drug Des. Discov.*, 14 (2017) 216-227.
- [74] B. Narayana, V. V. Salian, B. K. Sarojini, J. P. Jasinski, *Acta Cryst.* 70 (2014) 855.
- [75] R. Dennington, T. Kerth, J. Millam, *GaussView, Version 5*, Semicham.Inc., Shawnee Mission KS, 2009.
- [76] T. Lu, F. Chen, *Multiwfn: a multifunctional wave function analyzer*, *J. Chem. Inf. Comput. Chem.* 33 (2012) 580-592.
- [77] W. Humphrey, A. Dalke, K. Schulten, *VMD: Visual molecular dynamics* *J. Mol. Graph.* 14 (1996) 33-38.

- [78] O. Trott, A. J. Olson, AutoDock Vina: improving the speed and accuracy of docking with a new scoring function, efficient optimization and multithreading, *J. Comput. Chem.* 31 (2010) 455-461.
- [79] W.L. Delano, The PyMOL Molecular Graphics System, Schrodinger LLC.pymol.org.Version 1, 2002, <http://www.pymol.org>.doi:citeulike-id:240061.
- [80] Discovery studio 4.5 Guide, Accelrys Inc.,San Diego, 2009. <http://www.accelrys.com>.
- [81] S.H. Rosline Sebastian, M.A. Al-Alshaikh, El-Emam A Ali, C.Y. Panicker, J. Zitko, M. Dolezal, C. Van Alsenoy, *J. Mol. Struct.* 1119 (2016) 188-199.
- [82] A. F. Holleman, E. Wiberg, N. Wiberg, in: W. de Gruyter (Ed.), *Lehrbuch der Anorganischen Phyto remediation and biofortification: two sides of one coin, Chemie, Berlin, New York, 2007.*
- [83] S. Shana Parveen, Monirah A. Al-Alshaikh, C.Yohannan Panicker, Ali A. El-Emam, B. Narayana, Vinutha V. Saliyan, B.K. Sarojini, C. Van Alsenoy, *J.Mol.Struct*, 1112 (2016) 136-146.
- [84] Y.S. Mary, K. Raju, I. Yildiz, O. Temiz-Arpaci, H.I.S. Nogueira, C.M. Granadeiro, C. Van Alsenoy, *Spectrochim. Acta A: Mol. Biomol. Spectrosc.*, 96 (2012) 617-625.
- [85] P.S. Binil, Y.S. Mary, H.T. Varghese, C.Y. Panicker, M.R. Anoop, T.K. Manoj kumar, *Spectrochim. Acta A Mol. Biomol. Spectrosc.*, 94 (2012) 101-109.
- [86] K.R. Ambujakshan, H. Tresavarghese, S. Mathew, S. Ganguli, A. Kumar Nanda, C. Yohannan Panicker, *Orien. J. Chem.*, 24 (2008) 865-874.

- [87] L. Ushakumari, C.Y. Panicker, H. Tresavaraghese, Haseena, A. V. Vaidyan, N. Sudhakaran, K. Raju, *Orien. J. Chem.*, 24 (2008) 849-958.
- [88] S. Murugavel, C. Ravikumar, G. Jaabil, Ponnusamy Alagusundaram, *J. Mol. Struct*, 1176 (2019) 729-742.
- [89] Monirah A Al-Alshaikh, Y. Sheema Mary, C. Yohana Panicker, Mohamed I Attia, Ali A.El-emam, *J. Mol. Struct*, 1109 (2016) 130-138.
- [90] R. Minitha, Y. Sheenamary, Hema Tresa Varghese, Yohannan Panickers, Reena Ravindran, K. Raju, V. Manikandan Nair, *J. Mole.struct.*, 985 (2011) 316-322.
- [91] K.S. Resmi, Kabiru Haruna, Y. Sheena Mary, C. Yohannan Panicker, A. Tawfik Saleh, Abdulaziz A. Al-Saadi, Christian Van Alsenoy, *J. Mol. Struct.* 1098 (2015) 130.
- [92] G. Socrates, *Infrared Characteristic Group Frequencies*, Wiley, New York, 1980.
- [93] G. Varsanyi, *Vibrational Spectra of Benzene Derivatives*, Academic Press, New York, 1969.
- [94] P.B. Nagabalarubramanian, M. Karabacak, S. Periandy, *Spectrochim. Acta Part A* 82 (2011) 169–180.
- [95] I. Matulkova, I. Nemecek, K. Teubner, P. Nemecek, Z. Micka, *J Mol Struct*, 873 (2008) 46–60.
- [96] T. Beena, L. Sudha, A. Nataraj, V. Balachandran, D. Kannan, M.N. Ponnuswamy, *Chemistry Central Journal* 201711:6, <https://doi.org/10.1186/s13065-016-0230-8>.

- [97] Y. Sheena Mary, C. Yohannan Panicker, M. Sapnakumari, B. Narayana, B.K. Sarojini, Abdulaziz A. Al-Saadi, C. Van Alsenoy, Javeed Ahmad War, H.K. Fun, *Spectrochimica Acta A:Mol.Biomol. Spectrosc.*, 138 (2015) 529-538.
- [98] Shargina Beegum, Y. Sheena Mary, Hema Tresa Varghese, C. Yohannan Panicker, Stevan Armaković, Sanja J. Armaković, Jan Zitko, Martin Dolezal, C. Van Alsenoy, *J.Mol.Struct* , 1131 (2017) 1-15.
- [99] S. Sakthivel, T. Alagesan, S. Muthu, Christina Susan Abraham, E. Geetha, *J. Mol. Struct*, 1156 (2018) 645-656.
- [100] M. Tamil Elakkiya, S. PremKumar, M. Sathiyendran, P. Suresh, V. Shanmugaiyah, K. Anitha, *J. Mol. Struct*, 1173 (2018) 635-646.
- [101] S. Shana Parveen, Monirah A. Al-Alshaikh, C. Yohannan Panicker, Ali A. El-Emam, B. Narayana, Vinutha V. Saliyan, B.K. Sarojini, C. Van Alsenoy, *J. Mol. Struct*, 1112 (2016) 136-146.
- [102] Usha rani, N. Sundaraganesan, M. Kurt, M. Cinar, M. Karaback, *Spectrochim. Acta A: Mol.Biomol.Spectrosc.*, 75 (2010) 1523-1529.
- [103] K. Jayasheela, Lamyia H. Al-Wahaibi , S. Periandy , Hanan M. Hassan , S. Sebastian ,S. Xavier , Joseph C. Daniel , Ali A. El-Emam , Mohamed I. Attia , *J.Mol.Struct* 1159 (2018) 83-95.
- [104] E.F. Mooney, *Spectrochimica Acta* 20 (2009) 1343–1348.
- [105] A. Viji, V. Balachandran, S. Babiyana, B. Narayana, Vinutha V. Saliyan, *J Mol. Struct.* 1203 (2020) 127452.

- [106] Shaheen Fatma, Abha Bishnoi, Vineeta Singh, Fatmah A.M. Al-Omary, Ali A. El-Emam, Shilendra Pathak, Ruchi Srivastava, Onkar Prasad, Leena Sinha , J.Mol.Struct,1110 (2016) 128-137.
- [107] A. Viji, V. Balachandran, S. Babiyana, B. Narayana, Vinutha V. Saliyan, J Mol. Struct, 1215 (2020) 128244.
- [108] W.C. Harris, L.B. Knight, R.W. McNamee, Durig J R, Versuche zum stickst, Inorg. Chem. 13 (1974) 2297.
- [109] J. Coates, Interpretation of Infrared Spectra of Organic Structures, John Wiley, New York, 2000.
- [110] V.V. Aswathy, Y. Sheena Mary, P.J. Jojo, C. Yohannan Panicker, Anna Bielenica, Stevan Armaković, Sanja J. Armaković, Paulina Brzózka, Sylwester Krukowski, C. Van Alsenoy, J Mol Struct. 2860 (2017) 30016-9.
- [111] R.M. Silverstein, G.C. Bassler, T.C. Morrill, Spectrometric Identification of Organic Compounds, fifth ed., John Wiley and Sons Inc., Singapore, 1991.
- [112] N.B. Colthup, L.H. Daly, S.E. Wiberly, Introduction of Infrared and Raman Spectroscopy, Academic Press, New York, 1975.
- [113] L.J. Bellamy, The Infrared Spectrum of Complex Molecules, third ed., Chapman and Hall, London, 1975.
- [114] Tintu K. Kuruvilla, Johanan Christian Prasana, S. Muthu, Jacob George, J. Mol Struct., 1157 (2018) 519-529.
- [115] A. Therasa Alphonsa, C. Loganathan, S. Athavan Alias Anand, S. Kabilan, J. Mol. Struct., 1106 (2016) 277-285.

- [116] V.K. Rastogi, M.A. Palafox, I. Mittai, N. Perica, W. Kiefer, K. Lang, P. Ohja, J. Raman Spectrosc. 38 (2007) 1227-1241.
- [117] R. Mohamed Asath, S. Premkumar, T. Mathavan, A.Milton Franklin Benial, J.Mol.Struct., 1134 (2017) 143-156.
- [118] K. Fukui, Role of frontier orbitals in chemical reactions, Science 218 (1982) 747-754.
- [119] R.G. Parr, R.G. Pearson, Absolute hardness, companion parameter to absolute electronegativity, J. Am. Chem. Soc. 105 (1983) 7512-7516.
- [120] L. Sinha, O. Prasad, V. Narayan, S.R.Shukla, J. Mol. Simul. 37 (2011) 153-163.
- [121] E.D. Glendening, A.E. Reed, J.E. Carpenter, F. Weinhold, NBO version 3.1, Pittsburg, Theoretical chemistry institute and department of chemistry, University of Wisconsin, Madison, 1988.
- [122] J. Chocholousova, V. Vladimir spirko, P, Phys. Chem. Chem. Phys. 6 (2004) 37-41.
- [123] R.G. Parr, W. Yang, Functional Theory of Atoms and Molecules, Oxford University press, New York, 1989.
- [124] P.W.Ayers, R.G. Parr, Variational principals for describing chemical reactions: The Fukui function and chemical hardness revisted, J. Am. Chem. Soc. 122 (2000) 2010–2018.
- [125] P.K. Chattaraj, B. Maiti, U. Sarkar, Philicity: A unified treatment of chemical reactivity and selectivity, J. Phys. Chem. 107 (2003) 4973–4975.

- [126] E.R. Johnson, S. Keinan, P. Mori-Sanchez, J. Contreras-Garcia, A.J. Cohen, W. Yang, Revealing noncovalent interactions, *J. Am. Chem. Soc.* 132 (2010) 6498-6506.
- [127] Rozas, I. Alkorta, J. Elguero, Behavior of ylides containing N, O, and C atoms as hydrogen bond acceptors, *J. Am. Chem. Soc.* 122 (2000) 11154– 11161
- [128] C. Hansch, P.G. Sammes, J.B. Taylor, *Comprehensive Medicinal Chemistry*, vol.2, Pergomen Press, Oxford, UK, 1990 (chapter 7) 1.
- [129] M.D. McReynolds, J.M. Dougerty, P.R. Hanson, synthesis of phosphorus and sulfur heterocycles via ring-closing metathesis, *Chem. Rev.* 104 (2004) 2239-2258.
- [130] J.R. Lewis, Amaryllidaceae, Sceletium, muscarine, imidazole, oxazole, peptide and other miscellaneous alkaloids, *Nat. Prod. Rep.* 16 (1999) 389-416.
- [131] R.J. Nevagi, Biological and medical significance of 2-Aminothiazoles, *Der.Pharm.Lett.* 6 (2014) 134-150.
- [132] F. Haviv, J.D. Ratajczyk, R.W. DeNet, F.A. Kerdesky, R.L. Walters, S.P. Schmidt, J.H. Holms, P.R. Young, G.W. Carter, *J.Med.Chem.* 31 (1988) 1719-1728.
- [133] K.D. Hargrave, F.K. Hess, J.T. Oliver, *J.Med.Chem.* 26 (1983) 1158-1163.
- [134] M. Grimstrup, F. Zaragoza, *Eur.J.Org.Chem.*(2002) 2953-2960.
- [135] J.C. Jean, L.D. Wise, B.W. Caprathe, H. Tecle, S. Bergmeier, C.C. Humblet, T.G. Heffner, L.T. Meltzner, T.A. Pugsley, *J.Med.Chem.* 33 (1990) 311-317.

- [136] S. Annadurai, R. Martinez, D.J. Canny, T. Eidem, P.M. Dunman, M.A. Gharbia, *Bioorg. Med Chem.Lett.* 22 (2012) 7719-7725.
- [137] K.V. Sashidhara, K.B. Rao, V. Kushwaha, R.K. Modukuri, R. Verma, P.K. Murthy, *Brugia malayi*, *Eur.L.Chem.*81 (2014) 473-480.
- [138] S.E. Kazzouli, S.B. Rabin, A. Mouadbib, G. Guillaumet, Solid support synthesis of 2,4-disubstituted thizoles and aminothiazoles, *Tetrahedron Lett.* 43 (2002) 3193-3196.
- [139] A. A. C. Braga, N.H. Morgon, G. Ujaque, F. Maseras, *J.Am.Chem.Soc.*127 (2005) 9298-9307
- [140] A. A. C. Braga, G. Ujaque, F. Maseras, A DFT study of full catalytic cycle of the Suzuki-Miyaura cross-coupling on a model system, *organometallics* 34 (2006) 3647-3658.
- [141] G.M. Morris, D.S. Goodsell, R.S. Halliday, R. Huey, W.E. Hart, R.K. Belew, A.J. Olson, *J. Comput. Chem.* 19 (1998) 1639-1662.
- [142] S.S. Parveen, M.A. Al-Alshaikh, C.Y. Panicker, A. A. El-Emam, M. Arisoy, O. Temiz Arpacı, C. Van Alsenoy, *J. Mol. Struct.* 1115 (2016) 94-104.
- [143] Y.S. Mary, N.R. El-Brollosy, A.A. El-Emam, O.A. Al-Deeb, P.J. Jojo, C.Y. Panicker, C. Van Alsenoy, *Spectrochim. Acta A Mol. Biomol. Spectrosc.*, 133 (2014) 449-456.
- [144] Tintu K. Kuruvilla, S. Muthu, Johanan Christian Prasana, Jacob George, S. Sevvanthi, *J Mol.Struct.*, 1175 (2019) 163-174.

- [145] Tintu K. Kuruvilla, Johanan Christian Prasana, S. Muthu, Jacob George, *Int. J. Mater. Sci.* 12 (2017) 282-301.
- [146] S. Shana Parveen, Monirah A. Al-Alshaikh, C. Yohannan Panicker, Ali A. El-Emam, Mustafa Arisoy, Ozlem Temiz-Arpaci, C. Van Alsenoy, *J. of Mol. Struct.*, 1115 (2016) 94-104.
- [147] S. George, *Infrared and Raman Characteristic Group Frequencies e Tables and Charts*, third ed., Wiley, Chichester, 2001.
- [148] M. Arirazhagan, J. Senthil Kumar, *Spectrochim. Acta A Mol. Biomol. Spectrosc.*, 82 (2011) 228-234.
- [149] Reza soleymani, Yasin Mohammad salehi, Tahereh yousofzad, Maryam karimicheshmehali, *Oriental journal of chemistry* 28 (2012) 627-638.
- [150] A. Sarau Devi, V.V. Aswathy, Y. Sheena Mary, C. Yohannan Panicker, Stevan Armaković, Sanja J. Armaković, Reena Ravindran, C. Van Alsenoy, *J. Mol. Struct.*, 1148 (2017) 282-292.
- [151] Renjith Raveendran Pillai, Vidya V. Menon, Y. Shyma Mary, Stevan Armakovi, Sanja J. Armakovi, C. Yohannan Panicker, *J. of Mol. Struct.*, 1130 (2017) 208-222.
- [152] N.P.G. Roeges, *A guide to the complete interpretation to IR spectra of organic compounds*, Wiley, New York, 1994.
- [153] B. Smith, *Infrared Spectral Interpretation. A Systematic Approach*, CRC Press, Washington, DC, 1999.

- [154] C. Yohannan Panicker, Hema Tresa Varghes, P.S. Manjula, B.K. Sarojini, B. Narayana, Javeed Ahamad War, S.K. Srivastava, C. Van Alsenoy, Abdulaziz A. Al-Saadi, *Spectrochim. Acta, Mol. Biomol. Spectrosc.*, 151 (2015) 198-207.
- [155] N.B. Colthup, L.H. Daly, S.E. Wilberly, *Introduction to IR and Raman spectroscopy*, Academic press, NewYork 1990.
- [156] M. Barthes, G. De Nunzio, G. Ribet, *Polarons or proton transfer in chains of peptide*, *Synth. Met.* 76 (1996) 337-340.
- [157] Jilu Lukose, C. Yohannan Panicker, Prakash S. Nayak, B. Narayana, B.K. Sarojini, C. Van Alsenoy, Abdulaziz A. Al-Saadi, *Spectrochimica Acta Part A: Mol.Biomol. Spectrosc.*, 135 (2015) 608-616.
- [158] S. Sakthivel, T. Alagesan, S. Muthu, Christina Susan Abraham, E. Geetha, *J. Mol. Struct*, 1156 (2018) 645-656.
- [159] K.B.Benzon, Hema Tresa Varghese, C. Yohannan Panicker, Kiran Pradhan, Bipranch Kumar Tiwary, Ashis Kumar Nanda, C. Van Alsenoy, *Spectrochimica Acta Part A, Mol. Biomol. Spectrosc.*, 146 (2015) 307-322.
- [160] N. Sandhyarani, G. Skanth, S. Berchmanns, V. Yegnaraman, T. Pradeep, *J.Colloid Interface Sci.*209 (1999) 154-161.
- [161] K. Malek, A. Puc, G. Schroeder, V.I. Rybachenko, L.M. Proniewich, *Chem. Phys.* 327 (2006) 439-451.
- [162] J.B. Bhagyasree, J. Samuel, H.T. Varghese, C.Y. Panicker, M. Arisoy, O. Temiz-Arpaci, *Spectrochim. Acta, Mol.Biomol. Spectrosc.*, 115 (2013) 79-91.

- [163] W.C. Harris, L.B. Knight, R.W. McNamee, J.R. Durig, Vibrational spectra and structure of tetramethyltetrazine, *Inorg. Chem.* 13 (1974) 2297-2301.
- [164] L.G. Crane, D. Wang, L.M. Sears, B. Heyns, K. Carron, *Anal. Chem.* 67 (1995) 360-364.
- [165] A.C.S. Bezerra, Eduardo L De Sa, F.C. Nart, *J. Phys. Chem.* 101 (1997) 6443-6449.
- [166] M. El-Behery, H. El-Twigry, *Spectrochim. Acta A: Mol. Biomol. Spectrosc.*, 66 (2007) 28-36.
- [167] N. Sundaraganesan, S. Ayyappan, H. Umamaheswari, B.D. Joshua, *Spectrochim. Acta A: Mol. Biomol. Spectrosc.*, 66 (2007) 17-27.
- [168] J.S. Kwiatkowski, J. Leszczynski, I. Teca, *J. mol.struct.*, 436 (1997) 451-480.
- [169] Adel S. El-Azab, K. Jalaja, Alaa A.-M. Abdel-Aziz, Abdulrahman M. Al-Obaid, Y. Sheena Mary, C. Yohannan Panicker, C. Van Alsenoy, *J.Mol.Struct*, 1119 (2016) 451-461.
- [170] E.F. Mooney, The infra-red spectra of chloro- and bromobenzene derivatives II. nitrobenzenes, *Spectrochim. Acta* 20 (1964) 1021-1032.
- [171] K. Jug, Z.B. Maksic, in: Maksic Z B (Ed.), *Theoretical model of chemical bonding, Part 3*, Springer, Berlin, 1999.
- [172] S. Fliszer, *Charge distributions and chemical effects*, Springer, New York, 1983.
- [173] S. Chidangil, M.K. Shukla, P.C. Mishra, A molecular electrostatic potential mapping study of some Fluroquinolone anti-bacterial agents, *J. Mol. Modeling annual*, (1998) 250-258.

- [174] F.Javier Luque, J.M. Lopez, M. Orozco, Perspective on “Electrostatic interactions of a solute with a continuum. A direct utilization of ab initio molecular potentials for the prevision of solvent effects”, *Theor. Chem. Acc.* 103 (2000) 343-345.
- [175] I. Fleming, *Frontier Orbitals, Organic chemical Reactions*, Wiley, London, 1976.
- [176] A.E. Reed, F.Weinhold, Natural bond orbital analysis of near hartree-fock water dimer, *J. Chem. Phys.* 78 (1983) 4066-4073.
- [177] A. Michalak, F. De Proft, P. Geerlings, R.F. Nalewajski, *J. Phys. Chem.* 103A (1999) 762-771.
- [178] C. Morell, A. Grand, A. Toro-Labbe, New Dual Descriptor for Chemical reactivity *J. Phys. Chem. A* 109 (2005) 205-212.
- [179] Poornima Devi, Shaheen Fatma, Shraddha Shukla, Roop Kumar, Vineeta Singh, Abha Bishnoi, *Synthesis, J. Heliyon* 4 (2018) 01009.
- [180] E. Espinosa, E. Molins, C. Lecomte, Hydrogen bond strengths revealed by topological analyses of experimentally observed electron densities, *Chem. Phys. Lett.* 285 (1998) 170-173.
- [181] L.F. Matta, R.J. Boyd, *An Introduction of the Quantum Theory of Atom in Molecule*, Wiley-VCH Verlag Gmbh, 2007.
- [182] B.K. Sarojini, B.G. Krishna, C.G. Darshanraj, B.R. Bharath, H. Manjunatha. *Eur J Med Chem*, 45 (2010) 3490-3496.
- [183] B.K. Shoichet, S.L. McGovern, B. Wei, J.J. Irwin. Lead discovery using molecular docking, *Curr Opin Chem Bio*, 6(4) (2002) 439–446.
- [184] N.B. Patel, F.M. Shaih, *Sci Pharm* 78 (2010) 753-765.

- [185] L. Swellmeen, 1,3-Oxazole derivatives: a review of biological activities as antipathogenic, *Der pharma chemical*, 8 (2016) 269-286.
- [186] W. Zhang, W. Liu, X. Jiang, F. Jiang, H. Zhuang, L. Fu, *Eur. J med chem.*, 46 (2011) 3639-3650.
- [187] D. Kumar, N.M. Kumar, S. Sundaree, E.O. Johnson, K. Shah, *Eur. J med chem.*, 45 (2010) 1244-1249.
- [188] G.C. Moraski, M. Chang, A. Villegas-Estrada, S.G. Franzblau, M. Möllmann, M.J. Miller, *J med chem.*, 45 (2010) 1703-1716.
- [189] G. Eren, *Bioorg Med Chem.*, 18 (2010) 6367-6376.
- [190] W.T. Ashton, R.M. Sisco, H. Dong, K.A. Lyons, H. He, G.A. Doss, B. Leiting, R.A. Patel, J.K. Wu, F. Marsilio, N.A. Thornberry, A.E. Weber, Dipeptidyl peptidase IV inhibitors derived from β -aminoacylpiperidines bearing a fused thiazole, oxazole, isoxazole, or pyrazole, *Bioorg Med Chem.*, 15 (2005) 2253-2258.
- [191] R.D. Jadhav, K.S. Kadam, S. Kandre, T. Guha, M.M.K. Reddy, M.K. Brahma, N.J. Deshmukh, A. Dixit, L. Doshi, N. Potdar, A.A. Enose, R.A. Vishwakarma, H. Sivaramakrishnan, S. Srinivasan, K.V.S. Nemmani, A. Gupte, A.K. Gangopadhyay, R. Sharma, *Eur J med chem.*, 54 (2012) 324-342.
- [192] K.B. Benzon, Hema Tresa Varghese, C. Yohannan Panicker, Kiran Pradhan, Bipranch Kumar Tiwary, Ashis Kumar Nanda, C. Van Alsenoy, *Spectrochimica Acta Part A, Mol. Biomol. Spectrosc.*, 151 (2015) 965-979.

- [193] A. Lifshitz, C. Tamburu, A. Suslensky, F. Dubnikova, *J. Phys. Chem.* 110 (2006) 4607-4613.
- [194] G. Nadia Haress, A.M. Fatmah Alomary, A. Ali El-Emam, Y. Sheena Mary, C. Yohannan Panicker, A. Abdulaziz Al-Saadi, Javeed Ahmad War, Christian Van Alsenoy, *Spectrochimica Acta Part A, Mol. Biomol. Spectrosc.*, 135 (2015) 973-983.
- [195] H. Arslan, U. Florke, N. Kulcu, G. Binzet, *Spectrochimica Acta Part A, Mol. Biomol. Spectrosc.*, 68 (2007) 1347–1355.
- [196] P. Purkayastha, N. Chattopadhyay, *Phys. Chem. Chem. Phys.* 2 (2000) 203–210.
- [197] G. Varsanyi, *Assignments of Vibrational Spectra of Seven Hundred Benzene Derivatives*, Wiley, New York, 1974.
- [198] R.M. Silverstein, F.X. Webster, *Spectrometric Identification of Organic Compounds*, 6th ed., John Wiley, Asia, 2003.
- [199] R.T. Ulahannan, C.Y. Panicker, H.T. Varghese, C.V. Alsenoy, R. Musiol, J. Jampilek, P.L. Anto, *Spectrochimica Acta Part A, Mol. Biomol. Spectrosc.*, 121 (2014) 445-456.
- [200] H.T. Varghese, C.Y. Panicker, D. Philip, J.R. Mannekutla, S.R. Inamdar, *Spectrochimica Acta Part A, Mol. Biomol. Spectrosc.*, 66 (2007) 959-963.
- [201] G. Seda Sagdinc, Asli Esme, *Spectrochimica Acta Part A*, 75 (2010) 1380-1376.
- [202] S. Veena Kumar, Y. Sheena Mary, Kiran Pradhan, Dhiraj Brahman, Y. Shyma Mary, Renjith Thomas, M.S. Roxy, C. Van Alsenoy, *J. of Mol. Struct.*, 1199 (2020) 127035.

- [203] K. Felfoldi, M. Sutyinszky, N. Nagy, I. Palinko, *Synth. Commun.* 30 (2000) 1543-1553.
- [204] J.B. Bhagyasree, J. Samuel, H.T. Varghese, C.Y. Panicker, M. Arisoy, O. Temiz-Arpaci, *Spectrochimica Acta Part A, Mol. Biomol. Spectrosc.*, 115 (2013) 79-91.
- [205] Y.S. Mary, K. Raju, I. Yildiz, O. Temiz-Arpaci, H.I.S. Nogueira, C.M. Garandeiro, C. Van Alsenov, *J. Mol. Struct.* 1012 (2012) 22-30.
- [206] N. Sandhyarani, G. Skanth, S. Berchmanns, V. Yegnaraman, T. Pradeep, *J. Colloid Interface Sci.* 209 (1999) 154-161.
- [207] S. Suresh Kumar, S. Athimoolam, B. Sridhar, *Spectrochimica Acta Part A, Mol. Biomol. Spectrosc.*, 146 (2015) 204–213.
- [208] R. Mohamed Asath, S. Premkumar, T. Mathavan, A. Milton Franklin Benial, *J. Mol. Struct.* 1134 (2017) 143-156.
- [209] K. Fuji, Role of frontier orbitals in chemical reactions, *Science*, 218 (1982) 747-754.
- [210] D.E. Manolopoulos, J.C. May, S.E. Down, Theoretical studies of the fullerenes: C₃₄ to C₇₀, *Chem. Phys. Lett.* 181 (1991)105 - 111.
- [211] J. Aihara, *J. Phys. Chem. A* 103 (1999) 7487-7495.
- [212] Y. Ruiz - Morales, *J. Phys. Chem. A* 106 (2002) 11283-11308.
- [213] M. Sheikhi, E. Balali, H. Lari, *J. Phys. Theor. Chem.* 13 (2016) 155-171.
- [214] J.R. Cheeseman, G.W. Trucks, T.A. Keith, M.J. Frisch, *J. Chem. Phys.* 104 (1996) 5497-5509.

- [215] P. Nagabalasubramanian, M. Karabacak, S. Periandy, *Spectrochim. Acta A: Mol. Biomol. Spectrosc.* 85 (2012) 43-52.
- [216] E. Temel E, Alas, alvar C, Gokçe H, Güder A, Albayrak Ç, Alpaslan Y B, Alpaslan G, Dilek N, *Spectrochim. Acta A Mol. Biomol. Spectrosc.* 136 (2015) 534-546.
- [217] Shweta, Eram Khan, Poonam Tandon, Rakesh Maurya, Padam Kumar, *J. Mol. Struct.* 1183 (2019) 100-106.
- [218] R.F.W. Bader, *Atoms in Molecules, a Quantum Theory*, Oxford University Press, Oxford,, 1990 ISBN: 0198558651.
- [219] Milosz Ruszkowski, Joanna Sliwiak, Agnieszka Ciesielska, Jakub Barciszewski, Michal Sikorska and Mariusz, Jaskolska., *Acta Cryst.* 70 (2014). 2032–2041.
- [220] B. Kramer, M. Rarey, T. Lengauer, Evaluation of the FLEX incremental construction algorithm for protein–ligand docking, *Proteins Struct. Funct. Genet.* 37 (1999) 228-241.
- [221] W. Yan-mei, I.I Si-dong, Z. Jie-ping, Z. Wei-wang , *Fine Speciality Chem.* 15 (2007) 20-24
- [222] I. Yavri, A.R. Alborzi, B. Mohtat, *Dyes Pigments* 68 (2006) 85-88
- [223] Y. Yan, X. Su, Y. Liyang, J. Zhang, C. Shi, Y. Lu, L. Gu, I. Fu, Emodin azide methyl anthraquinone derivative triggers mitochondrial-dependent cell apoptosis involving in caspase-8-mediated Bid cleavage, *Mol. Cancer Ther.* 7 (2008) 1688-1697.

- [224] A.M. Ali, N.H. Ismail, M.M. Mackeen, L.S. Yazan, S.M. Mohamed, A.S.H. Ho, N.H. Lajis, Antiviral, Cytotoxic And Antimicrobial Activities Of Anthraquinones Isolated From The Roots Of *Morinda Elliptica*, *Pharm. Biol.* 38 (2000) 298-301.
- [225] N.P.D. Nanayakkara, K.K. Schrader, *J. Agric. Food Chem.* 56 (2008) 1002-1007
- [226] H. Gruen, H. Goerner, *Photochem. Photobiol. Sci.* 7 (2008) 1344 - 1352.
- [227] R.C. Francis, S.J. Shin, S. Omori, T.E. Amidon, R.J. Blain, J. Wood, Soda Pulping of Hardwoods Catalyzed by Anthraquinone and Methyl Substitute Anthraquinones, *Chem. Technol.* 26 (2006) 141-152.
- [228] G.V. Aguilar, X.H. Wang, S.F. Nelsen, J.I. Zink, *J. Am. Chem. Soc.* 128 (2006) 6180-6185.
- [229] G. Stewart, Y.G. Jiao, E.J. Valente, P.P. Fu, T.Q. Li, Z.Z. Hu, H.T. Yu, *J. Photoch. Photobio. A* 201 (2009) 39-44.
- [230] J.C.C. Atherton, S. Jones, Establishing cleavage conditions for an anthracene chiral auxiliary using a photochemical retro Diels- Alder reaction, *Tetrahedron Lett.* 43 (2002) 9097-9100.
- [231] Bouas H -Laurent, A. Castellan, J.P. Desvergne, R. Lapouyade, Photodimerization of anthracenes in fluid solution: structural aspects, *Chem.soc.rev.* 29 (2000) 43-55.
- [232] G. Nishimura, Y. Shiraishi, T. Hirai, A fluresent chemosensor for wide-range pH Detection, *Chem.Commun.*, 42 (2005) 5313-5315.
- [233] H. Bouas-Laurent, A. Castellan, J.P. Desvergne, R. Lapouyade, Photodimerization of anthracenes in fluid solutions: (part 2) mechanistic aspects of the

- photocycloaddition and of the photochemical and thermal cleavage Part 1: *Chem. Soc. Rev.* 30 (2001) 248-263.
- [234] X.C. Han, C. Li, M.D. Mosher, K.C. Rider, P.W. Zhou, R.L. Crawford, W. Fusco, A. Paszczyński, N.R. Natale, *Bioorg. Med.Chem.* 170 (2009) 1671-1680.
- [235] A.D. Becke, The quantum theory of atoms in molecules: From solid state to DNA and drug design, *J. Chem. Phys.*, 98 (1993) 5648-5652.
- [236] G.M. Morris, D.S. Goodsell, R.S. Halliday, R. Huey, W.E. Hart, R.K. Belew, A.J. Olson, *J. Comput. Chem.* 19 (1998) 1639-1662.
- [237] J.T. Mague, A. A-M Abdel-Aziz, A. S. El-Azab, M.A. El-Sherbeny, *Acta Cryst. E* 70 (2014) 248-249.
- [238] J.J. Nie, D.J. Xu, *Chin. Struct. J. Chem.* 21 (2002) 165-167. OK
- [239] P. Pavitha, J. Prashanth, G. Ramu, G. Ramesh, K. Mamatha, B. Venkatram Reddy, *J. Mol.Struct.*, 2860 (2017) 30876-1.
- [240] A. Chandran, Y.S. Mary, H.T.Varghese, C.Y. Panicker, P. Pazdera, G. Rajendran, *Spectrochim. Acta A* 79 (2011) 1584-1592.
- [241] Can Alaşalvar, Nuri Öztürk, Alaa A.-M. Abdel-Aziz, HalilGökce, Adel S. El-Azab, Manal A. El-Gendy, Yusuf Sert, *J. Mol.Struct.*, 1171 (2018) 696-705.
- [242] M. Gussoni, C.O. Castiglioni, *J.Mol.Struct.* 521 (2000) 1-18.
- [243] R.M. Silverstein, F.X. Webster, *Spectrometric Identification of Organic Compounds*, 6th ed., John Wiley Asia, 2003.

- [244] Y.S. Mary, P.J. Jojo, C. Van Alsenoy, M. Kaur, M.S. Siddegowda, H.S. Yathirajan, H.I.S. Nogueira, S.M.A.Cruz, *Spectrochim. Acta A: Mol. Biomol. Spectrosc.*, 120 (2014) 340-350.
- [245] S.Y. Lee, B.H. Boo, *Bull. Density functional theory study of vibrational spectra for anthracene neutral and radical Cation*, *Korean Chem. Soc.* 17 (1996) 754-759.
- [246] L.J. Bellamy, *The Infrared Spectra of Complex Molecules*, third ed., John Wiley & Sons, Inc., New York, 433 pages, 1975.
- [247] D. Käfer, G. Witte, P. Cyganik, A. Terfort, C. Wöll, *J. Am. Chem. Soc.* 128 (2006) 1723-1732.
- [248] X. Wang, G. Valverde-Aguilar, M.N. Weaver, S.F. Nelson, J.I. Zink, *J. Phys. Chem. A* 111 (2007) 5441-5447.
- [249] B.H. Stuart, *Infrared Spectroscopy: Fundamentals and Applications*, John Wiley & Sons, England, (2004) 244.
- [250] J.B. Lambert, H.F. Shurvell, R.G. Cooks, *Introduction to Organic Spectroscopy*, Macmillan Publish, New York, USA, 463 pages, 1987.
- [251] H. Gökce, S. Bahçeli, *Spectrochim. Acta Part A: Mol. Biomol. Spectrosc.*, 133 (2014) 741-751.
- [252] M. Durgun, Ü. Ceylan, Ş. P. Yalçın, H. Türkmen, N. Özdemir, I. Koyuncu, *J. Mol. Struct.* 114 (2016) 95-107.
- [253] A.E. Reed, F. wienhold, *J.Chem. Phys.* 83 (1985) 1736.
- [254] A.E. Reed, R.B. wienhold, F. wienhold, *J.Chem. Phys.* 83 (1985) 735.
- [255] J.P. Foster, F. wienhold, *J.Am.Chem. Soc.* 102 (1980) 7211.

- [256] J.O. Jenson, A. Banerjee, C.N. Merrow, D. Zeroka, J.M. Lochner, *J. Chem. Phys.* 68 (1978) 3801-3807.
- [257] H. Buyukuslu H, Akdogan M, Yildirim G, Parlak C, *Spectrochim. Acta Part A* 75 (2010) 1362-1369.
- [258] Parr R G, Szentpaly L V, Liu S, Electrophilicity index, *J. Am. Chem. Soc.* 121 (1999) 1922-1924.
- [259] Scrocco E, Tomasi J, Electronic molecular structure, reactivity and intermolecular forces: An euristic interpretation by means of electrostatic molecular potentials, *Adv. Quantum Chem.*, 11 (1978) 115-193.
- [260] Scrocco E, Tomasi J, The electrostatic molecular potential as a tool for the interpretation of molecular properties, *Curr. Chem.*, 7 (1973) 95-170 ;
- [261] Balachandran V, Lakshmi A, Janaki A, *J. Mol. Struct.* 1013 (2012) 75-85.
- [262] Runge E, Gross E K U, Density-Functional Theory for Time-Dependent Systems, *Phy. Rev. Lett.* 52 (1984) 997-1000.
- [263] F. De proft, J. M. L. Martin, P. Geerlings, Calculation of molecular electrostatic potentials and Fukui functions using density functional methods *Chem. Phys. Lett.* 256 (1996) 400-408.
- [264] E.F. Lee, P.E. Czabotar, B.J. Smith, K. Deshayes, K. Zobel, P.M. Colman, W.D. Fairlie, *Cell Death and Differentiation* 14 (2007) 1711–1719.
- [265] F.A. Tanius, *Biochem.* 31 (1992) 11632-11640.
- [266] S.K. Carter, Psuedourea; National Cancer Chemotherapy Institute, Clinical Brochure No. NSC56054, 2.

- [267] R.F. Pittillo, C. Woolley, *Appl Environ Microbiol.* 18 (1969) 519-521.
- [268] H.C. Becker, B. Norden, *J Am Chem Soc.* 121 (1999) 11947-11952.
- [269] W.D. Wilson, Interaction of unfused tricyclic aromatic cations with DNA: a new class of intercalators. *Biochem.* 28 (1989) 1984-1992.
- [270] B. Lambert, J.B. Lepecq, In *DNA-Ligand Interactions: From Drugs to Proteins*; Plenum Press, New York, USA, 197 (1986) 141-157.
- [271] D. Suh, J.B. Chaires, Criteria for the mode of binding of DNA binding agents, *Bioorg Med Chem.* 3 (1995) 723-728.
- [272] M.S. Tichenor, *J Am Chem Soc.* 129 (2007) 10858-10869.
- [273] R.C. Francis, S.J. Shin, S. Omori, T.E. Amidon, R.J. Skin, Wood, *Sustainable lignin for carbon fibers: Principles, techniques and applications.* *Technol.* 26 (2006) 141-152.
- [274] M.H. Jamroz, *Vibrational Energy Distribution Analysis VEDA 4*, 2004. Warsaw.
- [275] P. Sykes, *A Guide book to mechanism in organic chemistry*, 6th ed., Pearson Education, India, New Delhi, 2004.
- [276] V. Arjunan, A. Raj, S. Subramanian, S. Mohan, *Spectrochim. Acta A*, 110 (2013) 141-150.
- [277] S. Zilberg, Y. Hass, S. Shaik, *J. Phys. Chem.* 99 (1995) 16558–16565.
- [278] C. R. Renjith, Y. Sheena Mary, Hema Tresa Varghese, C. Yohannan Panicker, Thies Thiemann, Anas Shereef, A. Abdulaziz Al-Saadi, *J. Phy. and Chem. of Solids*, 87 (2015) 110-121..

- [279] Y. Sheena Mary, C. Yohannan Panicker, Thies Thiemann, Mariam Al-Azani, Abdulaziz A.Al-Saadi, C. Van Alsenoy, K. Raju, Javeed Ahmad War, S.K. Srivastava, *Spectrochimica Acta Part A: Mol. Biomol. Spectrosc.*, 151 (2015) 350-359.
- [280] Abhishek Kumar, Ambrish Kumar Srivastava, Shashi Gangwar, Neeraj Misra, Avijit Mondal, Goutam Brahmachari, *J. Mol. Struct.*, 1096 (2015) 94-101
- [281] Manu Vatsal, Vandna Devi, Pamita Awasthi, *J. Mol. Struct.*, 1157 (2018) 230-238.
- [282] M. Kurt, E. Babur Sas, M. Can, S. Okur, S. Icli, S. Demic, M. Karabacak, T. Jayavarthanam, N. Sundararganesan, *J.Mol Struct.*, 994 (2011) 179-193.
- [283] G. Vasanyi, *Assignments of vibrational spectra of seven hundred benzene derivatives*, vol.I, Adam Hilger, London, 1974.
- [284] T. Joseph, H.T. Varghese, C.Y. Panicker, T. Thiemann, K. Viswanathan, C.V. Alsenoy, *J. Mol. Struct.* 1005 (2011) 17-24.
- [285] T. Joseph, H.T. Varghese, C.Y. Panicker, T. Thiemann, K. Viswanathan., C.V. Alsenoy, T.K. Manojkumar, *Molecular and Biomolecular Spectroscopy*, *Spectrochim. Acta, A* 117 (2014) 413-421.
- [286] R.S. Mullican, *J. Chem, phys.*23 (1995) 1833-1840.
- [287] S. Gunasekaran, R.A. Balaji, S. Kumaresan, G. Anand, S. Srinivasan, *Can. J. Anal. Sci. spectrosc.*, 53 (2008) 149-160.

- [288] E.D. Glendening, A.E. Reed, J.E. Carpenter, F. Weinhold, NBO version 3.1, Pittsburg, Theoretical chemistry institute and department of chemistry, University of Wisconsin, Madison, 1988.
- [289] P. Politzer, J.S. Murray, D.L. Beveridge, R. Lavery, Theoretical Biochemistry and Molecular Biophysics, A comprehensive Survey, protein, Vol. 2, Adenine Press, Schenectady, New York, 1991.
- [290] J.S. Murray, K. Sen, Molecular electrostatic potentials, concepts and Applications, Elsevier, Amsterdam, 1996.
- [291] R.G. Parr, W. Yang, J. Am. Chem. Soc. 106 (1984) 4049-4050.
- [292] C. Morell, A. Grand, A. Toro-Labbe, J. Phys. Chem. A 109 (2005) 205-212.
- [293] G.M. Morris, D.S. Goodsell, R.S. Halliday, R. Huey, W.E. Hart, R.K. Belew, A.J. Olson, J. Comput. Chem. 19 (1998) 1639-1662.

Reprints



Scopus Preview

Author search Sources



Create account

Sign in

Sources

Title

Find sources

Title: [Journal Of Molecular Structure](#) x [Journal Of Information And Computational Science](#) x

Filter refine list

Apply

Clear filters

2 results

Download Scopus Source List [Learn more about Scopus Source List](#)

Page

Export to Excel

Save to source list

View metrics for year:

2019

Display options

Display only Open Access journals

Counts for 4-year timeframe

No minimum selected

Source title

CiteScore

Highest percentile

Citations 2016-19

Documents 2016-19

% Cited

1

Journal of Molecular Structure

4.0

64%

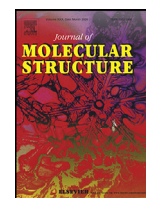
25/69

20,154

5,076

77

Inorganic Chemistry



FT-IR and FT-Raman investigation, quantum chemical analysis and molecular docking studies of 5-(4-Propan-2-yl)benzylidene)-2-[3-(4-chlorophenyl)-5[4-(propan-2-yl)phenyl-4,5-dihydro-1H-pyrazol-1-yl]-1,3-thiazol-4(5H)-one

K. Venil^a, A. Lakshmi^{a,*}, V. Balachandran^b, B. Narayana^c, Vinutha V. Salian^c

^a Department of Physics, Government Arts College (Affiliated to Bharathidasan University) Tiruchirappalli 621 222, India

^b Centre for Research, Department of Physics, Arignar Anna Government Arts College (Affiliated to Bharathidasan University), Musiri, Tiruchirappalli 621 211, India

^c Department of Studies in Chemistry, Mangalore University, Mangalagangothri 574 199, India

ARTICLE INFO

Article history:

Received 17 June 2020

Revised 10 August 2020

Accepted 11 August 2020

Available online 12 August 2020

Keywords:

Thiazole

Fukui function

RDG

Molecular docking

ABSTRACT

The FT-IR and FT-Raman spectra of 5-(4-Propan-2-yl)benzylidene)-2-[3-(4-chlorophenyl)-5[4-(propan-2-yl)phenyl-4,5-dihydro-1H-pyrazol-1-yl]-1,3-thiazol-4(5H)-one were recorded and analyzed. The fundamental vibrational wavenumbers, intensities of vibrational bands and the optimized geometrical parameters of the compound were evaluated using DFT (B3LYP) method with 6-31 G, 6-31G(d,p) basis sets. Stability of the molecule arising from hyper conjugative interactions, charge delocalization has been analysed using natural bond orbital (NBO) analysis. Information about the size, shape, charge density distribution and site of chemical reactivity of the molecule has been obtained by mapping electron density isosurface with molecular electrostatic potential (MEP) surface. The calculated HOMO-LUMO energies also show that the charge transfer occurs within the molecule. The global reactivity parameters which are obtained by frontier molecular orbital disclose that the molecule might be bioactive. To explain the chemical selectivity or the reactivity site in the molecule, the electron density-based local reactivity descriptors such as Fukui functions were calculated. The reduced density gradient of the title molecule was investigated by the interaction of the molecule. Molecular docking studies were also described. This study may also provide a further investigation of thiazole derivatives for pharmacological importance.

© 2020 Elsevier B.V. All rights reserved.

1. Introduction

Thiazole is used in the manufacturing of synthetic drugs, fungicides and dyes. The derivatives of thiazole like phenylthiazolyl, isothiazole are found to have a potent local anaesthetic, anti-inflammatory, analgesic and antipyretic activities [1-3]. Similarly, aminothiazoles are used to treat bacterial infections, inflammations, tumours [4-7] and play a vital role in insulin release [8-10]. Thiazole appears commonly in structures of various natural products and biologically active compounds, like thiamine (vitamin-B) and antibiotic drugs such as penicillin, micrococin which have revolutionized the therapy of bacterial diseases [11]. Phenyl and substituted phenyl-thiazoles are also common structures of a wide range of biologically active natural products [12]. Recently it has been found that phenyl-thiazole ring system provides a tem-

plate for the design and synthesis of antiviral agents which inhibit the flaviviruses by targeting their E-protein [13]. Dyes are also prepared by employing thiazoles, especially isothiazole orange, containing thiazole moiety in the form of benzothiazole which has the binding capability with nucleic acids and other uses in biosensors and imaging [14-16]. Thiazoles used in material science due to its applications in liquid crystals, sensors and molecular switches. As far as the pharmacological applications of 1,3-thiazoles are concerned, these scaffolds are antiviral [17], antifungal, antibacterial [18], anticancer [19], antitubercular [20] and anti-inflammatory [21]. Thiazoles are compounds which are used as antihyperglycemic compounds [22]. For this property, they have many applications in pharmacy and medicine industries [23].

In the present work, the vibrational spectral investigations of the title compound aided by density functional computations were described to elucidate the correlation between the molecular structure and biological activity, bonding features, electron delocalization and the intramolecular charge transfer interactions. The ener-

* Corresponding author.

E-mail address: laksharumugam13@gmail.com (A. Lakshmi).

gies, degrees of hybridization, population of the lone pairs of oxygen, energies of their interaction with the antibonding orbital of the rings and the electron density distributions and E(2) energies have been calculated by Natural Bond Orbital (NBO) analysis using Density Functional Theory (DFT) method to predict clear evidence of stabilization originating from the hyper-conjugation of various intra-molecular interactions. Reduced density gradient (RDG) analyses were carried out to investigate H-bond, steric effect and Van der Waals interaction are presented in the molecule. To evaluate the biological potential of the title compound molecular docking studies are reported here.

2. Experimental details

5-(4-Propan-2-yl)benzylidene)-2-[3-(4-chlorophenyl)-5[4-(propan-2-yl)phenyl-4,5-dihydro-1H-pyrazol-1-yl]-1,3-thiazol-4(5H)-one was synthesized as per the reported procedure [24–26]. The Fourier transform infrared spectrum of the title compound was recorded at room temperature within the interval at 4000–450 cm^{-1} in a resolution of $\pm 1 \text{ cm}^{-1}$ using an MCT detector with Perkin Elmer FT-IR spectrometer equipped for the Mid-IR range, and KBr pellets were utilized in the spectral measurements. The FT-Raman spectrum of the title compound was recorded on a BRUKER RFS-66 V model equipped with FRA-106 FT-Raman accessories within the interval at 4000–0 cm^{-1} using the 1064 nm line of an Nd: YAG laser device for excitation operated at 200 mW power.

3. Computational details

All calculations presented in this study were performed by using Gaussian 09 software [27] and Gauss view [28]. Several studies have been carried out regarding the calculations of vibrational spectra using B3LYP methods with the basis set 6–31 G and 6–31 G (d,p). RDG was calculated with the use of Multiwfn program [29] and plotted by visual molecule dynamics program (VMD) [30]. The reactivity descriptors, such as electrophilicity (ω), global hardness (η), the chemical potential (μ), ionization potential (I) and electron affinity (A) were determined from the energies of the frontier molecular orbital. The NBO and Mulliken population analysis is also reported for the local minima of the molecules. Molecular docking studies were made on Autodock 4.2 software [31] and the result of docking was analyzed using Pymol [32] and Discovery studio [33] visualization software.

4. Results and discussions

4.1. Optimized molecular geometrical parameters

The optimized molecular structure and the geometrical parameters of the title compound are shown in Fig. 1 and Table S1 (Supplementary material), respectively, by using the B3LYP method with 6–31 G, 6–31G(d,p) basis sets. The title compound contains 32 C–C bonds, 30 C–H bonds, 5 C–N bonds, 2 C–S bonds and single N–N, C–O and C–Cl bonds.

The DFT calculated bond length of the C–C bond of the benzene rings are found at 1.419–1.388 Å [34]. For our title compound, the C–C bond length for phenyl ring are C4–C5 = 1.4082/1.4042 Å, C4–C6 = 1.4121/1.4082 Å, C5–C7 = 1.3979/1.3933 Å, C6–C9 = 1.3932/1.3882 Å, C7–C11 = 1.392/1.393 Å, C9–C11 = 1.3963/1.3979 Å for the above basis sets which was very close to experimental value [34]. The bond lengths of thiazole ring for the title compound are C42=N43 = 1.30/1.30 Å, C40–N43 = 1.41/1.40 Å respectively. These C–N bond lengths were found to be shorter than the average value for a C–N single bond 1.47 Å,

but longer than a C = N double bond 1.22 Å [35], suggesting that some multiple bond character is presented. The bond lengths of both the phenyl rings and regular hexagon falls between the normal values for a single (1.54 Å) and a double (1.33 Å) bond [36]. For the title compound, bond lengths are C5–H8 = 1.0844/1.0851 Å, C6–H10 = 1.0835/1.0843 Å, C7–H12 = 1.0829/1.084 Å, C9–H13 = 1.0829/1.0841 Å. The reported values for C–S bond length are in the range 1.7675–1.8641 Å [37]. For the title compound, the C–S bond length for C39–S41 = 1.86/1.79 Å, C42–S41 = 1.84/1.78 Å, which are in agreement with literature [38]. C40–C39–S41 = 108.92/108.73°, S41–C39–C45 = 118.14/118.67°, N25–C42–N43 = 122.95/122.14° which shows the interaction between the C = S and the neighbouring groups. Similarly at C40 position of the thiazole ring, the angles C39–C40–O44 is increased by 4.72/4.83° and the angle N43–C40–C39 is reduced by 6.54/7.30° from 120° which shows the interaction between the neighbouring atoms. From Table S1 (Supplementary material), comparative analysis of the parameters such as bond length and bond angles was observed using DFT are in good agreement with each other.

4.2. Vibrational assignments

The title compound is constituted by 67 atoms and hence has 195 normal modes of vibration. The observed and calculated wavenumbers and potential energy distributions are discussed below. The fundamental modes of vibration were carried out and are depicted in Table S2 (Supplementary material). The comparison between theoretical and experimental FT-IR and FT-Raman spectra are given in Figs. 2 and 3, respectively.

4.2.1. C–H vibrations

C–H stretching vibrations usually observed in a heteroaromatic compound in the frequency range 3200–2850 cm^{-1} [39,40]. The in-plane bending vibrations appear in the range of 1300–1000 cm^{-1} [41] and the out-of-plane bending occurs in the region 1000–750 cm^{-1} [41]. Murugavel et al. [42] reported that the C–H stretching vibrations at 2993, 3024 and 3061 cm^{-1} in FT-IR and calculated at 2944, 3022 and 3065 cm^{-1} . Al-Alshaiikh et al. [43] observed the C–H stretching vibrations at 3079, 3042 cm^{-1} theoretically and experimentally at 3060 cm^{-1} in FT-IR and 3068 cm^{-1} in FT-Raman spectrum. Minitha et al. [44] reported the C–H stretching vibrations at 3195, 3157, 3106 3057 cm^{-1} in the FT-IR and at 3153, 3100, 3047 cm^{-1} in the FT-Raman spectrum. For the title compound, the C–H stretching vibrations observed experimentally at 2870 cm^{-1} in FT-IR, 3102 cm^{-1} in FT-Raman and theoretically at 3135, 3129, 3120, 3104, 3095, 3074, 3056, 2986, 2873 cm^{-1} by B3LYP/6–31 G and 3133, 3125, 3117 3100, 3093, 3070, 3055, 2986, 2871 cm^{-1} by B3LYP/6–31 G (d,p) methods. Murugavel et al. [42] reported that the in-plane bending vibration occurs at 1028 and 1282 cm^{-1} . Resmi et al. [45] reported that the in-plane C–H bands are assigned at 1262, 1140, 1116, 1029 cm^{-1} and at 1250, 1103 cm^{-1} in FT-IR, 1250, 1136, 1105 cm^{-1} in FT-Raman, 1249, 1139, 1101, 1028 cm^{-1} by theoretically. Al-Alshaiikh et al. [43] observed the in-plane bending at 1063, 1013 cm^{-1} in IR and 1285, 1161, 1139, 1066 cm^{-1} in the Raman spectrum. Minitha et al. [44] reported the C–H in-plane bending vibration occurs at 1514, 1425, 1287 cm^{-1} in IR spectrum, 1569, 1501, 1417, 1284 cm^{-1} in Raman spectrum and 1586, 1573, 1497, 1418, 1281 cm^{-1} observed by theoretically. In the present study, 1267, 1248 cm^{-1} and 1462, 1390, 1300, 1250 cm^{-1} are assigned to C–H in-plane bending mode at FT-IR and FT-Raman spectrum, respectively and 1473, 1466, 1456, 1391, 1360, 1329, 1304, 1294, 1256, 1235 cm^{-1} by B3LYP/6–31 G and 1473, 1463, 1450, 1388, 1355, 1325, 1301, 1290, 1249, 1231 cm^{-1} theoretically by B3LYP/6–31G(d,p) basis sets. C–H out-of-plane bending vibrations are observed at 756, 826, 899 and 984 cm^{-1} by Murugavel

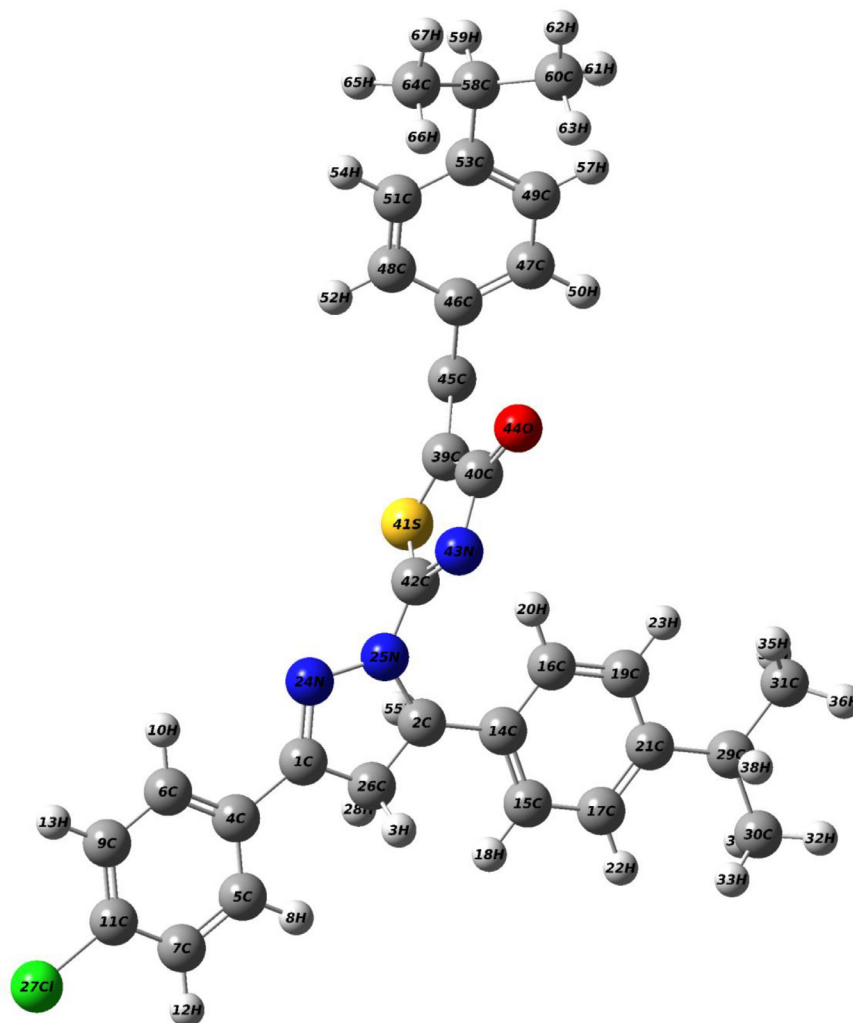


Fig. 1. Optimized molecular structure of 5-(4-Propan-2-yl)benzylidene)-2-[3-(4-chlorophenyl)-5[4-(propan-2-yl)phenyl-4,5-dihydro-1H-pyrazol-1-yl]-1,3-thiazol-4(5H)-one.

et al. [42]. Resmi et al. [45] reported that the out-of-plane C–H deformations are assigned at 938, 904, 745 cm^{-1} in FT-IR and 731 cm^{-1} in FT-Raman spectrum. Al-Alshaikh et al. [43] observed the out-of-plane bending vibrations are assigned at 907, 825 cm^{-1} in the IR spectrum and 905, 827 cm^{-1} in the Raman spectrum. Minitha et al. [44] reported the C–H out-of-plane bending vibration assigned at 964, 936, 881, 749 cm^{-1} in the IR spectrum, 989, 942, 744 cm^{-1} in Raman spectrum and 993, 931, 890, 731 cm^{-1} obtained by theoretically. For the title compound, the C–H out-of-plane bending vibrations occur at 908, 827 cm^{-1} in FT-IR and 910, 895, 810, 790 cm^{-1} in FT-Raman spectrum and 955, 928, 912, 906, 880, 856, 835, 816, 804 cm^{-1} by B3LYP/6-31 G, 953, 924, 909, 875, 850, 830, 812, 800 cm^{-1} theoretically observed by B3LYP/6-31 G (d,p) basis sets.

4.2.2. CH_3 vibrations

In general, the methyl group C–H stretching vibrations occur in the region 2975–3840 cm^{-1} [46,47]. Normally, CH_3 group deformations are found in between 1450 and 1400 cm^{-1} [48]. For the present study, the asymmetric stretching vibration occurs at 3023, and 2959 in FT-IR spectrum, 3040 in FT-Raman spectrum and computed values are 3053, 3045, 3031, 3016, 3003, 2996, 2975, 2964, 2930, 2910, 2904, 2896 cm^{-1} by B3LYP/6-31 G and 3049, 3041, 3032, 3025, 3012, 2999, 2991, 2972, 2960, 2928, 2906, 2900, 2891 cm^{-1} by B3LYP/6-31 G (d,p). The symmetric stretching modes calculated for the title molecule at 2945, 2930, 2910, 2904, 2896 cm^{-1} by B3LYP/6-31 G and 2941, 2928, 2906, 2900,

2891 cm^{-1} by B3LYP/6-31 G (d,p) and 2904 cm^{-1} observed in FT-Raman spectrum. In this study, the CH_3 in-plane bending vibrations are assigned at 1416 cm^{-1} in FT-IR spectrum. The computed wavenumbers are predicted by $\delta_{\text{ipb}} = 1419, 1412, 1406, 1402$ cm^{-1} , $\delta_{\text{opb}} = 1445, 1440, 1435, 1426$ cm^{-1} , $\delta_{\text{sb}} = 1365, 1366$ cm^{-1} , $\delta_{\text{ipr}} = 874, 866, 851, 849$ cm^{-1} by B3LYP/6-31 G and $\delta_{\text{ipb}} = 1415, 1409, 1404, 1399$ cm^{-1} , $\delta_{\text{opb}} = 1441, 1438, 1430, 1422$ cm^{-1} , $\delta_{\text{sb}} = 1363, 1360$ cm^{-1} , $\delta_{\text{ipr}} = 869, 861, 848, 845$ cm^{-1} by B3LYP/6-31 G (d,p) methods. In this present work, the CH_3 out-of-plane bending vibrations are assigned at 1010 cm^{-1} in FTIR spectrum. The theoretically predicted values by B3LYP/6-31 G $\gamma_{\text{opr}} = 1041, 1026, 1014, 1004$ cm^{-1} by B3LYP/6-31 G and 1038, 1024, 1010, 999 cm^{-1} by B3LYP/6-31 G (d,p) methods.

4.2.3. CH_2 vibrations

The CH_2 symmetric stretching vibrations are generally noticed in the vicinity of 2900–2800 cm^{-1} and asymmetric stretch will appear at 3000–2800 cm^{-1} [49,50]. Mary et al. [51] reported the stretching modes of CH_2 are assigned at 2971, 2925 cm^{-1} by theoretically and at 2974, 2921 cm^{-1} in the IR spectrum and the deformation modes of the CH_2 group are assigned at 1430, 1197, 1132 cm^{-1} theoretically and at 1434, 1191 cm^{-1} in the IR spectrum. Beegum et al. [52] reported that the CH_2 stretching vibrations are assigned at 2926, 1465, 1340 cm^{-1} in the IR spectrum, 2958, 2930, 1335 cm^{-1} in the Raman spectrum and 2956, 2922, 1467, 1338,

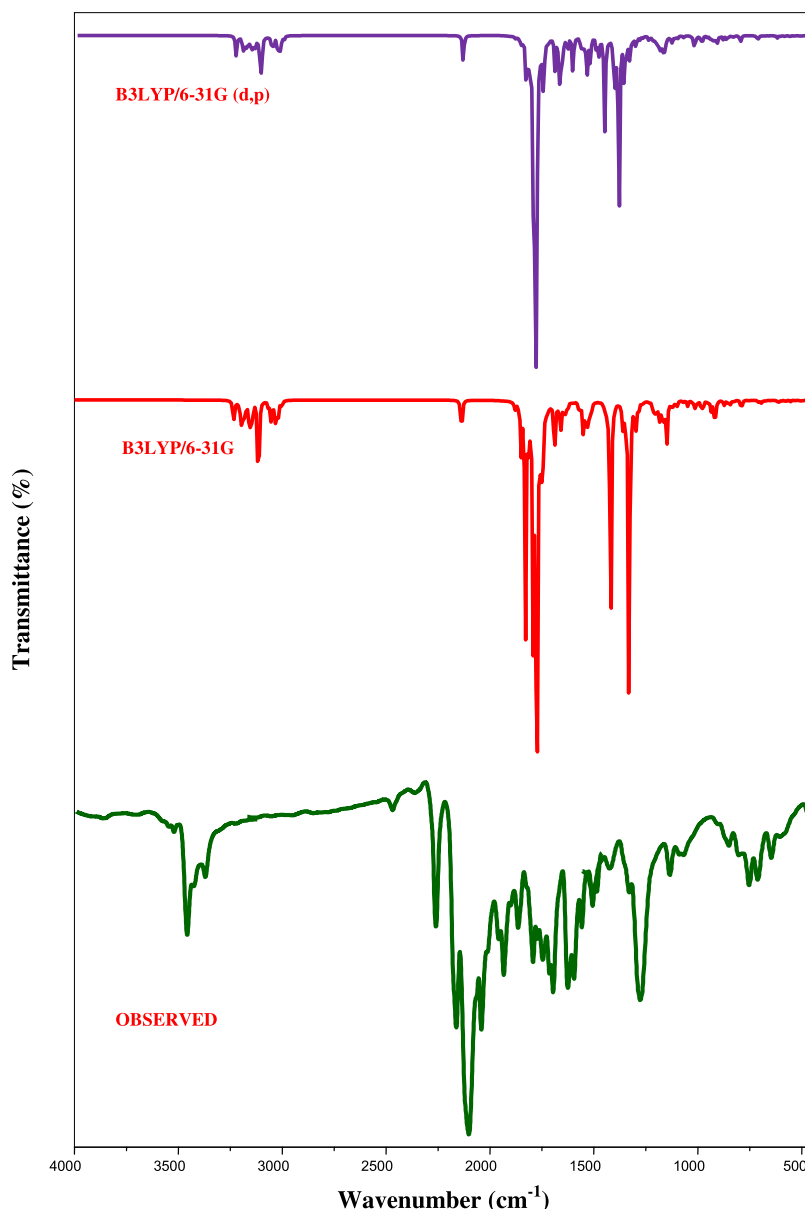


Fig. 2. Observed FT-IR and simulated spectra of 5-(4-Propan-2-yl)benzylidene)-2-[3-(4-chlorophenyl)-5[4-(propan-2-yl)phenyl]-4,5-dihydro-1H-pyrazol-1-yl]-1,3-thiazol-4(5H)-one.

1203, 947 cm^{-1} theoretically obtained. Al-Alshaiikh et al. [43] assigned the CH_2 stretching modes at 2965, 2921 cm^{-1} in the FT-IR spectrum, 2999, 2965, 2944, 2918 cm^{-1} in FT-Raman spectrum and the deformation modes of the CH_2 groups are assigned at 1444, 1415, 1366, 1294, 1269, 1252 cm^{-1} in the FT-IR spectrum, 1444, 1415, 1370, 1351, 1270 cm^{-1} in FT-Raman spectrum and at 1441, 1418 cm^{-1} for scissoring, 1362, 1355 cm^{-1} for wagging, 1296, 1267 cm^{-1} for twisting, 1254, 1132 cm^{-1} for rocking modes. For the title compound, the CH_2 stretching modes are observed at $\nu_{\text{ass}} = 3036 \text{ cm}^{-1}$, $\nu_{\text{ss}} = 2945 \text{ cm}^{-1}$, $\sigma_{\text{sci}} = 1398 \text{ cm}^{-1}$, $\rho_{\text{rock}} = 1206 \text{ cm}^{-1}$, $\tau = 1095 \text{ cm}^{-1}$, $\delta_{\text{wagg.}} = 935 \text{ cm}^{-1}$ by B3LYP/6-31 G, $\nu_{\text{ass}} = 3032 \text{ cm}^{-1}$, $\nu_{\text{ss}} = 2941 \text{ cm}^{-1}$, $\sigma_{\text{sci}} = 1395 \text{ cm}^{-1}$, $\rho_{\text{rock}} = 1203 \text{ cm}^{-1}$, $\tau = 1091 \text{ cm}^{-1}$, $\delta_{\text{wagg.}} = 931 \text{ cm}^{-1}$ by B3LYP/6-31 G (d,p) methods respectively.

4.2.4. C-O vibrations

The stretching mode of C-O is expected in the range of 1850–1550 cm^{-1} [53]. The in-plane and out-of-plane bending modes of C-O were reported in the ranges $725 \pm 95 \text{ cm}^{-1}$ and $595 \pm 120 \text{ cm}^{-1}$

[53]. The calculated C-O stretching vibrational modes was obtained theoretically at 1788 cm^{-1} , 1782 cm^{-1} and 1694 cm^{-1} at FT-IR and 1689 cm^{-1} in FT-Raman by Ellakiya et al. [54]. Parveen et al. [55] observed the bands at 1657 cm^{-1} in the IR spectrum, 1662 cm^{-1} in the Raman spectrum and the in-plane and out-of-plane bending modes of C-O are assigned at 606, 569 cm^{-1} theoretically. In the present work, C-O stretching vibrations observed at 1689 cm^{-1} , in-plane bending at 944 cm^{-1} and out-of-plane bending at 753 cm^{-1} in FT-IR spectrum and observed theoretically at $\nu = 1896$, $\delta = 948$, $\gamma = 755$, 748 cm^{-1} by B3LYP/6-31 G, $\nu = 1890$, $\delta = 945$, $\gamma = 751$, 745 cm^{-1} by B3LYP/6-31 G (d,p) basis sets.

4.2.5. C-Cl vibrations

The vibration between halogen atom attached to aromatic carbon is recognized around wave numbers 1285–485 cm^{-1} [56]. Generally, C-Cl absorption found in the vicinity 750–700 cm^{-1} [57] and C-Cl deformation bending around 460–175 cm^{-1} [58].

For Beegam et al. [52], the C-Cl stretching mode is observed at 673 cm^{-1} in the Raman spectrum and theoretically at 671

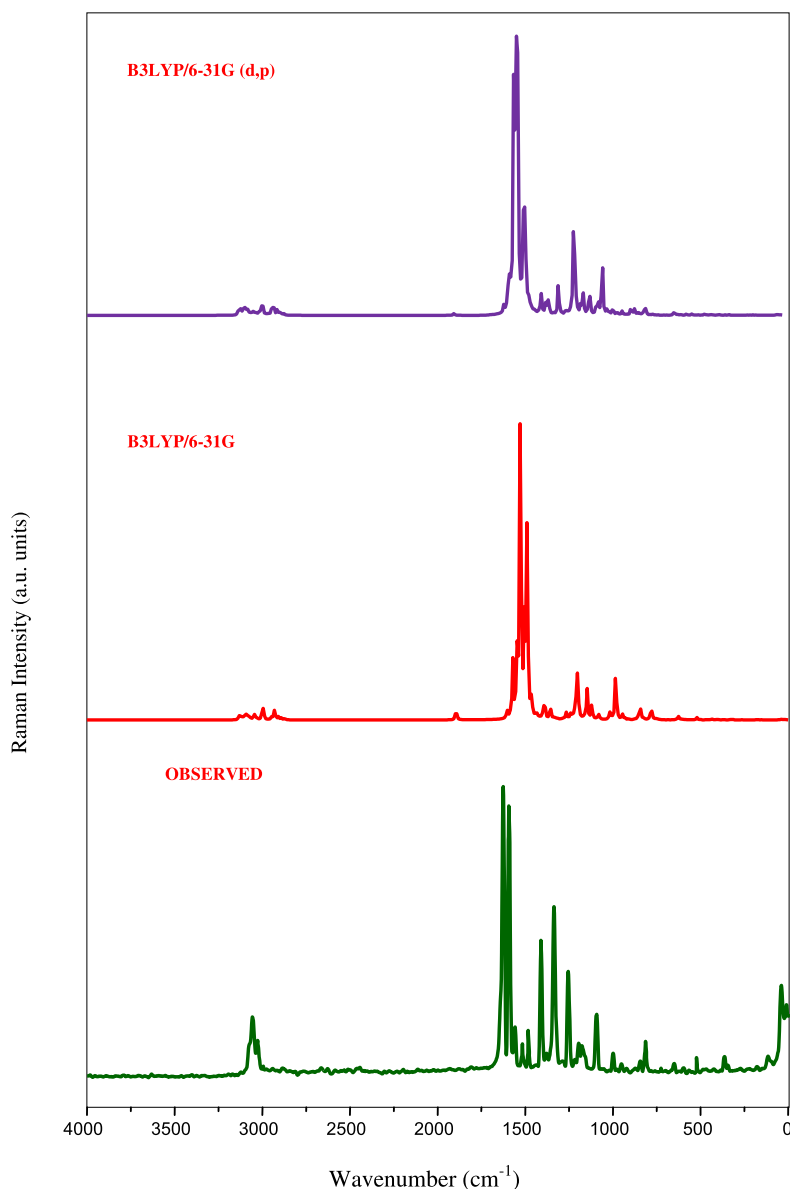


Fig. 3. Observed FT-Raman and simulated spectra of 5-(4-Propan-2-yl)benzylidene)-2-[3-(4-chlorophenyl)-5[4-(propan-2-yl)phenyl-4,5-dihydro-1H-pyrazol-1-yl]-1,3-thiazol-4(5H)-one.

cm^{-1} . Viji et al. [59] observed the C–Cl stretching vibrations experimentally at 414 cm^{-1} and calculated at $\nu=416, 415 \text{ cm}^{-1}$ observed theoretically. Sebastian et al. [34] observed this mode at 764 cm^{-1} in the IR spectrum and 760 cm^{-1} theoretically. For the C–Cl stretching mode, Resmi et al. [45] are assigned at $876, 644, 581 \text{ cm}^{-1}$ in Raman spectrum and $877, 646, 588 \text{ cm}^{-1}$ theoretically. For the title compound, the C–Cl stretching mode is observed theoretically at $\nu=690 \text{ cm}^{-1}$, $\delta=453 \text{ cm}^{-1}$, $\gamma=266, 160, 93 \text{ cm}^{-1}$ by B3LYP/6-31 G and at $\nu=685 \text{ cm}^{-1}$, $\delta=449 \text{ cm}^{-1}$, $\gamma=262, 155, 88 \text{ cm}^{-1}$ by B3LYP/6-31 G (d,p).

4.2.6. C–C vibrations

The C–C stretching vibrations usually occur at $1625\text{--}1465 \text{ cm}^{-1}$ [60]. Murugavel et al. [42] reported that the wavenumbers $1613, 1553, 1302, 1207, 1082$ and 1036 cm^{-1} are recognized as C–C stretching modes. Resmi et al. [45] reported that the C–C stretching vibrations are observed at $1570, 1545, 1284 \text{ cm}^{-1}$ in the IR spectrum and at 1571 cm^{-1} in the Raman spectrum and theoretically observed at $1278, 1264$ and 1571 cm^{-1} . For the title compound, the band observed in FT-IR spectrum at $1600, 1545, 1225, 1196, 1181,$

$1117, 1011 \text{ cm}^{-1}$ and FT-Raman spectrum at $1600, 1545, 1501, 1210, 1160, 1110 \text{ cm}^{-1}$. The computed values at $1601, 1584, 1573, 1549, 1525, 1507, 1234, 1223, 1201, 1192, 1124, 1104 \text{ cm}^{-1}$ by B3LYP/6-31 G and $1603, 1581, 1569, 1545, 1519, 1504, 1227, 1222, 1195, 1147, 1119, 1100 \text{ cm}^{-1}$ by B3LYP/6-31 G (d,p). Murugavel et al. [42] reported that and C–C in-plane deformation was found at $429, 514, 580, 627, 652 \text{ cm}^{-1}$ which is in accord with the experimental data at $428, 442, 459, 476, 515, 552, 575$ and 627 cm^{-1} . For the title compound, the C–C in-plane bending occurs at 409 cm^{-1} in FT-IR spectrum, $835, 640, 410 \text{ cm}^{-1}$ in FT-Raman spectrum and the computed values are $840, 836, 668, 644, 439, 424, 414, 396 \text{ cm}^{-1}$ by B3LYP/6-31 G and $837, 833, 666, 640, 438, 421, 410, 390 \text{ cm}^{-1}$ by B3LYP/6-31 G (d,p) methods.

4.2.7. Ring vibration

The thiazole and phenyl ring in-plane bending vibrations are theoretically calculated at $520, 469, 437, 426, 418, 402, 354, 317, 304 \text{ cm}^{-1}$ in B3LYP/6-31 G (d,p) and $515, 463, 433, 421, 415, 399, 352, 312, 302 \text{ cm}^{-1}$ in B3LYP/6-31 G observed by Viji et al. [61]. In the present work, the in-plane bending vibrations of thia-

zole ring are theoretically observed at 780, 767, 630, 621, 610, 605, 525, 515, 503, 490, 470, 376, 370, 335, 320, 83, 71, 60, 52, 45, 41, 36 cm^{-1} in B3LYP/6-31 G, 777, 763, 625, 616, 607, 602, 523, 512, 500, 487, 468, 374, 368, 333, 318, 80, 68, 57, 49, 40, 38, 32 cm^{-1} in by B3LYP/6-31 G (d,p) methods. The observed values at 608, 501 cm^{-1} in FT-IR spectrum and 600, 510, 375, 42 cm^{-1} in FT-Raman spectrum. The out-of-plane bending vibrations observed at 720, 556 cm^{-1} in FT-IR spectrum, 28 cm^{-1} in FT-Raman spectrum and computed values are 736, 725, 584, 560 551, 405 399, 385, 364, 306, 182, 173, 145 cm^{-1} in B3LYP/6-31 G, 732, 720, 581, 555, 544, 400, 394, 382, 361, 304, 179, 171, 142 cm^{-1} in by B3LYP/6-31 G (d,p) methods.

4.2.8. N-N vibrations

N-N stretching mode occurs at 1417–1372 cm^{-1} [62]. The N-N stretching mode is reported at 1120 cm^{-1} in the IR spectrum and 1130 cm^{-1} theoretically assigned by Parveen et al. [55]. In the present work, 981, 980 cm^{-1} observed by FT-IR and FT-Raman spectrum and 986, 982 cm^{-1} obtained by theoretically by B3LYP/6-31 G, 6-31 G (d,p) methods.

4.2.9. C-S vibrations

This vibration cannot be identified easily as it results in weak infrared bands, which is susceptible to coupling effects and is also of variable intensity. In general, the C-S stretching vibration was reported in 750–600 cm^{-1} [63]. In the present work, the C-S stretching vibration assigned at 854 cm^{-1} in the IR spectrum, 860, 786 cm^{-1} and 854, 785 cm^{-1} obtained theoretically by B3LYP/6-31 G, 6-31 G (d,p) methods. Aswathy et al. [64] observed the band at 728 cm^{-1} in the IR spectrum, 729 cm^{-1} in the Raman spectrum and 728 cm^{-1} theoretically is assigned as the C-S stretching mode.

4.2.10. C-N vibrations

According to literature, the C-N stretching modes are expected in the region 1100–1300 cm^{-1} [65–67]. Murugavel et al. [42] reported that the C-N stretching peaks appeared at 1188, 1222, 1229, 1440 and 1503 cm^{-1} . Kuruvilla et al. [68] observed the C-N stretching vibrations theoretically at 1537 and 966 cm^{-1} and experimentally observed at 1395 cm^{-1} in the FT-IR spectrum. The C-N vibration observed at 1612 cm^{-1} in the FT-Raman spectrum by Alphonsa et al. [69]. For our title molecule, the C-N stretching mode in the FT-IR spectrum exhibited at 1491, 1332 cm^{-1} . The calculated wavenumbers predicted at $\nu = 1530, 1493, 1485, 1336, 847 \text{ cm}^{-1}$, $\gamma = 593$ in B3LYP/6-31 G, $\nu = 1528, 1490, 1481, 1333, 840 \text{ cm}^{-1}$, $\gamma = 590 \text{ cm}^{-1}$ in by B3LYP/6-31 G (d,p) methods are assigned for C-N stretching vibrations.

4.3. Mulliken population analysis

The natural population analysis of the title compound obtained by Mulliken [70] population analysis with B3LYP level using 6-31 G and 6-31 G (d,p) basis sets. Mulliken atomic charge calculation has an important role in the application of quantum chemical calculation to the molecular system because of atomic charge effect, dipole moment, molecular polarizability, electronic structure and a lot of properties of molecule systems. The calculated Mulliken charge values are listed in Table S3 (Supplementary material). The charge changes with basis set due to polarization.

In the title compound, the Mulliken atomic charge of 8 carbon atoms, 30 hydrogen atoms and one sulphur atom exhibit a strong positive region and 22 carbon atoms, 3 nitrogen and one oxygen atoms are as a negative region. In the present structure, the carbon atoms have both positive and negative charges so they were highly influenced by their substituent atoms [71]. For our title molecule, C40 was highly positive (C40=4.489/0.361) because that atom was attached with the two electronegative

oxygen and nitrogen atoms and these two electronegative atoms withdrawing an electron charges from the carbon atom and become negative. The nitrogen atom N25 was more negative than other nitrogen which is due to the influence of surrounding hydrogen atoms is N24=-0.324/-0.198, N25=-0.458/-0.531 and N43=-0.465/-0.278. All the hydrogen atoms in the title molecule have a positive charge and among the atoms, H35, H55, H56, H63, H66 were highly positive. The eight positive carbon atoms C1=0.215/0.184, C2=0.119/0.032, C4=0.112/0.113, C14=0.126/0.16, C21= 0.14/ 0.126, C40=0.489/0.361, C46=0.102/0.036, C53= 0.13/ 0.116. The carbon present in the negative region depends upon the neighbouring atoms and the carbon-negative range are given as C5=-0.127/-0.155, C6=-0.097/-0.126, C7=-0.086/-0.112, C9=-0.9/-0.121, C11=-0.085/-0.26, C15=-0.145/-0.174, C30=-0.332/-0.417, C31=-0.332/-0.418 respectively. Atoms C127 and C42 have both positive and negative charges. Distribution of positive and negative charges is vital to increase or decreasing bond length between the atoms.

4.4. Molecular electrostatic potential (MEP) surface

For investigating chemical reactivity of the molecule, molecular electrostatic potential (MEP) surface is plotted over the optimized electronic structure of the title molecule using density functional B3LYP method with 6-31 G (d,p) basis set is shown in Fig. 4. The MEP generated in the molecule by the charge distribution is very helpful in understanding the reactive sites for the nucleophilic and electrophilic region in hydrogen bonding interactions. The colour scheme for the MEP surface is the red, electron-rich, partially negative charge; blue, slightly electron-deficient, partially positive charge; light blue, slightly electron-deficient region; yellow slightly electron-rich region respectively. The colour order of the MEP of the title compound originates with red colour (-7.132×10^{-2} a.u) and terminated with dark blue colour (7.132×10^{-2} a.u) which shows the separate values of the electrostatic potential at the exterior of the molecule. The MEP total density of the title molecule clearly shows the presence of more electron density around the carbonyl group is characterized by red colour. The predominance of the green region in the MESP surfaces corresponds to a potential halfway between the two extremes red and blue colour. As seen from the 2D diagram of MEP of the title molecule, more reactive sites are close to ketone (C=O) group which is present in thiazole group, the region having the most negative potential over oxygen atom O44 and the positive potential regions are most of the hydrogen atoms and it represents the possible site of the nucleophilic sites.

4.5. Molecular orbital studies

The most widely used theory by chemists is the molecular orbital (MO) theory. Ionization Potential (I), electron affinity (A), electronegativity (χ), electrophilic index (ω), hardness (η) and chemical potential (μ) must be put into a MO framework. The orbital energies of the Frontier orbital are given by Fig. 5. The FMO energy parameters and global reactivity descriptors at B3LYP/6-31 G (d,p) method are tabulated in Table 1. We focus on the HOMO and LUMO energies to determine interesting molecular/atomic properties and chemical quantities.

$$\text{Thesofenessofthemolecule } S = \frac{1}{2\eta}$$

$$\text{Thehardnessofthemolecule} = \frac{I + A}{2}$$

$$\text{Electrophilicindex } (\omega) \text{ or Global reactivity} = \frac{\mu^2}{2\eta}$$

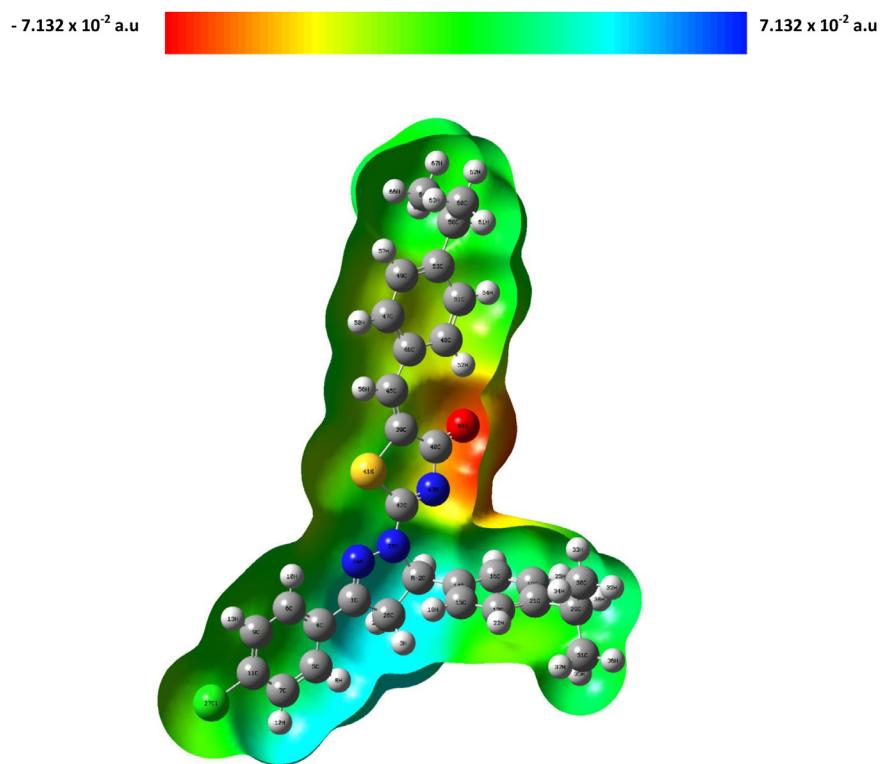


Fig. 4. Molecular electrostatic potential surfaces of 5-(4-Propan-2-yl)benzylidene)-2-[3-(4-chlorophenyl)-5[4-(propan-2-yl)phenyl]-4,5-dihydro-1H-pyrazol-1-yl]-1,3-thiazol-4(5H)-one.

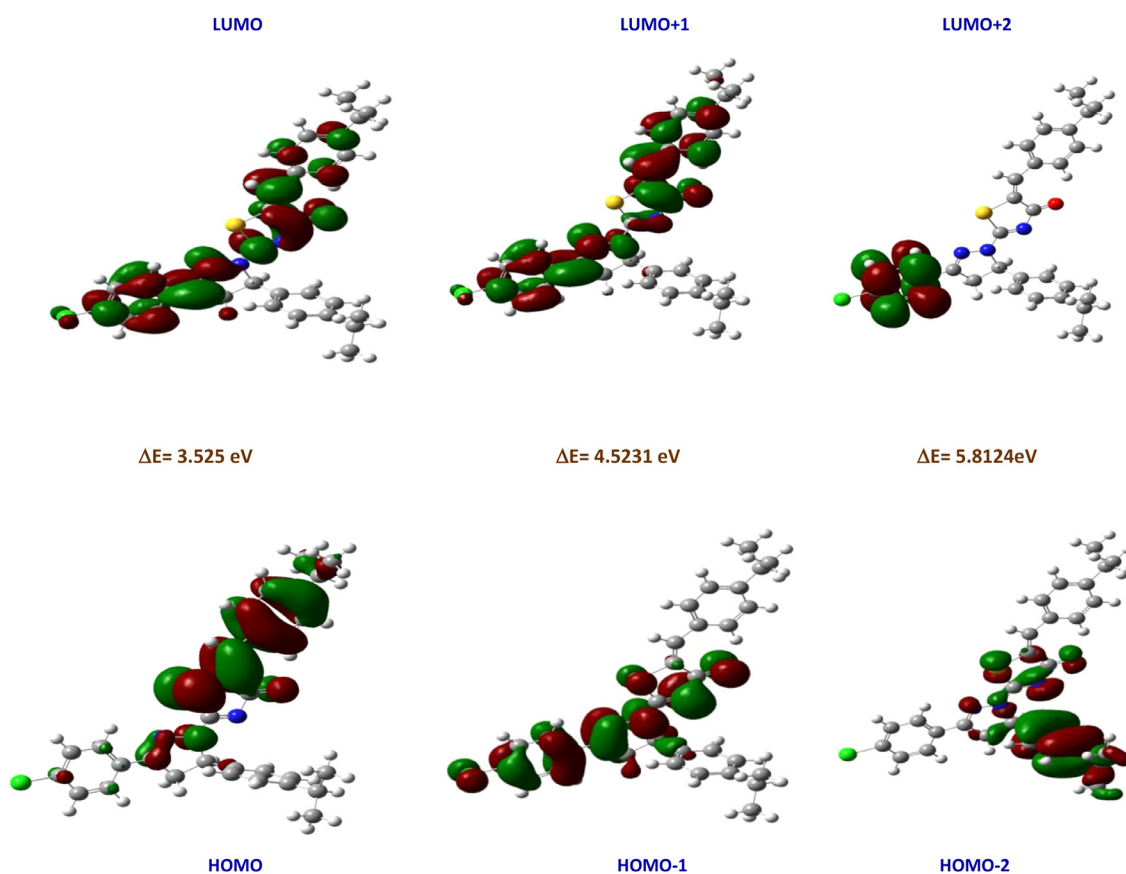


Fig. 5. Patterns of the principle highest occupied and lowest unoccupied molecular orbital of 5-(4-Propan-2-yl)benzylidene)-2-[3-(4-chlorophenyl)-5[4-(propan-2-yl)phenyl]-4,5-dihydro-1H-pyrazol-1-yl]-1,3-thiazol-4(5H)-one.

Table 1

HOMO-LUMO energies for 5-(4-Propan-2-yl)benzylidene)-2-[3-(4-chlorophenyl)-5[4-(propan-2-yl)phenyl]-4,5-dihydro-1H-pyrazol-1-yl]-1,3-thiazol-4(5H)-one by B3LYP/6-31(d,p) basis set.

Molecular properties	Energy (eV)	Energy gap (eV)	Ionisation potential (I)	Electron affinity (A)	Global hardness(η)	Electron negativity (χ)	Global softness (σ)	Chemical potential (μ)	Global Electrophilicity (ω)
E_{HOMO}	5.7579	3.5250	5.7579	2.2329	1.7625	3.995	0.5674	-3.9954	4.5286
E_{LUMO}	2.2329								
$E_{\text{HOMO-1}}$	6.1868	4.5231	6.1868	1.6637	2.2616	3.9252	0.4422	-3.9253	3.4064
$E_{\text{LUMO-1}}$	1.6637								
$E_{\text{HOMO-2}}$	6.5852	5.8124	6.5852	0.7725	2.9064	3.6789	0.3441	-3.6788	2.3282
$E_{\text{LUMO-2}}$	0.7725								

Table 2

Second order perturbation theory analysis of Fock matrix in NBO basis corresponding to intra molecular bands of 5-(4-Propan-2-yl)benzylidene)-2-[3-(4-chlorophenyl)-5[4-(propan-2-yl)phenyl]-4,5-dihydro-1H-pyrazol-1-yl]-1,3-thiazol-4(5H)-one.

Donor	Acceptor	E(2)(kcal/mol)BMP	E(j)-E(i) (a.u)BMP	F _(ij) (a.u)BMP
LP (1) N 24	BD*(1) C2 - N 25	4.81	0.82	0.056
LP (1) N 25	BD*(2) C1 - N 24	26.81	0.24	0.072
LP (1) N 25	BD*(1) C 2 - C 14	1.04	0.65	0.024
LP (1) N 25	BD*(1) C 2 - H 55	4.15	0.65	0.049
LP (1) N 25	BD*(1) S 41 - C 42	6.94	0.75	0.068
LP (1) N 25	BD*(1) C 42 - N 43	13.01	0.68	0.088
LP (1)Cl 27	BD*(1) C 7 - C 11	1.21	1.48	0.038
LP (1)Cl 27	BD*(1) C 9 - C 11	1.21	1.48	0.038
LP (2)Cl 27	BD*(1) C 7 - C 11	3.88	0.87	0.052
LP (2)Cl 27	BD*(1) C 9 - C 11	3.85	0.87	0.052
LP (3)Cl 27	BD*(2) C 7 - C 11	12.37	0.32	0.061
LP (1) S 41	BD*(1) N 25 - C 42	0.61	0.92	0.021
LP (1) S 41	BD*(1) C 39 - C 40	7.94	0.99	0.08
LP (1) S 41	BD*(1) C 40 - O 44	0.78	1.04	0.026
LP (1) S 41	BD*(1) C 42 - N 43	8.55	0.94	0.08
LP (2) S 41	BD*(2) C 39 - C 45	64.42	0.2	0.111
LP (2) S 41	BD*(1) S 41 - C 42	0.56	0.76	0.022
LP (2) S 41	BD*(2) C 42 - N 43	100.22	0.21	0.133
LP (1) N 43	BD*(1) N 25 - C 42	1.76	0.75	0.033
LP (1) N 43	BD*(1) C 39 - C 40	5.99	0.81	0.062
LP (1) N 43	BD*(1) C 39 - C 45	0.71	0.69	0.02
LP (1) N 43	BD*(1) C 40 - O 44	1.54	0.87	0.033
LP (1) N 43	BD*(1) S 41 - C 42	5.63	0.84	0.062
LP (1) O 44	BD*(1) C 39 - C 40	3.04	1.13	0.053
LP (1) O 44	BD*(1) C 40 - N 43	2.31	1.1	0.046
LP (2) O 44	BD*(1) C 39 - C 40	18.59	0.69	0.102
LP (2) O 44	BD*(1) C 40 - N 43	22.99	0.65	0.111

aE(2) means energy of hyperconjugative interactions (stabilization energy).

b Energy difference between donor and acceptor i and j NBO orbitals.

c F_(ij) is the Fock matrix element between i and j NBO orbitals.

where η is the chemical potential the electronegativity and hardness are used to make predictions about chemical behaviour and these are used to explain aromaticity in organic compounds [72]. A hard molecule has a large and a soft molecule has a small HOMO-LUMO gap. Like the same, soft molecule will be more reactive than the hard one. Based on a fully optimized ground state structure, the DFT/B3LYP/6-31 G calculation predicts one intense electronic transition from the ground to the first excited state and is mainly described by one electron excitation from the highest occupied molecular orbital (HOMO) to the lowest unoccupied molecular orbital (LUMO). The less value of ΔE confirms that the molecule is more polarized and has bioactivity [73,74]. Computed E_{HOMO} , E_{LUMO} and ΔE by DFT estimates that 401 molecular orbital with 139 occupied and remaining unoccupied for the title compound. Orbital 139 is identified as highest occupied HOMO orbital and 140 as lowest unoccupied LUMO orbital with energies 5.7579 eV and 2.2329 eV respectively. The HOMO-LUMO energy gap ΔE is 3.525 eV, Ionization potential (I) = 5.758 eV, Electron affinity (A) = 2.233 eV, Global hardness (η) = 1.763 eV, Softness (σ) = 0.567 eV, Chemical potential (μ) = -3.995 eV, Electrophilicity index (ω) = 4.529 eV. The values for chemical potential and electrophilicity index are small that indicates the reactive nature of the title compound which confirms the bioactivity of the title molecule by the positive value of chemical softness.

4.6. Natural bond orbital analysis

In quantum chemistry, a natural bond orbital (NBO) is a computed bonding orbital with maximum electron density. Natural bond orbital is used in computational chemistry to calculate bond orbital, donor-acceptor interactions and the distribution of electron density between atoms. The natural bond orbital (NBO) calculations were performed using NBO 3.1 program [75] as implemented in the Gaussian 09 package at the DFT/B3LYP level with 6-31 G (d,p) basis set in order to understand various second-order interactions and it provides an efficient method for studying interesting features of molecular structure and also provides a convenient basis for investigation charge transfer or conjugative interaction in the molecular system. The second-order Fock matrix was carried out to evaluate the donor-accepter interactions in the NBO analysis [76]. For each donor (i) and acceptor (j) the stabilization energy (E2) associated with the delocalization $i \rightarrow j$ is determined as

$$E(2) = \Delta E_{ij} = q_i \frac{(F_{i,j})^2}{(E_j - E_i)}$$

where q_i is the donor orbital occupancy, E_i, E_j are diagonal elements (orbital energies) and $F_{(i,j)}$ is the off-diagonal NBO Fock matrix element. All the interactions of the title compound were tabulated in Table 2. The important hyper-conjugative interac-

tions are C42-N43 from S41 of LP(2)S41 \rightarrow $\sigma^*(\text{C42-N43})$, C39-N45 from S41 of LP(2) S41 \rightarrow $\sigma^*(\text{C39-N45})$, C1-N24 from N25 of LP(1)N25 \rightarrow $\sigma^*(\text{C1-N24})$, C40-N43 from O44 of LP(2) O44 \rightarrow $\sigma^*(\text{C40-N43})$, C39-40 from O44 of LP(2) O44 \rightarrow $\sigma^*(\text{C39-C40})$, C39-C40 from O44 of LP(2) O44 \rightarrow $\sigma^*(\text{C39-C40})$, C42-N43 from N25 of LP(N25) \rightarrow $\sigma^*(\text{C42-N43})$ with stabilization energies, 100.22, 64.42, 26.81, 22.99, 18.59, 13.01 kJ/mol.

The perturbation energies of significant donor-acceptor interactions are presented in Table 3. The larger E(2) value the intensive is the interaction between electron donors (σ and π) and electron acceptors (σ^* and π^*). In Table 3, σ (C40-O44) orbital with 1.99418 a.u energy has 36.24% C40 character in SP^(2.02) hybrid and has 63.76% O44 character in SP^(1.74) hybrid. The idealized SP^(1.74) hybrid has 66.86%, 63.51% p-character and 33.16%, 36.46% s-character.

The two coefficients 0.6020 and 0.7985 are called polarization coefficients. σ C11-C127 orbital with 1.98945 a.u energy has 45.41% C11 character in SP^(3.42) hybrid and has 54.59% C127 character in SP^(5.04) hybrid. The idealized SP^(5.04) hybrid has 77.38%, 83.45% p-character and 22.62%, 16.55% s-character. The two coefficients 0.6739 and 0.7389 are called polarization coefficients. The oxygen (O44) has a larger percentage of this NBO, 63.76% and gives the larger polarization coefficient 0.6777 because it has a higher electronegativity. Similarly, the carbon (C48) has a larger percentage of this NBO, 62.63% and gives the larger polarization coefficient 0.6113. The carbon and nitrogen have a lesser percentage of NBO and give a lesser polarization coefficient. The carbon (C40) has a lower percentage of this NBO, 36.24% and gives the lesser polarization coefficient 0.6020.

Table 3

NBO analysis of bonding and antibonding orbit of 5-(4-Propan-2-yl)benzylidene)-2-[3-(4-chlorophenyl)-5[4-(propan-2-yl)phenyl-4,5-dihydro-1H-pyrazol-1-yl]-1,3-thiazol-4(5H)-one.

Band (A-B)	ED/Energy (a.u.)	ED%	ED%	NBO	S(%)	P(%)
BD (1) C 1 - C 4	1.9716	50.07	49.93	0.7076 SP ^(1.72)	36.83	63.17
	-0.63785			0.7066 SP ^(2.42)	29.21	70.79
BD (1) C 1 - N 24	1.98458	41.16	58.84	0.6416 SP ^(2.53)	28.3	71.7
	-0.8076			0.7671 SP ^(2.53)	35.15	64.85
BD (1) C 1 - C 26	1.97344	47.4	52.6	0.6884 SP ^(1.87)	34.83	65.17
	-0.71293			0.7253 SP ^(2.48)	28.73	71.27
BD (1) C 2 - C 14	1.96717	52.32	47.68	0.7233 SP ^(2.08)	32.46	67.54
	-0.62256			0.6905 SP ^(2.5)	28.53	71.47
BD (1) C 2 - N 25	1.97706	39.6	60.4	0.6293 SP ^(2.92)	25.51	74.49
	-0.79968			0.7772 SP ^(1.85)	35.07	64.93
BD (1) C 2 - C 26	1.96518	50.3	49.7	0.7092 SP ^(2.03)	33.04	66.96
	-0.71183			0.7050 SP ^(2.48)	28.73	71.27
BD (1) C 2 - H 55	1.89411	63.49	36.51	0.7968 SP ^(9.94)	9.14	90.86
	-0.45971			0.6042 S ⁽¹⁾	100	
BD (1) C 4 - C 5	1.97386	51.06	48.94	0.7146 SP ^(1.8)	35.68	64.32
	-0.71778			0.6996 SP ^(1.87)	34.85	65.15
BD (1) C 4 - C 6	1.97513	51.33	48.67	0.7146 SP ^(1.85)	35.11	64.89
	-0.71245			0.6977 SP ^(1.86)	34.98	65.02
BD (1) C 5 - C 7	1.96991	50.02	49.98	0.7072 SP ^(1.81)	35.55	64.45
	-0.71264			0.7070 SP ^(1.8)	35.76	64.24
BD (1) C 6 - C 9	1.97082	49.7	50.3	0.7050 SP ^(1.86)	34.99	65.01
	-0.70774			0.7092 SP ^(1.79)	35.82	64.18
BD (1) C 7 - C 11	1.98087	49.11	50.89	0.7008 SP ^(1.88)	34.78	65.22
	-0.73664			0.71334 SP ^(1.59)	38.64	61.36
BD (1) C 9 - C11	1.98117	48.98	51.02	0.6999 SP ^(1.89)	34.66	65.34
	-0.73613			0.7142 SP ^(1.58)	38.74	6.26
BD (1) C 11 - Cl 27	1.98945	45.41	54.59	0.6739 SP ^(3.42)	22.62	77.38
	-0.72439			0.7389 SP ^(5.04)	16.55	83.45
BD (1) C 14 - C 15	1.97179	51.33	48.67	0.7165 SP ^(1.78)	36.02	63.98
	-0.70373			0.6976 SP ^(1.88)	34.77	65.23
BD (1) C 14 - C 16	1.97342	51.24	48.76	0.7158 SP ^(1.83)	35.37	64.63
	-0.70241			0.6983 SP ^(1.88)	34.71	65.29
BD (1) C 15 - C 17	1.97468	50.24	49.76	0.7088 SP ^(1.78)	35.97	64.03
	-0.69235			0.7054 SP ^(1.83)	35.36	64.64
BD (1) C 21 - C 29	1.97443	49.85	50.15	0.7060 SP ^(2.34)	29.96	70.04
	-0.60045			0.7082 SP ^(2.34)	29.98	70.02
BD (1) N 24 - N 25	1.97516	44.85	55.15	0.6697 S ^(3.87)	20.53	79.47
	-0.78565			0.7456 SP ^(2.67)	27.25	72.75
BD (1) N 25 - C 42	1.98191	59.48	40.52	0.7713 SP ^(1.67)	37.41	62.59
	-0.84614			0.6365 S ^(2.05)	32.8	67.2
BD (1) C 31 - H 35	1.98711	61.78	38.22	0.7860 SP ^(2.93)	25.45	74.55
	-0.5137			0.6182 S ⁽¹⁾	100	
BD (1) C 39 - C 40	1.97996	54.86	45.14	0.7407 SP ^(2.03)	33.04	66.96
	-0.73079			0.6719 SP ^(1.84)	35.18	64.82
BD (1) C 39 - S 41	1.9775	53.45	46.55	0.7311 SP ^(1.98)	33.55	66.45
	-1.04732			0.6823 SP ^(2.03)	33.03	66.97
BD (1) C 39 - C 45	1.97473	54.08	45.92	0.7354 SP ^(2.00)	33.34	66.66
	-0.66995			0.6777 SP ^(2.10)	32.25	67.75
BD (1) C 40 - N 43	1.98023	41.39	58.61	0.6433 SP ^(2.21)	31.13	68.87
	-0.78333			0.7656 SP ^(2.28)	30.46	69.54
BD (1) C 40 - O 44	1.99418	36.24	63.76	0.6020 SP ^(2.02)	33.14	66.86
	-1.01591			0.7985 SP ^(1.74)	36.46	63.51
BD (1) S 41 - C 42	1.9822	47.49	52.5	0.6891 SP ^(2.07)	32.57	67.43
	-1.06292			0.7247 SP ^(1.77)	36.15	63.85

(continued on next page)

Table 4Fukui function (f_i^+ , f_i^- , Δf) for 5-(4-Propan-2-yl)benzylidene)-2-[3-(4-chlorophenyl)-5[4-(propan-2-yl)phenyl-4,5-dihydro-1H-pyrazol-1-yl]-1,3-thiazol-4(5H)-one.

Atoms	Natural atomic charges			Fukui functions(eV)			Electro-philicity	Nucleo-philicity
	qN	qN-1	qN+1	F+	F-	F0		
C 1	0.184	0.160	0.237	-0.077	0.024	-0.039	-0.102	0.102
C 2	0.032	0.037	0.010	0.026	-0.005	0.013	0.031	-0.031
H 3	0.163	0.138	0.245	-0.107	0.025	-0.053	-0.131	-0.131
C 4	0.113	0.115	0.113	0.001	-0.001	0.001	0.003	-0.003
C 5	-0.155	-0.163	-0.142	-0.021	0.007	-0.010	-0.028	0.028
C 6	-0.126	-0.132	-0.111	-0.022	0.006	-0.011	-0.028	0.028
C 7	-0.112	-0.114	-0.104	-0.011	0.003	-0.005	-0.013	0.013
H 8	0.149	0.140	0.160	-0.019	0.008	-0.010	-0.028	0.028
C 9	-0.121	-0.125	-0.114	-0.011	0.004	-0.006	-0.015	0.015
H 10	0.173	0.171	0.196	-0.025	0.002	-0.012	-0.027	0.027
C 11	-0.260	-0.263	-0.256	-0.008	0.003	-0.004	-0.011	0.011
H 12	0.157	0.137	0.191	-0.054	0.020	-0.027	-0.074	-0.074
H 13	0.159	0.142	0.194	-0.053	0.018	-0.026	-0.070	0.070
C 14	0.160	0.143	0.157	-0.014	0.016	-0.007	-0.031	0.031
C 15	-0.174	-0.176	-0.160	-0.016	0.003	-0.008	-0.019	0.019
C 16	-0.140	-0.137	-0.126	-0.012	-0.003	-0.006	-0.008	0.008
C 17	-0.175	-0.182	-0.160	-0.022	0.007	-0.011	-0.029	0.029
H 18	0.131	0.116	0.150	-0.034	0.015	-0.017	-0.049	0.049
C 19	-0.190	-0.200	-0.176	-0.025	0.010	-0.012	-0.035	0.035
H 20	0.135	0.196	0.160	0.036	-0.060	0.018	0.096	-0.096
C 21	0.126	0.127	0.128	-0.001	-0.001	0.000	0.000	0.000
H 22	0.130	0.107	0.168	-0.061	0.024	-0.031	-0.085	0.085
H 23	0.133	0.132	0.168	-0.035	0.001	-0.018	-0.036	0.036
N 24	-0.198	-0.193	-0.163	-0.031	-0.005	-0.015	-0.025	0.025
N 25	-0.531	-0.511	-0.474	-0.036	-0.020	-0.018	-0.016	0.016
C 26	-0.424	-0.410	-0.477	0.066	-0.014	0.033	0.080	-0.080
Cl 27	0.117	0.076	0.197	-0.121	0.041	-0.060	-0.162	0.162
H 28	0.182	0.158	0.240	-0.082	0.023	-0.041	-0.105	0.105
C 29	-0.208	-0.203	-0.222	0.019	-0.005	0.009	0.024	-0.024
C 30	-0.417	-0.417	-0.419	0.001	0.000	0.001	0.001	-0.001
C 31	-0.418	-0.417	-0.419	0.002	-0.001	0.001	0.003	-0.003
H 32	0.139	0.126	0.163	-0.037	0.013	-0.019	-0.051	0.051
H 33	0.143	0.141	0.147	-0.005	0.002	-0.003	-0.007	0.007
H 34	0.141	0.131	0.162	-0.031	0.011	-0.016	-0.042	0.042
H 35	0.147	0.155	0.149	0.006	-0.008	0.003	0.014	-0.014
H 36	0.139	0.124	0.163	-0.040	0.016	-0.020	-0.055	0.055
H 37	0.140	0.134	0.160	-0.027	0.006	-0.013	-0.033	0.033
H 38	0.194	0.188	0.217	-0.029	0.007	-0.015	-0.036	0.036
C 39	-0.287	-0.325	-0.309	-0.016	0.037	-0.008	-0.053	0.053
C 40	0.361	0.328	0.376	-0.048	0.033	-0.024	-0.082	0.082
S 41	0.488	0.386	0.521	-0.135	0.102	-0.067	-0.236	0.236
C 42	-0.013	-0.064	-0.015	-0.049	0.051	-0.025	-0.100	0.100
N 43	-0.278	-0.355	-0.265	-0.089	0.077	-0.045	-0.166	0.166
O 44	-0.404	-0.546	-0.372	-0.174	0.142	-0.087	-0.316	0.316
C 45	-0.043	-0.147	-0.009	-0.138	0.104	-0.069	-0.242	0.242
C 46	0.036	0.079	0.026	0.052	-0.042	0.026	0.095	-0.095
C 47	-0.115	-0.114	-0.115	0.001	-0.002	0.001	0.003	-0.003
C 48	-0.138	-0.142	-0.135	-0.007	0.005	-0.004	-0.012	0.012
C 49	-0.147	-0.159	-0.140	-0.018	0.012	-0.009	-0.030	0.030
H 50	0.139	0.114	0.146	-0.032	0.024	-0.016	-0.056	0.056
C 51	-0.151	-0.162	-0.145	-0.017	0.011	-0.009	-0.029	0.029
H 52	0.137	0.114	0.141	-0.027	0.023	-0.013	-0.049	0.049
C 53	0.116	0.118	0.116	0.002	-0.001	0.001	0.003	-0.003
H 54	0.135	0.097	0.152	-0.055	0.038	-0.027	-0.092	0.092
H 55	0.224	0.221	0.294	-0.072	0.003	-0.036	-0.075	0.075
H 56	0.174	0.091	0.197	-0.106	0.084	-0.053	-0.190	0.190
H 57	0.131	0.095	0.148	-0.053	0.036	-0.027	-0.089	0.089
C 58	-0.178	-0.171	-0.182	0.010	-0.007	0.005	0.017	-0.017
H 59	0.144	0.119	0.157	-0.038	0.025	-0.019	-0.063	0.063
C 60	-0.406	-0.402	-0.408	0.006	-0.004	0.003	0.010	-0.010
H 61	0.136	0.128	0.140	-0.012	0.008	-0.006	-0.020	0.020
H 62	0.131	0.106	0.145	-0.040	0.026	-0.020	-0.065	0.065
H 63	0.153	0.155	0.151	0.004	-0.002	0.002	0.006	-0.006
C 64	-0.402	-0.398	-0.404	0.006	-0.004	0.003	0.011	-0.011
H 65	0.134	0.127	0.138	-0.011	0.007	-0.005	-0.018	0.018
H 66	0.152	0.154	0.150	0.004	-0.002	0.002	0.006	-0.006
H 67	0.132	0.106	0.146	-0.040	0.026	-0.020	-0.067	0.067

Table 5
Binding affinity for docking in 5-(4-Propan-2-yl)benzylidene)-2-[3-(4-chlorophenyl)-5[4-(propan-2-yl)phenyl-4,5-dihydro-1H-pyrazol-1-yl]-1,3-thiazol-4(5H)-one.

Drug	Protein	Type of activity	Binding affinity(kcal/mol)	Etimated inhibition constant Ki(μM)	Bonded residues	Nature of bond	Bond distance (Å)	RMSD	
5-(4-Propan-2-yl)benzylidene)-2-[3-(4-chlorophenyl)-5[4-(propan-2-yl)phenyl-4,5-dihydro-1H-pyrazol-1-yl]-1,3-thiazol-4(5H)-one	4QXM	Antitubercular	-9.03	239.32 (Nm)	MET A:98	van der waals	3.12	45.171	
			-7.24	4.95 (M)	ILE A:47	van der waals	4.06	32.143	
			-7.23	5.06(M)	TYR A:158	van der waals	4.46	51.17	
			-7.03	7.05 (M)	ILE A:36	Alkyl	3.01	30.178	
			-6.73	11.75(M)	THR A:196	Conventional hydrogen bond	2.8	39.7	
	5T6N	Antiviral	-7.63	2.57	GLN A:210	Conventional hydrogen bond	3.49	46.93	
			-6.23	27.26	TRP A:234	π-π stacked	3.15	48.102	
			-5.71	65.29	GLN A:210	Conventional hydrogen bond	1.92	61.645	
			-5.67	69.34	TRP A:234	π-π stacked	3.13	49.815	
			-5.37	115.39	TRP A:234	π-π stacked	3.15	82.058	
			-6.47	18.02	GLN A:358	van der waals	2.21	262.039	
		4YJ3	Anticancer	-6.18	29.66	PRO A:364	van der waals	2.62	229.467
				-6.14	31.72	THR A:365	van der waals	2.81	269.206
				-6.12	32.56	GLY A:365	Pi-donor hydrogen bond	2.94	267.117
				-6.02	38.85	VAL A:26	Pi-alkyl	3.01	258.416
				-7.63	2.57	GLN A:210	Conventional hydrogen bond	3.49	46.93
				-6.23	27.26	TRP A:234	π-π stacked	3.15	48.102
	3S9Y	Anticancer	-5.71	65.29	GLN A:210	Conventional hydrogen bond	1.92	61.645	
			-5.67	69.34	TRP A:234	π-π stacked	3.13	49.815	
			-5.37	115.39	TRP A:234	π-π stacked	3.15	82.058	
			-7.52	3.07	ALA A:247	Conventional hydrogen bond	1.91	123.143	
			-7.09	6.37	LEU A:248	Conventional hydrogen bond	1.92	123.075	
			-7.06	6.64	TYR A:357	π-π stacked	3.01	114.455	
4I50	Anticancer	-7.03	7.01	TYR A:357	π-π stacked	3.21	113.872		
		-6.38	21.08	GLY A:246	van der waals	3.83	122.866		

4.7. Fukui function

In computational chemistry, the Fukui function describes the electron density when some electrons are added or removed from it. It is a local density functional descriptor, which helps in predicting the chemical reactivity and selectivity. The Fukui function helps one to predict the most reactive sites for electrophilic and nucleophilic sites within a molecule [77,78]. The condensed or atomic Fukui functions on the *r*th atomic site for an electrophilic f^-_r , nucleophilic f^+_r , and free radical f^0_r on the reference molecule can be defined as

$$\begin{aligned} f^+_k &= qk(N+1) - qk(N), \\ f^-_k &= qk(N) - qk(N-1) \\ f^0_k &= \frac{1}{2} \{qk(N+1) - qk(N-1)\} \end{aligned}$$

In these equations, q_r is the atomic charge (evaluated from Mulliken population analysis, electrostatic derived charge, etc.) at the *r*th atomic site in the neutral (N), anionic ($N+1$), cationic ($N-1$) chemical species [79]. Dual descriptor ($\Delta f(r)$) combines the two Fukui functions f^+_r and f^-_r as

$$\Delta f(r) = [f^+_r - f^-_r]$$

The dual descriptors $\Delta f(r)$ distinguishes between the nucleophilic and electrophilic attack at a particular site with their sign. If $\Delta f(r) > 0$, the site is favoured for a nucleophilic site, whereas if $\Delta f(r) < 0$, the site may be favoured for electrophilic sites. From Table 4, according to the condition for dual descriptor, important

some nucleophilic sites for the title compound are C127, N43, H56, S41, C45, O44 are positive values i.e. $\Delta f(r) > 0$. Similarly some electrophilic sites are C64, C2, C26, C46, H20 are negative values i.e. $\Delta f(r) < 0$. Among these nucleophilic and electrophilic sites, C46 and H20 have higher negative and positive charge values and O44, C45 are found in thiazole and phenyl group respectively of the title compound.

4.8. Reduced density gradient (RDG)

The reduced density gradient (RDG) can be used to reveal the intermolecular, intramolecular and even covalent interactions in real space based on the electron density and their derivatives as developed by Johnson et al. [80]. It is defined as

$$RDG(r) = \frac{1}{2(3\pi r^2)^{1/2}} \frac{|\nabla \rho(r)|}{\rho(r)^{4/3}}$$

In order to explore the features associated with small reduced gradients, we examined plots of RDG versus sign ($\lambda_2(r) \rho(r)$). The λ_2 sign was utilized to distinguish the bonded ($\lambda_2 < 0$) interactions from nonbonding ($\lambda_2 > 0$) interactions. The plot of the RDG versus the electron density ρ increased by the sign of λ_2 and visualization to a whole wide range of interactions types. The RDG spikes are found in the low gradient region and have low density and depicted in Fig. 6. According to the 2d graph, the strong interactive interaction indicates in blue colour which represents the interac-

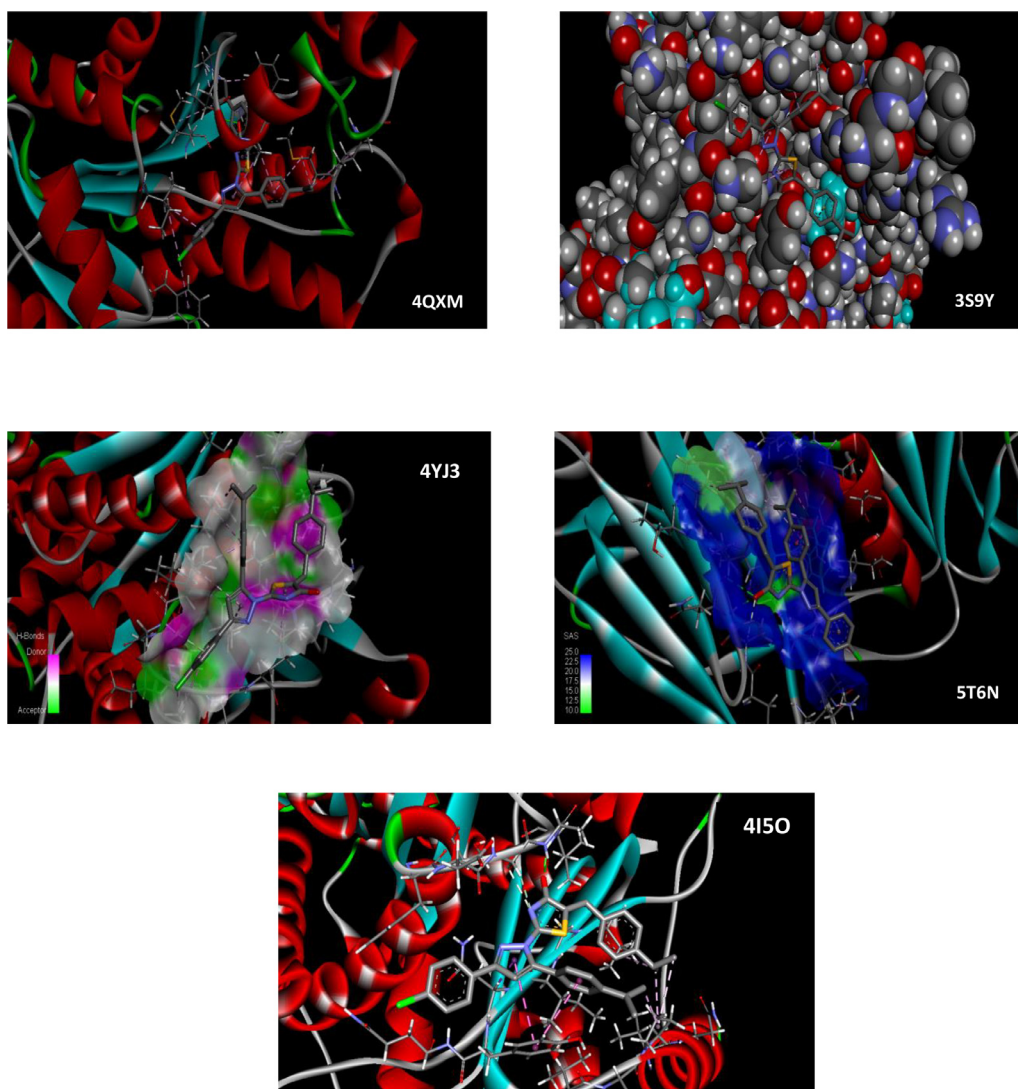


Fig. 7. Ligand 5-(4-Propan-2-yl)benzylidene)-2-[3-(4-chlorophenyl)-5[4-(propan-2-yl)phenyl-4,5-dihydro-1H-pyrazol-1-yl]-1,3-thiazol-4(5H)-one - Protein - 4YJ3.

tion between H-bond, C-Cl bonds, weak interaction represents in green colours such as van der Waals interaction and steric repulsion in red colour. The reduced density gradient, RDG is -0.010 a.u.

4.9. Molecular docking

Molecular docking is a powerful computational tool that predicts the preferred binding orientation, affinity and protein targets. Title compound can be used for treating microbacterial diseases and cancer. To explore the biological activity of the title molecule, molecular docking simulations have been performed using AutoDock/Vina software [81]. The title compound (ligand) was docked into the active site of the protein 4QXM, 5T6N, 4YJ3, 3S9Y and 4I50 associated with antitubercular, antiviral and anticancer activity. The 3D crystal structure of the protein was obtained from the protein data bank. Initially, the co-crystalline ligands co-factors and water molecules were removed from protein. using Auto Dock Tools (ADT) graphical user interface. Subsequently, polar hydrogen was attached and atomic charges were computed by Kollman and Gasteiger method. The active site of protein was defined with $60 \text{ \AA} \times 60 \text{ \AA} \times 60 \text{ \AA}$ grid size and the Lamarckian Genetic Algorithm (LGA) was used to carry out the process. The molecular docking binding energies (kcal/mol), intermolecular en-

ergy (kcal/mol) and inhibition constants (μm) were obtained and are tabulated in Table 5. Binding energy gives a measure of the affinity of ligand-protein complex whereas the intermolecular energy indicates the energy between non-bounded atoms. Interaction of antitubercular protein shows three van der waals and one conventional hydrogen bond was found in 4QXM interacting with amino acids (3.12 \AA ; MET A:98, 4.06 \AA ; ILE A:47, 4.46 \AA ; TYR A:158, 2.8 \AA ; THR A:196) with different binding energy (-9.03 , -7.24 , -7.23 , -6.73 kcal/mol), inhibition constant (239.32 nm, 4.95 mm, 5.06 mm, 11.75 mm) and RMSD values are (45.171, 32.143, 51.17, 39.7) \AA . Interaction of antiviral protein shows two conventional hydrogen bonds, three pi-pi stacked bonds were found in 5T6N interacting with amino acids (3.49 \AA ; GLN A-210, 1.92 \AA ; GLN A:210, 3.15 \AA ; TRP A:234, 3.13 \AA ; TRP A:234, 3.15 \AA TRP A:234) with different binding energies (-7.63 , -5.71 , -6.23 , -5.67 , -5.37) kcal/mol, inhibition constant (2.57, 65.29, 27.26, 69.34, 115.39 μm) and RMSD values are (46.93, 61.645, 48.102, 49.815, 82.058) \AA . Interaction of anticancerous protein shows existence of three van der waals interactions and Pi-donor hydrogen bond were found in 4YJ3 interacting with amino acids (2.21 \AA ; GLN A:358, 2.62 \AA ; PRO A:364, 2.81 \AA ; THR A:365, 2.94 \AA ; GLY A:365) with different binding energies (-6.47 , -6.18 , -6.14 , -6.12) kcal/mol, inhibition constant (18.02, 29.66, 31.72, 32.56) μm) and RMSD values are (262.039, 229.467, 269.206, 267.117) \AA . Interaction of an-

anticancerous protein shows three conventional hydrogen bonds and a van der Waals bond were found in 3S9Y interacting with amino acids (3.01 Å; ASP A:160, 3.03 Å; LYS A:158, 2.61 Å; ASP A:160; 2.93 Å; MET A:1) with different binding energies (−7.71, −7, −6.51, −7.79) kcal/mol, inhibition constant (2.24, 7.4, 16.78, 1.94) μm and RMSD values are (17.797, 56.79, 23.213, 39.362) Å. Two conventional hydrogen bonds, two pi-pi stacked interactions and a van der Waals bond were found in another anticancerous protein 4I50 with amino acids (1.91 Å; ALA A:247, 1.92 Å; LEU A: 248, 3.01 Å; TYR A:357, 3.21 Å; TYR A:357, 3.83; GLY A:246) with different binding energies (−7.52, −7.09, −7.06, −7.03, −6.38) kcal/mol, inhibition constant (3.07, 6.37, 6.64, 7.01, 21.08) μm and RMSD values are (123.143, 123.075, 114.455, 113.872, 122.855) Å. The docked ligand interactions with amino acids of the receptor and the ligand at the active sites of the receptor are stated in Fig. 7 and Table 5. These docked preliminary results suggest that the title compound might exhibit the inhibitory activity against protein inhibitors.

5. Conclusion

The optimized geometries and vibrational wavenumbers of the title compound have been determined using DFT/B3LYP/6–31 G and 6–31 G (d,p) basis sets. In HOMO and LUMO, the lower energy gaps i.e. 3.525 eV, depict the presence of biological activity of the title compound. From the MEP analysis, it is evident that the electrophilic regions are oxygen atoms and nucleophilic regions are mainly over hydrogen atoms. Stability of the molecule arising from hyper conjugative interaction and charge delocalization has been analysed using natural bond orbital analysis. The electron density between atoms revealed two relatively strong intramolecular noncovalent interactions. The molecular docking results refer that the compound might be an inhibitory activity against anticancerous and antiviral agents. The anticancerous protein 4YJ3 is having higher binding energy, inhibition constant and RMSD values such as −6.47 kcal/mol, 18.02 μM and 262.039 than 3S9Y, 4I50. Thus the title compound may be observed as an efficient antitubercular, anticancerous and antiviral drug.

CRedit author statement

The corresponding author is responsible for ensuring that the descriptions are accurate and agreed by all authors.

Declaration of Competing Interest

The authors declare that they have no known competing financial interests or personal relationships that could have appeared to influence the work reported in this paper.

Acknowledgement

BN thanks UGC for financial assistance through BSR one-time grant (SR/S/Z/–23/2010/32) for the purchase of chemicals.

Supplementary materials

Supplementary material associated with this article can be found, in the online version, at doi:10.1016/j.molstruc.2020.129070.

References

- N. Klose, K. Niedbolla, K. Schwartz, I. Bottcher, 4, 5Bis(4-methoxyphenyl)2-cycloalkylthioimidazole mit antiphlogistischer Wirkung, *Arch. Pharm.* 316 (1983) 941–951.
- R.K. Satsangi, S.M. Zaidi, V.C. Misra, 1-(4-substituted-thiazol-2-yl)hydantoin as anti-inflammatory and CNS-active agents, *Pharmazie* 38 (1983) 341–342.
- E. Daniel Lynch, Ian McClenaghan, E. Mark Light, L. Simon Coles, The Hydrogen-bonding networks of 2-amino-4-phenyl-1,3-thi zole derivatives, *Cryst. Eng.* 5 (2002) 123–136.
- C.T. Supuran, A. Scozzafava, B.C. Jurca, M.A. Lies, Carbonic anhydrase inhibitors-Part 49: synthesis of substituted ureido and thioureido derivatives of aromatic/heterocyclic sulfonamide with increased affinities for isozyme I, *Eur. J. Med. Chem.* 33 (1998) 83–93.
- G. Renzi, A. Scozzafava, C.T. Supuran, carbonic anhydrase inhibitors: topical sulfonamide antiglaucoma agents incorporating secondary amine moieties, *Bioorg. Med. Chem. Lett.* 10 (2000) 4570–4577.
- J.J. Li, D. Anderson, E.G. Burton, J.N. Cogburn, J.T. Collins, D.J. Garland, S.A. Gregory, H.C. Huang, P.C. Isakson, 1,2-Diarylcyclopentenes as selective Cyclooxygenase-2 inhibitors and orally active anti-inflammatory agents, *Med. Chem.* 38 (1995) 4570–4578.
- K. Asada, M. Watanabe, T. Nagasu, T. Tsukhara, K. Iijima, A.K. Kitoh, Novel sulfonamides as potential, systemically active antitumor agents, *Med. Chem.* 38 (1992) 2496–2497.
- A.K. Gadad, C.S. Maharajshetti, S. Nimbalkar, A. Raichurkar, synthesis and antibacterial activity of some 5-guanylhydrazone/thiocyanato-6-arylimido[2,1-b]-1,3,4-thiadiazole-2-sulfonamide derivatives, *Eur. J. Med. Chem.* (2000) 853–857.
- F. Zani, P. Vicini, Antimicrobial activity of some 1,2-benzisothiazoles having a benzenesulfonamide moiety, *Arch. Pharm.* (1998) 219–223.
- T.H. Maren, Relations between structure and biological activity of sulfonamides, *Ann. Rev. Pharmacol. Toxicol.* (1976) 309–327.
- M.J. Rogers, E. Cundliffe, T.F. Mccutchan, *Antimicrob. Agents Chemother.* 42 (1998) 715–716.
- M.C. Bagley, J.W. Dale, E.A. Merritt, X. Xiong, Thiopeptide antibiotics, *Chem. Rev.* 105 (2005) 685–714.
- A.S. Mayhoub, M. Khaliq, C. Botting, Z. Li, R.J. Kuhn, M. Cushman, *Bioorg. An investigation of phenylthiazole antiflaviviral agents*, *Med. Chem.* 19 (2011) 3845–3854.
- O. Seitz, F. Bergmann, D. Heindl, A Convergent Strategy for the Modification of Peptide Nucleic Acids: novel Mismatch Specific PNA Hybridization Probes, *Angew. Chem. Int. Ed.* 38 (15) (1999) 2203–2206.
- O. Köhler, D.V. Jarikote, O. Seitz, Forced intercalation probes (FIT Probes): thiazole orange as a fluorescent base in peptide nucleic acids for homogeneous single-nucleotide-polymorphism detection, *Chembiochem* 6 (1) (2005) 69–77.
- O. Köhler, O. Seitz, Thiazole orange as fluorescent universal base in peptide nucleic acids, *Chem. Commun.* (23) (2003) 2938–2939.
- O.I. El-Sabbagh, M.M. Baraka, S.M. Ibrahim, C. Pannecouque, G. Andrei, R. Snoeck, J. Balzarini, A.A. Rashad, Synthesis and antiviral activity of new pyrazole and thiazole derivatives, *Eur. J. Med. Chem.* 44 (9) (2009) 3746–3753.
- S.K. Bharti, G. Nath, R. Tilak, S. Singh, Synthesis, anti-bacterial and anti-fungal activities of some novel Schiff bases containing 2, 4-disubstituted thiazole ring, *Eur. J. Med. Chem.* 45 (2) (2010) 651–660.
- M.I. Soares, A.F. Brito, M. Laranjo, J.A. Paixão, M.F. Botelho, T.M.P. e Melo, Chiral 6, 7-bis (hydroxymethyl)-1H, 3H-pyrrolo [1, 2-c] thiazoles with anti-breast cancer properties, *Eur. J. Med. Chem.* 60 (2013) 254–262.
- F. Mjambili, M. Njoroge, K. Naran, C. De Kock, P.J. Smith, V. Mizrahi, D. Warner, K. Chibale, Synthesis and biological evaluation of 2-aminothiazole derivatives as antimycobacterial and antiplasmodial agents, *Bioorg. Med. Chem. Lett.* 24 (2) (2014) 560–564.
- M. Helal, M. Salem, M. El-Gaby, M. Aljahdali, Synthesis and biological evaluation of some novel thiazole compounds as potential anti-inflammatory agents, *Eur. J. Med. Chem.* 65 (2013) 517–526.
- H.W. Lee, B.Y. Kim, J.B. Ahn, S.W. Kang, J.H. Lee, J.S. Shin, S.K. Ahn, S.J. Lee, S.S. Yoon, Eur PPARs in cellular and whole body energy metabolism, *J. Med. Chem.* 40 (2005) 862.
- A. Ceriello, Oscillating Glucose Is More Deleterious to Endothelial Function and Oxidative Stress Than Mean Glucose in Normal and Type 2 Diabetic Patients, *Diab. Met. Res. Rev.* 24 (2008) 14.
- V.V. Salian, B. Narayana, B.K. Sarojini, M.S. Kumar, K. Sharath Chandra, A. G.Lobo, Tailor made biheterocyclic pyrazoline-thiazolidinones as effective inhibitors of *Escherichia coli* FabH: design, synthesis and structural studies, *J. Mol. Struct.* 1192 (2019) 91–104.
- V.V. Salian, B. Narayana, B.K. Sarojini, E.S. Sindhupriya, L.N. Madhu, S. Rao, Biologically potent pyrazoline derivatives from versatile (2)-1-(4-chlorophenyl)-3-[4-(propan-2-yl)phenyl]prop-2-en-1-one, *Lett. Drug Des. Discov.* 14 (2017) 216–227.
- B. Narayana, V.V. Salian, B.K. Sarojini, J.P. Jasinski, (2E)-1-(4-Chlorophenyl)-3-[4-(propan-2-yl)phenyl]prop-2-en-1-one, *Acta Cryst. E70* (2014) o855.
- Frisch M.J., Trucks G.W., Schlegel H.B., Scuseria G.E., Robb M.A., Cheeseman J.R., Scalmani G., Barone V., Mennucci B., Peterson G.A., Nakatsuji H., Caricato M., Li X., Hratchian H.P., Izmaylov F., Bloino J., Zheng G., Sonnenberg J.L., Hada M., Ehara M., Toyota K., Fukuda R., Hasegawa J., Ishida M., Nakajima T., Honda Y., Kitao O., Nagari H., Vreven T., Montgomery T.A.J., Peralta J.E., Ogliaro F., Bearpark M., Heyd J.J., Brothers E., Kudin K.N., Staroverov V.N., Kobayashi R.K., Normand J., Ragavachari K., Rendell A., Burant J.C., Iyengar S.S., Tomasi J., Cossi M., Rega N., Millam J.M., Klene M., Knox J.E., Cross J.B., Bakken V., Adamo C., Jaramillo J., Gomperts R.G., Stramann R.E., Yazyev O., Austin A.J., Cammi R., Pomelli C., Ochterski J.W., Martin R.L., Morokuma K., Zakrzewski V.G., Voth G.A., Salvador P., Dannenberg J.J., Dapprich S., Farkas O., Ortiz J.V., Cioslowski J., Fox D.J. Gaussian, Inc., Wallingford CT, 2009.
- R. Dennington, T. Kerth, J. Millam, GaussView, Version 5, Semichem, Inc., Shawnee Mission KS, 2009.

- [29] T. Lu, F. Chen, Multiwfn: a multifunctional wave function analyzer, *J. Chem. Inf. Comput. Chem.* 33 (2012) 580–592.
- [30] W. Humphrey, A. Dalke, K. Schulten, VMD: visual molecular dynamics, *J. Mol. Graph.* 14 (1996) 33–38.
- [31] O. Trotter, A.J. Olson, AutoDock Vina: improving the speed and accuracy of docking with a new scoring function, efficient optimization and multithreading, *J. Comput. Chem.* 31 (2010) 455–461.
- [32] W.L. Delano, The PyMol Molecular Graphics System, Schrodinger LLC, 2002. pymol.org. Version 1, <http://www.pymol.org>.doi:citeulike-id:240061.
- [33] Discovery Studio 4.5 Guide, Accelrys Inc., San Diego, 2009 <http://www.accelrys.com>.
- [34] S.H. Rosline Sebastian, M.A. Al-Alshaiikh, A. Ali El-Emam, C.Y. Panicker, J. Zitko, M. Dolezal, C. Van Alsenoy, - Spectroscopic, quantum chemical studies Fukui functions, in vitro antiviral activity and molecular docking of 5-chloro-N-(3-nitrophenyl)pyrazine-2-carboxamide, *J. Mol. Struct.* 1119 (2016) 188–199.
- [35] A.F. Holleman, E. Wiberg, N. Wiberg, W. de Gruyter (Ed.), *Chemie*, Berlin, New York, 2007.
- [36] S. Shana Parveen, A.Al-Alshaiikh Monirah, C. Yohannan Panicker, Ali A. El-Emam, B. Narayana, Vinutha V. Saliyan, B.K. Sarojini, C. Van Alsenoy, Vibrational and structural observations and molecular docking study on 1-[3-(4-chlorophenyl)-5-[4-(propan-2-yl)phenyl]-4,5-dihydro-1H-pyrazol-1-yl]-ethanone, *J. Mol. Struct.* 1112 (2016) 136–146.
- [37] Y.S. Mary, K. Raju, I. Yildiz, O. Temiz-Arpaç, H.I.S. Nogueira, C.M. Granadeiro, C. Van Alsenoy, Ft-IR, FT-Raman, SERS and computational study of 5-ethylsulphonyl-2-(o-chlorobenzyl)benzoxazole, *Spectrochim. Acta* 96 (2012) 617–625.
- [38] P.S. Binil, Y.S. Mary, H.T. Varghese, C.Y. Panicker, M.R. Anoop, T.K. Manoj kumar, Infrared and Raman spectroscopic analyses and theoretical computation of 4-butyl-1-(4-hydroxyphenyl)-2-phenyl-3,5-pyrazolidinedione, *Spectrochim. Acta* 94 (2012) 101–109.
- [39] K.R. Ambujakshan, H. Tresavarghese, S. Mathew, S. Ganguli, A. Kumar Nanda, C. Yohannan Panicker, Vibrational spectroscopic studies and theoretical calculations of 2-phenyl-4H-3,1-benzoxazin-4-one, *Orien. J. Chem.* 24 (2008) 865–874.
- [40] L. Ushakumari, C.Y. Panicker, H. Haseena Tresavaraghese, A.V. Vaidyan, N. Sudhakaran, K. Raju, Spectroscopic investigations of a substituted amide of pyrazine-2-carboxylic acid, *Orien. J. Chem.* 24 (2008) 849–958.
- [41] V. Balachandran, T. Karthick, S. Perumal, A. Nataraj, Vibrational spectroscopic studies, molecular orbital calculations and chemical reactivity of 6-nitro-m-tolonic acid, *Spectrochim. Acta* 92 (2012) 137–147.
- [42] S. Murugavel, C. Ravikumar, G. Jaabil, Alagusundaram Ponnusamy, Synthesis, crystal structure analysis, spectral investigations (NMR, FT-IR, UV), DFT calculations, ADMET studies, molecular docking and anticancer activity of 2-(1-benzyl-5-methyl-1H-1,2,3-triazol-4-yl)-4-(2-chlorophenyl)-6methoxy pyridine – A novel potent human topoisomerase II α inhibitor-, *J. Mol. Struct.* 2860 (2018) 31090–31091.
- [43] A. Al-Alshaiikh Monirah, Y. Sheena Mary, C. Yohanna Panicker, I. Atia Mohamed, Ali A. El-emam, Spectroscopic investigations Van Alsenoy C., spectroscopic investigations and molecular docking study of 3-(1H-imidazol-1-yl)-1-phenylpropan-1-one, a potential precursor tobioactive agents, *J. Mol. Struct.* 1109 (2016) 130–138.
- [44] R. Minita, Y. Sheenamary, Hema Tresa Varghese, Yohannan Panickers, Reena Ravindran, K. Raju, V. Manikandan Nair, FT-IR, FT-Raman, and computational study of 1H-2,2-dimethyl-1,3H-phenothiazin-4[10H]-one, *J. Mole. Struct.* 985 (2011) 316–322.
- [45] K.S. Resmi, Kabiru Haruna, Y. Sheena Mary, C. Yohannan Panicker, A. Tawfik Saleh, A.Al-Saadi Abdulaziz, Van Alsenoy Christian, Conformational, NBO, NLO, HOMO-LUMO, NMR, electronic spectral study and molecular docking study of N,N-Dimethyl-3-(10H-phenothiazin-10yl)-1-propanamine-, *J. Mol. Struct.* 1098 (2015) 130.
- [46] G. Socrates, *Infrared Characteristic Group Frequencies*, Wiley, New York, 1980.
- [47] G. Varsanyi, *Vibrational Spectra of Benzene Derivatives*, Academic Press, New York, 1969.
- [48] P.B. Nagabalasubramanian, M. Karabacak, S. Periandy, FT-IR, FT-Raman, ab initio and DFT structural, vibrational frequency and HOMO-LUMO analysis of 1-naphthaleneacetic acid methyl ester, *Spectrochim. Acta Part A* 82 (2011) 169–180.
- [49] I. Matulkova, I. Nemeč, K. Teubner, P. Nemeč, Z. Micka, Novel compounds of 4-amino-1,2,4-triazole with dicarboxylic acids—Crystal structures, vibrational spectra and non-linear optical properties, *J. Mol. Struct.* 873 (2008) 46–60.
- [50] Beena T., Sudha L., Nataraj A., Balachandran V., Kannan D., Ponnuswamy M.N., Synthesis, spectroscopic, dielectric, molecular docking and DFT studies of (3E)-3-(4-methylbenzylidene)-3,4-dihydro-2H-chromen-2-one: an anticancer agent, *Chem. Cent. J.* 201711:6, 10.1186/s13065-016-0230-8.
- [51] Sheena Mary Y., Yohannan Panicker C., Sapnakumari M., Narayana B., Sarojini BK., Abdulaziz A.Al-Saadi, Van Alsenoy C., Javeed Ahmad War, Fun H.K. Infrared spectrum, structural and optical properties and molecular docking study of 3-(4-Fluorophenyl)-5-phenyl-4,5-dihydro-1H-pyrazole-1-carbaldehyde, 1425 (2014) 1700–4.
- [52] Shargina Beegum, Y.Sheena Mary, Hema Tresa Varghese, C. Yohannan Panicker, Stevan Armarković, Sanja J. Armarković, Jan Zitko, Martin Dolezal, C. Van Alsenoy, Vibrational spectroscopic analysis of cyanopyrazine-2-carboxamide derivatives and investigation of their reactive properties by DFT calculations and molecular dynamics simulations, *J. Mol. Struct.* 2860 (2016) 31206–6.
- [53] S. Sakthivel, T. Alagesan, S. Muthu, Abraham Christina Susan, E. Geetha, Quantum mechanical, spectroscopic study (FT-IR and FT - Raman), NBO analysis, HOMO-LUMO, first order hyperpolarizability and docking studies of a non-steroidal anti-inflammatory compound, *J. Mol. Struct.* 1156 (2018) 645–656.
- [54] M. Tamil Elakkiya, S. Premkumar, M. Sathiyendran, P. Suresh, V. Shanmugaiah, K. Anitha, Structural, spectral, computational, thermal and antibacterial studies on a cocrystal: 2-aminopyrazine phthalic acid, *J. Mol. Struct.* 1173 (2018) 635–646.
- [55] Shana Parveen S., Monirah A.Al-Alshaiikh, Yohannan Panicker C., Ali A. El-Emam, Narayana B., Vinutha V. Saliyan, Sarojini B.K., Van Alsenoy C., Vibrational and structural observations and molecular docking study on 1-[3-(4-chlorophenyl)-5-[4-(propan-2-yl)phenyl]-4,5-dihydro-1H-pyrazol-1-yl]-ethanone, *J. Mol. Struct.*, 2860(16)30112-0.
- [56] Usha rani, N. Sundaraganesan, M. Kurt, M. Cinar, M. Karaback, FT-IR, FT-Raman, NMR spectra ad DFT calculations on 4-chloro-N-methylaniline, *Spectrochim. Acta* (2010) 1523–1529.
- [57] K. Jayasheela, Lanya H. Al-Wahaibi, S. Periandy, Hanan M. Hassan, S. Sebastian, S. Xavier, Joseph C. Daniel, Ali A. El-Emam, Mohamed I. Attia, Probing vibrational activities, electronic properties, molecular docking and Hirshfeld surfaces analysis of 4chlorophenyl ([[(1E)-3-(1Himidazol-1-yl)-1-phenylpropylidene]amino)oxy)methanone: a promising anti-Candida agent, *J. Mol. Struct.* 1159 (2018) 83–95.
- [58] Mooney E.F., The infrared spectra of chlorobenzene and bromobenzene derivatives—III. Toluenes, *Spectrochim. Acta* 20 (9) 1343–1348.
- [59] A. Viji, V. Balachandran, S. Babiyana, B. Narayana, V. Vinutha, Saliyan - Molecular docking and quantum chemical calculations of 4-methoxy-{2-[3-(4-chlorophenyl)-5-(4-(propane-2-yl) phenyl)-4, 5-dihydro-1H-pyrazol-1-yl]- 1, 3thiazol-4-yl}phenol, *J. Mol. Struct.* 2860 (2019) 31561–31563.
- [60] Shaheen Fatma, Abha Bishnoi, Vineeta Singh, A.M.Al-Omary Fatmah, Ali A. El-Emam, Shilendra Pathak, Ruchi Srivastava, Onkar Prasad, Leena Sinha, Spectroscopic and electronic structure calculation of a potential antibacterial agent incorporating pyrido-dipyrimidine-dione moiety using first principles, *J. Mol. Struct.* 1110 (2016) 128–137.
- [61] A. Viji, V. Balachandran, S. Babiyana, B. Narayana, V. Vinutha, Saliyan FT-IR and FT-Raman investigation, quantum chemical studies, molecular docking study and antimicrobial activity studies on novel bioactive drug of 1-(2,4-dichlorobenzyl)-3-[2-3(4chlorophenyl)-5-(4-propan-2-yl)phenyl]-4,5-dihydro-1H-pyrazol-1-yl]-4-oxo-4,5-dihydro-1,3-thiazol-5(4H)-ylidene]=2,3-dihydro-1H-indol-2-one, *J. Mol. Struct.* 1215 (2020) 128244.
- [62] W.C. Harris, L.B. Knight, R.W. McNamee, J.R. Durig, Versuche zum stickst, *Inorg. Chem.* 13 (1974) 2297.
- [63] J. Coates, *Interpretation of Infrared Spectra of Organic Structures*, John Wiley, New York, 2000.
- [64] V.V. Aswathy, Y. Sheena Mary, P.J. Jojo, C. Yohannan Panicker, Anna Bielenica, Stevan Armarković, J.Armaković Sanja, Brzózka Paulina, Krukowski Sylwester, C. Van Alsenoy, Investigation of spectroscopic, reactive, transport and docking properties of 1-(3,4dichlorophenyl)-3-[3-(trifluoromethyl)phenyl]thiourea (ANF-6): combined experimental and computational study, *J. Mol. Struct.* 2860 (2017) 30016–30019.
- [65] R.M. Silverstein, G.C. Bassler, T.C. Morrill, *Spectrometric Identification of Organic Compounds*, 5th edn., John Wiley and Sons Inc., Singapore, 1991.
- [66] N.B. Colthup, L.H. Daly, S.E. Wiberly, *Introduction of Infrared and Raman Spectroscopy*, Academic Press, New York, 1975.
- [67] L.J. Bellamy, *The Infrared Spectrum of Complex Molecules*, 3rd edn., Chapman and Hall, London, 1975.
- [68] Tintu K. Kuruvilla, Prasana Johanan Christian, S. Muthu, George Jacob, Vibrational spectroscopic (FT-IR, FT-Raman) and quantum mechanical study of 4-(2chlorophenyl)-2-ethyl-9-methyl-6H-thieno[3,2-f][1,2,4]triazolo[4,3-a][1,4] diazepine, *J. Mol. Struct.* 2860 (2018) 30001–30002.
- [69] A. Therasa Alphonsa, C. Loganathan, S. Athavan Alias Anand, S. Kabilan, Molecular structure, NMR, UV-Visible, Vibrational spectroscopic and HOMO, LUMO analysis of (E)-1-(2, 6-bis (4-methoxyphenyl)-3, 3-dimethylpiperidine-4-ylidene)-2-(3(3, 5-dimethyl-1H-pyrazol-1-yl) pyrazin-2-yl) hydrazine by DFT method, *J. Mol. Struct.* 2860 (2015) 30410–30415.
- [70] V.K. Rastogi, M.A. Palafox, I. Mittai, N. Perica, W. Kiefer, K. Lang, P. Ohja, FTIR,FT-Raman spectra and density functional computations of the vibrational spectra, molecular geometry and atomic charges of the biomolecule: 5-bromouracil, *J. Raman Spectrosc.* 38 (2007) 1227–1241.
- [71] R. Mohamed Asath, S. Premkumar, T. Mathavan, A. Milton, B. Franklin, Vibrational Spectroscopic, Molecular Docking and Quantum Chemical Studies on 6-aminocotinamide, *J. Mol. Struct.* 1134 (2017) 143–156.
- [72] K. Fukui, Role of frontier orbitals in chemical reactions, *Science* 218 (1982) 747–754.
- [73] R.G. Parr, R.G. Pearson, Absolute hardness, companion parameter to absolute electronegativity, *J. Am. Chem. Soc.* 105 (1983) 7512–7516.
- [74] L. Sinha, O. Prasad, V. Narayan, S.R. Shukla, Raman, FT-IR spectroscopic analysis and first order hyperpolarizability of 3-benzoyl-5-chlorouracil by first principles, *J. Mol. Simul.* 37 (2011) 153–163.
- [75] E.D. Glendening, A.E. Reed, J.E. Carpenter, F. Weinhold, NBO version 3.1, Pittsburgh, Theoretical Chemistry Institute and Department of Chemistry, University of Wisconsin, Madison, 1988.
- [76] J. Chocholousova, V. Vladimír spírk, Hobza First local minimum of th formic acid dimer exhibits simultaneously red-shifted O-H ...O and improper blue-shifted C-H...O hydrogen bonds, *P. Phys. Chem. Chem. Phys.* 6 (2004) 37–41.

- [77] R.G. Parr, W. Yang, *Functional Theory of Atoms and Molecules*, Oxford University press, New York, 1989.
- [78] P.W. Ayers, R.G. Parr, Variational principals for describing chemical reactions: the Fukui function and chemical hardness revisited, *J. Am. Chem. Soc.* 122 (2000) 2010–2018.
- [79] P.K. Chattaraj, B. Maiti, U. Sarkar, Philicity: a unified treatment of chemical reactivity and selectivity, *J. Phys. Chem.* 107 (2003) 4973–4975.
- [80] E.R. Johnson, S. Keinan, P. Mori-Sanchez, J. Contreras-Garcia, A.J. Cohen, W. Yang, Revealing noncovalent interactions, *J. Am. Chem. Soc.* 132 (2010) 6498–6506.
- [81] O. Trott, A.J. Olson, AutoDock Vina: improving the speed and accuracy of docking with a new scoring function, efficient optimization and multithreading, *J. Comput. Chem.* 31 (2010) 455–461.



Sources

Publisher

Publisher: Annals Romanian Society Cell Biology x

i Improved Citescore

We have updated the CiteScore methodology to ensure a more robust, stable and comprehensive metric which provides an indication of research impact, earlier. The updated methodology will be applied to the calculation of CiteScore, as well as retroactively for all previous CiteScore years (ie. 2018, 2017, 2016...). The previous CiteScore values have been removed and are no longer available.

[View CiteScore methodology.](#) >



Filter refine list

Apply Clear filters

1 result

All Export to Excel Save to source list

[Download Scopus Source List](#) [Learn more about Scopus Source List](#)

View metrics for year: 2019

Display options

Display only Open Access journals

Counts for 4-year timeframe

No minimum selected

Minimum citations

Source title ↓

CiteScore ↓ Highest percentile ↓

Citations 2016-19 ↓ Documents 2016-19 ↓ % Cited ↓

<input type="checkbox"/> 1	Annals of the Romanian Society for Cell Biology	0.3	3%	10	39	18
			167/172			
			Physiology			



Molecular Docking, Vibrational, Structural and Electronic Studies of 5-(4-Butoxybenzylidene)-2-[3-(4-Chlorophenyl)-5[4-(Propan-2-Yl)-4,5-Dihydro-1H-Pyrazol-1-Yl]-1,3-Thiazol-4(5H)-One

K.Venil^a, A.Lakshmi^a, V. Balachandran^b

^a Department of Physics, Government Arts College (Affiliated to Bharathidasan University), Trichy 621 222, TN, India.

^b Centre for Research, Department of Physics, Arignar Anna Government Arts College, Musiri ,621 211, TN, India

Abstract

Spectroscopic and structural investigations of 5-(4-Butoxybenzylidene)-2-[3-(4-chlorophenyl)-5[4-(propan-2-yl)-4, 5-dihydro-1H-pyrazol-1-yl]-1,3-thiazol-4(5H)-one are presented by using experimental (FT-IR and FT-Raman) spectra and theoretical (Density functional theory) calculations. The optimized geometrical assignments were made on the basis of potential energy distribution. The molecular electrostatic potential map was used to detect the electrophilic and nucleophilic sites in the molecule. The directly calculated ionization potential (I), electron affinity (A), electronegativity (χ), electrophilic index (ω), hardness (η) and chemical potential (μ) are all correlated from HOMO-LUMO energies with their molecular properties. The reduced density gradient of the title molecule was investigated by the interaction of molecule. Molecular docking studies were also described.

Keywords:DFT, Thiazole, Reduced Density Gradient and Docking.

1. Introduction

Thiazole is a heterocyclic compound that contains both sulphur and nitrogen and a large family of derivatives. Thiazole itself is a pale yellow liquid with a pyridine-like odor and they have extensive applications in agriculture and medicinal chemistry [1, 2]. Varieties of biologically active molecules accommodate the thiazole and its derivatives, aminothiazoles [3]. They are used as important fragments in different drugs related to anti-tuberculosis, anti-inflammatory, [4, 5, 6], anti-allergic [7], anti-hypertensive [8], schizophrenia [9], anti-bacterial, HIV infections [4, 10] and human

lymphatic filarial parasites [11]. Various thiazole derivatives are used as fungicides and herbicides and have numerous applications in agricultural field [12]. Hydantoin derivatives, in particular phenytoin, are important antiepileptic drugs.

In the present work, optimized molecular structure of the title compound is investigated. The vibrational spectroscopic investigations combined with DFT (Density functional theory) calculations are employed to provide comprehensive vibrational spectral assignments of the title compound. The molecular properties like dipole moment, polarizability, hyper polarizability and molecular electrostatic potential surface have been calculated to get a better understanding the properties of the title molecule. The non-covalent interactions like hydrogen bonding and Van der Waals interaction were identified from the molecular geometry and electron localization function. These interactions in molecules have been studied by using reduced density gradient (RDG) and graphed by Multiwfn. Molecular docking is a computer-assisted drug design (CADD) method used to predict the favourable orientation of a ligand (viz. drug) to a target (viz. receptor) when bound to each other to form a stable complex.

2. Experimental details

5-(4-Butoxybenzylidene)-2-[3-(4-chlorophenyl)-5[4-(propan-2-yl)-4, 5-dihydro-1H-pyrazol-1-yl]-1,3-thiazol-4(5H)-one was synthesized as per the reported procedure [13-15]. The Fourier Transform infrared (FT-IR) spectrum of the title compound was recorded using Perkin Elmer Spectrometer fitted with a KBr beam splitter around $4000-450\text{ cm}^{-1}$. The Bruker RFS 27 FT-Raman spectrometer in the region $4000-0\text{ cm}^{-1}$ using a 1064 nm Nd:YAG laser source was used to reported the FT-Raman spectrum. Both the spectral measurements were performed at the Sophisticated Analytical Instrumentation Facility (SAIF), IIT, Madras, India.

3. Computational details

All calculations of the title compound were carried out using Gaussian 09 program [16] was performed with Becke's three-parameter hybrid model and therefore the Lee-Yang-Parr correlation was a useful functional (B3LYP) in DFT [17, 18] technique. The electronic structure of the molecule has to be proven with the density functional theory. The visual representations for fundamental modes are also checked by the Gauss view program [19]. Electron density map and reduced density

gradient (RDG) were calculated with the use of Multiwfn program [20] and plotted by visual molecule dynamics program (VMD) [21]. The reactivity descriptors, such as electrophilicity (ω), global hardness (η), the chemical potential (μ), ionization potential (I) and electron affinity (A) were determined from the energies of frontier molecular orbitals. The molecular docking calculation was performed by the AutoDock 4.0.1 software [22], which was also applied to detect the docking input files and analyze the docking result. Using Discovery studio visualize software, one of the best active site was visualized for ligand-protein interaction.

4.0 Results and discussions

4.1 Optimized molecular geometrical parameters

The geometrical structure and parameters of 5-(4-Butoxybenzylidene)-2-[3-(4-chlorophenyl)-5[4-(propan-2-yl)-4,5-dihydro-1H-pyrazol-1-yl]-1,3-thiazol-4(5H)-one are depicted in Figure 1 and Table 1 by using B3LYP/6-31G and B3LYP/6-31G (d,p) methods.

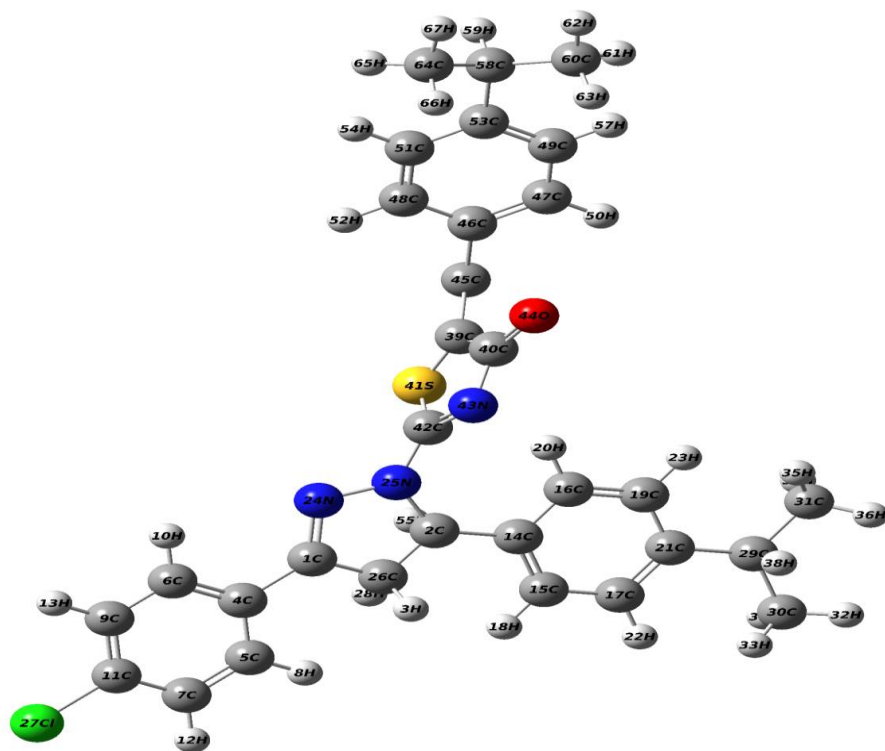


Figure 1: Optimized molecular structure of 5-(4-Propan-2-yl)benzylidene)-2-[3-(4-chlorophenyl)-5[4-(propan-2-yl)phenyl-4,5-dihydro-1H-pyrazol-1-yl]-1,3-thiazol-4(5H)-one

Table 1: Optimized structural parameters of 5-(4-Butoxybenzylidene)-2-[3-(4-chlorophenyl)-5[4-(propan-2-yl)-4,5-dihydro-1H-pyrazol-1-yl]-1,3-thiazol-4(5H)-one obtained by B3LYP/6-31G and B3LYP/6-31G (d,p) basis sets.

Parameters	Bond length (Å)		Parameters	Bond angle(°)		Parameters	Dihedral angle(°)	
	B3LYP/6-31G	B3LYP/6-31G(D,P)		B3LYP/6-31G	B3LYP/6-31G(d,p)		B3LYP/6-31G	B3LYP/6-31G(D,P)
C1-C4	1.4604	1.4628	C4-C1-N24	121.7147	121.788	N24-C1-C4-C5	179.171	178.663
C1-N24	1.3062	1.294	C4-C1-C26	125.171	125.091	N24-C1-C4-C6	-0.574	-1.023
C1-C26	1.5223	1.5184	N24-C1-C26	113.104	113.11	C26-C1-C4-C5	0.425	-0.056
C1-C14	1.5184	1.5174	C14-C2-N25	112.3446	112.421	C26-C1-C4-C6	-179.319	-179.743
C2-N25	1.5078	1.4931	C14-C2-C26	115.1468	114.938	C4-C1-N24-N25	-179.833	179.898
C2-C26	1.5576	1.5519	C14-C2-N25	109.2771	109.088	C26-C1-N24-N25	-0.948	-1.241
C2-H55	1.0919	1.0919	N25-C2-C26	100.1893	100.201	C4-C1-N26-C2	-174.604	-174.939
H3-C26	1.0937	1.0932	N25-C2-H55	107.2673	107.668	C4-C1-C26-H3	-54.509	-54.804
C4-C5	1.4082	1.4042	C26-C2-H55	121.7147	121.788	C4-C1-C26-H28	65.533	65.160
C4-C6	1.4121	1.4083	C1-C4-C5	125.171	125.091	N24-C1-C26-C2	6.557	6.245
C5-C7	1.3979	1.3933	C1-C4-C6	113.104	113.11	N24-C1-C26-H3	126.652	126.379
C5-C8	1.0844	1.0852	C5-C4-C6	112.3446	112.421	N24-C1-C26-H28	-113.306	-113.657
C6-C9	1.3932	1.3882	C4-C5-C7	115.1468	114.9386	N25-C2-C14-C15	68.304	64.354

C6-H10	1.0835	1.0843	C4-C5-H8	109.2771	109.088	N25-C2- C14-C16	-111.460	-115.788
C7-C11	1.392	1.3929	C7-C5-H8	100.1893	100.201	C26-C2- C14-C15	-45.540	-49.422
C7-H12	1.0829	1.084	C4-C6-C9	107.2673	107.668	C26-C2- C14-C16	134.697	130.437
C9-C11	1.3963	1.3978	C4-C6-H10	121.7147	121.788	H55-C2- C14-C15	-172.766	-176.292
C9-H13	1.083	1.0842	C9-C6-H10	125.171	125.091	H55-C2- C14-C16	7.471	3.566
C11-C127	1.8237	1.7554	C5-C7-C11	113.104	113.11	C14-C2- N25-N24	-113.650	-114.317
C14-C15	1.4058	1.4019	C5-C7-H12	112.3446	112.421	C14-C2- N25-C42	69.525	71.318
C14-C16	1.4006	1.3959	C11-C7- H12	115.1468	114.938	C26-C2- N25-N24	9.079	8.210
C15-C17	1.3957	1.3917	C6-C9-C11	109.2771	109.088	C26-C2- N25-C42	-167.745	-166.155
C15-H18	1.0867	1.0872	C6-C9-H13	100.1893	100.201	H55-C2- N25-N24	126.247	125.504
C16-C19	1.3982	1.3951	C11-C9- H13	107.2673	107.668	H55-C2- N25-C42	-50.578	-48.861
C16-H20	1.0849	1.0859	C7-C11-C9	121.7147	121.788	C14-C2- C26-C1	112.154	112.861
C17-C21	1.4076	1.4037	C7-C11- C127	125.171	125.091	C14-C2- C26-C3	-8.727	-7.907
C17-C22	1.086	1.0865	C9-C11- C127	113.104	113.11	C14-C2- C26-H28	-128.840	-128.348
C19-C21	1.4035	1.399	C2-C14- C15	112.3446	112.421	N25-C2- C26-C1	-8.582	-7.874
C19-H23	1.0862	1.087	C2-C14- C16	115.1468	114.939	N25-C2- C26-C3	-129.463	-128.642

C21-C29	1.5261	1.5226	C15-C14-C16	109.2771	109.088	N25-C2-C26-H28	110.424	110.917
N24-N25	1.3915	1.37	C14-C15-C17	100.1893	100.201	H55-C2-C26-C1	-122.075	-121.822
N25-C42	1.3483	1.3513	C14-C15-H18	107.2673	107.668	H55-C2-C26-C3	117.044	117.409
C26-H28	1.0969	1.096	C17-C15-H18	121.7147	121.788	H55-C2-C26-H28	-3.069	-3.032
C29-C30	1.5465	1.5402	C14-C16-C19	125.171	125.091	C1-C4-C5-C7	-179.695	-179.612
C29-C30	1.546	1.5402	C14-C16-H20	113.104	113.11	C1-C4-C5-H8	0.260	0.318
C29-H38	1.0993	1.0978	C19-C16-H20	112.3446	112.421	C6-C4-C5-C7	0.054	0.082
C30-H32	1.0965	1.0953	C15-C17-C21	115.1468	114.938	C6-C4-C5-C8	-179.991	-179.988
C30-H33	1.0953	1.094	C15-C17-H22	109.2771	109.088	C1-C4-C6-C9	179.712	179.627
C30-H34	1.0968	1.0955	C21-C17-H22	100.1893	100.201	C1-C4-C6-H10	-0.241	-0.339
C31-H35	1.0956	1.0944	C16-C19-C21	107.2673	107.668	C5-C4-C6-C9	-0.037	-0.066
C31-H36	1.0966	1.0954	C16-C19-H23	121.7147	121.788	C5-C4-C6-H10	-179.990	179.968
C31-H37	1.0968	1.0956	C21-C19-H23	125.171	125.091	C4-C5-C7-C11	-0.039	-0.047
C39-C40	1.493	1.5081	C17-C21-C19	113.104	113.11	C4-C5-C7-H12	179.976	179.971
C39-S41	1.8656	1.794	C17-C21-C29	112.3446	112.421	H8-C5-C7-C11	-179.994	-179.978
C39-C45	1.3602	1.3596	C19-C21-C29	115.1468	114.939	H8-C5-C7-H12	0.020	0.040

C40-N43	1.4066	1.3966	C1-N24-N25	109.2771	109.088	C4-C6-C9-C11	0.006	0.015
C40-O44	1.2485	1.2232	C2-N25-N24	100.1893	100.201	C4-C6-C9-H13	-179.979	-179.983
S41-C42	1.8391	1.776	C2-N25-C42	107.2673	107.668	H10-C6-C9-C11	179.958	179.981
C42-N43	1.3043	1.2987	N24-N25-C42	121.7147	121.788	H10-C6-C9-H13	-0.027	-0.018
C45-C46	1.4585	1.4571	C1-C26-C2	125.171	125.091	C5-C7-C11-C9	0.006	-0.006
C45-C56	1.0902	1.0904	C1-C26-H3	113.104	113.11	C5-C7-C11-C127	-179.973	-179.967
C46-C47	1.416	1.4105	C1-C26-H28	112.3446	112.421	H12-C7-C11-C9	179.992	179.977
C46-C48	1.4198	1.4156	C2-C26-H3	115.1468	114.939	H12-C7-C11-C127	0.013	0.016
C47-C49	1.3931	1.3906	C2-C26-H28	109.2771	109.088	C6-C9-C11-C7	0.010	0.021
C47-H50	1.0867	1.0872	H3-C26-H28	100.1893	100.201	C6-C9-C11-C127	179.989	179.982
C48-C51	1.3882	1.3839	C21-C29-C30	107.2673	107.668	H13-C9-C11-C7	179.995	-179.980
C48-H52	1.0817	1.082	C21-C29-C31	121.7147	121.788	H13-C9-C11-C127	-0.026	-0.019
C49-C53	1.4036	1.4017	C21-C29-H38	125.171	125.091	C2-C14-C15-C17	179.751	179.385
C49-H57	1.0828	1.0831	C30-C29-C31	113.104	113.11	C2-C14-C15-H18	-0.979	-1.326
C51-C53	1.4054	1.4049	C30-C29-H38	112.3446	112.421	C16-C14-C15-C17	-0.483	-0.476
C51-H54	1.0837	1.0851	C31-C29-H38	115.1468	114.939	C16-C14-C15-H18	178.787	178.813

C53-O58	1.3842	1.3595	C29-C30-H32	109.2771	109.088	C2-C14-C15-C19	-179.424	-179.063
O58-C59	1.4618	1.4285	C29-C30-H33	100.1893	100.201	C2-C14-C16-H20	2.293	2.184
C59-H60	1.0988	1.0996	C29-C30-H34	107.267	107.668	C15-C14-C16-C19	0.806	0.799
C59-H61	1.0988	1.0996	C40-C39-C45	113.104	113.11	C15-C14-C16-H20	-177.477	-177.954
C59-C62	1.5233	1.5217	S41-C39-C45	118.135	118.670	C14-C15-C17-C21	-0.126	-0.137
C62-H63	1.0976	1.0969	C39-C40-N43	113.471	112.705	C14-C15-C17-H22	179.731	179.737
C62-H64	1.0976	1.0969	C39-C40-O44	124.813	124.954	H18-C15-C17-C21	-179.403	-179.432
C62-C65	1.5402	1.5336	N43-C40-O44	121.716	122.339	H18-C15-C17-H22	0.454	0.442
C65-H66	1.1	1.0984	C39-S41-C42	86.313	87.757	C14-C16-C19-C21	-0.532	-0.522
C65-H67	1.1	1.0984	N25-C42-S41	119.688	119.294	C14-C16-C19-H23	-179.815	-179.889
C65-C68	1.5369	1.5315	N25-C42-N43	122.861	122.033	H20-C16-C19-C21	177.745	178.228
C68-H69	1.0969	1.0956	S41-C42-N43	117.447	118.672	H20-C16-C19-H23	-1.538	-1.139
C68-H70	1.0958	1.0945	C40-N43-C42	113.818	112.104	C15-C17-C21-C19	0.407	0.421
C68-H71	1.0969	1.0956	S41-C39-C45	118.135	118.670	C15-C17-C21-C29	179.921	-179.872

For the title compound, the C-C bond length for pyrazole ring of C1-C26, C2-C26 are 1.5223/1.5184, 1.5576/1.5519 Å, for thiazole ring for C39-C40 is 1.493/1.5081 Å for the B3LYP/6-31G and B3LYP/6-31G (d,p) methods and these values are in between the single and double bond (1.54 Å and 1.33 Å) [23]. In the present work, the C-O bond length are observed at

C40-O44=1.2485/1.2232 Å, C53-O58 = 1.3842 / 1.3595Å, O58-C59=1.4618/1.4285Å which are in good agreement with the reported values for a similar derivatives (1.3871 Å and 1.3653 Å) [24]. The C-N bond length for the title compound are C1-N24, C2-N25, N25-C42, C40-N43, C42-N43 are 1.3062/1.294 Å, 1.5078/1.4931 Å, 1.3483/1.3513 Å, 1.4066/1.3966 Å, 1.3043/1.2987 Å which are in agreement with the literature [25]. The C-S bond length for the title compound are 1.8656/1.794 Å for C39-S41 and for S41-C42 is 1.8656/1.794 Å, 1.8391 /1.776 Å and is similar to Kuruvilla et.al [26] observed the C-S value at C5-S9= 1.748 Å and C8-S9=1.733 Å theoretically and experimentally at 1.8642, 1.862 Å. In the case of C-H bond lengths, (DFT/XRD) it is observed that aromatic C-H bonds measure 1.10/1.09 Å, which is equal to the experimental value. For the title compound, the bond lengths for C2-H55, C6-H10, C9-H13, C31-H35, C47-H50, C65-H66, C68-H70, C68-H71 are 1.0919/1.0919, 1.0835/1.0843, 1.083/1.0842, 1.0956/1.0944, 1.0867/1.0872, 1.1/1.0984, 1.0958/1.0945 and 1.0969/1.0956 Å observed. It was also very confined to experimental value [27]. The N-N bond lengths (DFT/XRD) are reported in the range 1.3409-1.3886Å [28] and in the present case (BPT1), the N-N bond length is found at 1.3915/1.37 Å for N24-N25. The thiazole ring is tilted from the phenyl ring as is evident from the torsion angles C45-C39-C40-N43=179.99/179.97°, S41-C39-C40-H43 = -0.1457/-0.2921°, C40-C39-S41-C42= 0.3713/ 0.414° and C45-C39-S41-C42= -179.74/-179.81°.

For the title compound, the interactions between the thiazole and pyrazole groups are C40-C39-C45 = 132.917/132.571, S41-C39-C45 = 118.135/118.669, C39-C40-N43 = 113.471 /112.705, C39-C40-O44 = 124.813 / 124.954, N43-C40-O44 = 121.716/ 122.339, C39-S41-C42 = 86.313/87.757, N25-C42-S41= 119.688/119.294, N25-C42-N43 = 122.861 / 122.033, S41-C42-N43 = 117.447/118.672, C40-N43-C42 = 113.818 / 112.104 respectively.

4.2 Vibrational assignments

The title compound is consist of 71 atoms and has 207 fundamental modes of vibrations. The observed and simulated FT-IR and FT-Raman spectra of 5-(4-Butoxybenzylidene)-2-[3-(4-chlorophenyl)-5[4-(propan-2-yl)-4,5-dihydro-1H-pyrazol-1-yl]-1,3-thiazol-4(5H)-one at B3LYP level using 6-31G and 6-31G(d,p) basis sets are shown in Figures 2 and 3. The elaborated vibrational assignments of the title compound along with the calculated IR and Raman frequencies and normal mode descriptions are given in Table 2.

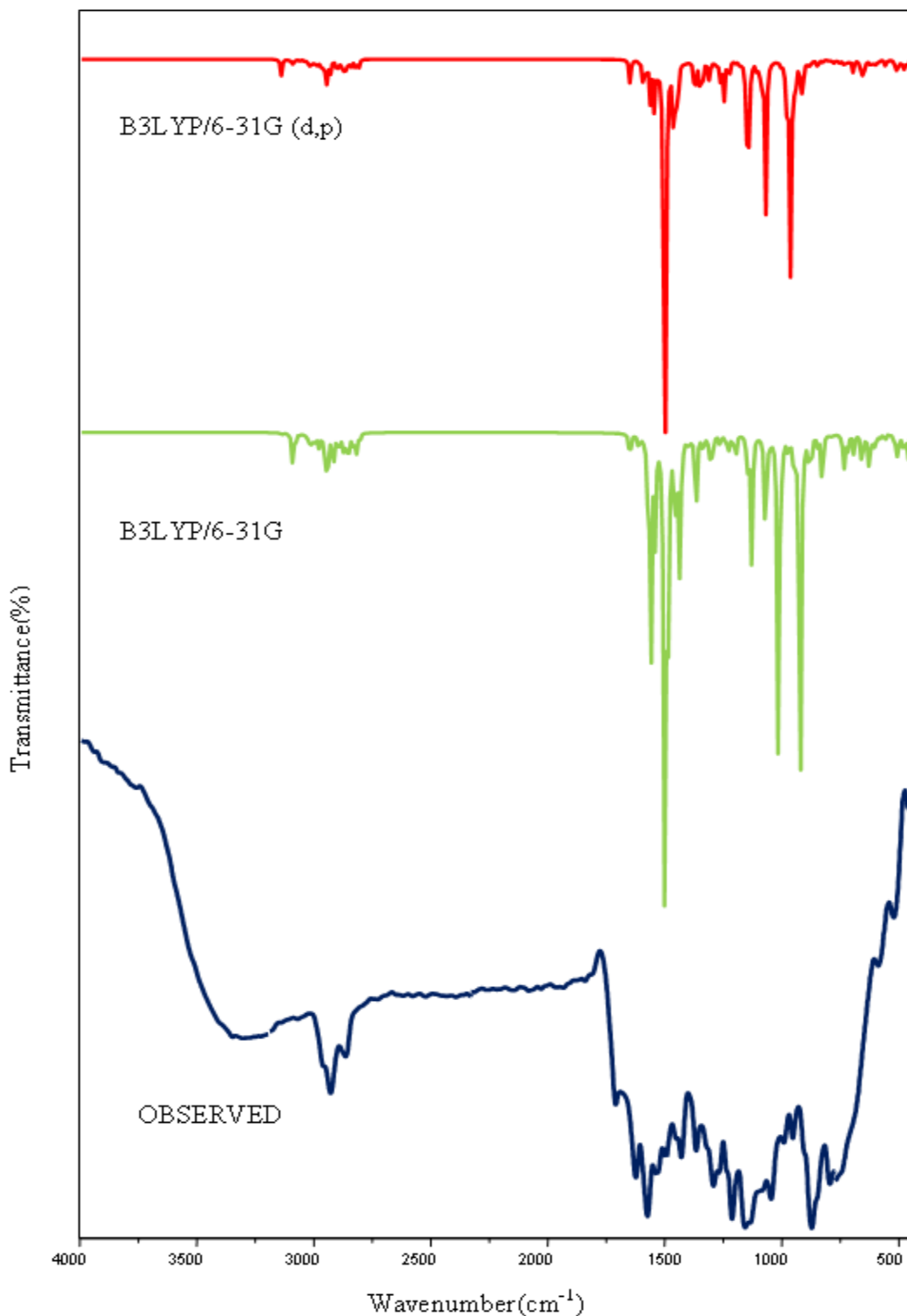


Figure 2: Observed FT-IR and simulated spectra of 5-(4-Butoxybenzylidene)-2-[3-(4-chlorophenyl)-5[4-(propan-2-yl)-4,5-dihydro-1H-pyrazol-1-yl]-1,3-thiazol-4(5H)-one

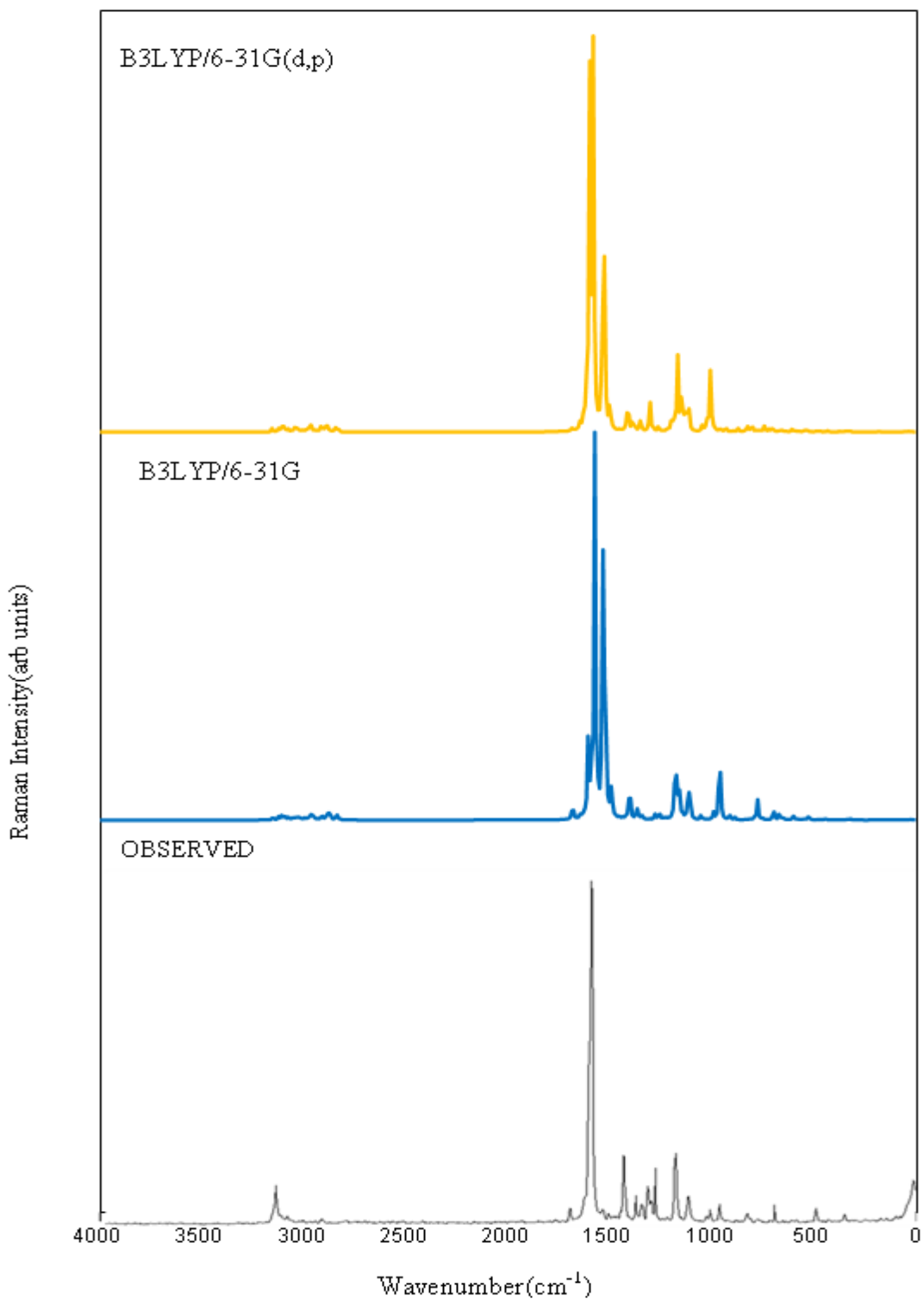


Figure 3: Observed FT-Raman and simulated spectra of 5-(4-Butoxybenzylidene)-2-[3-(4-chlorophenyl)-5[4-(propan-2-yl)-4,5-dihydro-1H-pyrazol-1-yl]-1,3-thiazol-4(5H)-one

Table 2: Vibrational assignments of 5-(4-Butoxybenzylidene)-2-[3-(4-chlorophenyl)-5[4-(propan-2-yl)-4,5-dihydro-1H-pyrazol-1-yl]-1,3-thiazol-4(5H)-one one by B3LYP/6-31G and B3LYP/6-31G (d,p) basis sets.

Modes	Observed wavenumbers (cm ⁻¹)		Calculated wavenumbers(cm ⁻¹)		Vibrational assignments
	FT-IR	FT-Raman	B3LYP/6-31G	B3LYP/6-31G(d,p)	
1		3150	3156	3152	νCH(98)
2			3125	3123	νCH(98)
3			3110	3107	νCH(98)
4			3099	3095	νCH(98)
5			3094	3088	νCH(98)
6		3075	3078	3074	νCH(98)
7			3058	3055	νCH(98)
8			3045	3043	νCH(98)
9			3038	3034	νCH(98)
10			3033	3029	νCH(98)
11			3026	3021	νCH(98)
12			3016	3011	νCH(98)
13		3002	3010	3003	νCH(98)
14			3001	2995	ν _{ass} CH ₃ (96)
15			2986	2983	ν _{ass} CH ₃ (97)
16			2976	2971	ν _{ass} CH ₃ (97)
17			2970	2966	ν _{ass} CH ₂ (95)
18			2964	2959	ν _{ass} CH ₃ (96)
19			2950	2947	ν _{ass} CH ₃ (97)
20			2936	2935	νCH(98)

21	2922		2930	2926	$\nu_{\text{assCH}_3}(98)$
22			2922	2919	$\nu_{\text{assCH}_2}(96)$
23		2910	2915	2912	$\nu_{\text{ssCH}_2}(96)$
24			2910	2906	$\nu_{\text{assCH}_2}(97)$
25			2896	2893	$\nu_{\text{ssCH}_2}(96)$
26			2888	2884	$\nu_{\text{ssCH}_3}(97)$
27			2882	2878	$\nu_{\text{ssCH}_3}(96)$
28			2872	2869	$\nu_{\text{assCH}_2}(97)$
29	2856		2860	2854	$\nu_{\text{ssCH}_3}(96)$
30			2846	2843	$\nu_{\text{CH}}(98)$
31			2841	2835	$\nu_{\text{ssCH}_2}(96)$
32			2830	2822	$\nu_{\text{ssCH}_2}(96)$
33	1679	1680	1683	1680	$\nu_{\text{CO}}(72), \nu_{\text{CC}}(20)$
34			1644	1641	$\nu_{\text{CC}}(70), \delta_{\text{CH}}(18)$
35			1625	1623	$\nu_{\text{CC}}(71), \delta_{\text{CH}}(20)$
36			1613	1604	$\nu_{\text{CC}}(70), \delta_{\text{CH}}(22)$
37	1591		1596	1590	$\nu_{\text{CC}}(68), \nu_{\text{CN}}(12), \delta_{\text{CH}}(10)$
38			1579	1572	$\nu_{\text{CN}}(65), \nu_{\text{CC}}(14), \delta_{\text{CH}}(10)$
39			1563	1559	$\nu_{\text{CC}}(64), \delta_{\text{CH}}(14), \delta_{\text{CC}}(11)$
40			1538	1533	$\nu_{\text{CC}}(60), \delta_{\text{CCl}}(18), \nu_{\text{CN}}(10)$
41	1541		1533	1529	$\nu_{\text{CN}}(65), \nu_{\text{CC}}(15), \delta_{\text{CH}}(12)$
42			1525	1517	$\nu_{\text{CN}}(65), \nu_{\text{CC}}(16), \delta_{\text{CH}}(12)$
43	1506	1510	1512	1508	$\delta_{\text{CH}}(64), \nu_{\text{CC}}(18)$

44			1499	1493	$\delta\text{CH}(64)$, $\nu\text{CC}(20)$
45	1485	1485	1490	1486	$\delta\text{CH}(65)$, $\nu\text{CC}(18)$
46			1481	1475	$\delta_{\text{opb}} \text{CH}_3(72)$
47			1477	1470	$\delta_{\text{opb}} \text{CH}_3(75)$
48			1472	1466	$\delta_{\text{opb}} \text{CH}_3(73)$
49			1455	1451	$\delta_{\text{ipb}} \text{CH}_3(73)$
50			1442	1436	$\delta_{\text{ipb}} \text{CH}_3(72)$
51			1437	1430	$\delta_{\text{ipb}} \text{CH}_3(72)$
52			1429	1422	$\sigma_{\text{sci}} \text{CH}_2(80)$
53		1415	1423	1415	$\sigma_{\text{sci}} \text{CH}_2(80)$
54			1420	1408	$\delta\text{CH}(65)$, $\nu\text{CC}(21)$
55			1414	1403	$\delta\text{CH}(66)$, $\nu\text{CC}(22)$
56		1400	1408	1399	$\sigma_{\text{sci}} \text{CH}_2(80)$
57	1394		1402	1395	$\sigma_{\text{sci}} \text{CH}_2(81)$
58			1388	1383	$\delta_{\text{sb}} \text{CH}_3(75)$
59			1385	1379	$\delta_{\text{sb}} \text{CH}_3(75)$
60			1376	1370	$\delta_{\text{sb}} \text{CH}_3(74)$
61			1370	1362	$\nu\text{CN}(64)$
62		1350	1356	1351	$\nu\text{CN}(65)$, $\delta\text{CH}(14)$
63			1346	1342	$\delta\text{CO}(67)$
64	1329		1335	1330	$\delta\text{CH}(67)$
65			1327	1323	$\delta\text{CH}(68)$
66		1310	1318	1312	$\delta\text{CH}(66)$, $\nu\text{CC}(14)$
67			1308	1302	$\delta\text{CH}(66)$, $\nu\text{CC}(15)$
68		1295	1301	1297	$\nu\text{CO}(66)$, $\delta\text{CH}(12)$
69		1280	1285	1281	$\delta\text{CH}(66)$, $\nu\text{CC}(12)$

70			1278	1275	$\delta\text{CH}(66)$, $\nu\text{CC}(12)$, $\nu\text{CN}(10)$
71			1266	1263	$\delta\text{CH}(64)$, $\nu\text{CN}(18)$, $\nu\text{CC}(10)$
72	1254	1250	1260	1254	$\nu\text{CO}(65)$, $\delta\text{CH}(17)$, $\nu\text{Ccl}(10)$
73			1248	1244	$\delta\text{CH}(66)$, $\nu\text{CC}(12)$, $\nu\text{CN}(10)$
74	1230		1236	1231	$\nu\text{CC}(63)$, $\delta\text{CH}(16)$, $\nu\text{CN}(12)$
75		1215	1221	1217	$\nu\text{CC}(65)$, $\delta\text{CH}(18)$
76			1214	1207	$\rho\text{rockCH}_2(70)$, $\delta\text{CH}(12)$
77		1200	1210	1200	$\rho\text{rockCH}_2(70)$, $\delta\text{CH}(12)$
78			1195	1191	$\nu\text{CC}(65)$, $\delta\text{CH}(14)$
79			1186	1182	$\nu\text{CC}(66)$, $\delta\text{CH}(15)$
80	1173		1179	1175	$\rho\text{rockCH}_2(70)$
81			1165	1163	$\rho\text{rockCH}_2(69)$
82			1162	1158	$\nu\text{CC}(68)$
83			1145	1143	$\nu\text{CC}(68)$
84			1140	1136	$\nu\text{CC}(68)$
85			1131	1127	$\nu\text{CC}(66)$
86	1118		1125	1120	$\nu\text{CC}(66)$
87			1118	1113	$\tau\text{CH}_2(75)$
88			1110	1105	$\tau\text{CH}_2(75)$
89			1102	1097	$\gamma\text{CH}(60)$
90			1093	1088	$\gamma\text{CH}(60)$
91			1080	1075	$\nu\text{CC}(65)$, $\delta\text{CH}(13)$
92			1056	1051	$\tau\text{CH}_2(75)$

93			1044	1040	$\tau\text{CH}_2(74)$
94			1032	1028	$\gamma\text{opr CH}_3(62)$, $\nu\text{CC}(10)$
95			1021	1017	$\gamma\text{opr CH}_3(63)$, $\nu\text{CC}(10)$
96			1013	1009	$\nu\text{CC}(74)$, $\nu\text{CO}(16)$
97	1002		1003	1000	$\gamma\text{opr CH}_3(64)$
98			992	989	$\nu\text{CC}(66)$, $\delta\text{CH}(15)$
99			984	980	$\delta\text{CO}(66)$, $\delta\text{CH}(14)$
100			965	963	$\delta\text{CO}(65)$, $\delta\text{CH}(12)$
101			960	956	$\gamma\text{CH}(58)$, $\gamma_{\text{ring}}(26)$
102	948	950	953	948	$\gamma\text{CH}(58)$, $\gamma_{\text{ring}}(26)$
103			935	933	$\gamma\text{CH}(58)$, $\gamma_{\text{ring}}(25)$
104			932	929	$\gamma\text{CH}(58)$, $\gamma_{\text{ring}}(21)$
105			925	921	$\nu\text{CC}(72)$, $\nu\text{CO}(15)$, $\delta\text{CH}(10)$
106			924	916	$\nu\text{CC}(63)$, $\delta\text{CH}(18)$
107	909	910	914	910	$\nu\text{CC}(64)$, $\delta\text{CH}(20)$
108			889	885	$\gamma\text{CH}(58)$, $\gamma_{\text{ring}}(18)$
109			883	879	$\nu\text{NN}(65)$, $\delta\text{CH}(18)$
110			867	865	$\gamma\text{CH}(55)$, $\gamma\text{CC}(18)$
111			845	842	$\gamma\text{CC}(18)$, $\delta\text{wagg CH}_2(12)$
112			840	834	$\gamma\text{CH}(62)$, $\gamma_{\text{ring}}(18)$
113	827		833	829	$\gamma\text{CH}(58)$, $\gamma\text{CC}(21)$
114			823	820	$\gamma\text{CH}(58)$, $\gamma\text{CC}(20)$
115			817	812	$\delta_{\text{wagg}} \text{CH}_2(58)$, $\gamma\text{CC}(20)$
116		800	805	802	$\delta_{\text{wagg}} \text{CH}_2(58)$, $\gamma\text{CC}(21)$
117			800	795	$\gamma\text{CH}(56)$, $\gamma\text{CC}(18)$

118			796	790	γ CH(55), γ CC(17)
119			792	786	δ CC(63), δ CH(18)
120			785	780	δ_{wagg} CH ₂ (57)
121			779	773	γ CH(58), γ_{ring} (18)
122			775	769	δ_{wagg} CH ₂ (58), γ CC(20)
123			768	765	δ_{ipr} CH ₃ (68)
124			760	756	δ_{ipr} CH ₃ (68)
125	747		741	748	δ_{ipr} CH ₃ (68)
126			738	731	ν CS(74), δ CH(20)
127		720	726	720	ν CN(64), ν CC(16)
128			715	711	δ CC(60), δ_{ipr} CH ₃ (19)
129			706	700	γ CH(58), γ_{ring} (16)
130			697	694	ν CS(75), δ CH(20)
131			690	688	δ CC(60), δ_{ipr} (17)
132			685	679	γ CO(58)
133			670	666	γ CC(68)
134			664	659	γ CC(68)
135			658	655	γ CC(68)
136			653	648	δ_{ring} (56)
137			646	643	δ_{ring} (56)
138			640	638	δ_{ring} (56)
139			635	631	γ CC(66)
140			630	626	γ CO(51), γ_{ring} (17)
141			625	620	γ CO(50), γ_{ring} (17)
142			616	612	δ CC(58)
143			608	603	δ CC(59)

144	597		602	598	$\cup\text{CCI}(68), \delta_{\text{ring}}(25)$
145			590	586	$\delta\text{CC}(58)$
146			588	580	$\delta_{\text{ring}}(52)$
147			575	573	$\delta\text{CC}(58)$
148			565	561	$\delta\text{CC}(58)$
149	551		553	550	$\delta_{\text{ring}}(52)$
150			545	541	$\delta_{\text{ring}}(53)$
151			539	535	$\delta\text{CC}(59)$
152			531	523	$\delta_{\text{ring}}(52)$
153			522	518	$\delta_{\text{ring}}(50)$
154			510	506	$\delta\text{CC}(58)$
155	503	502	503	500	$\delta\text{CC}(58)$
156			487	481	$\delta_{\text{ring}}(54)$
157			477	472	$\delta\text{CC}(59)$
158			480	466	$\delta\text{CC}(59)$
159	457		463	460	$\delta_{\text{ring}}(55)$
160	438		445	440	$\delta\text{CCI}(60), \delta_{\text{ring}}(15)$
161			427	422	$\delta_{\text{ring}}(52)$
162	411		417	410	$\delta_{\text{ring}}(54)$
163			407	401	$\delta_{\text{ring}}(50)$
164			392	389	$\delta_{\text{ring}}(52)$
165			381	375	$\delta_{\text{ring}}(52)$
166			371	366	$\delta\text{CC}(53)$
167			360	354	$\delta\text{CC}(54)$
168		345	349	345	$\delta\text{CC}(54)$
169			337	332	$\delta\text{CC}(54)$

170			330	325	$\gamma_{CC}(55)$
171			319	314	$\gamma_{CC}(54)$
172			303	299	$\gamma_{CC}(53)$
173			296	293	$\gamma_{CC}(55)$
174			291	286	$\gamma_{CC}(54)$
175			280	275	$\gamma_{CCl}(55)$
176			273	268	$\gamma_{CC}(50)$
177			262	259	$\gamma_{CC}(54)$
178			246	242	$\gamma_{CC}(50)$
179			230	221	$\tau_{CH_3}(55)$
180			218	212	$\tau_{CH_3}(54)$
181			210	206	$\tau_{CH_3}(54)$
182			197	191	$\gamma_{CC}(55)$
183			189	185	$\gamma_{CC}(55)$
184			176	173	$\gamma_{CC}(55)$
185			166	162	$\delta_{ring}(58)$
186		150	158	151	$\gamma_{CC}(55)$
187			146	142	$\delta_{ring}(55)$
188		135	141	136	$\gamma_{CC}(56)$
189			135	128	$\gamma_{ring}(56)$
190		120	126	120	$\gamma_{CC}(56)$
191			112	102	$\delta_{ring}(53)$
192		92	95	89	$\gamma_{ring}(54)$
193			86	79	$\gamma_{ring}(53)$
194			80	74	$\gamma_{ring}(54)$
195			75	69	$\gamma_{ring}(53)$

196			66	57	$\gamma_{\text{ring}}(51)$
197			60	49	$\delta_{\text{ring}}(58)$
198			52	46	$\delta_{\text{ring}}(58)$
199			48	43	$\delta_{\text{ring}}(58)$
200		35	41	35	$\gamma_{\text{ring}}(54)$
201			37	30	$\gamma_{\text{ring}}(53)$
202			30	24	$\gamma_{\text{ring}}(54)$
203			25	22	$\gamma_{\text{ring}}(54)$
204			23	20	$\gamma_{\text{ring}}(53)$
205			17	16	$\gamma_{\text{ring}}(54)$
206			12	10	$\gamma_{\text{ring}}(54)$
207			7	6	$\gamma_{\text{ring}}(54)$

ν -stretching, ν_{sym} -sym stretching, ν_{asym} -asym stretching, δ -in-plane bending, γ -out-of-plane bending, ρ -scissoring, ω -wagging, σ -rocking, τ -twisting.

4.2.1 C-H vibrations

The substituted aromatic structures show the presence of C-H stretching vibration in the region 3100-3000 cm^{-1} which is the characteristic region for the identification of C-H stretching vibrational modes [29-31].

Soleymani et al [32] observed the C-H vibrations at 3112, 3113 3071, 2978 cm^{-1} theoretically and 3050, 3128 cm^{-1} experimentally. Saruadevi et al [33] reported the C-H stretching modes are observed at 3096 cm^{-1} in the IR spectrum and at 3097, 3063, 3038 cm^{-1} in the Raman spectrum experimentally and at 3098, 3075, 3072, 3066, 3055, 3044 cm^{-1} theoretically. Renjith et al [34] reported the C-H stretching vibrations at 3097, 3086, 3081, 3057, 3055 cm^{-1} in the IR spectrum and 3077, 3064 cm^{-1} in the Raman spectrum. C-H stretching are found at 3090, 3062, 2964, 2940 cm^{-1} in FT-Raman and at 2934, 2771 cm^{-1} in FT-IR by Kuruvilla et.al. [26]. Kuruvilla et.al. [27] observed the C-H vibrations experimentally at 3050, 2900 cm^{-1} in FT-IR spectrum and 3042, 2976, 2891, 2850 cm^{-1} in FT- Raman

spectrum. For our title molecule, the C-H stretching vibrations observed at 3150, 3075, 3002 cm^{-1} for FT-Raman spectrum, 3156, 3125, 3110, 3099, 3094, 3078, 3058, 3045, 3038, 3033, 3026, 3016, 3010, 2936, 2846 cm^{-1} and 3152, 3123, 3107, 3095, 3088, 3074, 3055, 3043, 3034, 3029, 3021, 3011, 3003, 2935, 2843 cm^{-1} are calculated by B3LYP method with 6-31G and 6-31G(d,p) basis sets.

Jeyasheela et al [35] observed the C-H in-plane bending vibrations at 1179, 1059 cm^{-1} in Raman spectrum and at 1167, 1086, 1046 cm^{-1} in IR spectrum and computed bands appeared at 1318, 1170, 1094, 1059 cm^{-1} . Tamilelakkia et al [36] observed the C-H stretching mode at 1543, 1440 cm^{-1} in IR spectrum and 1540, 1477 cm^{-1} in Raman spectrum and was calculated in the range of 1511-1445 cm^{-1} . Saraudevi et al [33] reported the C-H bands theoretically at 1277, 1248, 1170, 1140, 1108, 1102, 1042 cm^{-1} and experimentally observed at 1250, 1114, 1044 cm^{-1} in IR spectrum and 1279, 1246, 1168, 1038 cm^{-1} in Raman spectrum. In our title molecule, the C-H in-plane bending vibrations occurs at 1506, 1485, 1329 and 1510, 1485, 1310, 1280 cm^{-1} observed in FT-IR and FT-Raman spectrum and calculated theoretically at 1512, 1499, 1490, 1420, 1414, 1335, 1327, 1308, 1285, 1278, 1266, 1248 and 1508, 1493, 1486, 1475, 1408, 1403, 1330, 1323, 1302, 1281, 1275, 1263, 1244 cm^{-1} for the same basis set.

Saraudevi et al [33] observed the CH out-of-plane bending vibrations theoretically at 930, 897, 895, 858, 818, 811, 731 cm^{-1} and experimentally at 931, 896, 855, 816 for IR, 788, 729 cm^{-1} for Raman spectrum. In the present work, the C-H out-of-plane bending vibrations occurs at 948, 827 and 950 for FT-IR and FT-Raman spectrum and calculated theoretically at 960, 953, 935, 932, 889, 840, 833, 823, 796, 779, 706 and 956, 948, 933, 929, 885, 865, 834, 829, 820, 795, 790, 773, 700 by B3LYP/6-31G and B3LYP/6-31G(d,p) respectively.

4.2.2 CH₃ vibrations

The CH₃ modes are occurs in the region 2900-3050 cm^{-1} [37]. Asymmetric and symmetric stretching modes of a methyl group attached to the benzene ring are usually downshifted because of electronic effects and are expected near 2925 and 2865 cm^{-1} for asymmetric and symmetric stretching vibrations [38].

The asymmetric stretching modes of the methyl group are calculated at 3047, 3039, 3022, 3003 cm^{-1} by Paniker et al [39]. For the title compound, asymmetric stretching vibrations observed at 2922 cm^{-1}

for IR spectrum, theoretically observed at 3001, 2986, 2976, 2964, 2950, 2930 cm^{-1} and 2995, 2983, 2971, 2959, 2947, 2926 cm^{-1} by B3LYP/6-31G and B3LYP/6-31G(d,p) respectively.

The symmetric modes are observed at 3038, 2946 cm^{-1} in the IR spectrum and theoretically observed at 2948, 2943 cm^{-1} by Paniker et al [39]. Saraudevi et al [33] reported the CH_3 stretching mode at 3027, 2970, 2908 cm^{-1} and experimentally observed at 3002, 2972, 2970 cm^{-1} . Parveen et.al [24] observed the CH_3 stretching modes are assigned at 3002, 2980, 2958, 2914 cm^{-1} in the IR spectrum, 2960, 2938 cm^{-1} in the Raman spectrum and theoretically occurs in the range 3032-2906 cm^{-1} . Murugavel et al [40] theoretically the C-H stretching modes of methyl group at 3056, 3022, 2984, 2964, 2944, 2917 and 2911 cm^{-1} is the experimental values 3024 and 2943 cm^{-1} . Alphonsa et al [41] reported CH_3 stretching mode for FT-IR spectrum at 2983, 2924 cm^{-1} and for FT-Raman at 2983, 2944, 2923 cm^{-1} and asymmetric and symmetric stretching vibrations observed at 3059, 3053 cm^{-1} for FT-IR, Raman spectrum and theoretically at 3012 cm^{-1} . For the title compound, symmetric stretching vibrations observed at 2856 cm^{-1} for IR spectrum, theoretically observed at 2888, 2882, 2860 cm^{-1} and 2884, 2878, 2854 cm^{-1} by B3LYP/6-31G and B3LYP/6-31G(d,p) respectively.

In this work, the CH_3 in-plane bending vibrations theoretically observed at $\delta_{\text{opb}} = 1481, 1477, 1472$ cm^{-1} , $\delta_{\text{ipb}} = 1455, 1442, 1437$ cm^{-1} , $\delta_{\text{sb}} = 1388, 1385, 1376$ cm^{-1} , $\delta_{\text{ipr}} = 768, 760, 741$ cm^{-1} , $\tau_{\text{CH}_3} = 230, 218, 210$ cm^{-1} by B3LYP/6-31G method and $\delta_{\text{opb}} = 1475, 1470, 1466$ cm^{-1} , $\delta_{\text{ipb}} = 1436, 1430, 1422$ cm^{-1} , $\delta_{\text{sb}} = 1383, 1379, 1370$ cm^{-1} , $\delta_{\text{ipb}} = 765, 756, 748$ cm^{-1} , $\tau_{\text{CH}_3} = 221, 212, 206$ cm^{-1} by B3LYP/6-31G(d,p) method. For the title compound, the out-of-plane bending vibration occurs at 1002 cm^{-1} for FT-IR spectrum. The theoretically predicted values by B3LYP/6-31G $\gamma_{\text{opr}} = 1032, 1021, 1003$ cm^{-1} by B3LYP/6-31G and 1028, 1017, 1000 cm^{-1} by B3LYP/6-31G (d,p) methods.

4.2.3 CH_2 group

The stretching vibrations of the CH_2 group and deformation modes of CH_2 group (scissoring, wagging, twisting and rocking modes) appears in the regions $3000 \pm 20, 2900 \pm 25, 1450 \pm 30, 1330 \pm 35, 1245 \pm 45, 780 \pm 55$ cm^{-1} respectively [37, 42,30].

Parveen et.al [24] observed the CH_2 stretching modes at 2923 cm^{-1} in the Raman spectrum and at 2926, 2966 cm^{-1} theoretically. The deformation modes of CH_2 are assigned at 1439, 1295, 1220, 1148 cm^{-1} in the IR spectrum, 1146 cm^{-1} in the Raman spectrum. Murugavel et al [40] the CH_2 stretching

vibrations are calculated at 2991 cm^{-1} (asymmetric) and 2944 cm^{-1} (symmetric). Asymmetric bending of is found at 1275 cm^{-1} which is consistent with the DFT value of 1274 cm^{-1} . Minithra et al [43] observed CH_2 asymmetric and symmetric stretching at $2982, 2932\text{ cm}^{-1}$ and $2905, 2893\text{ cm}^{-1}$ and assigned at $2978, 2930, 2885\text{ cm}^{-1}$ in the IR spectrum and at $2971, 2935, 2898\text{ cm}^{-1}$ in the Raman spectrum. For the title compound, the asymmetric CH_2 stretching calculated at $2970, 2922, 2910, 2872$ by B3LYP/6-31G method and $2933, 2919, 2906, 2869$ by B3LYP/6-31G(d,p) method. The symmetric CH_2 stretching observed at 2910 in FT-Raman spectrum and the computed values are $2915, 2896, 2841, 2830$ by B3LYP/6-31G method and $2912, 2893, 2835, 2822$ by B3LYP/6-31G(d,p) method. For the title compound, CH_2 scissoring band observed at 1394 , rocking at 1173 in the IR spectrum and scissoring at $1415, 1400$, rocking at 1200 , wagging at 800 in the Raman spectrum. For the title compound, the CH_2 stretching modes are observed at $\sigma_{\text{sci}} = 1429, 1423, 1408, 1402\text{ cm}^{-1}$, $\rho_{\text{rock}} = 1214, 1210, 1179, 1165\text{ cm}^{-1}$, $\tau = 1118, 1110, 1056, 1044\text{ cm}^{-1}$, $\delta_{\text{wagg.}} = 817, 805, 785, 775\text{ cm}^{-1}$ by B3LYP/6-31G, $\sigma_{\text{sci}} = 1422, 1415, 1399, 1395\text{ cm}^{-1}$, $\rho_{\text{rock}} = 1207, 1200, 1175, 1163\text{ cm}^{-1}$, $\tau = 1113, 1105, 1051, 1040\text{ cm}^{-1}$, $\delta_{\text{wagg.}} = 812, 802, 780, 769\text{ cm}^{-1}$ by B3LYP/6-31G (d,p) methods respectively.

4.2.4 C-O vibrations

The C-O stretching vibrations [44, 37] are expected in the region $1715\text{-}1600\text{ cm}^{-1}$. The in-plane deformation of C-O found in the region $625 \pm 70\text{ cm}^{-1}$ and out-of-plane bending is in the range $540 \pm 80\text{ cm}^{-1}$ [37].

Lucose et al [45] observed C-O stretching vibrations at 1632 cm^{-1} in IR spectrum and theoretically at 1636 cm^{-1} (DFT). In-plane bending at 569 cm^{-1} in IR and 555 cm^{-1} in DFT is assigned as this mode and out-of-plane bending at $673, 676\text{ cm}^{-1}$ in the IR spectrum.

The C=O stretching vibration appears both in the FT-IR and FT-Raman spectra due to intra molecular charge transfer from donor atom to acceptor atom through σ and π bonds conjugated path, which can induce large variation in dipole and molecular polarizability of the molecule and hence high activity in both spectra [37]. Renjith et al [34] observed the C-O modes at 1625 at IR and $1614, 1626\text{ cm}^{-1}$ at Ramanspectrum. The C-O stretching modes are reported at $1786, 1603, 1027\text{ cm}^{-1}$ and at $1726, 1629\text{ cm}^{-1}$ in the FT-IR, Raman spectrum and $1184, 1083, 1010, 974, 696\text{ cm}^{-1}$ assigned theoretically by Sakthivel et al [46]. Benzon et al [47] reported the C-O stretching mode at 1212 cm^{-1}

(IR), 1228 cm^{-1} (Raman) and at 1229 cm^{-1} theoretically. For the title molecule, C-O stretching vibrations observed at 1679, 1254 cm^{-1} in IR spectrum and 1680, 1295 cm^{-1} in Raman spectrum. The reported values for $\nu\text{C-O} = 1683, 1301, 1260 \text{ cm}^{-1}$, $\delta\text{CO} = 1346, 984, 965 \text{ cm}^{-1}$, $\gamma\text{CO} = 685, 630, 620 \text{ cm}^{-1}$ by B3LYP/6-31G method, $\nu\text{C-O} = 1680, 1297, 1254 \text{ cm}^{-1}$, $\delta\text{CO} = 1342, 980, 963 \text{ cm}^{-1}$, $\gamma\text{CO} = 679, 626, 620 \text{ cm}^{-1}$ by B3LYP/6-31G (d,p) methods respectively.

4.2.5 C-C vibrations

C-C stretching vibrations occur in the range of 1625-1465 cm^{-1} [48]. The in-plane and out-of plane bending modes of C-C were reported at 725 ± 95 and $595 \pm 120 \text{ cm}^{-1}$ [49].

The C-C band observed by Kuruvilla et al [26] at 1579, 1531, 1439, 1380, 1123 for FT-Raman and for FT-IR bands at 1428, 1235, 1002 cm^{-1} . Soleymani et.al [32] observed C-C band at 1625, 1590, 1575, 1540, 1470, 1465, 1430, 1380, 1280 cm^{-1} . Tamil elakkiya et al [36] observed the C-C band at 1313, 1039 cm^{-1} and calculated at 1600, 1625, 1319, 1054 cm^{-1} . In the present work, the C-C vibrations observed at 1591, 1230, 1118, 909 in IR spectrum, 1215, 910 in Raman spectrum. The reported values at 1644, 1625, 1613, 1596, 1538, 1236, 1221, 1195, 1186, 1162, 1145, 1140, 1131, 1125, 1080, 1013, 992, 925, 924, 914, 845 cm^{-1} by B3LYP/6-31G method, 1641, 1623, 1604, 1590, 1533, 1231, 1217, 1191, 1182, 1158, 1143, 1136, 1127, 1120, 1075, 1009, 989, 921, 916, 910, 842 cm^{-1} by B3LYP/6-31G (d,p) methods respectively. The C-C in-plane bending observed at 503 and 502, 345 in IR and Raman spectrum and the reported values are 792, 715, 690, 616, 608, 590, 575, 565, 539, 510, 503, 477, 480, 360, 349 cm^{-1} by B3LYP/6-31G method, 786, 711, 688, 612, 603, 586, 573, 561, 535, 506, 500, 472, 466, 354, 345 cm^{-1} by B3LYP/6-31G (d,p) methods. The C-C out-of-plane bending vibration assigned at 150, 135, 120 in Raman spectrum and the calculated values are at 330, 319, 303, 296, 291, 273, 262, 246, 197, 189, 176, 158, 141, 126 cm^{-1} by B3LYP/6-31G method, 325, 314, 299, 293, 286, 275, 268, 242, 191, 185, 173, 151, 136, 120 cm^{-1} by B3LYP/6-31G (d,p) methods.

4.2.6 C-N vibrations

The CN stretching modes are expected in the region 1400-1200 cm^{-1}

Sandhyarani et al [50] reported the C-N stretching mode at 1319 cm^{-1} . Benzoni et al [47] reported at 1247, 129, 938 cm^{-1} theoretically, 1268, 11135, 926 cm^{-1} in the Raman spectrum and 924 cm^{-1} in the IR spectrum. The C-N stretching modes were reported at 1268, 1220, 1151 cm^{-1} theoretically by Malek

et.al [51]. Al-Alshaikh et.al.[52] observed C-N stretching mode at 1329, 1092, 997 cm^{-1} in the IR spectrum, 1328 cm^{-1} in the Raman spectrum and theoretically at 1479, 1472, 1331, 1097, 998 cm^{-1} . Bhagyasree et al [53] reported C-N stretching modes at 1247 and 1236 cm^{-1} and Mary et al [14] reported the C-N stretching modes at 1233, 1209 cm^{-1} by theoretically and 1238 cm^{-1} by Raman spectrum. shanaparveen et al [28] assigned the C-N stretching mode at 1579 cm^{-1} and IR spectrum at 1553 cm^{-1} . In the present work, C-N stretching vibrations observed at 1541 and 1350, 720 in IR and Raman spectrum. The predicted values at 1579, 1533, 1525, 1370, 1356, 726 and 1572, 1529, 1517, 1362, 1351, 720 cm^{-1} by B3LYP/6-31G and 6-31G(d,p) methods.

4.2.7 N-N vibrations

N-N stretching mode occurs at 1417-1372 cm^{-1} [54].The ν N-N has been reported at 1151 cm^{-1} by Crane et al [55], 1121 cm^{-1} by Bezerra et al [56] and 1130 cm^{-1} El-behery and El-Twigry [57] and 1083 cm^{-1} theoretically by Sundaragensan et al [58]. Binil et al [59] reported the N-N stretching mode at 1138 cm^{-1} in IR, 1139 cm^{-1} in Raman and 1136 cm^{-1} theoretically. For Murugavel et al [40], N-N stretching vibrations allocated at 1083, 1119 cm^{-1} by DFT technique and experimentally at 1082 cm^{-1} in FTIR spectrum. For the title molecule, N-N stretching mode is calculated at 883 and 879 cm^{-1} by B3LYP/6-31G and 6-31G(d,p) methods respectively.

4.2.8 C-S vibrations

This vibration cannot be identified easily as it results in weak infrared bands, which is susceptible to coupling effects and is also of variable intensity. In general, the C-S stretching vibration was reported in 750-600 cm^{-1} [60].

Benzon et al [27] reported value this mode at 1515 cm^{-1} in the IR spectrum, 1520 cm^{-1} in the Raman spectrum, 1517 cm^{-1} theoretically. The C-S stretching mode observed for Sarau et al [23] are assigned at 759, 660 cm^{-1} theoretically and experimentally observed at 756, 665 cm^{-1} and 756, 658 cm^{-1} in the IR and Raman spectrum. Kuruvilla et al [33] observed these vibrations at 822,608 cm^{-1} and theoretically at 714 cm^{-1} . The C-S stretching modes were observed by Coates [53] in the range 710-687 cm^{-1} while Kwastkowski et al [61] reported the vibration at 839 and 608 cm^{-1} . The C-S stretching vibrations are reported at 783, 632 cm^{-1} and 633 cm^{-1} IR, Raman spectrum and 785, 635 cm^{-1} theoretically found by El-Azab et al [62]. The C-S stretching vibrations are reported at 770 cm^{-1} in the

IR spectrum, and at 770, 636 cm^{-1} theoretically assigned by ShaheenFatma et al [48]. In the present work, C-S vibrations calculated at 738, 697 and 731, 694 cm^{-1} by B3LYP/6-31G and 6-31G(d,p) methods respectively.

4.2.9 C-Cl vibrations

The vibrations belong to C-Cl absorption is obtained in the region between 850-550 cm^{-1} [63].

Kuruvilla et al [26] observed theoretically at C-Cl vibration at 694 and 415 cm^{-1} and experimentally at 710-505 cm^{-1} . Jayasheela et al [35] reported this band at 725 and 720 cm^{-1} 4-chlorophenyl (([(1E)-3-(1Himidazol-1-yl)-1-phenylpropylidene]amino}oxy) methanone for theoretically and experimentally. For the title compound, the vibrations occurs at for $\nu\text{C-Cl}= 597$, $\delta\text{C-Cl}=438$ in FT-IR spectrum and theoretically at $\nu\text{C-Cl}=602$ and 598 cm^{-1} , $\delta\text{C-Cl}=473$ and 440 cm^{-1} , $\gamma\text{C-Cl}=280$ and 275 cm^{-1} by B3LYP/6-31G and 6-31G(d,p) methods respectively.

4.2.10 Ring vibration

The thiazole ring in-plane bending vibrations are observed at 551, 457, 411 by FT-IR spectrum and theoretically at 588, 553, 545, 531, 522, 487, 463, 427, 417, 407, 392, 381, 166, 146, 112, 52, 48 cm^{-1} by B3LYP/6-31G method and 580, 550, 541, 523, 518, 481, 460, 422, 410, 401, 389, 375, 162, 142, 102, 49, 46, 43 cm^{-1} by B3LYP/6-31G(d,p) method. The ring out-of-plane bending observed at 35 in FT-Raman spectrum, theoretically at 135, 95, 86, 80, 75, 66, 41, 37, 30, 25, 23, 17, 12, 7 cm^{-1} by B3LYP/6-31G method and 128, 89, 79, 74, 69, 57, 35, 30, 24, 22, 20, 16, 10, 6 cm^{-1} by B3LYP/6-31G(d,p) method.

4.3 Molecular electrostatic potential (MEP) surface analysis

Molecular electrostatic potential at a point in space around a molecule gives information about the net electrostatic effect produced at that point by total charge distribution (electron + proton) of the molecule and correlates with dipole moments, electro-negativity, partial charges and chemical reactivity of the molecules. It provides a visual method to understand the relative polarity of the molecule [64, 65]. An electron density iso-surface mapped with electrostatic potential surface depicts the size, shape, charge density and site of chemical reactivity of the molecules. Figure 4 illustrates the charge distributions of the molecule two dimensionally. As it can be seen from the figure, the different

values of the electrostatic potential at the surface are represented by different colours; red represents region of most electronegative electrostatic potential, blue represents region of the most positive electrostatic potential and green represents region of zero potential. Potential increases in the order red < orange < yellow < green < blue. Blue indicates the strongest attraction and red indicates the strongest repulsion. Region of negative potential are usually associated with the lone pair of electronegative atoms. As can be seen from the MEP map of the title molecule, more reactive sites are close to C=O (C40-O44) groups, the region having the most negative potential over oxygen atom O44 and O58, then all the hydrogen atoms have positive potential. The negative potential which is represented by red colour corresponds to an interaction of a proton by aggregate the electron density of the molecule represented by red yellow shade and blue region is positive which corresponds to the repulsion of the proton represented by blue shades.

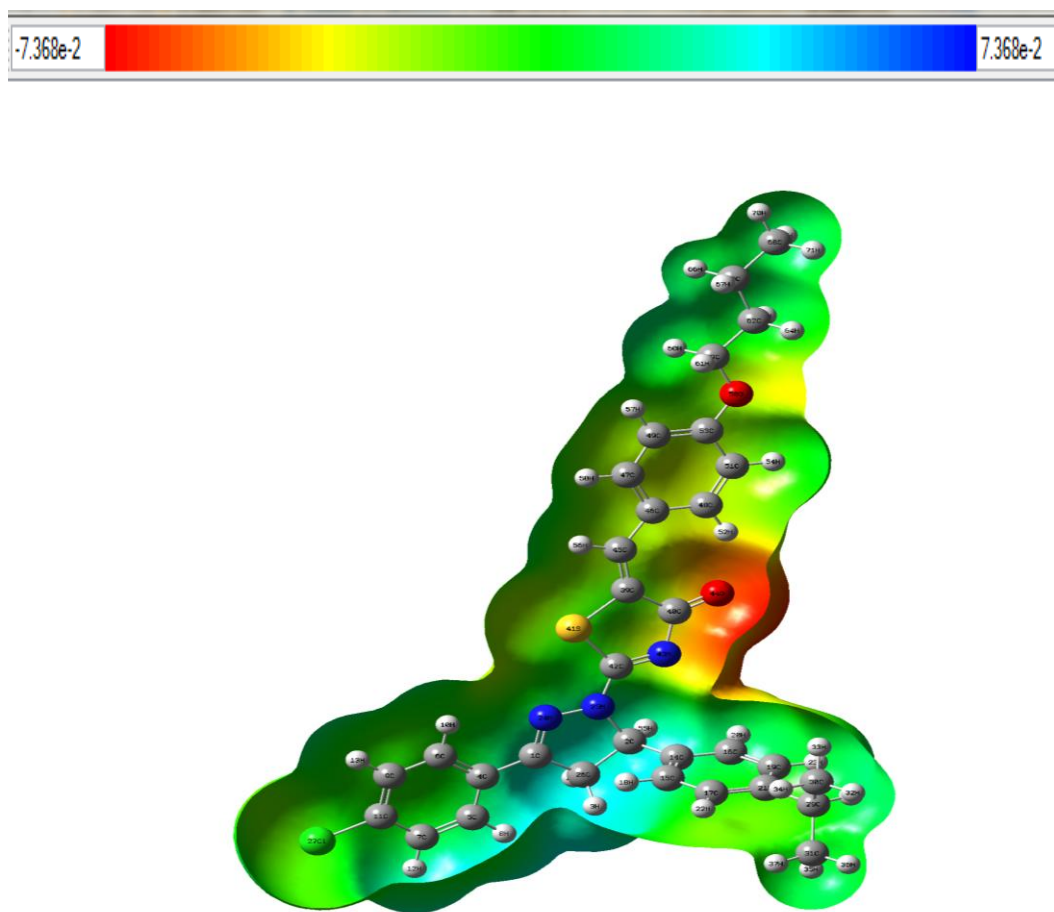


Figure 4: Molecular electrostatic potential surfaces of 5-(4-Butoxybenzylidene)-2-[3-(4-chlorophenyl)-5[4-(propan-2-yl)-4,5-dihydro-1H-pyrazol-1-yl]-1,3-thiazol-4(5H)-one

The strong negative region spread over the phenyl rings, nitrogen atom and oxygen atom of the hydroxyl group and these are possible sites of electrophilic sites. The positive electrostatic potential regions are fully covered all the hydrogen atoms and it represents the possible site of the nucleophilic sites in the MEP plot.

4.4 Frontier molecular orbital (FMO) study

DFT method with 6/31G(d,p) basis set is applied to compute the energy of HOMO and LUMO levels and the energies are shown in Table 3. The Frontier molecular orbitals (FMO) play a significant function in the electric and quantum chemistry [66]. The pictorial demonstration of these different FMOs is shown in Figure 5. The HOMO is the donor and LUMO is acceptor orbital and the energy difference between HOMO and LUMO have been used to investigate the global reactivity descriptors. The electrophilic index (ω), hardness (η) and chemical potential (μ) are known reactivity parameters. These parameters are considered as highly successful descriptors for biological activity. Moreover, electronegativity (χ), electron affinity (A), ionization potential (I) are also determined using the energies of frontier molecular orbitals and these reactivity parameters used in understanding the site selectivity and the reactivity. The compounds that possess positive electron affinity are known as electron acceptors and might participate in charge transfer reactions. The electron donation strength for any donor compound can be measured using ionisation potential is the energy which need to take off an electron from the HOMO. Electronegativity is known as one for the most important chemical properties which defined as power of species to attract electrons towards itself. The large $E_{\text{HOMO}} - E_{\text{LUMO}}$ differences define a hard species, which means compound is more stable and less reactive. While, small $E_{\text{HOMO}} - E_{\text{LUMO}}$ gap defines a soft species is less stable and more reactive. The calculated energy of HOMO is -5.3304 eV and LUMO is -1.9783 eV and the energy gap for the title compound is 3.3521 eV and is a hard one. Ionization potential (I) = 5.3304 eV, Electron affinity (A) = 1.9783 eV, Global hardness (η) = 1.6761 eV, Softness (η) = 0.5966 eV, Chemical potential (μ) = -3.6544 eV, Electrophilicity index (ω) = 3.9838 eV. The values for chemical potential and electrophilicity index are small that indicates the reactive nature of the title compound which confirms the bioactivity of the title molecule by the positive value of chemical softness.

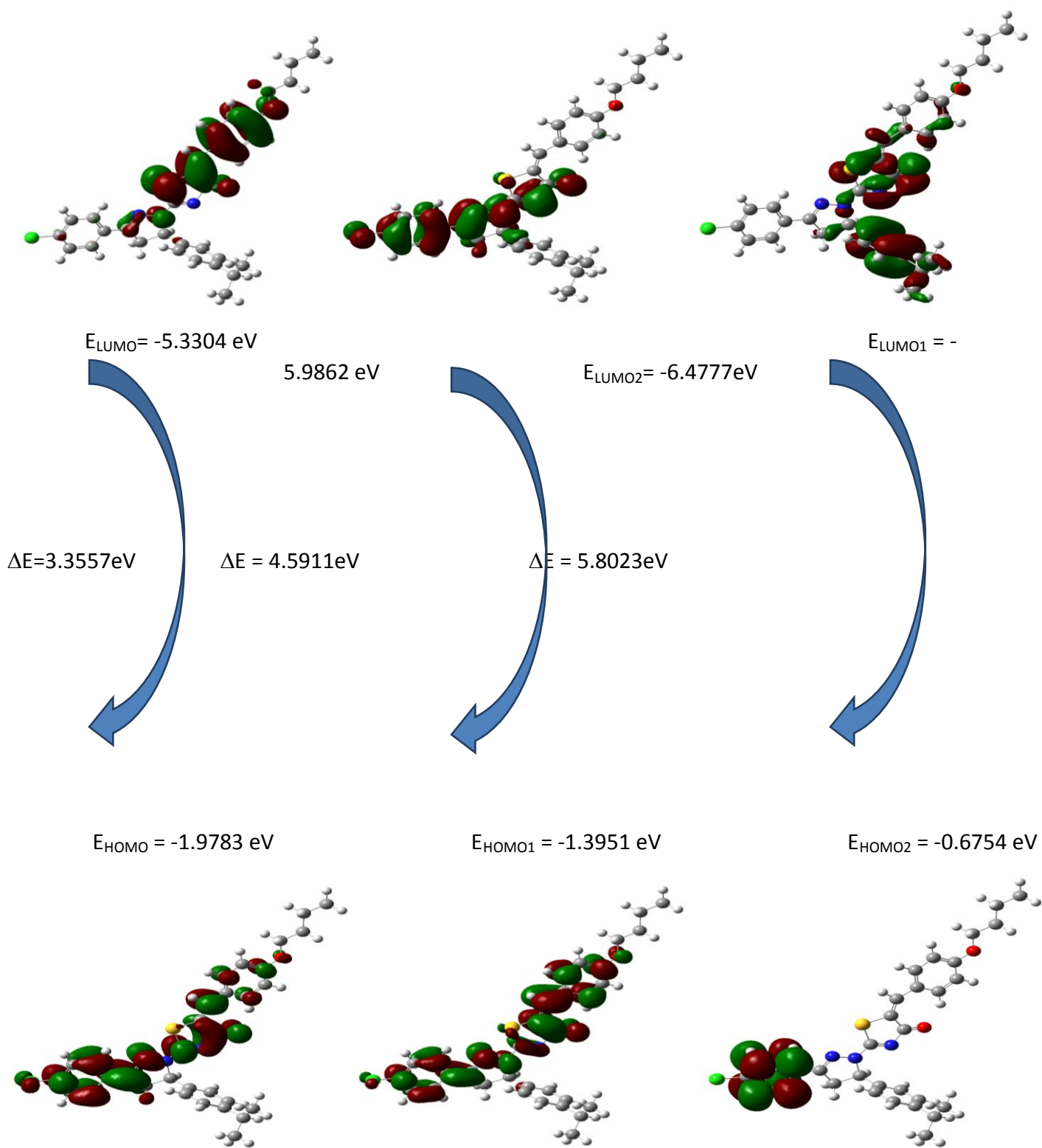


Figure 5: Patterns of the principle highest occupied and lowest unoccupied molecular orbital 5-(4-Butoxybenzylidene)-2-[3-(4-chlorophenyl)-5[4-(propan-2-yl)-4,5-dihydro-1H-pyrazol-1-yl]-1,3-thiazol-4(5H)-one

Table 3 HOMO-LUMO energies for 5-(4-Butoxybenzylidene)-2-[3-(4-chlorophenyl)-5[4-(propan-2-yl)-4,5-dihydro-1H-pyrazol-1-yl]-1,3-thiazol-4(5H)-one by B3LYP/6-31G (d,p) basis set

Molecular properties	Energy (eV)	Energy gap (eV)	Ionisation potential (I)	Electron affinity (A)	Global hardness (η)	Global softness (σ)	Chemical potential (μ)	Global Electroplicity (ω)
E_{HOMO}	5.3304	3.3521	5.3304	1.9783	1.6761	0.5966	-3.6544	3.9838
E_{LUMO}	1.9783							
$E_{\text{HOMO-1}}$	5.9862	4.5911	5.9862	1.3951	2.2955	0.4356	-3.6907	2.9669
$E_{\text{LUMO-1}}$	1.3951							
$E_{\text{HOMO-2}}$	6.4777	5.8023	6.4777	0.6754	2.9012	0.3447	-3.5765	2.2045
$E_{\text{LUMO-2}}$	0.6754							

4.5 Reduced density gradient

RDG is a pictorial visualization of various kinds of non-covalent interactions directly in the real space using Multiwfn and plotted by visual molecular dynamics (VMD) program [20,21]. Noncovalent interactions are very weak when compared with covalent bonds and hence play a vital role in nature. To understand the nature of inter molecular interaction of the title compound, RDG analyses were carried out and the resultant graphs are shown in Figure 6.

According to this graph, the green regions represent weak attractive interactions ($\lambda_2 \approx 0$) such as Van der Waals interaction; strong attractions like H-bond, C-Cl bonds are represented by blue colour. The red colour represents steric repulsion appears in the inside of phenyl rings, pyrazole, and 4-Butoxybenzylidene while van der waals interactions took place near 4(propan-2-yl) and over hydrogen atoms. The negative values of $\lambda(2)\rho$ indicates strong attractive interactions, while the positive values mean the repulsive interactions.

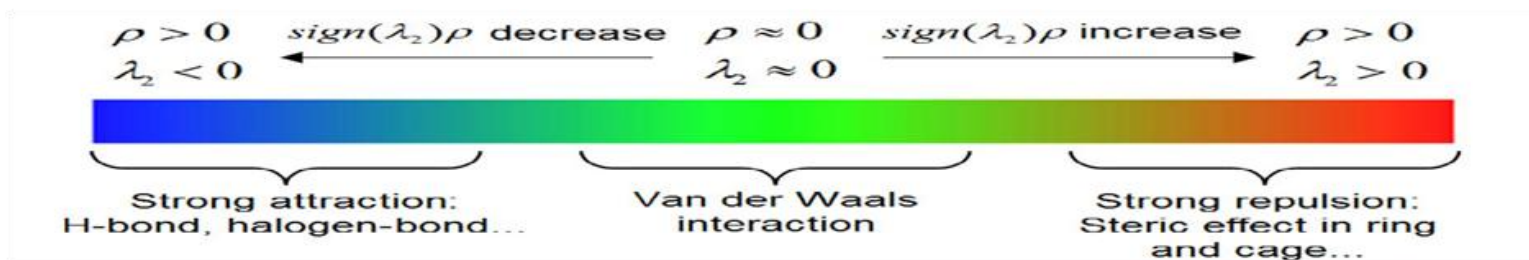
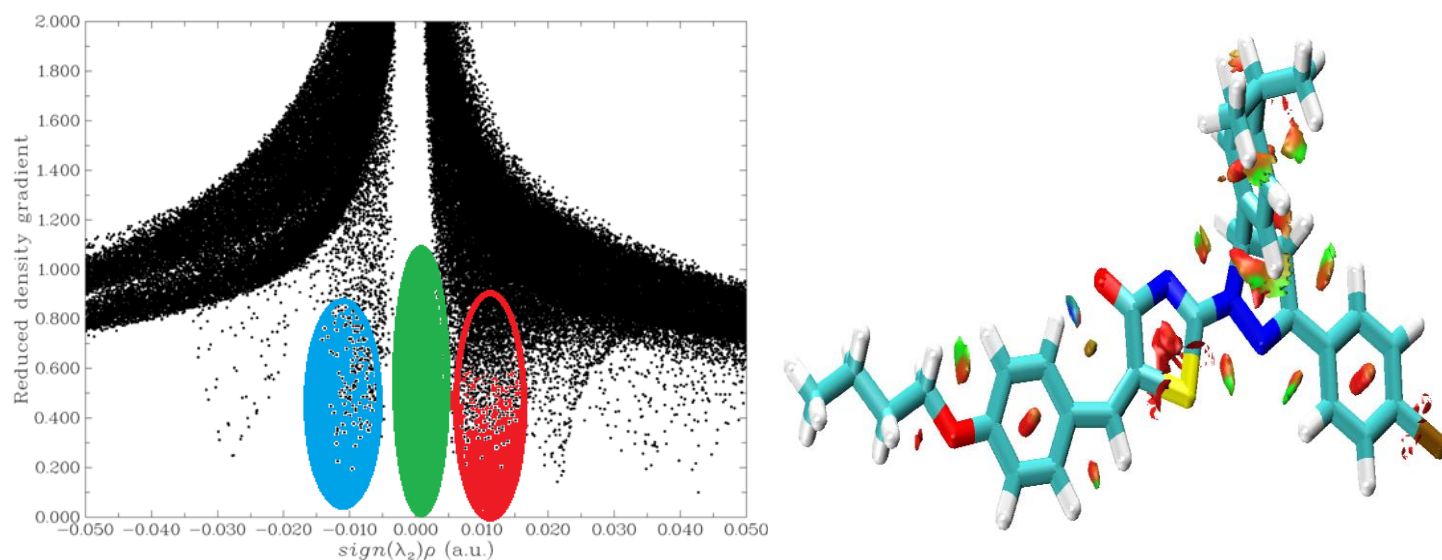


Figure 6: Plots of the RDG versus $\lambda(2)\rho$ of 5-(4-Propan-2-yl)benzylidene)-2-[3-(4-chlorophenyl)-5[4-(propan-2-yl)phenyl-4,5-dihydro-1H-pyrazol-1-yl]-1,3-thiazol-4(5H)-one

4.6 Molecular docking

Molecular docking is a computer-assisted drug design (CADD) method used to predict the favourable orientation of a ligand (drug) to a target (receptor) when bound to each other to form a

stable complex. By understanding the favoured orientation can be used to find out the strength of binding affinity between ligand and target site, e.g. by docking score [67]. Moreover, docking study can be used to find out type of interactions between ligand and receptor like hydrogen bonding and hydrophobic interactions. Hence, molecular docking can be considered as first-line technique for a pharmaceutical lead discovery [68]. Molecular docking studies were carried out to understand the binding profile of thiazole derivatives and to support the in vitro anticancerous activity. Automated docking was used to determine the orientation of inhibitors bound in the active site of Tubulin (PDB ID=4YJ2), which the protein has anti-cancerous activity. Protein 4YZJ has antiviral and 1OQE, 4YJE has anti tumor activity. A Lamarckian genetic algorithm method, implemented in the program AutoDockVina software was employed. The ligand used for docking was the optimized structure at B3LYP/6-31G (d, P). The files were prepared in a pdb format. The protein structure file (PDB ID: 4YZJ) taken from RCSB Protein Data Bank (PDB) was prepared for docking by removal of water molecules, adding polar hydrogens and Kollman charges to the structure file. In silico prediction of amino acids involved in the active site of protein responsible for binding with the ligands are obtained from the co-crystallized endogenous ligand from the PDB file. The ligand was docked in the functional sites of the selected protein and minimum docking energy value was examined. Docked conformation which had the lowest binding energy was chosen to scrutinize the molecule mode of binding. The molecular docking binding energies and inhibition constants were also obtained and listed in Table 4 The title compound taken as the ligand interactions with proteins are shown in Figure 7.

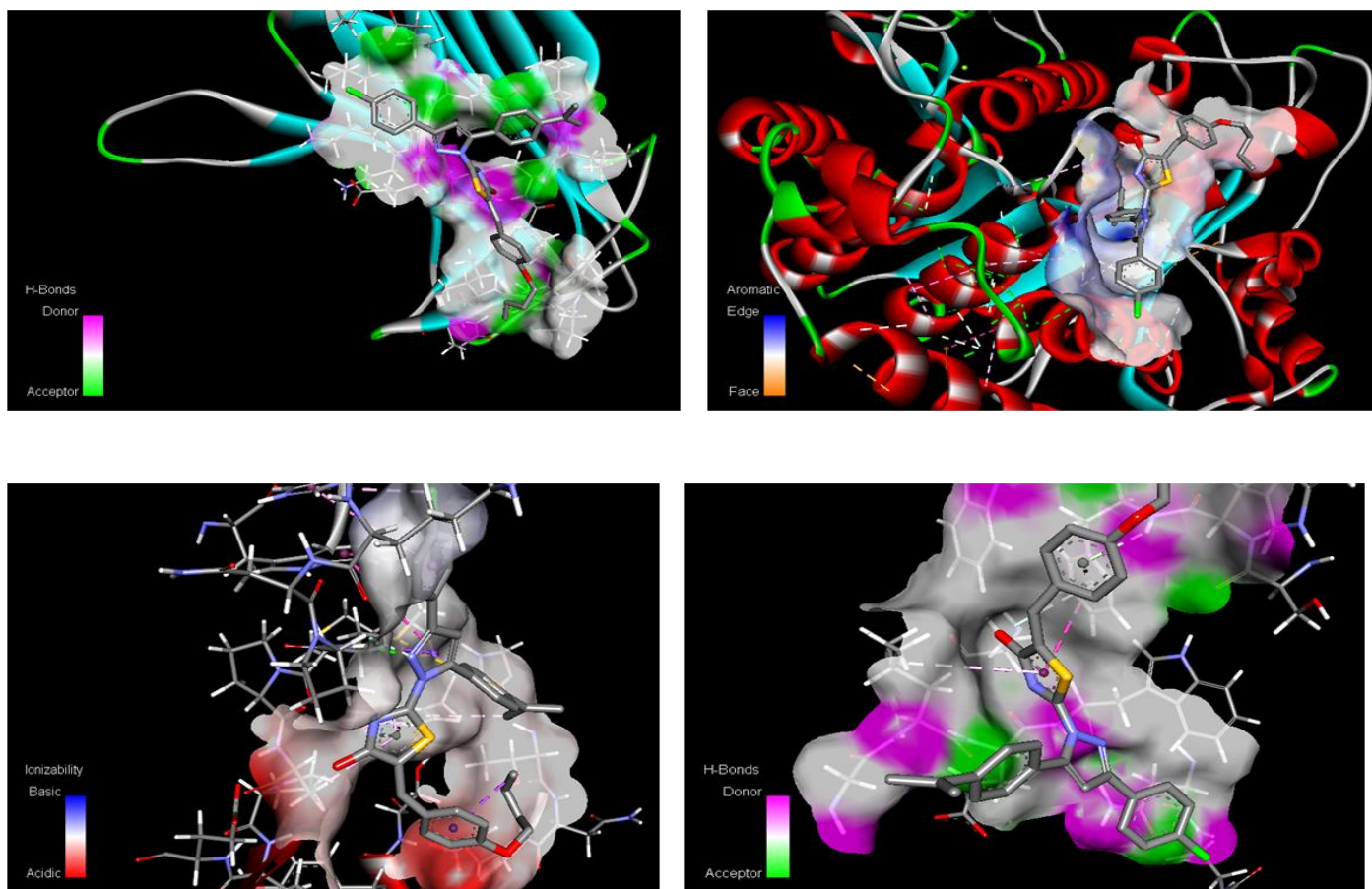


Figure 7: Ligand - 5-(4-Butoxybenzylidene)-2-[3-(4-chlorophenyl)-5[4-(propan-2-yl)-4,5-dihydro-1H-pyrazol-1-yl]-1,3-thiazol-4(5H)-one, Proteins – 1JH5,1OQE, 4YJ2 and 4JZJ

Table 4: Binding affinity for docking in 5-(4-Butoxybenzylidene)-2-[3-(4-chlorophenyl)-5[4-(propan-2-yl)-4,5-dihydro-1H-pyrazol-1-yl]-1,3-thiazol-4(5H)-one

Drug	Protein	Type of activity	Binding affinity (kcal/mol)	Estimated inhibition constant K_i (μ M)	Bonded residues	Nature of bond	Bond distance (\AA)	RMS D
5-(4-chlorophenyl)-2-[3-(4-chlorophenyl)-5[4-(propan-2-yl)-4,5-dihydro-1H-pyrazol-1-yl]-1,3-thiazol-4(5H)-one]			-4.7	360.43	ASN A-42	Conventional hydrogen bond	3.31	87.206
			-4.33	667.85	PRO A-15	Alkyl	4.1	71.635

	1OQE	Antitumer	-4.19	845.86	ILE A-15	Alkyl	4.17	78.414
			-3.97	1.23(mM)	GLU A-41	Conventional hydrogen bond	4.32	81.106
			-3.8	1.64 (mM)	ASN A-42	Conventional hydrogen bond	4.55	82.083
	4YJ2	Anticancer	-4.7	358.4	LEU A-397	Alkyl	3.72	80.983
			-4.6	426.72	PRO A-175	Alkyl	3.82	121.029
			-4.21	817.23	PRO A-173	π -alkyl	4.24	111.228
			-4.57	447.01	PRO A-184	π -alkyl	4.39	87.283
			-4.53	482.07	GLN A-176	Carbon hydrogen bond	4.55	94.627
	4YJE	Antitumer	-5.42	106.41	MET A-438	Conventional hydrogen bond	3.64	49.944
			-5.42	106.79	MET A-438	Conventional hydrogen bond	3.8	47.995
			-5.32	126.67	TYR A-486	carbon hydrogen bond	3.89	48.812
			-5.2	155.59	MET A-438	Conventional hydrogen bond	4.02	33.732
			-4.95	234.91	MET A-438	Conventional hydrogen bond	4.17	25.064
	4JZJ	Antiviral	-5.17	163.56	PHE A: 107	van der waals	3.85	36.106
			-4.95	236.07	TRP A: 47	van der waals	4.65	36.427
-4.49			514.73	PHE A:	van der waals	4.94	30.37	

					107			4
			-4.23	790.86	TRP A: 106	π - π Stacked	5.05	38.12 3
			-4.2	838.87	LEU A: 45	π - π Stacked	5.08	32.47 1

4.6.1 Anti-tumor activity

Interaction of antitumor protein 1OQE shows the existence of many conventional bonds such as three conventional hydrogen bonds and two alkyl bond interaction with amino acid (ASN A: 42, GLU A: 41, ASN A: 42, PRO A: 15, ILE A: 15) with different binding energies (-4.7, -3.97, -3.8, -4.33, -4.19)kcal/mol, inhibition constants (360.43, 1.23 (mM), 1.54 (mM), 667.85, 845.86)ki(μ M) RMSD values are (87.206, 81.106, 82.083, 71.635, 78.414) \AA . Interaction of antitumor protein 4YJE shows the existence of many conventional bonds such as five conventional hydrogen bond interaction with amino acid (MET A: 438, MET A: 438, TYR A: 486, MET A: 438, MET A: 438) with different binding energies (-5.42, -5.32, -5.2, -4.95, -4.45)kcal/mol, inhibition constants (106.41, 126.67, 155.59, 234.91, 544.29)ki(μ M) RMSD values are (49.944, 48.812, 33.732, 25.064, 25.158) \AA .

4.6.2 Anticancer activity

Interaction of anticancerous protein 4YJ2 shows the existence of many conventional bonds such as one Alkyl bonds, two π -alkyl bond and one carbon hydrogen bond interaction with amino acid (LEU A: 397, PRO A: 175, PRO A: 173, PRO A: 184, GLN A: 176) with different binding energies (-4.7, -4.6, -4.21, -4.57, -4.53)kcal/mol, inhibition constants (358.4, 426.72, 817.23, 447.01, 482.07)ki(μ M) RMSD values are (80.983, 121.029, 111.228, 87.283, 94.627) \AA .

4.6.3 Antiviral activity

Interaction of antiviral protein 4JZJ shows the existence of many conventional bonds such as three van der waals bonds and two π - π stackedbond interaction with amino acid (PHE A: 107, TRP A: 47, PHE A: 107, TRP A: 105, LEU A: 45) with different binding energies (-5.17, -4.95, -4.49, -4.23, -

4.2)kcal/mol, inhibition constants (163.56, 236.07, 514.73, 790.86, 838.87)ki(μ M) RMSD values are (36.106, 36.427, 30.374, 38.123, 32.471) \AA .

5. Conclusion

Structures of the title compounds were investigated using high-level quantum chemistry calculation. The optimized geometrical parameters and vibrational frequency assignment of the fundamental modes of title compounds have been obtained from DFT/B3LYP/6-31G and DFT/B3LYP/6-31G(d, p) level of calculation. The HOMO and LUMO analysis are used to determine the charge transfer within the molecule and the calculated HOMO and LUMO energies show the chemical activity of the molecule. The energy gap of the title molecule is $\Delta E = 3.3557\text{eV}$. From the molecular electrostatic potential plot, it is evident that the negative charge covers the carbonyl group and the positive region is over the remaining groups and the more electronegativity in the carbonyl group makes it the most reactive part of the molecule. Weak interaction profile shows that the presence of Van der Waals interactions and steric effect are present in the molecule. Molecular docking analysis reveals that the title molecule can act as a good inhibitor against the proteins 1JH5, 1OQE, 4YJ2 and 4JZJ.

Reference

- [1] C. Hansch, P. G. Sammes, J. B. Taylor, "in: Comprehensive Medicinal Chemistry", vol.2, Pergomen Press, Oxford, UK, 1990, (chapter 7) pp.1.
- [2] M. D. McReynolds, J. M. Dougerty, P. R. Hanson, "synthesis of phosphorus and sulfurheterocycles via ring-closing metathesis", Chem. Rev. vol. 104 2004, pp.2239-2258.
- [3] J. R. Lewis, "Amaryllidanceae, Scelletium, muscarine, imidazole, oxazole, peptide and other miscellaneous alkaloids", Nat. Prod. Rep. vol. 16 1999, pp.389-416.
- [4] R. J. Nevagi, "Biological and medical significance of 2-Aminothiazoles", Der.Pharm.Lett. vol. 6, 2014, pp. 134-150.
- [5] M. H. M. Helal, M. A. Salem, M. S. A. El-Gaby, M. Aljahdali, "Synthesis and biological evaluation of some novel thiazole compounds as potential anti-inflammatory agents", Eur.J.Med .Chem. vol. 65, 2013, pp. 517-526.
- [6] F. Haviv, J. D. Ratajczyk, R. W. DeNet, F. A. Kerdesky, R. L. Walters, S. P. Schmidt, J. H. Holms, P. R. Young, G. W. Carter, "3-[1-(2-enxazolyl)hydrazine]propanenitrile derivatives: inhibitors of immune complex induced inflammation", J.Med.Chem. vol. 31, 1988, pp. 1719-1728;

- [7] K. D. Hargrave, F. K. Hess, J. T. Oliver, "N-(4-substituted-thiazolyl)oxamic acid derivatives, a new series of potent , orally active antiallergy agents", *J.Med.Chem.*,vol. 26, 1983, pp. 1158-1163.
- [8] M. Grimstrup, F. Zaragoza, "Solid-phase synthesis of 2-Amino-5-sulfanythiazoles", *Eur.J.Org.Chem.*, 2002,pp. 2953-2960.
- [9] J. C. Jean, L. D. Wise, B. W. Caprathe, H. Tecle, S. Bergmeier, C. C. Humblet, T. G. Heffner, L. T. Meltzner, T. A. Pugsley, "4-(1,2,5,6-Tetrahydro-1-alkyl-3-pyridinyl)-2-thiazolamines: a novel class of compounds with central dopamine agonist properties", *J.Med.Chem.* vol. 33, 1990,pp. 311-317.
- [10] S. Annadurai, R. Martinez, D. J. Canny, T. Eidem, P. M. Dunman, M. A. Gharbia, "Design and synthesis of 2-Aminothiazole based antimicrobials targeting MRSA", *Bioorg. Med Chem.Lett.*,vol. 22, 2012 pp. 7719-7725.
- [11] K. V. Sashidhara, K. B. Rao, V. Kushwaha, R. K. Modukuri, R. Verma, P. K. Murthy, "synthesis and antifilarialactivityofchlocone-thiazole derivatives against a human lymphatic filarial parasite, *Brugiamalayi*", *Eur.L.Chem.*, vol. 81, 2014, pp. 473-480.
- [12] S. E. Kazzouli, S. B. Rabin, A. Mouadbib, G. Guillaumet, "Solid support synthesis of 2,4-disubstituted thizoles and aminothiazoles", *Tetrahedron Lett.*,vol. 43, 2002, pp. 3193-3196.
- [13] V. V. Salian, B. Narayana, B. K. Sarojini, M. S. Kumar, K. Sharath Chandra, A. G. Lobo, "Tailor made biheterocyclicpyrazoline-thiazolidinones as effective inhibitors of *Escherichia coli* FabH: design, synthesis and structural studies", *Journal of Molecular Structure*,vol. 1192, 2019, pp. 91-104.
- [14] V. V. Salian, B. Narayana, B. K. Sarojini, E. S. Sindhupriya, L. N. Madhu, S. Rao, "Biologically potent pyrazoline derivatives from versatile (2)-1-(4-chlorophenyl)-3-[4-(propan-2-yl)phenyl]prop-2-en-1-one", *Lett. Drug Des.Discov.*,vol. 14, 2017, pp. 216-227.
- [15] B. Narayana, V. V. Salian, B. K. Sarojini, J. P. Jasinski, "(2E)-1-(4-Chlorophenyl)-3-[4-(propan-2-yl)phenyl]prop-2-en-1-one", *ActaCryst.*, vol. 70, 2014, pp. 855.
- [16] M. J. Frisch, G. W. Trucks, H. B. Schlegel, G. E. Scuseria, M. A. Robb, J. R. Cheeseman, G. Scalmani, V. Barone, B. Mennucci, G. A. Peterson, H. Nakatsuji, M. Caricato, X. Li, H. P. Hratchain, F. Izmaylov, J. Bloino, G. Zheng, J. I. Sonnenberg, M. Hada, M. Ehara, K. Toyota, R. Fukuda, J. Hasegawa, M. Ishida, T. Nakajima, Y. Honda, O. Kitao, H. Nagari, T. Vreven, T. A. Montgomery Jr., J. E. Peralta, F. Ogliaro, M. Bearpark, J. J. Heyd, .Brothers E, Kudin K N, V. N. Staroverov, R. K. Kobayashi, J. Normand, K. Ragavachari, A. Rendell, J. C. Burant, S. S.B Iyengar, J. Tomasi, M. Cossi, N. Rega, J. M. Millam, M. Klene, J. E. Knox, J. B. Cross, V. Bakken, C. Adamo, J. Jaramillo, R. G. Gomperts, R. E. Strarmann, O. Yazyev, A. J. Austin, R. Cammi, C. Pomelli, J. W. Ochterski, R. I. Martin, K. Morokuma, V. G. Zakrzewski, G. A. Voth, P. Salvador, J. J. Dannenberg, S. Dapprich, O. Farkas, J. V. Ortiz, J. Cioslowski, D. J. Fox Gaussian, Inc., Wallingford CT, 2009.

- [17] A. A. C. Braga, N. H. Morgon, G. Ujaque, F. Maseras, "Computational characterization of the role of the base in the Suzuki-Miyaura cross-coupling reaction", *J. Am. Chem. Soc.*, vol. 127, 2005, pp. 9298-9307
- [18] A. A. V. Braga, G. Ujaque, F. Maseras, "A DFT study of full catalytic cycle of the Suzuki-Miyaura cross-coupling on a model system", *organometallics.*, vol. 34, 2006, pp. 3647-3658.
- [19] R. Dennington, T. Keith, J. Millam, "Gauss view, Version 5", Semichem Inc., ShawneeMission, KS, 2009.
- [20] T. Lu, F. Chen, "Multiwfn: a multifunctional wave function analyzer", *J. Chem. Inf. Comput. Chem.*, vol. 33, 2012, pp. 580-592.
- [21] W. Humphrey, A. Dalke, K. Schulten, "VMD: Visual molecular dynamics", *J. Mol. Graph.*, vol. 14, 1996, pp. 33-38.
- [22] G. M. Morris, D. S. Goodsell, R. S. Halliday, R. Huey, W. E. Hart, R. K. Belew, A. J. Olson, "Automated Docking Using a Lamarckian Genetic Algorithm and Empirical Binding Free Energy Function", *J. Comput. Chem.*, vol. 19, 1998, pp. 1639-1662.
- [23] Y. S. Mary, K. Raju, I. Yildiz, O. Temiz-Arpaci, H. I. S. Nogueira, C. M. Granadeiro, C. Van Alsenoy, "FT-IR, FT-Raman, SERS and computational study of 5-ethylsulphonyl-2-(o-chlorobenzyl)benzoxazole", *Spectrochim. Acta A: Molecular and Biomolecular Spectroscopy*, vol. 96, 2012, pp. 617-625.
- [24] S.S. Parveen, M.A. Al-Alshaikh, C.Y. Panicker, A. A. El-Emam, M. Arisoy, O. Temiz-Arpaci, C. Van Alsenoy, "Synthesis, vibrational spectroscopic investigations, molecular docking, antibacterial and antimicrobial studies of 5-ethylsulphonyl-2-(p-aminophenyl)benzoxazole", *Journal of Molecular Structure*, vol. 1115, 2016, pp. 94-104.
- [25] Y.S. Mary, N.R. El-Brollosy, A. A. El-Emam, O.A. Al-Deeb, P.J. Jojo, C.Y. Panicker, C. Van Alsenoy, "Vibrational spectra, NBO analysis, HOMO-LUMO and first hyperpolarizability of 2-[[2-Methylprop-2-en-1-yl]oxy]methyl-6-phenyl-2,3,4,5-tetrahydro-1,2,4-triazine-3,5-dione, a potential chemotherapeutic agent based on density functional theory calculations", *Spectrochim. Acta A: Molecular and Biomolecular Spectroscopy*, vol. 133, 2014, pp. 449-456.
- [26] Tintu K. Kuruvilla, S. Muthu, Johanan Christian Prasana, Jacob George, S. Sevvanthi, "Spectroscopic (FT-IR, FT-Raman), quantum mechanical and docking studies on methyl[(3S)-3-(naphthalen-1-yloxy)-3-(thiophen-2-yl)propyl]amine", *Journal of Molecular structure*, vol. 1175, 2019, pp. 163-174.
- [27] Tintu K. Kuruvilla, Johanan Christian Prasana, S. Muthu, Jacob George, "Quantum Mechanical Calculations and Spectroscopic (FT-IR, FT Raman) Investigation on 1-cyclohexyl-1-phenyl-3-(piperidin-1-yl)propan-1-ol, by density functional method", *Int. J. Mater. Sci.*, vol. 12, 2017, pp. 282-301.
- [28] S. Shana Parveen, A. Monirah Al-Alshaikh, C. Yohannan Panicker, Ali A. El-Emam, Mustafa Arisoy, Ozlem Temiz-Arpaci, C. Van Alsenoy, "Synthesis, vibrational spectroscopic investigations, molecular docking, antibacterial and antimicrobial studies of 5-ethylsulphonyl-2-(p-aminophenyl)benzoxazole" – *Journal of Molecular Structure.*, vol. 1115, 2016, pp. 94-104.

- [29] S. George, "Infrared and Raman Characteristic Group Frequencies e Tables and Charts", third ed., Wiley, Chichester, 2001.
- [30] M. Silverstein, G. Glayton Basseler, C. Morrill, "Spectrometric Identification of Organic Compounds", Wiley, New York, 1991.
- [31] M. Arirazhagan, J. Senthil Kumar, "Vibrational analysis of 4-amino pyrazole (3,4-d)pyrimidine A joint FTIR, Laser Raman and scaled quantum mechanical studies", *Spectrochim. Acta A: Molecular and Biomolecular Spectroscopy*, vol. 82, 2011, pp.228-234.
- [32] Reza soleymani, Yasin Mohammad salehi, Tahereh yousofzad, Maryam karimicheshmehali, "Synthesis, NMR, Vibrational and Mass Spectroscopy with DFT/HF Studies of 4-(4-Bromophenyl) -2Mercaptothiazole Structure", *Oriental journal of chemistry*, vol.28, 2012, pp.627-638.
- [33] A. Sarau Devi, V.V. Aswathy, Y. Sheena Mary, C. Yohannan Panicker, Stevan Armaković, J. Sanja. Armaković, Reena Ravindran, C. Van Alsenoy, "Synthesis, XRD single crystal structure analysis, vibrational spectral analysis, molecular dynamics and molecular docking studies of 2-(3-methoxy-4-hydroxyphenyl) benzothiazole", *Journal of Molecular Structure*, vol.1148, 2017, pp.282-292.
- [34] Renjith Raveendran Pillai, Vidya V. Menon, Y. Shyma Mary, Stevan Armakovi, Sanja J. Armakovi, C. Yohannan Panicker, "Vibrational spectroscopic investigations, molecular dynamic simulations and molecular docking studies of N'-diphenylmethylidene-5-methyl-1H-pyrazole-3-carbohydrazide", *Journal of Molecular Structure*, vol.1130, 2017, pp. 208-222.
- [35] K. Jayasheela, H. Lamy, AlWahaibi, S. Periyandi, Hanan M Hassan, S. Sebastian, S. Xavier, Joseph C. Daniel, Ali A. El-Emam, Mohamed I Attia – "Probing vibrational activities, electronic properties, molecular docking and Hirshfeld surfaces analysis of 4-chlorophenyl({[1E]-3-(1H-imidazole-1yl)-1-phenylpropylidene]amino}oxy)methanone: A promising anti-candida agent", *Journal of Molecular Structure*, vol.1159, 2018, pp.83-95.
- [36] M. Tamil Elakkiya, S. Prem Kumar, M. Sathiyendran, P. Suresh, V. Shanmugaiah, K. Anitha, "Structural, spectral, computational, thermal and antibacterial studies on a cocrystal: 2-aminopyrazine phthalic acid", *Journal of Molecular Structure*, vol.1173, 2018, pp. 635-646.
- [37] N. P. G. Roeges, "A guide to the complete interpretation to IR spectra of organic compounds", Wiley, New York, 1994.
- [38] B. Smith, "Infrared Spectral Interpretation. A Systematic Approach", CRC Press, Washington, DC, 1999.
- [39] C. Yohannan Panicker, Hema Tresa Varghes, P.S. Manjula, B.K. Sarojini, B. Narayana, Javeed Ahamad War, S.K. Srivastava, C. Van Alsenoy, Abdulaziz A. Al-Saadi, "FT-IR, HOMO-LUMO, NBO, MEP analysis and molecular docking study of 3-Methyl-4-((E)-[4-(methylsulfanyl)-benzylidene]amino) 1H-1,2,4-triazole-5(4H)-thione", *Spectrochim. Acta, Molecular and Biomolecular Spectroscopy*, vol.151, 2015, pp.198-207.

- [40] S. Murugavel, C. Ravikumar, G. Jaabil, Ponnusamy Alagusundaram, "Synthesis, crystal structure analysis, spectral investigations (NMR, FT-IR, UV), DFT calculations, ADMET studies, molecular docking and anticancer activity of 2-(1-benzyl-5-methyl-1H-1,2,3-triazol-4-yl)-4-(2-chlorophenyl)-6-methoxypyridine – A novel potent human topoisomerase II α inhibitor", vol.1176, 2019, pp. 729-742.
- [41] A. Therasa Alphonsa, C. Loganathan, S. Athavan Alias Anand, S. Kabilan, "Molecular structure, NMR, UV-Visible, Vibrational spectroscopic and HOMO, LUMO analysis of (E)-1-(2,6-bis (4-methoxyphenyl)-3,3-dimethylpiperidine-4-ylidene)-2-(3-(3,5-dimethyl-1H-pyrazol-1-yl)pyrazin-2-yl)hydrazine by DFT method", Journal of Molecular Structure, vol. 1106, 2016, pp. 277-285.
- [42] N.B. Colthup, L.H. Daly, S.E. Wilberly, "Introduction to IR and Raman spectroscopy", Academic press, New York 1990.
- [43] R. Minitha, Y. Sheenamary, Hema Tresa Varghese, Yohannan Panickers, Reena Ravindran, K. Raju, V. Manikandan Nair, "FT-IR, FT-Raman, and computational study of 1H-2,2-dimethyl-3H-phenothiazin-4[10H]-one", Journal of Molecular Structure, vol. 985, 2011, pp. 316-322.
- [44] M. Barthes, G. De Nunzio, G. Ribet, "Polarons or proton transfer in chains of peptide", Synth. Met. Vol.76, 1996, pp. 337-340.
- [45] Jilu Lukose, C. Yohannan Panicker, Prakash S. Nayak, B. Narayana, B.K. Sarojini, C. Van Alsenoy, Abdulaziz A. Al-Saadi, "Synthesis, structural and vibrational investigation on 2-Phenyl-N-(pyrazin-2-yl)acetamide combining XRD diffraction, FT-IR and NMR spectroscopies with DFT calculations", Spectrochimica Acta Part A: Molecular and Biomolecular Spectroscopy, vol. 135, 2015, pp. 608-616
- [46] S. Sakthivel, T. Alagesan, S. Muthu, Christina Susan Abraham, E. Geetha, "Quantum mechanical, spectroscopic study (FT-IR and FT - Raman), NBO analysis, HOMO-LUMO, first order hyperpolarizability and docking studies of a non-steroidal anti-inflammatory compound", Journal of Molecular Structure, vol. 1156, 2018, pp. 645-656.
- [47] K.B. Benzoni, Hema Tresa Varghese, C. Yohannan Panicker, Kiran Pradhan, Biprakash Kumar Tiwary, Ashis Kumar Nanda, C. Van Alsenoy, "Spectroscopic investigation (FT-IR and FT-Raman), vibrational assignments, HOMO-LUMO, NBO, MEP analysis and molecular docking study of 2-(4-hydroxyphenyl)-4,5-dimethyl-1H-imidazole 3-oxide", Spectrochimica Acta Part A: Molecular and Biomolecular Spectroscopy, vol. 146, 2015, pp. 307-322.
- [48] Shaheen Fatma, Abha Bishnoi, Vineeta Singh, Fatmah A.M. Al-Omary, Ali A. El-Emam, Shilendra Pathak, Ruchi Srivastava, Onkar Prasad, Leena Sinha, "Spectroscopic and electronic structure calculation of a potential antibacterial agent incorporating pyrido-dipyrimidine-dione moiety using first principles", Journal of Molecular Structure, vol.1110, 2016, pp.128-137.
- [49] L.J. Bellamy, "The Infrared Spectrum of Complex Molecules", third ed., Chapman and Hall, London, 1975.

- [50] N. Sandhyarani, G. Skanth, S. Berchmanns, V. Yegnaraman, T. Pradeep, "A combined surface-enhanced raman-x-ray photoelectron spectroscopic study of 2-mercaptobenzothiazole monolayers on polycrystalline Au and Ag films", *Journal of Colloid Interface Sci.*, vol.209, 1999, pp. 154-161.
- [51] K. Malek, A. Puc, G. Schroeder, V.I. Rybachenko, L.M. Proniewich, "FT-IR and FT-Raman spectroscopies and DFT modelling of benzimidazolium salts", *Chem. Phys.* Vol. 327, 2006, pp. 439-451.
- [52] A. Monirah, Al-Alshaikh, Y. Sheena mary, C. Yohannanpaniker, Mohamed I. Attia, Ali A. El-Emam, C. Van Alsenoy, "Spectroscopic investigations and molecular docking study of 3-(1H-imidazole-1-yl)-1-phenylpropan-1-one, a potential precursor to bioactive agents", *Journal of Molecular Structure*, vol. 1109, 2016, pp. 131-138.
- [53] J. B. Bhagyasree, J. Samuel, H.T. Varghese, C.Y. Panicker, M. Arisoy, O. Temiz-Arpaci, "Synthesis, FT-IR investigation and computational study of 5-[(4-bromophenyl)acetamido]-2-(4-tert-butylphenyl) benzoxale", *Spectrochim. Acta, Molecular and Biomolecular spectroscopy*, vol. 115, 2013, pp. 79-91.
- [54] W.C. Harris, L.B. Knight, R.W. McNamee, J.R. Durig, "Vibrational spectra and structure of tetramethyltetrazine", *Inorg. Chem.*, vol.13, 1974, pp. 2297-2301.
- [55] L.G. Crane, D. Wang, L.M. Sears, B. Heyns, K. Carron, "SERS surfaces modified with a 4-(2-pyridylazo)resorcinol disulfide derivative: detection of copper, lead and cadmium", *Anal. Chem.* 67 (1995) 360-364.
- [56] A. C. S. Bezerra, Eduardo L De Sa, F.C. Nart, "In situ vibrational study of the initial steps during urea electrochemical oxidation", *Journal of Physics and Chemistry*, vol. 101, 1997, pp. 6443-6449.
- [57] M. El-Behery, H. El-Twigry, "Synthesis, magnetic, spectral and antimicrobial studies of Cu(II), Ni(II), Co(II), Fe(II) and UO₂(II) complexes of a new Schiff base hydrazone derived from 7-chloro-4-hydrazinoquinoline", *Spectrochim. Acta Part A: Molecular and Biomolecular spectroscopy*, vol. 66, 2007, pp. 28-36.
- [58] N. Sundaraganesan, S. Ayyappan, H. Umamaheswari, B.D. Joshua, "FTIR, FT-Raman spectra and ab initio, DFT vibrational analysis of 2,4-dinitrophenylhydrazine", *Spectrochim. Acta*, vol.66, 2007, pp. 17-27.
- [59] P.S. Binil, Y.S. Mary, H.T. Varghese, C.Y. Panicker, M.R. Anoop, T.K. Manojkumar, "Infrared and Raman spectroscopic analyses and theoretical computation of 4-butyl-1-(4-hydroxyphenyl)-2-phenyl-3,5-pyrazolidinedione", *Spectrochimica Acta Part A: Molecular and Biomolecular Spectroscopy*, vol.94, 2012, pp. 101-109.
- [60] J. Coates, "Interpretation of Infrared Spectra of Organic Structures", John Wiley, New York, 2000.
- [61] J.S. Kwiatkowski, J. Leszczynski, I.Teca, "Molecular structure and infrared spectra of furan, thiophene, selenophene and their 2,5-N and 3,4-N derivatives: density functional theory and

conventional post-Hartree-Fock MP2 studies”, *Journal of molecular structure*, vol.436, 1997,pp.451-480.

[62] S. Adel. El-Azab, K. Jalaja, Alaa A.-M. Abdel-Aziz, M. Abdulrahman, Al-Obaid, Y. Sheena Mary, C. YohannanPanicker, C. Van Alsenoy, “Spectroscopic analysis (FT-IR, FT-Raman and NMR) and molecular docking study of ethyl 2-(4-oxo-3-phenethyl-3,4-dihydroquinazolin-2-ylthio)-acetate”, *Journal of Molecular Structure*, vol.1119, 2016, pp. 451-461.

[63] E.F. Mooney, “The infra-red spectra of chloro- and bromobenzenederivativesII. Nitrobenzenes”, *Spectrochim. Acta*, vol. 20, 1964, pp. 1021-1032.

[64] S. Chidangil, M.K. Shukla, P.C. Mishra, “A molecular electrostatic potential mapping study of some Fluoroquinolone anti-bacterial agents”, *J. Mol. Modeling annual*, 1998, pp. 250-258.

[65] F.JavierLuque, J.M. Lopez, M. Orozco, Perspective on “Electrostatic interactions of a solute with a continuum. A direct utilization of ab initio molecular potentials for the prevision of solvent effects”, *Theor.Chem. Acc.* Vol. 103, 2000, pp.343-345.

[66] I.Fleming, “Frontier Orbitals, Organic chemical Reactions”, Wiley, London, 1976.

[67] B.K. Sarojini, B.G. Krishna, C.G. Darshanraj, B.R. Bharath, H. Manjunatha. “Synthesis, characterization, in vitro and molecular docking studies of new 2,5-dichloro thienyl substituted thiazole derivatives for antimicrobial properties”. *Eur J Med Chem*, vol. 45, 2010, pp.3490-3496.

[68] B.K. Shoichet, S.L. McGovern, B. Wei, J.J. Irwin.”Lead discovery using molecular docking”, *Curr Opin Chem Bio*, vol.6, 2002, pp. 439–446.

Already have a manuscript?

Use our Manuscript Matcher to find the best relevant journals!

Find a Match

Refine Your Search Results

0130-7673

Search

Sort By: Title (A-Z)

Search Results

Found 1 results (Page 1)

Share These Results

Exact Match Found

NOVI MIR

Publisher: IZD STVO IZVESTIYA , PUSHKINSKAYA PL 5, MOSCOW, RUSSIA, K-6

ISSN / eISSN: 0130-7673

Web of Science Core Collection: Arts & Humanities Citation Index

Additional Web of Science Indexes: Current Contents Arts & Humanities

Filters

Clear All

Web of Science Coverage

Open Access

Category

Country / Region

FT-IR and FT-Raman Investigation, Quantum Chemical Analysis and Molecular Docking of (4Z)-4-(4-Methylbenzylidene)-2-phenyl-1,3-oxazol-5(4H)-one

K.Venil¹, A. Lakshmi^{2,*}, V. Balachandran³

¹Department of Physics, Government Arts College, Tiruchirappalli 621 222, India.

²Department of Physics, Government Arts College, Tiruchirappalli 621 222, India.

³Centre for Research, Department of Physics, Arignar Anna Government Arts College, Musiri, Tiruchirappalli 621 211, India.

¹venilr@yahoo.in, ²laksharumugam13@gmail.com, ³brsbala66@gmail.com

Abstract

The FT-IR and FT-Raman spectra were recorded and analyzed for (4Z)-4-(4-Methylbenzylidene)-2-phenyl-1,3-oxazol-5(4H)-one molecule. Quantum chemical calculations of the equilibrium geometry and the theoretical vibrational wavenumber were carried out using DFT method (B3LYP) with 6-31G (d,p) basis set. The frontier molecular orbital analysis is used to determine the charge transfer within the molecule. The stability of the molecule arising from hyper-conjugative interaction and charge delocalization has been analyzed using natural bonding orbital analysis. Molecular docking studies were also carried out.

Keywords: Vibrational spectra, MEP and Molecular Docking.

1. Introduction

The biological study of heterocyclic compounds has been interesting field for a long time [1] and oxazole is one such moiety which has gained attention in recent times due to its increasing importance in the field of medicinal chemistry. Oxazole derivatives play a pivotal role in delineating the biological activities like antimicrobial [2], anticancer [3], antitubercular [4] anti-inflammatory [5], antidiabetic [6], antiobesity [7] and antioxidant [8]. Oxazole derivatives play a pivotal role in delineating the biological activities. The aim of this work was to investigate the title molecule by spectroscopic characterization by computational studies. The vibrational spectroscopic investigations combined with DFT calculations are employed to provide comprehensive vibrational spectral assignments. The natural bond orbital, NBO, analysis has been carried out to elucidate information regarding the intra molecular charge transfer within the molecule. The electrophilic and nucleophilic sites are reported with the help of MEP surface. The study of frontier molecular orbitals, HOMO and LUMO has been used to represent how the charge takes place in the molecule and global reactive descriptors are studied. Molecular docking is a powerful tool for predicting the binding affinity of a ligand with the protein and used for structure –based drug designing.

2. Experimental details

Fourier transform infrared (FT-IR) spectrum of (4Z)-4-(4-Methylbenzylidene)-2-phenyl-1,3-oxazol-5(4H)-one was recorded employing the Perkin Elmer spectrometer fitted with a KBr beam splitter around

4000-400 cm^{-1} . Bruker RFS 27 FT-Raman spectrometer was used to report the FT-Raman spectrum in the region 4000-0 cm^{-1} using a 1064 nm Nd: YAG laser source. Both the spectral measurements were performed at the Sophisticated Analytical Instrumentation Facility (SAIF), IIT, Chennai, India.

3. Computational details

All calculations presented in this study were performed with the Gaussian 09W program [9] and Gauss view [10]. By DFT calculations, B3LYP functional combined with 6-31G and 6-31G (d,p) basis sets to predict the molecular structure and vibrational wave numbers. The natural bonding orbital calculations were performed using the NBO program as implemented in Gaussian 09 Package. The molecular docking calculations were performed with the Autodock Tools version 1.5.6 software package [11] and the docking results were analyzed using Pymol [12] and Discovery studio [13] visualization software. The three dimensional crystal structure of DNA was obtained from the Protein data bank PDB ID.

4. Results and discussions

4.1 Molecular geometry

The optimized geometrical structure and parameters of the title compound obtained using DFT at B3LYP/6-31G and B3LYP/6-31G (d,p) level are shown in Figure 1 and Table 1 respectively. The title compound contains 17 C-C bonds, 12 C-H bonds, 3 C-O bonds and 2 C-N bonds.

Table 1. Optimized Structural Parameters of (4Z)-4-(4-Methylbenzylidene)-2-phenyl-1,3-oxazol-5(4H)-one

Parameter s	Bond Length		Parameters	Bond angle		Parameters	Dihedral angle	
	B3LYP/6-31G	B3LYP/6-31G(d,p)		B3LYP/6-31G	B3LYP/6-31G(d,p)		B3LYP/6-31G	B3LYP/6-31G(d,p)
C1-C2	1.3965	1.3932	C2-C1-C6	120.1941	120.1864	C6-C1-C2-C3	-0.0001	0.0015
C1-C6	1.4003	1.396	C2-C1-H7	119.7215	119.7025	C6-C1-C2-H8	180.0005	-179.999
C1-H7	1.0849	1.0857	C5-C1-H7	120.0845	120.1111	H7-C1-C2-C3	179.9999	-179.999
C2-C3	1.4071	1.4034	C1-C2-C3	119.7765	119.8103	H7-C1-C2-H8	0.0007	-0.0001
C2-H8	1.0834	1.0841	C1-C2-H8	120.837	120.6321	C2-C1-C6-C5	0.0002	-0.0017
C3-C4	1.4088	1.405	C2-C3-H8	119.3865	119.5577	C2-C1-C6-H11	180.0003	179.9971
C3-C12	1.4529	1.4608	C2-C3-C4	119.9757	119.9049	H7-C1-C6-C5	180	179.9992
C4-C5	1.394	1.3903	C2-C3-C12	120.7341	120.887	H7-C1-C6-H11	0.0001	-0.002
C4-H9	1.084	1.0845	C4-C3-C12	119.2902	119.2081	C1-C2-C3-C4	0.0002	-0.0002
C5-C6	1.4026	1.3986	C3-C4-C5	119.8256	119.8754	C1-C2-C3-C12	179.9995	-179.998
C5-H10	1.085	1.0857	C3-C4-H9	118.9188	118.8525	H8-C2-C3-C4	180.0004	-180
C6-H11	1.0854	1.086	C5-C4-H9	121.2556	121.272	H8-C2-C3-C12	-0.0011	0.0031
C12-N13	1.3003	1.2894	C4-C5-C6	120.1699	120.1597	C2-C3-C4-C5	-0.0003	-0.0008
C12-O14	1.4204	1.3833	C4-C5-H10	119.7888	119.7752	C2-C3-C4-H9	179.9995	-180
N13-C15	1.4354	1.416	C6-C5-H10	120.0413	120.0651	C12-C3-C4-C5	179.9996	179.9965
O14-C16	1.4316	1.4015	C1-C6-C5	120.0582	120.0633	C12-C3-C4-H9	0.0002	-0.0023
C15-C16	1.4987	1.5023	C1-C6-H11	119.9885	119.9712	C2-C3-C12-N13	180.0027	-179.974

C15-C18	1.3172	1.3152	C5-C6-H11	119.9532	119.9656	C2-C3-C12-O14	0.0004	0.0307
C16-O17	1.2189	1.1976	C3-C12-N13	127.9771	126.7808	C4-C3-C12-N13	0.002	0.0284
C18-C19	1.3737	1.3692	C3-C12-O14	117.0539	116.6691	C4-C3-C12-O14	179.9997	-179.967
C19-C20	1.4361	1.4327	N13-C12-O14	114.969	116.5501	C3-C4-C5-C6	0.0003	0.0006
C19-C21	1.436	1.4333	C12-N13-C15	106.6147	105.3947	C3-C4-C5-H10	180.001	-179.998
C20-C22	1.3857	1.3823	C12-O14-C16	106.1513	106.2689	H9-C4-C5-C6	179.9995	179.9994
C20-H23	1.0841	1.0845	N13-C15-C16	108.106	107.9065	H9-C4-C5-H10	0.0012	0.0007
C21-C24	1.3858	1.3814	N13-C15-C18	126.3724	127.5269	C4-C5-C6-C1	-0.0003	0.0006
C21-H25	1.0841	1.0846	C16-C15-C18	125.5216	124.5665	C4-C5-C6-H11	179.9996	-179.998
C22-C26	1.4122	1.4079	O14-C16-C15	104.1591	103.8798	H10-C5-C6-C1	180.0009	179.9993
C22-H27	1.0863	1.087	O14-C16-O17	122.5165	122.6714	H10-C5-C6-H11	-0.0011	0.0005
C24-C26	1.4122	1.4089	C15-C16-O17	133.3244	133.4487	C3-C12-N13-C15	180.0066	-179.986
C24-H28	1.0863	1.0871	C15-C18-C19	171.1948	179.9605	O14-C12-N13-C15	-0.0044	0.009
C26-C29	1.5093	1.5069	C18-C19-C20	121.2321	121.2464	C3-C12-O14-C16	180.0039	179.9899
C29-H30	1.0952	1.0938	C18-C19-C21	121.236	121.2185	N13-C12-O14-C16	0.002	-0.0056
C29-H31	1.0995	1.098	C20-C19-C21	117.5283	117.5336	C12-N13-C15-C16	0.005	-0.0086
C29-H32	1.0952	1.0944	C19-C20-C22	120.5149	120.4589	C12-N13-C15-C18	179.9974	-179.992

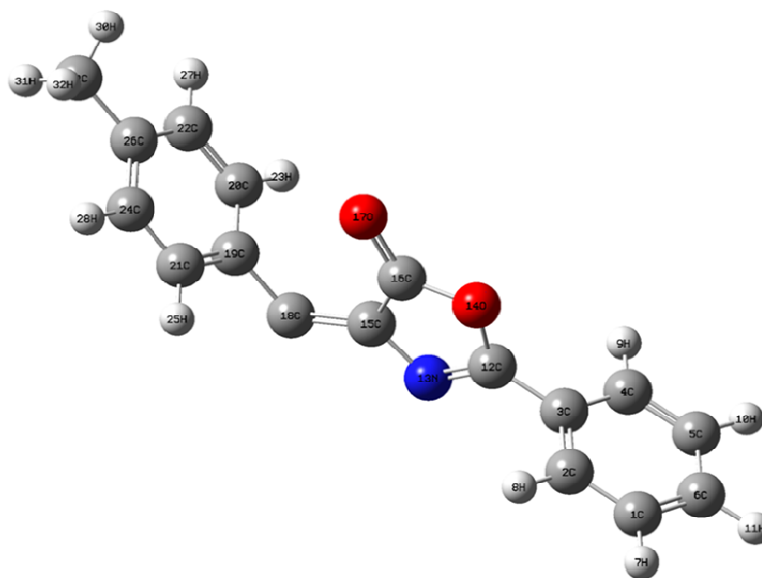


Figure 1. Optimized Structural Parameters of (4Z)-4-(4-Methylbenzylidene)-2-phenyl-1, 3-oxazol-5(4H)-one

The bond length C1-C2, C1-C6, C2-C3, C5-C6, C15-C16, C19-C20, C19-C21, C22-C26, C24-C26 are 1.3965 / 1.3932, 1.4003 / 1.396, 1.4071 / 1.4034, 1.4026 / 1.3986, 1.4987 / 1.5023, 1.4361 / 1.4327,

1.436 / 1.4333, 1.4122 / 1.4089 which are high due to the presence of benzene ring and also are good agreement with Benzon et al [14] that C22-C24, C21-C23 are 1.4988 and 1.4923 Å. For the title molecule, C18-C19, C20-C22, C21-C24 has bond length as 1.3737/1.3692, 1.3857/1.3823, 1.3858/1.3814 are good agreement with the reported value [15].

The C–H bond length lies between 1.08 and 1.09 Å for the phenyl ring. Here for the title compound, C1-H7, C2-H8, C4-H9, C5-H10, C6-H11, C20-H23, C21-H25, C22-H27, C24-H28, C29-H30, C29-H31, C29-H32 are 1.0849/1.0857, 1.0834/1.0841, 1.084/1.0845, 1.085/1.0857, 1.0854/1.086, 1.0841/1.0845, 1.0841/1.0846, 1.0863/1.087, 1.0863/1.0871, 1.0952/1.0938, 1.0995/1.098, 1.0952/1.0944 are very close to the reported value. The C–O bond length of the title molecule of C12-O14, C16-O14, C16-O17 are 1.4204/1.3899, 1.4316/1.4015, 1.2189/1.1976 which are in close agreement with reported values C3–O11 = 1.3959 Å and C12–O11 = 1.4565 Å [16].

The C–N bond distance for the title molecule, C12-N13, N13=C15 has 1.3003/1.2894, 1.4354/1.416 Å was found to be much shorter than the average value for a C–N single bond (1.47Å) but significantly longer than a C=N double bond (1.22Å) [17], suggesting that some multiple bond character is presented. Haress et al [16] assigned the C–N bond length of C24-N5 = 1.2951/1.2933 Å and C7-N4 = 1.2947/1.2923 Å which are close to our title molecule. Purkayastha and Chattopadhyay [18] reported N14-C13, N14-C19 bond lengths as 1.3270 Å, 1.400 Å which are close related to our title compound.

For the title compound, the bond angle for C2-C1-C6, C1-C2-C3 is 120.19/120.18°, 119.77/119.81° which is in good agreement with the reported values (120.4° and 120°) and C3-C4-C5, C1-C6-C5 has 119.83°/119.87°, 120.05°/120.06° are close to Benzon et al [14] observed at 120.7° and 118.1°. For the title molecule, N13-C15-C16 = 108.11°/107.91°, N13-C15-C18 = 126.37°/127.53°, C16-C15-C18 = 126.52°/124.56° which is due to the interaction between the oxazole and the benzene ring. It is clearly seen that the dihedral angles C4-C3-C12-O14, C2-C3-C12-N13 are 180° and C2-C3-C12-O14, C4-C3-C12-N13 are 0°. This indicates that the benzene ring and the oxazole ring moieties of the title compound is planner.

4.2 Vibrational analysis

The title compound is constituted by 32 atoms and has 90 normal modes of vibrations. Among 90 fundamental modes of vibrations are classified into 36 stretching and the remaining is divided into in-plane and out-of-plane bending vibrations. The observed and simulated FT-IR and FT-Raman spectra of the title compound at DFT-B3LYP level using 6-31G and 6-31G (d,p) basis sets are shown in Figures 2 and 3. The elaborated vibrational assignments of the title compound along with the calculated IR and Raman frequencies and normal mode descriptions are given in Table 2.

Table 2. Vibrational assignments of (4Z)-4-(4-Methylbenzylidene)-2-phenyl-1,3-oxazol-5(4H)-one

Modes	Observed wavenumbers (cm ⁻¹)		Calculated wavenumbers (cm ⁻¹)		Vibrational assignments
	FT-IR	FT-Raman	B3LYP/6-31G	B3LYP/6-31G (d,p)	
1		3095	3095	3091	νCH (98)
2		3010	3015	3010	νCH (99)
3	3001		3006	3001	νCH (98)

4			2991	2989	ν CH (98)
5		2940	2945	2941	ν CH (99)
6	2900		2910	2905	ν CH (98)
7			2896	2891	ν CH (98)
8			2870	2866	ν CH (99)
9	2802		2802	2800	ν CH (98)
10			2796	2791	ν_{ass} CH ₃ (97)
11		2785	2790	2786	ν_{ass} CH ₃ (97)
12			2788	2780	ν_{ss} CH ₃ (97)
13	1680	1682	1685	1680	ν CO(78), ν CC (16)
14	1602	1605	1607	1603	ν CC(84), ν CO (12)
15	1580		1576	1573	ν CC (78), δ CH (17)
16		1545	1549	1542	ν CN (76), δ CC (19)
17	1510		1520	1514	ν CC (76), δ CH (18)
18		1502	1504	1500	ν CC (76), δ CH (18)
19			1491	1487	ν CC (78), δ CH (16)
20	1455	1460	1464	1458	δ CH (69), ν CC (22)
21			1453	1447	δ CH (68), ν CC (20)
22			1435	1431	δ_{opp} CH ₃ (88)
23		1420	1426	1422	δ_{ipb} CH ₃ (86)
24	1411		1420	1412	δ CH (68), δ CC (19)
25		1386	1391	1385	δ CH (70), ν CC (21)
26	1374		1380	1374	δ_{sb} CH ₃ (86)
27			1351	1340	ν CC (75), δ CH (21)
28			1337	1332	ν CO (69), δ CH (13), ν CC (10)
29	1300	1304	1309	1304	δ CH (72), ν CO (13)
30		1295	1300	1296	δ CH (69), ν CC (13)
31	1250	1251	1254	1250	ν CC (76), δ CH (18)
32		1190	1196	1192	ν CC (68), δ CH (12)
33	1183		1183	1180	ν CC (70), δ CH (12), δ CC (10)
34			1170	1167	δ CH (78)
35	1135		1140	1134	δ CH (75)
36	1100	1102	1115	1101	δ CH (73)
37	1056		1064	1057	δ CH (75)
38			1028	1025	ν CN (66), ν CC (13), δ CO (10)
39		1007	1011	1009	δ CO (67), ν CC (12), δ CH (10)
40			1004	1000	δ CH (68)
41		991	993	990	δ_{opr} CH ₃ (70)
42	980		982	978	ν CC (72), δ CH (14)
43		968	970	967	Ring breathing (75)
44			954	950	δ ring (69)
45			933	931	γ CH (64)
46	911		915	912	δ_{ipr} CH ₃ (69), δ CH (10)
47	902		906	902	δ ring (70)
48	888		890	886	γ CH (65)

49		875	879	877	γ CH (65)
50	861		863	860	γ CH (65)
51		836	841	838	γ CH (66)
52			830	824	δ CO (72), δ ring (16)
53	812		815	812	δ ring (66)
54			805	802	γ CH (67)
55			801	795	γ CH (67)
56		785	790	786	γ CH (67)
57			765	763	δ ring (70)
58	733		738	735	γ CH (68)
59			722	718	γ CH (68)
60	693	694	700	695	δ ring (72)
61			648	643	γ CH (68)
62			631	627	γ ring (63), γ CC (14)
63			615	612	γ CC (66), γ ring (15)
64		602	606	600	δ ring (68)
65			590	587	δ ring (68)
66	563		571	565	δ CC (60), δ CO (18)
67			560	554	δ ring (66)
68		527	535	530	δ ring (65)
69	503		506	501	δ ring (65)
70			491	488	γ ring (62)
71			470	467	γ ring (62)
72			431	428	δ ring (66)
73	402		408	401	γ ring (63)
74			376	373	γ ring (62)
75			353	348	δ CC (68)
76			312	309	γ CC (62)
77			290	285	δ CCH ₃ (64)
78		224	228	225	δ CC (66)
79			211	208	δ CC (66)
80			195	189	δ ring (68)
81			170	166	γ CC (61)
82			128	123	γ ring (60)
83		101	110	102	δ ring (65)
84			89	85	δ ring (65)
85		65	72	67	δ CC (66)
86			61	56	γ ring (60)
87			47	40	δ CC (58)
88			38	31	τ CH ₃ (67)
89			29	25	γ CC (62)
90			13	10	γ CC (60)

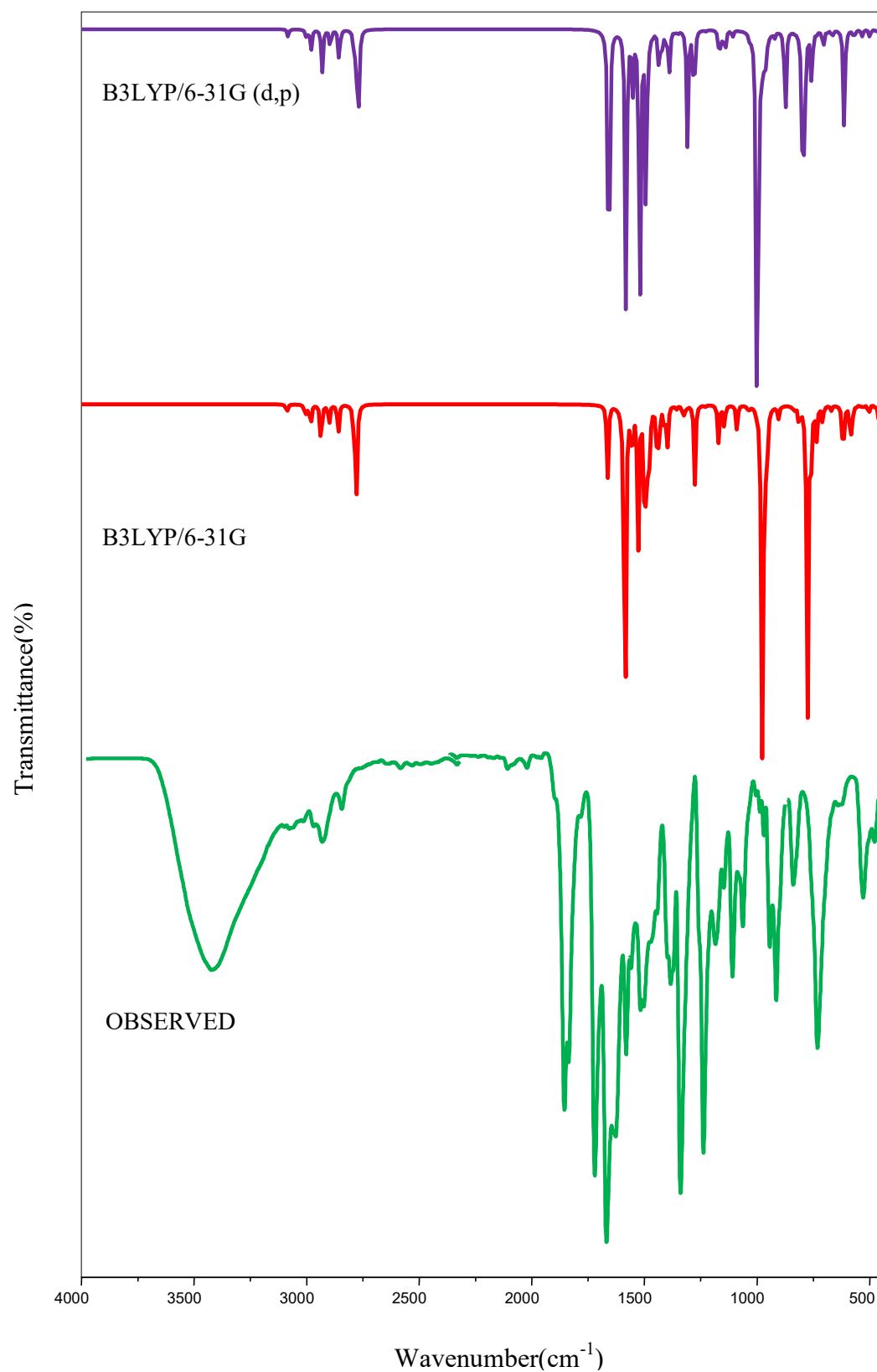


Figure 2 Observed FT-IR and simulated spectra of (4Z)-4-(4-Methylbenzylidene)-2-phenyl-1,3-oxazol-5(4H)-one

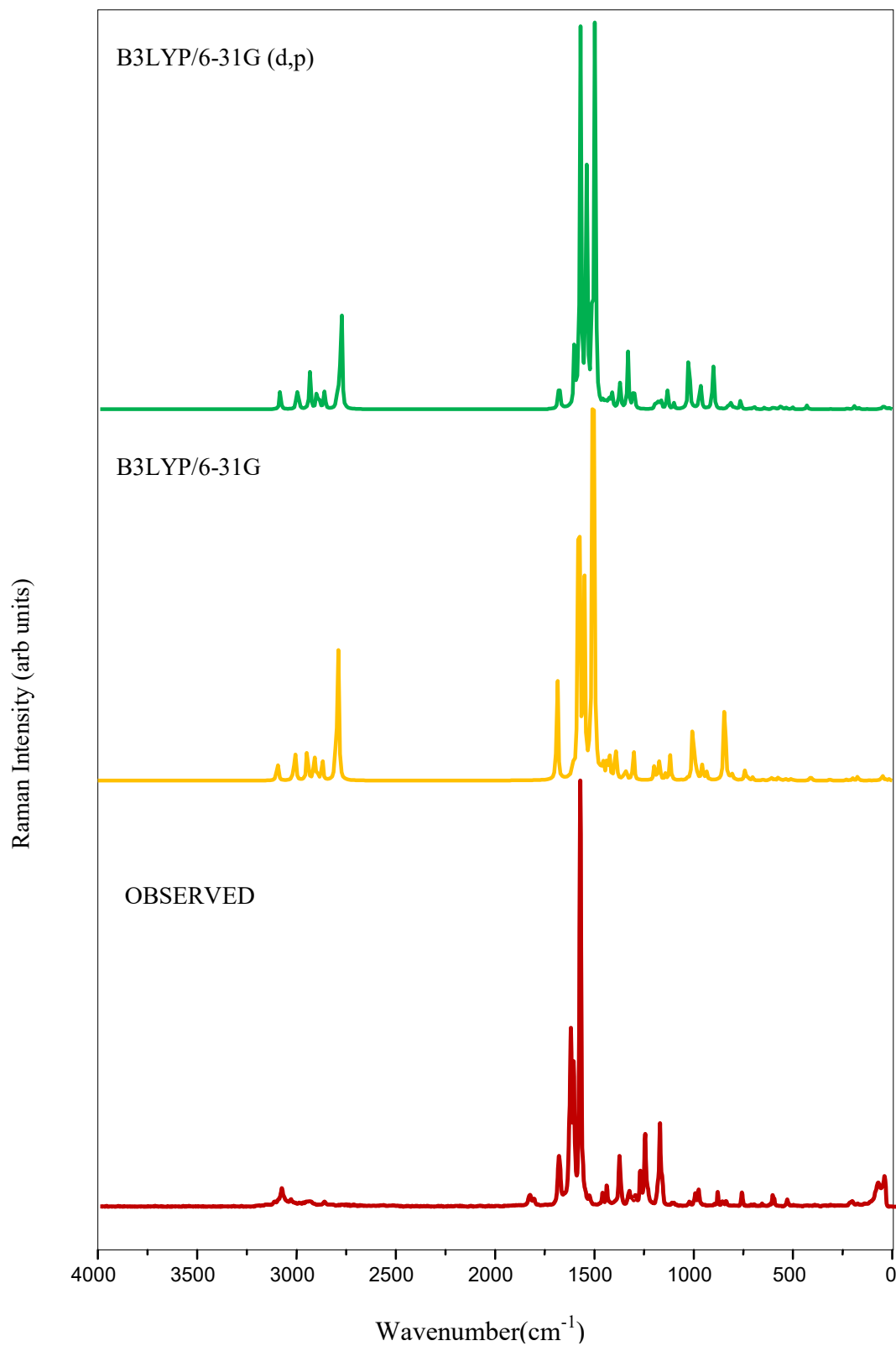


Figure. 3 Observed FT-Raman and Simulated Spectra of (4Z)-4-(4-Methylbenzylidene)-2-phenyl-1,3-oxazol-5(4H)-one

4.2.1 CH₃ vibrations

The stretching vibrations of CH₃ are expected in the range 3050-2850 cm⁻¹ for asymmetric and symmetric vibrations [19, 20]. The deformed modes of methyl group are expected in the range of 1485-1355 cm⁻¹. The methyl rocking wavenumbers are expected in the range 1100±95 cm⁻¹ and 1080± 80 cm⁻¹ [19].

Benzon et al [21] assigned the asymmetric CH₃ stretching vibrations at 3023, 2997, 2961 cm⁻¹ in IR spectrum, 3037, 3016, 2992, 2967 cm⁻¹ in Raman spectrum and for symmetric CH₃ stretching vibrations at 2934, 2916 cm⁻¹ theoretically and 2924 cm⁻¹ for IR spectrum, 2928, 2903 cm⁻¹ at Raman spectrum. Parveen et al [22] observed the CH₃ vibrations at 2980 cm⁻¹ and 2978 cm⁻¹ in the IR and Raman spectrum and theoretically observed at 3011, 2988, 2925 cm⁻¹. Benzon et al [14] asymmetric CH₃ groups are theoretically obtained at 3063, 2996 cm⁻¹ and experimentally observed at 3063 cm⁻¹ in IR spectrum, 2998 cm⁻¹ in Raman spectrum. For our title compound, the assCH₃ stretching vibrations occurs 2785 cm⁻¹ in FT-Raman spectrum and theoretically observed at 2796, 2790 cm⁻¹ and 2791, 2786 cm⁻¹ for B3LYP/6-31G and B3LYP/6-31G (d,p) basis sets. The symmetric stretching vibrations observed at 2788 cm⁻¹ and 2780 cm⁻¹ for the same basis sets.

Benzon et al [14] observed the CH₃ deformation modes at 1458, 1455, 1450, 1435 cm⁻¹ by theoretically and 1442, 1446 in FT-IR, FT-Raman spectrum. Parveen et al [22] observed the deformed methyl group at 1355 cm⁻¹ at IR and theoretically at 1449, 1434, 1358 cm⁻¹. Benzon et al [21] observed the CH₃ modes at 1468 cm⁻¹ (IR), 1470, 1435 cm⁻¹ (Raman) and calculated at 1464, 1458, 1455, 1435 cm⁻¹. In the present work, the CH₃ in-plane bending vibrations are assigned at 1374, 911 cm⁻¹ and 1420, 991 cm⁻¹ in FT-IR and FT-Raman spectrum. The computed wavenumbers are predicted by B3LYP/6-31G method at $\delta_{opb} = 1435$ cm⁻¹, $\delta_{ipb} = 1426$ cm⁻¹, $\delta_{sb} = 1380$ cm⁻¹, $\delta_{opr} = 993$ cm⁻¹, $\delta_{ipr} = 915$ cm⁻¹ and for B3LYP/6-31G (d,p) method at $\delta_{opb} = 1431$ cm⁻¹, $\delta_{ipb} = 1422$ cm⁻¹, $\delta_{sb} = 1374$ cm⁻¹, $\delta_{opr} = 990$ cm⁻¹, $\delta_{ipr} = 913$ cm⁻¹. In this study, the out-of-plane twisting vibration is observed at 38/31 cm⁻¹ for the above basis sets.

4.2.2 C-H stretching

The C-H stretching vibrations occur at 3120-3000 cm⁻¹ [19]. The C-H in-plane and out-of-plane bending occurs at 1315-995 cm⁻¹ and 1000-700 cm⁻¹ [19].

Parveen et al [22] observed the C-H stretching vibrations at 3088, 3038 cm⁻¹ in IR spectrum and 3102, 3072, 3035 cm⁻¹ in Raman spectrum. Haress et al [16] reported the C-H stretching at 2921, 2917, 2915 cm⁻¹. Renjith et al [23] observed the CH stretching vibration at 3081 cm⁻¹ and 3077, 3064 cm⁻¹ in IR and Raman spectrum, observed theoretically in the range of 3097-3057 cm⁻¹. For the title molecule, the CH stretching vibrations observed at 3001, 2900, 2802 cm⁻¹ in FT-IR spectrum, 3095, 3010, 2940 cm⁻¹ in FT-Raman spectrum and theoretically at 3095, 3015, 3006, 2991, 2945, 2910, 2896, 2870, 2802 cm⁻¹ by B3LYP/6-31G and 3091, 3010, 3001, 2989, 2941, 2905, 2891, 2866, 2800 cm⁻¹ by B3LYP/6-31G (d,p) methods.

The C-H in-plane bending for IR spectrum observed at 1294, 1145, 1115, 1035 cm⁻¹ and 1288, 1148 cm⁻¹ for FT-Raman spectrum for Parveen et al [22]. Haress et al [16] observed the in-plane bending for 2-(Adamantan-1-yl)-5-(4-nitrophenyl)-1,3,4-oxadiazole at 1349, 1299, 1085 cm⁻¹ theoretically. Renjith et al [23] observed the in-plane bending at 1272, 1202, 1077 cm⁻¹ in IR spectrum and 1266, 1197, 1174, 1150 cm⁻¹ in Raman spectrum. In the present work, the in-plane bending vibrations observed at 1455, 1411, 1300, 1135, 1100, 1056 cm⁻¹ in FT-IR spectrum and 1460, 1386, 1304, 1295, 1102 cm⁻¹ in FT-Raman spectrum and theoretically obtained at 1464, 1453, 1420, 1391, 1309, 1300, 1170, 1140, 1115, 1064, 1004 cm⁻¹ by B3LYP/6-31G and 1458, 1447, 1412, 1385, 1304, 1296, 1167, 1134, 1101, 1057, 1000 cm⁻¹ by B3LYP/6-31G (d,p) methods.

The out-of-plane bending by Parveen et al [22] assigned at 947, 922, 820, 808 cm^{-1} for IR spectrum and 820, 920 cm^{-1} for Raman spectrum. Haress et al [16] reported the out-of-plane bending at 943, 845, 821 cm^{-1} theoretically. Renjith et al [23] observed the out-of-plane bending for IR spectrum at 1272, 1202, 1077 and Raman spectrum at 1266, 1197, 1174, 1150. In the present work, the out-of-plane bending vibrations occurs at 888, 861, 733 cm^{-1} in FT-IR spectrum, 875, 836, 785 cm^{-1} in FT-Raman spectrum and 933, 890, 879, 863, 841, 805, 801, 790, 738, 722, 648 cm^{-1} by B3LYP/6-31G and 931, 886, 877, 860, 838, 802, 795, 786, 735, 718, 643 cm^{-1} by B3LYP/6-31G (d,p) methods.

4.2.3 C-O vibrations

The C-O band is expected in the region $1220 \pm 40 \text{ cm}^{-1}$ [20, 24, 25]. Benzon et al [21] reported the stretching of C-O appears at 1212 cm^{-1} in the IR spectrum, 1228 cm^{-1} in Raman spectrum and the calculated value is 1229 cm^{-1} . Ulahannan et al [26] reported that the stretching of C-O at 1215 cm^{-1} in IR and theoretically at 1208 cm^{-1} . Varghese et al [27] reported the C-O stretching at 1255 cm^{-1} in both IR and Raman spectra. Sagdinc et al [28] reported the C-O vibration at 1680, 1725, 1717 cm^{-1} for IR spectrum, at 1723 cm^{-1} Raman spectrum and at 1726 cm^{-1} observed theoretically. Veenakumar et al [29] assigned the C-O stretching vibrations at 1214, 1050 and 1396, 1208, 1050 in IR and Raman spectrum. For the title compound, the C-O stretching vibrations reported at 1680 and 1682 in FT-IR and FT-Raman spectrum. Theoretically at 1685, 1337 and 1680, 1332 in B3LYP/6-31G and B3LYP/6-31G (d,p) methods. The in-plane bending vibrations occurs at 1007 in FT-Raman spectrum, 1011, 830 and 1009, 824 in B3LYP/6-31G and B3LYP/6-31G (d,p) methods.

4.2.4 C-C vibrations

The C-C stretching is expected around $1600 \pm 50 \text{ cm}^{-1}$ [30]. Benzon et al [21] is observed at 1653 cm^{-1} , 1647 cm^{-1} in IR, Raman spectrum and assigned theoretically at 1630 cm^{-1} . Felfoldi et al [31] reported the C-C stretching vibrations at 1625 cm^{-1} theoretically. For the title molecule, C-C vibrations observed at 1602, 1580, 1510, 1251, 1183, 980 in FT-IR spectrum, 1605, 1502, 1304, 1251, 1190 in FT-Raman spectrum and theoretically at 1607, 1576, 1520, 1504, 1491, 1351, 1254, 1196, 1183, 982 and 1603, 1573, 1514, 1500, 1487, 1340, 1250, 1192, 1180, 978 B3LYP/6-31G and B3LYP/6-31G (d,p) methods. The in-plane bending vibrations observed at 563 and 224,65 in FT-IR and FT-Raman spectrum and 571, 353, 228, 211 and 565, 348, 225, 208 in the B3LYP/6-31G and B3LYP/6-31G (d,p) methods. The out-of-plane bending vibrations observed at 648, 312, 170, 29, 13 and 612, 309, 166, 25, 10 at B3LYP/6-31G and B3LYP/6-31G (d,p) methods.

4.2.5 C-N vibrations

Normally C-N stretching vibrations of aromatic rings are observed in the region at 1330-1260 cm^{-1} due to stretching of the phenyl carbon-nitrogen bond [20].

Parveen et al [22] assigned the C-N stretching modes at 1211, 1208 cm^{-1} in the IR, Raman and at 1270, 1209 cm^{-1} theoretically. Bhagyasree et al [32] reported C-N stretching modes at 1247 and 1236 cm^{-1} and Mary et al [33] reported the C-N stretching modes at 1238 cm^{-1} in Raman spectrum and theoretically at 1233, 1209 cm^{-1} . Sandhyarani et al [34] reported the C-N stretching at 1318 cm^{-1} and Benzon et al [21] C-N is assigned at 1247, 1183, 1131, 1122 cm^{-1} theoretically and experimentally observed at 1247, 1181, 1140, 1120 cm^{-1} in Raman spectrum, 1153 in IR spectrum. Veenakumar et al [29] reported the C-N stretching mode at 1609, 1132 for IR spectrum and 1605, 1520, 1288, 1170, 1009, 971 at FT-Raman spectrum, and observed theoretically in the range of 1607-969. Hareeas et al [16] observed the C-N stretching at 1535, 1520 cm^{-1} and 1540, 1521 cm^{-1} in the IR and Raman spectra and calculated wavenumber at 1531, 1516 cm^{-1} . For the title molecule, the C-N vibrations observed at 1545 in FT-Raman spectrum and theoretically at 1549, 1028 and 1542, 1025 at B3LYP/6-31G and B3LYP/6-31G (d,p) methods.

4.2.6 Ring vibrations

The ring breathing mode of the 1,4-disubstituted benzenes with entirely different substituent [24] has been reported in the interval 780-880 cm^{-1} . Mary et al [35] reported the ring breathing modes are assigned at 977, 748 cm^{-1} for benzene ring theoretically. For our title compound, the ring breathing modes are observed at 968 in FT-Raman spectrum, 970 and 967 assigned theoretically by B3LYP method with 6-3.1G and 6-31G (d,p) basis sets.

For the title molecule, the in-plane bending vibrations of oxazole and benzene rings are observed at 902, 812, 693, 503 in FT-IR spectrum and 694, 602, 527,101 in FT-Raman spectrum and theoretically reported at 954, 906, 815, 765, 700, 606, 590, 560, 535, 506, 431, 195, 110, 89 cm^{-1} in B3LYP/6-31G and 950, 902, 812, 763, 695, 600, 587, 554, 530, 501, 428, 189, 102, 85 cm^{-1} in B3LYP/6-31G (d,p) methods. The out-of-plane bending vibrations observed at 402 in IR spectrum and obtained theoretically at 631, 491, 470, 408, 376, 128, 61 cm^{-1} in B3LYP/6-31G, 627, 488, 467, 401, 373, 123, 56 cm^{-1} in B3LYP/6-31G (d,p) methods.

4.5. Natural bond orbital analysis

The natural bond orbital (NBO) analysis is an effective tool for determining the chemical interpretation of hyper conjugative interactions and electron density transfer from filled lone pair orbital of one subsystem to a vacant orbital of another subsystem. The DFT calculations are used to analyze various second order interactions between the filled and vacant orbital's of a system which gives a measure of delocalization and hyper conjugation [36]. The hyper conjugation interaction energy can be obtained from the second order perturbation method [37] as follows:

$$E(2) = \Delta E_{ij} = q_i \left(\frac{F_{i,j}}{E_j - E_i} \right)^2 \quad (1)$$

where q_i is the donor orbital occupancy, E_i and E_j are the diagonal elements and $F(i, j)$ is the off diagonal NBO Fock matrix element. The NBO analysis shows the various possible donors and acceptors in the molecule with their occupancy value in each position are tabulated in Table 4. The important hyper-conjugative interactions are C12-N13 from O14 of LP(2) $O14 \rightarrow \sigma^*(C12-N13)$, C16-O17 from O14 of LP(2) $O14 \rightarrow \sigma^*(C16-O17)$, O14-C16 from O17 $\rightarrow \sigma^*(O14-C16)$, C12-O14 from N13 $\rightarrow \sigma^*(C12-O14)$, C15-C16 from C18 $\rightarrow \sigma^*(C15-C16)$ with stabilization energies 19.37, 16.14, 11.1, 4.66, 4.09 kJ/mol.

Table 3. Second Order Perturbation Theory Analysis of Fock Matrix in NBO Basis Corresponding to Intra Molecular Bands of (4Z)-4-(4-Methylbenzylidene)-2-phenyl-1, 3-oxazol-5(4H)-one

Donor	Acceptor	E(2)(kcal/mol) BMP	E(J)-E(i) (a.u) BMP	F _(ij) (a.u) BMP
LP (1) N 13	BD*(1) C 12 - O 14	4.66	0.62	0.068
LP (1) N 13	BD*(1) C 15 - C 16	2.71	0.82	0.06
LP (1) N 13	BD*(1) C 15 - C 18	0.35	0.72	0.02
LP (1) N 13	BD*(1) C 16 - O 17	0.4	0.63	0.02
LP (1) O 14	BD*(1) C 12 - N 13	1.89	0.99	0.055
LP (1) O 14	BD*(1) C 15 - C 16	1.58	1.04	0.051
LP (1) O 14	BD*(1) C 16 - O 17	0.39	0.84	0.023

LP (2) O 14	BD*(2) C 12 - N 13	19.37	0.31	0.1
LP (2) O 14	BD*(2) C 16 - O 17	16.14	0.29	0.089
LP (1) O 17	BD*(1) O 14 - C 16	0.86	1.02	0.038
LP (1) O 17	BD*(1) C 15 - C 16	1.48	1.23	0.054
LP (2) O 17	BD*(1) O 14 - C 16	11.1	0.5	0.094
LP (2) O 17	BD*(1) C 15 - C 16	2.95	0.71	0.059
LP (2) O 17	BD*(2) C 19 - C 20	0.28	0.28	0.012
LP (1) C 18	BD*(1) N 13 - C 15	0.6	0.77	0.027
LP (1) C 18	BD*(1) C 15 - C 16	4.09	0.82	0.073
LP (1) C 18	BD*(1) C 19 - C 20	0.34	0.93	0.023
LP (1) C 18	BD*(2) C 19 - C 20	4	0.38	0.054
LP (1) C 18	BD*(1) C 19 - C 21	0.35	0.93	0.023

a E(2) means energy of hyperconjugative interactions (stabilization energy).

b Energy difference between donor and acceptor i and j NBO orbitals.

c F(i,j) is the Fock matrix element between i and j NBO orbitals.

Also, the various possible transitions among these donors and acceptors are provided. The larger the E (2) values the more intense will be the interaction between the electron donors and electron acceptor groups i.e. more electron donating tendency and greater the extent of conjugation of the whole system tabulated on Table 5. σ (C15-C16) orbital with 0.99659 a.u. energy has 50.91% C15 character in SP^(1.98) hybrid and has 49.08% C16 character in SP^(1.44) hybrid. The idealized SP^(1.44) hybrid has 66.49%, 58.95% p-character and 33.51%, 41.05% s-character. The two coefficients 0.7136 and 0.7006 are called polarization coefficients. σ (C16-O17) orbital with 0.99543 a.u energy has 40.43% C16 character in SP^(1.99) hybrid and has 59.57% O17 character in SP^(3.85) hybrid. The idealized SP^(3.75) hybrid has 66.61%, 79.37% p-character and 33.39%, 20.63% s-character. The two coefficients 0.6358 and 0.7718 are called polarization coefficients. The oxygen (O17) has a larger percentage of this NBO, 79.37% and gives the larger polarization coefficient 0.7718 because it has a higher electronegativity. Similarly, the carbon (C29) has a larger percentage of this NBO, 74.12% and gives the larger polarization coefficient 0.6988. The carbon and nitrogen have a lesser percentage of NBO and give a lesser polarization coefficient. The carbon (C16) has a lower percentage of NBO, 25.22% and gives the lesser polarization coefficient 0.5514.

Table 4. NBO Analysis of Bonding and Antibonding Orbit of (4Z)-4-(4-Methylbenzylidene)-2-phenyl-1,3-oxazol-5(4H)-one

Band (A-B)	ED/Energy (a.u.)	ED %	ED %	NBO	S(%)	P(%)
σ C 1-C 2	0.98877	49.7	50.3	0.7050 sp ^(1.85)	35.12	64.88
				0.7092 sp ^(1.81)	35.59	64.41
σ C 1-C 6	0.99014	50.01	49.99	0.7072 SP ^(1.84)	35.26	64.74
				0.7070 SP ^(1.84)	35.26	64.75
σ C 2-C 3	0.9825	48.22	51.78	0.6944 SP ^(1.88)	34.74	65.26
				0.7178 SP ^(1.83)	35.17	64.83
σ C 3-C 4	0.98248	51.79	48.21	0.7196 SP ^(1.85)	35.13	64.87
				0.6944 SP ^(1.88)	34.71	65.29

σ C 3-C 12	0.98717	50.62	49.38	0.7115 SP ^(2.37)	29.67	70.33
				0.7027 SP ^(1.31)	43.28	56.72
σ C 3-C 12	0.98879	50.29	49.71	0.7092 SP ^(1.81)	35.61	64.39
				0.7050 SP ^(1.85)	35.14	64.86
σ C 4-C 5	0.98879	50.29	49.71	0.7092 SP ^(1.81)	35.61	64.39
				0.705 SP ^(1.85)	35.14	64.86
σ C 5-C 6	0.99013	50.01	49.99	0.7072 SP ^(1.84)	35.24	64.76
				0.707 SP ^(1.84)	35.25	64.75
σ C 12-N 13	0.99155	41.08	58.92	0.641 SP ^(2.13)	31.98	68.02
				0.7676 SP ^(2.13)	31.91	68.09
σ C 12-O 14	0.99353	30.56	69.44	0.5528 SP ^(3.04)	24.77	75.23
				0.8333 SP ^(2.17)	31.58	68.42
σ N 13-C 15	0.99006	58.41	41.59	0.7643 SP ^(2.07)	32.58	67.42
				0.6449 SP ^(2.34)	29.93	70.07
σ O14-C 16	0.9935	69.59	30.41	0.8342 SP ^(2.38)	29.58	70.42
				0.5514 SP ^(2.97)	25.22	74.78
σ C 15-C 16	0.99659	50.91	49.08	0.7136 SP ^(1.98)	33.51	66.49
				0.7006 SP ^(1.44)	41.05	58.95
σ C 15-C 18	0.98694	54.63	45.37	0.7391 SP ^(1.74)	36.43	63.57
				0.6736 SP ^(2.43)	29.2	70.8
σ C 16-O 17	0.99543	40.43	59.57	0.6358 SP ^(1.99)	33.39	66.61
				0.7718 SP ^(3.85)	20.63	79.37
σ C 18-C 19	0.9882	46.62	53.38	0.5828 SP ^(2.19)	31.31	68.69
				0.7306 SP ^(2.55)	28.16	71.84
σ C 19-C 20	0.98691	50.97	49.03	0.714 SP ^(1.78)	35.92	64.08
				0.7002 SP ^(1.86)	35.02	64.98
σ C 19-C 21	0.9869	50.97	49.03	0.714 SP ^(1.78)	35.92	64.08
				0.7002 SP ^(1.85)	35.03	64.97
σ C 20-C 22	0.98822	50.25	49.75	0.7098 SP ^(1.82)	35.49	64.51
				0.7053 SP ^(1.85)	35.07	64.93
σ C 21-C 24	0.98821	50.25	49.75	0.7089 SP ^(1.82)	35.46	64.54
				0.7053 SP ^(1.85)	35.05	64.95
σ C 22-C 26	0.98822	49.26	50.74	0.7019 SP ^(1.83)	35.32	64.68
				0.7123 SP ^(1.87)	34.9	65.1

4.6. Molecular electrostatic potential functions

Molecular electrostatic potential (MEP) is related to the electronic density which is very useful descriptor in understanding nucleophilic and electrophilic sites as well as hydrogen bonding interaction [38]. This analysis is also used to predict the biological activity of a molecule as well as its ability to form hydrogen bonding with its target protein. To predict the reactive sites such as electrophilic and nucleophilic sites for the title molecule, MEP at the B3LYP/6-31G (d,p) optimized geometry was calculated. The color range of the MEP diagram of the title molecule is shown in Fig.4 which starts with red color and ends with dark blue color which means different values of electrostatic potential at the surface of the molecule in the following decreasing order: Red > orange > yellow > blue > green, red, blue and green represent the regions of most negative, most positive and zero electrostatic potential respectively. The negative electrostatic potential corresponds to an attraction of the proton by the aggregate electron density in the molecule (shades of red), while the positive electrostatic potential corresponds to the repulsion of the proton by the atomic nuclei (shade of blue). The negative, (red) region of MEP were related to electrophilic reactivity and the positive (blue) regions to nucleophilic reactivity. From the MEP plot of the title molecule, it is evident that the negative charge covers the nitrogen in the oxazole ring and the positive region is over all the hydrogen atoms in the methylbenzylidene and benzene ring. The more electronegativity in the nitro group makes it the more reactive part in the molecule.

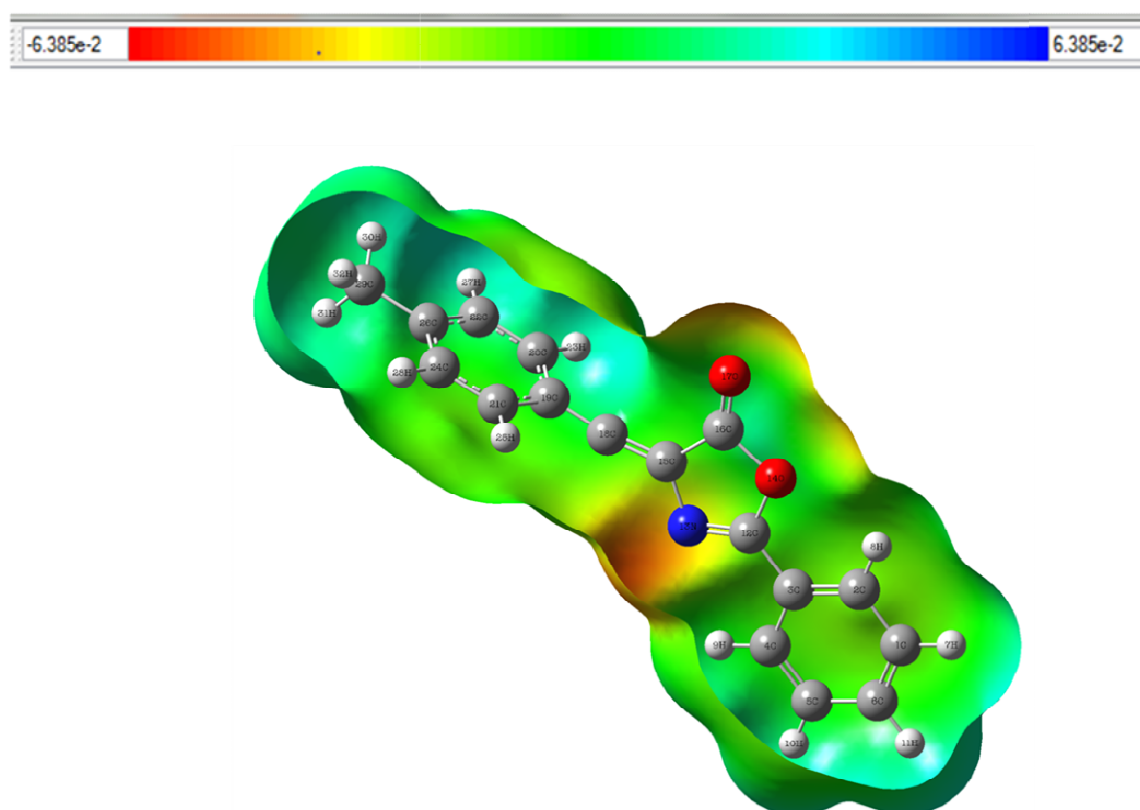


Figure 4. Molecular Electrostatic Potential Surfaces (4Z)-4-(4-Methylbenzylidene)-2-phenyl-1,3-oxazol-5(4H)-one

4.10. Molecular docking

The molecular interactions between the lead molecule and target protein of biological interest have become great importance within the field of drug design. Title molecule can be used for treating cancer, tubercular and convulsant. To explore the biological activity of the title molecule, molecular docking studies were carried out. The molecular mechanism of selectivity [39] can be observed by docking analysis of the lead molecule with many protein targets. The title molecule was docked into the active sites of proteins 5FDC, 1EOU, 5H8V, 1PCV, 2RER and 1NNU associated with convulsant, cancer, fungal, tubercular and human lymphatic filarial parasites activity. . The molecular docking binding energies (kcal/mol), intermolecular energy (kcal/mol) and inhibition constants (μM) were obtained and are tabulated in Table 5. The proteins were downloaded from the protein data bank website. The docking macromolecule i.e protein was prepared by removing the water, co-factors, co-crystallized ligands and AutoDock tools (ADT) graphical computer program was accustomed calculate Kollman charges and polar hydrogens. The active site of the macromolecule was defined to incorporate residues of the active site within the grid size of $60\text{\AA} \times 60\text{\AA} \times 60\text{\AA}$. The common method to evaluate the quality of docking result is to calculate the Root Mean Square Deviation (RMSD) between the docked cause and the well known crystal structure conformation. RMSD values up to 2\AA are considered reliable for a docking protocol [40]. Amongst the docked conformations of the co-crystallized ligand and scored well was visualized for ligand-protein interactions in Discovery Studio Visualizer 4.1 software. The docked ligand interactions with amino acids of the receptor and the ligand at the active sites of the receptor are stated in Fig.7

4.10.1. Anticonvulsant

Interaction of anticonvulsant proteins shows existence of many conventional bonds which are as follows: two Conventional hydrogen bond and one van der Waals bond was found in 5FDC interacting with amino acids (1.92\AA ; TYR A: 7, 2.01\AA ; HIS A:64, 3.14\AA ; GLY A:63) with different binding energy(-7.05 , -6.71 , -5.99) kcal/mol, inhibition constant (6.85 , 12.12 , 40.43) μM and RMSD value is (8.468 , 25.279 , 13.263) \AA . One conventional bond, one π -donor hydrogen bond and one van der waals bond was found in 1EOU interacting with amino acids (2.3\AA ; ASN A:11, 2.93\AA ; TYR A:7, 3.5\AA ; GLY A:63) with different binding energy(-7.23 , -6.42 , -6.23) kcal/mol, inhibition constant (5.02 , 19.84 , 27.11) μM and RMSD value is (9.016 , 13.611 , 8.945) \AA .

4.10.2 Anticancer

Interaction of anticancer proteins shows existence of many conventional bonds which are as follows: three Conventional hydrogen bond and one π - π stacked bond was found in 5H8V interacting with amino acids (2.26\AA ; LEU A:160, 2.18\AA ; TYR A:219, 3.66\AA ; ALA A:161, 3.21\AA ; VAL A:194) with different binding energy(-7.97 , -7.63 , -5.3 , -5.18) kcal/mol, inhibition constant (1.44 , 2.53 , 129.56 , 158.36) μM and RMSD value is (27.135 , 26.811 , 9.135 , 19.745) \AA .

4.10.3. Antifungal

Interaction of antifungal proteins shows existence of many conventional bonds which are as follows: two Conventional hydrogen bond, two van der Waals bond and one π - π stacked bond was found in 1PCV interacting with amino acids (1.97\AA ; ARG A:44, 2.62\AA ; ARG A:44, 2.74\AA ; PHE A:95, 3.12\AA ; MET A: 42, 2.12\AA ; TRP A: 75) with different binding energy (-6.6 , -5.97 , -5.7 , -5.63 , -6.14) kcal/mol, inhibition constant (14.5 , 42.39 , 65.97 , 73.29 , 31.45) μM and RMSD value is (35.044 , 44.564 , 46.382 , 46.842 , 32.706) \AA .

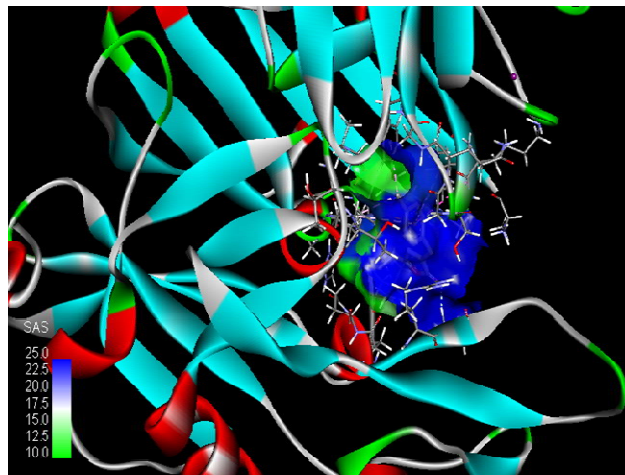
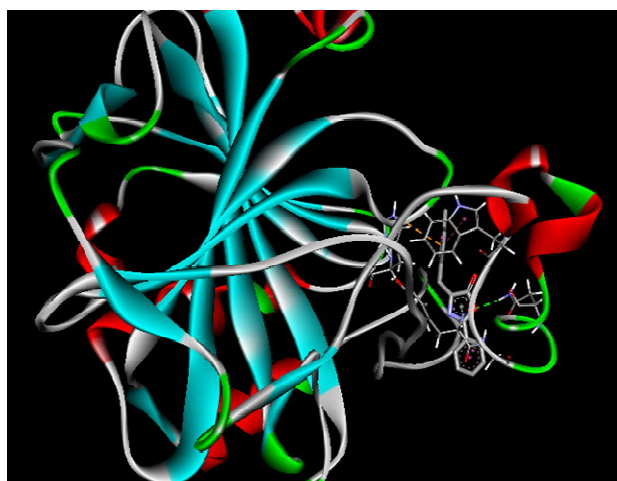
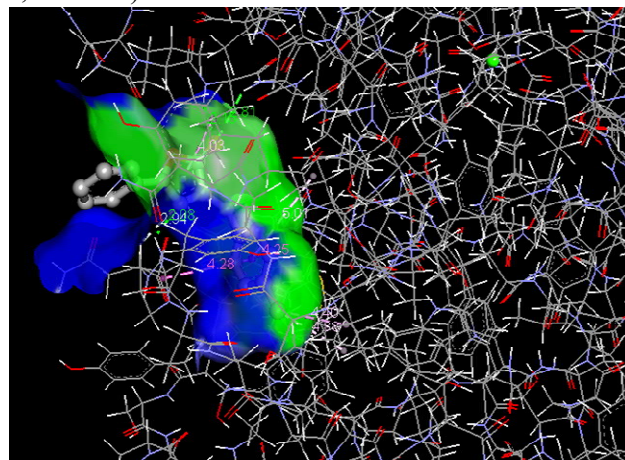
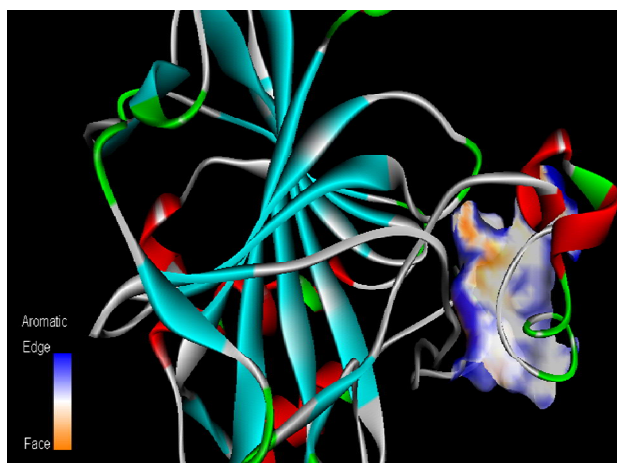
4.10.4. Antitubercular

Interaction of antitubercular proteins shows existence of many conventional bonds which are as follows: two Conventional hydrogen bond and one carbon-hydrogen bond was found in 2RER interacting with amino acids (1.83\AA ; ARG A:82, 2.22\AA ; ARG A:82, 2.35\AA ; PRO A:87) with different binding

energy(-7.61, -7.34, -6.95) kcal/mol, inhibition constant (2.63, 4.14, 8.03) μM and RMSD value is (49.626, 55.046, 53.908) \AA .

4.10.5. Human lymphatic filarial parasites

Interaction of human lymphatic filarial parasites proteins shows existence of many conventional bonds which are as follows: two carbon-hydrogen bond and two van der Waals bond was found in INNU interacting with amino acids (2.03 \AA ; ALA A:169, 2.01 \AA ; SER A:170, 2.12 \AA ; GLY A:104, 4.1 \AA ; ASN A:218) with different binding energy (-7.67, -7.01, -7.49, -6.71) kcal/mol, inhibition constant (2.37, 7.31, 3.23, 11.99) μM and RMSD value is (99.845, 111.129, 103.844, 108.043) \AA .



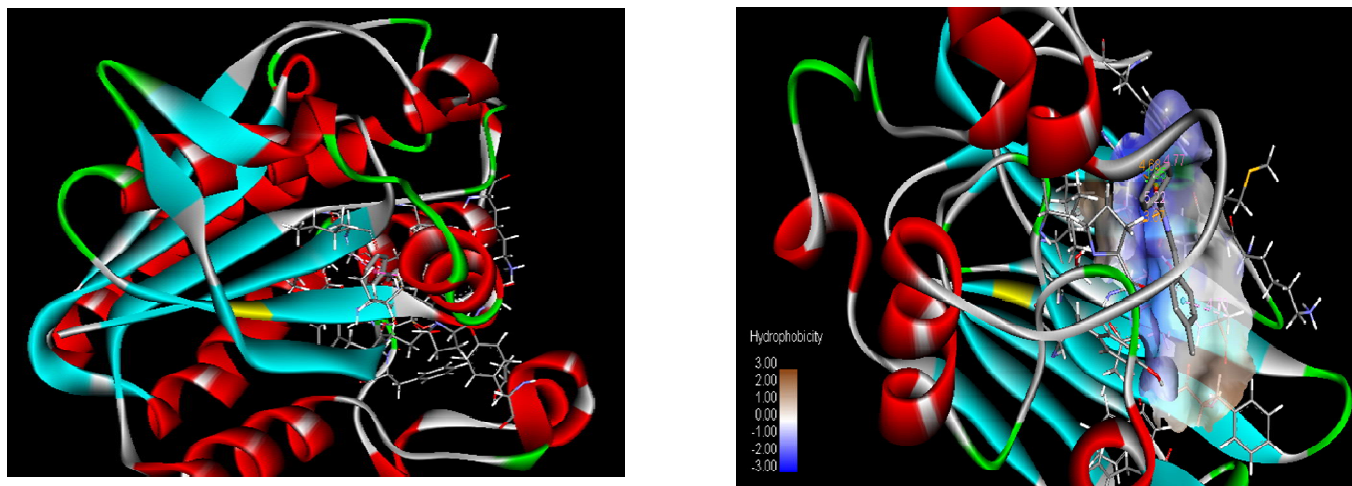


Figure 5. Binding site between Protein – 5FDC, 5H8X, 1PCV, 2OHM, 1NNU, 1EOU, 2RER and Ligand (4Z)-4-(4-Methylbenzylidene)-2-phenyl-1,3-oxazol-5(4H)-one

Table 5. Binding affinity for docking in (4Z)-4-(4-Methylbenzylidene)-2-phenyl-1,3-oxazol-5(4H)-one

Drug	Protein	Type of activity	Binding affinity (kcal/mol)	Etimated inhibition constant Ki(μ M)	Bonded residues	Nature of bond	Bond distance (\AA)	RMSD
(4Z)-4-(4-Methylbenzylidene)-2-phenyl-1,3-oxazol-	5FDC	Anticonvulsant	-7.05	6.85	TYR A:7	Conventional Hydrogen bond	1.92	8.468
			-6.71	12.12	HIS A:64	Conventional Hydrogen bond	2.01	25.279
			-6.25	26.17	GLY A: 6	π -Anion	3.02	13.607
			-5.99	40.43	GLY A: 63	Van der waals	3.14	13.263
			-5.78	58.01	PHE A: 231	π - π Alkyl	3.16	35.532
	5H8X	Anticancer	-7.97	1.44	LEU A: 160	Conventional Hydrogen bond	2.26	27.135
			-7.63	2.53	TYR A: 219	Conventional Hydrogen bond	2.18	26.811
			-5.3	129.56	ALA A:161	Conventional Hydrogen bond	3.66	9.135
			-5.18	158.36	VAL A: 194	π - π Stacked	3.21	19.745
			-4.99	221.37	LEU A: 194	Alkyl	2.76	14.536
			-4.96	232.75	HIS A: 197	Amide-Pi Alkyl	4.37	14.701
			-4.86	273.78				19.569
	-4.77	318.57				19.938		
-4.73	342.15				20.54			
1PCV	Antifungal	-6.6	14.5	ARG A: 44	Conventional Hydrogen bond	1.97	35.044	

5(4H)-one			-6.14	31.45	TRP A: 75	π - π Stacked	2.12	32.706
			-5.97	42.39	ARG A:44	Conventional Hydrogen bond	2.62	44.564
			-5.7	65.97	PHE A:95	Van der waals	2.74	46.382
			-5.64	73.29	MET A:42	Van der waals	3.12	46.842
			-5.63	74.76	GLU A:84	π -Anion	5.4	21.728
			-5.59	80.5	ALA A;86	π -Alkyl	5.37	47.042
	1EOU	Anticonvulsant	-7.23	5.02	ASN A: 11	Conventional Hydrogen bond	2.3	9.016
			-7.01	7.29	HIS A: 64	π -Cation	2.93	11.272
			-6.42	19.84	TYR A: 7	π -Donor Hydrogen bond	3.27	13.611
			-6.23	27.11	GLY A: 63	Van der waals	3.5	8.945
			-6.03	37.84	TYR A: 5	π - π T-Stacked	5.02	16.602
	2RER	Antitubercular	-7.61	2.63	ARG A: 82	Conventional Hydrogen bond	1.83	49.626
			-7.34	4.14	ARG A: 82	Conventional Hydrogen bond	2.22	55.046
			-7.2	5.27	TRP A: 63	π - π Stacked	2.24	53.799
			-6.95	8.03	PRO A: 87	Carbon - Hydrogen Bond	2.35	53.908
			-6.65	13.4	TRP A: 65	π -Sigma	4.12	53.525
	1NNU	Human lymphatic filarial parasites	-7.67	2.37	ALA A: 169	Carbon - Hydrogen Bond	2.03	99.845
			-7.49	3.23	GLY A: 104	Van der waals	2.12	103.844
			-7.01	7.31	SER A: 170	Carbon Hydrogen Bond	2.01	111.129
			-6.94	8.12	LYS A:240	π -Cation	2.6	107.16
			-6.78	10.74	ASP A: 168	π -Anion	3.3	105.347
-6.71			11.99	ASN A:218	Van der waals	4.1	108.043	

5. Conclusion

The FT-IR and FT-Raman spectral measurements have been performed for (4Z)-4-(4-Methylbenzylidene)-2-phenyl-1,3-oxazol-5(4H)-one. In the present work, to calculate the geometrical parameters of the optimized structure, quantum chemical techniques have been used. The stability of the molecule arising hyper-conjugative interaction and charge delocalization has been studied using NBO analysis. The HOMO-LUMO analysis is used to determine the charge transfer within the molecule the calculated HOMO-LUMO energies show the chemical reactivity of the molecule. The energy gap (ΔE) is 2.8969 eV. From the MEP plot, it is evident that the negative charge covers the nitrogen in the oxazole group and the positive region is over all the hydrogen atoms. Molecular docking studies were carried out for various proteins such as 5FDC, 1EOU, 5H8V, 1PCV, 2RER and 1NNU.

References

- [1] N. B. Patel, F. M. Shaih, "4-thiazolidinones of nicotinic acid with 2-amino-6-methyl benzothiazole and their biological activity", *Sci Pharm* vol.no.78 (2010) 753-765.
- [2] L. "Swellmeen, 1,3-Oxazole derivatives: a review of biological activities as antipathogenic", *Der pharma chemical*, vol.no.8 (2016) 269-286.
- [3] W. Zhang, W. Liu, X. Jiang, F. Jiang, H. Zhuang, L. Fu, "synthesis and antimicrobial activity of chiral 2-emica, (substituted-hydroxyl)-3-(benzo[d]oxazol-5-yl)propanoic acid derivatives", *Eur. Journal of med. chem.*, vol.no.46 (2011) 3639-3650.
- [4] D. Kumar, N.M. Kumar, S. Sundaree, E.O. Johnson, K. Shah, "An expeditious synthesis and anticancer activity of novel 4-(3'-indolyl)oxazole", *Eur. Journal of med. chemical.*, vol.no.45 (2010) 1244-1249.
- [5] G.C. Moraski, M. Chang, A. Villegas-Estrada, S.G. Franzblau, M. Möllmann, M.J. Miller, "Structure-activity relationship of new anti-tuberculosis agents derived from oxazoline and oxazole benzyl esters", *Journal of med. chemical.*, vol.no.45 (2010) 1703-1716.
- [6] G. Eren, "Synthesis, biological evaluation, and docking studies of novel heterocyclic diaryl compounds as selective COX-2 inhibitors". *Bioorg Med Chemistry.*, vol.no.18 (2010) 6367-6376.
- [7] W.T. Ashton, R.M. Sisco, H. Dong, K.A. Lyons, H. He, G.A. Doss, B. Leiting, R.A. Patel, J.K. Wu, F. Marsilio, N.A. Thornberry, A.E. Weber, "Dipeptidyl peptidase IV inhibitors derived from β -aminoacylpiperidines bearing a fused thiazole, oxazole, isoxazole, or pyrazole", *Bioorg Med. Chemistry.*, vol.no.15 (2005) 2253-2258.
- [8] R.D. Jadhav, K.S. Kadam, S. Kandre, T. Guha, M.M.K. Reddy, M.K. Brahma, N.J. Deshmukh, A. Dixit, L. Doshi, N. Potdar, A. A. Enose, R. A. Vishwakarma, H. Sivaramakrishnan, S. Srinivasan, K.V.S. Nemmani, A. Gupte, A. K. Gangopadhyay, R. Sharma, "Synthesis and biological evaluation of isoxazole, oxazole, and oxadiazole containing heteroaryl analogs of biarylureas as DGATI inhibitors", *Eur Journal of med chemistry.*, vol.no.54 (2012) 324-342.
- [9] M.J. Frisch, G.W. Trucks, H.B. Schlegel, G.E. Scuseria, M.A. Robb, J.R. Cheeseman, G. Scalmani, V. Barone, B. Mennucci, G.A. Peterson, H. Nakatsuji, M. Caricato, X. Li, H.P. Hratchian, F. Izmaylov, J. Bloino, G. Zheng, J.I. Sonnenberg, M. Hada, M. Ehara, K. Toyota, R. Fukuda, J. Hasegawa, M. Ishida, T. Nakajima, Y. Honda, O. Kitao, H. Nagari, T. Vreven, T.A. Montgomery Jr., J.E. Peralta, F. Ogliaro, M. Bearpark, J.J. Heyd, E. Brothers, K.N. Kudin, V.N. Staroverov, R.K. Kobayashi, J. Normand, K. Ragavachari, A. Rendell, J.C. Burant, S.S. Iyengar, J. Tomasi, M. Cossi, N. Rega, J.M. Millam, M. Klene, J.E. Knox, J.B. Cross, V. Bakken, C. Adamo, J. Jaramillo, R.G. Gomperts, R.E. Strarmann, O. Yazyev, A.J. Austin, R. Cammi, C. Pomelli, J.W. Ochterski, R.I. Martin, K. Morokuma, V.G. Zakrzewski, G.A. Voth, P. Salvador, J.J. Dannenberg, S. Dapprich, O. Farkas, J.V. Ortiz, J. Cioslowski, D.J. Fox, Gaussian, Inc., Wallingford CT, (2009).
- [10] R. Dennington, T. Kerth, J. Millam, "GaussView, Version 5", Semicham. Inc., Shawnee Mission K S, (2009).
- [11] O. Trott, A. J. Olson, "AutoDock Vina: improving the speed and accuracy of docking with a new scoring function, efficient optimization and multithreading" *Journal of. Comput. Chemistry.*, vol.no.31 (2010) 455-461.

- [12] W.L. Delano, "The PyMol Molecular Graphics System, Schroedinger LLC.pymolorg",. Version 1, (2002), <http://www.pymol.org.doi:citeulike-id:240061>.
- [13] Discovery studio 4.5 Guide, Accelrys Inc.,San Diego, (2009). <http://www.accelrys.com>.
- [14] K.B. Benzon, Hema Tresa Varghese, C. Yohannan Panicker, Kiran Pradhan, Bipranch Kumar Tiwary, Ashis Kumar Nanda, C. Van Alsenoy, " Spectroscopic and theoretical characterization of 2-(4-methoxyphenyl)-4,5-dimethyl-1H-imidazole 3-oxide", Spectrochimica Acta Part A, Mol. Biomol. Spectrosc., vol.no.151 (2015) 965-979.
- [15] A. Lifshitz, C. Tamburu, A. Suslensky, F. Dubnikova, "Thermal reactions of benzoxazole, Single pluse shock tube experiments and quantum chemical calculations", Journal of Phys. Chemistry., vol.no.110 (2006) 4607-4613.
- [16] G. Nadia Haress, A.M. Fatmah Alomary, A. Ali El-Emam, Y. Sheena Mary, C. Yohannan Panicker, A. Abdulaziz Al-Saadi, Javeed Ahmad War, Christian Van Alsenoy, "Spectroscopic investigation (FT-IR and FT-Raman), vibrational assignments, HOMO-LUMO analysis and molecular docking study of 2-(Adamantan-1-yl)-5-(4-nitrophenyl)-1,3,4-oxadiazole", Spectrochimica Acta Part A, Mol. Biomol. Spectroscopy., vol.no.1425 (2014) 1158-5.
- [17] H. Arslan, U. Florke, N. Kulcu, G. Binzet, "The molecular structure and vibrational spectra of 2-chloro-N-(diethylcarbamothioyl)benzamide by hartree-fock and density functional methods", Spectrochimica Acta Part A, Mol. Biomol. Spectroscopy., vol.no.68 (2007) 1347–1355.
- [18] P. Purkayastha, N. Chattopadhyay, "Role of rotamerisation and excited state intramolecular proton transfer in the photophysics of 3-(2'-hydroxyphenyl)benzoxazole, 2-(2'-hydroxyphenyl)benzimidazole and 2-(2'-hydroxyphenyl)benzothiozole: a theoretical study", Phys. Chem. Chem. Physics. vol.no.2 (2000) 203–210.
- [19] N.P.G. Roeges, "A Guide to the Complete Interpretation of Infrared Spectra of Organic Structures", John Wiley and Sons Inc., New York, (1994).
- [20] N.B. Colthup, L.H. Daly, S.E. Wiberly, "Introduction of Infrared and Raman Spectroscopy", Academic Press, New York, (1990).
- [21] K.B. Benzon, Hema Tresa Varghese, C. Yohannan Panicker, Kiran Pradhan, Bipranch Kumar Tiwary, Ashis Kumar Nanda, C. Van Alsenoy, "Spectroscopic investigation (FT-IR and FT-Raman), vibrational assignments,HOMO-LUMO, NBO, MEP analysis and molecular docking study of 2-(4-hydroxyphenyl)-4,5-dimethyl-1H-imidazole 3-oxide", Spectrochimica Acta Part A, Mol. Biomol. Spectroscopy., vol.no.1425 (2015) 359-5.
- [22] S. Shana Parveen, A. Monirah . Al-Alshaikh, C.Yohannan Panicker, Ali A. El-Emam, Mustafa Arisoy, Ozlem Temiz-Arpaci, C. Van Alsenoy, "Synthesis, vibrational spectroscopic investigations, molecular docking, antibacterial and antimicrobial studies of 5-ethylsulphonyl-2-(p-aminophenyl)benzoxazole", Journal of Mol.Structure., vol.no.1115 (2016) 94-104.
- [23] Renjith Raveendran Pillai, V. Vidya Menon, Y. Shyma Mary, Stevan Armakovi, J. Sanja Armakovi, C. Yohannan Panicker, "Vibrational spectroscopic investigations, molecular dynamic simulations and molecular docking studies of N''-diphenylmethylidene-5-methyl-1H-pyrazole-3-carbohydrazide", Journal of mol. Structure., vol.no.1130 (2017) 208-222.
- [24] G. Varsanyi, "Assignments of Vibrational Spectra of Seven Hundred Benzene Derivatives", Wiley, New York, (1974).

- [25] R.M. Silverstein, F.X. Webster, "Spectrometric Identification of Organic Compounds", 6th ed., John Wiley, Asia, (2003).
- [26] R.T.VUlahannan, C.Y. Panicker, H.T. Varghese, C.V. Alsenoy, R. Musiol, J. Jampilek, P.L. Anto, "Vibrational spectroscopic, ¹H NMR and quantum chemical computational study of 4-hydroxy-2-oxo-1,2-dihydroquinoline-8-carboxylic acid", *Spectrochimica Acta Part A, Mol. Biomol. Spectroscopy.*, vol.no.121 (2014) 445-456.
- [27] H.T. Varghese, C.Y. Panicker, D. Philip, J.R. Mannekutla, S.R. Inamdar, "IR, Raman and SERS studies of methyl salicylate", *Spectrochimica Acta Part A, Mol. Biomol. Spectroscopy.*, vol.no.66 (2007) 959-963.
- [28] G. Seda Sagdinc, Asli Esme, "Theoretical and vibrational studies of 4,5-diphenyl-2-2 oxazole propionic acid (oxaprozin)", *Spectrochimica Acta Part A*, 75 (2010) 1380-1376.
- [29] S. Veena Kumar, Y. Sheena Mary, Kiran Pradhan, Dhiraj Brahman, Y. Shyma Mary, M.S. Renjith Thomas, Roxy, C. Van Alsenoy, "Synthesis, spectral properties, chemical descriptors and light harvesting studies of a new bioactive azo imidazole compound", *Journal of Mol. Structure.*, vol.no.1199 (2020) 127035.
- [30] G. Socrates, "Infrared Characteristic Group Frequencies", John Wiley and Sons, New York, (1980).
- [31] K. Felfoldi, M. Sutyinszky, N. Nagy, I. Palinko, "Synthesis of E- and Z-o-methoxy-substituted 2,3-diphenyl prepenoic acids and its methyl esters", *Synth. Commun.* vol.no.30 (2000) 1543-1553.
- [32] J.B. Bhagyasree, J. Samuel, H.T.Varghese, C.Y. Panicker, M. Arisoy, O. Temiz-Arpaci, "Synthesis, FT-IR investigation and computational study of 5-[(4-bromophenyl)acetamido]-2-(4-tert-butylphenyl)benzoxazole", *Spectrochimica Acta Part A, Mol. Biomol. Spectroscopy.*, vol.no.115 (2013) 79-91.
- [33] Y.S. Mary, K. Raju, I. Yildiz, O. Temiz-Arpaci, H.I.S. Nogueira, C.M. Garandeiro C. Van Alsenov, "FT-IR, FT-Raman, surface enhanced Raman scattering and computational study of 2-(p-fluorobenzyl)-6-nitrobenzoxazole", *Journal of Mol. Structure.*, vol.no.1012 (2012) 22-30.
- [34] N. Sandhyarani, G. Skanth, S. Berchmanns, V. Yegnaraman, T. Pradeep, "A combined Surface - Enhancement Raman-X-ray photoelectron spectroscopic study of 2-mercaptobenzothiazole monolayers on polycrystalline Au and Ag films", *Journal of Colloid Interface Science.*, vol.no.209 (1999) 154-161.
- [35] Y. Sheena Mary, C. Yohannan Panicker, M. Sapnakumari, B. Narayana, B.K. Sarojini, A. Abdulaziz Al-Saadi, C. Van Alsenoy, H.K. Javeed Ahmad War, "Infrared spectrum, structural and optical properties and molecular docking study of 3-(4-Fluorophenyl)-5-phenyl-4,5-dihydro-1H-pyrazole-1-carbaldehyde", *Spectrochimica Acta Part A, Mol. Biomol. Spectroscopy.*, vol.no.138 (2015) 529-538.
- [36] J.R. Cheeseman, G.W. Trucks, T.A. Keith, M.J. Frisch, "A comparison of models for calculating nuclear magnetic resonance shielding tensors", *Journal of Chem. Physics.*, vol.no.104 (1996) 5497-5509.
- [37] P. Nagabala Subramanian, M. Karabacak, S. Periandy, "Molecular structure, polarizability, hyperpolarizability analysis and spectroscopic characterization of 1-(chloromethyl)-2-methylnaphthalene with experimental (FT-IR and FT-Raman) techniques and quantum chemical calculations", *Spectrochim, Acta A: Mol. Biomol. Spectroscopy.*, vol.no.85 (2012) 43-52.

- [38] E. Temel, Alas, C. alvar, H. Gokçe, A. Güder, Ç. Albayrak, Y.B. Alpaslan, D. Alpaslan , N. Dilek, “ DFT calculations, spectroscopy and antioxidant activity studies on (E)-2-nitro-4-[(phenylimino) methyl] phenol”, Spectrochim. Acta A Mol. Biomol. Spectroscopy., vol.no.136 (2015) 534-546.
- [39] Milosz Ruszkowski, Joanna Sliwiak, Agnieszka Ciesielska, Jakub Barciszewski, Michal Sikorska and Mariusz, Jaskolska., “Specific binding of gibberellic acid by Cytokinin Specific Binding Proteins: a new aspect of plant hormone-binding proteins with the PR-10 fold”, Acta Cryst., vol.no.70 (2014) 2032–2041.
- [40] B. Kramer, M. Rarey, T. Lengauer, “Evaluation of the FLEX incremental construction algorithm for protein–ligand docking, Proteins”, Struct. Funct. Genet. vol.no.37 (1999) 228-241.



Create account

Sign in

Sources

Title

[Find sources](#)

Title: [Journal Of Information And Computational Science](#) x

Filter refine list

Apply

Clear filters

Display options

Display only Open Access journals

Counts for 4-year timeframe

No minimum selected

1 result

Download Scopus Source List [Learn more about Scopus Source List](#)

Page Export to Excel Save to source list

View metrics for year: 2019

Source title ↓

CiteScore ↓ Highest percentile ↓

Citations ↓ Documents ↓ % Cited ↓

<input checked="" type="checkbox"/> 1	Journal of Information and Computational Science	N/A	N/A	N/A	N/A
---------------------------------------	--	-----	-----	-----	-----

PhD_Synopsis_Sub....pdf

Show all

Vibrational, structural and electronic studies of (2e)-1-(anthracene-9-yl)-3-(4-ethoxyphenyl) prop-2-en-1-one

K.Venil^a, A.Lakshmi^{a,*}, V. Balachandran^b

^a Department of Physics, Government Arts College, Trichy 620 022, India.

^b Centre for Research-Department of Physics, Arignar Anna Government Arts College, Musiri, 621 211, India.

Corresponding author E.Mail: laksharumugam13@gmail.com

Abstract

The FT-IR and FT-Raman spectra of (2E)-1-(Anthracene-9-Yl)-3-(4-ethoxy phenyl) prop-2-en-1-one (ABP) were recorded and analyzed. The vibrational wavenumbers were calculated using density functional theory (DFT) with B3LYP method and 6-31G, 6-31G(d,p) basis sets. The data obtained from wavenumber calculations are used to assign vibrational bands obtained in infrared and Raman spectra. The HOMO and LUMO analysis are used to determine the charge transfer within the molecule. A detailed molecular picture of the title compound and its interactions were obtained from NBO analysis. Local reactivity properties have been assessed using MEP surfaces.

Keywords

FT-IR, FT-Raman spectra, DFT, Anthracene

1. Introduction

Anthracene derivatives, such as Anthraquinone, are a significant building block for the synthesis of dyes and pigments [1,2] pharmaceuticals[3,4], agrochemicals[5], light-emitting devices [6], additives of paper making [7] as well as potentially used as a significant insecticide since it is postulated as the chemical which gives teak its resistance to insect and fungi attacks. Anthracene finds applications as photoelectric material in areas of photo-induced electron transfer, photochemical reactions and photon absorption [8-10]. They also have been widely used as fluorescent sensors, electronic donor or receptors with chromospheres, triple state sensitization agent and polymer of energy transfer detection agent 3-D memory material [11-14]. Hence, anthracene and its derivatives have been the subject matter for ongoing spectroscopic and theoretical investigations from the viewpoint of application and basic science.

The present study describes the vibrational spectral investigations of the title compound aided by density functional computations to elucidate the correlation between the molecular structure and biological activity, bonding features, electron delocalization and the intermolecular charge-transfer interactions. The molecular species which are responsible for chemical stability and chemical reactivity of the molecule were also identified by natural bond orbital (NBO) analysis and molecular electrostatic potential (MEP) surface analysis, respectively.

2. Experimental details

The infrared and Raman spectra of (2E)-1-(Anthracene-9-Yl)-3-(4-ethoxy phenyl)prop-2-en-1-one was recorded at Sophisticated Analytical Instrumentation Facility (SAIF), Indian Institute of Technology, Chennai. The FT-IR spectrum of the title compound was recorded in the frequency region 4000-400 cm^{-1} at a resolution of $\pm 1 \text{ cm}^{-1}$ Perkin Elmer spectrometer equipped with an MCT detector, a KBr beam splitter and global source. The spectrum of FT-Raman has been recorded using the 1064 nm line of an Nd-YAG laser as excitation wavelength in the region of 3500-100 cm^{-1} BRUKER model interferometer. The reported wavenumbers are expected to be accurate within ± 1 resolution with 250 mW of power at the sample in both techniques.

3. Computational details

The quantum chemical computations have been carried out to determine the molecular structure, vibrational frequencies with intensities and characteristics of the molecule using density functional triply-parameter hybrid model DFT/B3LYP [15,16] employing 6-31G and 6-31G(d, p) basis sets by Gaussian 09w software package [17]. The natural bonding orbital (NBO) calculations were performed using NBO 3.1 [18] program as implemented in Gaussian 09W [17] package at the 6/31G(d,p) level to understand various second-order interactions between another subsystem which is the measure of the intramolecular delocalization or hyper-conjugation. The HOMO-LUMO analysis was also investigated with the same level, to confirm the intramolecular charge transfer and also molecular electrostatic potential (MEP) contour map shows the various electrophilic region of the title molecule.

4. Results and discussions

4.1 Optimized molecular geometrical parameters

The title compound is optimized using the B3LYP method with the 6-31G and 6-31G (d,p) basis set. The complete geometrical optimization was accomplished by accepting the C1 point group symmetry. The experimental and calculated molecular geometrical parameters were given in Table 1 and the observed and calculated bond parameters are compatible with each other. The molecular structure of the title compound is shown in Fig.1. The experimental value of C-C bond length in the range of 1.4747-1.356 Å, which is much shorter than the typical C-C single bond

(1.54Å) and longer than the C=C double bond (1.34Å) [20, 21]. The title compound contains 28 C-C bonds, 21 C-H bonds, 3 C-O bonds and a single H-O bond. For the title compound, C1-C2, C1-C6, C3-C4, C5-C6, C7-C10, C9-C10, C11-C13, C14-C15, C24-C26, C26-C28, C28-C30, C30-C32, C31-C33, C32-C35 and C35-C37 bond length are computed as 1.3727, 1.4258, 1.4486, 1.3754, 1.4005, 1.4497, 1.372, 1.3748, 1.4747, 1.356, 1.4571, 1.411, 1.3885, 1.3942 and 1.4055 Å for the basis set B3LYP/6-31G and for 6-31G(d,p) basis set the bond length are observed as 1.3685, 1.4233, 1.4451, 1.3709, 1.3977, 1.4459, 1.3678, 1.3703, 1.4814, 1.3513, 1.4558, 1.4067, 1.3848, 1.3905 and 1.4045Å respectively. The C=O bond length (1.1988Å) given by DFT calculation agree with the reported literature values [27] and for the title compound is C24=O25= 1.2587/1.2298 Å.

According to the calculations for the title compound, the exocyclic angle C8-C24-O25 and O25-C24-C26 are reduced by 1.0° which shows the interaction between C24 and O25 (C8-C24-O25 = 121.1°/121.06° and O25-C24-C26 = 121.19°/ 121.92°) for the B3LYP/6-31G and /6-31G(d,p) basis sets. This departure of the exocyclic angles from 120° can be found in the crystal structure of the anthraquinone [28]. For the title compound, the bond angle for C33-C37-O40,

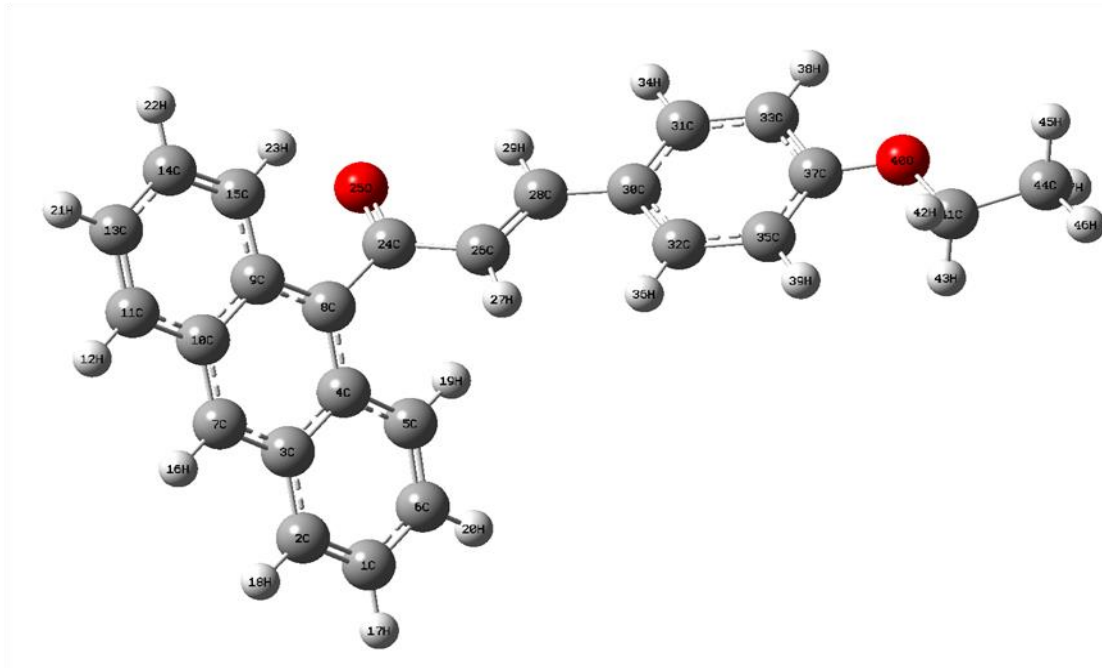


Fig. 1 Optimized molecular structure of (2E)-1-(Anthracene-9-yl)-3-(4-ethoxyphenyl)prop-2-en-1-one

Table 1 : Optimized structural parameters of (2E)-1-(Anthracene-9-yl) -3- (4ethoxyphenyl) prop-2-en-1-one

Parameter	Bond length (Å)		Parameter	Bond angle (degrees)		Parameter	Dihedral angle (degrees)	
	B3LYP/6-31G	B3LYP/6-31G(d,p)		B3LYP/6-31G	B3LYP/6-31G(d,p)		B3LYP/6-31G	B3LYP/6-31G(d,p)
C1-C2	1.373	1.365	C2-C1-C6	119.798	120.447	C6-C1-C2-C3	-0.653	0.161
C1-C6	1.426	1.426	C2-C1-H17	120.516	120.959	C6-C1-C2-H18	178.648	179.972
C1-H17	1.085	1.100	C6-C1-H17	119.679	118.594	H17-C1-C2-C3	-179.690	-179.854
C2-C3	1.433	1.433	C1-C2-C3	121.125	120.764	H17-C1-C2-H18	-0.389	-0.043
C2-H18	1.086	1.101	C1-C2-H18	120.695	121.155	C2-C1-C6-C5	0.980	0.001
C3-C4	1.449	1.429	C3-C2-H18	118.177	118.081	C2-C1-C6-H20	-178.164	179.909
C3-C7	1.400	1.399	C2-C3-C4	119.410	118.790	H17-C1-C6-C5	-179.975	-179.984
C4-C5	1.436	1.433	C2-C3-C7	121.245	121.701	H17-C1-C6-H20	0.881	-0.077
C4-C8	1.421	1.399	C4-C3-C7	119.343	119.509	C1-C2-C3-C4	-1.068	-0.253
C5-C6	1.375	1.365	C3-C4-C5	117.372	118.787	C1-C2-C3-C7	178.379	179.764
C5-C6	1.375	1.365	C3-C4-C5	117.372	118.787	C1-C2-C3-C7	178.379	179.764
C5-H19	1.083	1.101	C3-C4-C8	119.496	119.515	H18-C2-C3-C4	179.614	179.931
C6-H20	1.085	1.100	C5-C4-C8	123.092	121.699	H18-C2-C3-C7	-0.939	-0.052
C7-C10	1.401	1.399	C4-C5-C6	121.411	120.765	C2-C3-C4-C5	2.403	0.184
C7-H16	1.087	1.101	C4-C5-H19	119.192	118.076	C2-C3-C4-C8	-179.832	-179.923
C8-C9	1.42	1.399	C6-C5-H19	119.381	121.15	C7-C3-C4-C5	-177.054	-

	3				9			179.83 3
C8-C24	1.50 3	1.540	C1-C6-C5	120.838	120.44 8	C7-C3-C4-C8	0.710	0.061
C9-C10	1.45 0	1.429	C1-C6-H20	119.400	118.56 3	C2-C3-C7-C10	-178.066	- 179.95 3
C9-C15	1.43 6	1.433	C5-C6-H20	119.756	120.99 0	C2-C3-C7-H16	1.225	-0.021
C10- C11	1.43 3	1.433	C3-C7-C10	121.868	120.97 6	C4-C3-C7-C10	1.381	0.064
C11- H12	1.08 6	1.101	C3-C7-H16	119.073	119.49 9	C4-C3-C7-H16	-179.328	179.99 6
C11- C13	1.37 2	1.365	C10-C7- H16	119.056	119.52 5	C3-C4-C5-C6	-2.129	-0.028
C13- C14	1.42 6	1.426	C4-C8-C9	120.457	120.97 6	C3-C4-C5-H19	176.396	- 179.98 0
C13- H21	1.08 5	1.100	C4-C8-C24	120.270	119.49 9	C8-C4-C5-C6	-179.807	- 179.91 9
C14- C15	1.37 5	1.365	C9-C8-C24	119.265	119.52 5	C8-C4-C5-H19	-1.281	0.129
C14- H22	1.08 5	1.100	C8-C9-C10	119.150	119.51 0	C3-C4-C8-C9	-3.287	-0.097
C15- H23	1.08 1	1.101	C8-C9-C15	123.293	121.69 5	C3-C4-C8-C24	175.679	179.99 9
H19- C26	2.52 9	1.536	C10-C9- C15	117.535	118.79 5	C5-C4-C8-C9	174.344	179.79 4
H23- O25	2.27 7	2.036	C7-C10-C9	119.580	119.51 4	C5-C4-C8-C24	-6.690	-0.111
C24- O25	1.25 9	1.227	C7-C10- C11	120.998	121.70 4	C4-C5-C6-C1	0.465	-0.067
C24- C26	1.47 5	1.540	C9-C10- C11	119.422	118.78 2	C4-C5-C6-H20	179.606	- 179.97 3
C26- H27	1.08 5	1.070	C10-C11- H12	118.188	118.07 5	H19-C5-C6-C1	-178.058	179.88 3
C26- C28	1.35 6	1.540	C10-C11- C11	121.011	120.76 8	H19-C5-C6- H20	1.083	-0.023

C28-H29	1.09 0	1.070	H12-C11-H12	120.800	121.15 8	C3-C7-C10-C9	-0.893	-0.152
C28-C30	1.45 7	1.790	C11-C13-C14	119.826	120.44 9	C3-C7-C10-C11	179.193	179.90 0
C30-C31	1.41 6	1.395	C11-C13-H21	120.485	120.97 3	H16-C7-C10-C9	179.816	179.91 6
C30-C32	1.41 1	1.395	C14-C13-H21	119.689	118.57 8	H16-C7-C10-C11	-0.098	-0.032
C31-C33	1.38 9	1.395	C13-C14-C11	121.048	120.44 2	C4-C8-C9-C10	3.761	0.009
C31-H34	1.08 6	1.100	C13-C14-H22	119.317	118.58 0	C4-C8-C9-C15	-177.992	- 179.92 0
C32-C35	1.39 4	1.395	C15-C14-H22	119.634	120.97 7	C24-C8-C9-C10	-175.215	179.91 3
C32-H36	1.08 5	1.100	C9-C15-C14	121.158	120.76 4	C24-C8-C9-C15	3.033	-0.016
C33-C37	1.40 5	1.395	C9-C15-H23	118.799	118.07 3	C4-C8-C24-O25	129.436	126.86 1
C33-H38	1.08 3	1.100	C14-C15-H23	120.017	121.16 3	C4-C8-C24-C26	-54.308	-0.002
C35-C37	1.40 6	1.395	C8-C24-O25	121.120	91.051	C9-C8-C24-O25	-51.586	-53.045
C35-H39	1.08 3	1.100	C8-C24-C26	117.575	115.55 0	C9-C8-C24-C26	124.670	- 179.90 8
C37-O40	1.38 4	1.430	O25-C24-C26	121.196	122.22 5	C8-C9-C10-C7	-1.682	0.115
O40-C41	1.46 4	1.430	C24-C26-H27	117.112	109.47 1	C8-C9-C10-C11	178.233	- 179.93 5
C41-H42	1.09 8	1.070	C24-C26-C28	120.960	109.47 1	C15-C9-C10-C7	179.970	- 179.95 4
C41-H43	1.09 8	1.070	H27-C26-C28	121.907	109.47 1	C15-C9-C10-C11	-0.115	-0.004
C41-C44	1.51 9	1.540	C26-C28-H12	115.950	120.00 0	C8-C9-C15-C14	-178.256	179.91 1
C44-H45	1.09 4	1.070	C26-C28-C30	128.050	120.00 0	C8-C9-C15-H23	3.601	-0.101

C44-H46	1.09 6	1.070	C29-C28-C30	116.001	120.00 0	C10-C9-C15-C14	0.018	-0.019
C44-H47	1.09 4	1.070	C28-C30-C31	118.933	120.00 8	C10-C9-C15-H23	-178.125	179.97 0

C37-O40-C41, and O40-C41-C44 has $115.7^\circ/115.9^\circ$, $119.7^\circ/119.1^\circ$ and $106.7^\circ/107.5^\circ$ is reduced by 4.3° , 0.3° and 3.3° due to the interaction between the C37 and O40. C35-C37-O40 is increased by 4.3° due to the interaction between the ethoxy group and O40. O40-C41-H42, O40-C41-H43 ($=109.3^\circ/109.7^\circ$, $109.3^\circ/109.7^\circ$) is reduced by 0.3° , 0.7° due to the interaction between H42 and O40.

4.2 Vibrational assignments

The title compound has 47 atoms and 135 modes of fundamental vibrations which span the irreducible representation as A. The observed and simulated FT-IR and FT-Raman spectra of the title compound at DFT-B3LYP level using 6-31G and 6-31G (d, p) basis sets are shown in Figs. 2 and 3. The experimental and theoretical wavenumbers along with their intensities are given in Table 2. The assignments of fundamental modes are based on the reported literature and Gauss View visualization program. The observed and calculated wavenumber and potential energy distribution are discussed below.

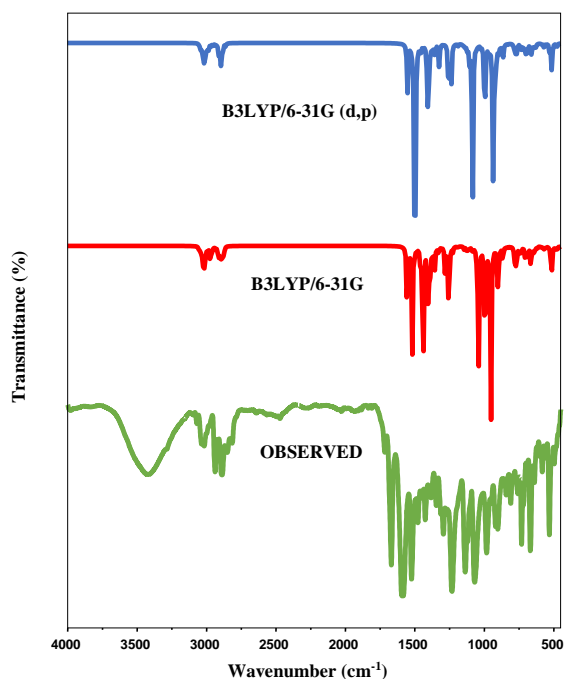


Fig.2 Observed FT-IR and simulated spectra of (2E)-1-(Anthracene-9-yl)-3-(4ethoxyphenyl) prop-2-en-1-one

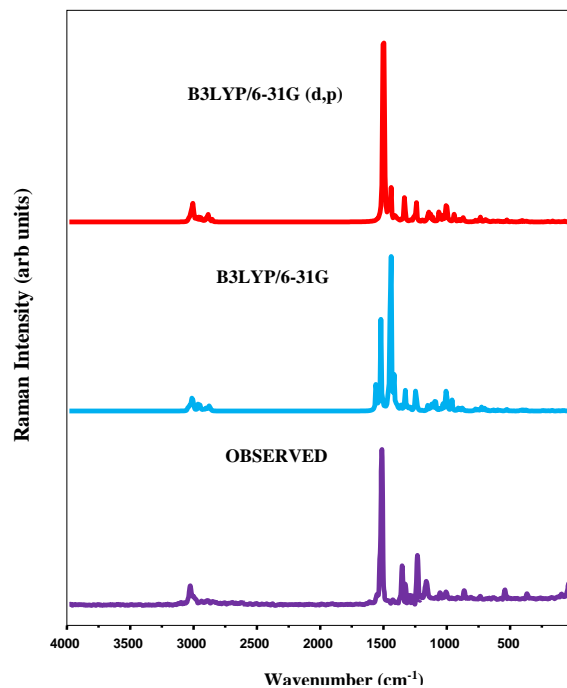


Fig.3 Observed FT-Raman and simulated spectra of (2E)-1-(Anthracene-9-yl)-3-(4ethoxyphenyl) prop-2-en-1-one

Table 2 : Vibrational assignments of-(2E)-1-(Anthracene-9-Yl) -3- (4ethoxyphenyl) prop-2-en-1-one

Modes	Observed wavenumber (cm ⁻¹)		Calculated (Scaled) wavenumbers (cm-1)		Vibrational assignment (%)
	FT-IR	FT-Raman	B3LYP/	B3LYP/	
			6-31G	6-31G(d,p)	
1		3060	3065	3062	vCH(98)
2	3050		3055	3051	vCH(98)
3			3045	3043	vCH(98)
4			3038	3036	vCH(98)
5			3032	3029	vCH(97)
6			3025	3022	vCH(98)
7			3017	3015	vCH(99)
8			3010	3007	vCH(98)
9	3000		3002	2999	vCH(98)
10		2980	2986	2982	vCH(97)
11	2973		2978	2975	vCH(98)
12			2971	2966	vCH(99)
13			2960	2957	vCH(98)
14			2948	2945	vCH(98)
15			2940	2936	vCH(98)
16			2928	2925	v _{ass} CH ₃ (96)
17	2923		2920	2918	v _{ass} CH ₃ (96)
18		2900	2910	2907	v _{ss} CH ₃ (96)
19		2890	2898	2896	v _{ass} CH ₂ (98)
20	2885		2889	2887	v _{ss} CH ₂ (98)
21		1580	1585	1581	vCO(69), vCC(20), δCH(10)
22			1571	1566	vCC(68), □CH(22)
23		1565	1560	1557	vCC(68), □CH(22)
24			1549	1545	vCC(72), vCO(12), □CH(10)
25			1531	1528	vCC(70), □CH(23)
26		1515	1518	1516	vCC(72), □CH(20)
27			1489	1487	vCC(72), □CH(22)
28			1471	1469	□CH(68), vCC(22)
29	1443		1445	1442	□CH(69), vCC(22)
30	1313	1435	1440	1438	ssClCH ₂ (21)

31			1433	1431	\square CH(68), $s_{\text{Sci}}\text{CH}_2(21)$
32	1424		1429	1425	$s_{\text{Sci}}\text{CH}_2(83)$
33			1420	1417	$v\text{CC}(70)$, \square CH(13)
34		1408	1415	1410	$\square_{\text{opb}}\text{CH}_3(69)$, $s_{\text{Sci}}\text{CH}_2(13)$
35			1406	1401	$\square_{\text{IPB}}\text{CH}_3(74)$
36			1392	1390	\square CH(69), $v\text{CC}(14)$
37	1387		1388	1385	\square CH(69), $v\text{CC}(14)$
38			1366	1362	$v\text{CC}(72)$, \square CH(16)
39	1356	1355	1358	1355	$v\text{CC}(74)$, \square CH(12)
40			1340	1337	$\square_{\text{SB}}\text{CH}_3(71)$, $r_{\text{rock}}\text{CH}_2(10)$
41		1325	1327	1325	\square CH(68), $v\text{CC}(18)$
42	1313		1315	1312	\square CH(72), $v\text{CC}(14)$
43		1294	1289	1288	$r_{\text{rock}}\text{CH}_2(68)$, $\square_{\text{SB}}\text{CH}_3(13)$
44			1273	1270	$v\text{CC}(67)$, $\square\text{CO}(13)$, \square CH(10)
45	1257	1259	1260	1258	\square CH(67), $v\text{CC}(18)$, $v\text{CO}(10)$
46			1225	1221	$v\text{CC}(69)$, \square CH(16)
47	1174	1216	1179	1175	$v\text{CC}(68)$, \square CH(18)
48			1160	1158	\square CH(68), $v\text{CC}(16)$
49		1173	1145	1141	\square CH(68), $v\text{CC}(15)$
50			1131	1129	$v\text{CC}(68)$, \square CH(12)
51	1116		1120	1118	$\square_{\text{opr}}\text{ch}_3(76)$, $t\text{CH}_2(13)$
52		1109	1091	1089	$v\text{CO}(60)$, \square CH(18)
53			1078	1075	$v\text{CC}(66)$, \square CH(16)
54			1060	1059	\square CH(68), $v\text{CC}(18)$
55	1041		1043	1040	$v\text{CC}(68)$, \square CH(18)
56			1040	1036	\square CH(65), $v\text{CC}(20)$
57		1033	1033	1032	\square CH(66), $v\text{CC}(18)$
58			1030	1027	\square CH(65), $v\text{CC}(21)$
59			1024	1020	$v\text{CC}(66)$, \square CH(18)
60	1012	1013	1015	1012	$\square_{\text{ipr}}\text{CH}_3(74)$, $r_{\text{rock}}\text{CH}_2(12)$
61			1007	1001	$v\text{CC}(66)$, \square CH(18)
62	985		989	986	$v\text{CO}(62)$, \square CH(13)
63			980	979	$v\text{CC}(63)$, \square CH(16)
64	970	970	973	970	$v\text{CC}(63)$, \square CH(18)
65			958	953	$v\text{CC}(66)$, $v\text{CO}(18)$,

					\square CH(10)
66			943	941	vCC(68), vCO(20)
67			939	935	vCC(68), \square CH(18)
68			934	930	vCC(66), \square CH(16)
69			930	928	\square CH(58)
70			926	923	vCC(66), \square CH(13)
71	918		924	918	\square CH(58)
72			905	903	\square CH(59)
73	890		896	892	vCC(67), vCO(14)
74		880	885	881	γ CH(59)
75			870	867	\square CH(60)
76	846		849	845	\square CH(60)
77			825	823	\square CH(62)
78	816		818	815	vCC(60), \square CH(16)
79			810	809	vCC(70), vCO(12)
80			806	804	\square CH(69)
81	798	800	802	799	\square CC(61), \square CO(12)
82			788	785	\square CH(67)
83			784	779	\square CH(68)
84			775	771	$\square_{\text{rin}}\square(58)$
85	765		770	765	\square CH(66)
86			758	752	$\square_{\text{rin}}\square(58)$
87			745	741	$\square_{\text{wa}}\square\text{CH}_2(65)$
88	734	732	735	733	\square CH(68)
89			734	729	\square CH(68)
90			728	722	\square CO(57)
91			718	715	\square CC(66)
92			707	703	\square CH(67)
93	696		697	695	\square CC(59)
94			682	681	\square CC(60)
95	669		673	670	$\square_{\text{rin}}\square(52)$
96			661	657	\square CO(58)
97	643		648	645	\square CC(52)
98			636	632	$\square_{\text{rin}}\square(62)$
99	623		628	625	$\square_{\text{rin}}\square(63)$
100			615	613	$\square_{\text{rin}}\square(63)$
101	599	600	600	597	$\square_{\text{rin}}\square(63)$
102			575	571	$\square_{\text{rin}}\square(62)$
103	557	557	559	555	\square CO(58)

104	530		535	521	□CO(53)
105			520	519	□CC(52)
106			500	497	□CC(53)
107			474	470	□ _{rin} □(52)
108	456	450	455	451	□CC(59)
109			439	436	□ _{rin} □(50)
110	436		431	427	□ _{rin} □(57)
111			420	418	□ _{rin} □(51)
112		400	406	401	□ _{rin} □(58)
113			388	385	□ _{rin} □(57)
114			360	361	□ _{rin} □(57)
115			338	334	□ _{rin} □(52)
116			304	301	□CC(58)
117		280	285	282	□ _{rin} □(58)
118			275	271	□CC(51)
119			260	258	Butterfly(55)
120			241	239	□CC(50)
121			228	226	□CC(51)
122			202	199	□CC(58)
123		190	194	192	tCH ₃ (68)
124			163	160	Butterfly(55)
125			150	149	□ _{rin} □(51)
126		120	125	121	tCH ₂ (66)
127			120	117	□ _{rin} □(52)
128			105	103	□ _{rin} □(51)
129			98	95	□ _{rin} □(53)
130		82	82	80	□ _{rin} □(51)
131			65	62	□ _{rin} □(52)
132			45	40	□ _{rin} □(52)
133			34	29	□ _{rin} □(51)
134			20	17	□ _{rin} □(51)
135			13	10	□ _{rin} □(50)

4.2.1 C-H vibrations

The C-H stretching vibrations of aromatic compounds are exhibit in the region 3100-2800 cm⁻¹[30]. The C-H in-plane bending and out-of-plane bending vibrations occur at 1300-1000 cm⁻¹ and 1000-700 cm⁻¹ [30].

In the present work, the CH stretching vibrations, the band appeared at 3127vw, 3050 vw, 2971 vw, 2923 vw, 2885 vw, 2851 vw cm^{-1} in IR spectrum and 3060s, 2990 vw, 2950 vw, 2860 vw, 2758 vw cm^{-1} in Raman spectrum. The computed values by B3LYP/6-31G method are 3065, 3055, 3045, 3038, 3032, 3025, 3017, 3010, 3002, 2986, 2978, 2971, 2960, 2948, 2940 cm^{-1} and 3062, 3051, 3043, 3036, 3029, 3022, 3015, 3007, 2999, 2982, 2975, 2966, 2957, 2936, 2918, 2907, 2896, 2887 cm^{-1} obtained by B3LYP/6-31G(d,p) method. Alaşalvar et al [22] reported that the CH in-plane bending modes are found at 1466, 1458, 1377, 1264, 1181, 1169, 1160, 1118, 1091, 1078, 1017 cm^{-1} for IR spectrum and 1467, 1385, 1186, 1162, 1123, 1093, 1078 cm^{-1} for Raman spectrum. In the present work, the C-H in-plane bending vibrations reported at 1443, 1313, 1174, 1041 cm^{-1} in the IR spectrum and 1435, 1325, 1216, and 1033 cm^{-1} in the Raman spectrum. The computed values by B3LYP/6-31G method are predicted at 1471, 1445, 1440, 1406, 1392, 1340, 1327, 1273, 1179, 1160, 1078, 1043, 1040 cm^{-1} for B3LYP/6-31G and 1469, 1442, 1438, 1401, 1390, 1337, 1325, 1270, 1175, 1158, 1075, 1040, 1036, 1032 cm^{-1} obtained by B3LYP/6-31G(d,p) method. The CH out-of-plane bending modes are observed at 727, 813, 841, 846, 864, 905, 919 cm^{-1} for IR spectrum and 817, 841, 863, 924 for Raman spectrum by Alaşalvar et al [22]. In the present work, the C-H out-of-plane bending vibrations are assigned to 918, 890, 864, 798, 734 cm^{-1} in FT-IR and 880, 800, 732 cm^{-1} in FT-Raman. The computed values by B3LYP/6-31G method are 926, 924, 896, 885, 870, 849, 810, 802, 788, 775, 745, 735, 718 cm^{-1} and 930, 923, 918, 892, 881, 867, 845, 809, 799, 785, 771, 741, 733, 715 cm^{-1} obtained by B3LYP/6-31G(d,p) method.

4.2.2 Ring vibrations

The anthracene ring and phenyl ring in-plane bending vibrations were calculated at 784, 770, 648, 636, 628, 615, 600, 439, 420, 406, 388, 304, 125, 105 cm^{-1} for B3LYP/6-31G and 779, 765, 645, 632, 613, 597, 436, 418, 401, 385, 301, 121, 103 obtained by B3LYP/6-31G(d,p) method. The peaks were observed at 696, 643, 623, 599 for IR and 765, 600, 450, 400, 120 for Raman spectrum was assigned to ring in-plane bending vibrations. The ring out-of-plane bending vibrations were calculated at 682, 500, 455, 431, 360, 163, 120, 98, 82, 65, 45, 34, 20, 13 cm^{-1} for B3LYP/6-31G and 681, 497, 451, 427, 361, 160, 117, 95, 80, 62, 40, 29, 17, 10 cm^{-1} obtained by B3LYP/6-31G (d,p) method and the Raman spectrum was observed at 82 cm^{-1} .

4.2.3 Carbon -Oxygen vibration

The C=O stretching mode is expected in the region 1750-1680 cm^{-1} [37, 38]. The in-plane and out-of-plane C=O bending modes are expected in the regions 625 ± 70 and 540 ± 80 cm^{-1} , respectively. In the present work, C=O stretching mode, in-plane bending and out-of-plane bending vibrations are observed at 1116 cm^{-1} , 669 cm^{-1} and 557 cm^{-1} by FT-IR and at $\nu=1580$ cm^{-1} and $\gamma=557$ cm^{-1} by FT-Raman. Hence in the present work, the calculated CO stretching vibrations by B3LYP/6-31G method at $\nu=1585$, 1120, 1007 cm^{-1} , CO in-plane bending = 734, 673, 575 cm^{-1} , CO out-of-plane bending = 559 cm^{-1} and $\nu\text{CO}=1581$, 1118, 1001 cm^{-1} , $\delta\text{CO}=729$, 670, 571 cm^{-1} , $\gamma\text{CO}=555$ cm^{-1} by B3LYP/6-31G (d, p).

4.2.4 CH₃ vibrations

The wavenumber of the vibrational modes of methoxy group is known to be influenced by a many interactions such as electronic effects, intermolecular hydrogen bonding and Fermi resonance [40]. Electronic effect such as back donation and induction mainly caused by the presence of oxygen atom adjacent to CH₃ group that can shift the position of CH stretching and bending modes [41,42]. $\nu_{as}CH_3$ absorb with a weak medium intensity ($2985\pm 25\text{ cm}^{-1}$ and $2970\pm 30\text{ cm}^{-1}$) and regularly seen above 3000 cm^{-1} . In the present work, CH₃ stretching vibrations for the title compound, the bands appeared at $\nu_{ass}=2923\text{vw cm}^{-1}$ in FT- IR spectrum and 2900, 2890cm^{-1} for FT- Raman spectrum. The computed values for $\nu_{ass} = 2928, 2920\text{ cm}^{-1}$, $\nu_{ss}= 2910$, $\delta_{opb}=1420\text{ cm}^{-1}$, $\delta_{sb}=1358, 1315\text{ cm}^{-1}$, $\delta_{ipb}=1415\text{ cm}^{-1}$, $\gamma_{opr}=1131\text{ cm}^{-1}$, $\delta_{ipr}=1024\text{ cm}^{-1}$ computed wave-numbers by B3LYP/6-31G method and at $\nu_{ass}=2925, 2918$ $\delta_{opb}=1417\text{ cm}^{-1}$, $\delta_{ipb}=1410\text{ cm}^{-1}$, $\delta_{sb}=1355, 1312\text{ cm}^{-1}$, $\gamma_{opr}=1129\text{ cm}^{-1}$ computed wavenumber by B3LYP/6-31G(d,p) method.

4.2.5 CH₂ vibrations

The main fundamental vibrations associated with each CH₂ group is classified as CH₂ symmetric stretching, CH₂ asymmetric stretching, CH₂ rocking and scissoring modes belong to in-plane vibration, whereas CH₂ twisting and wagging modes assigned to out-of-plane bending vibration. This CH₂ symmetric and asymmetric stretching vibrations occur in the range $3000\text{-}2800\text{ cm}^{-1}$ [43]. For the title compound, the methyl group, symmetric stretching is observed at $\nu_{ss}CH_2 = 2889, 2887\text{ cm}^{-1}$ and $\nu_{as}CH_2 = 2898, 2896\text{ cm}^{-1}$ theoretically obtained by B3LYP/6-31G and B3LYP/6-31G(d,p) methods. Scissoring modes reported at 1313 cm^{-1} (IR), 1435 cm^{-1} (Raman) and $1440, 433, 1420\text{ cm}^{-1}$ observed theoretically for B3LYP/6-31G, $1438, 1431, 1417\text{ cm}^{-1}$ for B3LYP/6-31G(d,p). Rocking modes are observed at $1356, 1313\text{ cm}^{-1}$ for IR spectrum and 1355 cm^{-1} for Raman spectrum. Theoretically δ_{rock} observed at $1358, 1315, 1024\text{ cm}^{-1}$ by B3LYP/6-31G, $1355, 1312, 1188\text{ cm}^{-1}$ $\gamma_{wag} = 758, 752\text{ cm}^{-1}$ by B3LYP/6-31G (d,p) methods. $\tau CH_2 = 1131, 1129\text{ cm}^{-1}$ for the same basis set. Varasanyi et al [44] observed the τCH_2 scissoring mode at $1465, 1420\text{ cm}^{-1}$ and CH₂ twisting and wagging at $1350, 1150\text{ cm}^{-1}$. For methyl group, two asymmetric stretching modes are calculated at $2974, 2975, 2978$ and 3006 cm^{-1} , while one symmetric stretching vibrational frequency is observed at 2921 and 2926 cm^{-1} by Alasalvar et al [22].

4.2.6 C-C vibration

The C-C stretching vibrations in aromatic rings generally appear at $1600\text{-}1400\text{ cm}^{-1}$ [45-50]. In the present work, the C-C stretching vibrations observed at $1424, 1387, 1257$ in FT-IR and $1565, 1515, 1294, 1259\text{ cm}^{-1}$ in FT-Raman spectrum. These C-C stretching modes are calculated at $1571, 1560, 1549, 1531, 1518, 1489, 1429, 1388, 1366, 1289, 1260, 1145\text{ cm}^{-1}$ B3LYP/6-31G method and $1566, 1557, 1545, 1528, 1516, 1487, 1425, 1385, 1362, 1288, 1258, 1221, 1141\text{ cm}^{-1}$ by B3LYP/6-31G(d,p) method. In the present study, The C-C in-plane deformation were calculated at $806, 728, 707, 474, 338, 228\text{ cm}^{-1}$ by B3LYP/6-31G method and $804, 722, 703, 470,$

334, 226 cm^{-1} by B3LYP/6-31G (d,p) method. The C-C out-of-plane deformation were calculated at 661, 535, 520, 285, 260, 241 cm^{-1} for B3LYP/6-31G and 657, 531, 519, 282, 258, 239 cm^{-1} for B3LYP/6-31G (d,p).

4.5 Mulliken atomic charges

The natural population analysis of the title compound is obtained by Mulliken [54] population analysis with B3LYP level using 6-31G and 6-31G(d,p) basis sets. The Mulliken charge values are tabulated in Table 3. The calculation has an important role in the application of quantum chemical calculation to the molecular system because of atomic charge effect, dipole moment, molecular polarizability and electronic structure. The charge changes with the basis set to polarization. For example, the charge of C(24) and C(37) atoms has 0.22 a.u, 0.32 a.u and 0.3 a.u, 0.36 a.u for the B3LYP /6-31G and B3LYP /6-31G (d,p) basis set are more positive, which are acceptor atoms. The charge distribution for C(33) and C(35) atoms has -0.13 a.u, -0.12 a.u and -0.14 a.u, -0.13 a.u charges. The charges of O(25) and O(40) atoms have -0.45 a.u, -0.49 a.u and -0.56 a.u, -0.52 a.u are more negative which are donor atoms. MEP and Mulliken charge analysis can be used for interpreting and predicting the reactive sites of a wide variety of chemical systems in both nucleophilic and electrophilic reactions.

Table 3 : Mulliken atomic charges for (2E)-1-(Anthracene-9-Yl)-3- (4ethoxyphenyl) prop-2-en-1-one calculated at B3LYP/6-31G and B3LYP/6-31G

Atoms	B3LYP/ 6-31G	B3LYP/ 6-31G(d,p)	Atoms	B3LYP/ 6-31G	B3LYP/ 6-31G(d,p)
C1	0.13	-0.10	O25	0.45	-0.49
C2	0.15	-0.12	C26	0.14	-0.16
C3	0.06	0.11	H27	0.14	0.09
C4	0.05	0.08	C28	0.13	-0.08
C5	0.15	-0.14	H29	0.17	0.12
C6	0.13	-0.10	C30	0.09	0.13
C7	0.22	-0.20	C31	0.17	-0.13
C8	0.04	-0.05	C32	0.15	-0.13
C9	0.05	0.08	C33	0.13	-0.12
C10	0.06	0.11	H34	0.14	0.10
C11	0.15	-0.12	C35	0.14	-0.13
H12	0.13	0.08	H36	0.14	0.09
C13	0.13	-0.09	C37	0.30	0.36
C14	0.13	-0.10	H38	0.15	0.10
C15	0.13	-0.12	H39	0.14	0.09
H16	0.13	0.08	O40	0.56	-0.52

H17	0.13	0.09	C41	0.02	0.05
H18	0.13	0.09	H42	0.15	0.11
H19	0.15	0.10	H43	0.15	0.11
H20	0.13	0.09	C44	0.41	-0.34
H21	0.13	0.09	H45	0.16	0.13
H22	0.13	0.09	H46	0.14	0.11
H23	0.17	0.12	H47	0.16	0.13
C24	0.22	0.32			

4.6 NBO analysis

The natural bond orbital (NBO) calculations for the title compound were performed using NBO 3.1 program [18] as implemented in the Gaussian 09 package at the DFT / B3LYP level with 6-31G (d,p) basis set. The NBO method demonstrates the bonding concept like atomic charge, Lewis structure, bond type, hybridization, bond order, charge transfer and resonance possibility. The stabilization of orbital interaction is proportional to the energy difference between interacting orbitals. The bonding – antibonding stabilization energies within the molecule are calculated, to investigate the intermolecular interactions. The bonding - antibonding interactions can be qualitatively described employing second-order perturbation interaction energy $E^{(2)}$ [55-59]. This energy represents the estimate of the off-diagonal NBO Fock matrix elements and the Fock matrix was carried out to evaluate donor (i) and acceptor (j). The stabilization energy $E^{(2)}$ associated with delocalization $i \rightarrow j$ is estimated as follows

$$E^{(2)} = \Delta E_{ij} = \frac{q_i F_{2(i,j)}}{\epsilon_j - \epsilon_i}$$

where q_i is the donor orbital occupancy ϵ_j and ϵ_i are diagonal elements and $F(i,j)$ is the off-diagonal NBO Fock matrix element.

The occupancy of bond orbitals, atomic and hybrid contributions of different bonds of the title compound are presented in Table 4. The NBO analysis BD (C37-O40) orbital with 1.99005 electrons has 33.04% C37 character in a $sp^{1.14}$ hybrid and has 66.96% O40 character in a $sp^{2.33}$ hybrid. The $sp^{1.14}$ hybrid on C37 has 75.64 p-character and the $sp^{2.33}$ hybrid on O40 has 69.97 p-character. For BD (C41-C44) orbital with 1.98962 electrons has 50.54% C41 character in a $sp^{2.55}$ hybrid and has 49.46% C44 character in a $sp^{2.9}$ hybrid. The $sp^{2.55}$ hybrid on C41 has 71.87% p-character and the $sp^{2.9}$ hybrid on C44 has 74.33% p-character for the title compound. The two coefficients, 1.99005 and 1.98962 are called polarization coefficients. The sizes of these coefficients show the importance of the two hybrids in the formation of the bond. The oxygen has a larger percentage of this NBO, 66.96% and gives the larger polarization coefficient 0.8183 because it has the higher electronegativity. Similarly, BD (C5-H19), BD (C1-H17), BD (C2-H18) has a lesser percentage of NBO and give the lesser polarization coefficients as compared to

BD (C37-O40) bond. This shows that oxygen and carbon in the above bonding orbitals have less electronegativity as compared to BD (C37-O40).

The donor-accepter interaction can be estimated by the second-order perturbation theory. Table 5 lists the calculated second-order interaction energies $E^{(2)}$ between the donor-acceptor orbital of the title compound. The most important interaction energies related to the resonance in the anthracene ring are electron-donating from the BD (C1-C2), BD (C3-C4), LP(2) O25, LP(2) O25, LP(2) O40, LP(2) O40 to the anti-bonding acceptor BD*(2) C3-C4, BD*(2) C8-C9, BD*(1) C24-C26, BD*(1) C8-C24, BD*(2) C35-C37, BD*(1) C41-H43, orbitals and their corresponding energies are 24.47, 44.72, 19.57, 8.82, 8.35 and 5.56 kcal/mol, respectively. These interactions indicate that the strongest interaction increase in the stabilization energy of electron delocalization occurs due to the substitution of the molecule.

Table 4: NBO analysis of bonding and antibonding orbit of (2E)-1-(Anthracene-9-Yl) -3-(4ethoxyphenyl) prop-2-en-1-one in C1 conformer B3LYP/6-31G method.

Band (A-B)	ED/Energy (a.u.)	ED %	ED %	NBO	S(%)	P(%)
s C1-C2	1.98066	49.84	50.16	0.7060 SP ^(1.73)	36.64	63.36
	-0.93974			0.7082 SP ^(1.71)	36.96	63.04
s C2-C3	1.97394	48.47	51.53	0.6962 SP ^(1.97)	33.65	66.35
	-0.87357			0.7179 SP ^(2.02)	33.1	66.9
s C4-C5	1.97022	51.74	48.26	0.7193 SP ^(2.04)	32.9	67.1
	-0.86633			0.6947 SP ^(2.11)	32.15	67.85
s C7-C10	1.97451	48.7	51.3	0.6978 SP ^(1.82)	35.4	64.6
	-0.90144			0.7163 SP ^(1.9)	34.51	65.49
s C8-C24	1.97312	51.47	48.53	0.7174SP ^(2.66)	27.31	72.69
	-0.80745			0.6966 SP ^(2.16)	31.63	68.37
s C9-C15	1.97195	51.85	48.15	0.7201 SP ^(2.04)	32.91	67.09
	-0.86421			0.6939 SP ^(2.03)	32.98	67.02
s C13-C14	1.97925	50.16	49.84	0.7083 SP ^(1.94)	34.04	65.96
	-0.87604			0.7060 SP ^(1.97)	33.69	66.31
s C24-O25	1.99274	34.52	65.48	0.5875 SP ^(2.38)	29.56	70.44
	-1.32438			0.8092 SP ^(1.68)	37.29	62.71
s C28-C30	1.98055	50.6	49.4	0.7113 SP ^(2.53)	28.32	71.68
	-0.6963			0.7029 SP ^(3.21)	23.78	76.22
s C35-C37	1.97967	50.28	49.72	0.7091 SP ^(1.87)	34.79	65.21
	-0.95682			0.7051 SP ^(1.66)	37.56	62.44
s C37-O40	1.99005	33.04	66.96	0.5748 SP ^(3.14)	24.36	75.64

	-1.07088			0.8183 SP ^(2.33)	30.03	69.97
s O40-C41	1.98638	30.64	30.64	0.8329 SP ^(2.32)	30.11	69.89
	-1.05031			0.5535 SP ⁽⁴⁾	20.02	79.98
s C41-C44	1.98962	50.54	49.46	0.7109 SP ^(2.55)	29.13	71.87
	-0.79316			0.7033 SP ^(2.9)	25.67	74.33
s C5-H19	1.93	63.92	36.08	0.7995 SP(2.23)	30.99	69.01
	-0.67659			0.6006 S ⁽¹⁾		100

Table 5: Second-order perturbation theory analysis of Fock matrix in NBO basis corresponding to intramolecular bands of (2E)-1-(Anthracene-9-Yl) -3- (4ethoxyphenyl) prop-2-en-1-one at B3LYP/6-31G basis set.

Donor	Acceptor	E(2)(kcal/mol)	E(J)-E(i) (a.u)	F _(ij) (a.u)
		BMP	BMP	BMP
p (2) O25	s*(2) C8-C9	2.8	0.68	0.043
p (2) O25	s*(1) C8-C24	8.82	1.08	0.088
p (2) O25	s*(1) C14-C15	0.58	1.42	0.026
p (2) O25	s*(2) C14-C15	1.02	0.71	0.025
p (2) O25	s*(1) C24-C26	19.57	1.06	0.13
p (2) O25	s*(1) C26-H27	0.57	1.19	0.023
p (2) O40	s*(1) C33-C 37	3.02	1.4	0.058
p (2) O40	s*(1) C 35-C 37	8.4	1.4	0.097
p (2) O40	s*(2) C 35-C 37	1.16	0.72	0.028
p (2) O40	s*(1) C41-H 42	7.65	1.31	0.09
p (2) O40	s*(1) C41-H 43	1.49	1.31	0.04
p (2) O40	s*(1) C41-C 44	0.92	1.17	0.029
p (2) O40	s*(1) C33-C37	3.8	1.51	0.068
p (2) O40	s*(2) C35-C37	8.35	0.83	0.081
p (2) O40	s*(1) C41-H43	5.56	1.42	0.08
p (2) O40	s*(1) C41-C44	1.03	1.28	0.033
s(1) C1-C2	s*(1) C6-H20	2.28	1.66	0.055
s(2) C3-C4	s*(2) C8-C9	44.72	0.45	0.129
s(2) C1-C2	s*(2) C3-C4	24.47	0.49	0.107
s(1) C2-H18	s*(1) C3-C4	5.13	1.51	0.079
s(2) C3-C4	s*(1) C2-C3	4.11	1.68	0.074
s(2) C4-C5	s*(1) C6-H20	3.18	1.59	0.064
s(2) C30-C32	s*(1) C26-C28	1.2	0.92	0.032
s(2) C30C32	s*(2) C 35-C 37	37.8	0.49	0.122

aE(2) means the energy of hyperconjugation interactions (stabilization energy).

bEnergy difference between donor and acceptor i and j NBO orbitals.

cF(i,j) is the Fock matrix element between i and j NBO orbitals.

4.7 Frontier molecule orbitals

The highest occupied molecular orbital (HOMO) and lowest unoccupied molecular orbital (LUMO) are called as the frontier molecule orbitals (FMOS) that have an important role in chemical reactions [60]. The HOMOs and LUMOs can be considered as donor and acceptor groups occupied, unoccupied by electrons respectively [61]. The energy values between HOMO and LUMO also determines the molecular electronic properties such as ionization potential ($I = -E_{\text{HOMO}}$), electron affinity ($A = E_{\text{LUMO}}$), chemical hardness ($\eta = (I-A)/2$), Chemical softness ($\varepsilon = 1/2(I-A)$), Chemical potential ($\mu = -(I+A)/2$), Electronegativity ($\chi = (I+A)/2$), electrophilicity index ($\omega = \mu^2/2\eta$) chemical reactivity and chemical stability that are important parameters in a quantum chemistry [62-64]. To understand the bonding schemes of the title compound, the surfaces of FMOs are given in Fig.4 and Table 6. The energy gap, the difference between H-L, H-1-L-1, H-2-L-2 orbital are the parameters in determining molecular electrical transport properties because it is a measure of electronic conductivity and the energy gaps were calculated as 3.1197, 4.3785 and 6.1495eV respectively. This energy gap also indicates the colour of these compounds as electrons are constantly shifting between these orbitals and further dictates their interaction with receptor site at the cellular level. Simultaneously, it also explains that charge transfer interactions are occurring within the molecules. From the energy gap, one can find whether the molecule is hard or soft. The molecules having a large energy gap are known as hard and having small energy gap are known as soft. The energy gap of the title molecule is 3.12 eV. Hence we conclude that the title molecule belongs to hard material. The soft molecules are more polarizable than the hard one because they need small energy for excitation. The calculated values of the hardness and softness of the molecules were 0.115eV and 8.722eV. The chemical potential of the title compound is negative and it means that the compound is stable.

4.8 Molecular electrostatic potential

The molecular electrostatic potential (MEP) has been used to predict the behaviour and reactivity of the molecule. It is very useful in understanding the potential sites for electrophilic (negative region) and nucleophilic (negative region) reactions [65] MEP is also well suited for analyzing process based on the “recognition” of one molecule by another, as in drug-receptor and enzyme-substrate interactions because it is through their potential that the two species first “see” each other [66]. To predict reactive sites for electrophilic and nucleophilic sites for the investigated molecule, MEP is calculated at the B3LYP/6-31G(d,p) optimized geometries and shown in Fig. 5. The colour scheme for the MEP surface is, red represents a rich region which is an absolute negative charge, yellow represents the slightly electron-rich region, light blue represents a slightly electron-deficient region, green represents the neutral region and blue

represents electron-deficient which is a partially positive charge. Potential increases in the order red < orange < yellow < green < blue [67].

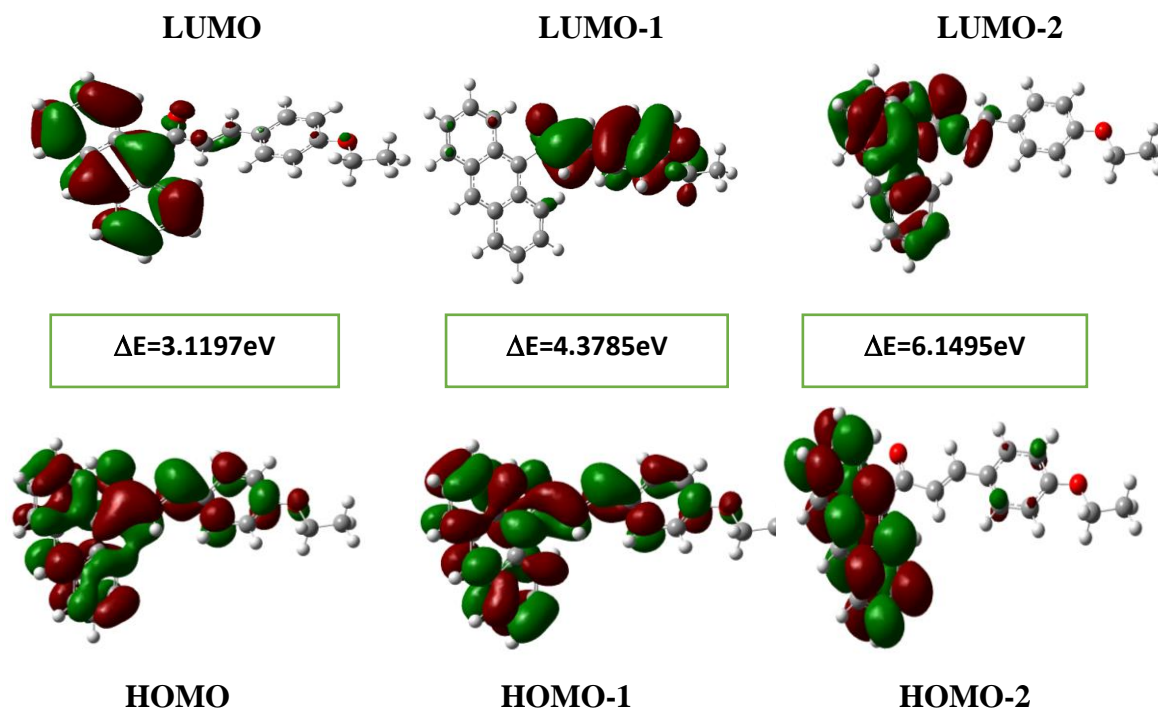


Fig.4 Patterns of the principle highest occupied and lowest unoccupied molecular orbital of (2E)-1-(Anthracene-9-yl)-3-(4ethoxyphenyl) prop-2-en-1-one

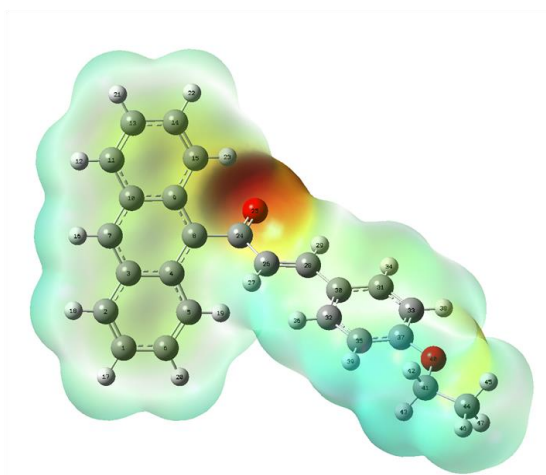


Fig.5 Molecular electrostatic potential surfaces of (2E)-1-(Anthracene-9-yl)-3-(4ethoxyphenyl) prop-2-en-1-one

For the title compound, more reactive sites are close to the C=O group, the regions having the most negative potential over the oxygen atom O₂₅ ketone group then all the hydrogen atoms have positive potential. The red colour is a negative potential which corresponds to the interaction of a proton and blue region is positive which corresponds to the repulsion of the proton. It is seen that negative electrostatic potential (red) is located maximum around oxygen atom and the hydrogen atoms attached to the ethylene group possess the bang of positive charge (blue).

Table 6: HOMO-LUMO energies for (2E)-1-(Anthracene-9-Yl) -3- (4ethoxyphenyl) prop-2-en-1-one calculated at B3LYP/6-31G(d,p)

Energy (eV)	Energy gap (eV)	Ionisation potential (I)	Electron affinity (A)	Global hardness (h)	Electron negativity (c)	Global softness (s)	Chemical potential (m)	Global Electroplicity (w)
5.2966	3.1197	0.19465	0.08	0.11465	0.1373	8.7222	-0.1373	0.0822
2.1769								
5.8787	4.3785	0.21604	0.05513	0.16091	0.1356	6.2146	-0.1356	0.05713
1.5002								
6.4559	6.1495	0.23725	0.01126	0.22599	0.1242	4.4249	-0.1242	0.03413
0.3064								

5 Conclusions

The FT-IR and FT-Raman spectra of (2E)-1-(Anthracene-9-Yl) -3-(4-ethoxy phenyl) prop-2-en-1-one was recorded and the vibrational spectra have been investigated experimentally and theoretically by using B3LYP and 6-31G, 6-31G (d,p) methods. Experimentally observed frequencies are in good agreement with the theoretical values. The stability of the molecule arising from hyper-conjugative interaction and charge delocalization has been analyzed using NBO analysis. The LUMO and HOMO energy provides information regarding ionization potential, chemical potential and other chemical descriptors. As can be seen from the MEP map of the title molecule, negative region is mainly localized over the C=O group, anthracene ring and the maximum positive region is localized on the phenyl groups. Weak interaction profile shows that the presence of Van der Waals interactions and the steric effect is present in the molecule.

References

- [1] Yan-mei W, Si-dong I I, Jie-ping Z, Wei-wang Z, *Fine Speciality Chem.* 15 (2007) 20-24
- [2] Yavri I, Alborzi A R, Mohtat B, *Dyes Pigments* 68 (2006) 85-88
- [3] Yan Y, Su X, Liyang Y, Zhang J, Shi C, Lu Y, Gu L, Fu I, *Mol. Cancer Ther.* 7 (2008) 1688-1697.
- [4] Ali A M, Ismail N H, Mackeen M M, Yazan L S, Mohamed S M, Ho A S H, Lajis N H, *Pharm. Biol.* 38 (2000) 298-301.
- [5] Nanayakkara N P D, Schrader K K, *J. Agric. Food Chem.* 56 (2008) 1002-1007
- [6] Gruen H, Goerner H, *Photochem. Photobiol. Sci.* 7 (2008) 1344 – 1352.
- [7] Francis R C, Shin S J, Omori S, Amidon T E, Blain R J, Wood J, *Chem. Technol.* 26 (2006) 141 – 152.
- [8] Aguilar G V, Wang X H, Nelsen S F, Zink J I, *J. Am. Chem. Soc.* 128 (2006) 6180-6185.
- [9] Stewart G, Jiao Y G, Valente E J, Fu P P, Li T Q, Hu Z Z, Yu H T, *J. Photoch. Photobio. A* 201 (2009) 39-44.
- [10] Atherton J C C, Jones S, *Tetrahedron Lett.* 43 (2002) 9097-9100.
- [11] Bouas H-Laurent, Castellan A, Desvergne J P, *Chem. Soc. Rev.* 29 (2000) 43–55.
- [12] Nishimura G, Shiraishi Y, Hirai T, *Chem. Commun.* 42 (2005) 5313–5315.
- [13] Bouas-Laurent H, Castellan A, Desvergne J P, Lapouyade R, *Chem. Soc. Rev.* 30 (2001) 248-263.
- [14] Han X C, Li C, Mosher M D, Rider K C, Zhou P W, Crawford R L, Fusco W, Paszczyński A, Natale N R, *Bioorg. Med. Chem.* 17 (2009) 1671-1680.
- [15] Becke A D, *J. Chem. Phys.*, 98 (1993) 5648-5652.
- [16] Lee C, Yang W, Parr R G, *Phys. Rev. B*, 37 (1988) 785-789.
- [17] Frisch M J, Trucks G W, Schlegel H B, Scuseria G E, Robb M A, Cheeseman J R, Scalmani G, Barone V, Mennucci B, Peterson G A, Nakatsuji H, Caricato M, Li X, Hratchian H P, Izmaylov F, Bloino J, Zheng G, Sonnenberg J I, Hada M, Ehara M, Toyota K, Fukuda R, Hasegawa J, Ishida M, Nakajima T, Honda Y, Kitao O, Nagari H, Vreven T, Montgomery T A Jr., Peralta J E, Ogliaro F, Bearpark M, Heyd J J, Brothers E, Kudin K N, Staroverov V N, Kobayashi R K, Normand J, Ragavachari K, Rendell A, Burant J C, Iyengar S S, Tomasi J, Cossi M, Rega N, Millam J M, Klene M, Knox J E, Cross J B, Bakken V, Adamo C, Jaramillo J, Gomperts R G, Strarmann R E, Yazyev O, Austin A J, Cammi R, Pomelli C, Ochterski J W, Martin R I, Morokuma K, Zakrzewski V G, Voth G A, Salvador P, Dannenberg J J, Dapprich S, Farkas O, Ortiz J V, Cioslowski J, Fox D J *Gaussian, Inc., Wallingford CT, 2009.*
- [18] Glendening E D, Reed A E, Carpenter J. E, Weinhold F, *NBO version 3.1*, Pittsburg, Theoretical chemistry institute and department of chemistry, University of Wisconsin, Madison, 1988.
- [19] Morris G M, Goodsell D S, Halliday R S, Huey R, Hart W E, Belew R K, Olson A J, *J. Comput. Chem.* 19 (1998) 1639-1662.

- [20] Mague J T, Abdel-Aziz A A-M, El-Azab A S, El-Sherbeny M A, *Acta Cryst. E* 70 (2014) 248-249.
- [21] Nie J J, Xu D J, *Chin. Struct. J. Chem.* 21 (2002) 165-167.
- [22] Arjunan V, Raj A, Subramanian S, Mohan S, *Spectrochim. Acta* 110A (2013) 141-150.
- [23] Murthy BVR, *Kristallogr.Z* 113 (1960) 445-465.
- [24] Roeges N P G, *A Guide to the complete interpretation of the Infrared Spectra of organic structures*, Wiley, NY, 118 (1994) 3543-3543.
- [25] Can Alaşalvar, Nuri Öztürk, Alaa A.-M. Abdel-Aziz, HalilGökce, Adel S. El-Azab, Manal A. El-Gendy, Yusuf Sert, *J. Mol. Struct.* 1171 (2018) 696-705.
- [26] Gussoni M, Castiglioni C O, *J.Mol.Struct.* 521 (2000) 1-18.
- [27] Pavitha P, Prashanth J, Ramu G, Ramesh G, Mamatha K, Venkatram Reddy B, *Journal of Molecular Structure*, PII: S0022-2860(17)30876-1.
- [28] Chandran A, Mary Y S, Varghese H T, Panicker C Y, Pazdera P, Rajendran G, *Spectrochim. Acta* 79A (2011) 1584-1592.
- [29] Mary Y S, Jojo P J, Van Alsenoy C, Kaur M, Siddegowda M S, Yathirajan H S, Nogueira H I S, Cruz S M A, *Spectrochim. Acta* 120 (2014) 370-380.
- [30] Lee S Y, Boo B H, *Bull, Korean Chem. Soc.* 17 (1996) 754-759.
- [31] L.J. Bellamy, *The Infrared Spectra of Complex Molecules*, third ed., John Wiley & Sons, Inc., New York, 433 pages, 1975.
- [32] Colthup N B, Daly L H, Wiberly S E, *Introduction to IR and Raman spectroscopy*, Academic Press, New York 1990.
- [33] Käfer D, Witte G, Cyganik P, Terfort A, Wöll C, *J. Am. Chem. Soc.* 128 (2006) 1723-1732.
- [34] G. Varasanyi, *Assignments for Vibrational Spectra of Seven Hundred Benzene Derivatives*, Vol. I, Adam Hilger, London, 1974, pp 334.
- [35] Wang X, Valverde G.-Aguilar, Weaver M N, Nelson S F, Zink J I, *J. Phys. Chem. A* 111 (2007) 5441-5447.
- [36] Mulliken R S, *J.Chem. Phys.* 23 (1995) 1833-1840.
- [37] Reed A E, wienhold F, *J.Chem. Phys.* 83 (1985) 1736.
- [38] Reed A E, wienhold R B, wienhold F, *J.Chem. Phys.* 83 (1985) 735.
- [39] Reed A E, wienhold F, *J.Chem. Phys.* 78 (1983) 4066.
- [40] Foster J P, wienhold F, *J.Am.Chem. Soc.* 102 (1980) 7211.
- [41] Jenson J O, Banerjee A, Merrow C N, Zeroka D, Lochner J M, *J.Mol.Struct. (Theochem.)* 531 (2000) 323.
- [42] Fuji K, *Science* 218 (1982) 747-754.
- [43] Buyukuslu H, Akdogan M, Yildirim G, Parlak C, *Spectrochim. Acta Part A* 75 (2010) 1362-1369.
- [44] Parr R G, Donnelly R A, Levy M, Palke W E, *J. Chem. Phys.* 68 (1978) 3801-3807.
- [45] Parr R G, Pearson R G, *J. Am. Chem. Soc.* 105 (1983) 7512-7516.
- [46] Parr R G, Szentpaly L V, Liu S, *J. Am. Chem. Soc.* 121 (1999) 1922-1924.

- [47] (a) Scrocco E, Tomasi J, *Adv. Quantum Chem.*, 11 (1978) 115-193.
(b) Luqul F J, Lopez J M, Orozco M, *Theor. Chem. Acc.*, 2000, 103, 343.
- [48] (a) Scrocco E, Tomasi J, *Curr. Chem.*, 7 (1973) 95-170 ;
(b) Li Y, Liu Y, Wang H, Xiong X, Wei P, Li F, *Molecules*, 18 (2013) 877-893.
- [49] Balachandran V, Lakshmi A, Janaki A, *J. Mol. Struct.* 1013 (2012) 75-85.